16th International Benchmark Workshop on Numerical Analysis of Dams

Proceedings

Mateja Klun
Andrej Kryžanowski
Nina Humar

Ljubljana, 5th - 6th April, 2022

16TH INTERNATIONAL BENCHMARK WORKSHOP ON NUMERICAL
ANALYSIS OF DAMS- PROCEEDINGS
16. MEDNARODNA KONFERENCA O NUMERČNI ANALIZI PREGRAD- ZBORNIK PRISPEVKOV

Ljubljana, 2024

ICOLD Technical Committee A
Computational Aspects of
Analysis and Design of Dams

SLOCOLD

FGG
UNIVERZA V LJUBLJANI | Fakulteta za gradbeništvo in geodezijo

Univerza v Ljubljani

UNESCO katedra za zmanjševanje
tveganj ob vodnih ujmah
Univerza v Ljubljani

unesco
Katedra

Sponsors and supporters:

CIMNE
International Centre
for Numerical Methods in Engineering

KTH
VETENSKAP
OCH KONST

Hydro Québec

eDF

Geoportal

ZAG 75 LET

iC ELEA
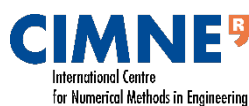
Mateja Klun, Faculty of civil and geodetic engineering of Ljubljana
Andrej Kryžanowski, Faculty of civil and geodetic engineering of Ljubljana
Nina Humar, Slovenian national committee on large dam

We are pleased to present you the proceedings of the 16th International Benchmark Workshop on Numerical Analysis of Dams, held in Ljubljana on April 5th and 6th, 2022. Organised by Slovenian national committee on large dams (SLOCOLD), under the auspices of the International Commission on Large Dams' Technical Committee on Computational Aspects of Analysis and Design of Dams, this workshop brought together experts and practitioners from around the globe to exchange insights, innovative approaches and best practices in the numerical analysis of dams.

ICOLD has long been at the forefront of progress of the dam engineering science and has contributed greatly to the development and advance of dam design, safety, and performance evaluation. In this spirit, the Benchmark Workshops serve as vital platforms for fostering collaboration, refining methodologies, and addressing emerging challenges in the field, as well as a reference for the global dam community, offering valuable insights and benchmarks for engineers, researchers, and stakeholders alike. They are particularly valuable for young engineers, providing them with essential resources and challenges as they contribute to the critical task of ensuring dam safety and resilience in the face of evolving environmental and societal demands.

The benchmarking activities of the Technical Committee on Computational Aspects of Analysis and Design of Dams have attracted significant participation from technicians operating in the dam sector, with attendance consistently reaching up to 190 participants in recent workshops. Despite the fact that 16th benchmark workshop was only held online, due to the uncertain situation triggered by the COVID-19 pandemic, it attracted a participation of significant number of contributors and gained the attendance of over 100 participants from all over the world. For the first time, we tackled topics such as Dam behaviour prediction and fitting to actual measurements, modelling of AAR affected dams and Behaviour of the embankment dam, right after the rehabilitation works.

The proceedings herein encapsulate the collective knowledge and expertise shared during the 16th International Benchmark Workshop, by formulators, contributors and participants. From innovative modelling approaches to practical application, these papers offer valuable insights and perspectives for researchers, engineers, and stakeholders involved in dam design, surveillance and management.

We extend our gratitude to all the contributors, presenters, and attendees whose dedication and enthusiasm have made this workshop a resounding success. It is our hope that these proceedings will serve as a lasting resource for advancing the state-of-the-art in the numerical analysis of dams and contribute to the ongoing efforts to ensure the safety and resilience of dam infrastructure worldwide.

Nina Humar,
President of Slovene national committee on large dams SLOCOLD

TABLE OF CONTENTS

Dam behaviour prediction

Theme A

BEHAVIOUR PREDICTION
OF A CONCRETE ARCH DAM

Description and Synthesis of Theme A

Formulators:

Fernando Salazar
CIMNE, Spain

Alexandre Simon,
EDF Hydro, France

Richard Malm
KTH Royal Institute of Technology, Sweden

Rikard Hellgren
KTH Royal Institute of Technology, Sweden

Mateja Klun
University of Ljubljana, Slovenia

1 INTRODUCTION

Dam monitoring is an important part of the dam safety work to obtain a greater understanding of the dam and is essential to identify changes in its behavior that can occur during their service life. Proper assessment of the aging dams increases the knowledge of their current safety and allows for better planning of renovation and rebuilding investments.

Prediction of measurements and interpretation of future dam behavior, based on the data gained with measurements, can therefore be considered as a common task for dam engineers nowadays. Previous research has shown that the behavior of concrete dams is, to a great extent, governed by the ambient variation in temperature and water level. Thereby, utilizing different type of behavior models that can account for these variations in ambient conditions has great potential to capture the expected response of a dam.

Moreover, these behavior models are often a crucial part of dam safety systems. With the help of various prediction models, engineers can evaluate dams' performance, estimate its response to actual load conditions and define warning levels. In recent years, a vast development has occurred in the field of prediction models, especially regarding data-based and machine learning approaches. In addition to data-based models, numerical models based on the finite element method (FEM), are widely used to estimate displacements, stresses, and strains of dams and therefore predict their response. These models are based on the physical laws that govern the processes. Due to the increased computer power, both data-based and numerical models gained in their level of detail and accuracy but also in their complexity. Both are used by dam specialists, and it is therefore important to study the capabilities of these methodologies for assessing the dam behavior and predict the expected future behavior of the dam.

The Technical Committee A "Computational Aspects of Analysis and Design of Dams" within International Commission of Large Dams (ICOLD) has organized international Benchmark Workshops (BW) on the topic of numerical analysis of dams since 1990. The purpose of these is to share knowledge and experience regarding numerical modelling within the fields of dam safety, planning, design, construction as well as operation and maintenance of dams. In the 6th ICOLD BW in 2001, interpretation of the measurements at the Schlegeis dam was one theme at the workshop. Years later, in 2017, at the 14th ICOLD BW, a theme was focused on predicting the dam behavior, including cracking, caused by seasonal temperature variations. The aim of the current theme for the 2022 ICOLD BW is to build from the experience of past workshops and see how modern tools can be used in the prediction of dam behavior.

1.1 *Focus of this benchmark problem*

In this benchmark problem, denoted as Theme A in the 2022 ICOLD BW, a double curvature arch dam, located in the south of France and owned by the EDF (Électricité de France) is used as a case study. The name of the dam remains undisclosed. The aim of the theme was to establish a prediction model for the dam. For this task, all types of models were welcome to use (statistical, hybrid, deterministic, machine learning, finite element modelling) from the simplest to the most complex ones.

The geometry and material properties of the dam and foundation were delivered by the formulators. The participants were also given the monitoring data from the dam for the period 2000-2012. The provided data has been pre-processed and so it could be directly used for the analysis, e.g. no further cleaning was necessary. Furthermore, the data was provided without any modification of the actual time series and is measured with different frequencies. The participants were asked to build a model, calibrate it, and use it for long-term and short-term predictions using the provided data and by making their assumptions and choose suitable approaches to solve the problem.

Theme A consists of mandatory and optional tasks that are divided among three cases: calibration (Case A), short-term predictions (Case B), and long-term predictions (Case C). For the participants, it was mandatory to consider the radial displacement from two pendulums, evaluate them and provide results for all three cases. Other variables (crack opening, piezometric level, and seepage) are provided as well, while interpretation and prediction of them were optional.

1.2   *General basic assumptions*

The focus of the theme is on the following variables:
- Radial displacement (two pendulums in the central block of the dam)
- Crack opening displacement (sensor at the rock-concrete interface)
- Piezometric levels (vibrating wire piezometers at the rock-concrete interface)
- Seepage (weir at the downstream toe of the dam).

The material properties that were considered in the design studies of the dam are provided by the formulators. The geometry of the dam is provided in different CAD formats.

1.3   *Deliverables*

All participants were requested to deliver their solution to the defined problem including output data, description of modelling assumptions, used software, etc. For the mandatory tasks, the participants were asked to provide both predictions and warning levels for the monitored phenomenon.

In addition to delivering the requested results, all participants were required to provide a paper describing the problem and the chosen solution methods. The participants presented their results during the Workshop.

2   FORMULATION OF THE THEME

2.1   *Description of the dam*

The studied dam is owned by EDF (Électricité de France) and it is named 'Dam_EDF' in the following text. Dam_EDF was constructed between 1957 and 1960. It is a double curvature arch dam, which is asymmetric because of the shape of the valley. Dam_EDF is made of concrete with cement dosage at 300 kg/m^3 and it consists of 13 blocks:
- 1 block of 12 m wide on the right bank
- 11 blocks of 12.5 m wide
- 1 block of 17 m wide on the left bank

In Figure 1 and Figure 2, illustrations of the dam are presented. The foundation of Dam_EDF consists of laminated metamorphic slate which have a high compressive strength. However, the anisotropy of foundation confers a higher deformability to the left bank.
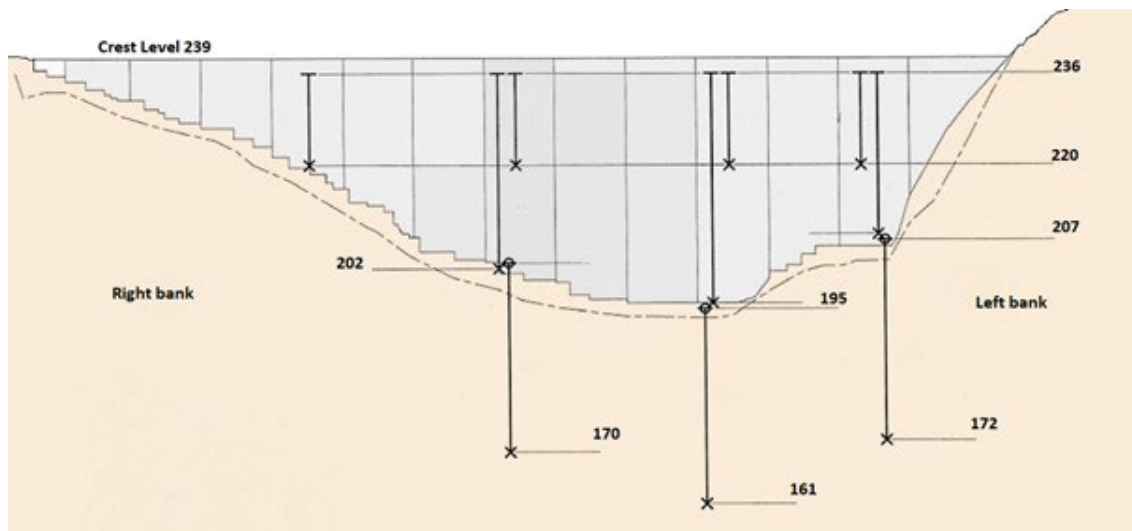
Figure 1. Downstream view of Dam_EDF.
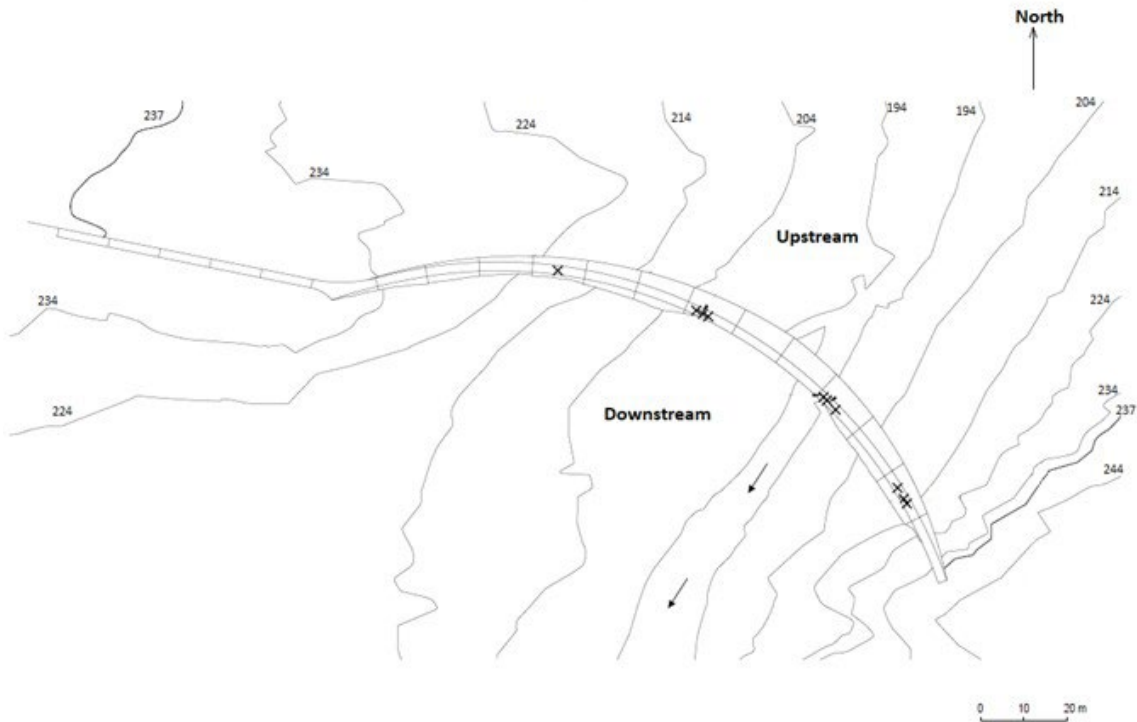
Figure 2. View from the top. The crosses indicate the position of the pendulums.

2.1.1 Dam Geometry

The main technical data are:
- Dam height above foundation   45 m
- Crest thickness   2 m
- Base thickness   6 m
- Crest radius   110 m (90°)
- Crest length   166 m
- Normal Water Level *   237 m
- Crest Level *   239 m

* In the following text, all altitudes refer to a common arbitrary reference point, which is not the sea level. Water levels in the reservoir, altitudes of pendulums and piezometric levels all refer to this point. The unit of altitude is meter [m]. It should be noted that the real altitude of the Dam_EDF is approximately 2000 m above sea level.

2.1.2 Material properties

Dam_EDF is made of concrete with cement dosage at 300 kg/m^3. The average value of compressive strength is 34 MPa (after 90 days) with values varying from 22 MPa to 45 MPa.

2.2   *Measurements*

2.2.3 Introduction

Dam_EDF is equipped with a comprehensive monitoring system, including pendulums, crack opening displacement sensors, piezometers and seepage measurements. Only the valid measurements are stored in the database. Thus, the provided data in this benchmark is the reference and valid data for behavior analysis and does not need any further cleaning.

2.2.4 Water level

Time series of water levels were provided for the period 1995 to 2017. The time format is common to all time series given in this benchmark: day/month/year hour:minutes:seconds (dd/mm/yyyy hh:mm:ss). For water level in the reservoir, there is at least one value per day. The unit of water level is meter [m]. When the water level is lower than +196 m, the complete upstream surface is exposed the air. This can happen because Dam_EDF is located on the top of a glacial threshold. Hence, when water level is lower than +196 m, there is only water in a lake located below the upstream toe of Dam_EDF.
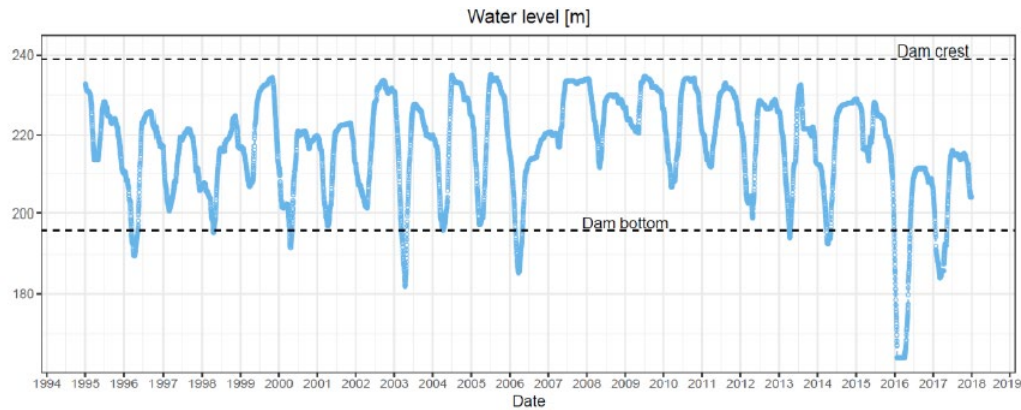
Figure 3. Time series of water level in the reservoir.

2.2.5 Air temperature

The air temperature is not measured at the location of the dam. However, two time series of daily air temperature are given:

- T_a, which is a time series of measurements located in the area of the dam. Measurements are carried out according to the standard of WMO (World Meteorological Organization) and are located 50 km from the dam, at a different altitude.
- T_b, which is a time series calculated by interpolation from several air temperature measuring stations. The interpolation takes into account the altitude of the dam and is calculated on a mesh of 1 square kilometer.

Time series of air temperature were provided for the period 1995 to 2017 and the unit is °C (degree Celsius).
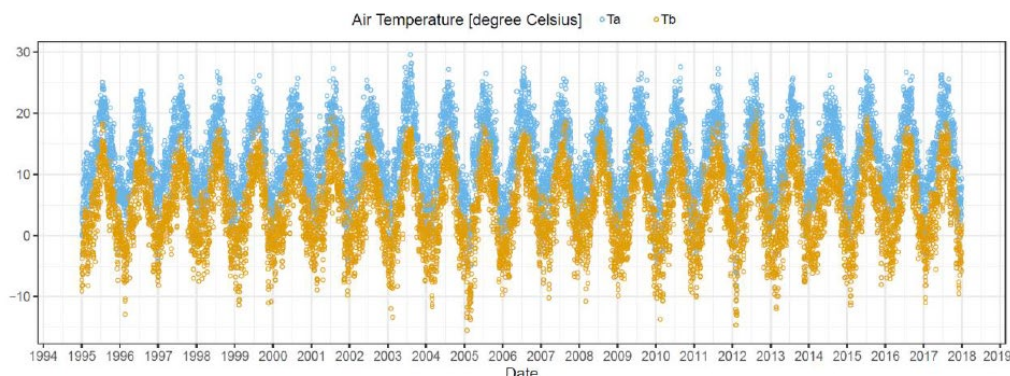
Figure 4. Time series of air temperature T_a and T_b.

2.2.6 Rainfall

Data from a rain gauge located about 5 km from Dam_EDF were provided. The daily cumulative precipitation time series was provided for the period 1995 to 2017. The unit of precipitation is mm.
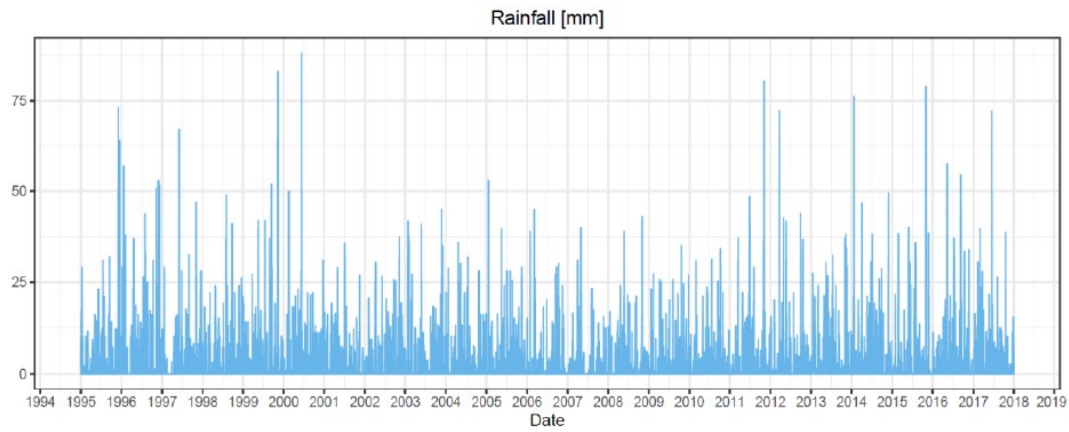
Figure 5. Time series of daily rainfall (mm).

2.2.7 Pendulums (downstream and upstream displacements between two points)

The dam is equipped with several pendulums, as illustrated in Figure 6 below.
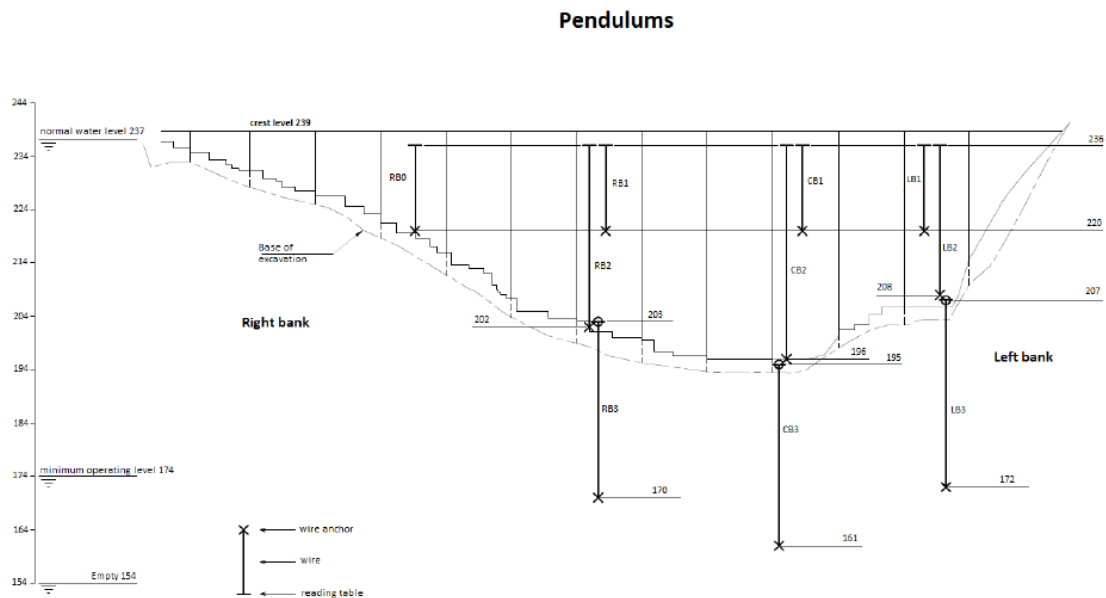
Figure 6. Location of pendulums (downstream view).

For this benchmark, only the measurements of pendulums on the Central Block (CB) were given. CB2 is the radial displacement between the altitudes 236m (just under the crest of Dam_EDF) and 196 m (toe of Dam_EDF). CB3 is the radial displacement in the foundation between the altitudes 195 m and 161 m. An increasing radial displacement indicates a movement of the highest point in the downstream direction.
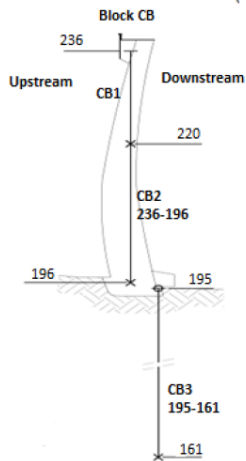
Figure 7. View of block CB and location of pendulums.

The provided radial displacements measured using the pendulums is presented in Figure 8. An increasing radial displacement indicates a movement of the highest point in the downstream direction. The unit of displacements is mm.
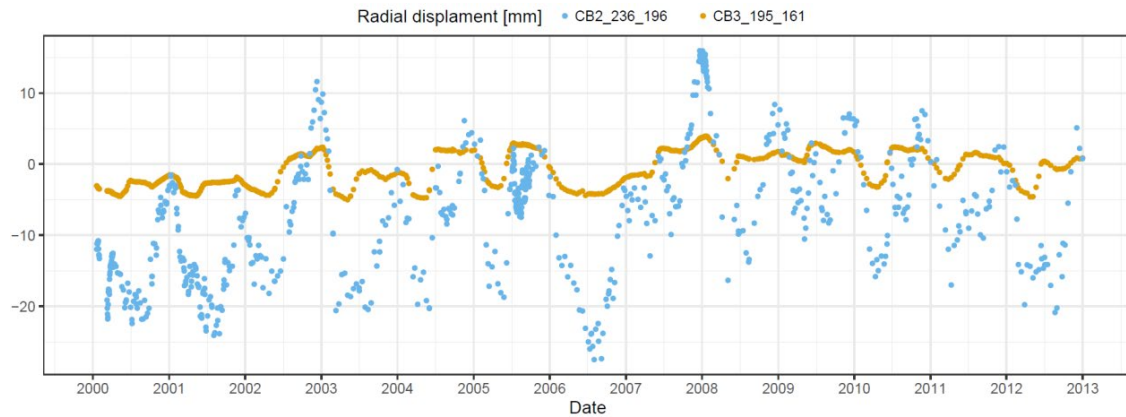
Figure 8. Time series of pendulums CB2 and CB3.

2.2.8 Crack opening displacements sensor

A crack opening displacement sensor is located at the rock concrete interface of the Central Block (CB). The sensor measures the opening between C4 (in the foundation) and C5 (in the concrete, at the toe of the dam). The location of the sensor is illustrated on the Figure 9. An increasing value of C4-C5 means that the distance between C4 and C5 is increasing.
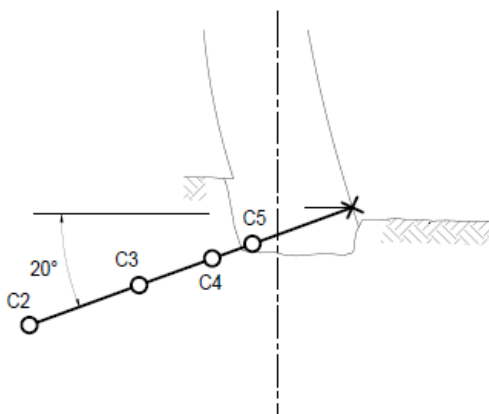
Figure 9. Location of crack opening displacements sensor in the block CB.

The time series of the relative distance between C4-C5 is given in the Excel file. The data is given from 2000 to 2012 as seen in Figure 10. An increasing value of C4-C5 means that the distance between C4 and C5 is increasing. The unit of displacement is mm.
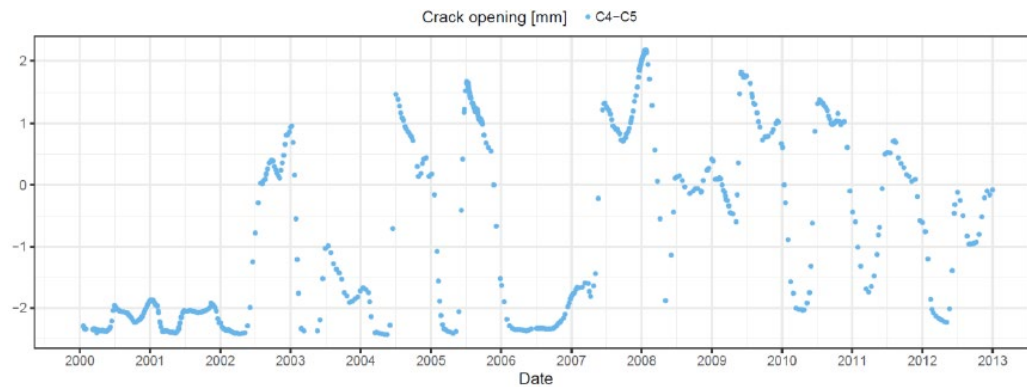
Figure 10. Time-series of crack opening displacements.

2.2.9 Piezometers

For this benchmark only piezometers located in the block CB were provided. Their locations in the block CB are indicated on the Figure 11 below.
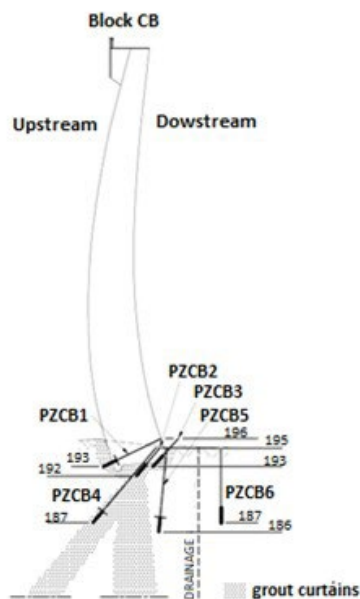
Figure 11. Location of piezometers in the block CB.

PZCB4, PZCB5 and PZCB6 are embedded deeply in the foundation and will not be analyzed. PZBC1 is located at the upstream of the grout curtain and thus its levels are quite equal to the hydraulic head. Consequently, PZCB1 is not analyzed in this benchmark.

Time series of piezometric levels PZCB2 and PZCB3 are given from 2000 to 2012. The unit of piezometric levels is meter (m). The reference for altitude is the same as for water level and elevations (see Figure 3).

Time series of PZBC3 contains missing values from the 5th of February 2008 to the 10th of September 2008. A leakage in the standpipe of piezometer PZBC3 was observed during this period that is why measurements were removed. In September 2008, a cleaning of the drainage system was carried out. This has to be considered when analyzing the monitoring data.
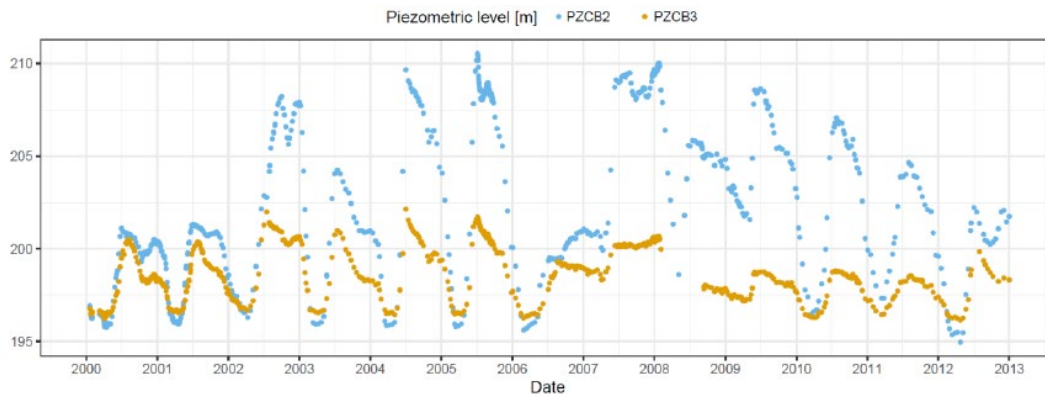
Figure 12. Time series of piezometric levels.

2.2.10   Seepage

The total seepage flowrate of Dam_EDF were also provided. The flowrate is measured using a weir located in the gallery at the downstream toe of Dam_EDF. The measured total seepage is the total amount of water originated from different locations such as the surrounding rock, moisture transport in concrete, potential leakages in concrete cracks and the drainage system. Times series of flowrate are given from 2000 to 2012 and the unit is $L.min^{-1}$ (Liter per minute).
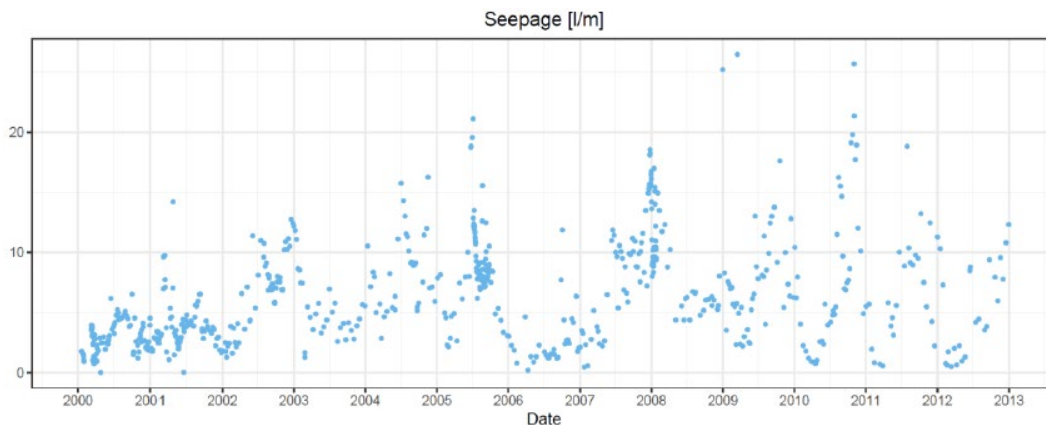
Figure 13 – Time series of seepage.

2.3   *Delivered data from the formulators*

2.3.1 Data preparation

Variables are measured with different and irregular frequency. One of the goals of this Theme is to compare criteria to handle the data preparation caused by issues that may appear in practice such as resampling, missing values, etc. Therefore, the dataset was provided without any modification of the actual time series. The main features of the data are summarized in Table 1.

Table 1. Summary of the main features of the provided data.

Variable type [units]	Variable name	Period	Average reading frequency	# Measurements
Water Level [m]	Water Level	1995-2017	1 day	9736
Air Temperature [ºC]	T_a	1995-2017	1 day	8401
	T_b	1995-2017	1 day	8401
Rainfall [mm]	Rainfall	1995-2017	1 day	8401
Radial displacement [mm]	CB2_236_196	2000-2012	1.5 weeks	703
	CB3_195_161	2000-2012	1.5 weeks	698
Crack opening [mm]	C4-C5	2000-2012	1.5 weeks	676
Piezometric level [m]	PZCB2	2000-2012	1.5 weeks	705
	PZCB3	2000-2012	1.5 weeks	670
Seepage [l/min]	seepage	2000-2012	1.5 weeks	672

The most appropriate format of the time series depends on the chosen model (either FEM or data-based) and the software tool used. The participants received the data in three different versions to facilitate the analysis:

- An excel file with each variable in a different sheet ('ThemeA_data_fmt01.xlsx'). It should be noted that the time vector differs among variables, due to the different reading frequency and reading period.
- An excel file with all variables in one sheet ('ThemeA_data_fmt02.xlsx'). The time vector encompasses all time stamps from all variables. Since this includes the hour, several rows appear for the same day in case more than one record was taken at different hours.
- An excel file with all variables in one sheet with a common time vector in the format dd/mm/yyyy ('ThemeA_data_fmt03.xlsx'). This is a transformation of the original dataset: if more than one record is available for some variable within one day, the mean value is taken. As a result, the number of records is lower than in the original dataset.

In all versions, the cells in the forecasting period for the output variables were left blank. Participants were able to explore the provided data by loading either the second or the third versions into the free online app: https://cimnetest.shinyapps.io/PREDATOR/. The participants are free to use any version of the data for each part of the analysis.

2.3.2 Data-based models

Participants were free to use their preferred software or algorithm to compute predictions and warning levels. The most popular data-based approach for dam monitoring analysis is the hydrostatic-seasonal-time (HST) model. It was first proposed by Willm and Beaujoint in 1967 [1] to predict displacements in concrete dams, and has been widely applied ever since. Other statistical methods have also been used for this purpose. Examples include neural networks [2], [3], support vector machines [4] and boosted regression trees [5], among others [4], [6].

2.3.3 Numerical FE model

The participants were free to perform the finite element analyses in any way that they find suitable. A geometrical model was developed by the formulators and was provided to the participants. The geometry consists of two separate parts; the concrete arch dam (including the abutment), and the rock foundation. In this geometry, the dam is described as a monolithic structure.

2.3.3.1 Geometry files

The geometry of the dam were provided in different CAD-based file formats that can be imported into most of the existing finite element codes
- ACIS .sat
- STEP .stp
- IGES .igs
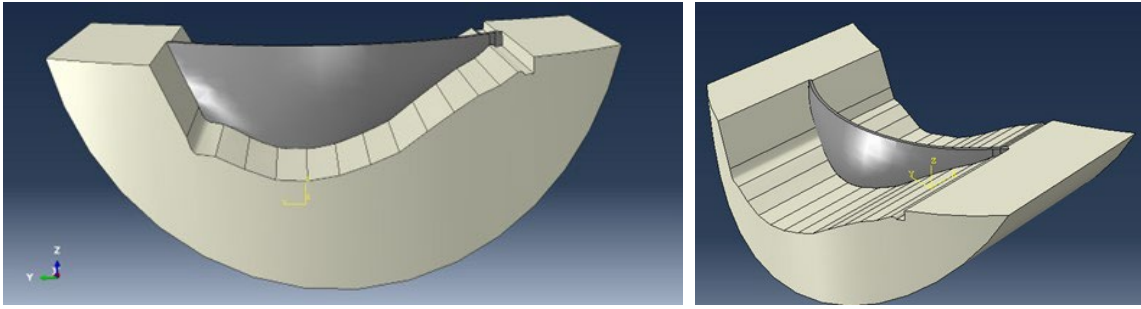
Figure 14. Illustration of the geometry of the arch dam and foundation used as a case-study for the theme.

2.3.3.2 Mesh file

An input-file in ASCII code (.inp) was provided with the raw data of the coordinates of all nodes and the topology of the elements in the FE-model. The dam has been meshed with 4-node linear tetrahedron elements (C3D4 in Abaqus), with a typical length of about 1.0 m. The concrete parts consist of 32195 nodes and 155780 elements. The rock foundation has been meshed with 4-node linear tetrahedron elements (c3D4 in Abaqus), with a typical length of about 1.0 m at the rock-concrete interface and 20 m near its exterior surfaces. The rock parts consist of 7224 nodes and 31073 elements.

Defining a suitable mesh is an important part of numerical analyses, and the requirement of the mesh, regarding the size of the elements, depends on many factors, such as defined material behavior, type of loads considered etc. Therefore, even though the formulators provided one suggestion for mesh, the participants could define a mesh of their own that was suitable for their analyses.
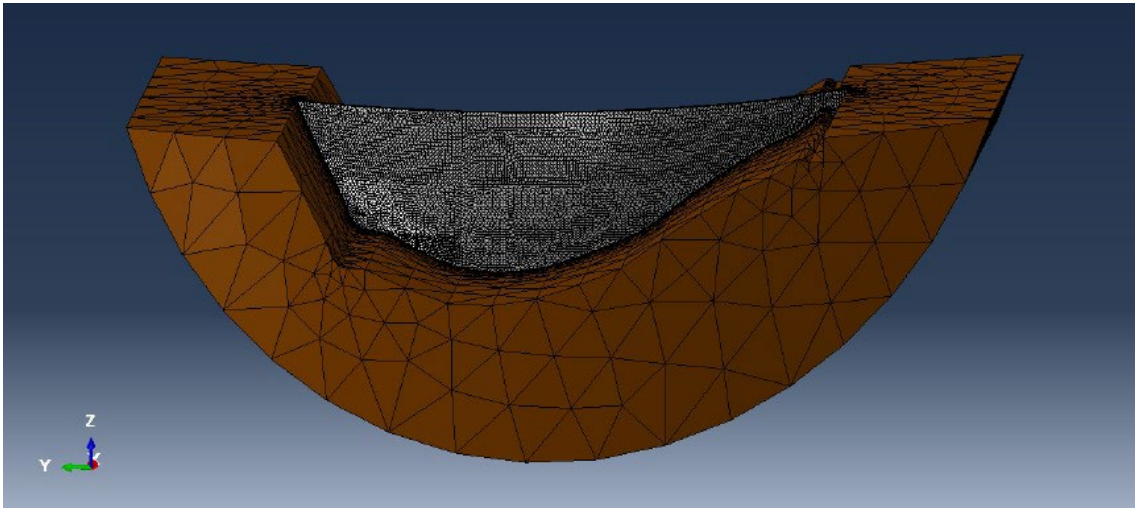
Figure 15. Illustration of the geometry of the arch dam and foundation used as a case-study for the theme.

2.4 *Case studies and tasks*

The tasks are divided into three Cases, in accordance with the period of analysis.
- Calibration (**Case A**): 2000-2012
- Short term prediction (**Case B**): January 2013 - June 2013
- Long term prediction (**Case C**): July 2013 - December 2017.

For all cases and each output variable (pendulums, crack opening displacements, piezometers, and seepage), the participants were requested to submit:

- A vector of the predictions, with one value for each time stamp in the provided time series
- Two vectors of lower and upper warning thresholds.

The time series for both the input variables and the dam responses were provided for the period 2000-2012. They can be used to calibrate the parameters of the models: material properties, boundary conditions and other features of FEM, and training parameters for data-based models. Records of rainfall, water level and air temperature are provided from 1995. Participants using FEM models may find this information useful for computing the thermal and stress field of the dam at the beginning of the calibration period. Predicted values should be the best estimate of the dam response in terms of each of the output variables. These predictions will be compared to the actual measurements by the formulators. Participants are free to define the warning thresholds with their own criterion.

In addition to the predictive task, it was requested to perform one interpretive task. The interpretation task should be considered as a general analysis of the dam, measurements, data, and modelling in the context of dam safety. The participants were asked to explain how their analysis and results could teach us anything about the dam's performance, if the model can provide support for the decision-making process, etc. This task was considered as very open where the participants could decide to perform risk analysis, assess maintenance needs, failure simulations, establish link between external load and monitored phenomenon, or any other approach based on their judgement, experience, and motivation. All tasks are summarized in Table 2.

Table 2. Summary of the mandatory and optional tasks.

Interpretation		Case A: calibration		Case 2: Short term		Case 3: Long term	
		Prediction	Warning levels	Prediction	Warning levels	Prediction	Warning levels
CB2_236_196	Mandatory	Mandatory	Mandatory	Mandatory	Mandatory	Mandatory	Mandatory
CB3_195_161	Mandatory	Mandatory	Mandatory	Mandatory	Mandatory	Mandatory	Mandatory
C4-C5		Optional	Optional	Optional	Optional	Optional	Optional
PZCB2		Optional	Optional	Optional	Optional	Optional	Optional
PZCB3		Optional	Optional	Optional	Optional	Optional	Optional
Leakage		Optional	Optional	Optional	Optional	Optional	Optional

In summary, six output variables and three different time periods were considered. All records corresponding to the Case A (calibration; 2000-2012) were available to the participants. Therefore, the results for this period are described and discussed in detail in each paper and only a general summary is included in this report. In contrast, the actual measurements for Case B (January-June 2013) and Case C (July 2013 – December 2017) were not provided before the benchmark. These results are considered as more relevant and will be analyzed in more depth in this synthesis.

2.4.4 Required output from the participants

The participants delivered their results to the formulators of the theme via the provided excel template files. In these template files, the first section was used for participants to provide general information about their group, which will help with the synthesis of the results (experience, software used, consumption of time, etc.).

For Cases A, B, and C, the spreadsheets contain time stamps for each variable, where the participants are asked to copy their prediction vectors, with one value for each time stamp, and two vectors for the lower and upper thresholds, respectively. Radial displacement results were mandatory, while other variables are optional.

The formulators analyzed the data provided in the excel spreadsheets and the papers prepared by the participants in which the modelling assumptions, calibration process, pre-processing, etc. were explained. The participants were also asked to highlight the specific information regarding the lessons learned and specific steps to solve the tasks.

3 DESCRIPTION OF CONTRIBUTIONS

3.1 *Statistics*

In total, 18 teams participated in theme A and provided 23 solutions to the formulators. The participants were from the following countries: Austria, Canada, China, France, Iran, Italy, North Macedonia, Portugal, Russian Federation, Spain, Switzerland, and United States of America. In average 3 authors collaborated in a team that provided a contribution. By composition, 11 groups were from consultancy or a dam owner, 5 groups from universities or research centers, and the authors of 2 groups were from combined affiliations.

The participants were asked to submit the results and 6 tasks were marked as obligatory, while there were also 15 optional tasks that could be performed. The formulators received 18 full solutions of the obligatory tasks and 5 partials. Additionally, 3 groups provided also all the optional tasks, while the formulators also received 12 partial solutions for the optional tasks. Time spent by the participants varied substantially, from 3 days to 124 days, while the average time spent per solution was 30.5 days (see Figure 16). Majority of the solutions were provided using 2 inputs for prediction of pendulums and joint opening (20 solutions), all of them used water level, while 16 used air temperature measured 50 km from the dam (Tb), 4 used interpolated air temperature (Ta), and 2 used precipitation time series, only 3 solutions were provided using 3 input parameters. Similarly, for the optional results for the pores pressures and water seepage, 3 solutions were provided using only water level, 5 solutions used water level and Tb, or Ta, or rain, and 3 solutions were provided using 3 or more input parameters.
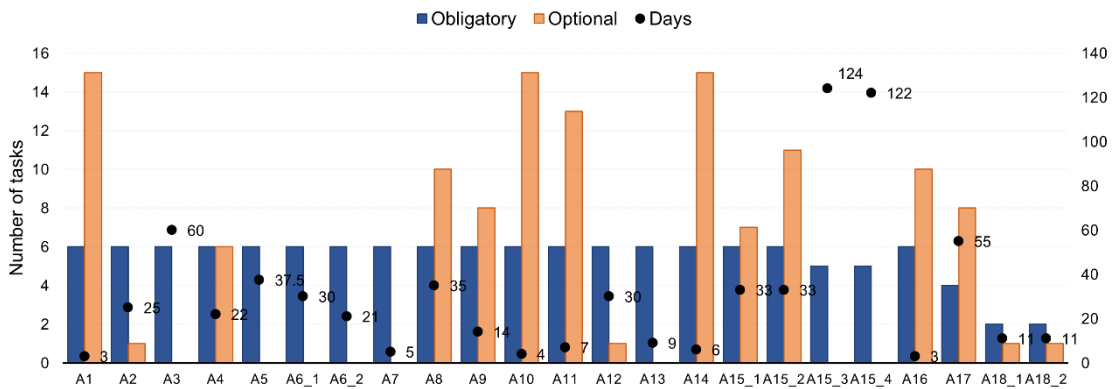
Figure 16. Number of tasks performed and time spent to provide solution.

The motivation to participate and provide results were in 38% to expand and share expertise, in 29% to test new methods and compare results with others, in 19% to learn from others, and in 14% the participants didn't report on their motivation to participate. 7 groups have already participated in previous Benchmark workshops, while 11 groups participated for the first time. Participants were also asked to report on their confidence in the provided result in percentage, not all groups reported on their confidence, and for those who did, the lowest confidence level was 10%, and only one group was 100% confident in their results, while the average reported confidence level was at 60%.

3.2 *Summary of methods used by the participants*

Table 3 shows a summary of the submissions received for all Cases and variables, classified by the approach used. Overall, 3 submissions were based on FEM, 8 on machine learning (one of which added an analytical formula), 6 employed an analytical approach and 5 a hybrid method, correcting the outcome of a FEM model with machine learning (1) or with an analytical model (4).

Table 3. Summary of methods used and variables considered by each participant.

Participant	Approach	Variables						# vars. Considered
		CB2	CB3	C4C5	PZCB2	PZCB3	Seep.	
A01	AN	X	X	X	X	X	X	6
A02	HY-ML	X	X	X				3
A03	ML	X	X					2
A04	ML	X	X				X	3
A05	ML	X	X					2
A06_1	ML	X	X					2
A06_2	HY-AN	X	X					2
A07	AN	X	X	X				3
A08	HY-AN	X	X	X	X	X	X	6
A09	AN	X	X	X	X			4
A10	ML	X	X	X	X	X	X	6
A11	ML	X	X	X	X	X	X	6
A12	HY-AN	X	X	X				3
A13	HY-AN	X	X					2
A14	ML+AN	X	X	X	X	X	X	6
A15_1	AN	X	X	X	X	X		5
A15_2	AN	X	X	X	X	X		5
A15_3	FEM	X	X					2
A15_4	FEM	X	X					2
A16	AN	X	X	X	X	X		5
A17	FEM	X	X	X	X	X	X	6
A18	ML	X	X					2

Method	# Contributions
AN	6
FEM	3
HY-AN	4
HY-ML	1
ML	7
ML+AN	1
Total	22

Participant 1 (France): analytical model with user-defined correlation functions. Simultaneous Perturbation Stochastic Approximation (SPSA) method for calibration (10 parameters). Threshold function added for joint opening. For piezometers, 14 parameters were used, four of which are included to model a change in behavior after August 2008. During Case A, the authors observed a decrease in accuracy in 2002 attributed to a rapid increase in water level, different from other years. The authors recommend to re-calibrate the model yearly to adjust to the time variation of the response (they observed a drop in piezometric levels for a given reservoir level). Accuracy for seepage in Case A is clearly lower than for other variables. The authors hypothesize that part of the seepage may come from runoff due to rainfall, and that the precipitation data taken 5 km far from the dam may represent the precipitation at the dam incorrectly. In conclusion, they state that the use of an analytical approach including correlation functions, defined based on engineering knowledge, allows for a better interpretation of dam behavior. However, such functions are complex and not easy to associate to physical phenomena, which, in turn, are complex and dependent.

Participant 2 (Austria): FEM model including thermal and mechanical effects. The results are fed, together with the monitoring data, into a Long-Short Term Memory (LSTM) neural network. The data provided for the calibration period (Case A) is divided into a training set (95% initial period) and a test set (5% final records). They used Tensorfolw/Keras in the Python environment. Forecasts are submitted for displacements and joint openings. The authors noticed lower accuracy during unloading periods.

Participant 3 (Iran): hybrid approach using moving averages and gradients of inputs as predictors. Radial displacements are predicted with a polynomial of fourth degree dependent on the reservoir level. The results are corrected with a Gradient Boosted Regression based on all inputs except level. The resulting approach is named Hydrostatic Machine Learning. The models are interpreted using word clouds and partial dependence plots. The process for computing variable importance is unclear, since inputs associated to reservoir level are considered differently (in a polynomial) to the others (which are fed into a GBR model).

Participant 4 (China-USA): data-driven model. Inputs are taken from HST (polynomial of 4th degree for the hydrostatic load). The temperature effect is considered from average temperatures

along a number of periods (e.g., last 2 days, previous week, previous month, etc.). The time effect is also included as a polynomial. The final model has 14 inputs. For the seepage, an additional term is added, depending on the rainfall, also over different time periods, adding 6 additional coefficients to the model. They used "Kernel Extreme learning machine", described as a version of neural networks. In addition to the coefficients to be fit for the network, this approach requires adjusting the parameters related to a kernel. Particle Swarm Optimization (PSO) was used for calibration. The warning levels were defined assuming a normal distribution of residuals and a bandwidth corresponding to 99% of the samples, i.e., predictions plus/minus 2.58 times the standard deviation. The model interpretation was performed using a version of global sensitivity analysis, grouping the inputs by loads (hydrostatic, temperature, time, rainfall). Only displacements and seepage were considered.

Participant 5 (Canada): Bayesian dynamic linear model (BDLM) coupled with Bayesian long-short-term memory (LSTM) neural network. The authors claim that their method does not require re-training, which allows for detecting anomalies that evolve over years. Only displacements are considered. Moving averages of temperature, up to 54 days, are used for the BDLM, while the LSTM considers raw data for reservoir level and temperature. The authors developed the OpenBDLM library for BDLM. They concluded that a change in behavior occurred between February 2004 and 2007 for CB3, based on the visual exploration of the residuals of the model and on the plot of probability of switching regime. They introduced artificial anomalies on the raw data to verify their model's detection capability. The effect of inputs is evaluated based on the BDLM, showing the hydrostatic load as the most important effect.

Participant 6 (Russia): HST for CB3 and neural network (multilayer perceptron) for CB2 using Keras. They defined the warning intervals based on the predicted value +/- 3 times the standard deviation of the residuals, which encompasses 99.7 % of values in a perfect Gaussian distribution. The histogram of residuals is close to a normal distribution for CB2 (HST model), but that is not the case for CB3 (NN). The author also considered a FEM model using Simulia Abaqus. First, the thermal problem was solved with a time step of one day. Then, the resulting deformation was added to that obtained from the mechanical calculation resulting from the application of the hydrostatic load with a time increment of one week. The accuracy of the FEM model was reported to be lower for both outputs considered.

Participant 7 (USA): First, a finite element model based on LS-DYNA software was developed, but not used for generating predictions. Displacements and crack opening were considered. Two-week moving average of temperatures were taken as input. The time series of crack opening was taken to segment the data, as a function of the state of the crack, i.e., closed, moderately open (<1.85 mm) or wide open (>1.85 mm). The data were further subdivided according to the pool level. For each of the final sets, the effect of the temperature was seen to be close to linear. As a result of the approach used, the crack opening needs to be estimated before predicting displacements. This is done by means of curve fitting based on pool level and temperature. Warning levels were defined so that they contained around 90% of the data.

Participant 8 (Portugal): finite element analysis with consideration of joints and solar radiation. Some assumptions were made for the thermal analysis: T_b was applied and the orientation of the dam was estimated. Different models with varying degrees of complexity were developed. The results of a thermal analysis in an elastic FE model are fed into an analytical model (Separation of Effects, SEM). The result resembles an HST in which the thermal effect is modelled by the FEM results (instead of the conventional term). The warning levels were defined based on the predictions +/- 3 times the standard deviation of the residuals. The authors mention 5 times the standard deviation as an additional warning (maybe alarm) threshold. For pendulums, using the FE instead of the regular HST resulted in an improvement in R^2 from 0.93 to 0.95.

Participant 9 (Italy): ensemble model, based on a weighted combination of a multi-linear regression model and a Seasonal Autoregressive Integrated Moving Average (SARIMA) model. Pendulums, crack opening and one piezometer were considered. The authors mention that Case C (5-year prediction) is a challenging task, not often considered in practice. The weights for each

model are defined based on engineering judgement. Warning levels are based on the 95% confidence intervals, i.e., 1.96 times the standard deviation of the residuals. The temperature records provided were not considered, because they were not taken at the dam site and thus the authors assumed that they would not represent the local peaks. Rainfall was also discarded, in view of the correlation matrix. The water level is modified, assuming a constant value equal to 195 m when the actual record is lower (and thus below the dam toe). PZCB3 was not considered due to the reported change in behavior during the training period.

Participant 10 (Spain): machine learning model based on boosted regression trees (BRT). Moving averages of different periods of water level and temperatures were considered as inputs. Predictions were provided for all proposed outputs. A preliminary variable selection process was followed, after which T_a was selected and T_b discarded; the modified water level (with a lower bound in 195 m) was taken instead of the original series; rainfall was neglected. Then, for each output, a calibration process was followed, which included 100 pseudo-random selections of inputs and 36 combinations of model parameters for each input set. The final models were selected in view of the accuracy on the training set (2000-2010) and on the test set (2011-2012) selected by the authors. The predictions for Case B and C were computed from these final models with a bias correction. The warning levels were defined on the basis of the corrected predictions and the 100% quantile range of the residuals. The models were interpreted to draw practical hints on dam behavior.

Participant 11 (Spain): machine learning approach. Several ML algorithms were considered, namely random forest (RF), generalized linear regression, bayesian neural network, hydrostatic-season-time (HST), neural networks (NN), support vector machines (SVM) and BRT. Synthetic variables were generated to be considered as inputs: moving averages, aggregates (sum of values along the period) and variation ratio. Variable selection was later performed on the basis of the importance computed from an SVM model. Model parameters were calibrated with cross validation. Year 2012 was considered for validation. The warning levels were defined as the predictions ±2 times the standard deviation of the residuals. As a result, 95% of the records are expected to be within the interval. Model interpretation suggests a long-term inertia of CB2 (180 days). The authors analyzed the similarity among years in terms of load values. The final models used were based on SVM for pendulums, on BRT for piezometers and on NN for crack opening and seepage.

Participant 12 (Switzerland): 3D numerical model. Joints among blocks and between dam and foundation were considered. T_b was used to account for the thermal effects in a transient analysis, assuming 1D thermal flow. The displacement due to hydrostatic load was computed from an analytical expression, i.e., a polynomial of 4th order of the reservoir level. The contribution of the thermal load was considered from the results of the numerical model. The material properties were calibrated with an in-house software. As a result, the final values used are slightly different to those mentioned in the formulation of the Theme. The warning levels are defined as the envelope of the maximum differences between predictions and observations for the calibration period.

Participant 13 (Portugal): combination of an analytical approach (HTT) and a deterministic calculation (ANSYS software). The authors also mention "brief implementations" of gradient boosted trees and neural networks, with "promising" results. A sensitivity analysis on mesh size was performed, showing that coarser meshes result in stiffer models. Material properties were calibrated based on results for CB2. Predictions were computed ass the sum of the result obtained from the FEM, which account for hydrostatic and thermal loads, and those from the HTT model, to consider the time effect. In the thermal calculation, air temperature was assumed to be equal to T_b and a different value was considered for the wetted part of the upstream face. For the calibration period, the authors reported the highest differences between predictions and observations during periods of decreasing water level. Predictions for Case B and C were generated assuming constant time effect for CB2 and linear evolution for CB3. The warning levels were computed as predictions ±3 times the RMSE for each output.

Participant 14 (Portugal): combination of multi-linear regression and neural networks was used for displacements and crack opening. The hybrid approach includes predictions based on HST corrected by a NN model, which estimates the residuals. For other outputs, HST model was applied. An exploratory analysis was made to check the effect of the cleaning of the drainage system performed in 2008. Some data for PZCB3 were excluded from the training set because of some abnormal behavior identified. The authors noticed that some load combinations in the prediction period (Case B and C) were not presented during the calibration period, which may result in less accurate predictions.

Participant 15 (France): two analytical models (HST and HSTT) model and two versions of a deterministic model based on FLAC3D software (with different conditions for the foundation) are used. For the analytical models, predictions are provided for all outputs except for seepage. As for the FEM model, only the displacements are considered. The time series of water level was modified, as other participants did, by bounding the lower limit to the bottom of the dam (195 m). Warning levels are computed as predictions ±2.5 times the standard deviation of the corrected data (which are computed as the observations minus the hydrostatic and thermal effects). Since they are based on the corrected data, these results couldn't be evaluated. The material properties of the concrete and foundation were calibrated to approximate the output of the HSTT model. Both the vertical and the dam-foundation joints are reproduced with numerical shear keys, which allow opening but not sliding. A transient thermal analysis was carried out to reproduce the thermal load, with a time step of one day. The predictions of the deterministic model are in good agreement with those of the analytical approaches for CB2. As for CB3, results diverge, in particular for low water levels. The authors perform a safety analysis of the dam.

Participant 16 (France): thermal HST for displacements; a non-linear version of HST for crack opening displacements; a physically based and non-linear version of HST for piezometers at the rock concrete interface; artificial neural networks for leakages. T_a is used instead of T_b. They use the "corrected measurements" concept, i.e., the result of subtracting the reversible effects from the raw measurements. They are useful for identifying trends. Some deviation from the overall trend is observed for CB2 in 2003 and 2012, which is attributed to the limitations of the HST model used. For crack opening, a non-linear term is added based on the observed behavior. Predictions for seepage are not provided. Warning levels are generated from 2 times the standard deviation of the residuals.

Participant 17 (North Macedonia): deterministic model based on FEM (Sofistik software). The dam is considered monolithic. The model is calibrated by focusing on the maximum and minimum displacements along the training period (Case A). Results for CB3 are less accurate, though with a similar trend. As for the crack opening, the authors considered a kinematic constraint, which resulted in lower variation than observed. They suggest that the behavior may be better captured with interface elements. Piezometric levels were computed with 2D hydraulic models. The permeability of the material was calibrated based on the observed values for the maximum water level. The grout curtain was considered in a simplified way, which is mentioned as a potential source of discrepancy between model predictions and observed values. The model also underestimated the seepage flow values recorded.

Participant 18 (France): first, a simple HST model was applied; then, an HST-T model was used to better capture the thermal effects. Predictions for CB2 were improved, but those for CB3 (less affected by temperature), did not change. Also, ML algorithms were explored, namely SVM, LSTM and RF. The HST models were fit with a software developed by the authors, which includes a process for selecting the terms in the final model. No term associated with time was included. As for the ML models, 30% of the data in 2000-2010, taken at random, has been used for selecting model parameters via cross-validation. The final models were later evaluated by comparing predictions with observations for 2011-2012. Although the submitted predictions are based on LSTM, the authors use HST and HSTT as references. They focus on some specific load combinations and interpret all three models from an engineering perspective. Warning levels are based on 2.5 times the standard deviation of the residuals.

4 EVALUATION OF THE RESULTS FROM THE CONTRIBUTIONS

4.1 *Tasks:*

During the discussion, we will mention the approach used by the contributors. In this regard, we grouped the methodologies as follows:
- Pure machine learning, solely based on data (ML)
- Pure analytical, similar to Hydrostatic-Season-Time (AN)
- Finite element method (FEM)
- Hybrid models, which combine two or more of the previous three methods (HY).

4.2 *Predictions*

4.2.5 Case B

Load conditions during Case B are similar to those observed during the calibration phase in a number of years, with a decrease in water level followed by an increase at the end of the semester. The air temperature was also within the observed values for the first six months of the year. As a result, good prediction accuracy was expected from many models.
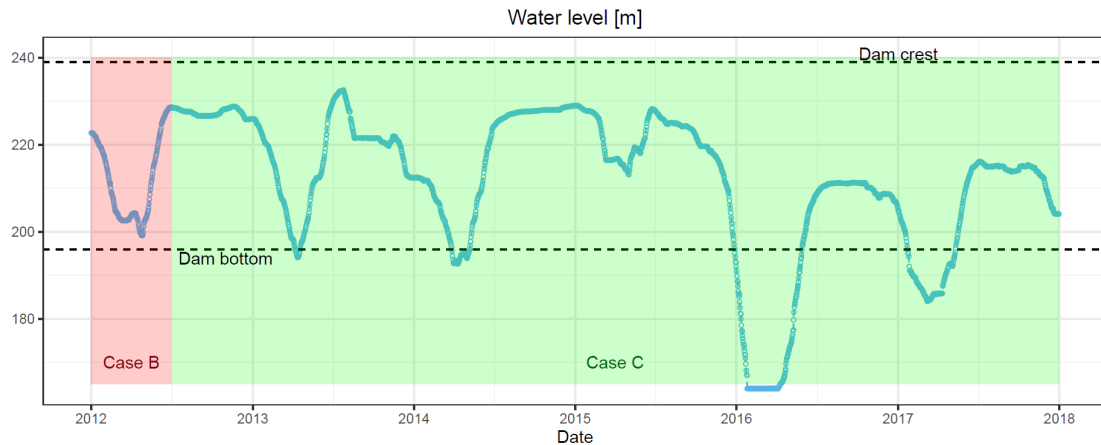
Figure 17. Water level variation during prediction periods for Case B (red) and Case C (green).

4.2.5.1 Radial displacements

The radial displacement for the period follows a similar trend to that observed in previous years: the dam deforms towards the upstream side during the first 3 months in response to the decrease in reservoir level. In the second half of the period, the records are sensibly stable, because the increase in water level is compensated by the increase in air temperature —which has an opposite effect—. This applies to both variables considered of this kind (CB2 and CB3), though the range of variation is –obviously– much lower for the foundation (CB3). This behavior was captured by all participants, though with varying accuracy.

For CB2, the median MAE is close to 2 mm, which is a useful value, since it represents around 10% of the variation of the observations in the period. The more accurate results correspond to A03 (MAE 1.05 mm), with three more contributions with MAE below 1.2 mm (A01, A10, A15.1). Interestingly, these 4 contributions were generated with different approaches, namely ML (A03 and A10), analytical (A01), and FEM+AN (A15.1). The lowest accuracy was registered for A06.2, based on ML, probably due to some degree of overfitting. However, relatively high errors were also obtained for a hybrid approach based on FEM and AN (A13), and strictly on FEM (A17).
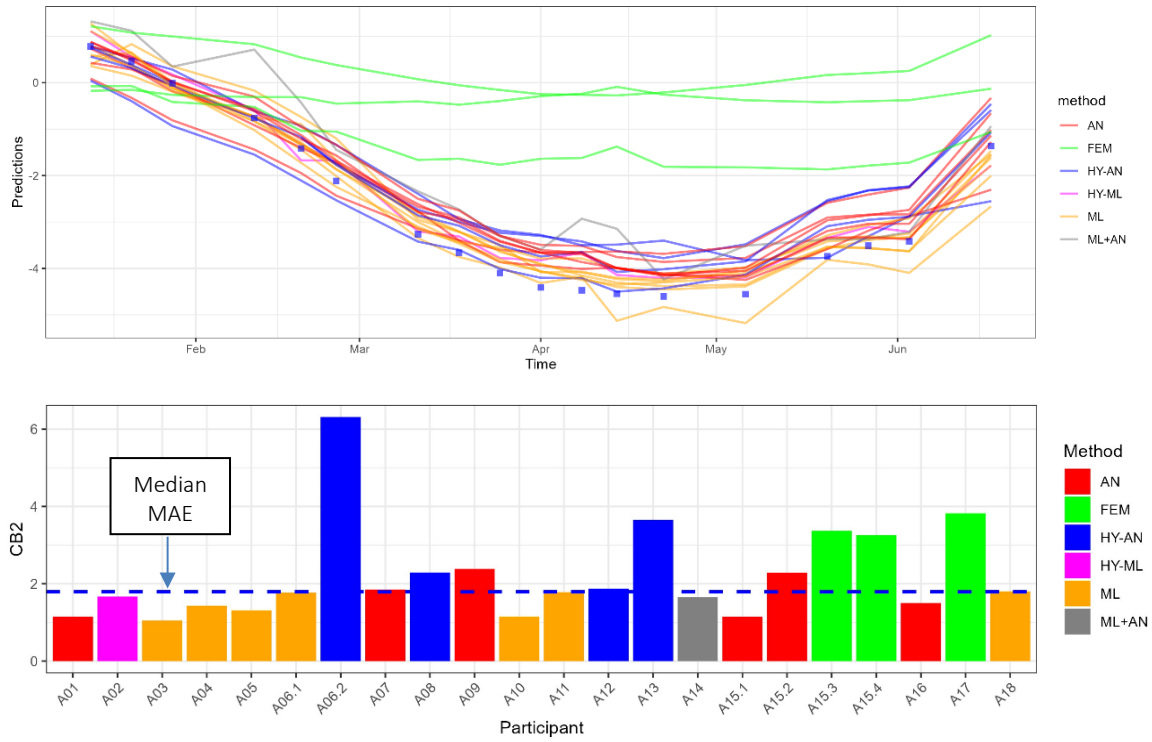
Figure 18. Radial displacement at CB2. Top: Predictions (lines) versus observations (squares) Bottom: Mean Absolute Error (MAE) for predictions and median of all contributions (dashed line).

As regards the displacements in the foundation (CB3), predictions are in general more accurate, with only three participants clearly off the observed series. In this case, the highest accuracy was obtained by A05 (MAE 0.19 mm), with a method based on ML. Nonetheless, similar accuracy was obtained by A06.1 using FEM and all predictions except the three mentioned can be considered as useful and accurate (median MAE was 0.43 mm).
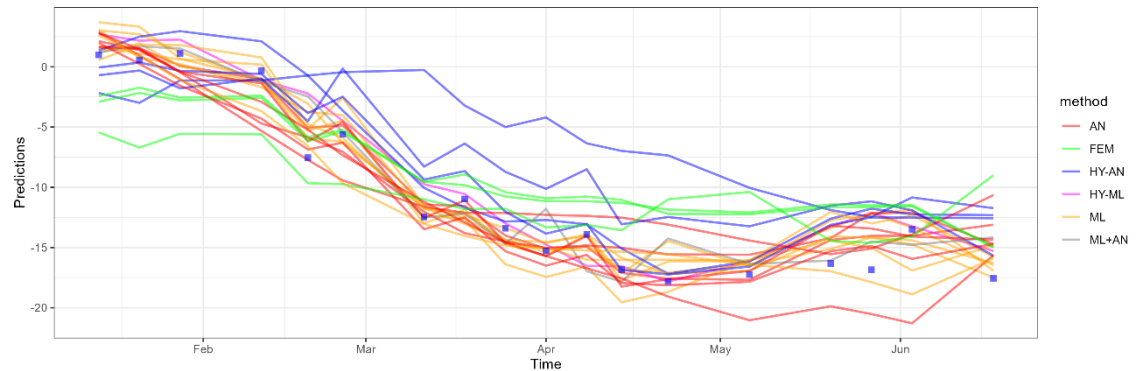
Figure 19. Radial displacement at the foundation (CB3). Predictions (lines) versus observations Mean Absolute Error (MAE) for predictions and median of all contributions (dashed line).
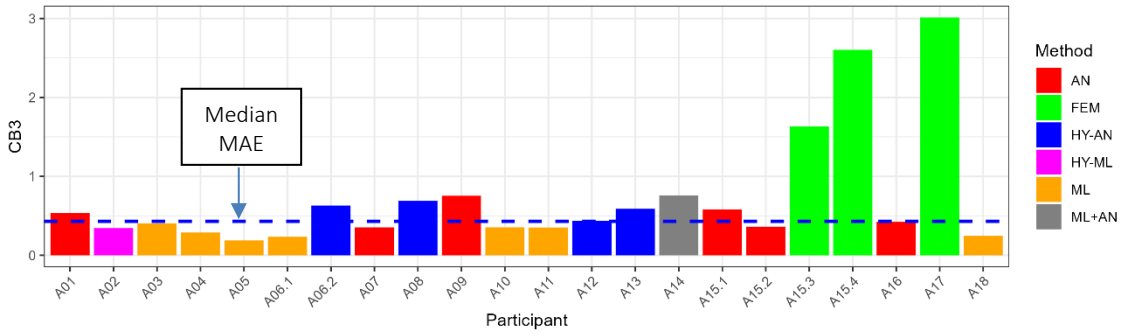
Figure 20. Mean Absolute Error (MAE) for predictions and median of all contributions (dashed line).

4.2.5.2   *Joint opening – C4_C5*

The evolution of joint opening for Case B is similar to that of the displacements previously discussed, with closing from January to mid-March and barely constant value from then on, except for the last record at the end of June. This trend was correctly captured by all submitted contributions (12 from 11 participants) but A12 (AN for joint opening[1]) and A17 (FEM).
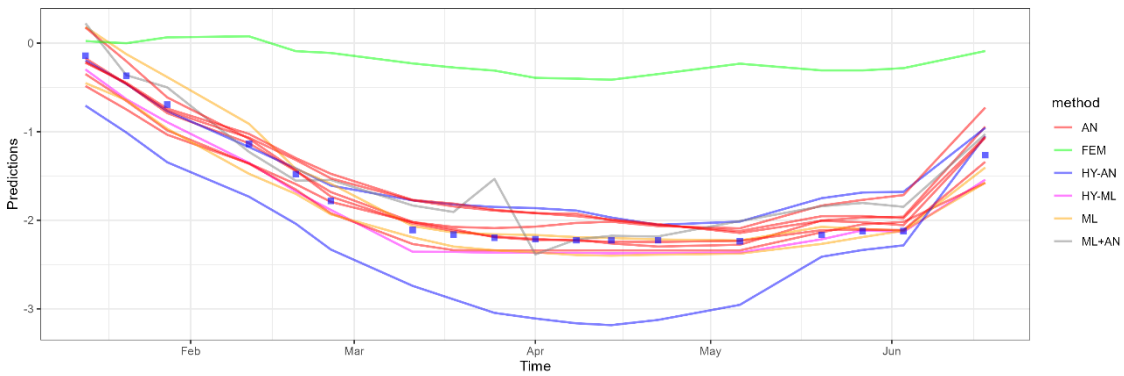
Figure 21. Predictions vs observations for Case B and C4-C5.
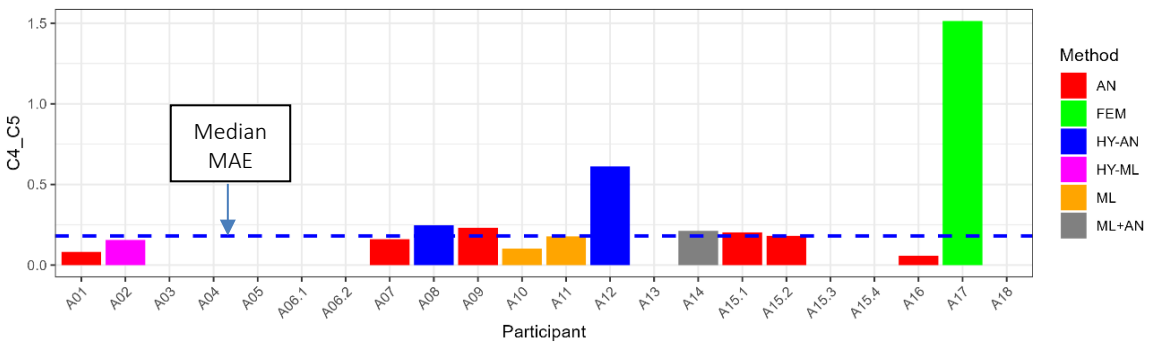
Figure 22. Accuracy of all contributors for C4-C5, Case B.

The most accurate predictions were provided by A16 (ML; MAE 0.06 mm), with two other participants having a MAE in the environment of the accuracy of the device (0.1 mm): A01 (AN; MAE 0.08 mm) and A10 (ML, MAE 0.10 mm). It is worth mentioning that only one participant submitted predictions of joint opening using FEM (A17), and the results were less accurate than all other approaches, based on AN or ML.

---

[1] A12 used a hybrid approach for displacement, combining FEM (for thermal load) and AN (for hydrostatic load).

4.2.5.3 Piezometers

Ten contributions were received for piezometers from nine participants. Again, only A17 was computed with FEM, which, as before, was the less accurate. The other predictions were computed with ML (A10, A11, A16) or AN (A01, A08[2], A09 and A15). Results are clearly different between the piezometers considered. While predictions are accurate in general for PZCB2 and capture the observed evolution, differences are higher among participants for PZCB3. It should be mentioned that the variation of the latter in the period considered is much lower. The best results for piezometers were obtained by A01 (AN), A10 (ML), and A11 (ML).
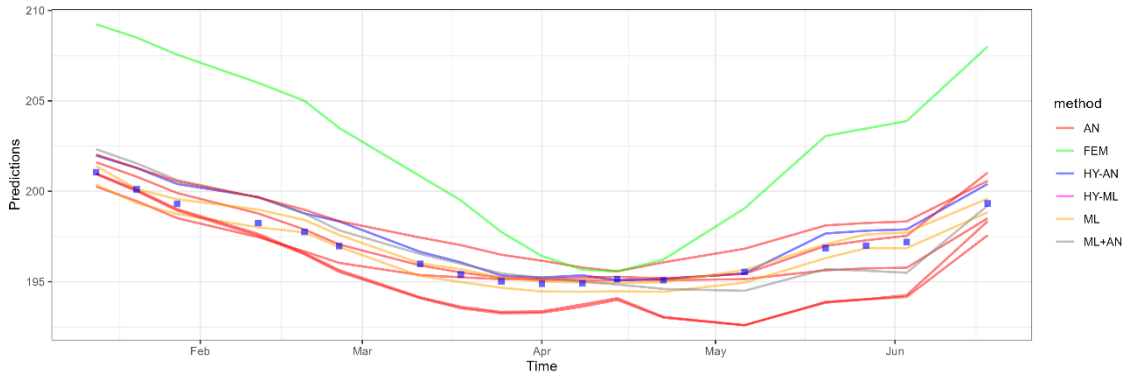
Figure 23. Predictions vs observations for Case B and PZCB2.
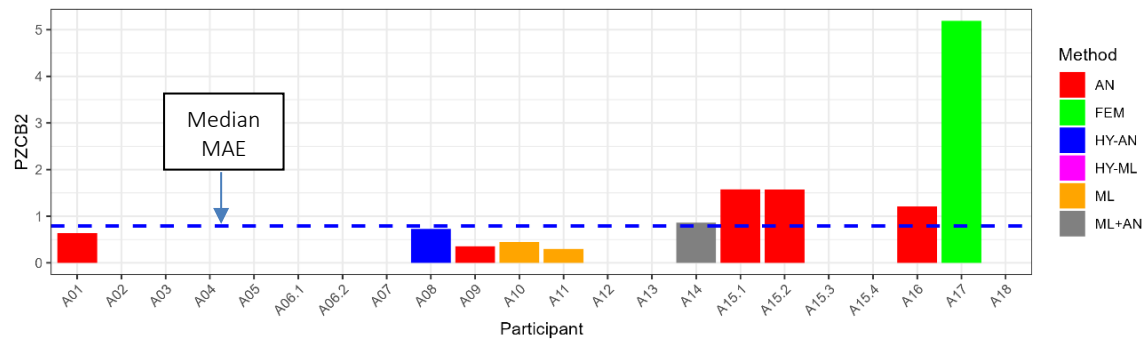
Figure 24. Accuracy of all contributors for PZCB2, Case B.
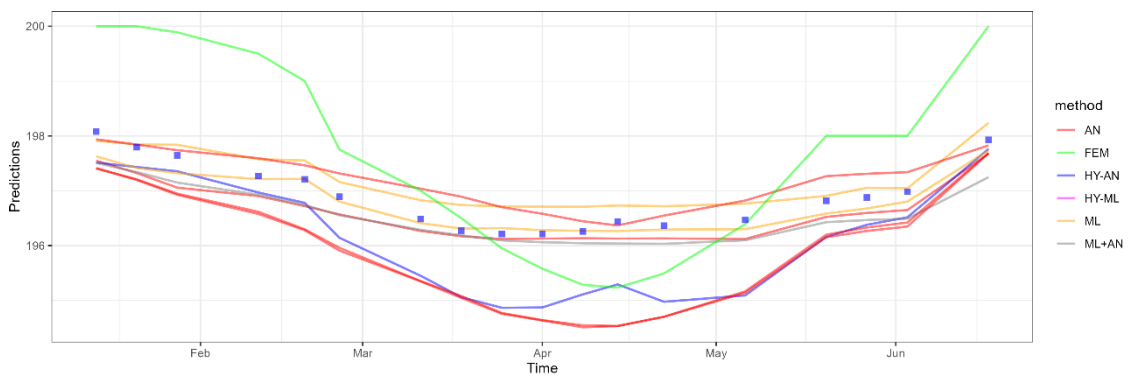
Figure 25. Predictions vs observations for Case B and PZCB3.

---

[2] A08 used a hybrid approach for displacements, adding the results of FEM to a HST model
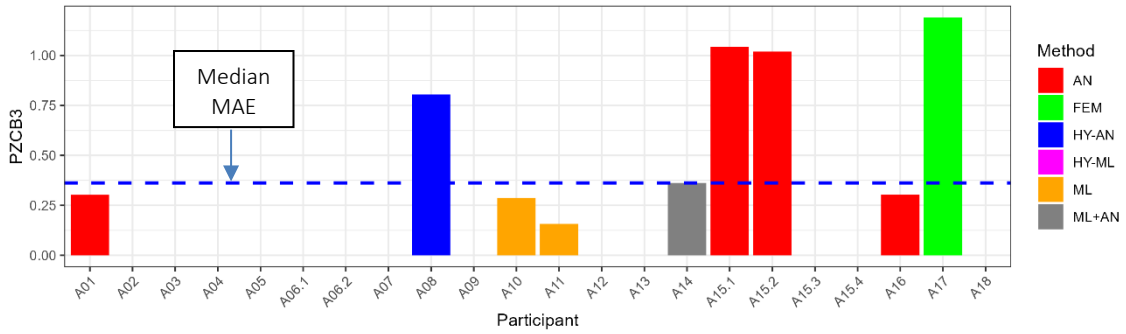
Figure 26. Accuracy of all contributors for PZCB3, Case B.

4.2.5.4 Seepage

The recorded time series for seepage is clearly noisier than all other variables considered in the benchmark. This can be derived from the observation of the records in the calibration period and was pointed out by all participants who considered this output. Such feature results in less accurate predictions in general, as can be seen in Figure 27.
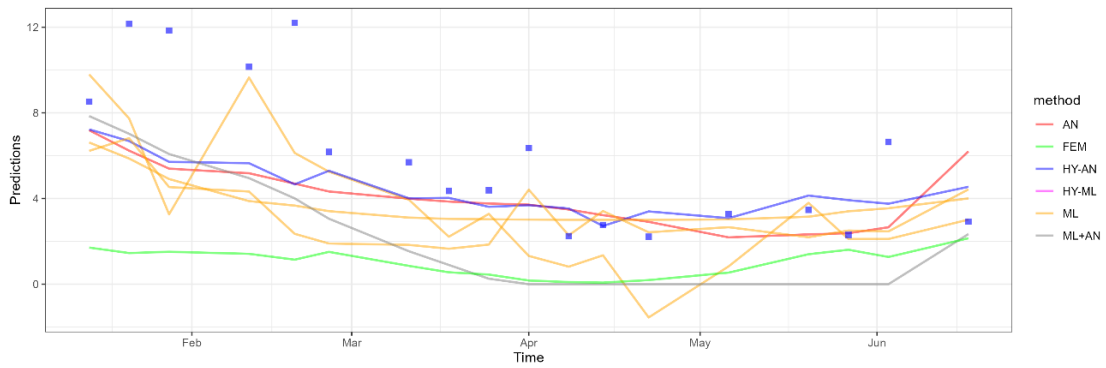
Figure 27. Predictions vs observations for Case B and seepage flow.

Only 7 contributions were received, generated with AN (A01, A08), ML (A04, A10, A11), a hybrid approach combining AN and ML (A14), and FEM (A17). All participants underestimated the seepage flows observed during the first two months of the period. This suggests that some important driver of seepage exists, which is not included among the input variables available.
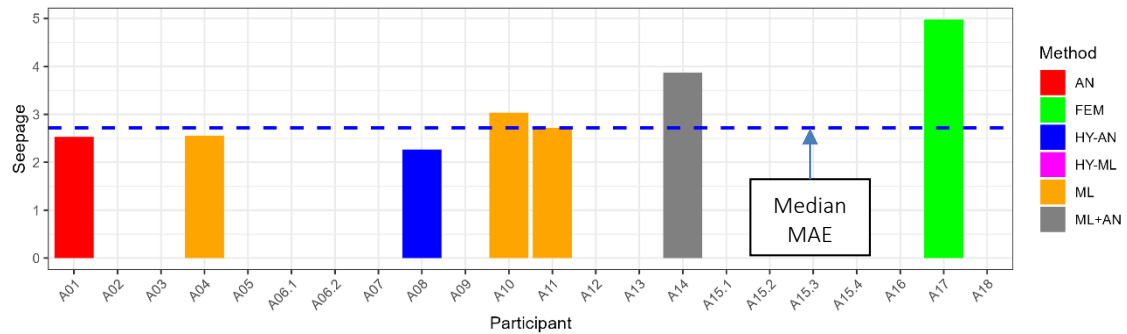
Figure 28. Accuracy of all contributors for seepage flow, Case B.

4.2.6 Case C

This task is more challenging than Case B, not only because the forecasting period is longer and further from the last available observed record, but also due to the irregular evolution of reservoir level for some years. While for 2013 and 2014 the loading conditions followed the more frequent trend, i.e., drawdown in the first quarter, followed by a fast filling and high levels during the second semester, there was a longer and greater emptying during 2015 and —not so important—

2016. As a result, prediction accuracy is expected to be lower in general. In addition to that, some of the output variables may undergo some change during such long prediction period, which would also negatively affect the forecasting accuracy.

4.2.6.1 Radial displacements

All participants submitted predictions for both displacements and Case C. As before, most of them were able to capture the evolution of the observed behavior. In this case, A09 (AN) resulted as the less accurate, in particular after mid-2015. Other models also failed to reproduce the behavior during the abnormal drawdown in early 2016, namely A11 (ML) and A16 (ML).
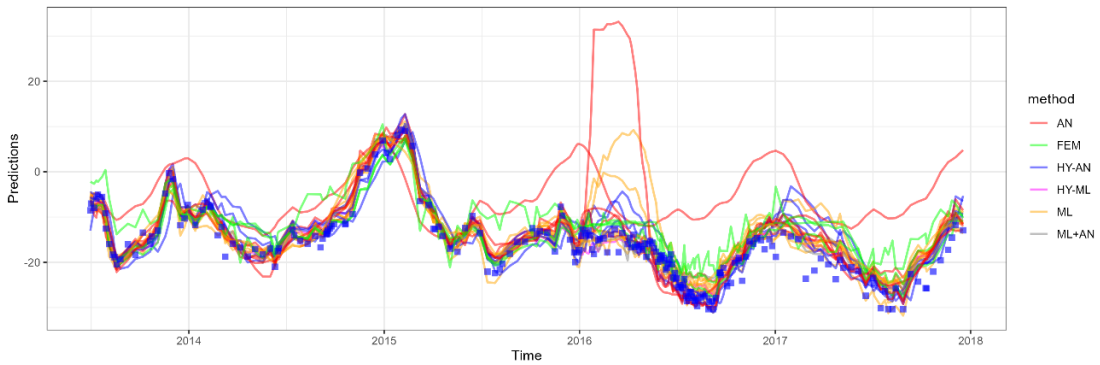
Figure 29. Predictions vs observations for Case C and CB2. Many participants captured the general trend, except A09. Some models failed to correctly predict the response during the abnormal emptying of the reservoir during the first semester of 2016 (A11, A16, both ML).
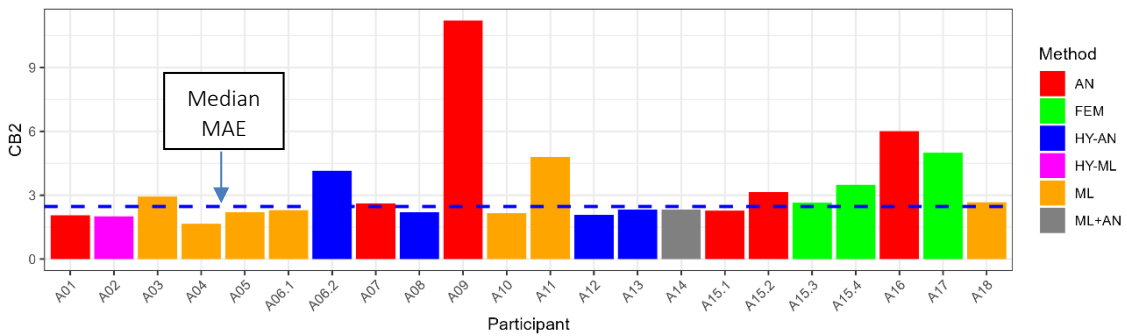
Figure 30. Accuracy of all contributors for CB2, Case C.

As for CB3, all three the contributions based solely on FEM (A15.3, A15.4 and A17) provided results clearly off the observed behavior. The same applies to A04 (ML). Both A03 (ML), A11 (ML) and A16 (AN) provided highly accurate predictions until early 2016 and poor estimates from there on, with special problems to reproduce the response during the first semester of 2016.
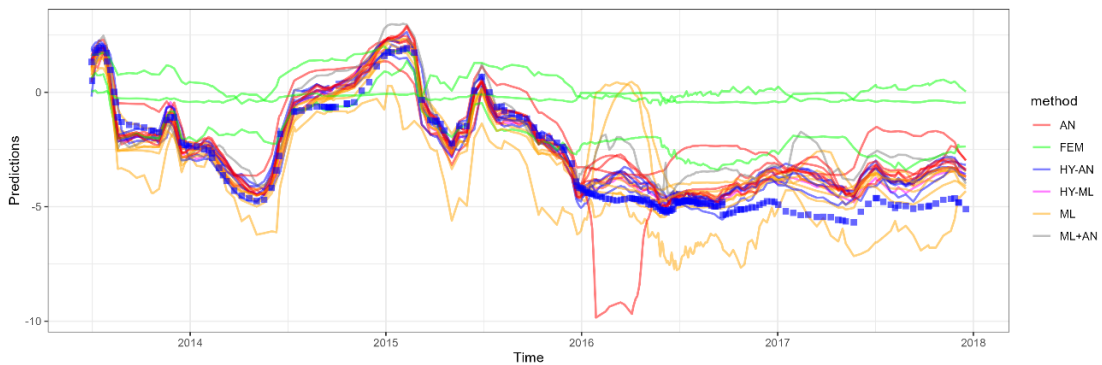
Figure 31. Predictions vs observations for Case C and CB3.
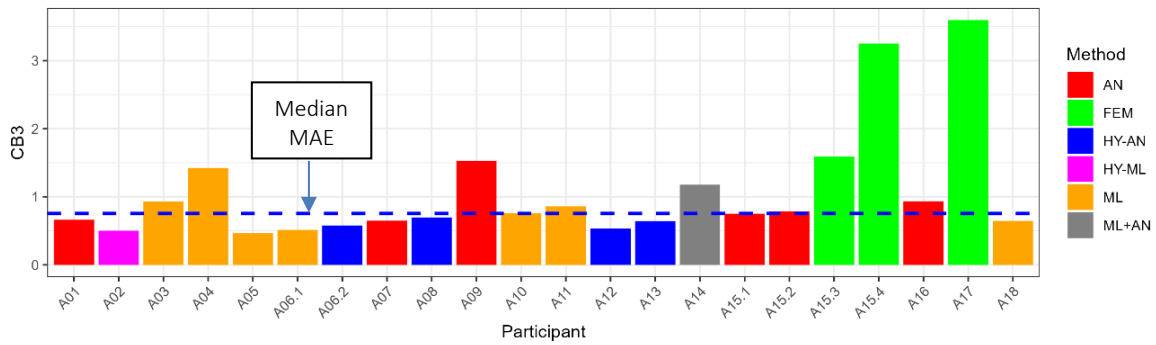
Figure 32. Accuracy of all contributors for CB3, Case C.

In general, accuracy decreased after January 2016. Not only during the abnormal emptying, but also —to a lesser extent— in the subsequent years. Even the predictions of the most accurate models (A02, A05, A06.1, and A12) depart from the observed trend after October 2016. Interestingly, they all predicted values higher than observations for such period, which may indicate a change in dam behavior. Figure 33 shows the observations and these predictions.
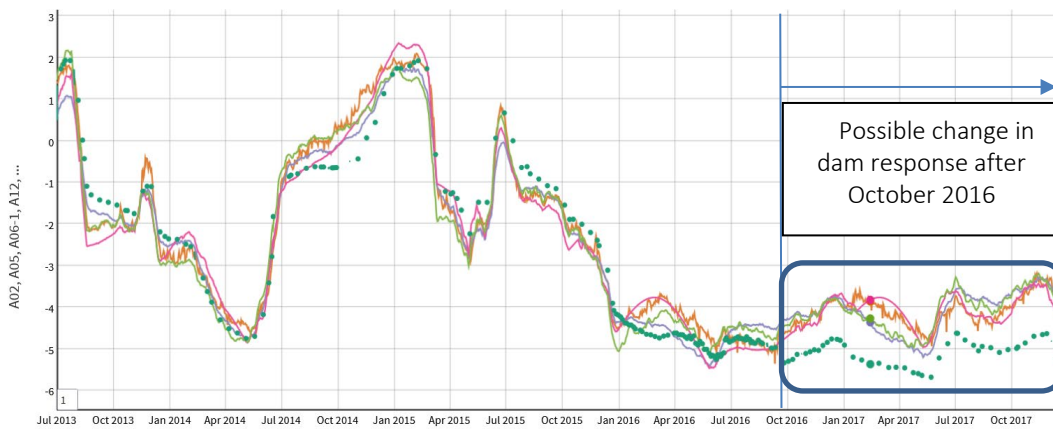
Figure 33. Best predictions (lines) for CB3, Case C, suddenly depart from observations (green dots) after October 2016.

4.2.6.2 Joint opening

As observed for Case B, observations for joint opening follow a similar trend to that for radial displacements. However, this only applies to the first period, before the mentioned drawdown in early 2016. This can be observed in Figure 34, which shows that joint opening remains almost constant from 2016 until the end of the period considered.

Twelve participants submitted a total of 13 predictions for this output and period. A17 (FEM) failed to capture the observed evolution, while predictions by A09 (AN), A12 (HY) and A16 (ML) are close to observations only for the first six months. All other participants (A01, A02, A07, A08, A10, A11, A14, A15.1 and A15.2) basically capture the evolution before 2016 with varying accuracy. Nonetheless, even the more accurate predictions overestimate the response between October and November 2014. Again, this may indicate some change in dam behavior.

Interestingly, the period of abnormal low water level is correctly predicted by A01, A02, A07, A10 and A11. Errors are higher after July 2017, when observations remain stable while all models predict some variations over the period.
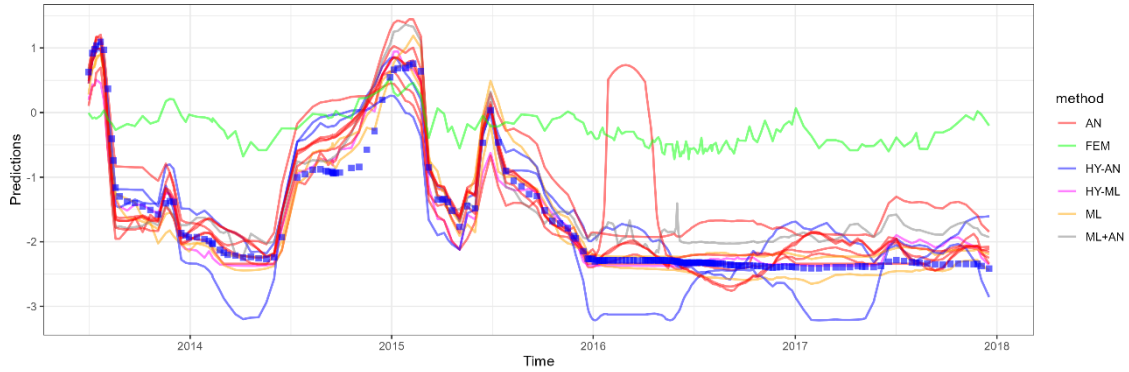
Figure 34. Predictions vs observations for Case C and C4-C5.
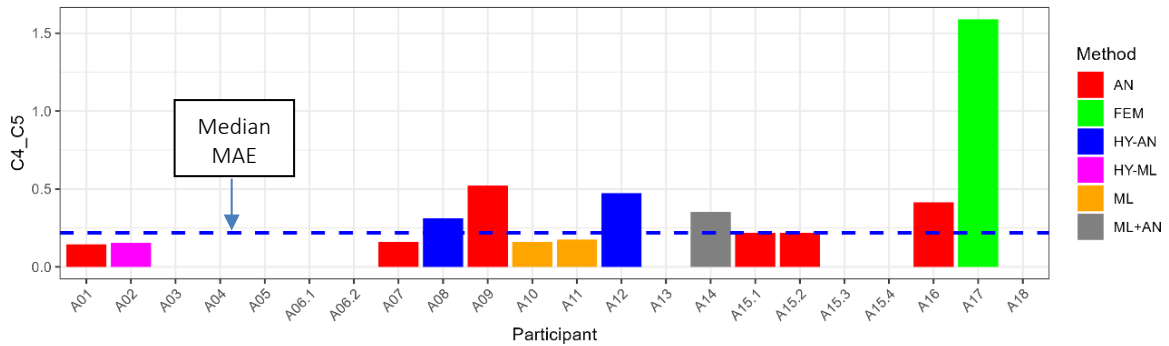
Figure 35. Accuracy of all submitted contributions for C4-C5, Case C.

4.2.7 Piezometers

Only 9 participants submitted a total of 10 forecasts for piezometers and Case C, though A15.1 and A15.2 are almost identical in this case. As shown in Figure 36, predictions from A17 (FEM) are far from observations for most of the interval. A15.1, A15.2 and A16 captured the evolution until the end of 2015. Again, the exceptionally low water level negatively affects to their accuracy.

The best models for PZCB2 were A01 (AN), A08 (HY), A09 (AN), A10 (ML), A11(ML) and A14 (ML+AN). They reproduced qualitatively the observed records even during the first 6 months of 2016. All of them also reproduced the evolution during the last period, except A01 and A14, which predictions were almost constant and thus did not follow the observed behavior in the last year.
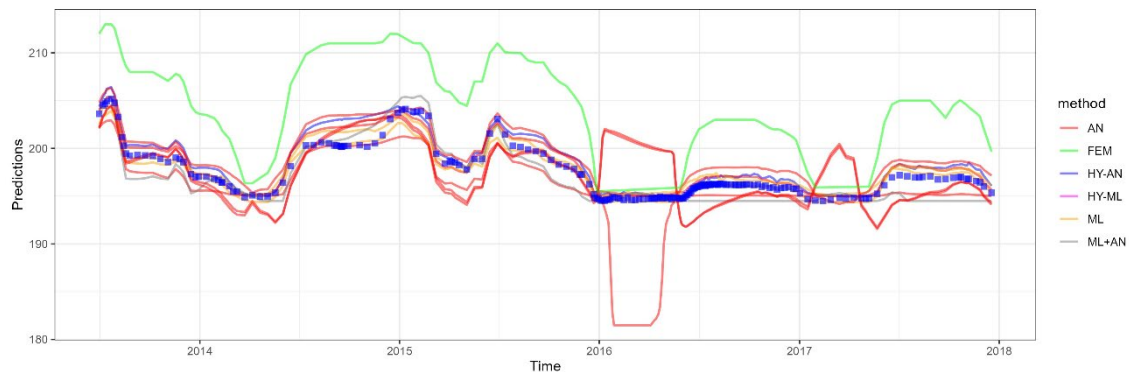
Figure 36. Predictions vs observations for Case C and PZCB2.
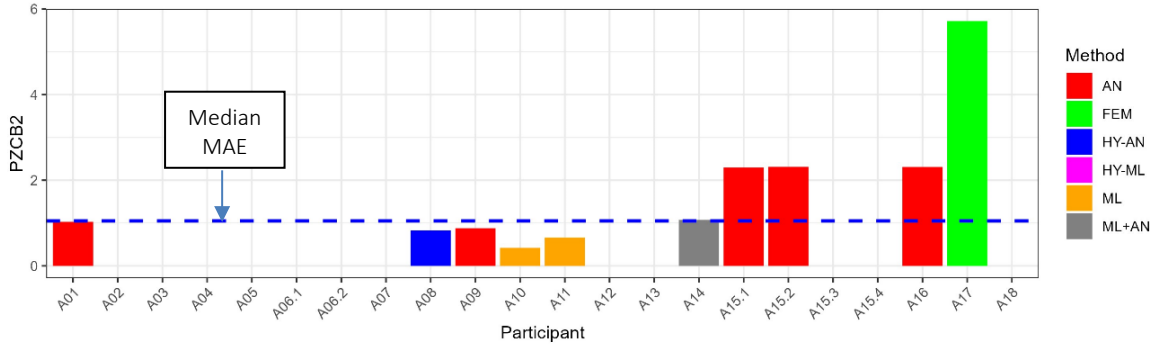
Figure 37. Accuracy of all submitted contributions for PZCB2, Case C.

As for PZCB3, accuracies are in general lower. Although the median MAE is similar (around 1 m), such error is more important for PZCB3, because the range of variation is lower (4 m, while the range for PZCB2 was 11 m). Even the more accurate models (A10 and A11, both ML) failed to correctly capture the observed evolution for some periods (January-July 2013, July 2014-February 2015, May-September 2016).
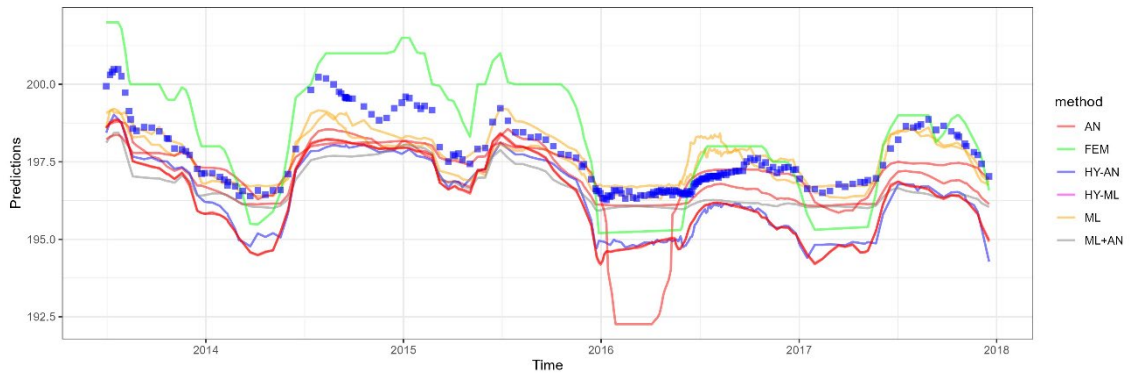
Figure 38. Predictions vs observations for Case C and PZCB3.
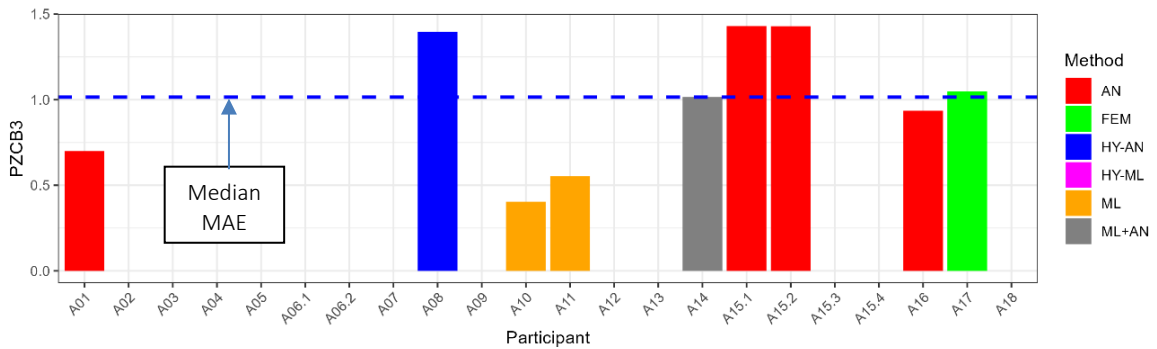
Figure 39. Accuracy of all submitted contributions for PZCB3, Case C.

4.2.7.1 Seepage

As for Case B, forecasts for seepage flow were in general less accurate than for the other outputs. The median MAE for Case C is much lower than for Case B, which is due to the lower ratio of high flows observed. In particular, all records after mid-2016 are lower than 10 l/s, in accordance with the relatively low water levels occurred. It can be concluded that predictions are more accurate for low hydrostatic load.

None of the models were capable of capturing the higher flows observed in the period. Only A04 (ML) approached some high flows in early 2015, but its predictions were consistently lower than observations during 2016. Even A10 and A11 (both ML), which featured relatively low error (around 0.5 l/s), cannot be considered useful for detecting anomalies, since they fail to estimate the majority of records above 10 l/s.

Results for Case C confirm that the inputs considered exclude some important information that has a clear influence on the observed seepage.
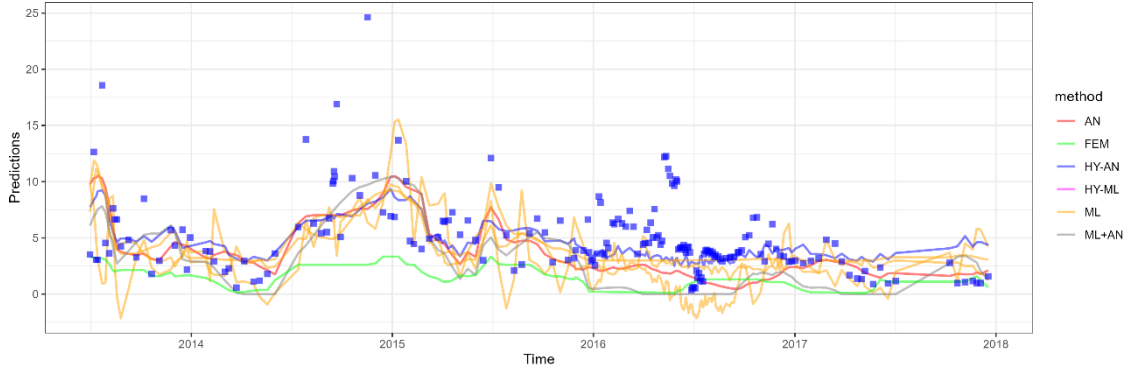
Figure 40. Predictions vs observations for Case C and seepage flow
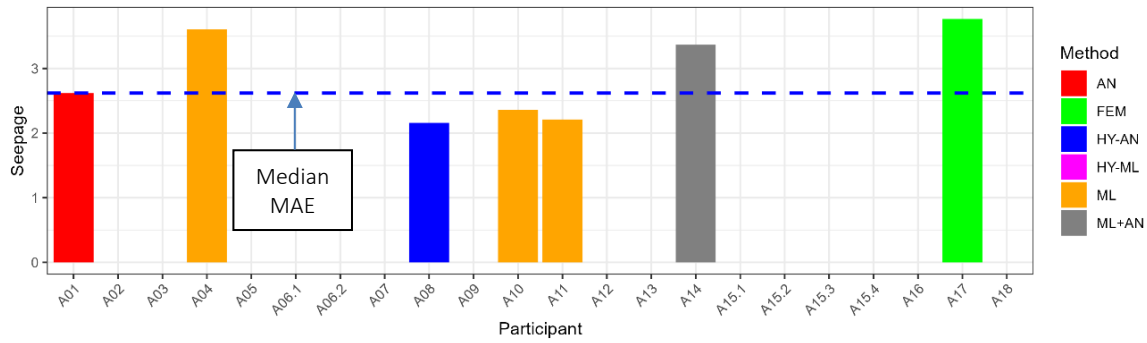
Figure 41. Accuracy of all submitted contributions for Seepage flow, Case C.

4.2.8 Overall assessment of model accuracy

Table 4 shows the summary of results in terms of model accuracy (MAE) for each task. Each column is colored in accordance with the corresponding MAE (from dark green for lowest error to dark red for highest MAE).

Table 4. Summary of submitted forecasts: participants, approaches used and MAE for each period and output. The colors of numerical columns correspond to the rank of each model within each output and Case.

Participant	Approach	CASE B - SHORT TERM						CASE C - LONG TERM					
		CB2	CB3	C4C5	PZCB2	PZCB3	Seep.	CB2	CB3	C4C5	PZCB2	PZCB3	Seep.
A01	AN	1.15	0.54	0.08	0.64	0.3	2.53	2.06	0.66	0.14	1.03	0.7	2.62
A02	HY-ML	1.67	0.34	0.16				2.01	0.5	0.15			
A03	ML	1.05	0.41					2.93	0.93				
A04	ML	1.43	0.29				2.56	1.65	1.42				3.6
A05	ML	1.32	0.19					2.19	0.47				
A06_1	ML	1.77	0.23					2.3	0.51				
A06_2	HY-AN	6.31	0.63					4.15	0.58				
A07	AN	1.85	0.35	0.16				2.61	0.65	0.16			
A08	HY-AN	2.29	0.69	0.25	0.73	0.8	2.27	2.19	0.7	0.31	0.83	1.4	2.16
A09	AN	2.39	0.75	0.23	0.36			11.2	1.53	0.52	0.88		
A10	ML	1.15	0.35	0.1	0.45	0.29	3.04	2.15	0.76	0.16	0.42	0.4	2.36
A11	ML	1.78	0.35	0.18	0.3	0.16	2.72	4.8	0.86	0.18	0.66	0.55	2.21
A12	HY-AN	1.87	0.44	0.61				2.07	0.53	0.47			
A13	HY-AN	3.65	0.59					2.32	0.64				
A14	ML+AN	1.65	0.76	0.21	0.86	0.36	3.87	2.33	1.18	0.35	1.07	1.02	3.37
A15_1	AN	1.15	0.58	0.2	1.58	1.04		2.27	0.75	0.22	2.3	1.43	
A15_2	AN	2.29	0.36	0.18	1.57	1.02		3.15	0.78	0.22	2.31	1.43	
A15_3	FEM	3.37	1.63					2.65	1.59				
A15_4	FEM	3.26	2.6					3.49	3.25				
A16	AN	1.5	0.42	0.06	1.21	0.3		6.01	0.93	0.41	2.31	0.94	
A17	FEM	3.82	3.01	1.51	5.19	1.19	4.98	4.99	3.6	1.59	5.72	1.05	3.76
A18	ML	1.8	0.25					2.67	0.65				

A strict quantitative comparison of model accuracy is neither feasible nor the objective of the benchmark. Accuracy is not the unique criterion for assessing models. Instead, robustness, flexibility, complexity, and interpretability must also be considered. In addition, the rank among models cannot be considered as the unique criterion for model assessment: a model with low ranking may be useful —in case many models provided highly accurate results— and vice versa, as is the case for seepage flows, for which all models were basically incapable of predicting high flows. It should also be remembered that MAE is measured in the same units as the output considered and, therefore, it cannot be compared between variables of different nature. Nonetheless, some conclusions can be drawn from the overall picture of accuracy for all tasks proposed:

- For the problems in this theme, FEM was not the optimal approach for accurately estimating the behavior of the arch dam. Among the three contributions based on FEM, they ranked lower in terms of accuracy when compared to other models. Furthermore, only one of these FEM-based models provided predictions for outputs beyond radial displacements, and even those predictions lacked significant accuracy. Although FEM remains invaluable for other purposes, such as estimating the dam response under extraordinary loads, data-based approaches clearly demonstrated higher accuracy in predicting observed dam behavior for all problems in this theme.
- FEM resulted to be very useful as part of hybrid models, which ranked among the top accurate models for some tasks (e.g., A02 for Case C and CB2, CB3 and C4-C5).
- Only four teams submitted predictions for all outputs and periods proposed. Among them, A01 (AN) and A10 (ML) can be considered as the most accurate overall. They succeeded in modelling the results for all outputs during the exceptional load combination occurred in the final period for Case C.
- Radial displacements are the most frequently controlled variables in dam safety. They are essential in identifying anomalies and can be estimated with FEM models. All participants submitted predictions for both variables of this kind. If only these outputs are considered, A01 and A10 are still among the more accurate, but other models provided similar results, namely A02 (HY-ML), A05 (ML) and A06.1 (ML).

4.3 *Warning thresholds*

The participants were also asked to provide prediction intervals with the aim of being used to detect anomalies. This task was more open to interpretation than pure predictions, and, therefore, more difficult to evaluate. The submissions received included low and high thresholds for each output, obviously based on the previous predictions, for both Case B and Case C. In principle, we assumed that the corresponding contributor considers any observed record that does not lie within the thresholds as an anomaly. Also based on the information from the dam owner, the dam underwent no relevant safety issue. Therefore, all observations for all outputs and periods are considered as normal and should be within the warning thresholds. As a result, submissions are evaluated considering the number of observations out of the intervals as errors, i.e., the "perfect" prediction interval would include all the observations. Table 5 show the summary of all contributions received.

Table 5. Summary of submitted warning levels: participants, approaches used, outputs considered and criterion for defining the warning thresholds.

Participant	Approach	CB2	CB3	C4C5	PZCB2	PZCB3	Seep.	Criterion Warning levels
A01	AN							99% percentile
A02	HY-ML							99% percentile
A03	ML							2 std dev.
A04	ML							2.58 std dev.
A05	ML							2 std dev.
A06_1	ML							3 std dev.
A06_2	HY-AN							3 std dev.
A07	AN							90% percentile
A08	HY-AN							3 std dev.
A09	AN							95% percentile
A10	ML							100% percentile
A11	ML							2 std dev.
A12	HY-AN							100% percentile
A13	HY-AN							3 std dev.
A14	ML+AN							3 std dev.
A15_1	AN							2.5 std dev.
A15_2	AN							2.5 std dev.
A15_3	FEM							2.5 std dev.
A15_4	FEM							2.5 std dev.
A16	AN							2 std dev.
A17	FEM							NA
A18	ML							2.5 std dev.

More precisely, we excluded isolated errors, i.e., if some record falls out of the prediction interval but the subsequent value returns and is thus considered as normal, it was not counted for the final sum. In addition, we also considered the width of the submitted ranges. This is a relevant issue from a practical viewpoint: since the final goal is detecting anomalies, a method which results in a very wide interval would success in including all observations, but would also be less useful for detecting anomalies, because these would also lie inside the interval and would thus be taken as normal values.

The width of the interval is considered in relative terms, i.e., as the ratio between the average width and the range of variation of each variable in the period. This allows for comparing approaches and variables of different kind. In the next subsections, the results are presented two ways: first, observations are plotted along with the upper and lower thresholds from all participants, to show a general view of the submissions; then, the number of observed values outside of the prediction interval is shown for each participant —with a dashed line indicating the 95%—, together with the relative width of the intervals —with a dashed line highlighting the median width for each case and output—.

4.3.1 Case B

4.3.1.1 Radial displacements

All contributors but 15.1 and 15.2 (both AN) submitted intervals following the observed evolution of CB2, as expected from the predictions previously analyzed. 12 out of the 22 total submissions succeeded in having all observations within the prediction interval. They are based on different approaches. None of the intervals generated with FEM resulted as valid (i.e., having more than 95% of observed values in range). Indeed, both of them (15.3 and 15.4) used narrow intervals and were not among the more accurate contributions, which explains the outcome.

Submissions A01 (AN) and A16 (ML) can be considered as the more useful, since they provided the narrowest intervals among those having all observations between the upper and lower thresholds. On the other hand, contribution A06.2, though having all observed values inside the range, used an interval width greater than the range of variation of the output, which reduces the capability for anomaly detection. Very similar results were obtained for CB3, with the same amount of solutions with all observations in range and similar interval widths.

Figure 42. Prediction intervals and observations for Case B, CB2

Figure 43. Percentage of observations inside prediction interval for Case B, CB2, along with the corresponding interval width.

Figure 44. Prediction intervals and observations for Case B, CB3.

Figure 45. Percentage of observations inside prediction interval for Case B, CB3, along with the corresponding interval width.

4.3.1.2 *Joint opening – C4_C5*

Eight out of the 10 submitted contributions for joint opening encompassed all observations for Case B, as shown in figure 47. Only A16 (AN) and A07 (AN) provided predictions intervals considered as invalid with the criterion applied. In both cases, the width is clearly below the median value. However, while for A16 this is the reason of the poor result, A07 provided values clearly off the observations, therefore, the outcome would have been similar with a wider interval.

A12 stands out for using the greater width among all contributions, which helps in avoiding false anomalies at the cost of lower potential for detecting anomalies. For this output, A11 provided the narrowest interval among all participants with all observations in range.

Figure 46. Prediction intervals and observations for Case B, C4-C5

Figure 47. Percentage of observations inside prediction interval for Case B, C4-C5, along with the corresponding interval width.

4.3.1.3 Piezometers

Only 9 submissions were received for piezometers, 4 of which are considered as valid, i.e., free of false detected anomalies. As before, A15.1 and A15.2 are clearly off the observed values. The high number of observations out of range for A14 (ML+AN) is due to the use of a narrow interval, much smaller than all other participants. A11 (ML) can be considered as the best model for piezometers, since all observations lied within the prediction interval for both PZCB2 and PZCB3, being the width lower than other submissions. The result for A10 is similar (except for a slightly wider interval for PZCB3), while A12 again avoided false positives by using a very wide interval.

Figure 48. Prediction intervals and observations for Case B, PZCB2

Figure 49. Percentage of observations inside prediction interval for Case B, PZCB2, along with the corresponding interval width.

Figure 50. Prediction intervals and observations for Case B, PZCB3

Figure 51. Percentage of observations inside prediction interval for Case B, PZCB3, along with the corresponding interval width.

4.3.1.4 *Seepage*

All participants observed high variability in seepage flow and poor prediction accuracy, which led to the use of relatively wide prediction intervals. Four out of the 6 submitted contributions were based on intervals wider than the range of variation of the output in the period, even though most of them limited the lower threshold to avoid negative values (in accordance with the physical meaning of the data). This results in less useful models. In this sense, it is worth mentioning A04 (ML), which was capable of having more than 80% of the observations in range despite using a very narrow interval. In turn, A14 again failed to capture the observations because of the narrow interval.

Figure 52. Prediction intervals and observations for Case B, Seepage.

Figure 53. Percentage of observations inside prediction interval for Case B, Seepage, along with the corresponding interval width.

4.3.2 Case C

This task is more difficult than Case B, not only because of the longer time period (with more observations), but also because predictions are made based on information taken as far as 5 years before. In addition, we already verified that the abnormal emptying of the reservoir at the beginning of 2016 resulted in poor predictions for some participants. Finally, there is higher probability that some indicators underwent some change in behavior over the long period considered. In this regard, the comparative analysis among participants is more interesting.

4.3.2.1 Radial displacements

For CB2, only 7 out of the 22 submissions succeeded in having more than 95% of the observations inside the prediction interval. Four of them are based on hybrid approaches, two on ML and one on an analytical model. It is worth mentioning that all of them except A01 (AN) used an interval wider than the median of all contributions. Nonetheless, they can be considered as useful: although they are above the median width, they range between 0.3 and 0.5 times the range of variation of the output.
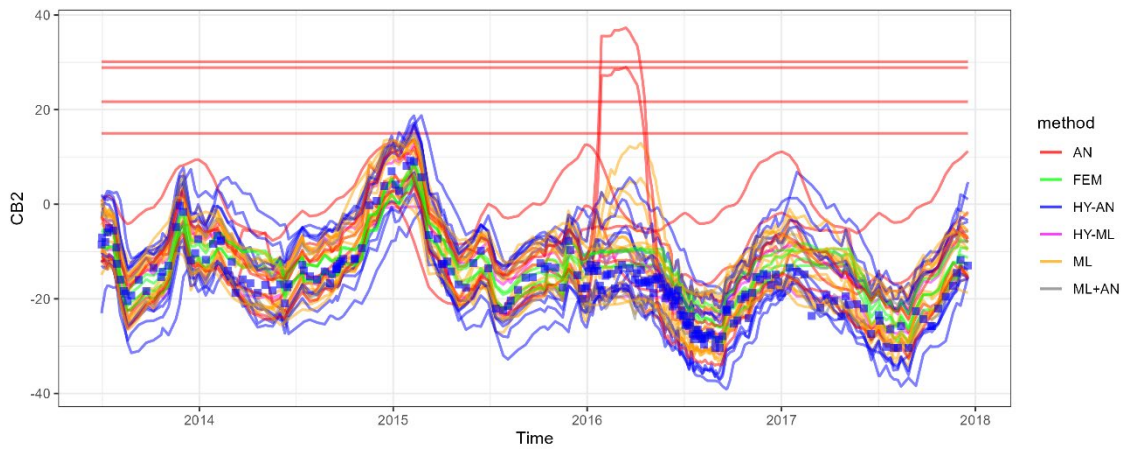
Figure 54. Prediction intervals and observations for Case C, CB2
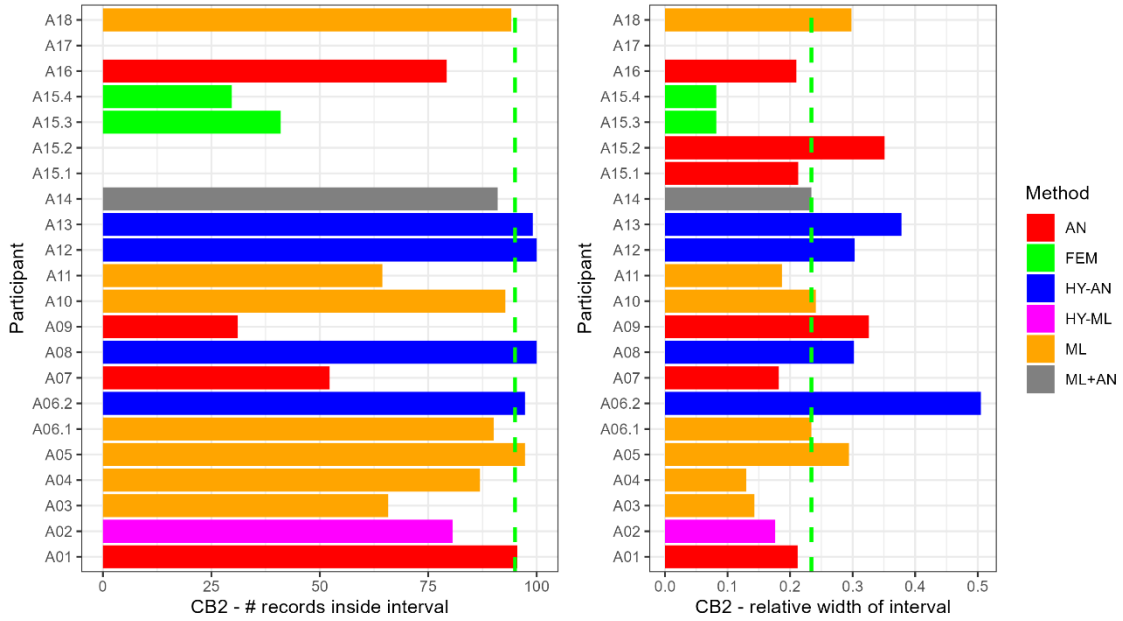
Figure 55. Percentage of observations inside prediction interval for Case C, CB2, along with the corresponding interval width.

As for CB3, only 5 contributions are considered valid, again with relatively wide intervals if compared with other participants. Still, also as for CB2, the relative width of the ranges is around 0.3-0.5. These results are closely related to those for prediction: again, A15.1 and A15.2 are far off the observations, and many of the problems appear during and after the anomalous period early in 2016. However, the observed behavior in the last period, which was considered as potentially anomalous in view of the predictions of the best models (Figure 33), is now considered as normal: the recorded values fall inside the intervals, though close to the lower threshold.
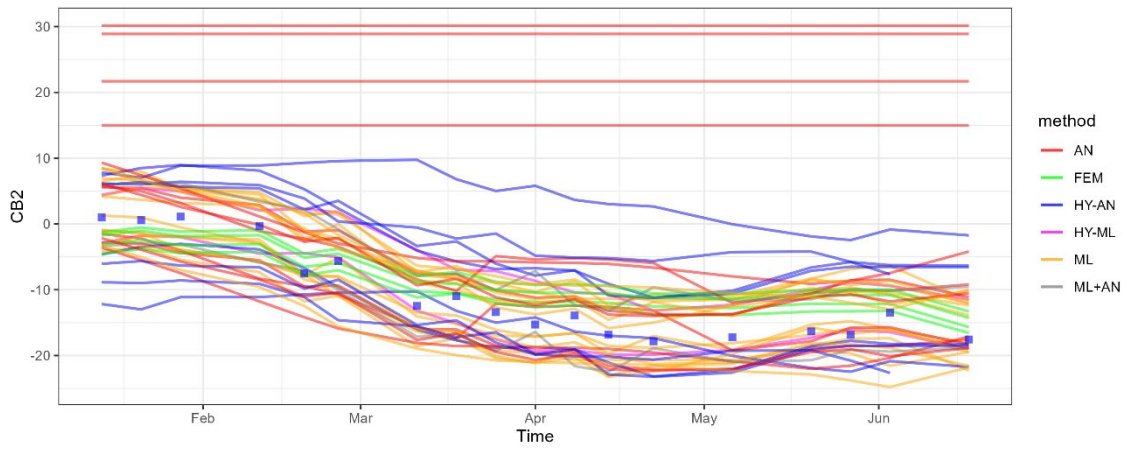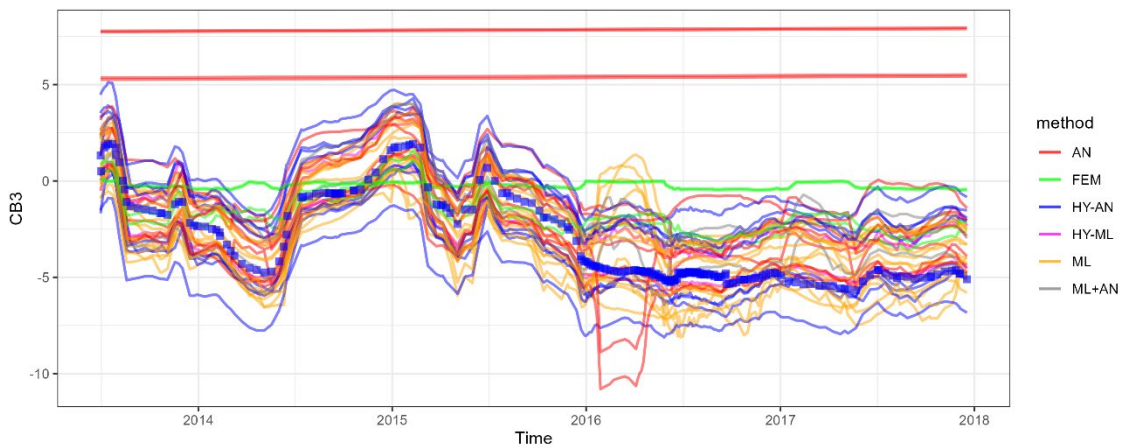

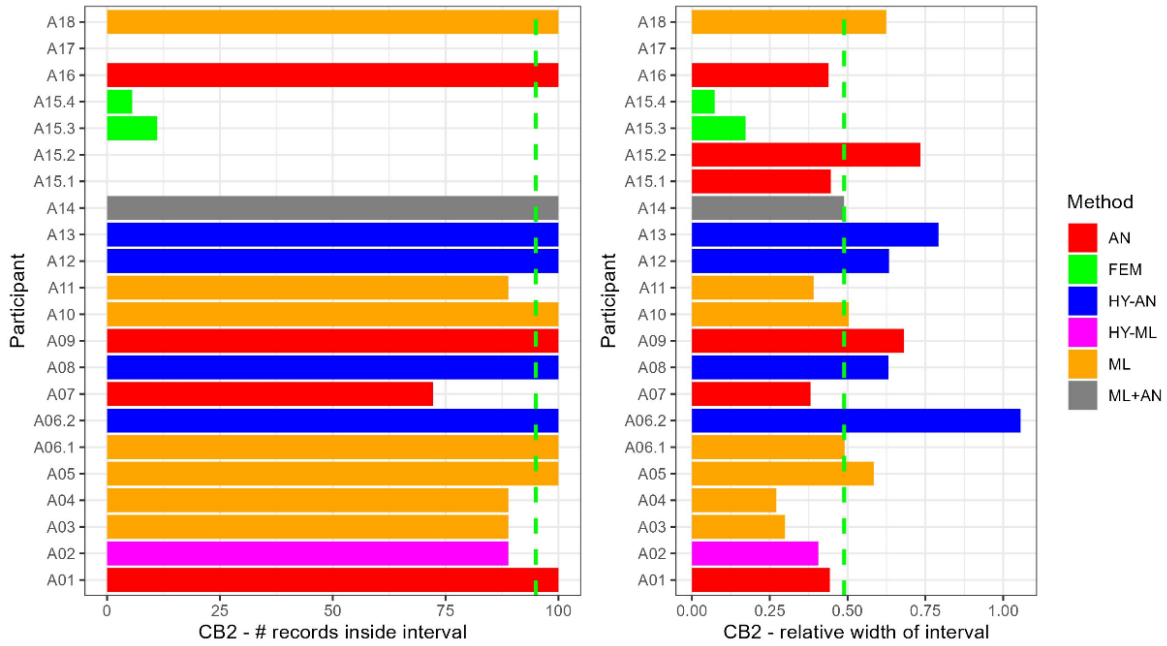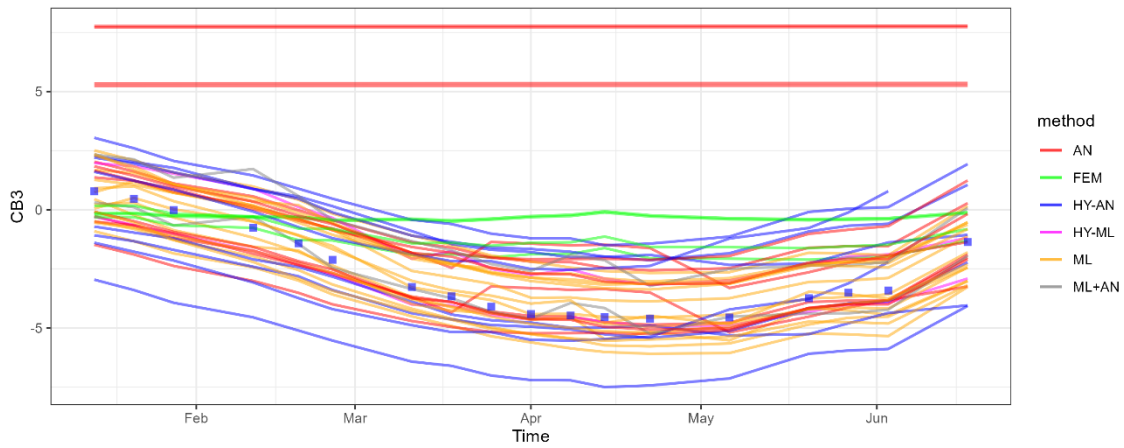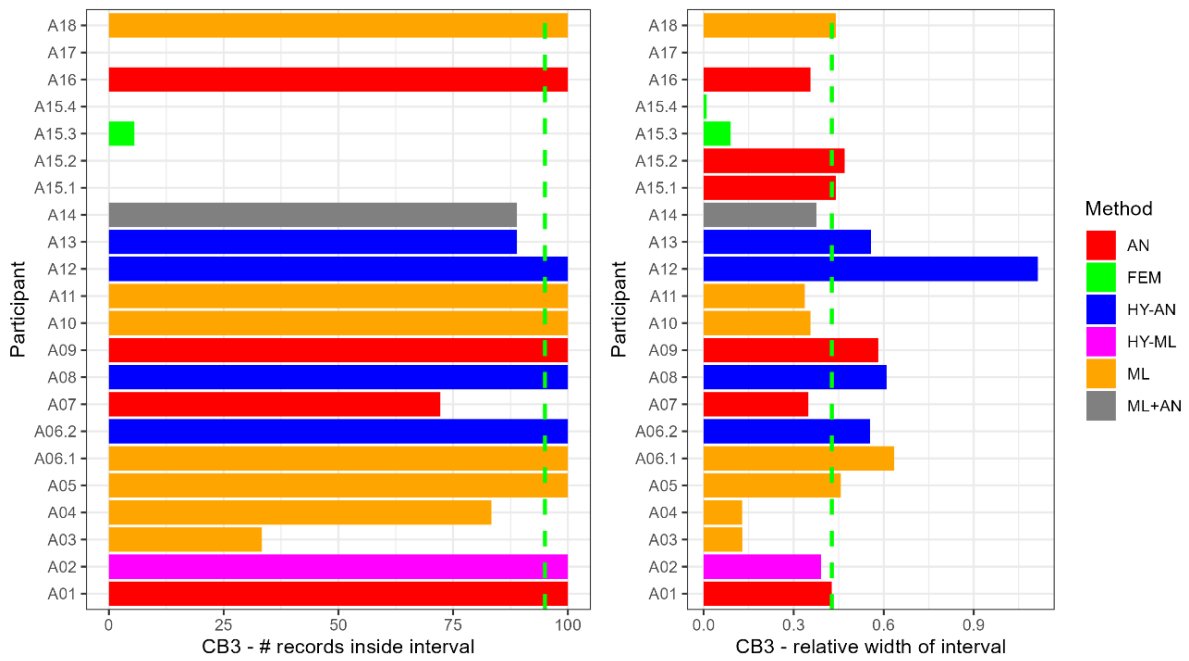Figure 56. Prediction intervals and observations for Case C, CB3.
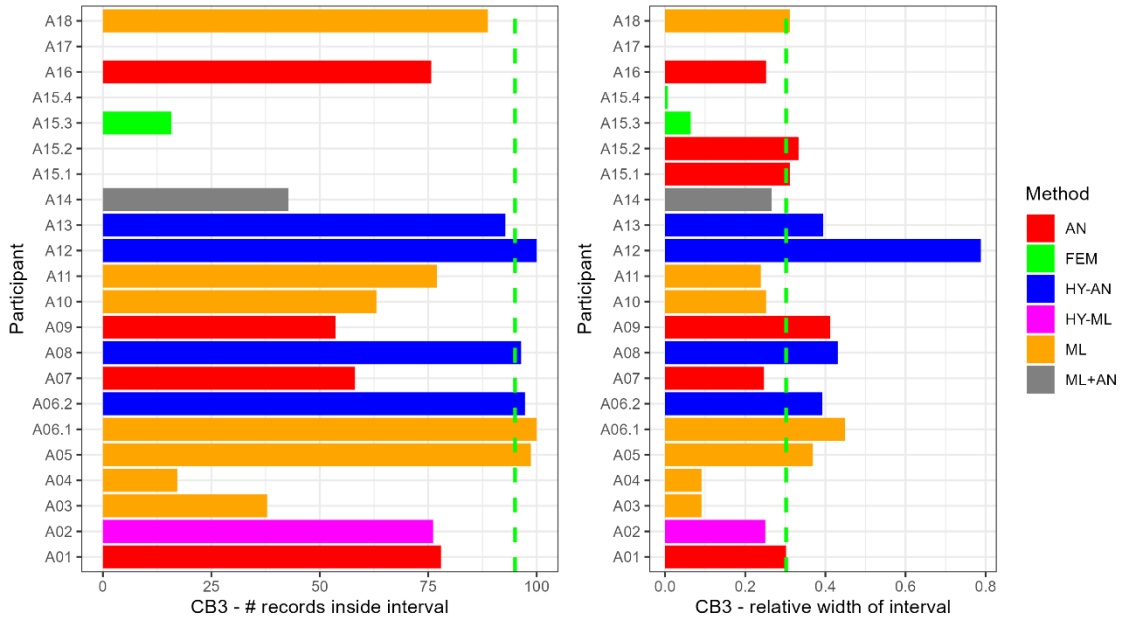
Figure 57. Percentage of observations inside prediction interval for Case C, CB3, along with the corresponding interval width.

4.3.2.2 Joint opening – C4_C5

As before, results for C4-C5 from A08 and A12 (both AN) are valid but based on wide intervals. In this case, two contributions based on ML (A10 and A11), as well as A02 (HY-ML), succeeded in capturing the observations with a relative width below 0.3, clearly narrower. Likewise, A01 (AN) identified near 95% of the observations, also with a narrow interval.
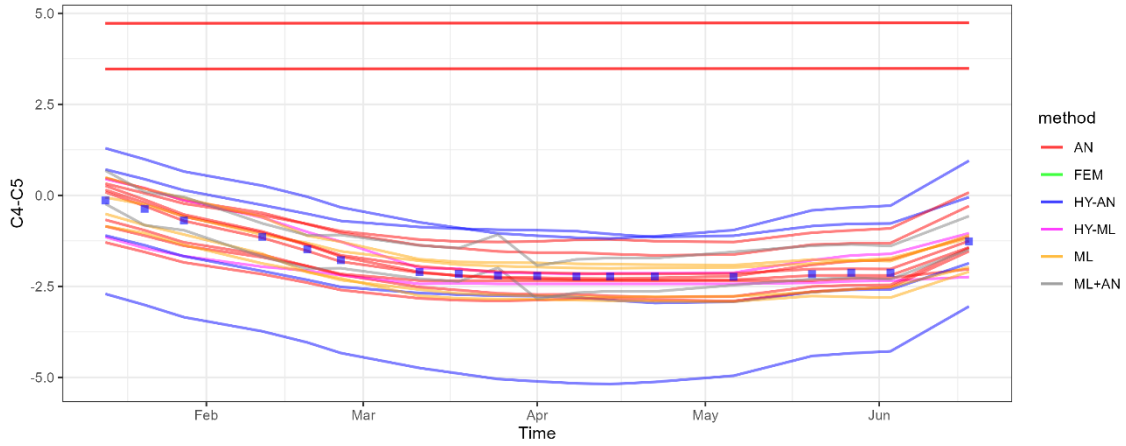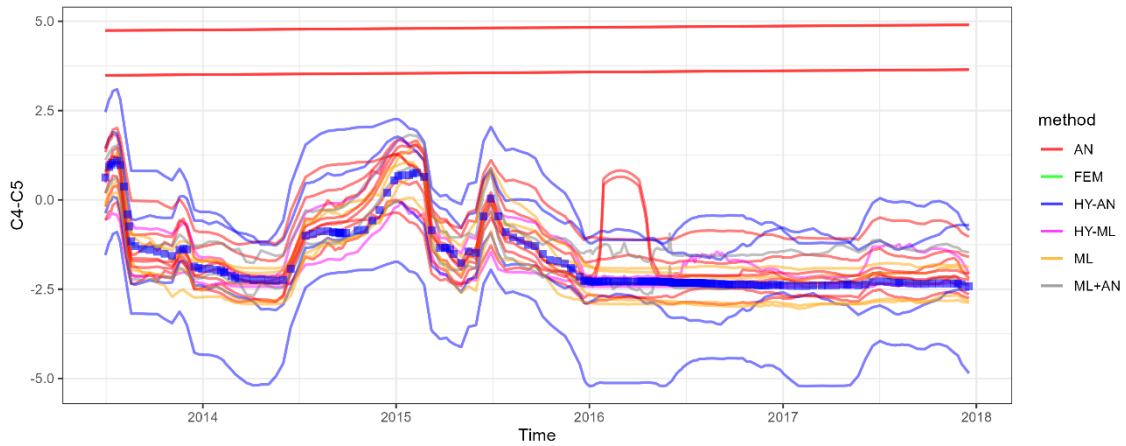

Figure 58. Prediction intervals and observations for Case C, C4-C5
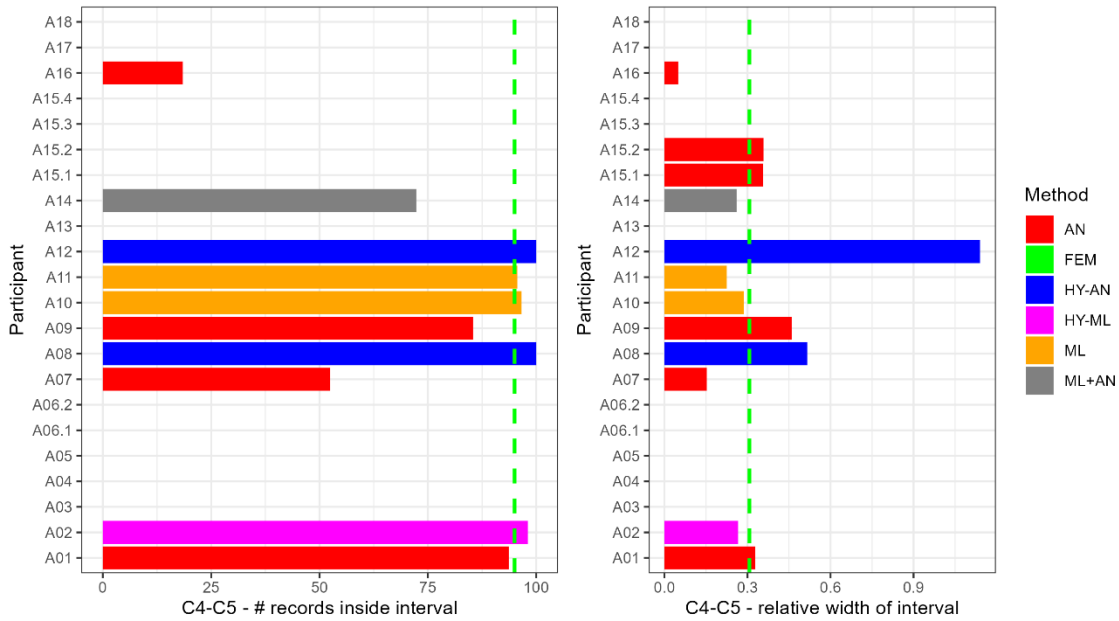
Figure 59. Percentage of observations inside prediction interval for Case C, C4-C5, along with the corresponding interval width.

4.3.2.3 Piezometers

Only 7 participants considered these outputs for Case C. For PZCB2, four of them approached the 95% threshold: two based on ML with narrow intervals (A10 and A11), one based on AN (A09) and, as before, A12 (HY-AN) with a very wide prediction interval. All these four models can be considered as useful. Predictions from A15.1 and A15.2 are barely constant and far from the observed values, as for other outputs. Upper and lower limits from A16 (ML) are reasonable except for the first semester of 2016. Figure 60. Prediction intervals and observations for Case C, PZCB2.
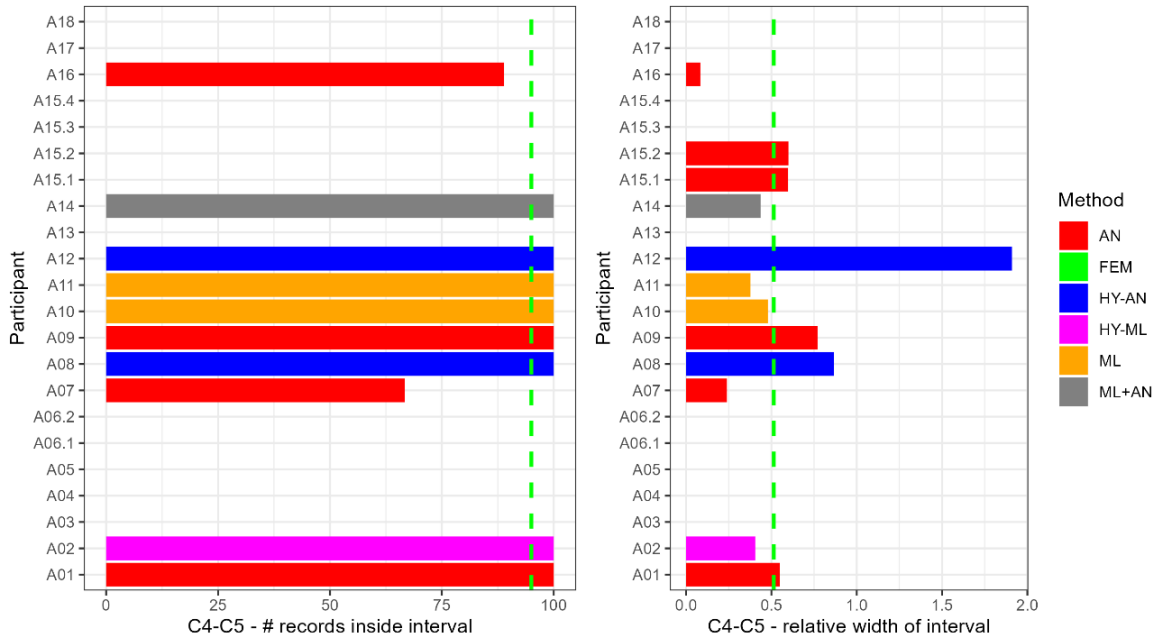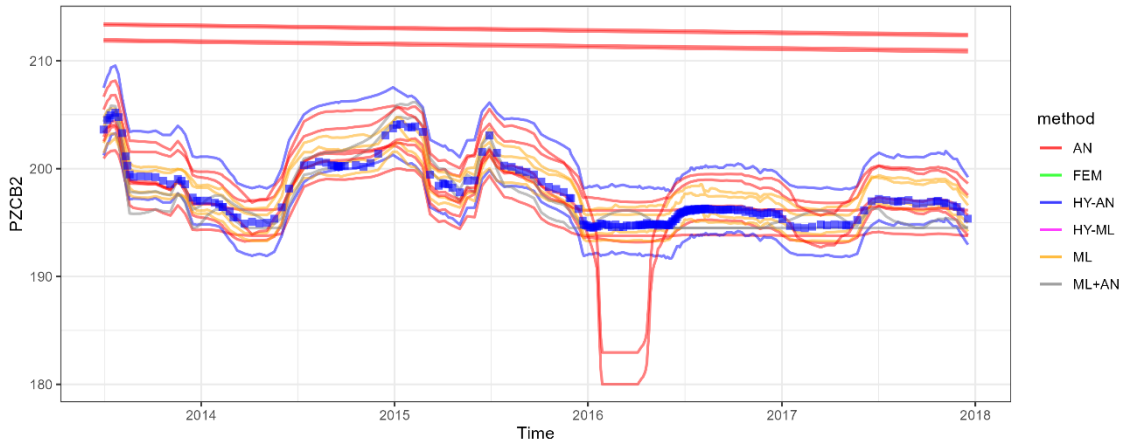

Figure 60. Prediction intervals and observations for Case C, PZCB2.
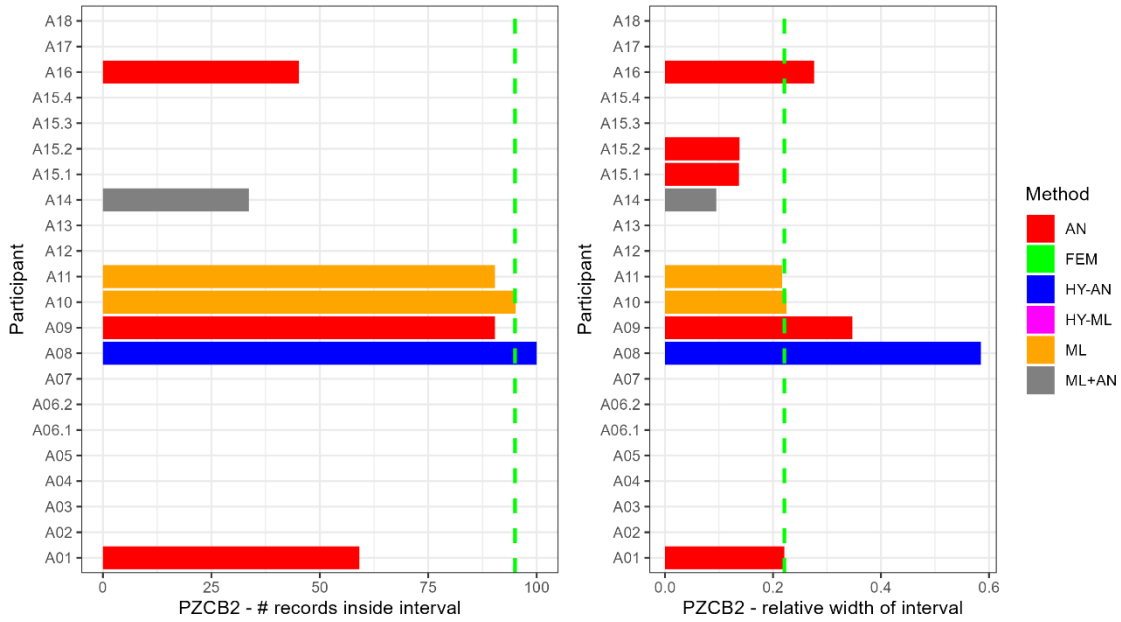
Figure 61. Percentage of observations inside prediction interval for Case C, PZCB2, along with the corresponding interval width.

Results are poorer for PZCB3. Only A08 was capable of taking all observations in range, at the cost of a very wide interval, within the same order of magnitude of the range of variation of the output. Interestingly, both A10 and A11 considered observations in July-August 2016 as out of range, while both A11 and A01 took also the first observations in 2015 as anomalous.
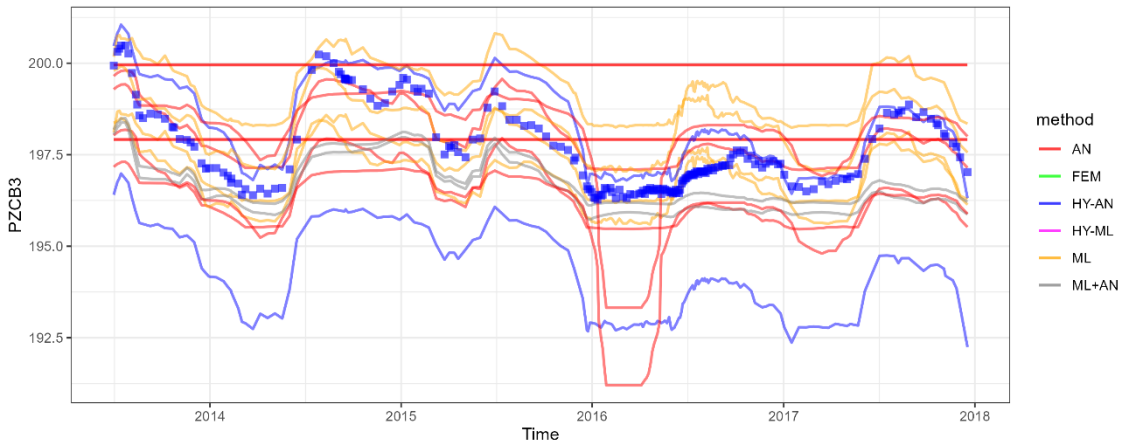
Figure 62. Prediction intervals and observations for Case C, PZCB3.
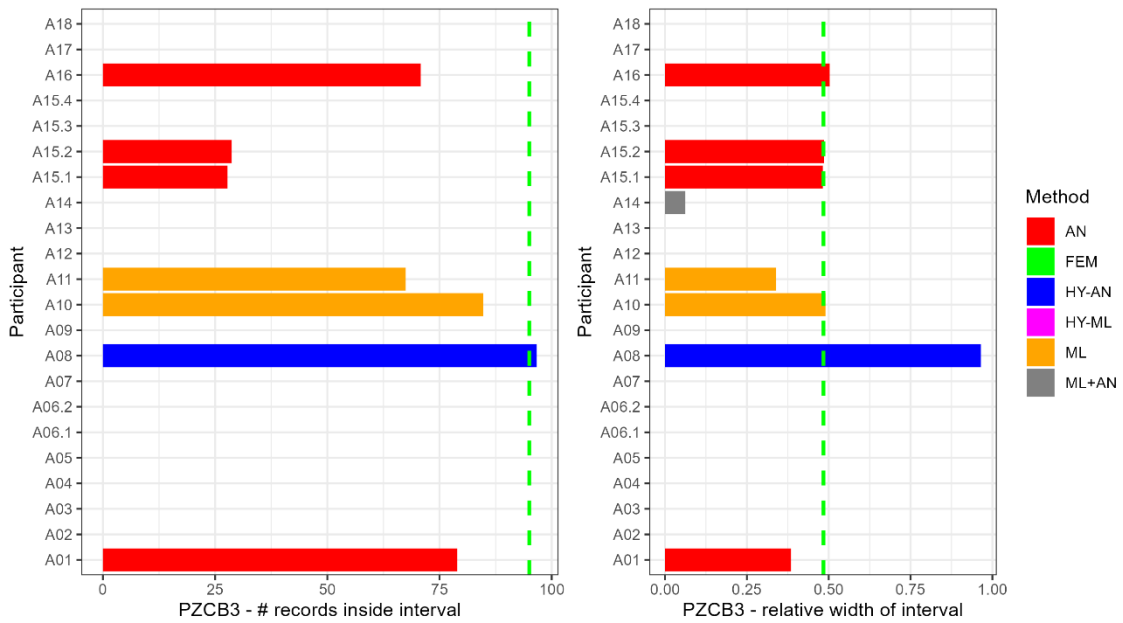
Figure 63. Percentage of observations inside prediction interval for Case C, PZCB3, along with the corresponding interval width.

4.3.2.4 *Seepage*

As for Case B, seepage was difficult to predict and thus also to generate useful warning thresholds. Still, 4 contributions were capable of considering all observed values inside the warning thresholds, with interval widths of around 0.5 times the range of variation of the seepage in the period. In this case, all valid models (A01, A08, A10, and A11) used similar widths. Interestingly, as for other outputs, different approaches were used for the best models.
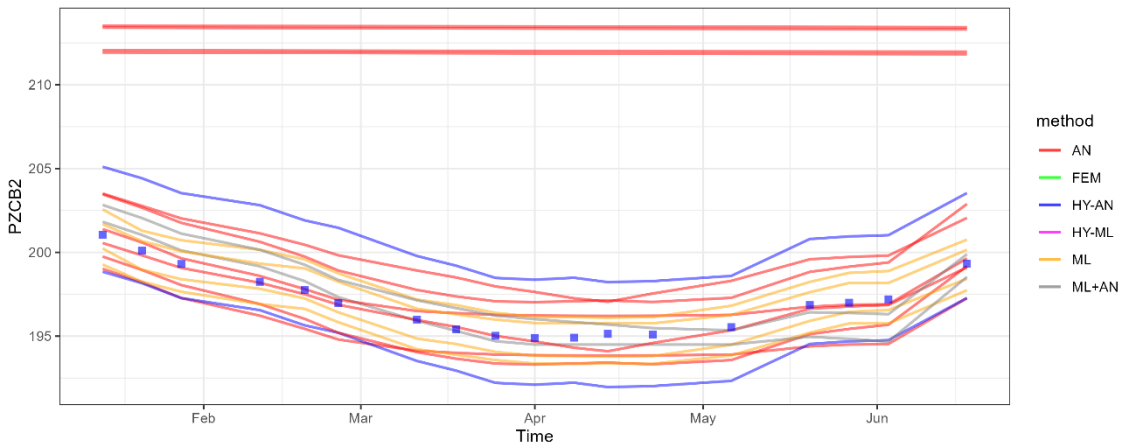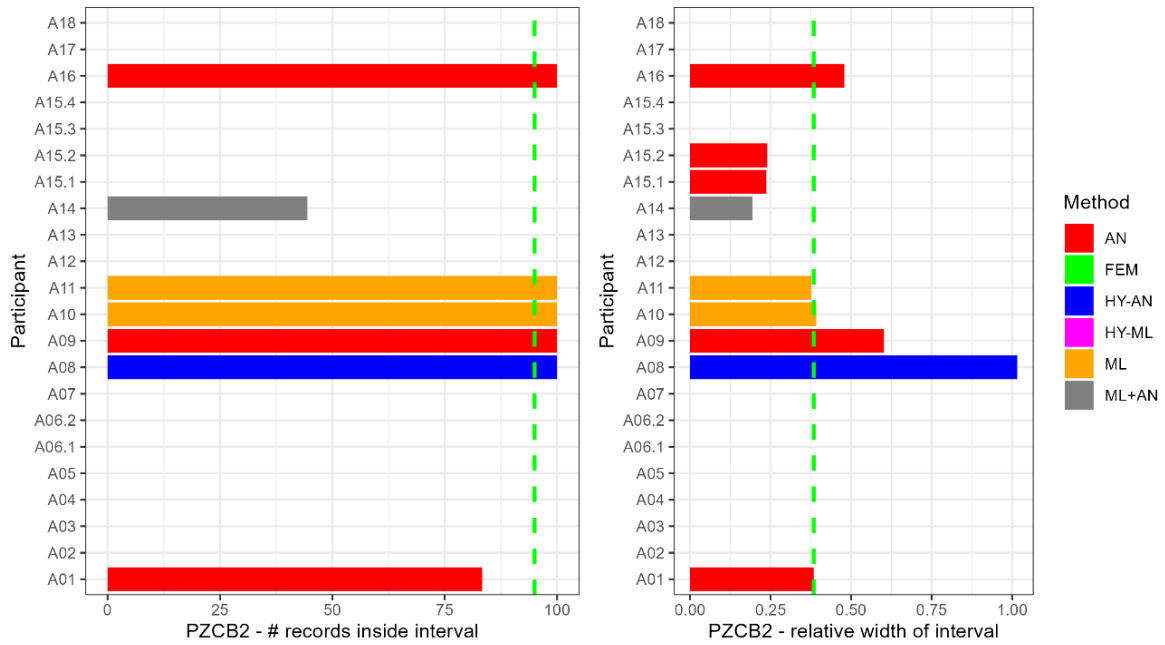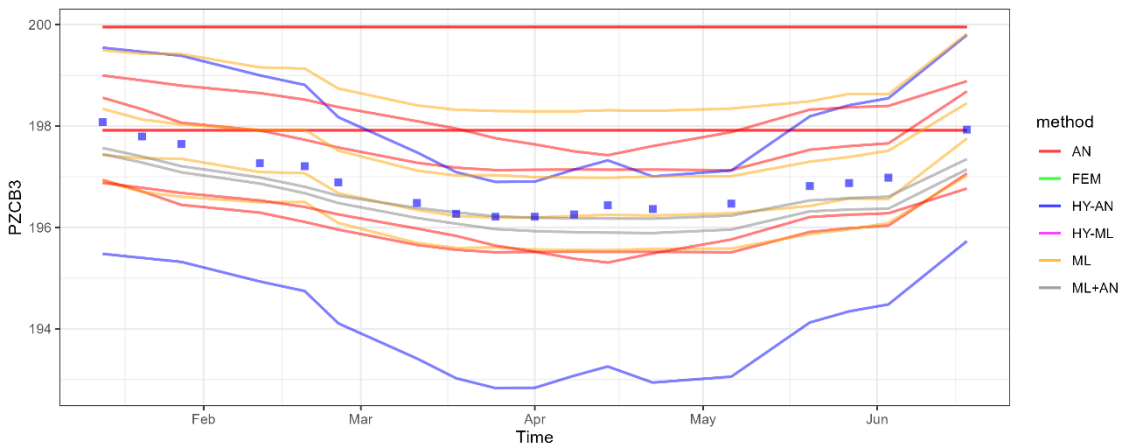

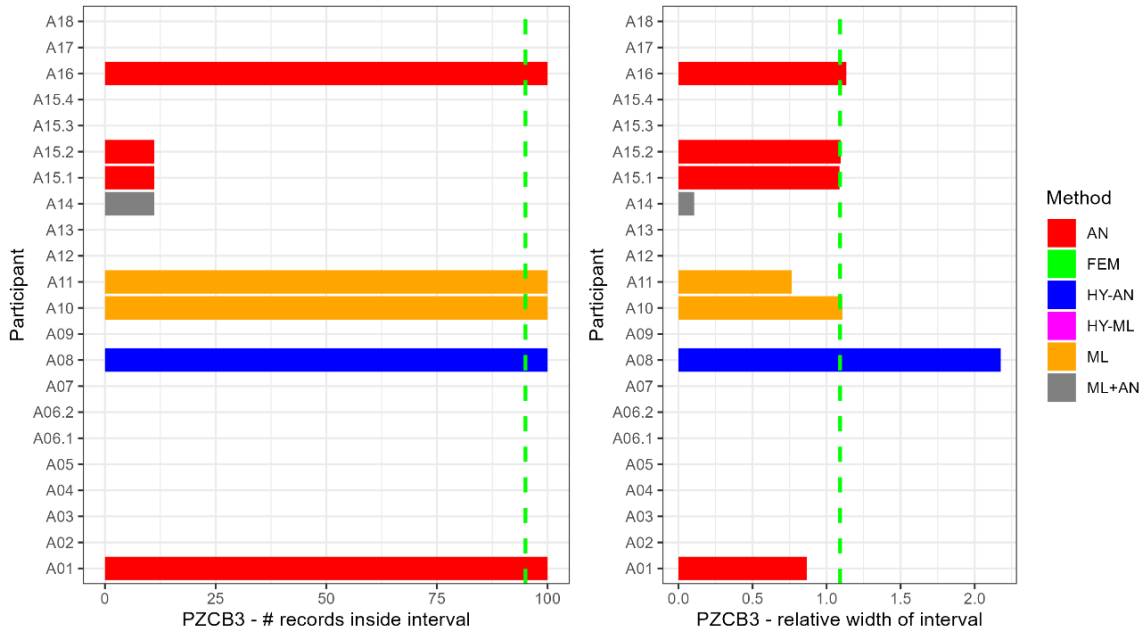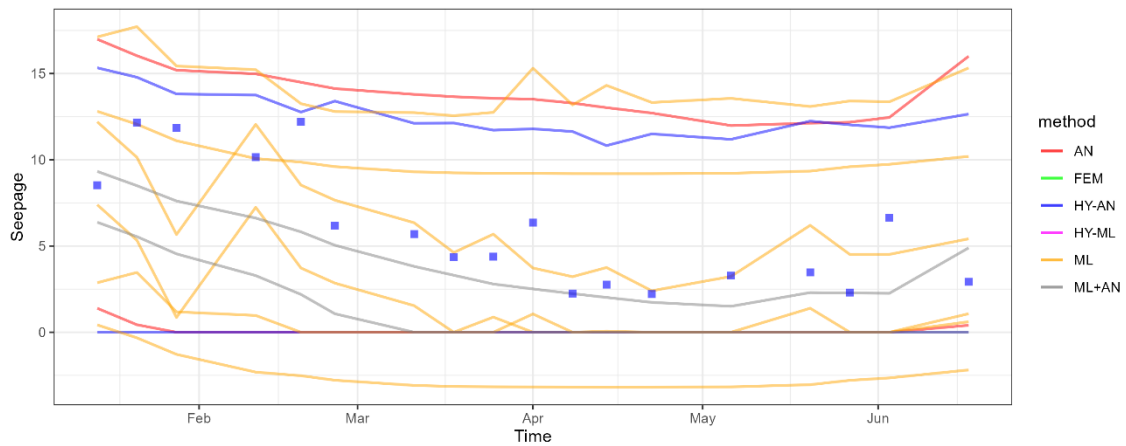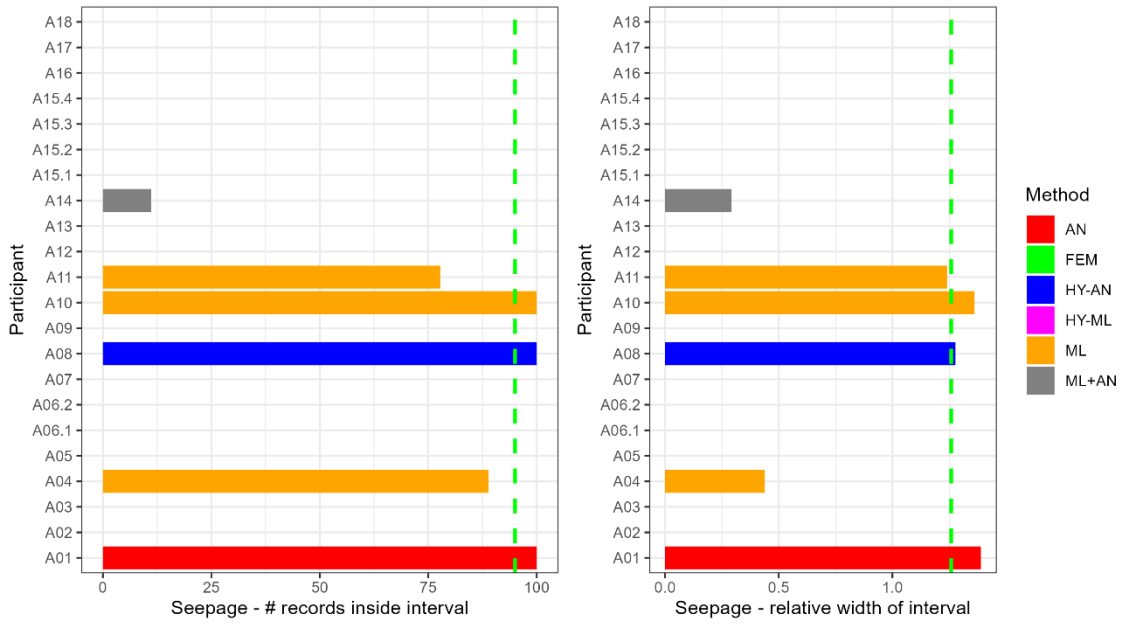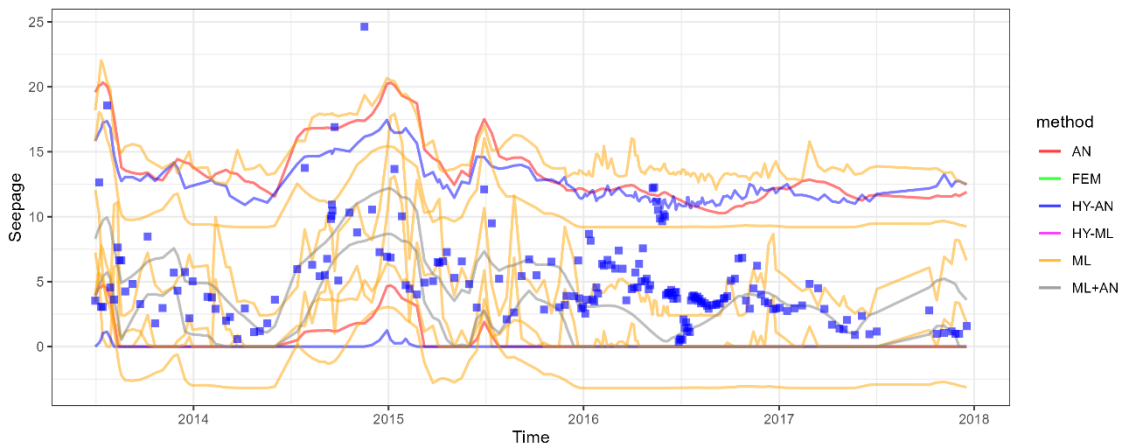Figure 64. Prediction intervals and observations for Case C, Seepage
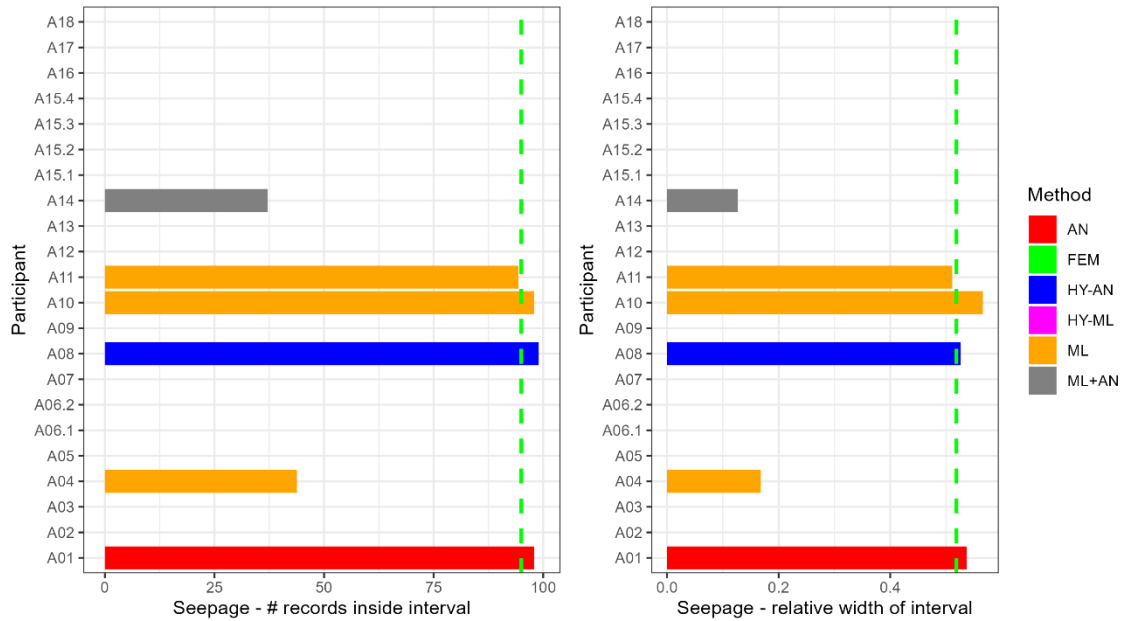
Figure 65. Percentage of observations inside prediction interval for Case C, Seepage, along with the corresponding interval width.

4.3.3 General comments on warning thresholds

As mentioned before, the main criterion for evaluating the warning thresholds is the percentage of observed records that fall within the prediction interval, i.e., between the upper and lower threshold. The dam owner reported that no anomalous behavior has been verified neither in period B nor in period C. Hence, all records should be considered as normal by a good model, i.e., inside the normal range.

Nonetheless, such outcome is easier to achieve by a model using a wide prediction interval, which, at the same time, is less useful for detecting anomalies. As a result, we also analyzed the width of the interval for those models with high percentage of values inside the range: for a similar result in terms of correct classification of records, narrow intervals are more useful.

Table 6 includes the summary of the percentage of correct classification for each participant, period and variable. As before, the colors depict the order for each task. In this case, green is used for 100 % of correct records and red for low percentages. It can be seen that A08 is the only contribution that succeeded in considering over 95% of records as normal for all scenarios. Results are better in general for Case B, for which A10 also provided perfect classification. In addition, A05, A06.1, A06.2, A09, A12, and A18 achieved similar results, although neither of them considered all outputs. For Case C, the percentage of correct classification is lower in general, although A05, A06.2 and A12 correctly classified over 95% of records from the outputs analyzed (which exclude piezometers and seepage).

Table 6. Summary of results for prediction intervals: participants, approaches used and percentage of records correctly considered as normal. The colors of numerical columns correspond to the rank of each model within each output and Case.

Participant	Approach	CASE B - SHORT TERM						CASE C - LONG TERM					
		CB2	CB3	C4C5	PZCB2	PZCB3	Seep.	CB2	CB3	C4C5	PZCB2	PZCB3	Seep.
A01	AN	100	100	100	83	100	100	96	78	94	59	79	98
A02	HY-ML	89	100	100				81	76	98			
A03	ML	89	33					66	38				
A04	ML	89	83				89	87	17				44
A05	ML	100	100					97	99				
A06_1	ML	100	100					90	100				
A06_2	HY-AN	100	100					97	97				
A07	AN	72	72	67				52	58	52			
A08	HY-AN	100	100	100	100	100	100	100	96	100	100	97	99
A09	AN	100	100	100	100			31	54	85	90		
A10	ML	100	100	100	100	100	100	93	63	97	95	85	98
A11	ML	89	100	100	100	100	78	64	77	96	90	67	94
A12	HY-AN	100	100	100				100	100	100			
A13	HY-AN	100	89					99	93				
A14	ML+AN	100	89	100	44	11	11	91	43	72	34	0	37
A15_1	AN	0	0	0	0	11		0	0	0	0	28	
A15_2	AN	0	0	0	0	11		0	0	0	0	29	
A15_3	FEM	11	6					41	16				
A15_4	FEM	6	0					30	0				
A16	AN	100	100	89	100	100		79	76	18	45	71	
A17	FEM												
A18	ML	100	100					94	89				

A more detailed analysis has been made considering the interval width. The contributions with over 95% of correct classifications were ordered as a function the interval width. Table 7 shows the results for Case B, with some contributors highlighted.

Table 7. Ranking of contributor for Case B, considering the percentage of correct classification and the width of the prediction interval.

Contrib	Method		CB2 Thres.
A16	ML	100	0.439
A01	AN	100	0.443
A14	ML+AN	100	0.489
A06_1	FEM+AN+ML	100	0.49
A10	ML	100	0.504
A05	ML	100	0.584
A18	ML	100	0.624
A08	HY-AN	100	0.632
A12	HY-AN	100	0.633
A09	AN	100	0.681
A13	HY-AN	100	0.792
A06_2	FEM+AN+ML	100	1.056

Contrib	Method		CB3 Thres.
A11	ML	100	0.337
A10	ML	100	0.356
A16	ML	100	0.356
A02	HY-ML	100	0.391
A01	AN	100	0.427
A18	ML	100	0.44
A05	ML	100	0.457
A06_2	FEM+AN+ML	100	0.554
A09	AN	100	0.582
A08	HY-AN	100	0.61
A06_1	FEM+AN+ML	100	0.635
A12	HY-AN	100	1.114

Contrib	Method	C4C5 Thres.	
A11	ML	100	0.377
A02	HY-ML	100	0.405
A14	ML+AN	100	0.437
A10	ML	100	0.479
A01	AN	100	0.549
A09	AN	100	0.771
A08	HY-AN	100	0.866
A12	HY-AN	100	1.91

Contrib	Method	PZCB2 Thres.	
A11	ML	100	0.377
A10	ML	100	0.392
A16	ML	100	0.479
A09	AN	100	0.602
A08	HY-AN	100	1.016

Contrib	Method	PZCB3 Thres.	
A11	ML	100	0.764
A01	AN	100	0.867
A10	ML	100	1.106
A16	ML	100	1.133
A08	HY-AN	100	2.176

Contrib	Method	Leak Thres.	
A08	HY-AN	100	1.277
A10	ML	100	1.361
A01	AN	100	1.389

Both A08 (HY-AN, green) and A10 (ML, light blue) achieved perfect classification for all outputs, the latter having the narrower interval. A01 (AN, orange) obtained perfect classification for 5 out of the 6 variables with an interval width similar to that from A10, while A11 (ML, yellow) correctly classified all observations for 4 out of the 6 outputs, always with the narrowest interval.

The same result is shown for Case C in Table 8. As before, A08 (HY-AN, green) achieved perfect results with wide intervals. In this case, A10 (ML, light blue) was only valid for 3 out of the 6 outputs, with intervals much narrower (around half of those from A08) except for seepage (similar widths).

Table 8. Ranking of contributors for Case C, considering the percentage of correct classification and the width of the prediction interval

Contrib	Method	CB2	Thres.
A01	AN	95.5	0.212
A05	ML	97.3	0.294
A08	HY-AN	100	0.302
A12	HY-AN	100	0.303
A13	HY-AN	99.1	0.378
A06_2	FEM+AN+ML	97.3	0.505

Contrib	Method	CB3	Thres.
A05	ML	98.65	0.369
A06_2	FEM+AN+ML	97.3	0.392
A08	HY-AN	96.4	0.431
A06_1	FEM+AN+ML	100	0.449
A12	HY-AN	100	0.788

Contrib	Method	C4C5	Thres.
A11	ML	95.63	0.225
A02	HY-ML	98.06	0.266
A10	ML	96.6	0.286
A08	HY-AN	100	0.516
A12	HY-AN	100	1.14

Contrib	Method	PZCB2	Thres.
A10	ML	95.19	0.225
A08	HY-AN	100	0.585

Contrib	Method	PZCB3	Thres.
A08	HY-AN	96.65	0.965

Contrib	Method	Leak	Thres.
A08	HY-AN	98.97	0.526
A01	AN	97.94	0.537
A10	ML	97.94	0.566

Piezometers, and specially PZCB3, were the variables more difficult to control for Case C. Only one participant sent intervals including all records, and the interval used was as wide as the range of variation of the output. In addition, even for this model, the time series could be interpreted as anomalous, as see in Figure 66.
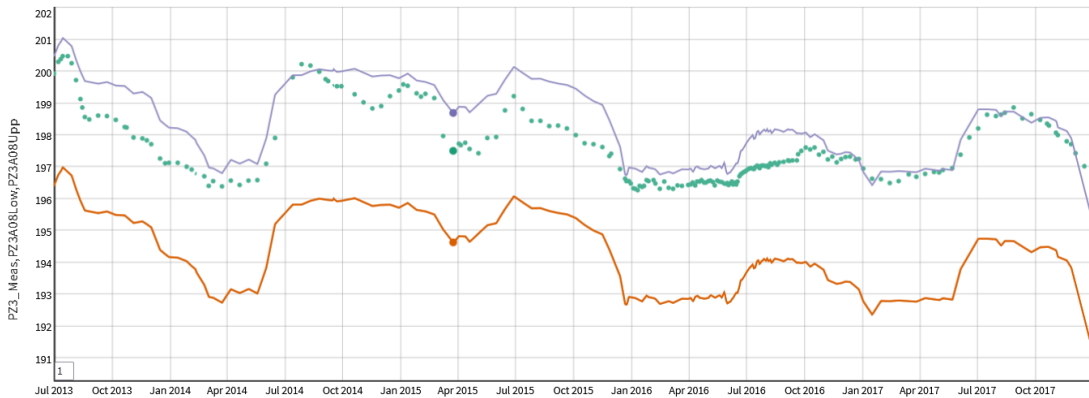
Figure 66. PZCB3. Observations (dots) and warning thresholds (lines) from the only valid model (A08, lines). Although more than 95% of the records fall within the normal interval, they are close to the upper threshold, occasionally above, which could be considered as anomalous.

This might indicate some change in behavior of the piezometric level. However, results from other models differ, with observations far from the upper threshold and different periods of records out of prediction interval. We consider the results for Case B as more relevant, since predictive models —as well as warning thresholds— are typically updated over time. The frequency with which this is done may vary, but once a year can be a reasonable value. As a result, usefulness in practice of any model is better evaluated from the results for Case B (six months' prediction period) than for Case C (four and a half years). For such period, a number of models provided what can be considered as good warning thresholds for variables free from anomalies, with reasonably narrow intervals and over 95% of observations included. Some examples are shown below.

Figure 67. Warning thresholds provided by A01 (AN) for Case B, CB2.
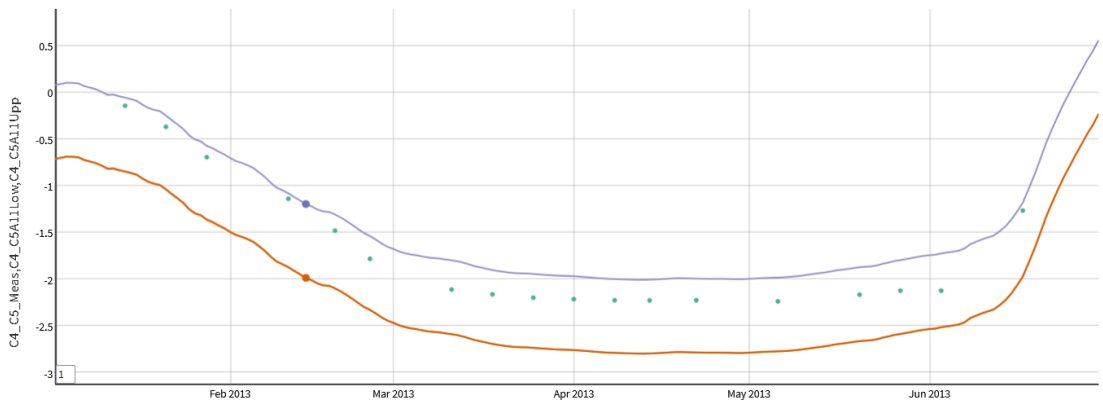
Figure 68. Warning thresholds provided by A11 (ML) for Case B, C4-C5.

Although results are poorer for Case C, still some models also offered reasonable predictions, as shown in the examples below.
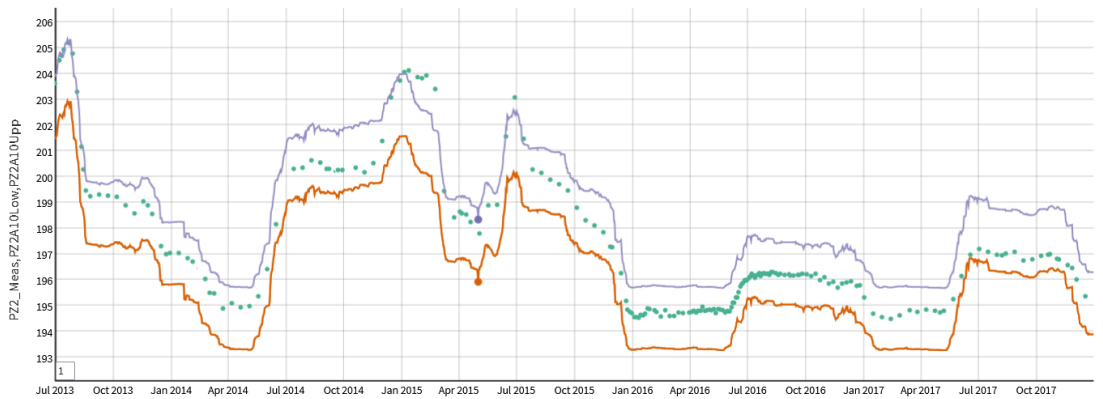
Figure 69. Warning thresholds provided by A10 (ML) for Case B, PZCB2.

All predictions and warning thresholds received can be explored in the interactive plots provided in the supplementary material. Overall, none of the contributors prevailed over the rest for all periods and outputs. There is neither a clear result as for the best approach, which suggests that various methods can be equally useful, provided that they are correctly applied. This also confirms that neither model of any nature shall be applied without the contribution of experienced engineers, with deep knowledge on dam engineering and in particular on the specific features of the dam under consideration. Models are powerful tools, which should always be used by high-skilled engineers.

4.4 *Interpretation*

4.4.1 Introduction

The task of interpretation was not formally described in the formulation document. It was simply asked to demonstrate how the analyses and the results could teach us elements on the functioning of the dam, its evolution over the time, its safety margins, etc. Thus, for example in the formulation document, when using the classical HST model, the contribution of each load can be interpreted to better understand the functioning of the structure. This type of analysis can also be reproduced with all types of complex analyses used by participants. However, this kind of analysis was not compulsory for the benchmark.

This section compares the interpretations given by the participants as precisely as possible, given the fact that it is not possible to carry out a comparison by quantitative estimators. In order to organize the restitution, it is proposed to focus initially on the identification of the explanatory variables. This step is crucial because it determines the sequence of possible interpretations. Then, the different sensitivity studies proposed by the participants will be discussed. Finite element analyzes occupy a special place in the interpretation, so that a paragraph will be devoted to them. Finally, and since the comparison of interpretations is a complex task, the last subsection includes some interpretations that may be interesting to share within the framework of this synthesis.

4.4.2 Identification of explanatory variables

For the analysis of monitoring measurements, the selection of the explanatory variables is among the most important steps, which greatly impacts the results of the model and the interpretation. First, the choice of the nature of the physical phenomena which accounts for the explanatory processes: should we take into account the rain, the effect of the temperature, the effect of the aging of the materials?

Secondly, the transformation of the measurement of the physical phenomenon into an explanatory variable can take different forms: the measurement can be integrated directly into the model (water level for example) or be transformed with the aim of better showing certain effects such as a threshold. We could also create a variable that incorporates a historical effect with the technique of moving averages, etc. The trickiest explanatory variable transformation is the one concerning the delayed effects, for phenomena such as temperature or water diffusion.

It is not possible to directly compare the techniques and the transformations of the explanatory variables used by the different participants. Different tests and statistical criteria can be used to select the explanatory variables and it is not possible to compare them directly with each other. But it is interesting to share the visual means that make it possible to select the explanatory variables. Regarding the choice of explanatory variables, there is no fixed criterion adopted by the profession, we must do the best and demonstrate pragmatism. The following figures show different visualization techniques provided by the participants.
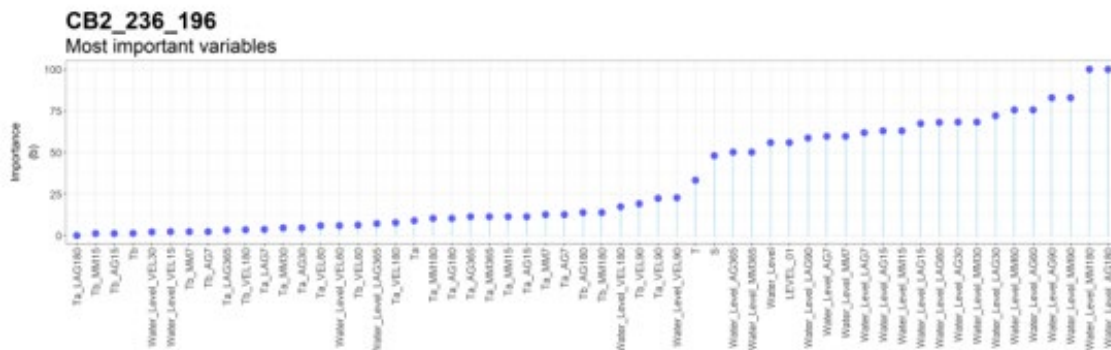
Figure 70. Example of selection of most important variables. In this case, the number of explanatory variables is high.

Some participants built numerous explanatory variables, such as moving averages (several values tested) or threshold effects. The next challenge is to find a statistical criterion that specifies from what threshold we can keep an explanatory variable in the final model. Defining this threshold is not obvious and often involves user experience.
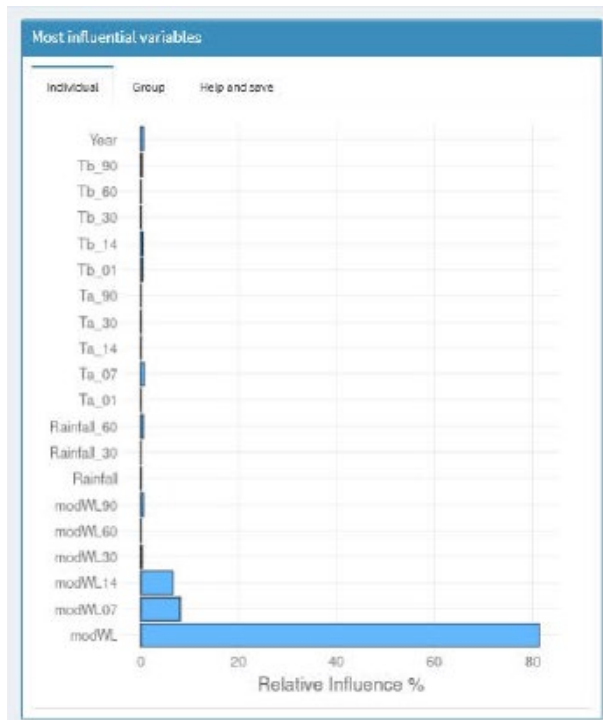
Figure 71. Selection of explanatory variables. On this example, the choice of the most influential variables is obvious.

In some cases, the most influential variables are easy to rank, and it follows an easy selection of the most significant variables.
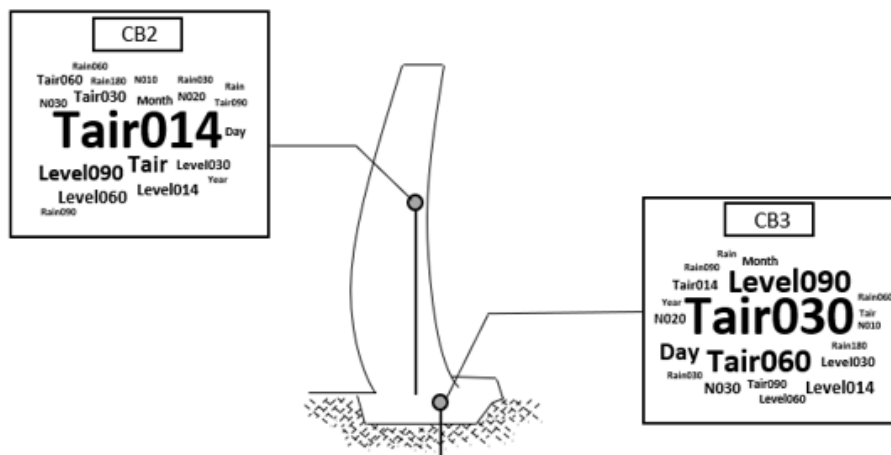
Figure 72. Synoptic diagram of the most influential variables

With the aim of facilitating the identification of the most significant explanatory variables, synoptic diagrams can be very useful to quickly understand which are the explanatory variables that most influence what is measured at different positions in the dam (see Figure 72).

4.4.3 Sensitivity studies

Sensitivity studies make it possible to study the specific effect of an explanatory variable on the monitoring measurement. These studies are calibrated on monitoring measurements. Consequently, their modeling reproduces exactly the real effects undergone by the structure within the uncertainty of the model. Sensitivity studies are therefore of great importance for interpretation. Care must be taken to remain within the range of validity of the calculated effects and to explain the sensitivities in relation to the physics of the phenomenon being monitored. It may also be interesting to ensure that these effects do not change over time.
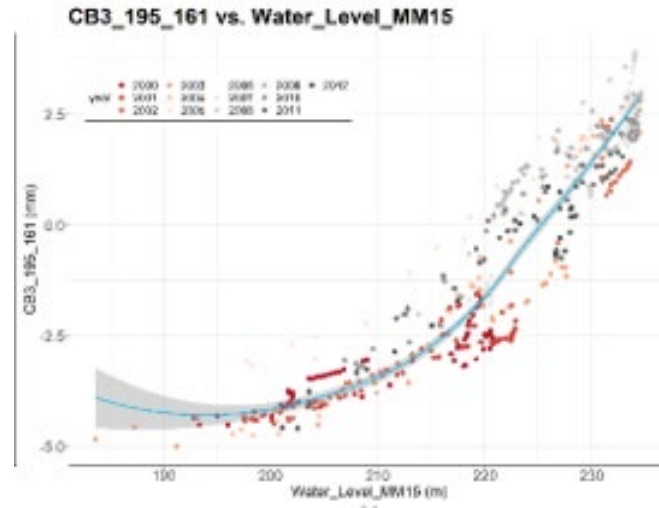
Figure 73. Example of the effect of the 15-day moving average water level on the displacements. The display of monitoring measurements and the uncertainty of the model are precious to interpret the graph.
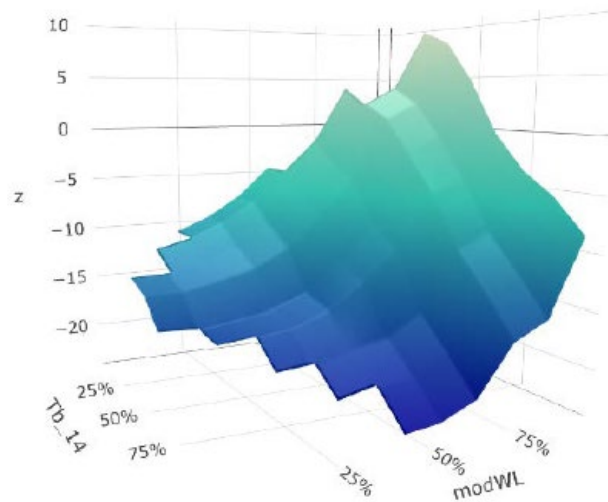
Figure 74. When several parameters influence the monitoring measurements, it may be of interest to use a 3D-vizualisation. In this case the 14-day moving average of the air temperature and the modified (with a threshold) water level influence the monitoring measurement.
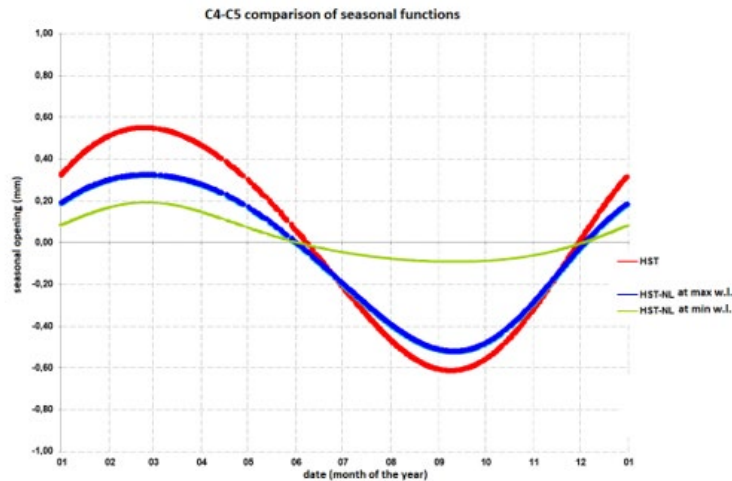
Figure 75. Seasonal effect which depends on the water level to better explain the crack opening displacement.

4.4.4 Finite element Analysis

Three contributions performed finite element analysis. The prediction from these models were less accurate than the models based on the data, but they allow easier access to interpretable physical quantities. For example, while a model based on the data only reproduces the displacement, a finite element analysis provides the calculation of the stresses in the concrete. These stress values are much easier to interpret by a dam engineer and can be compared to a safety criterion. Nevertheless, the calibration of a finite element model is a complex task which integrate many uncertainties. This issue is the subject of numerous ICOLD bulletins whose analysis goes beyond the scope of this benchmark.
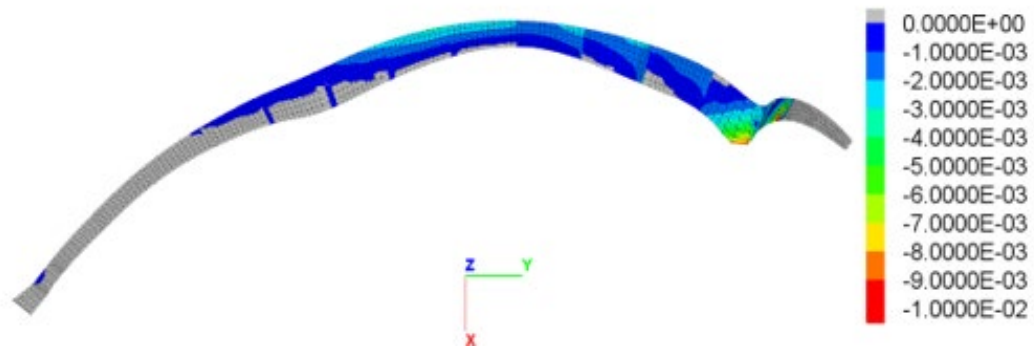
Figure 76. Example of crack opening displacement at the rock-concrete interface at normal water level. The use of finite element analysis provides spatial information between measuring devices and simultaneously considers the information of several sensors.

4.4.5 Focus on some interpretations

Regarding the thermal effects, many participants checked that the value of thermal diffusion calibrated on the monitoring data is consistent with the dam thickness and the physical properties of the dam. For participant A11 the short-term average temperature is correlated with CB2 and the long-term average is correlated with CB2. This result is somehow surprising because the thickness of concrete (and thus the thermal inertia) is greater in the displacement measured around CB3.

To interpret the irreversible effects, some participants (A15, A16) used the "corrected" or "compensated" measurements. These terms refer to raw data which are removed from reversible effects.

Regarding the structural behavior, some analyses are interesting to share:
- Participant A12: the behavior of CB2 could be explained with an opening of the vertical contraction joints in wintertime with a low water level. In this case, the arch effect is reduced, and the structure is more deformable than the monolithic one. With higher water level, joints are closing, and the full stiffness of the monolithic structure is restored.
- Numerical models confirm the crack opening at the upstream toe of the dam, and consequently the propagation of uplift pressure in the crack.
- Thanks to the use of finite element analysis, participant A15 was able to carry out a comparison of different dam / foundation shear parameters, as regard to the French guideline and then proposed a discussion about the sliding of the dam. This discussion covers topics such as keying of the dam and seasonal and drawdown cycles.
- For participant A12, Dam_EDF seems more rigid for higher water levels and less rigid for lower water levels.

Some participants could provide a combined interpretation i.e., an interpretation which combined two different kinds of monitored phenomenon:
- Participant A07 noted the correlation between displacements and crack opening displacements.
- Participant A09 highlighted that the crack opening is strongly correlated with piezometric levels (PZCB2 and PZCB3) which is a good indication of the response of the rock mass.

Participant A12 carried out a detailed analysis of the rock modulus obtained from the calibration process. This rock modulus is quite low. The dam behavior is basically reversible, without any drift or irreversible displacements. Only a modest delay between models and measurements is visible for CB3, indicating that the rock mass behavior is affected by some viscous effect. Numerical model also estimates the maximum compressive stress in the arch, which is far below the compressive maximum strength of concrete.

Regarding the piezometric levels PZCB3, participant A10 detected a change in 2008 (given in the description of the theme and detected by other participants), but also in 2012. This change in 2012 is also confirmed in the dam's owner safety report without confirming whether the cause is the sensor or the end of the benefit of the drainage refection operated in 2008.

Leakages are difficult to model as they are subjected to non-linearities which are described by the law of Poiseuille, thresholds and cross effects (participant A15). Several attempts of models were made by considering the rainfall, but without any success (participant A08). Participant A10 noted that the accuracy is low in high leakage flows essentially due to low reading frequency. Two outliers were detected (> 25 L/min) in the period Dec-2008/Mar 2009. Participant A17 also mentioned that the calculated values of seepage are lower than measured, which is an indication for additional leakage occurrence that affects the seepage process.

4.4.6 Overall remarks

The analysis of the comments provided by the participants on the conclusions drawn from the models on the dam behavior was of great interest. There was a great variety of interpretations, both regarding which outputs were assessed and on the insights mentioned.

All kinds of approaches were allowed for interpreting the response of the dam. In this regard, FEM has greater capabilities, since it allows for simulating extreme scenarios. Nonetheless, participants using data-driven approaches also provided reasonable interpretations regarding possible changes in behavior and relations between loads and responses. Some tools are also available for these models, from conventional sensitivity analysis to more complex measures of importance of inputs. In this regard, it is worth to mention that all conclusions were made also making use of the knowledge on dam behavior, the physical phenomena involved in arch dams, etc. This confirms the impression that engineering knowledge is the key asset when performing this kind of analysis. In other words, different approaches can be useful, but a skilled engineering team is always necessary.

5 SUMMARY AND CONCLUSIONS

In this Theme, tasks have been proposed to predict the behavior of a double curvature arch dam in terms of displacements, crack opening, piezometric levels and seepage, in two different time horizons, i.e., 6 months and 4.5 years.

Some participants have noted that behavior models are usually updated on an annual basis, which implies that long-term prediction does not correspond to usual practice. This is true, but in the context of the benchmark, the aim was to pose a difficult problem, to assess the limits of the predictive capabilities of the different approaches.

Although the behavior of the dam, according to the information provided by the owner, has not undergone relevant changes in the period considered, the loads did register exceptional values, with an extraordinary draw-down of the reservoir, which has been a problem for some participants.

Thus, although machine learning (ML) models have a higher risk of overfitting, which can result in erroneous predictions in the face of new input data, the results of the analysis show that, in general, the predictions are good and the used calibration processes have succeeded in avoiding this problem. No relevant difference is observed in this sense between these models and other approaches —which, in principle, are less sensitive to overfitting—. Up to 4 teams that have used ML have only considered displacements. In principle, once the data is prepared and an ML model selected, the effort required to consider other outputs should be small. Participants may not have been very confident in the prediction of piezometric levels and seepage.

A wide variety of approaches have been used. As for ML-based solutions, different algorithms have been employed: boosted regression trees, two versions of long-short-term memory neural networks, kernel extreme learning machine, random forests, and support vector machines; and two programming languages, R and Python. Regarding those based on FEM, different software tools have been used, namely: Sofistik, Ansys, Abaqus, LS-DYNA, FLAC-3D, and an in-house developed code (Parmac3D-PAVK). In this sense, a great advance is observed with respect to the last benchmark problem that can be considered similar, which was proposed in 2003. This reflects the advance in available technologies that has occurred in recent years, and that these new techniques are already entering the professional practice of dam engineering.

If we order the participants from highest to lowest prediction accuracy, taking into account only the displacements —the mandatory task that all have answered— Table 9 is obtained, which shows the low precision for the three FE-models. The 5 approaches with the lowest average error are based on ML, except for the second, which uses a hybrid approach (also with ML).

Table 9. Ranking of contributions by accuracy for displacements.

Participant	Approach	Ranking				Average ranking	Overall ranking
		CASE B		CASE C			
		CB2	CB3	CB2	CB3		
A01	AN	2	13	3	9	6.8	5
A02	HY-ML	9	5	2	2	4.5	2
A03	ML	1	10	15	15	10.3	11
A04	ML	6	4	1	18	7.3	6
A05	ML	5	1	6	1	3.3	1
A06_1	ML	10	2	9	3	6.0	3
A06_2	HY-AN	22	16	18	5	15.3	18
A07	AN	13	6	12	7	9.5	10
A08	HY-AN	15	17	6	10	12.0	12
A09	AN	17	18	22	19	19.0	20
A10	ML	2	6	5	12	6.3	4
A11	ML	11	6	19	14	12.5	13
A12	HY-AN	14	12	4	4	8.5	7
A13	HY-AN	20	15	10	6	12.8	14
A14	ML+AN	8	19	11	17	13.8	17
A15_1	AN	2	14	8	11	8.8	8
A15_2	AN	15	9	16	13	13.3	15
A15_3	FEM	19	20	13	20	18.0	19
A15_4	FEM	18	21	17	21	19.3	21
A16	AN	7	11	21	15	13.5	16
A17	FEM	21	22	20	22	21.3	22
A18	ML	12	3	14	7	9.0	9

This shows the high capability of data-driven models once a long enough period of records is available. As mentioned before, FEM models have other advantages and are essential during the design stage and for other purposes. The results confirm the greater flexibility of data-based models, and in particular those of ML, to consider variables of different types: of the 18 participating teams, only 6 have submitted solutions for all tasks, only one of which was based solely on FEM The FE-model had lower accuracy in general. This can be seen in Table 10 that presents the ranking of all teams that have offered solutions for all the variables.

Table 10. Ranking of participants which sent solutions for all outputs, based on prediction accuracy.

Participant	Approach	Ranking												Average ranking	Overall ranking
		CASE B - SHORT TERM						CASE C - LONG TERM							
		CB2	CB3	C4C5	PZCB2	PZCB3	Seep.	CB2	CB3	C4C5	PZCB2	PZCB3	Seep.		
A01	AN	1	3	1	3	3	2	1	1	1	4	3	4	2.3	2
A08	HY-AN	5	4	5	4	5	1	3	2	4	3	6	1	3.6	4
A10	ML	1	1	2	2	2	4	2	3	2	1	1	3	2.0	1
A11	ML	4	1	3	1	1	3	5	4	3	2	2	2	2.6	3
A14	ML+AN	3	5	4	5	4	5	4	5	5	5	4	5	4.5	5
A17	FEM	6	6	6	6	6	6	6	6	6	6	5	6	5.9	6

Regarding the definition of warning thresholds, the proposed approaches can be considered conventional, based on prediction error statistics for the calibration phase. Specifically, between 2 and 3 times the standard deviation of said error, or according to some percentile of the residuals. Perhaps the formulation of the topic was oriented towards the use of this conventional approach. The design of the task may also be considered less realistic than that for prediction, since decisions in dam safety are usually made in real time, i.e., in view of some potentially anomalous record, instead of by looking at a long period.

The evaluation of the contributions was made based on the number of observations captured within the warning thresholds, conditioned to the width of the interval. The results were related

to the prediction accuracy, with some influence of the approach used for the warning thresholds. In particular, A08 was the only solution that captured over 95% of the records inside the thresholds, despite not being among the more accurate models, due to the use of a wide interval (3 times the standard deviation of the residuals).

Among the future lines of research, which have not been considered by any of the participating teams, it is worth mentioning the possibility of jointly considering several outputs. This can apply to the prediction task (multivariate prediction approaches are available), but also to the definition of anomalies. Likewise, additional criteria can be considered to detect abnormal values or behavior changes, such as the observation of trends. For instance, a set of consecutive records out of the interval may be more relevant than a set —of the same size— of isolated anomalies. This was partially considered during the synthesis (isolated errors were discarded). Another option would be to visually explore the observations in reference to the warning thresholds: some trend could be identified, which may reveal some change in behavior, before any value falls out of the interval. This applies in particular when wide intervals are used. Overall, this task was more difficult to evaluate. A specific Theme could be designed to specifically address this topic in some future benchmark.

The main conclusion that can be drawn from the analysis of the submitted solutions is that none of the techniques clearly stands out as the best in all the evaluated aspects: prediction accuracy, flexibility to consider different results and ability to adapt to different scenarios of load combination. As expected, the experience of the modelers and their ability to make appropriate decisions during modeling and calibration are very important to obtain useful results.

The need for engineering knowledge was further verified by the analysis of the interpretation of the models. All participants who answered this question provided reasonable, sophisticated explanations on the possible origin of the observed behavior and of the analysis of their predictive models. This was clearly driven by the participation of high-skilled professionals teaming up with experts in modeling.

A limitation of these results is that they correspond to a given typology and a well-instrumented dam. In addition, the past related Theme posed in 2003 was based on a dam of the same type. Future endeavors of the Committee might be oriented towards posing some similar themes based for different type of dams, possibly with more issues regarding the monitoring records.

REFERENCES

[1] Willm G, Beaujoint N (1967) Les méthodes de surveillance des barrages au service de la production hydraulique d'Electricité de France-Problèmes ancients et solutions nouvelles. In: 9th ICOLD Congres, pp 529–550, q34-R30. [in French]

[2] Mata, J. "Interpretation of concrete dam behaviour with artificial neural network and multiple linear regression models." Engineering Structures 33.3 (2011): 903-910.

[3] Hellgren R, Malm R, Ansell, A. "Performance of data-based models for early detection of damage in concrete dams." Structure and Infrastructure Engineering 17.2 (2021): 275-289.

[4] Tinoco, J., de Granruth M, Días D, Miranda T, Simon, A-G.. "Piezometric level prediction based on data mining techniques." Neural Computing and Applications (2019): 1-16.

[5] Salazar, F., Toledo M.A, González, J.M, Oñate E. "Early detection of anomalies in dam performance: A methodology based on boosted regression trees." Structural Control and Health Monitoring 24.11 (2017): e2012.

[6] Salazar, F, Morán R, Toledo M.A, Oñate E. "Data-based models for the prediction of dam behaviour: a review and some methodological considerations.
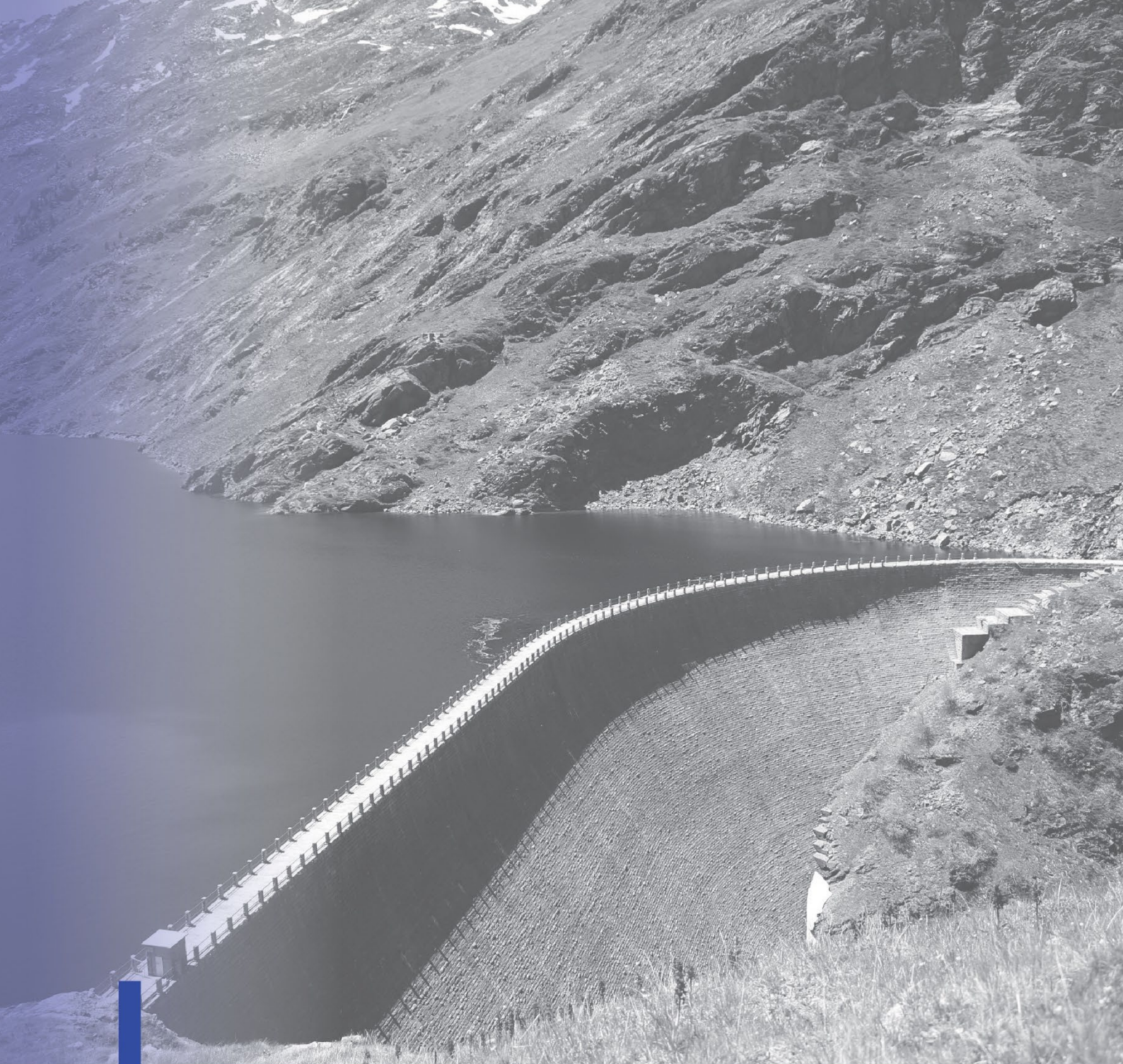
Dam behaviour prediction

Recieved papers for Theme A

DATA-BASED STATISTICAL MODEL WITH PHYSICALLY SOUND ANALYSIS AND CORRELATION FUNCTIONS

Moez Jellouli
ISL Ingénirie, Paris, France

Frédéric Dufour
ISL Ingénierie, Lyon, France

ABSTRACT: Dam safety assessment is a key societal issue to keep the risk as low as possible. To this end, several measurements are performed on site (displacement, piezometric head and seepage are the most common ones). Based on these data, an efficient model must be constructed to analyze the time evolution of the dam behavior and detect as early as possible some irreversible effects. For this purpose, in this contribution, we propose an original analytical model halfway between pure statistical model and pure physical FE model. Based on expert judgements, some physically sound correlation functions are proposed in the view of minimizing the total number of parameters. These functions link the data of interest with several environmental phenomena such as the water level in the reservoir, the air and water temperatures, the rainfall. Of course, except for the water level, which is perfectly known, those data bring some uncertainties in the statistical process since they are not usually directly measured on site. Indeed, both temperatures are estimated by means of a model. Some thermal phenomena such as convection and radiation are disregarded or roughly approximated which may further affect the estimation of the dam temperature. Those functions are calibrated for each time series of measured data to provide predictive estimation. Except for the seepage data, the coefficient of determination is very good, and the physical statistically calibrated parameters are in the expected range. Both checking gives us good confidence for the model prediction.

1 INTRODUCTION

Safety is a very important issue for dam management. On one hand, the structural vulnerability may increase with the dam ageing (for instance due to creep, swelling or cracking), and on the other hand, due to the climate change the environmental loading may increase (for instance, temperature increase, higher frequency of exceptional floods, heat wave). Those phenomena may increase the failure risk and highlight the need for the monitoring of dams to ensure their safety over the long term. Dam surveillance mainly consists of analyzing gathered data to verify that the dam is functioning as expected, to detect any possible anomalies, and to warn of any change which could endanger its safety. Displacements, internal pressures, and seepages are classical measures. A precise enough and efficient model is needed to compare its prediction with the measures to detect any change in the dam behavior. This model can be either based on physics (for instance, Finite Element Model - FEM) or on data (for instance, digital twin).

In a FEM, the geometry of the dam and its foundation, the boundary conditions, the loads, and the material behavior must be described explicitly for all thermal and mechanical phenomena (Leger and Leclerc, 2007; Leger et al., 1993). This numerical model must be calibrated on the data to improve its predictability. However, due to the number of parameters, the associated uncertainties, the spatial and time variabilities, the mesh size needed to capture short term thermal effects, some hypotheses are made. Therefore, although the model construction is rather expensive, the results are not fully satisfactory.

A digital twin construction, such as the worldwide known HST (Hydrostatic, Season, Time) method from Ferry and Willm (1958), Willm and Beaujoint (1967), and Lugiez et al. (1970), and its derivatives (see for instance, Tatin et al. 2015 and 2018 who added the water temperature effect) is based on correlation functions between data and external loads, and a statistical calibration process of the parameters. For instance, a polynomial of order 4 is generally proposed for the hydrostatic effect on the displacement. Once the twin model and its parameters have been calibrated during the learning period, it can easily predict some estimation at nearly no cost. Besides, the construction itself of the twin model is much cheaper than a physically based model.

To the authors' viewpoint, a FEM model is required in two conditions; (a) the period to predict the dam behavior contains some loading conditions which have never been met in the past and (b) the safety margin is addressed in terms of stress state. These conditions are not met in the present ICOLD benchmark. We thus have chosen to provide predictions solely based on data analysis. After some mathematical tools, the physical-based functions are introduced, and the results of the calibration process are analyzed.

2 ORIGINAL FUNCTIONS AND CALIBRATION METHODOLOGY

2.1 *Convolution product*

Most of the phenomena for very large structures such as dams highlight a response to a load which is not instantaneous. Therefore, a time convolution product is introduced as:

$$[f \otimes g](t) = \sum_{u=t-t_0}^{t} g(t-u) f(u) \tag{1}$$

Where g is the convolution function, f the time series and the parameter to be calibrated t_0 is the time duration of the effect, usually few hundreds of days for dam analysis.

2.2 *Convolution function g1 without time delay*

In practice, the convolution function $g1$ without a time delay is introduced to convolute a time series so that the effect is diffused in time. For instance, it may be used to compute the mean concrete temperature in the bulk with respect to the boundary values.

$$g1_{tc1}(t) = \frac{A}{t_{c1}} \sum_{n=1}^{3} \exp\left(-\frac{(1+2n)^2 \cdot t}{t_{c1}}\right) \tag{2}$$

Where t_{c1} is the characteristic time of the phenomenon, and A is added so that the integral of $g1$ is unit (see Figure 1(a)).

2.3 *Convolution function g2 with time delay*

Compared to the previous function $g1$, the function $g2$ (see Figure 1(b)) is built to introduce a time delay in some physical phenomena. For instance, for diffusion problem, such as the piezometric pressure as a function of the water level in the reservoir, or the temperature at some points in the dam as a function of the air temperature, a time shift t_{c2} is introduced as follows:

$$g2_{tc2}(t) = g1_{tc1}(t). erfc\left(\frac{t}{t_{c2}}\right) \tag{3}$$
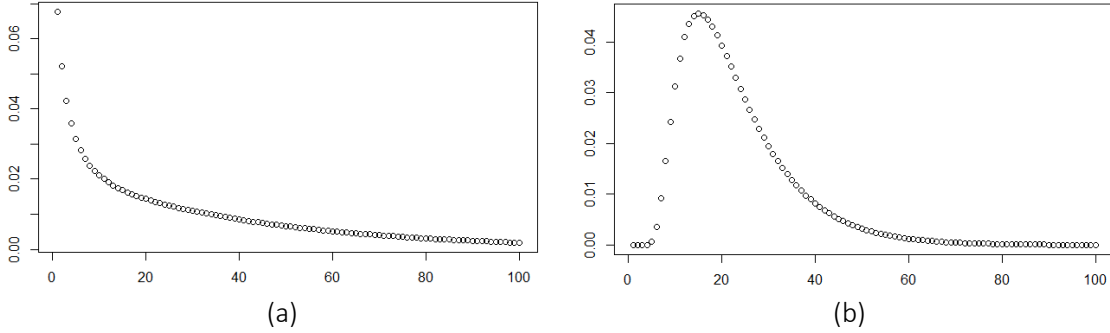
Figure 1. Typical convolution functions, (a) without time delay and a characteristic time length of t_{c1} = 40 days, and (b) with a time delay of t_{c2} = 10 days.

2.4 *Threshold function*

A threshold effect is observed in some phenomena. For instance, in the present benchmark, although the water height in the reservoir is always measured, it applies a hydrostatic pressure only down to the level 196 m NGF. Thus, to build the correlation between the water height and the horizontal displacement, one needs to introduce a cut-off effect in the time series. In the present work, it is done by means of the following function:

$$f(v) = ln\big(1 + exp(v)\big) \tag{4}$$

It has the property to be nearly null below -2 and to value the identity above 2 (see Figure 2).
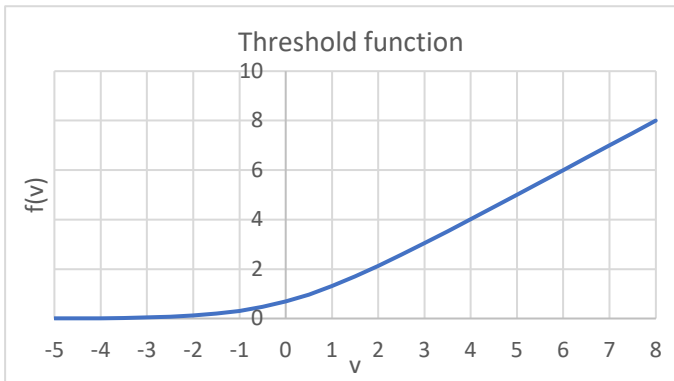
Figure 2. Activation function with a threshold.

2.5 *Calibration methodology*

All the model parameters are calibrated simultaneously. Although it does not prevent compensation between different effects, it avoids giving an emphasis to one of the phenomena.

The numerical algorithm is based on Simultaneous Perturbation Stochastic Approximation (SPSA) method developed by Spall (1992). The main ingredient is a minimizing cost process based on gradients. It is capable to find a global minimum from an initial guess.

3 PHYSICAL ANALYSIS

3.1 *Hydrostatic effect*

The dependency of a data on the hydrostatic pressure is introduced by means of a single monomial, in contrary to HST method which uses a 4th order polynomial. This minimizes the number of parameters to be calibrated while keeping the physical meaning.

3.2 *Thermal effect*

3.2.1 Air temperature

The external air temperature is computed based on the provided raw data T_b which are extrapolated and corrected from a weather station at 50 km away. Although an altitude correction is performed, the absence of recorded air temperature on site introduces some uncertainties. This is particularly true in the alpine context where temperature may vary daily from one valley to another and depending on the hillslope orientation. According to Tatin (2014), the solar radiation may play a significant role in the concrete temperature. Thus, an arbitrary increase of 2°C in winter and 8°C in summer at $t=t_s$ is added to the air temperature as follows:

$$T_{air} = T_b + \left(5 + 3\,cos\left(\frac{2\pi(t-t_s)}{365}\right)\right) \tag{5}$$

After calibration, t_s has been fixed to the 10th of July with a low sensitivity to the results.

3.2.2 Water temperature

According to Tatin et al. (2015), the mean water temperature T_w is accounted for. It is estimated as the mean between the top surface temperature and the bottom one. The latter has been chosen as 4°C which is the temperature of maximum density at a depth P_0 of 100 m. This depth was initially part of the learning process and has been finally fixed to a value close to the optimal one.

The top temperature varies during the season following where the temperature parameters (5°C and 6°C) have been calibrated once for all before hand:

$$T_{top} = max\left[0;\ 5 + 6\,cos\left(\frac{2\pi(t-t_s)}{365}\right)\right] \tag{6}$$

3.2.3 Concrete temperature

For a given day, the mean concrete temperature T_c of the arc dam is the convolution without time delay of a linear weighted function of both the air and the water temperatures:

$$T_{mc} = [\alpha.T_{air} + (1-\alpha)T_w]\otimes g1 \tag{7}$$

The weighting coefficient α depends on the water level of the reservoir to account for the coupling between the water level and the temperature distribution. If the reservoir is empty, then $\alpha = 1$, otherwise $0 < \alpha < 1$. In details, α is computed according to the relation:

$$\alpha = 1 - P_1.Z^{P_2} \tag{8}$$

Where Z is the relative water level varying from 0 for an empty reservoir and 1 for the maximum absolute water level, and P_1 and P_2 two parameters to calibrate. One example of such a function is provided in Figure 3.
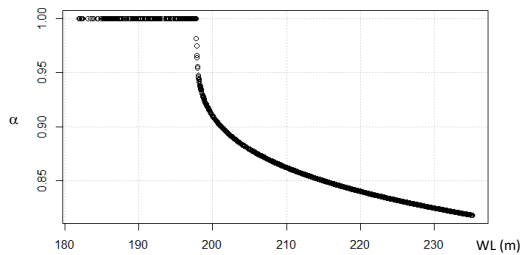
Figure 3. Weighting coefficient α as a function of the water level in the reservoir.

Since we have chosen here the convolution without the time delay, only the characteristic time tc is to be calibrated for each sensor. For the diffusion thermal problem, the initial guess for tc can be taken as $L^2/\pi^2.D$ where D is the concrete thermal diffusivity taken approximatively as 0.08 m²/day, and L is the mean dam thickness.

4 RESULTS AND ANALYSIS

4.1 *Pendulum displacement*

The pendulum displacement is computed as the sum of 4 effects detailed in the following table.

Table 1. The correlation functions for the displacement and the parameters to be calibrated.

Effects	Mathematical relation	Parameters to be calibrated
Hydrostatic pressure	$C_1 + C_2.(WL - Z_{min})^{C_3}$	C_1, C_2, C_3, Z_{min}
Mean dilation	$C_4.T_{mc}$	C_4, P_1, P_2, t_c
Thermal gradient	$C_5.Z.(T_w - T_{mc})$	C_5
Time	$C_6.(t - t_0)$	C_6

Where $t-t_0$ is the time duration since the beginning of the provided time series and WL is the absolute water level floored to Z_{min}.

4.1.1 Calibration and prediction for the pendulum CB2

The calibration process yields the following parameter values.

Table 2. Calibrated parameters for the pendulum CB2.

Parameter	C_1	C_2	C_3	C_4	C_5	C_6	P_1	P_2	Z_{min}	t_c
Value	-13.33	0.008137	2.2382	-1.4768	1.508	0.03	21.5	0.2356	194.15	14.8
Unit	mm	mm	(-)	mm/°C	mm/°C	mm/year	%	(-)	m NGF	days

Remark: According to the rough estimation of the characteristic diffusion time, 14.8 days corresponds to a width of 3.4 m which agrees with the dam thickness of 2 m at the crest and 6 m at bottom.

This set of parameters yields the following time series.

(a)   (b)

Figure 4. Learning process on the pendulum CB2; (a) raw time series with dots for the on-site measures and thick line for the digital twin, and (b) the time series of the difference between the model and the data.

The coefficient of determination is R²=0.964 and the standard deviation is 1.78 mm. The confidence intervals are $[-2.9; \; 3.0]$ and $[-4.5; \; 3.9]$ in mm for 95% and 99% respectively.

Due to the sake of conciseness, only the model for CB2 is analyzed in detail. However, since all the calibrated parameters are provided, the interested reader can easily construct the corresponding functions.
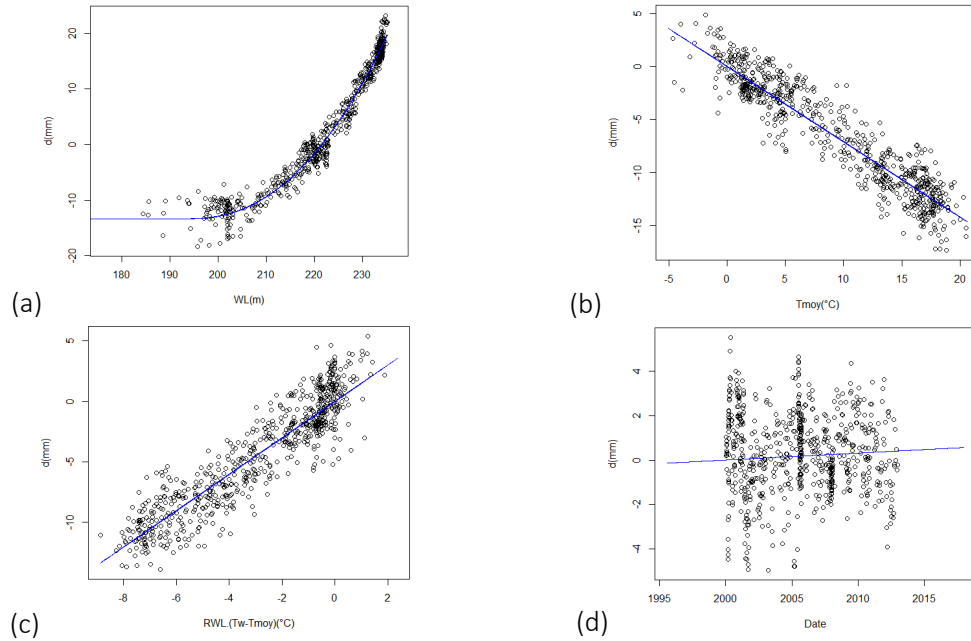
Figure 5. For each physical phenomenon which affects the pendulum CB2 displacement, comparison between the calibrated function and the data: (a) hydrostatic, (b) mean temperature, (c) thermal gradient, and (d) irreversible.

4.1.2 Calibration and prediction for the pendulum CB3

The calibration process yields the following parameter values.

Table 3. Calibrated parameters for the pendulum CB3.

Parameter	C_1	C_2	C_3	C_4	C_5	C_6	P_1	P_2	Z_{min}	t_c
Value	-3.68	0.00423	2.0594	-0.1798	-0.107	0.035	8.5	0.056	194.95	65
Unit	mm	mm	(-)	mm/°C	mm/°C	mm/year	%	(-)	m NGF	days

This set of parameters yields the following time series.

Figure 6. Learning process on the CB3 pendulum; (a) raw time series with dots for the on-site measures and thick line for the digital twin, and (b) the time series of the difference between the model and the data.

The coefficient of determination is R²=0.966 and the standard deviation is 0.498 mm. The confidence intervals are $[-0.76; 0.78]$ and $[-1.0; 1.3]$ in mm for 95% and 99% respectively.

4.2 *Calibration and prediction of the joint openings*

The joint opening is computed as the pendulum displacement since it is also a kinematic variable. Two differences are included:

- a delay on hydrostatic pressure term with convolution function $g1_{tc2}$ to consider delayed elastic behavior of the structure,
- a threshold effect to account for the closing effect with a minimum value dx_{min}.

Thus, the joint opening dx reads:

$$dx = dx_{min} + ln(1 + exp(v)) \tag{10}$$

where v here stands for:

$$C_1 + C_2.(WL \otimes g1_{tc2} - Z_{min})^{C_3} + C_4.T_{mc} + C_5.Z.(T_w - T_{mc}) + C_6.(t - t_0) \tag{11}$$

Table 4. Calibrated parameters for the joint openings.

Parameter	C_1	C_2	C_3	C_4	C_5	C_6	P_1	P_2	Z_{min}	t_c	t_{c2}	dx_{min}
Value	-1.05	499.10⁻⁵	1.982	-0.128	0.047	0.050	49.1	0.23	197.25	172	6.5	-2.67
Unit	mm	mm	(-)	mm/°C	mm/°C	mm/year	%	(-)	m NGF	days	days	mm

This set of parameters yields the following time series.

(a) (b)

Figure 7. Learning process on the joint opening; (a) raw time series with dots for the on-site measures and thick line for the digital twin, and (b) the time series of the difference between the model and the data.

The coefficient of determination is R²=0.984 and the standard deviation is 0.200 mm. The confidence intervals are $[-0.31; 0.31]$ and $[-0.51; 0.56]$ in mm for 95% and 99% respectively.

4.3 *Piezometric head*

For the piezometric head, the first tries have shown a change in the behavior from August 2008. Thus, a head decrease has been modelled from this date. The piezometric head is computed as the sum of 6 effects detailed in the following table.

Table 5. The correlation functions for the piezometric head and the parameters to be calibrated.

Effect	Mathematical relation	Parameters to be calibrated
Hydrostatic pressure	$C_1 + C_2.(WL \otimes g2_{tc1} - Z_{min})^{C_3}$	$C_1, C_2, C_3, t_{c1}, Z_{min}$
Drainage	$C_4.(WL \otimes g2_{tc2} - Z_{min})^{C_5}$	C_4, C_5, t_{c2}
Seasonal due to air temperature	$C_6.T_b \otimes g2_{tc3}$	C_6, t_{c3}
Rainfall	$C_7.RF \otimes g2_{tc4}$	C_7, t_{c4}
Time	$C_8.(t - t_0)$	C_8
Behavior change from 08/08	$C_9.(1 - exp(C_{10}.(t_{08} - t))).max[C_{11}/C_9 ; WL^{C_3}]$	C_9, C_{10}, C_{11}

Where $t - t_0$ and $t_{08} - t$ are the time durations since the beginning of the provided time series and the start of the piezometric head decrease respectively.

The threshold effect to account for dry piezometer with a minimum value PZ_{min} is added at the end. Thus, the piezometric head PZ reads:

$$PZ = PZ_{min} + ln(1 + exp(v)) \qquad (12)$$

where v here stands for:

$$C_1 + C_2.(WL \otimes g2_{tc1} - Z_{min})^{C_3} + C_4.(WL \otimes g2_{tc2} - Z_{min})^{C_5} + C_6.T_b \otimes g2_{tc3} + C_7.RF \otimes g2_{tc4} + C_8.(t - t_0) + C_9.(1 - exp(C_{10}.(t_{08} - t))).\max\left[\frac{C_{11}}{C_7}; WL^{C_3}\right] \qquad (13)$$

4.3.1 Calibration and prediction of the piezometer PZCB2

Table 6. Calibrated parameters for the piezometric head PZCB2.

Parameter	C_1	C_2	C_3	C_4	C_5	C_6	C_7	C_8	C_9	C_{10}	C_{11}
Value	1.182	0.0115	1.94	-0.011	0.863	-0.08	0	0.100	-5.04	-0.527	-4.79
Unit	m	(-)	(-)	(-)	(-)	m/°C	m/mm	m/year	m	(-)/year	m

Parameter	Z_{min}	t_{c1}	t_{c2}	t_{c3}	t_{c4}		PZ_{min}
Value	195.7	0.75	36	28	0 (no correlation)		195
Unit	m NGF	days	days	days	days		m NGF

This set of parameters yields the following time series.
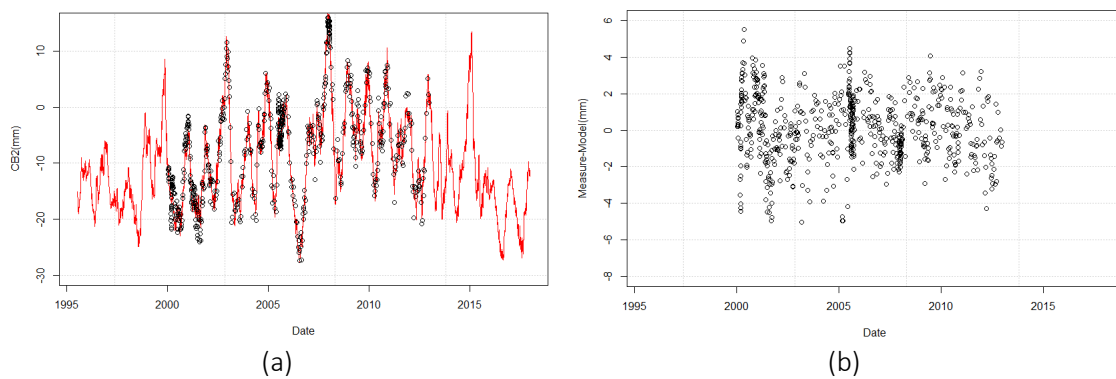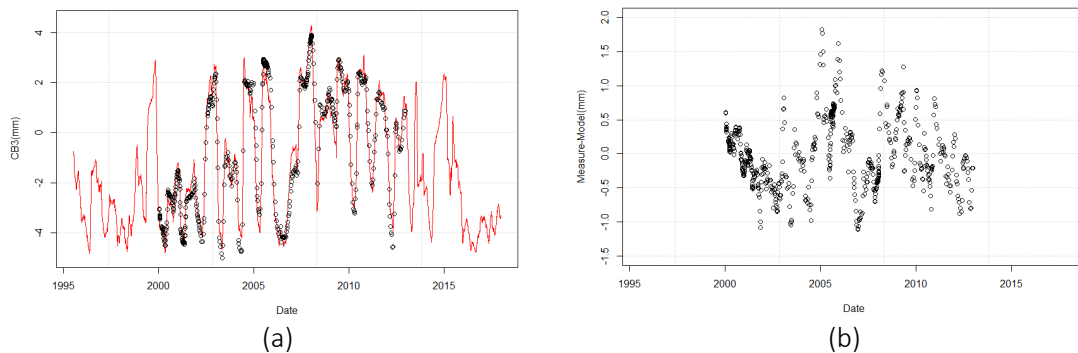

Figure 8. Learning process on the piezometer PZBC2; (a) raw time series with dots for the on-site measures and thick line for the digital twin, and (b) the time series of the difference between the model and the data.

The coefficient of determination is R²=0.988 and the standard deviation is 0.511 m. The confidence intervals are $[-0.85; 0.77]$ and $[-1.3; 1.09]$ in m for 95% and 99% respectively. The large discrepancy in 2002 is due to a fast water level increase in the reservoir. This is typical of an exceptional event for which statistical models only provide a rough estimate due to the lack of similar data during the learning process. One can notice that drainage and rainfall terms (downstream effects) are almost null for this piezometer. At the end, after few weeks, the model is back to good quality for the prediction. Indeed, after august 2008, the measures dropped significantly. Until the last measure in 2012, the model still detects a decrease of the piezometric level. It is not easy to extrapolate the measure until 2017 since the drop is not yet stabilized. From a practical viewpoint, it is recommended to calibrate the model yearly until the drop begins to stabilize.

4.3.2 Calibration and prediction of the piezometer PZCB3

For PZCB3, the first calibration tries showed that the drop initiated in august 2008 is stopped or extremely faded in the last months of provided data. We took the hypothesis of stopping the drop term starting from July 2012.

Table 7. Calibrated parameters for the piezometric head PZCB3.

Parameter	C_1	C_2	C_3	C_4	C_5	C_6	C_7	C_8	C_9	C_{10}	C_{11}
Value	1.382	0.2154	0.956	-0.475	0.460	-0.0246	0.029	-0.0436	-2.14	-1344	-1.34
Unit	m	(-)	(-)	(-)	(-)	m/°C	m/mm	m/year	m	(-)/year	m

Parameter	Z_{min}	t_{c1}	t_{c2}	t_{c3}	t_{c4}	PZ_{min}
Value	203.8	0.75	56	8	26	196
Unit	m NGF	days	days	days	days	m NGF

This set of parameters yields the following time series.
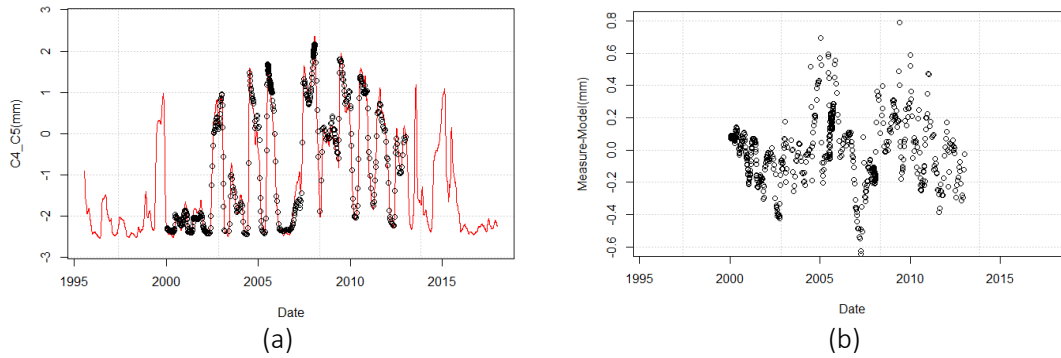

(a)   (b)

Figure 9. Learning process on the piezometer PZBC3; (a) raw time series with dots for the on-site measures and thick line for the digital twin, and (b) the time series of the difference between the model and the data.

The coefficient of determination is R^2=0.972 and the standard deviation is 0.265 m. The confidence intervals are $[-0.40; 0.41]$ and $[-0.71; 0.77]$ in m for 95% and 99% respectively. Compared to PZCB2, the drainage and rainfall terms are not null. Their amplitudes are respectively 2.0 m and 0.3 m.

4.4 *Calibration and prediction of the seepage*

For the seepage predictive model, we use the same set of functions as for the piezometric head. Unfortunately, so far, the results are not that good. The seepage prediction is much more complex. Indeed, if part of the seepage comes from the runoff along the hillslopes, this may introduce several characteristic times depending for instance on the ground hydric state. Furthermore, the rainfall data provided are measured 5 km away from the dam. As for the air temperature, in alpine regions, 5 km may change a lot the water quantities thus inducing uncertainties in the input data.

Nevertheless, a statistical model has been calibrated.

Table 8. Calibrated parameters for the seepage.

Parameter	C_1	C_2	C_3	C_4	C_5	C_6	C_7	C_8	C_9
Value	2.50	0.0399	1.70	-0.18	0.43	~0	0.95	-285	~0
Unit	l/min	(-)	(-)	l/min/°C	l/min/mm	l/min/year	l/min	(-)/year	l/min

Parameter	Z_{min}	t_{c1}	t_{c2}	t_{c3}	PZ_{min}
Value	208.5	~0	16	22	0
Unit	m NGF	days	days	days	l/min

This set of parameters yields the following time series.
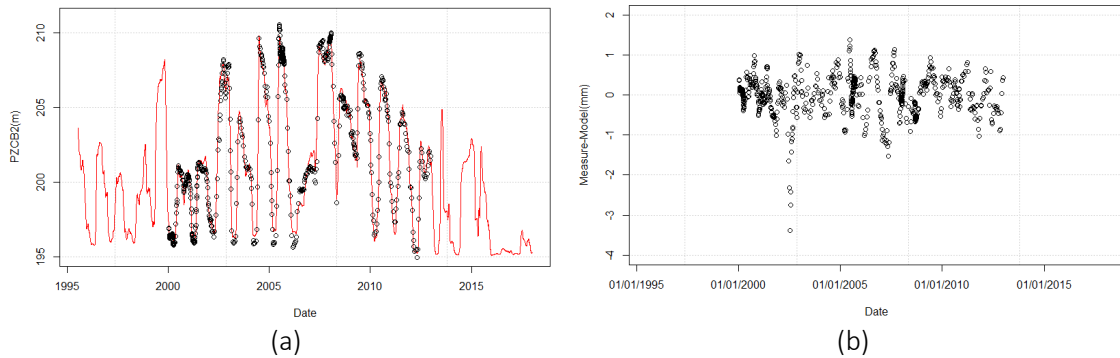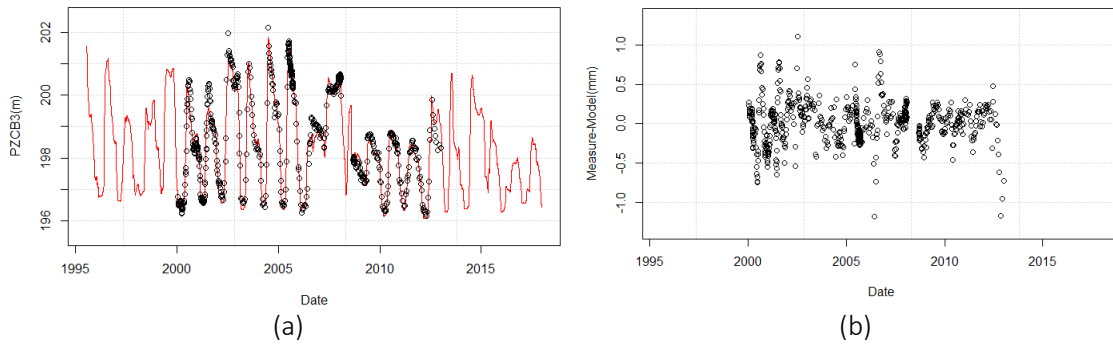

(a)   (b)
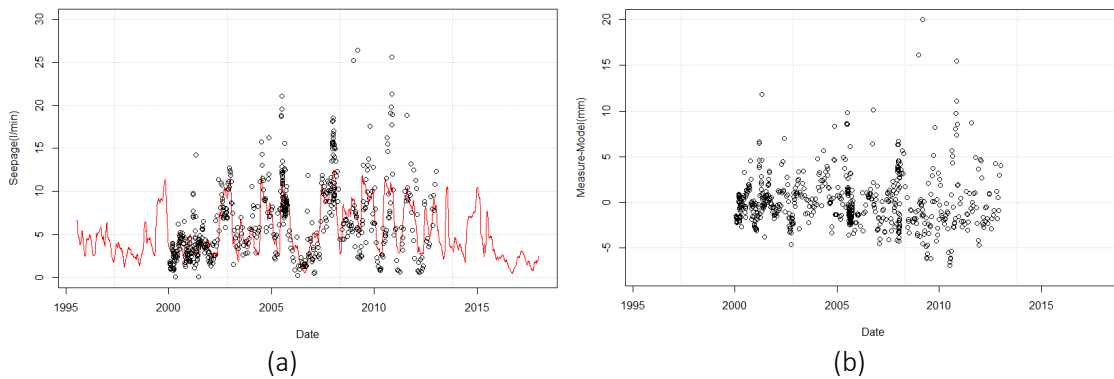
Figure 10. Learning process on the seepage; (a) raw time series with dots for the on-site measures and thick line for the digital twin, and (b) the time series of the difference between the model and the data.

The coefficient of determination is $R^2=0.567$ and the standard deviation is 2.88 l/min. The confidence intervals are $[-3.37; \ 4.80]$ and $[-5.8; \ 9.8]$ in l/min for 95% and 99% respectively.

5 CONCLUSION

In this contribution, we have proposed a statistical data-based model which is supported by physically sound functions. Some phenomena have been accounted for based on expert judgement yielding some specific correlation functions. They are different from the bibliography, and we do believe that their physical meaning is stronger. In contrary to neural network, for instance, the physical meaning can be evaluated a posteriori, after the calibration process, to eventually propose improvements. For instance, the characteristic times calibrated are systematically analyzed in view of the physics to check their coherency with the diffusivity of the concrete and the characteristic size of the dam. Besides, we have restricted ourselves to the minimum number of parameters required by the physics. Further parameters may be added to statistically improved the model at the risk of losing the physical meaning and introducing cross correlation between parameters. Except for the seepage, the coefficients of determination are above 0.95 which shows the very good quality of our approach.

On the other hand, this work, although innovative, has taken 3 days of work in total including the definition of the correlation functions, their calibrations, and the validation of the results. This is by far less than a FE model for a result we believe of the same quality.

In the next future, this innovative approach should be used on several other dams to determine some reference correlation functions depending on the dam typology and the type of sensors.

REFERENCES

Ferry, S. & Willm, G. 1958. Méthodes d'analyse et de surveillance des déplacements observés par le moyen de pendules dans les barrages. In VIth International Congress on Large Dams: 1179-1201. New-York. In French.

Leger, P. & Leclerc, M. 2007. Hydrostatic, Temperature, Time-Displacement Model for Concrete Dams. *Journal of Engineering Mechanics* 133(3): 267–277.

Leger, P., Venturelli, J. & Bhattacharjee, S.S. 1993. Seasonal temperature and stress distributions in concrete gravity dams. *Canadian Journal of Civil Engineering* 20(6): 999–1029.

Lugiez, F., Beaujoint, N. & Hardy, X. 1970. L'auscultation des barrages en exploitation au service de la production hydraulique d'Électricité De France, des principes aux résultats. In X[th] International Congress on Large Dams: 577-600. Montréal. In French.

Spall, J. C. 1992. Multivariate Stochastic Approximation Using a Simultaneous Perturbation Gradient Approximation. *IEEE Transactions on Automatic Control* 37(3), 332–341.

Tatin M. 2014. L'auscultation des barrages béton : amélioration des modèles de comportement thermiques et mécaniques. Univ. Grenoble Alpes.

Tatin, M., Briffaut, M., Dufour, F., Simon, A. & Fabre, J.P. 2015. Thermal Displacements of Concrete Dams: Accounting for Water Temperature in Statistical Models. *Engineering Structures* 91: 26-39. https ://dx.doi.org/10.1016/j.engstruct.2015.01.047

Tatin, M., Briffaut, M., Dufour, F., Simon, A. & Fabre, J.-P. 2018. Statistical modelling of thermal displacements for concrete dams: Influence of water temperature profile and dam thickness profile, *Engineering Structures* 165: 63-75. https ://doi.org/10.1016/j.engstruct.2018.03.010.

Willm, G. & Beaujoint, N. 1967. Les méthodes de surveillance des barrages au service de la production hydraulique d'Électricité De France. In IXth International Congress on Large Dams: 529-550. Istanbul. In French.

HYBRID ANALYSIS OF AN ARCH DAM
WITH A QUANTILE REGRESSION NEURAL NETWORK

Manuel Pirker
Institute for the hydraulic engineering and water resource management, Graz, Austria

Gerald Zenz
Institute for the hydraulic engineering and water resource management, Graz, Austria

ABSTRACT: Prediction and interpretation of deformation measurements based on data obtained from previous monitoring is one of the most common tasks for dam engineers to assess dam safety today. Deterministic and statistical approaches are used to solve these tasks. Finite element models offer the possibility to study the behavior of dams in great detail when mechanical parameters as well as geotechnical and geological information is available. However, compared to statistical models, they often lack predictive accuracy due to rheological time-dependent behavior and the lack of information on the geological conditions. This is especially the case when limited data is available to calibrate material models and body interactions, e.g., between individual blocks or to the foundation. Hybrid modeling combines the advantages of both approaches. The ICOLD Technical Committee on Computational Aspects of Analysis and Design of Dams called for a workshop on the behavior and predictive analysis of a double-curvature arch dam. For the given task, a finite element model is created and calibrated using available monitoring data. A recurrent neural network is then trained using the same data and the results of the finite element analysis to compensate for its lack of predictive accuracy. It is shown that this procedure not only improves the quality of modeling but also reveals deficiencies of the mechanical model alone. Furthermore, prediction intervals are derived from quantile regression neural networks to define warning levels and identify anomalies in the monitoring data.

1 INTRODUCTION

Prediction and interpretation of monitoring data is one of the most important tasks of a dam engineer today. This is done either by data-driven models or deterministic models such as finite element analysis (FEA). It is also possible to combine both approaches by performing a hybrid analysis. The knowledge gained from these analyses is critical for estimating the current safety condition of the dam, monitoring time-dependent changes over the years and coping with ageing. While FEA is best suited to provide insight into the behavior of the dam, statistical models are usually better at predicting it. These predictions can be used to detect anomalies in the measured data. Based on these detections, the responsible dam engineer must decide whether countermeasures must be taken. One method that can be used for this time series prediction is Long-Short-Term-Memory (LSTM) presented by Hochreiter & Schmidhuber (1997).

LSTMs are a further development of Recurrent Neural Networks (RNN), which were originally developed to represent the temporal relationship within data sequences. However, they have one major drawback. During the training process, weights are updated at each iteration based on the gradient of the error function. Sometimes this gradient can become so small that the weights no longer change or even the entire network can no longer be trained. One advantage of LSTMs is that they do not suffer from this vanishing gradient problem.

However, prediction of monitoring data alone is not sufficient. Suitable warning levels must be derived to detect abnormal behavior. One possibility is to derive them from alarm levels based on failure analysis of the monitored structure. Another approach is to derive them purely from measured data. In this case, the prediction intervals must be determined based on the underlying statistical model. For time series, this usually requires dealing with inhomogeneous variances. One method to achieve this is Quantile Regression (QR). QR does not assume identical, independent, and normally distributed individual values, as is the case with ordinary least squares models. The use of this method in neural networks leads to the Quantile Regression Neural Network (QRNN), as proposed by Taylor (2000).

This paper is a contribution to Theme A of the 16th International Benchmark Workshop on Numerical Analysis of Dams, organized by ICOLD in Ljubljana. The aim of this workshop is to interpret and predict measured data collected over a period of 13 years of a double-curvature arch dam. The prediction itself is to be performed for two cases. First, a short-term period from January to June 2013 will be predicted. Second, a prediction is needed for a long-term period from July 2013 to December 2018. In this paper, a combination of deterministic and statistical approaches is presented to achieve the most accurate predictions possible.

Firstly, a thermal-structural FEA is conducted to interpret the dam's behavior. Then a LSTM network is used to improve the predictive capability of the FEA. Finally, QRNNs are used to derive appropriate warning levels for monitoring.

2 METHODS

2.1 *Finite Element Analysis*

The FEA is performed with Ansys Mechanical Workbench (2020). The dam body is separated into 11 blocks (Fig. 1), which are connected by contact interfaces. Therefore, a bounded contact setting – no separation, no sliding – and a multi-point constraint formulation are used. Frictional contacts are used for the base joint, except for the embankment blocks. There, bonded contacts with a multi-point constraint are used.

A mesh with a total number of 10353 elements and 22656 nodes is used. The mesh of the dam body consists of quadratic hexahedral elements in both thermal and structural analysis. The foundation was discretized by quadratic tetrahedral elements. Displacement boundary conditions are applied to the edges of the foundation block. The lowest element quality – ratio of smallest to largest element axis – is 0.31 and is located within the rock mass. The same mesh is used for thermal and structural analysis.

According to the description in the assignment sheet, the rock foundation is divided into three parts: Left slope, middle slope, and right slope (Fig. 2). The left embankment's slope is used as the rock joint orientation since no other information about the rock joints is available. An

orthotropic linear elastic material model is used. The material properties normal and parallel to the assumed joints were taken from the task sheet.

The results of the analysis are extracted from the nodes at the central block at an elevation of 236 m for CB2 and 195 m for CB3. Deformations C4-C5 are extracted from the upstream base joint opening (Fig. 1-2).
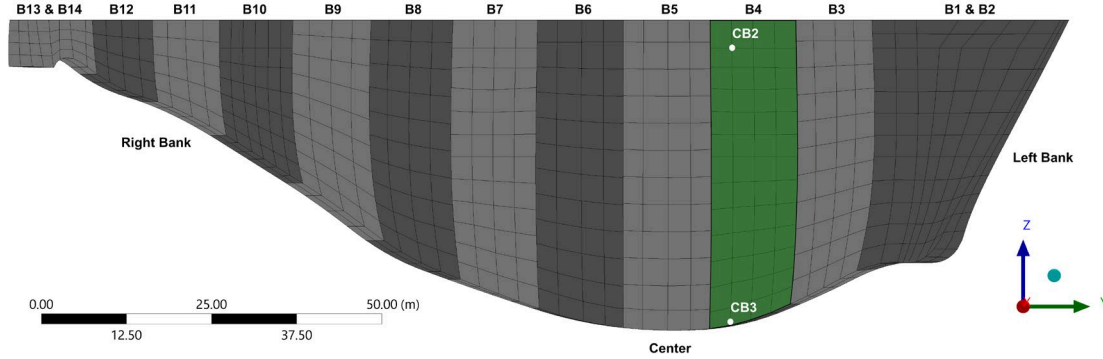
Figure 1. Dam body mesh with investigated nodes at the central block.
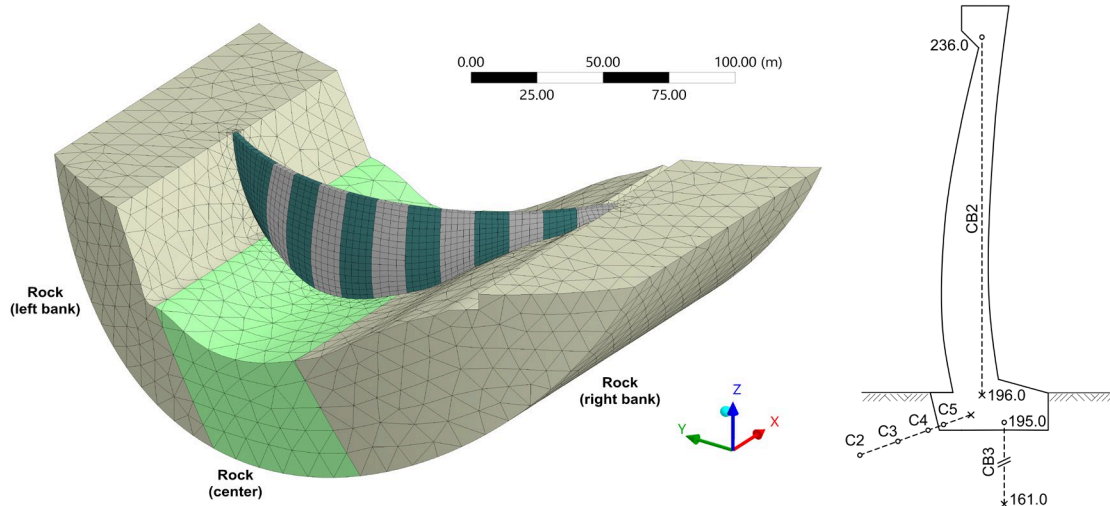
Figure 2. Mesh of the rock foundation with the dam body (left) and cross section showing positions of monitoring devices at the central block (right).

2.1.1 Thermal Modelling

The thermal load is considered by convection on all free surfaces of discretized domain. The necessary parameters for convection between media and thermal properties such as conductivity and specific heat capacity are taken from the task sheet. Since no information is available on the orientation of the dam, radiation is considered only on the downstream side of the dam. A typical emission factor for concrete of 0.91 is used. The ambient air temperature is varied over time according to the reference temperature $T_{b,air}$. The ambient temperature and the conductivity of the water-contacting surfaces are updated at each time step as a function of the current water level in the reservoir. For simplicity, the water temperature T_w results from a functional relation of the air temperature $T_{b,air}$:

$$T_{water} = max \begin{cases} 0 \\ 0.7 \cdot T_{b,air} \end{cases} \tag{1}$$

The transient thermal analysis is performed with a constant time step of 1 day. The results are then used as input for a subsequent structural analysis.

2.1.2 Structural Modelling

This analysis is divided into four steps. In the first step, the dam body alone is loaded by gravity, with only the base joint contacts being active. In the second step, the block joint contacts are activated. In the third step, the thermal load is applied and simulated for the period from 1995 to 2000. In the last step, the hydrostatic load is applied to the upstream side of the dam and the upstream valley. The hydrostatic pressure head and temperature distribution within the dam body are updated at each time step. The hydrostatic pressure acting within the block and bottom joints is not considered. The static analysis is performed with a constant time step of 7 days.

The concrete material parameters Young's modulus and the coefficient of thermal expansion (Tab. 1) are optimized to minimize the sum of squared errors from the calculated deformation in CB2 and the reference. Further material properties were taken from the task sheet.

Table 1. Optimized concrete material parameters.

Coefficient of Thermal Expansion m/m°C	Young' Modulus GPa
1.15e-5	24.0

2.2 *Long-Short-Term Memory*

LSTMs were introduced by Hochreiter & Schmidhuber (1997) as further development of RNNs. RNNs were developed to represent the temporal relationship within data sequences. They have the ability to pass information from one time step to the next. According to the representation in Figure 3, the output from the previous time step h_{t-1} and the input of the current time step X_t are combined via an activation function, e.g. *tanh*, to create the new output h_t, which is also passed on to the next time step.
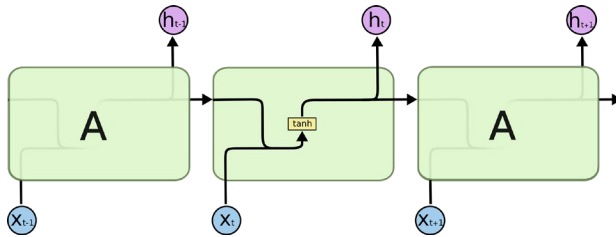
Figure 3. Unrolled RNN containing a single layer, depiction by Colah (2015).

During the training process, the weights are updated at each iteration based on the gradient of the error or loss function. Sometimes this gradient can become so small that the weights no longer change or even the entire network can no longer be trained.

LSTMs were introduced to solve the vanishing gradient problem. Each LSTM unit is composed of a cell that stores values over a period of time and three gates which regulate the flow of information to and from this cell. According to the representation in Figure 4, the first gate decides, based on the previous output h_{t-1} and the current input X_t, which parts of the passed cell state C_{t-1} should to be forgotten and which parts should be remembered. To do this, it uses multiplication with a sigmoid function. The next gate updates the cell state by adding new information. The third gate produces the actual output of the current time step h_t. This output and the new cell state C_t are again passed on to the next time step.
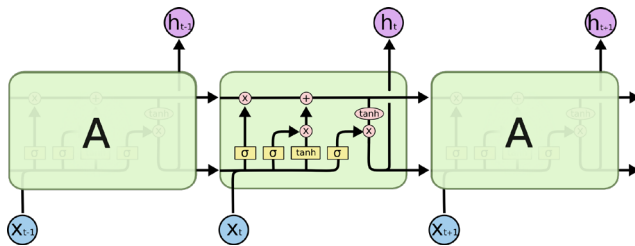
Figure 4. LSTM contains four interacting layers, depiction by Colah (2015).

2.2.1 Quantile Regression

QR models the relationship between a set of predictor variables and specific percentiles of a target value. In contrast to ordinary least squares, QR does not depend on assumptions about the distribution of the target value and also tends to resist the influence of outliers, Koenker et al. (1978).

In machine learning, QR is often used to create prediction intervals, e.g., for predicting upcoming demand or price changes on the stock exchange. Following Taylor (2000), the corresponding minimization problem can be stated as:

$$minimize \left(\max\left(\theta(y_i - \hat{y_i}), \ (\theta - 1)(y_i - \hat{y_i})\right)\right) \tag{2}$$

Where the θ-th quantile is derived from y_i and $\hat{y_i}$ is the predicted value. Setting $\theta = 0.5$ leads to the prediction of the median.

To use this approach in neural networks, the function presented has to be defined as a user-defined loss function. In this work, the 97.5% quantile is used as the upper bound and the 2.5% quantile as the lower bound of the prediction interval.

2.2.2 Data Preparation and Training

The provided data for the pendulums and the extensometer were previously cleaned and have a temporal resolution of 1.5 weeks. FEA provides results at weekly intervals. These time series are resampled by linear interpolation to daily resolution to account for the frequency of water level, precipitation and air temperature measurements. Prediction is also done on a daily basis.

Figure 5 shows a flowchart of the hybrid model process. After resampling, the data is scaled to the same magnitudes. Temperature and the FEA data are standardized, i.e. zero mean and unit variance. Water level and precipitation data are normalized between zero and one while maintaining the original scale of the structural response measurements.

After scaling the data, a training set is created ranging from January 1, 2000 to May 10, 2012 (95.0% of the data) and a validation set is created ranging from May 11, 2012 to December 31, 2012 (5.0% of the data). Initially, the model is trained on the training data only. The hyperparameters, i.e. network depth, number of neurons per layer, dropout rate and activation functions, are adjusted based on the determined losses in the training and evaluation set. After the adjustment process is performed and the final model is selected, training continues with the validation set. Finally, the obtained model is used to predict the monitoring values and their warning levels.
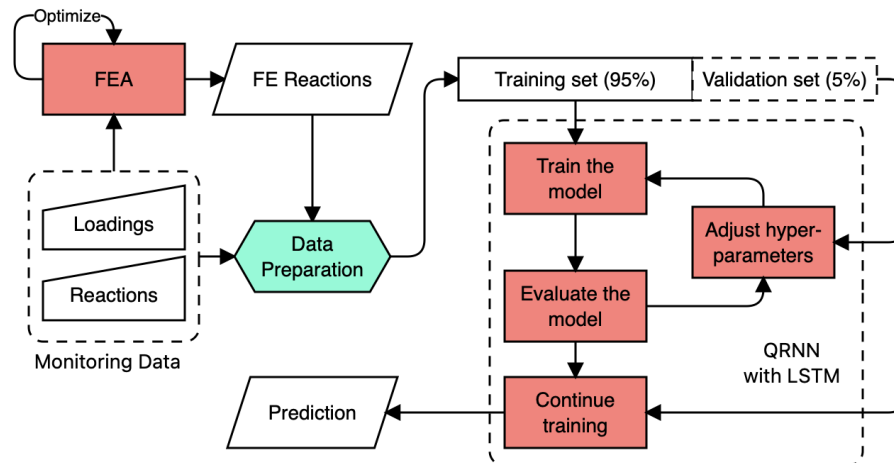
Figure 5. Flowchart for hybrid modelling.

During the training process, the weights and bias of the neural network are updated by backpropagation depending on the gradient of the loss function. There are several optimization methods for this process. In this work, a stochastic gradient descent method that is based on an

adaptive estimation of first and second order momentums called "Adam" is used, Kingma et al. (2015). In addition, a learning rate scheduler with exponential decay is defined.

A total of 9 models are trained – three for each measured value – using the Tensorflow/Keras framework within Python provided by Chollet (2015).

3 RESULTS

3.1 *Interpretation of FE Results*

The thermal field is extracted from the transient thermal analysis. Figure 6 clearly shows the difference in surface temperature between water-contacted and air-contacted faces. Moreover, the downstream surface of the dam has slightly higher temperatures than the upstream surface due to the applied radiation.
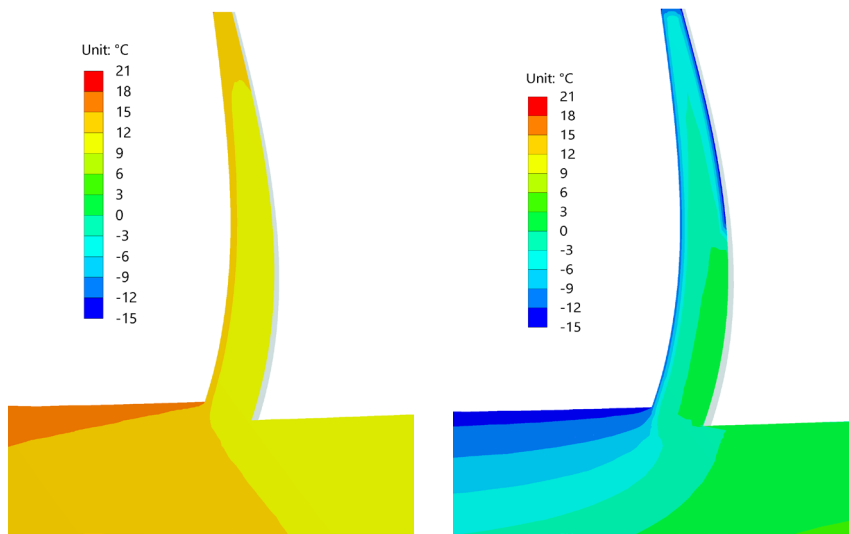
Figure 6. Temperature distributions in °C within central block for on 29th of August 2010 (left: during summer with high water level) and 11th of February 2010 (right: during winter with low water level).

Deformation and stress distributions provide further important information on the behavior of the dam. The maximum downstream displacement of the central block was measured on July 30, 2006, when summer temperatures were high and the reservoir was full (Fig. 7). The stress distribution at this time shows that tensile hoop stresses develop in the lower part of the block (Fig. 9). This is due to the unfavorable rock conditions in the center of the valley, resulting in the downstream deformations recorded by pendulum CB3.

Figure 8 shows the maximum upstream deformation occurring on December 31, 2007, during winter and when the reservoir was almost empty. The stress distribution in the central block (Fig. 9) shows that almost the entire cross section is under compression.
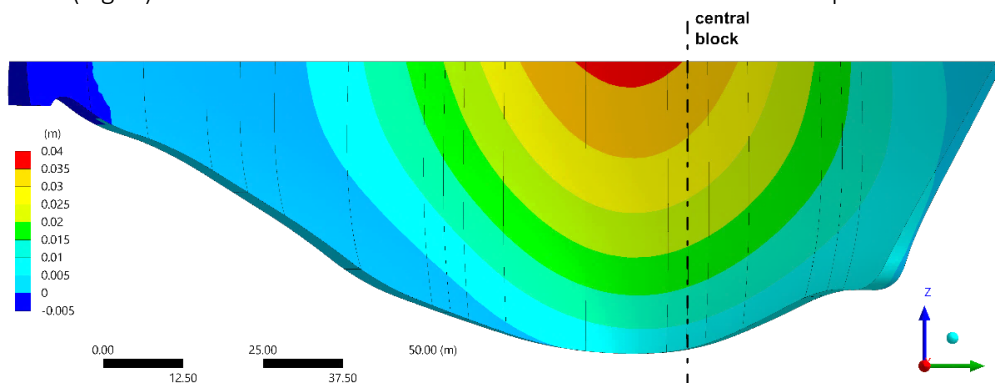
Figure 7. Deformation on time maximum downstream deformation – high temperature, high water level on July 30, 2006. Positive values indicate movement in downstream direction.
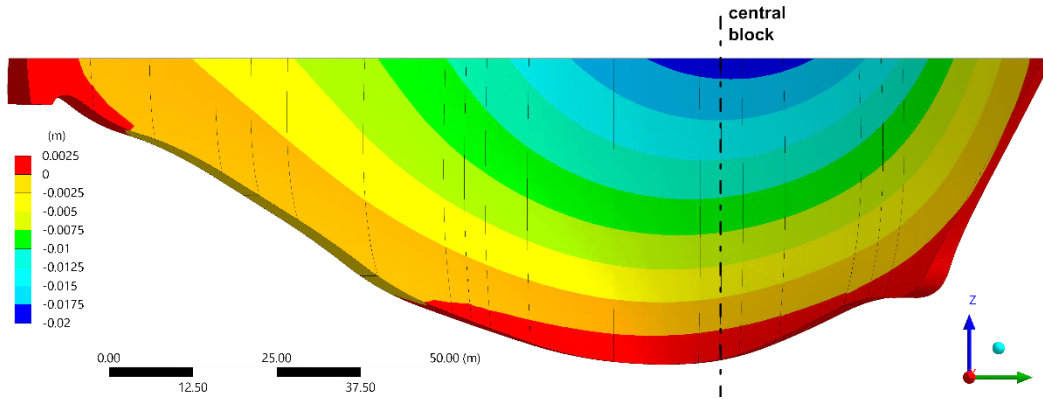
Figure 8. Deformation on time maximum upstream deformation – low temperature, low water level on 31, 2007. Positive values indicate movement in downstream direction.
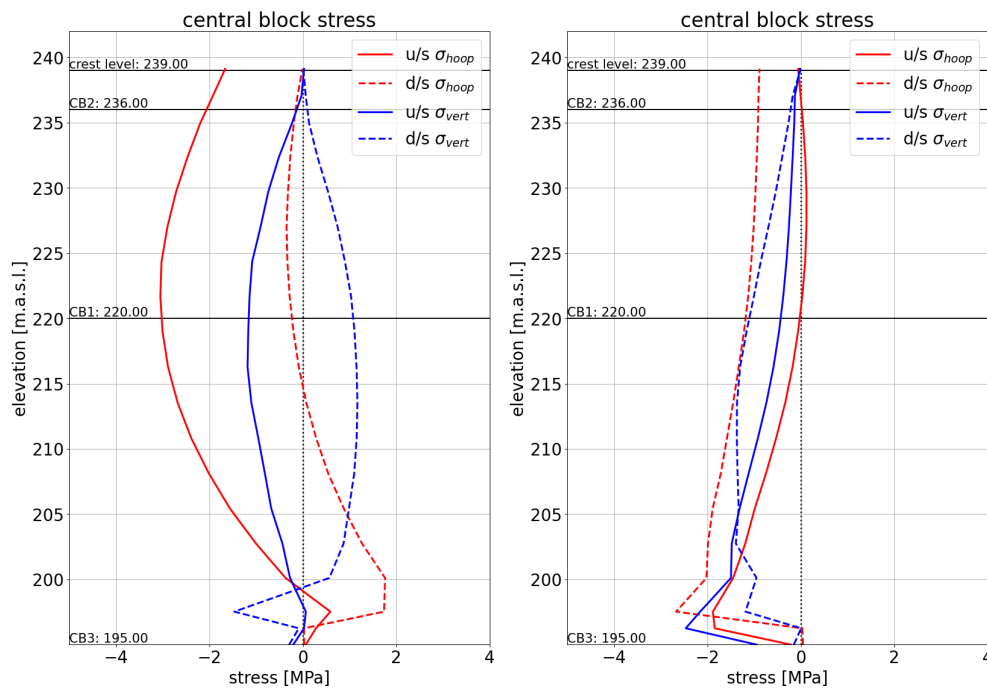
Figure 9. Vertical and hoop stresses in the central block for high temperature, high water level on July 30, 2006 (left) and low temperature, low water level on of December 31, 2007 (right).

3.2 *Predictions and Warning Levels*

In Figure 10, the FE results for CB2 show a delayed response to decreasing hydrostatic pressure, while loading periods are quite well captured. The largest errors are observed during the first quartiles of 2002 to 2004 and in 2012, when the water level in the reservoir reached its lowest level.

The median prediction using of the LSTM model reduces the mean absolute error from the FE calculation by 42.1% to 1.50 mm during the calibration period. The evaluation of anomalies in this period shows slight differences between the desired quantiles (2.5% - 97.5%) and the quantiles estimated by the models (2.7% - 97.7%). Similar results are obtained for CB3 and C4-C5 as well.
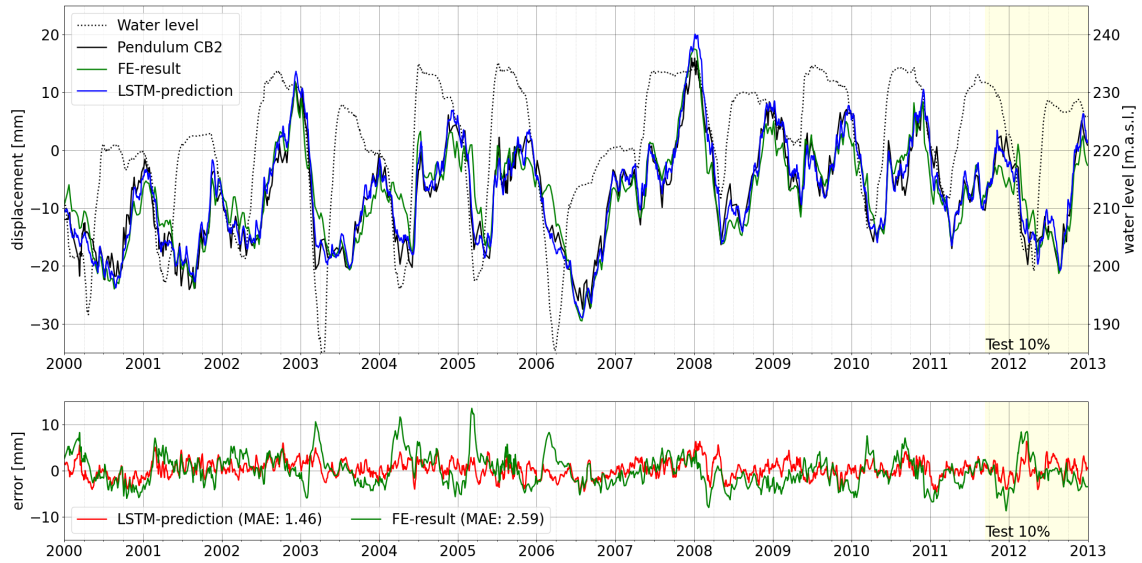
Figure 10. Calibration period with 10% evaluation split showing results from FEA and predictions of LSTM with their error compared to measurements.

The accuracy of the prediction can be significantly improved by additional use of the LSTM model. As the scatter plots in Figure 11 show, the total variance due to the non-linear behavior of CB2 can be decreased compared to the pure FE-results.
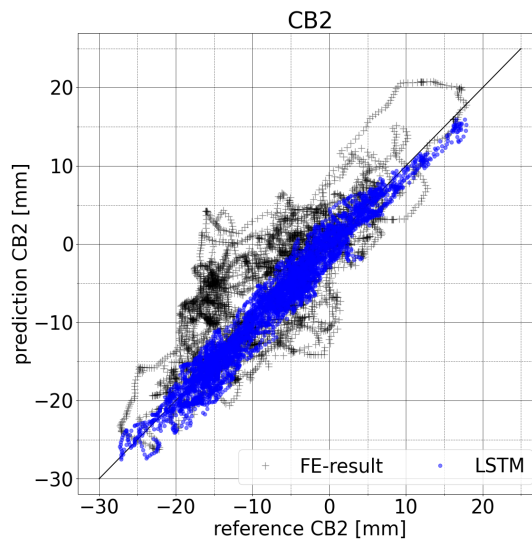
Figure 11. Scatter plots of reference measurements vs. LSTM predictions and initial FE results for CB2 (left).

Figure 12 shows anomalies identified from the 95% prediction interval. 205 anomalies were detected during the training process from 2000 to 2011, while 33 anomalies were detected in the testing process during the year 2012. Figure 13 and 14 show the final prediction with warning levels for pendulum measurements CB2 and CB3. The presented results for the short-term (case B) and long-term prediction periods (case C) have be evaluated and compared with participants during the benchmark workshop.
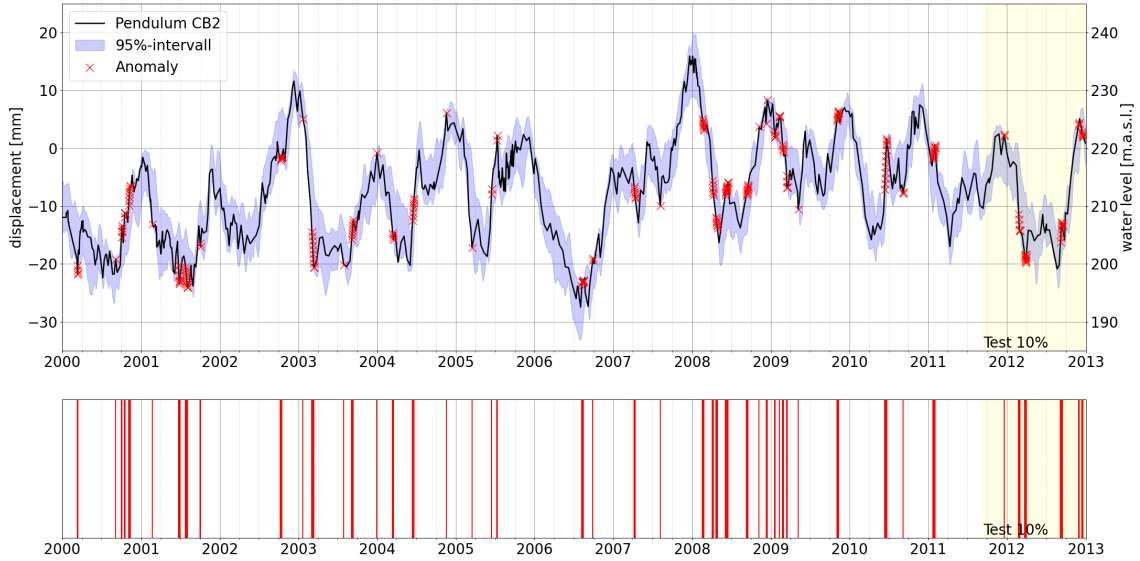
Figure 12. Identified anomalies from the 95% prediction interval for pendulum motion CB2 in the training and 10% test set (case A).
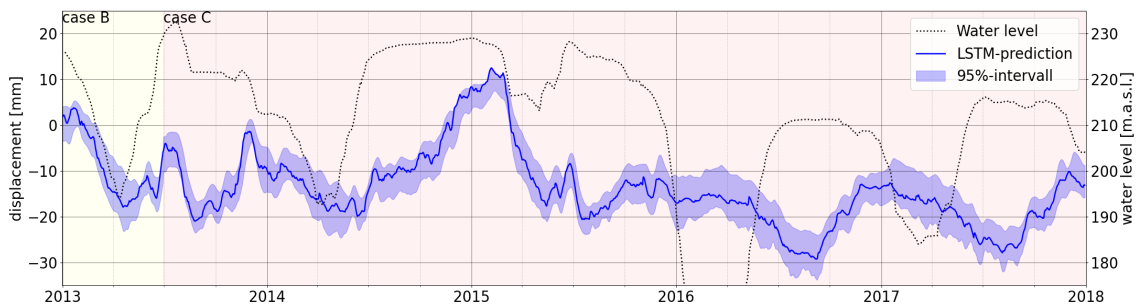
Figure 13. CB2 predictions including warning levels (95% prediction intervals) for all cases B and C compared with FE results and reference measurements.
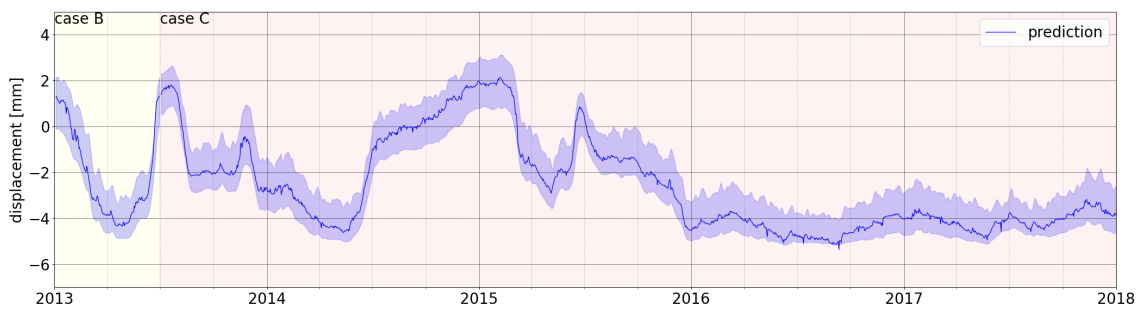
Figure 14. CB3 predictions including warning levels (95% prediction intervals) for all cases B and C compared with FE results and reference measurements.

4 CONCLUSION

In summary, hybrid analysis combines the advantages of the deterministic approach to describe mechanical behavior with FEA and those of the statistical approach to account for uncaptured time-dependent effects.

Finite element modelling provides important information about the behavior of the dam. In this case, the model is calibrated using measurements on one block only. Therefore, additional measurements are crucial to verify the deformations calculated by the FEA. Some essential

information to allow a more advanced numerical modelling is not given by the formulator - or unfortunately in general not available. Especially information on the geotechnical aspects such as joint orientation and spacing is necessary to further improve FE results. Lack of data on the thermal field within the dam body further complicates calibration, as additional assumptions must be made. The largest error is found during unloading periods, indicating a delayed response of the rheology of the surrounding rock that is not captured by the FE model. Similar deviations were found by Zenz (2003) when investigating the Zillergründl arch dam.

The LSTM model improves the prediction quality of the FE results. It is also capable to provide predictions intervals without making assumption about the parameter distributions in the FE analysis, such as Young's modulus or density. The latter requires data that is often scarce, especially for dams built decades ago. In the presented work, the linear material behavior and base joint interactions are captured in the FEA, while the LSTM model considers nonlinearities and time depending behavioral changes such as creep and rheological effects that are not captured.

REFERENCES

Ansys Mechanical Workbench. 2020. Academic research mechanical, release 2020 R1

Chollet, F. & others. 2015. Keras. Available at: https://github.com/fchollet/keras. (visited 17.01.2021)

Colah. 2015. Colah's blog. Available at: https://colah.github.io/posts/2015-08-Understanding-LSTMs/. (visited 17.01.2021)

Hochreiter S. & Schmidhuber J. 1997. Long short-term memory. *Neural computation* 9: 1735–1780

Kingma D.P. & Ba J. 2015. Adam: A method for stochastic optimization. *Conference for learning Representations.*

Koenker, R. & Basset, G. Jr. 1978. Regression quantiles. *Econometrica* 46: 33-50

Oberhuber P. & Perner F. 2005. Displacements in concrete dams caused by temperature variation. *Hydropower & dams* 5.

Taylor, J.W. 2000. A quantile regression neural network approach to estimating the conditional density of multiperiod returns. *Journal of forecasting* 19: 299-311

Zenz G. & others. 2003. Arch dam foundation bearing behaviour. *Felsbau.*

HYDROSTATIC MACHINE LEARNING MODEL FOR PREDICTION OF CONCRETE DAM BEHAVIOUR

Farrokh Mojtaba
Advanced structures research lab., K. N. Toosi University of Tech.,Tehran, Iran

Mohammad Moradabbasi
Advanced structures research lab., K. N. Toosi University of Tech.,Tehran, Iran

Sina Hadadi Ahangar Kolaee
Advanced structures research lab., K. N. Toosi University of Tech.,Tehran, Iran

ABSTRACT: Health monitoring of dams is based on measuring significant quantities that characterize their behavior (like Crack opening displacement, radial displacements, etc.) and on visualization inspections of the structures. Predictive models are essential in dam safety assessment. They have been conventionally based on simple statistical tools such as the hydrostatic-seasonal-time (HST) model. In recent years, examples of machine learning and related techniques are becoming more frequent as alternatives to HST. In this work, the most popular machine learning techniques such as gradient boosting regression, support vector machines, neural networks are utilized to predict radial displacements of a double curvature arch dam. The possibilities of model explanation are explored: the relative influence of each predictor is computed, and a new combination method is constructed based on HST and machine learning algorithms and called the Hydrostatic Machine Learning (HML) model. This study shows a comparison between HML and other machine learning tools for the description of dam behavior under environmental loads. This study indicates that HML models can be a powerful tool that can efficiently identify concrete dam behavior performance changes with higher flexibility and reliability than simple regression models.

1 INTRODUCTION

Dam monitoring is essential to ensure the satisfactory operation and long-term safety. In terms of safety, the aim of controlling a concrete dam is to guarantee the functions for which it was built by maintaining its functionality and structural integrity. Monitoring activities and model analysis are tools by which safety control is being carried out [1]. One of the main tasks to be performed is to compare the expected responses registered by the monitoring system, understand the dam behavior, and detect potential anomalies [2]. The actual responses of dams are compared with the prediction models aiming to detect anomalies and prevent failures. Such predictive methods can be classified into four scopes: Deterministic, Statistic, Hybrid, and Mixed Models [3]. Deterministic models such as FE models based on mechanical principles are often challenging to construct. Although numerical models based on the FEM provide a proper estimation of dam displacements and stresses, this method faces a significant degree of uncertainty in the characterization of the materials, especially concerning the dam foundation [3]. Such numerical tools are of great essentiality during the initial stages of the structure's life cycle unless there are enough data available to build data-based predictive models. However, their results are often not accurate enough for a precise dam safety assessment [3].

There are still quite a few dams with slightly observed data. However, there is a consistent trend towards the installation of a larger number of devices with higher data collection frequency. Data that is driven by tools allows for building predictive models based on monitoring data without explicitly considering the physical properties of the dam and the foundation. Many in-operation dams have quite a few monitoring and recording devices. Various indicators are acquired, such as displacement, the temperature in multiple levels, water temperature, leakage flow, and pore water pressure. This being the case, an increasing amount of information is available on the dam performance, which makes it interesting to study the ability of machine learning (ML) tools to process them, build and predict behavior models, and extract useful information.

1.1 *Statistical models*

1.1.1 HST

The hydrostatic-seasonal-time (HST) model is the most widely applied and generally accepted by practitioners in which three effects are taken into account: 1) A reversible effect of the hydrostatic loads, 2) A reversible seasonal thermal influence of the temperature, and 3) An irreversible term due to the evolution of the dam response over time [3]. The coherence of these assumptions is evident in the observed behavior of many concrete dams in terms of displacements [3]. De Sortis and Paoliani [4] and Léger and Leclerc [5] successfully obtained structural identification techniques using a very complex procedure. The main disadvantages of HST and other methods based on linear regression are as follows [1], [3]:

- The functions have to be defined in advance and thus may not represent the actual behavior of the structure.
- Some of the governing variables have been proven to be correlated. However, they are seemingly independent.
- They are not well-suited to model non-linear interactions between input variables.

HST also characterizes conceptual limitations that impact the prediction accuracy and may lead to misinterpretation of the results since the hydrostatic load and the temperature are considered to be independent, while these variables are coupled in reality. The thermal field in the dam structure, especially in the vicinity of the water surface, heavily relies on the temperature of the water in the upstream face [2]. In turn, the thermal load influences the stress and displacement fields. Various modifications to the original HST model have been proposed to tackle its drawbacks. They focus on improving the consideration of the thermal load by taking into account the actual air temperature instead of the historical mean [2] or how the water temperature affects the upstream face [6], [7].

1.1.2 HTT:

HTT (hydrostatic, temperature, time) [5] is another statistical model which interprets concrete dam-recorded pendulum displacements. In the HTT model, the thermal loads are arbitrary and contain temperature drift or unusual temperature conditions to analyze recorded concrete dam displacements. The HTT model uses thermometric data to compute effective linear temperature differences across dam sections and their effects on dam displacements.

1.1.3 Multiple linear regression and Multilayer Perceptron:

In recent years, non-parametric techniques have appeared as an alternative to HST data-based behavior models [8]. Support vector machines (SVM) [9], neural networks (NN) [1], adaptive neuro-fuzzy systems (ANFIS) [10] can be pointed out. In general, these tools are perfectly proper for non-linear cause-effect relations modeling and interacting among external variables, as previously mentioned between hydrostatic load and temperature. On the contrary, they are typically more difficult to interpret, leading them to be called *black box* models. Most of the published work focused on the accuracy of such predictive models, which was generally higher than what was offered by HST [1], [3], [11]. Although the HST model is simple, many exceptions were made by Santillán et al.[12], Mata [1], and Cheng and Zheng [13]. Therefore, a dilemma is posed to engineers. The HST model is perfectly known, used, and easily interpretable; however, it is based on some incorrect assumptions, and its accuracy can be increased. On the other hand, more flexible and accurate models are available, but they have difficulties in implementation and analysis.

For analyzing multifactor effects, the multi-linear regression (MLR) model is one of the statistical techniques used to a great extent. An MLR model is a statistical technique for investigating and modeling the relationship between variables and their correlation. MLR models have a long-standing history in dam engineering and were otherwise known as quantitative analysis models. The regression equation is only a reasonable approximation to the actual relationship between the variables in almost all applications of regression [1]. Researchers are frequently innovating techniques to improve the HST results. For instance, Bonelli and Radzicki [14] used an impulse-response function to predict the dam body pore pressure. Li et al. [11] proposed a method based on cointegration theory to improve HST. Having tested the stationarity of the monitoring data series, they fitted a multi-linear regression (MLR) model [3].

Both MLR and Neural network (NN) approaches are of great potential for assessing the behavior of the control variables that support the safety assessment of the concrete dam. One obvious disadvantage of linear regression that causes inadequacy is that it cannot reproduce nonlinear relationships between variables. To overcome this inadequacy, introducing higher-order terms of the covariates must be applied [3]. NN is a constructive alternative for this issue whose flexibility and capability to adapt to highly complex interactions have made them popular in several fields of engineering, including dam monitoring [1], [15]–[17]. Some worth-mentioning research studies related to NN, such as Perner et al. [18], Gomes and Awruch [19], Fedele et al. [20], Z. Wu et al. [21], Bakhary et al. [22], Wang and He [23], Wen et al. [24], Liu et al. [25], Joghataie and Dizaji [26], and Yi et al. [27]. However, NN has some drawbacks [3]:

- The results depend on how well the weights are initialized.
- The best network architecture, number of hidden layers and neurons in each layer, is not known in advance.
- The model is subjected to being over-fitted.
- The training process is prone to reach a local minimum of the error function.

Several techniques have been developed to overcome these shortcomings, and there is no way to bear the increase in the computational cost [28]. Despite this, NN stands out as the most popular ML tool in dam engineering, and the results are encouraging [15]. ANFIS models [29], principal component analysis [30], NARX (nonlinear autoregressive with exogenous input) models [31], or K-nearest neighbors [32] have also been applied to dam monitoring. However, such mentioned tools are rarely used in practice, where HST still prevails. Moreover, most previous studies are limited to one single variable of specific dams [1], [17]. Therefore, the results are not generally applicable. A further singularity of dams is that the early years of operation often gears to a transient state, which is not representative of the quasi-stationary response afterward [33]. In such a case, eliminating those years for training a predictive model

would be advisable. It might lead to questioning the optimal size of the training set in achieving the best accuracy [3]. De Sortis [4] carried out sensitivity analysis and maintained that at least 10 years were needed to acceptable predictions come true. However, his study was limited to the radial displacement predictions in one particular location of a specific dam by using HST. Similar work was run by Chouinard and Roy [34]. In recent years, some tools that can perform cognitive tasks such as pattern recognition and function approximation have been introduced in Artificial Intelligence [1].

1.2 *Objectives*

The study aims to assess the prediction accuracy of some ML algorithms, most of which have been used in dam engineering. Specifically, the algorithms selected are: gradient boosted regression (GBR), Extreme Gradient Boosting (XGBoost), support vector machines (SVM), Hydrostatic GBR and Hydrostatic NN. With the help of these prediction models, we can evaluate the dam's performance, estimate the response of the dam for its actual load conditions and define warning levels. The aim of using current algorithms for the considered dam is to build a model from the past year's data to see how modern tools can be used in the prediction of dam behavior.

2 CASE STUDY AND VARIABLE SELECTION

A double curvature arch dam located in the south of France is used as a case study in this study. Theme A of the 16th International Benchmark Workshop on Numerical Analysis of Dams has introduced this dam [35]. The theme aims to establish a prediction model for the dam. Table 1 shows some statistics of the target variables. The location of each monitoring device is depicted in Fig. 1. The monitoring data for the dam has been presented from 2000 to 2012. This paper uses the data from 2000 to 2009 to train the considered models. The remaining data has been used for testing models.

Table 1. Summary of the main features of the provided data.

Variable Type	units	Variable Name	Period	Frequency
Water Level	m	Water Level	1995-2017	1 day
Air Temperature	ºC	Ta	1995-2017	1 day
Air Temperature	ºC	Tb	1995-2017	1 day
Rainfall	mm	Rainfall	1995-2017	1 day
Radial displacement	mm	CB2_236-196	2000-2012	1.5 weeks
Radial displacement	mm	CB3_195-161	2000-2012	1.5 weeks
Crack Opening	mm	C4-C5	2000-2012	1.5 weeks
Piezometric level	m	PZCB2	2000-2012	1.5 weeks
Piezometric level	m	PZCB3	2000-2012	1.5 weeks
Seepage	l/min	Seepage	2000-2012	1.5 weeks

The main focus of this paper is to build the predictive models for the pendulums located in the central block of the dam shown in Fig. 1 (b): CB2 and CB3. In addition, three raw environmental variables measured at the dam site have been depicted in Fig. 2. It is obvious in Fig. 2 (a) that the reservoir's surface has gone beneath Dam Bottom (level 195) a few times. The water levels below the Dam Bottom are replaced with 195 since water levels less than this, due to the topography of the reservoir, do not affect the structure's displacements or movements in for creating predictive models in this paper.
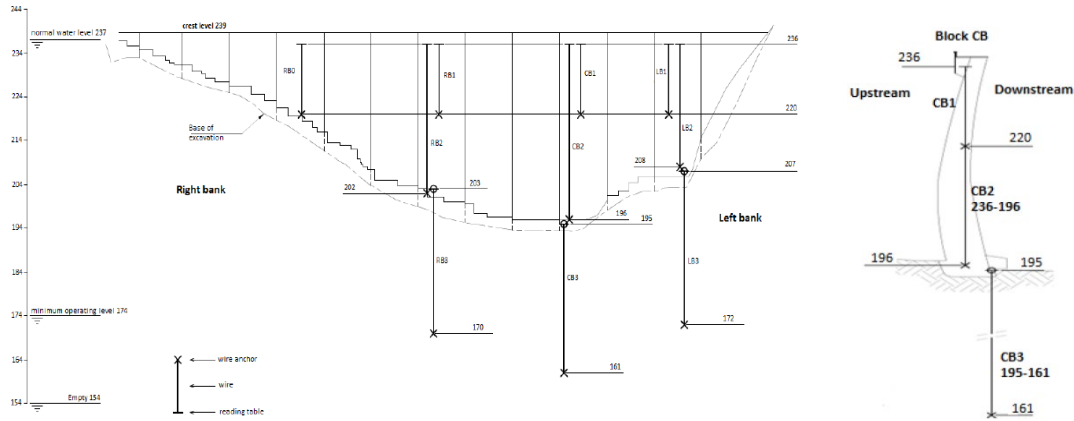
Figure 1. Location of pendulums: a) Downstream view and b) View of block CB and pendulums.

The predictor variables have been selected based on dam engineering performance [3]. Both displacements and leakage strongly depend on the hydrostatic load. Air temperature is well known to affect displacements in the form of delayed action. Other contributing factors are moving averages of reservoir level and its fluctuation velocity over different periods. The year and number of days from the first impounding are considered for the irreversible displacement of the structure. Table 2 summarizes the 21 considered predictor variables.

Table 2. Predictor variables.

Code	Group	Type	Period (days)
Level	Hydrostatic load	Original	–
Lev014	Hydrostatic load	Moving average	14
Lev030			30
Lev060			60
Lev090			90
Tair	Air temperature	Moving average	1
Tair014			14
Tair030			30
Tair060			60
Tair090			90
Rain	Rainfall	Accumulated	1
Rain030			30
Rain060			60
Rain090			90
Rain180			180
NDay	Time	Original	–
Year			–
Month	Season	Original	–
n010	Hydrostatic load	Rate of variation	10
n020			20
n030			30
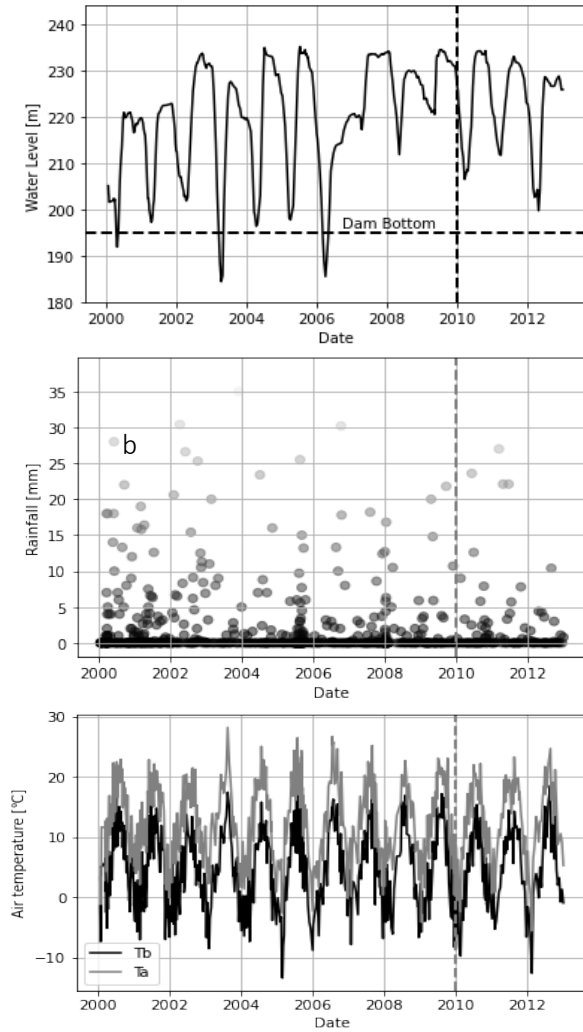
Figure 2. Time series of environmental variables at the dam site. From top to bottom: water level (a), air temperature (b), and daily rainfall (c). The vertical dashed line marks the division between training and test periods.

3 METHODS

In this section, the algorithms chosen to create the prediction models are briefly described. Although the detailed mathematical description is beyond the purpose of the paper, a short description, the most relevant features, and some key references are included. All the models have been built by using Python programming environment and some of its packages.

3.1 *HST Model*

A conventional HST model was fitted for comparison purposes:

$$\hat{Y} = F(t, h, s) = Y_h + Y_t + Y_s$$
$$= a_0 + a_1 h + a_2 h^2 + a_3 h^3 + a_4 h^4 + a_5 e^{-t} + a_6 t + a_7 \cos(s) + \cdots$$
$$a_8 \sin(s) + a_9 \sin^2(s) + a_{10} \sin(s) \cos(s) \tag{1}$$

where:

$$s = 2\pi \frac{d}{365.25} \tag{2}$$

where d is the number of days since 1 January, t is the elapsed time (years), h is the reservoir level, and a_0, a_1, …, and a_{10} are the coefficients to fit.

3.2 *Gradient Boosted Regression (GBR)*

Gradient boosting is a model that learns the boosting algorithm by ensemble learning for the decision tree. Although other models focus on it to boost performance, in this model, the gradient divulges the weaknesses of the model that have been learned so far. One advantage of gradient boosting is that the other loss functions can be used as much as possible. The character of the loss function is automatically reflected in learning through the gradient [5]. The main steps of the original boosting algorithm for regression trees and the squared error loss function can be found in Ref. [36].

3.3 *XGBoost Model*

With the rapid growth of opportunities in the advancement of computer technology, an advanced supervised machine learning algorithm named "extreme gradient boosting (XGBoost)" is developed by Chen and Guestrin [37]. The XGBoost is a novel extended version of the commonly used gradient tree boosting, which has been widely used in machine learning and data mining competitions due to its advantages of high efficiency and sufficient flexibility.

3.4 *SVR*

Support vector machine (SVM) is a new technique for solving pattern classification and regression in many areas [38]. Support vector regression (SVR) has been used for dam behavior identification [9]. The SVR goal is to find an optimal function $f(x)$, which represents the nonlinear mapping relationship between the dependent variable $y \subset R$ and the independent variables $x \in R^m$, such as dam displacement variable and corresponding influence variables, from a given training sample data set $\{(x_1, y_1), \ . \ . \ ., (x_n, y_n)\}$, where m and n represent the number of independent variables and the number of sample data, respectively.

3.5 *Hydrostatic Machine Learning Model*

A hybrid model has been proposed in this paper to separate the effects of water pressure from the other contributory factors on the displacement of the dam body. In this model by inspiration of HST model, first, the radial displacement is predicted using five variables related to the reservoir head by $a_0 + a_1h + a_2h^2 + a_3h^3 + a_4h^4$. The coefficients a_0 to a_4 are defined by using a regression technique. Next, a machine learning tool such as GBR or NN, is utilized to learn the residual displacement in an ensemble manner. The predictor of the ML tool has 20 variables. The reservoir water level is excluded from the input because the hydrostatic polynomial has considered its effect in the previous step.

4 VARIABLE IMPORTANCE

Variable importance refers to a class of techniques for assigning scores to input variables (features) of a predictive model that indicates the relative importance of each variable when making a prediction. Variable importance scores can be calculated for problems that involve predicting a numerical value, called regression, and those problems that include predicting a class label, called classification. Variable importance scores play an essential role in dimensionality reduction and feature selection that can improve the efficiency and effectiveness of a predictive model. Fig. 3 depicts the relative influence of the predictors for each radial displacement of the central block of the considered dam. Tair14 and Tair030 are the most relevant thermal input for CB2 and CB3, respectively. As we can see, the hydrostatic loads (reservoir level and average velocity of reservoir level) are more influential than Daily rainfall in both CB2 and CB3 measurements.
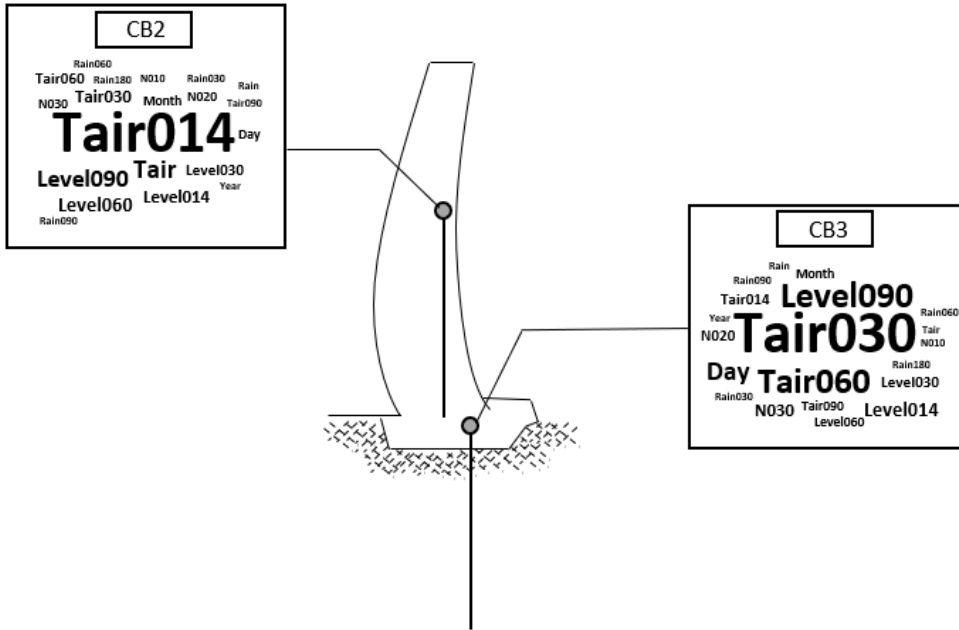
Figure 3. Word clouds for the radial displacements analyzed, using for Hyd GBR algorithm.

5 PARTIAL DEPENDENCE

In the conventional HST model, each external load's contribution can be associated with the value of the coefficient in the calibrated model. Fig. 4 displays the partial dependence plots for both radial displacements CB2 and CB3. The effect of the hydrostatic load illustrates that high levels imply more significant load and displacement towards downstream and vice-versa.
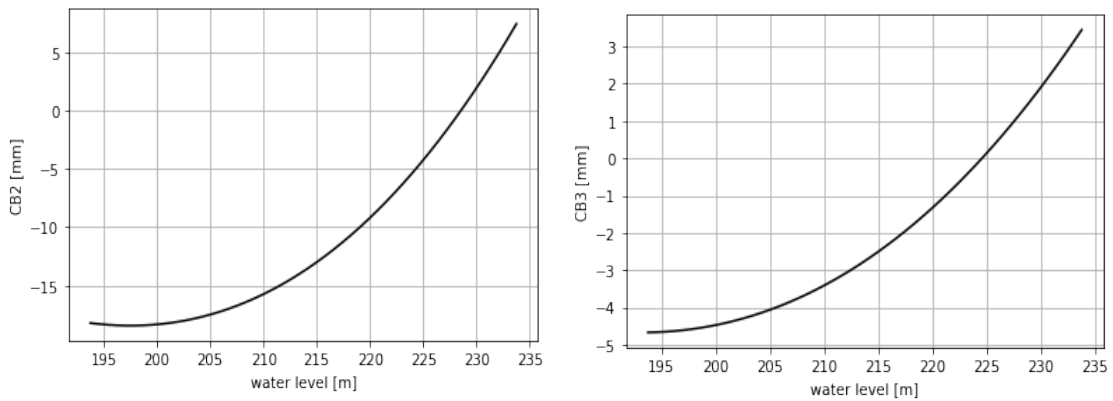
Figure 4. Partial dependence plot for the contribution of the environmental variables from an HST model for a radial displacement. Left: CB2, Right: CB3
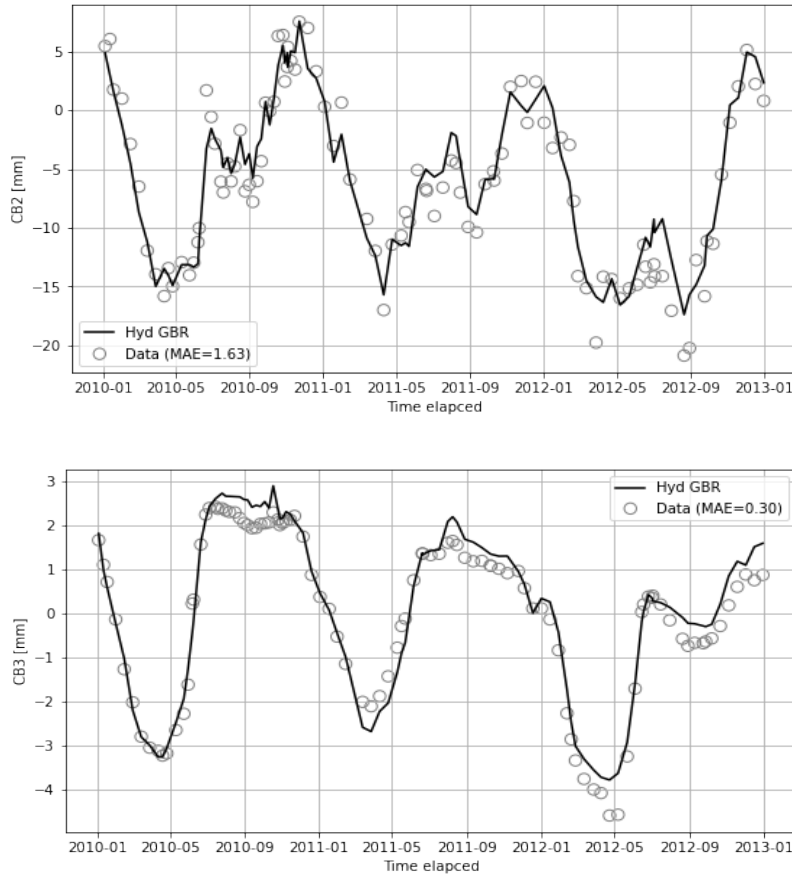
Figure 5. Measured data (circles) versus the Hyd GBR model (lines) for the test period. From top to bottom: CB2 and CB3.

6 MEASURES OF ACCURACY

Root Mean Squared Error (RMSE) and Mean Absolute Error (MAE) are metrics used to evaluate a prediction model. These metrics demonstrate our predictions' accuracy and the deviation from the actual values. Here, errors are the differences between predicted and actual values. It is calculated as follows:

$$MAE = \frac{\sum_{i=1}^{N} |y_i - F(x_i)|}{N} \tag{3}$$

where N is the size of the training (or test) set, y_i are the observed outputs and $F(x_i)$ the predicted values. In this paper, several predictive models have been used to predict the dam body's radial displacements. Tables 3 and 4 compare these methods' performance in training and test. The Hyd GBR clearly outweighs the others in test data. Fig. 5 compares the predictions of the Hyd GBR model with the measured data that does not take part in the training.

Table 3. MAE for each output and model, fitted on the whole training set (10 years). The minimum MAE are also underlined.

Target	HST	Hyd GBR	Hyd NN	GBR	XGboost	SVR
CB2	1.88	0.90	0.95	0.71	<u>0.38</u>	0.59
CB3	0.39	0.11	0.10	<u>0.09</u>	0.14	0.25

Table 4. MAE for each output and model, fitted on the test set (3 years). The minimum MAE are also underlined.

Target	HST	Hyd GBR	Hyd NN	GBR	XGboost	SVR
CB2	2.40	<u>1.63</u>	2.35	2.15	2.11	1.88
CB3	0.49	<u>0.30</u>	0.54	0.47	0.43	0.48

7 INTERVAL PREDICTION

A prediction interval is a quantification of the uncertainty on a prediction. It provides probabilistic upper and lower bounds on estimating an outcome variable. The main practical utility of Prediction intervals is the early detection of anomalies. It is necessary to compare the predictions with measured data and verify whether they fall within a predefined range. A prediction interval is calculated based on the variance of the predictive model residuals. For example, Kao and Loh [39] presented the 99% prediction intervals for models based on NN. Jung et al. [40] tested 1, 2, and 3 standard deviations of the residuals as the width of the prediction interval. The prediction interval in this work was set to $[\mu - 2\sigma, \mu + 2\sigma]$, being μ and σ the mean and the standard deviation of residuals, respectively. Fig. 6 shows that the test data for the case study of this paper is more or less in the range of the prediction intervals of the predictive model.
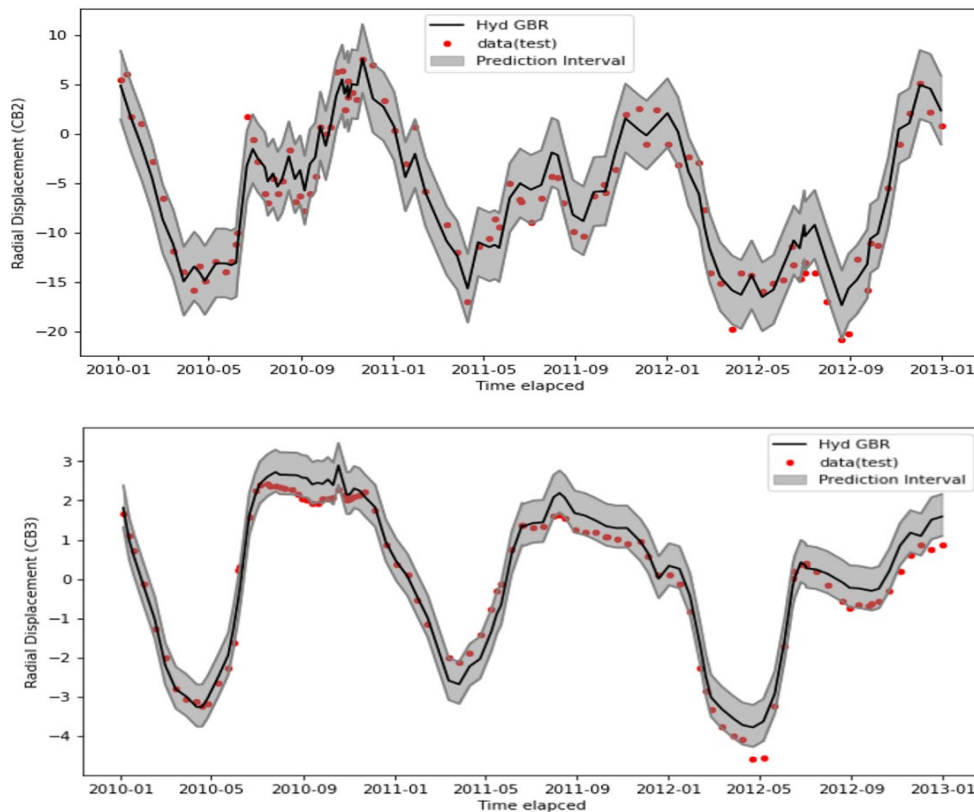
Figure 6. Typical output plot, with the test data (circles), the predictions (black line), and the prediction interval (shaded area).

8 NOVELTY DETECTION

One-Class SVM [41] is employed to conduct novelty detection in dam loading to prove our predictions fulfill the dam's behavior. For this purpose, the upstream reservoir level and the 14-day average air temperatures from 2000 to 2009 have been considered as input features for training. As shown in Fig. 7a, the trained one-class SVM covers most of the training data. Fig. 7b

shows a few novelties of the test data from 2010 to 2013. Thus, it shows that the test data is in the range of the training data, and the prediction should be in accordance with the measured data unless the current state of the dam differs from its state during the period between 2000 and 2009.
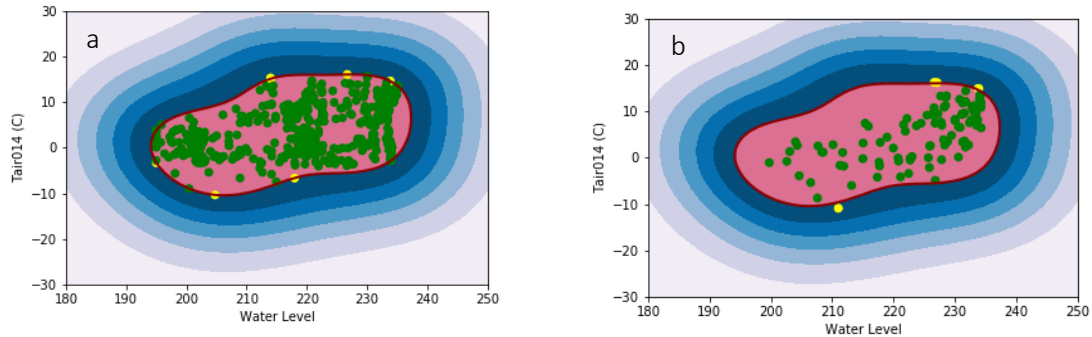
Figure 7. Novelty detection by utilizing One-Class SVM classification for training (a) and test (b) dataset proves the functionality of prediction.

9 SUMMARY AND CONCLUSIONS

In this study, different regression models were adopted and compared to predict the behavior of a double curvature arch dam. The dam is located in the south of France. Its data was presented in Theme A of the 16th International Benchmark Workshop on Numerical Analysis of Dams. It turned out that the machine learning techniques such as GBR, XGBoot, and SVR performed better than the conventional HST model for predicting the radial displacements of the central block of the dam. The authors proposed a hybrid model called the Hydrostatic Machine Learning (HML) model to have the advantages of the HST model and the machine learning techniques together. In this new model, the effect of the hydrostatic loads on the displacements is determined by a polynomial equation, and the impacts of the other contributory factors such as temperature, time, rainfall, etc., learned by a machine learning technique. In this study, Hyd. GBR and Hyd. NN models were utilized, and their results indicate that the Hyd. GBR can outperform the others in predicting the radial displacements of the dam body. Variable importance analysis showed that the most effective load with ignoring the hydrostatic load's effect is the dam's temperature. The novelty detection analysis revealed that the dam loads in the prediction period were in the range of the loads for which the predictive models had been trained. Thus, the measured displacements were expected to be in the prediction interval of the predictors.

REFERENCES

[1]   J. Mata, "Interpretation of concrete dam behaviour with artificial neural network and multiple linear regression models," Eng. Struct., vol. 33, no. 3, pp. 903–910, 2011, doi: 10.1016/j.engstruct.2010.12.011.

[2]   F. Salazar, M. T. Toledo, E. Oñate, and B. Suárez, "Interpretation of dam deformation and leakage with boosted regression trees," *Eng. Struct.*, vol. 119, pp. 230–251, 2016, doi: 10.1016/j.engstruct.2016.04.012.

[3]   F. Salazar, M. A. Toledo, E. Oñate, and R. Morán, "An empirical comparison of machine learning techniques for dam behaviour modelling," *Struct. Saf.*, vol. 56, pp. 9–17, 2015, doi: 10.1016/j.strusafe.2015.05.001.

[4]   A. De Sortis and P. Paoliani, "Statistical analysis and structural identification in concrete dam monitoring," *Eng. Struct.*, vol. 29, no. 1, pp. 110–120, 2007, doi: 10.1016/j.engstruct.2006.04.022.

[5]   P. Léger and M. Leclerc, "Hydrostatic, Temperature, Time-Displacement Model for Concrete Dams," *J. Eng. Mech.*, vol. 133, no. 3, pp. 267–277, 2007, doi: 10.1061/(asce)0733-9399(2007)133:3(267).

[6]   M. Tatin, M. Briffaut, F. Dufour, A. Simon, and J. P. Fabre, "Thermal displacements of concrete dams: Accounting for water temperature in statistical models," *Eng. Struct.*, vol. 91, pp. 26–39, 2015, doi: 10.1016/j.engstruct.2015.01.047.

[7]   F. Salazar and M. Toledo, "Discussion on 'Thermal displacements of concrete dams: Accounting for water temperature in statistical models,'" *Eng. Struct.*, vol. 171, pp. 1071–1072, 2018, doi: 10.1016/j.engstruct.2015.08.001.

[8]   F. Salazar, R. Morán, M. Toledo, and E. Oñate, "Data-Based Models for the Prediction of Dam Behaviour: A Review and Some Methodological Considerations," *Arch. Comput. Methods Eng.*, vol. 24, no. 1, pp. 1–21, 2017, doi: 10.1007/s11831-015-9157-9.

[9]   V. Ranković, N. Grujović, D. Divac, and N. Milivojević, "Development of support vector regression identification model for prediction of dam structural behaviour," *Struct. Saf.*, vol. 48, pp. 33–39, 2014, doi: 10.1016/j.strusafe.2014.02.004.

[10]   M. T. Cihan, "Comparison of artificial intelligence methods for predicting compressive strength of concrete," *Gradjevinar*, vol. 73, no. 6, pp. 617–632, 2021, doi: 10.14256/JCE.3066.2020.

[11]   F. Li, Z. Wang, and G. Liu, "Towards an Error Correction Model for dam monitoring data analysis based on Cointegration Theory," *Struct. Saf.*, vol. 43, pp. 12–20, 2013, doi: 10.1016/j.strusafe.2013.02.005.

[12]   D. Santillán, J. F. Miguel, and Á. Toledo, "Predicción de lecturas de aforos de filtraciones de presas bóveda mediante redes neuronales artificiales," *Tecnol. y ciencias del agua*, vol. 5, no. 3, pp. 81–96, 2014.

[13]   L. Cheng and D. Zheng, "Two online dam safety monitoring models based on the process of extracting environmental effect," *Adv. Eng. Softw.*, vol. 57, pp. 48–56, 2013, doi: 10.1016/j.advengsoft.2012.11.015.

[14]   S. Bonelli and K. Radzicki, "Impulse response function analysis of pore pressures in earthdams," *Eur. J. Environ. Civ. Eng.*, vol. 12, no. 3, pp. 243–262, 2008.

[15]   A. Simon, M. Royer, F. Mauris, and J. Fabre, "Analysis and interpretation of dam measurements using artificial neural networks," 2013.

[16]   F. Riquelme, J. Fraile, D. Santillán, R. Morán, and M. Toledo, "Application of artificial neural network models to determine movements in an arch dam," in *Proceedings of the 2nd international congress on dam maintenance and rehabilitation. Zaragoza, Spain*, 2011, pp. 117–123.

[17]   D. Santillán, J. Fraile-Ardanuy, and M. Á. Toledo, "Prediction of gauge readings of filtration in arch dams using artificial neural networks," *Tecnol. y ciencias del agua*, vol. 5, no. 3, pp. 81–96, 2014.

[18]   F. Perner, W. Koehler, and P. Obernhuber, "Interpretation of Schlegeis dam crest displacements," in *Proceedings of the 6th International Benchmark Workshop on Numerical Analysis of Dams. Salzburg, Austria*, 2001, pp. 17–19.

[19]   H. M. Gomes and A. M. Awruch, "Comparison of response surface and neural network with other methods for structural reliability analysis," *Struct. Saf.*, vol. 26, no. 1, pp. 49–67, 2004.

[20]   R. Fedele, G. Maier, and B. Miller, "Health assessment of concrete dams by overall inverse analyses and neural networks," *Int. J. Fract.*, vol. 137, no. 1–4, pp. 151–172, 2006.

[21]   Z. Wu and M. Abe, *Structural Health Monitoring and Intelligent Infrastructure: Proceedings of the First International Conference on Structural Health Monitoring and Intelligent Infrastructure, 13-15 November 2003, Tokyo, Japan*, vol. 1. Taylor & Francis, 2003.

[22]   N. Bakhary, H. Hao, and A. J. Deeks, "Damage detection using artificial neural network with consideration of uncertainties," *Eng. Struct.*, vol. 29, no. 11, pp. 2806–2815, 2007.

[23]   B. S. Wang and Z. C. He, "Crack detection of arch dam using statistical neural network based on the reductions of natural frequencies," *J. Sound Vib.*, vol. 302, no. 4–5, pp. 1037–1047, 2007.

[24]   C. M. Wen, S.-L. Hung, C.-S. Huang, and J. C. Jan, "Unsupervised fuzzy neural networks for damage detection of structures," *Struct. Control Heal. Monit. Off. J. Int. Assoc. Struct. Control Monit. Eur. Assoc. Control Struct.*, vol. 14, no. 1, pp. 144–161, 2007.

[25]   J. Liu, G. Wang, and Y. Chen, "Research and application of GA neural network model on dam displacement forecasting," in *Earth & Space 2008: Engineering, Science, Construction, and Operations in Challenging Environments*, 2008, pp. 1–9.

[26]   A. Joghataie and M. S. Dizaji, "Nonlinear analysis of concrete gravity dams by neural networks," in *Proceedings of the World Congress on Engineering*, 2009, vol. 2.

[27]   X. D. Yi, F. Xu, and C. K. Jiang, "Research on dam deformation forecast model based on genetic algorithm neural network," in *ISTM/2009: 8th international symposium on test and measurement*, 2009, pp. 1536–1539.

[28]   C. M. Bishop, "Neural networks: a pattern recognition perspective," 1996.

[29]   V. Ranković, N. Grujović, D. Divac, N. Milivojević, and A. Novaković, "Modelling of dam behaviour based on neuro-fuzzy identification," *Eng. Struct.*, vol. 35, pp. 107–113, 2012.

[30]   F. Restelli, "Systemic evaluation of the response of large dams instrumentation," *ICOLD Proceeding*, 2013.

[31] L. Piroddi and W. Spinelli, "Long-range nonlinear prediction: a case study," in *42nd IEEE International Conference on Decision and Control (IEEE Cat. No. 03CH37475)*, 2003, vol. 4, pp. 3984–3989.

[32] V. Saouma, E. Hansen, and B. Rajagopalan, "Statistical and 3d nonlinear finite element analysis of Schlegeis dam," in *Proceedings of the sixth ICOLD benchmark workshop on numerical analysis of dams*, 2001, pp. 17–19.

[33] G. Lombardi, "Advanced data interpretation for diagnosis of concrete dams," *CISM Udine, Italy*, 2004.

[34] L. Chouinard and V. Roy, "Performance of statistical models for dam monitoring data," in *Joint international conference on computing and decision making in civil and building engineering, Montreal*, 2006, pp. 14–16.

[35] R. Malm, R. Hellgren, M. Klun, A. Simonm, and F. Salazar, "Theme A: Behaviour prediction of a concrete arch dam," 16th International Benchmark Workshop on Numerical Analysis of Dams, 2021.

[36] H. Rao *et al.*, "Feature selection based on artificial bee colony and gradient boosting decision tree," *Appl. Soft Comput. J.*, vol. 74, pp. 634–642, Jan. 2019, doi: 10.1016/j.asoc.2018.10.036.

[37] T. Chen and C. Guestrin, "XGBoost: A Scalable Tree Boosting System," *Proc. 22nd ACM SIGKDD Int. Conf. Knowl. Discov. Data Min.*, doi: 10.1145/2939672.

[38] A. Widodo *et al.*, "Fault diagnosis of low speed bearing based on relevance vector machine and support vector machine," *Expert Syst. Appl.*, vol. 36, no. 3, pp. 7252–7261, Apr. 2009, doi: 10.1016/J.ESWA.2008.09.033.

[39] C. Y. Kao and C. H. Loh, "Monitoring of long-term static deformation data of Fei-Tsui arch dam using artificial neural network-based approaches," *Struct. Control Heal. Monit.*, vol. 20, no. 3, pp. 282–303, Mar. 2013, doi: 10.1002/STC.492.

[40] I. S. Jung, M. Berges, J. H. Garrett, and B. Poczos, "Exploration and evaluation of AR, MPCA and KL anomaly detection techniques to embankment dam piezometer data," *Adv. Eng. Informatics*, vol. 29, no. 4, pp. 902–917, Oct. 2015, doi: 10.1016/J.AEI.2015.10.002.

[41] B. Schölkopf, J. C. Platt, J. Shawe-Taylor, A. J. Smola, and R. C. Williamson, "Estimating the support of a high-dimensional distribution," *Neural Comput.*, vol. 13, no. 7, pp. 1443–1471, 2001.

INTERPRETABLE KELM DATA-DRIVEN MODEL FOR THE PREDICTION AND MONITORING OF ARCH DAM BEHAVIOUR

Chaoning Lin

College of Water Conservancy and Hydropower Engineering, Hohai University, Nanjing, Jiangsu, China
College of Civil and Transportation Engineering, Hohai University, Nanjing, Jiangsu, China

Siyu Chen

Nanjing Hydraulic Research Institute, Nanjing, Jiangsu, China
College of Water Conservancy and Hydropower Engineering, Hohai University, Nanjing, Jiangsu, China

  chen.siyu@hhu.edu.cn

Mohammad Amin Hariri-Ardebili

University of Colorado, Boulder, CO, USA
University of Maryland College Park, MD, USA

ABSTRACT: This paper presents a kernel extreme learning machine (KELM)-based nonlinear data-driven model for the dam behavior (i.e., radial displacement and seepage) prediction, where the model hyperparameters are determined using particle swarm algorithm (PSO) and internal cross-validation to overcome overfitting. The model inputs are composed of the reservoir water height, measured temperature, and rainfall variables. The global sensitivity analysis coupled with the KELM model is proposed for the model interpretation. The warning thresholds of the arch dam radial displacement and seepage are determined via the confidence interval method based on the fitting results.

1 INTRODUCTION

Concrete dams play important roles in the social and economic fields by flood control, power generation, water supply, and irrigation. During the service period, dams are subjected to a variety of operational and environmental loads and occasionally encounter some unconventional events or extreme loads (such as excessive flooding, droughts, earthquakes, etc.). Moreover, the overall performance of the concrete structures may decrease over time due to age-related deterioration, hydraulic erosion, and other factors. If a dam is not well managed and maintained, failures may occur, leading to economic and life losses in reservoir regions.

The displacement and seepage are two critical indicators that can intuitively reflect the operational status of a dam. With the rapid development of artificial intelligence (AI) since the end of the past century, there has been growing interest in adopting machine learning (ML) methods in dam engineering. Many ML methods have been adopted for dam behavior prediction and monitoring, such as auto-associative neural networks (Kao et al., 2013), support vector regression (Rankovic et al., 2014), boosted regression trees (Salazar et al., 2015), random forest (Belmokre et al., 2019; X. Li et al., 2019), Gaussian process regression (Lin et al., 2019), and long short-term memory network (Liu et al., 2020).

This study establishes a kernel extreme learning machine (KELM)-based nonlinear data-driven model to predict the dam displacement and seepage. The model hyperparameters are optimized using a particle swarm algorithm (PSO) and cross-validation. To mine the influencing factors of model inputs and provide support for decision-making, the global sensitivity analysis coupled with the KELM model is implemented for the model interpretation. The warning thresholds of the dam radial displacement and seepage are determined using the confidence interval method.

The rest of the paper is summarized as follows: Section 17 describes the statistical model of dam behavior and inputs. The theory of the KELM prediction model, warning thresholds of dam behavior, and model interpretation method are then introduced in Section 3. Results and discussion are presented in Section 4. Finally, Section 5 summarizes the findings.

2 STATISTICAL MODEL OF DAM BEHAVIOR

2.1 *Statistical model of dam displacement*

Displacement (denoted by δ) is a key indicator for evaluation of the dam behavior. In general, the displacements of the arch dam are assumed to be dependent on hydrostatic load, temperature, and time, which can be quantitatively interpreted and approximated as:

$$\delta = \delta_H + \delta_T + \delta_\theta \tag{1}$$

where δ_H, δ_T, and δ_θ represents the hydrostatic component, temperature component and time component, respectively.

Under the action of water pressure, hydrostatic component δ_H can be described by a polynomial function consisting of reservoir water height H and coefficients a_i $(i = 0 \sim 4)$ (Mata, 2011):

$$\delta_H = a_0 + a_1 H + a_2 H^2 + a_3 H^3 + a_4 H^4 \tag{2}$$

Temperature component δ_T describes the displacement caused by the temperature changes in bedrock and dam concrete. The temperature variation of the dam is mainly influenced by changes of air temperature. Meanwhile, there is a hysteresis effect between the air temperature and the dam internal temperature. Therefore, if the air temperatures are available and continuous, the temperature component δ_T can be quantitatively represented by a polynomial function consisting of segmented air temperature T_{A-B} (Kang et al., 2019), as:

$$\delta_T = \sum_{i=1}^{n} b_i T_{A-B} \tag{3}$$

where T_{A-B} denotes the average ambient temperatures A to B days before the day of observation, b_i $(i = 1 \sim 6)$ are coefficients. In this paper, T_0, T_{1-2}, T_{3-7}, T_{8-15}, T_{16-30}, and T_{31-60} are

selected as the temperature factors. It is noted that T_0 represents the temperature of the observation day.

Time component δ_θ reflects the irreversible deformation of the dam body or dam foundation toward a certain direction over time. According to the previous research (Lin et al., 2019; Y. Q. Shi et al., 2018), different and strictly monotone functions can be used for modelling the time component δ_θ, as:

$$\delta_\theta = c_1\theta + c_2\ln\theta + c_3(1 - e^{-\theta}) + c_4(\theta/\theta + 1) \tag{4}$$

where $\theta = t/100$, and t denotes number of days since the beginning of the analysis, c_1, c_2, and c_3 are coefficients.

Thus, the expression of statistical model for arch dam displacement analysis is as follows:

$$\delta = a_0 + a_1H + a_2H^2 + a_3H^3 + a_4H^4 + b_1T_0 + b_2T_{1-2} + b_3T_{3-7} + b_4T_{8-15} + b_5T_{16-30} + b_6T_{31-60} + \\ c_1\theta + c_2\ln\theta + c_3(1 - e^{-\theta}) + c_4(\theta/\theta + 1) \tag{5}$$

2.2 *Statistical model of dam seepage*

Excluding the hydrostatic load, temperature and time effects, the seepage (denoted by S) of the arch dam is also dependent on the rainfall effect, and the seepage response can be quantitatively interpreted and approximated by the following equation:

$$S = S_H + S_T + S_R + S_\theta \tag{6}$$

where S_H, S_T, and S_θ represent the hydrostatic component, temperature component, and time component, respectively, sharing the same form as shown in Equation (2)~(4). S_R denotes the rainfall component. Considering the lag effect between the rainfall and the external seepage changes, a polynomial function consisting of segmented rainfall factors R_{A-B} are utilized to simulate the rainfall component:

$$S_R = \sum_{i=1}^{m} d_i R_{A-B} \tag{7}$$

where R_{A-B} denotes the average rainfall A to B days before the response day of the observation. In this paper, R_0, R_{1-2}, R_{3-7}, R_{8-15}, R_{16-30}, and R_{31-60} are selected as the segmented rainfall factors, where R_0 denotes the rainfall of the observation day.

Thus, the expression of statistical model for arch dam seepage analysis is as follows:

$$S = a_0 + a_1H + a_2H^2 + a_3H^3 + a_4H^4 + b_1T_0 + b_2T_{1-2} + b_3T_{3-7} + b_4T_{8-15} + b_5T_{16-30} + b_6T_{31-60} + \\ R_0 + R_{1-2} + R_{3-7} + R_{8-15} + R_{16-30} + R_{31-60} + c_1\theta + c_2\ln\theta + c_3(1 - e^{-\theta}) + c_4(\theta/\theta + 1) \tag{8}$$

3 METHODOLOGY OF DAM BEHAVIOR PREDICTION AND WARNING

3.1 *Optimized kernel extreme learning machine*

Extreme learning machine (ELM) is an extension algorithm of the single layer feedforward network (SLFN) that can be used for regression, classification, and clustering (Huang et al., 2006). As opposed to the traditional artificial neural network based on gradient descent learning algorithm, ELM has a stochastic nature. It randomly assigns the input weights and the hidden layer biases, and then keep them fixed without iteratively tuning. In recent years, a novel variant of ELM called kernel extreme learning machine (KELM) has been proposed by (Huang et al., 2012), which integrates the advantages of ELM and kernel trick. The KELM was shown to achieve a better prediction performance and stability than prototype ELM with less computational cost (Ding et al., 2013).

The output of the ELM for generalized SLFNs can be written as

$$F_t = \sum_{i=1}^{N} \beta_i \mathbf{h}\left(a_i \cdot x_j + b_i\right)_j, \; j = 1,\ldots,N \tag{9}$$

where a_i denotes the weight vector linking ith hidden node and the input nodes; $\boldsymbol{\beta}_i$ presents the weight vector connecting jth hidden node and the output nodes; b_i is the threshold of ith hidden node. $\mathbf{h}$ refers to the activation functions.

The training goal is to find the best output weight $\boldsymbol{\beta}$, which can be computed by the least square method:

$$\boldsymbol{\beta} = \mathbf{H}^\dagger \mathbf{T} \tag{10}$$

where $\mathbf{H}^\dagger$ denotes the Moore-Penrose (MP) generalized inverse of the hidden layer output, and $\mathbf{T} = [t_1, t_2, \ldots, t_N]^T$ presents the target vector.

For complex prediction task, hidden layer feature mapping is typically unknown. Thus, the kernel function is introduced to replace the feature mapping function. On the basis of the orthogonal projection method, the MP generalized inverse matrix $\mathbf{H}^\dagger$ can be calculated by $\mathbf{H}^\dagger = \mathbf{H}^T\left(\mathbf{HH}^T\right)^{-1}$, and the output weight β can be computed by adding a positive constant, $1/C$. Therefore, the output function of KELM can be briefly described given by

$$F(x) = \mathbf{h\beta} = \mathbf{h}(x)\mathbf{H}^\dagger \left(\frac{I}{C} + \mathbf{HH}^\dagger\right)^{-1} \mathbf{T} = \begin{bmatrix} K(x_1, x) \\ \mathrm{M} \\ K(x_N, x) \end{bmatrix}^T \left(\frac{\mathbf{I}}{C} + \Omega_{ELM}\right)^{-1} T \tag{11}$$

where $K(x_i, x)$ is the kernel function and should satisfy the Mercer condition. In this study, Gaussian kernel $K(x_i, x) = \exp(-\|x_i - x\|^2 / 2\gamma^2)$ and linear kernel $K(x_i, x) = x_i^T \cdot x + \gamma$ are used in KELM modelling. Therefore, the main parameters of KELM herein are regularization parameter C, and kernel parameters γ.

The performance of the KELM model is controlled by hyperparameters C and γ. To make sure the model brings good generalization and robust performance, particle swarm optimizer (PSO) (Y. H. Shi et al., 1998) was combined with 3-fold cross-validation to determine the optimal parameters. In 3-fold cross-validation, the training data is divided into an internal validation set and an internal training set. For the PSO algorithm, the population size is set to 20, and the maximal iteration is set to 20 as the stopping criteria. In each iteration, P is the dimensions of the hyperparameters to be optimized, the position vector $\mathbf{X}_i = \left[x_i^1, x_i^2, \ldots, x_i^P\right]$ and the velocity vector $\mathbf{V}_i = \left[v_i^1, v_i^2, \ldots, v_i^P\right]$ are updated once by the following equations:

$$v_i^P = v_i^P + c_1 \cdot rand_1^P \cdot \left(pbest^P - x_i^P\right) + c_2 \cdot rand_2^P \cdot \left(nbest_i^P - x_i^P\right)$$
$$x_i^P = x_i^P + v_i^P \tag{12}$$

where c_1 and c_2 are two acceleration coefficients with the values are set as 2.0. $rand_1^P$ and $rand_2^P$ denote the two random numbers generated independently within [0, 1]. $pbest_i^P$ denotes the position with the best-known fitness of the ith particle, and $nbest^P$ represents the best global position in $pbest_i^P$.

In each iteration, the error function of PSO is evaluated by mean squared error of prediction ($MSEP_{cv,k}$), as shown in Equation (13):

$$MSEP_{cv,k} = \frac{1}{n}\sum_{k=1}^{K}\sum_{i=1}^{n}\left(\hat{y}_i - y_i\right)^2 \tag{13}$$

where n represents the number of samples, K represents the number of folds. $\hat{y}_i$ is the predicted value of the internal validation samples, y_i is the measured value of the internal validation samples.

3.2 *Warning thresholds of dam behavior*

The confidence interval method (B. Li et al., 2019) is used for dam behavior monitoring and determine the warning thresholds. If the measured value falls within the interval range, it is

regarded as a safe value. Otherwise, it is regarded as anomalous and may raise alarm. The expression of the confidence interval (CI) is given in Equation (14):

$$CI = [(\hat{y} - \alpha\sigma), (\hat{y} + \alpha\sigma)]; \ \sigma = \sqrt{\sum_{i=1}^{N_t} (e_i - \bar{e})^2 \bigg/ N_t - 1} \tag{14}$$

where $\hat{y}$ represents the fitted or predicted value of dam behavior, σ is the standard deviation, N_t represents the number of the training samples. $e_i = (y_i - \hat{y}_i)$, where $\bar{e}$ is the mean value of e_i, y_i is the measured value of dam behavior, and $\hat{y}_i$ is the fitted value of dam behavior.

It is noted that abnormal values may not be identified if the confidence interval is relatively wide. In contrast, if the range is too narrow, many values may be deemed as abnormal mistakenly (Wu, 2003), thereby resulting in many false positives. In general, the effectiveness of confidence interval is influenced by the input selection, performance of the KELM model, and hyperparameters tuning, which need to be determined with caution. Considering the dam status and risk level, the extreme case scenario is considered, the significance level is set as 1%, and therefore, $\alpha \approx 2.58$.

3.3 *Global sensitivity analysis for model interpretation*

KELM predictive model contains the disadvantages of black box characteristics, and the trained date-driven model is typically difficult to be understood. Inspired by (Chen et al., 2020; Cortez et al., 2013) pioneer work, we combined global sensitivity analysis (GSA) with the PSO-KELM to interpretate the dam behavior prediction model. This method allows us to compute the relative importance of input variables or any group combination of them. The main idea of the GSA is to hold all input variables at given value except the specific variable to be computed, and then calculate the output weight of the corresponding input by the available formula. The detailed procedure of the GSA is described in Table 5, where m and n are the number of input attributes and samples, respectively. M is the number of subgroups (each subgroup contains at least one input attribute). $\mathbf{X}^{(k)}$ is the generated meta-inputs by holding all input variables at their mean values except k th attributes, and $k \leq M$. $\hat{\mathbf{y}}^{(k)}$ represents the obtained output via inputting the $\mathbf{X}^{(k)}$ to the trained model, and $\tilde{y}$ denotes the median value of the measured leakage $\mathbf{Y}^{(n \times 1)}$. In principle, the proposed GSA can be applied to any supervised machine learning algorithm for regression tasks.

Table 5. Global sensitivity analysis for model interpretation.

Inputs: Training samples $\mathbf{X}^{(n \times m)}, \mathbf{Y}^{(n \times 1)}$
Outputs: Relative importance $\mathbf{RI}$

Divide $\mathbf{x}$ into k groups of attributes, $k \in [1, M]$
for $k = 1, \ldots, M$
    Build $\mathbf{X}^{(k)}$ by holding each input variables at their mean values except k th attributes
    $\hat{\mathbf{y}}^{(k)} = f(\mathbf{X}^{(k)})$
    $z_k = \sum_{i=1}^{n} |\hat{y}_i^{(k)} - \tilde{y}| / (n - 1)$
end for
for $k = 1, \ldots, M$
    $RI_k = z_k / \sum_{k=1}^{M} z_k \times 100\%$
end for

---

4 RESULTS AND DISCUSSION

4.1 *Case study*

4.1.1 Brief introduction of dam project

The case study of the benchmark is a double curvature arch dam called Dam_EDF, which is located in the south of France. The dam was constructed between 1957 and 1960. The maximum dam height above the foundation is about 45m, with the crest length being 166 m. To monitor the dam service status, the dam is equipped with a comprehensive monitoring system and instruments. Figure 1 presents the illustrations of the dam project.
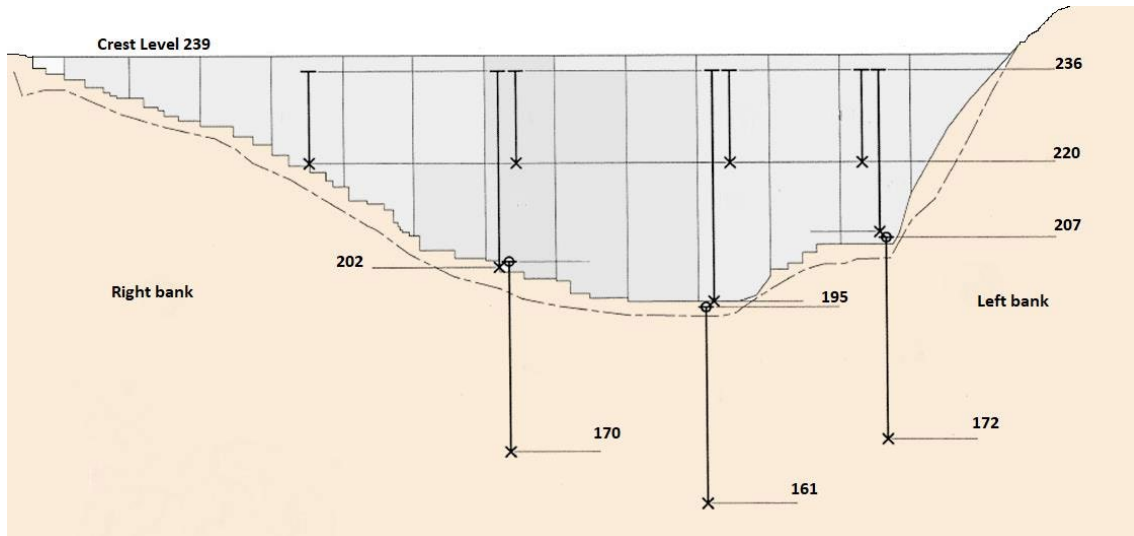
Figure 1. Downstream view of Dam_EDF.

4.1.2 Data collection

In this benchmark, the radial dam displacement and seepage are used for analysis. For the radial dam displacement (unit is mm), the measurements of pendulums on the Central Block (CB) are provided for analysis, where CB2 is the radial displacement between the altitudes 236 m (dam crest) and 196 m (dam toe), while CB3 is the radial displacement in the foundation between the altitudes 195 m and 161 m. For the seepage (unit is L.min^{-1}), the flowrate is measured using a weir located in the gallery at the downstream dam toe. The time series of dam behavior data are provided from 2000 to 2012.

The corresponding ambient data includes the water level, temperature, and rainfall (see Figure 2 ~Figure 4). The water level of the reservoir is collected per day. Since Dam_EDF is located on the top of a glacial threshold, the reservoir water height is 0 once the water level is lower than +196 m. The air temperature is not measured at the dam location, therefore, the provided calculated temperature called 'T_b' is used herein for temperature factors generation. 'T_b' is calculated by interpolation from several air temperature measuring stations. The interpolation takes into account the altitude of the dam and is calculated on a mesh of 1 square kilometer. Daily rainfall precipitation is collected from a rain gauge located about 5 km from Dam_EDF. The time series of the ambient data is provided from 1995 to 2017. It is noted that the provided data of the benchmark is automatically checked, and there is no need for any further cleaning.

Figure 2. Time series of the reservoir water height.
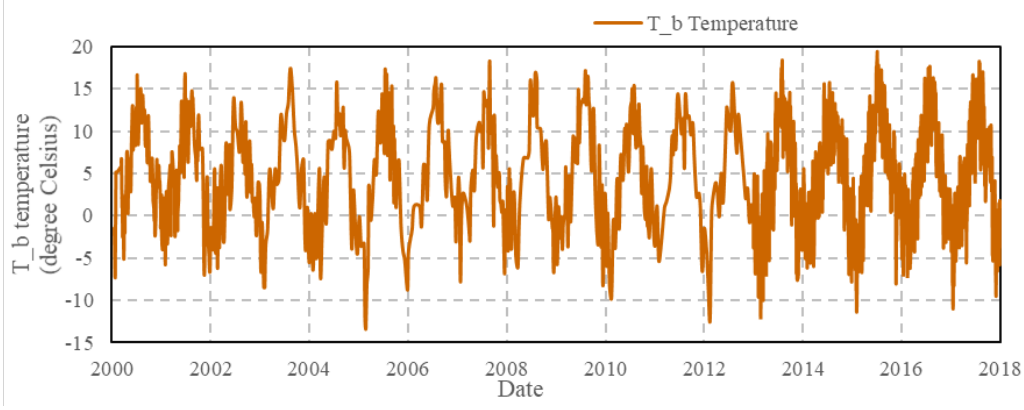
Figure 3. Time series of the T_b air temperature.
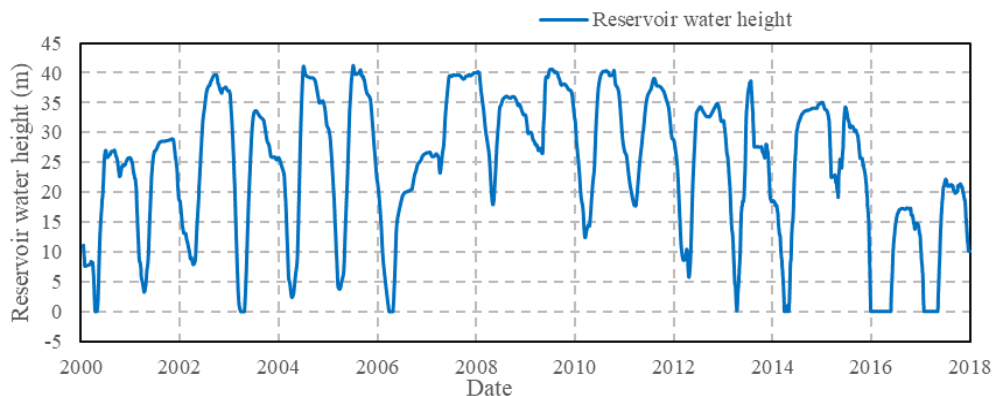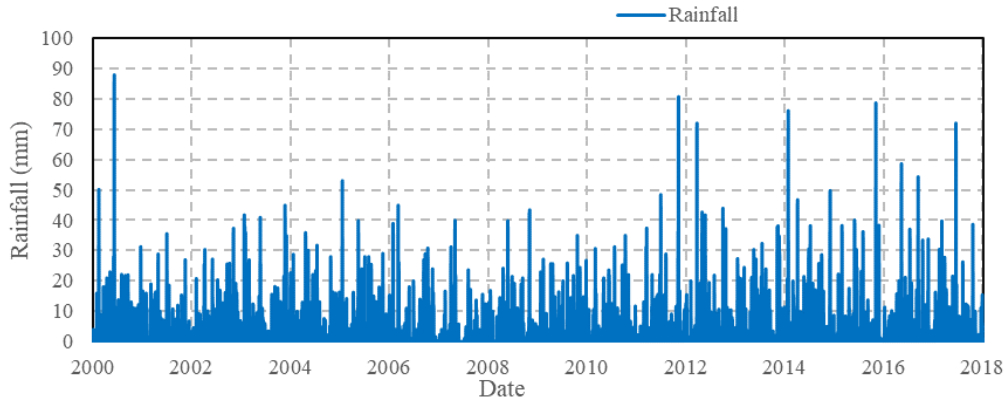

Figure 4. Time series of the daily rainfall.

4.2 *Model calibration and prediction*

Considering the fact that the dam construction was finished in 1960, and the initial modelling year is 2000, time component variables are not chosen for model inputs in this study. According to the relevant contents summarized in Section 96, the model input variables of dam displacement $\mathbf{x}_\delta$ and seepage $\mathbf{x}_S$ are shown as follows:

$$\mathbf{x}_\delta = \left\{ H, H^2, H^3, H^4, T_0,\ T_{1-2}, T_{3-7}, T_{8-15}, T_{16-30}, T_{31-60}, \right\} \tag{15}$$

$$\mathbf{x}_S = \left\{ H, H^2, H^3, H^4, T_0,\ T_{1-2}, T_{3-7}, T_{8-15}, T_{16-30}, T_{31-60}, R_0,\ R_{1-2}, R_{3-7}, R_{8-15}\ , R_{16-30}, R_{31-60} \right\} \tag{16}$$

where the time component factors are generated.

Prior to model implementation, all the inputs should be normalized within the range of [0,1] by Equation (17), where x_i is i th individual variable in input matrix $\mathbf{x}$.

$$m(x_i) = \frac{x_i - \min(\mathbf{x})}{\max(\mathbf{x}) - \min(\mathbf{x})} \tag{17}$$

The measured radial displacement and seepage from 2000-01-19 to 2012-12-31 are utilized for model training and calibration, and the rest measured radial displacement from 2013-01-01 to 2017-12-31 are utilized for validation of prediction performance. By implementing the model introduced in Section 1.25, the hyperparameters C and γ are tuned within the range of (0,1000] and (0,10], respectively. The obtained hyperparameters for KELM prediction model are listed in Table 6. The calibration and prediction results of CB2 displacement, CB3 displacement, and seepage are shown in Figure 5 ~ Figure 7, respectively.

Table 6. The hyperparameters of PSO-KELM data-driven models.

Hyperparameters	CB2 displacement	CB3 displacement	Seepage
C	970.04	692.26	246.36
γ	7.61	0.64	9.09

Figure 5. Performance of the PSO-KELM model for CB2 displacement simulation. (Linear kernel is used in KELM)

Figure 6. Performance of the PSO-KELM model for CB3 displacement simulation. (Linear kernel is used in KELM)
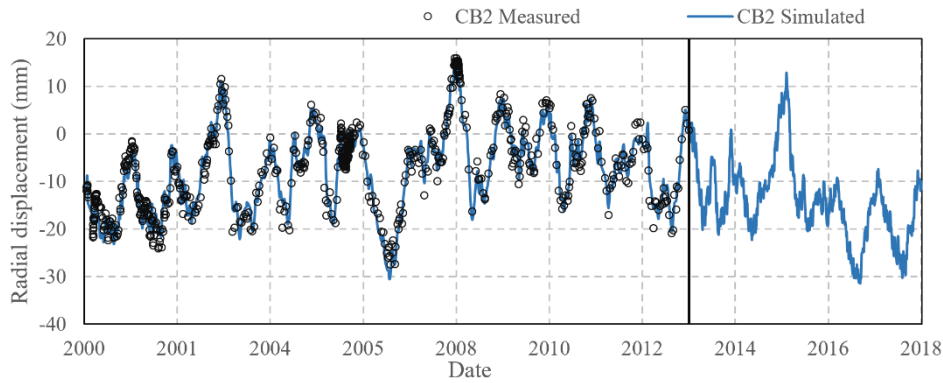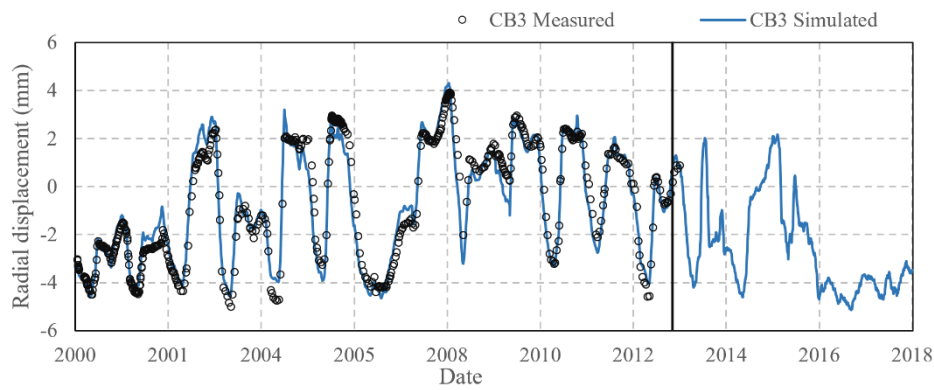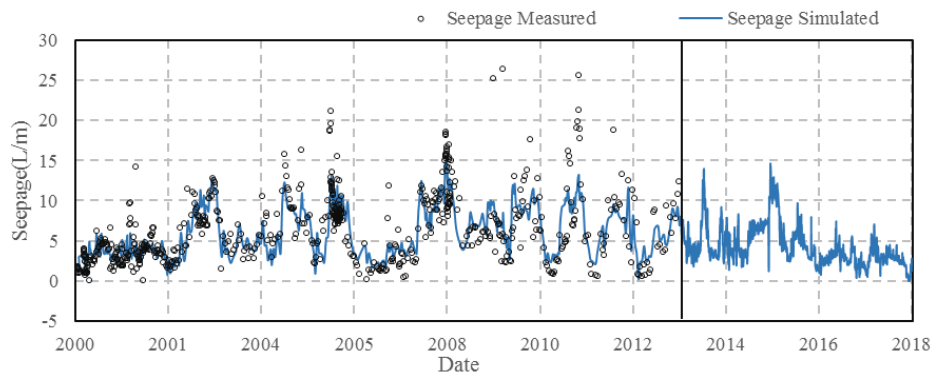

Figure 7. Performance of the PSO-KELM model for seepage simulation. (Gaussian kernel is used in KELM)

The calibration results of displacement and seepage are validated in terms of the mean absolute error and normalized root mean squared error (NRMSE), see Table 7.

$$\text{MAE} = \frac{1}{N} \sum_{i=1}^{N} |Y_i - P_i| \tag{18}$$

$$\text{NRMSE} = \frac{\sqrt{\sum_{i=1}^{N} (Y_i - P_i)^2 \Big/ N}}{Y_{max} - Y_{min}} \tag{19}$$

where N is the number of time stamps in the corresponding period, Y_{max} and Y_{min} are maximum and minimum measured value of dam behavior in the corresponding period, Y_i denotes the measured value of dam behavior, and P_i denotes the simulated value of dam behavior.

From the obtained results shown above, the PSO-KELM model provides satisfactory fitting performance of dam behavior. Most of the measured values are within the interval range except the very few measurements at the peak value.

Table 7. The metrics of calibration results.

Metrics	CB2 displacement	CB3 displacement	Seepage
MAE	1.470	0.432	1.710
NRMSE	0.044	0.045	0.095

4.3 *Model interpretation*

The relative importance of input factors via PSO-KELM coupled with GSA method is depicted in Figure 8, where the relative importance of two top dominated input variables in each kind of component is shown by the bar plot. It is found that the hydrostatic component plays a crucial role in the state of dam displacement and seepage, followed by the temperature component. However, the seepage of the dam is not sensitive to the rainfall variables, indicating that the rainfall component of the dam seepage is negligible. It must be explained with great caution that the obtained results herein are not able to quantitatively assess each input contributes for dam behaviors, but only the relative sensitivity degree of the dam behavior to each input variable.
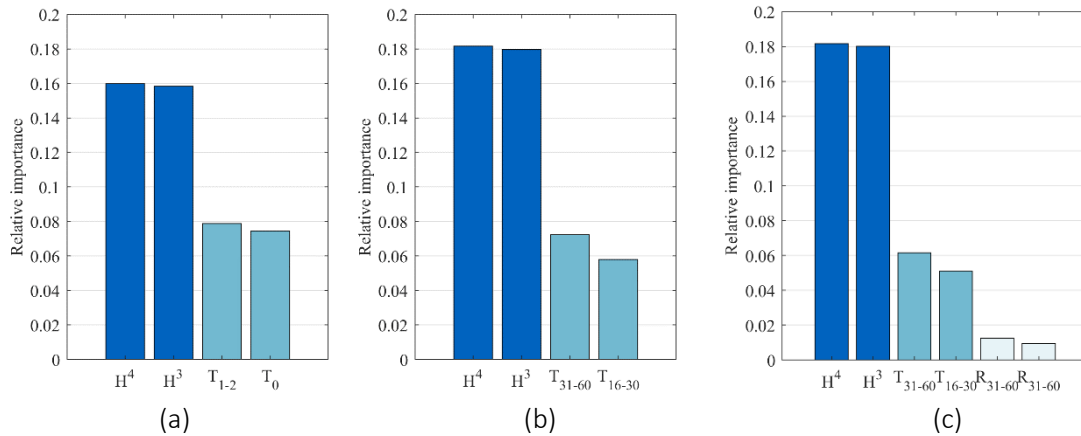
Figure 8. Relative importance of input factors via PSO-KELM model coupled with GSA method: (a) CB2 displacement, (b) CB3 displacement, (c) Seepage

5 CONCLUSIONS

In this paper, we proposed an interpretable PSO-KELM data-driven model for the prediction and monitoring of arch dam behavior (i.e., displacement and seepage). The effects of the reservoir water height, daily temperature, daily rainfall, and time were considered for inputs factors generation. By combining the PSO and 3-folds cross-validation with KELM, the hyperparameters were adaptively determined to guarantee the model generalization. Benefitting from the powerful nonlinear mapping and interpretable capability, the model provided satisfactory simulation

performance and reasonable interpretations. It could be learned from the results that the hydrostatic component accounts most for the dam displacement and seepage, while the temperature component came second. The rainfall component of seepage was negligible.

REFERENCES

Belmokre, A., Mihoubi, M. K., & Santillan, D. 2019. Analysis of Dam Behavior by Statistical Models: Application of the Random Forest Approach. *KSCE Journal of Civil Engineering,* 23(11), 4800-4811.

Chen, S. Y., Gu, C. S., Lin, C. N., Wang, Y., & Hariri-Ardebili, M. A. 2020. Prediction, monitoring, and interpretation of dam leakage flow via adaptative kernel extreme learning machine. *Measurement,* 166.

Cortez, Paulo, & Embrechts, Mark J. 2013. Using sensitivity analysis and visualization techniques to open black box data mining models. *Information Sciences,* 225, 1-17.

Ding, S. F., Zhao, H., Zhang, Y. N., Xu, X. Z., & Nie, R. 2013. Extreme learning machine: algorithm, theory and applications. *Artificial Intelligence Review,* 44(1), 103-115.

Huang, G. B., Zhou, H., Ding, X., & Zhang, R. 2012. Extreme learning machine for regression and multiclass classification. *IEEE Trans Syst Man Cybern B Cybern,* 42(2), 513-529.

Huang, G. B., Zhu, Q. Y., & Siew, C. K. 2006. Extreme learning machine: Theory and applications. *Neurocomputing,* 70(1-3), 489-501.

Kang, F., Li, J. J., Zhao, S. Z., & Wang, Y. J. 2019. Structural health monitoring of concrete dams using long-term air temperature for thermal effect simulation. *Engineering Structures,* 180, 642-653.

Kao, C. Y., & Loh, C. H. 2013. Monitoring of long-term static deformation data of Fei-Tsui arch dam using artificial neural network-based approaches. *Structural Control & Health Monitoring,* 20(3), 282-303.

Li, B., Yang, J., & Hu, D. X. 2019. Dam monitoring data analysis methods: A literature review. *Structural Control and Health Monitoring,* 27(3).

Li, X., Wen, Z. P., & Su, H. Z. 2019. An approach using random forest intelligent algorithm to construct a monitoring model for dam safety. *Engineering with Computers*.

Lin, C. N., Li, T. C., Chen, S. Y., Liu, X. Q., Lin, C., & Liang, S. L. 2019. Gaussian process regression-based forecasting model of dam deformation. *Neural Computing & Applications,* 31(12), 8503-8518.

Liu, W. J., Pan, J. W., Ren, Y. S., Wu, Z. G., & Wang, J. T. 2020. Coupling prediction model for long‐term displacements of arch dams based on long short‐term memory network. *Structural Control and Health Monitoring,* 27(7).

Mata, J. 2011. Interpretation of concrete dam behaviour with artificial neural network and multiple linear regression models. *Engineering Structures,* 33(3), 903-910.

Rankovic, V., Grujovic, N., Divac, D., & Milivojevic, N. 2014. Development of support vector regression identification model for prediction of dam structural behaviour. *Structural Safety,* 48, 33-39.

Salazar, F., Toledo, M. A., Onate, E., & Moran, R. 2015. An empirical comparison of machine learning techniques for dam behaviour modelling. *Structural Safety,* 56, 9-17.

Shi, Y. H., & Eberhart, R. 1998. A modified particle swarm optimizer. *1998 Ieee International Conference on Evolutionary Computation - Proceedings*, 69-73.

Shi, Y. Q., Yang, J. J., Wu, J. L., & He, J. P. 2018. A statistical model of deformation during the construction of a concrete face rockfill dam. *Structural Control & Health Monitoring,* 25(2).

Wu, Z.R. 2003. *Safety monitoring theory and its application of hydraulic structures*. Beijing: Higher Education.

DAM BEHAVIOUR PREDICTION USING AN ENSEMBLE OF BAYESIAN DYNAMIC LINEAR MODEL AND BAYESIAN LSTM NETWORKS

Bhargob Deka[1]
Department of Civil Engineering, Polytechnique Montreal, Montreal, Canada

Van-Dai Vuong[2]
Department of Civil Engineering, Polytechnique Montreal, Montreal, Canada

James-A. Goulet
Department of Civil Engineering, Polytechnique Montreal, Montreal, Canada

Patrice Côté
Direction of Dams and Infrastructure Expertise, Hydro-Québec, Montreal, Canada

Benjamin Miquel
Direction of Dams and Infrastructure Expertise, Hydro-Québec, Montreal, Canada

ABSTRACT: In this paper, we present our submission to the ICOLD benchmark for the two pendulum datasets (CB2 & CB3). Our approach relies on the ensembling of a *Bayesian dynamic linear model* (BDLM) along with *Bayesian long short-term memory* (LSTM) neural networks that use the *tractable approximate Gaussian inference method* (TAGI) for learning its parameters. We provide through our probabilistic ensembling method, the explainability of BDLMs as well as the accuracy and ease of use of Bayesian LSTM. Although the benchmark focusses on prediction accuracy and threshold value definition for the purpose of anomaly detection, one should keep in mind that this way of envisioning anomaly detection is only one approach among many others. We show in this paper that with our probabilistic regime switching method we expect to be able to detect anomalies of 0.5mm for CB2 and 0.15mm for CB3, where both cases, anomalies can develop over the span of years.

[1] equal contribution

[2] equal contribution

1 INTRODUCTION

Sensor-based structural health monitoring (SHM) is an established tool for informing dam owners and managers about the occurrence of abnormal events as well as the general condition of the structure. Although it is a routine task to measure structural responses such as displacements, inclinations, pressure, or flow rates using commercial technologies, it is much harder to extract information and knowledge from data. In the context of dam monitoring, the hydrostatic-seasonal-time (HST) method (Salazar et al., 2017) is the most common approach to model the dependency between structural responses and water level, seasonal components and time. The HST method has passed the test of time, nevertheless, it has several limitations; (1) it has a limited forecasting capacity when the relationship between the explanatory variables or their components are non-linear, or affected by a phase shift; (2) it is an offline method, i.e., the model is built using a training set so that it requires periodic retraining in order to adapt to new conditions not covered during training. This affects the capacity to detect anomalies that are building up over years as model re-training will capture a part of the anomaly in the model itself. The research community is still figuring out what are the options to overcome these limitations. In this context, the ICOLD workshop on dam behaviour prediction aims at comparing various methods with respect to their *predictive capacity, anomaly detection capacity* and *interpretability*.

In this paper, we present our submission to the ICOLD benchmark for the two pendulum datasets (CB2 \& CB3). Our approach relies on the ensembling of a *Bayesian dynamic linear model* (BDLM) (Gaudot et al., 2019) along with Bayesian *long short-term memory* (LSTM) neural networks (Goodfellow et al., 2016) that rely on the *tractable approximate Gaussian inference* method (TAGI) (Goulet et al., 2021) for learning its parameters. BDLMs enables non-linear dependencies between model sub-components, is an online method capable of updating itself as new data comes in, is inherently probabilistic so that it can handle epistemic and aleatory uncertainties, and it allows explaining the dependencies within the model. LSTMs excel at forecasting without requiring feature engineering regarding the interactions between structural responses, explanatory variables and other latent variables and its coupling with the TAGI method makes it inherently probabilistic as well. Ensembling (Sagi & Rokach, 2018) is a common approach in order to aggregate the predictions from several models with the objective of improving the accuracy through the cancellation of the model errors in the case they are statistically independent.

The paper is organized as follow: Section 2 presents the dataset employed as well as the pre-processing steps we applied on the data. Section 3 presents the methodologies behind the BDLM, LSTM, and ensembling methods. Section 4 presents the results regarding validation, forecasting, and model interpretation where we also investigate anomaly detectability.

2 DATASETS AND PREPROCESSING

In this paper, we are building models for the pendulum time-series CB2 and CB3, measuring the dam's radial displacement [mm] from the bottom to crest, and foundation to bottom, respectively. To model these time series, we rely on the reservoir water level [m] as well as the temperature data TB [^{o}C]. The data acquisition for the displacements CB2/3 has been made with an average frequency of 1.5 week, whereas the average frequency of the reservoir water level as well as the temperature TB is daily. We use daily data in our models both in training and forecasting which means that there are many missing data points in the CB2/CB3 displacement datasets.

For BDLM models, the water level data below 196m have been truncated to that value to account for the physical constrain associated with the bottom of the dam. In addition, instead of using the raw data itself, we account for the thermal inertia of the dam by using a {1,7,14} (CB2) & {14,28,54} (CB3) days moving averages for the residual of temperature TB where the yearly periodic pattern has been removed. Here, for each sensor, we selected the moving average periods which led to significant contribution for the displacement predictions among the set {1,7,14,28,54}. Note that the one day moving average is equivalent to the raw data.

For LSTM models, we use the raw data of the reservoir water level and the temperature TB. This is because the corrected pattern introduced by the truncation of the water level is detrimental to the accuracy of the LSTMs prediction. Furthermore, LSTM models can take into account the lagging effect of the temperature on the dam's displacement automatically by using a lookback period larger than one. Figure 1 presents the data that is employed as input to build the BDLM and TAGI-LSTM models.
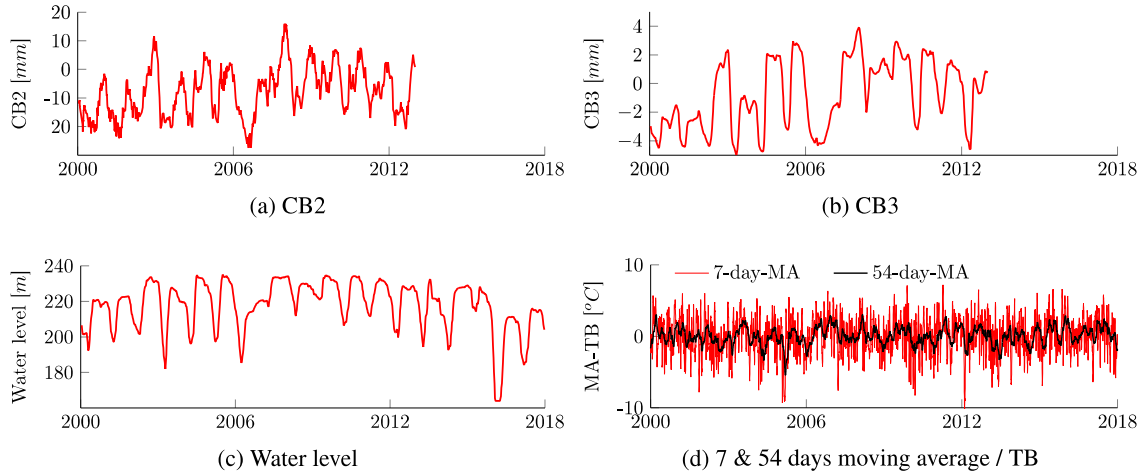

Figure 1. CB2/3 displacements, water level, and examples of moving averages fot the temperature TB.

3 METHODOLOGY

This section presents the theoretical foundations behind Bayesian dynamic linear models, the coupling between tractable approximate Gaussian inference and LSTMs, as well as the Gaussian mixture method for aggregating the predictions from multiple models.

3.1 *Bayesian Dynamic Linear Models (BDLM)*

Linear regression and neural networks are categorized as parametric methods because the relationships within the model are controlled by the estimation of parameters. On the other hand, BDLMs fall in the non-parametric category as the relationships within the model are learnt probabilistically through constraints describing the transition of hidden state variables through time, as well as their observability. For example in order to model the position x_t in time t of an object in free-fall, rather than trying to adjust the parameters of a function in order to fit through observations of the tuples (time, position), i.e. a parametric approach, BDLM would model the dependency through time $h(\boldsymbol{x}_t|\boldsymbol{x}_{t-1})$ using the classic kinematic equations for the hidden states $\boldsymbol{x} = [x, \dot{x}, \ddot{x}]^T$; the position x, speed $\dot{x}$ and acceleration $\ddot{x}$, and their observability by defining that only the position is observable, i.e. $y_t = x_t$. From these constraints on the transition and observability, we can then employ the Kalman filter (Kalman, 1960) (i.e., the Gaussian conditional equations) to infer the posterior probability density function $f(x_1|y_1, y_2, \ldots, y_t)$ of the hidden states given the data.

As stated in introduction, the main advantage of such an approach is that it allows updating the model online as the data become available, without needing to re-learn the model parameters. In practice, one can rely on a collection of predefined sub-components, each modelling a specific behaviour present in a time series, and which can be assembled in order to create powerful, yet simple, models. Another key aspect of BDLMs is their capacity to handle regime switches over time, where models describing different regimes (e.g., a constant regime versus a linearly changing one) can compete against each other and are ranked according to their prior probability, the probability to switch from one regime to another, and the likelihood of each at explaining the data. This regime switching algorithm is the backbone of anomaly detection in the context of BDLMs (Nguyen & Goulet, 2018a; Khazaeli et al., 2021) whereas a switch between

regimes can be used as a proxy indicating the presence anomalies. The complete details regarding the BDLM theory can be found in (Goulet, 2020) examples of its application to SHM datasets can be found in (Nguyen et al., 2019; Goulet & Koo, 2018; Nguyen & Goulet, 2018b; Goulet, 2017; Nguyen & Goulet, 2017), and the OpenBDLM library (Gaudot et al., 2019) can be found on GitHub (https://github.com/CivML-PolyMtl/OpenBDLM).

For this submission, the architecture of our model can be subdivided according to each time series, i.e., displacement, water level and temperature moving average. The selection of the model's components and their dependencies were defined iteratively to remove any distinguishable pattern from the model residual term. The water level uses a local level to model the average value, a local trend to extract the long-term non-periodic tendency ($\approx$ 5 years), and an autoregressive process to capture the short-term ($\approx$ 1 year) non-periodic changes in water level. The temperature is modelled using a local level to model the average value, a Fourrier-form periodic component to extract the long-term stationary pattern and an a white-noise process to capture the non-periodic changes in temperature. The displacement time series CB2/3 are modelled using a local level to represent the average value, two state-based non-linear dependencies on the water level (1) mean-centered values and (2) its long-term pattern, a linear dependency over the non-periodic changes in temperature, and an autoregressive process to capture the time-dependent model errors. The mathematical formulation for the matrices defining the transition and observation models are presented in Appendix A and the BDLM code for reproducing the results presented in this paper has been made available on GitHub (https://github.com/CivML-PolyMtl/OpenBDLM/tree/ICOLD_benchmark).

3.2 *TAGI-Long Short-Term Memory neural networks (TAGI-LSTM)*

LSTM is the classic neural network architecture for modelling time-series data. It models the dependency between explanatory variables and target outputs using a cell state enabling to consider long-term dependencies, layers of hidden variables defining the neural networks and gates (i.e., forget, input and output) enabling the combination of the information coming from the hidden and cell states. A key advantage of LSTM over BDLM or HST methods is that it does not require a specific architecture setup for defining the possible dependencies with respect to explanatory variables, thus enabling it to be quickly applied to many time series.

The parameters of LSTMs are typically learnt deterministically using gradient-based optimization. The drawback of such an approach is that it disregards the epistemic uncertainty associated with parameter estimation. To overcome this limitation, we rely on the tractable approximate Gaussian inference method (TAGI) (Goulet et al., 2021) in order to perform Bayesian estimation for the LSTM network parameters. The specific network architecture and the hyperparameters employed in this submission are presented in Appendix B.

Like other neural network architectures, LSTM networks are sensitive to the values employed to initialize model parameters before their estimation. Given the ease to evaluate multiple models having different initial model parameters, we choose to combine ten models in order to further improve the prediction accuracy. The ensembling method to combine these ten models along with the BDLM one is presented in the next subsection.

3.3 *Gaussian Mixture Ensembling*

The ensembling method we use in this submission relies on the moment matching Gaussian mixture of models (Runnalls, 2007). Here, we want to aggregate the BDLM and ten LSTM models where each has a Gaussian output as characterized by their respective expected value μ_i and variance σ_i^2, making them natively suited for the Gaussian mixture ($\mathbf{GM}$). A $\mathbf{GM}$ combines several Gaussian probability density functions according to the probability associated with each model. In the case of the moment matching $\mathbf{GM}$, we approximate the resulting mixture distribution by a Gaussian random variable whose moments ($\mu_{\mathbf{GM}}, \sigma_{\mathbf{GM}}^2$) matching those of the true mixture distribution and which can be computed using the relations

$$\mu_{\mathbf{GM}} = \sum_{i=1}^{N} w_i \mu_i$$

$$\sigma_{\mathbf{GM}}^2 \;=\; \sum\nolimits_{i=1}^{N} w_i \left[\sigma_i^2 + \left(\mu_i - \mu_{\mathbf{GM}}\right)^2\right],$$

where for N models, the $\mathbf{GM}$ expected value is the weighted sum of the individual μ_i and the $\mathbf{GM}$ variance is the weighted sum of the variance σ_i^2 plus a term to account for the discrepancy between each model's expected value.

In a Bayesian context, the weights should be computed according to their posterior probability $w_i = p(m_i|\mathcal{D})$ as defined by

$$p(m_i|\mathcal{D}) = \frac{p(\mathcal{D}|m_i).\,p(m_i)}{\sum_i p(\mathcal{D}|m_i).\,p(m_i)}$$

Here, we rely on the simplifying assumption that $p(\mathcal{D}|m_i) = ln\mathcal{L}(m_i)^{-1}$ is equal to the inverse log-likelihood of each model measured between 2012-2013, whose values are reported in Appendix C. The prior probability $p(m_i)$ for the BDLM model is equal to 0.5, and to 0.05 for each of the TAGI-LSTM models making their aggregated prior probability also equal to 0.5.

4 RESULTS

We divided the presentation of the results into three parts; first, we present the relative performance of each individual model, i.e., BDLM vs TAGI-LSTM by training each of them on a subset of the training data available, and then predicting the last three years of data available; second, we present the forecasted data aggregating the prediction of one BDLM and 10 TAGI-LSTM models; third, we present the model interpretation where we identify the sources and nature of the dependencies between time series. Finally, we present how the regime switching capacity of BDLM is better at detecting anomalies than threshold-based alarm triggers.
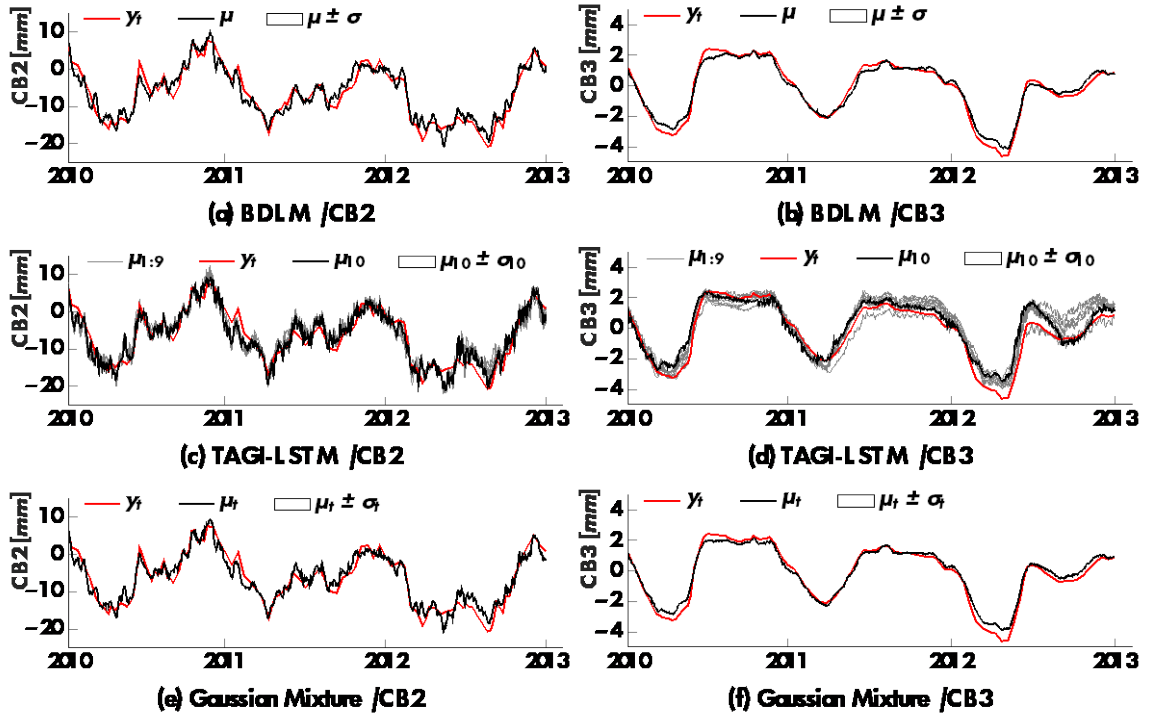
4.1 *Validation*

Figure 2. Comparative performance of BDLM, 10 instances of TAGI-LSTM, and the Gaussian mixture from BDLM and 10 instances ($\{\mu_1, \mu_2, \cdots, \mu_1\}$) of TAGI-lstm for both the CB2-3 sensors.

Figure 2 compares the predictions for the last three years of the training data available, obtained for each model and for the Gaussian mixture of all models. These results show that both methods offer a comparable performance with a slight edge for the BDLM method. In terms of computational time, both methods are comparable with a total training time in the order of an hour. Once trained, both models can be used to predict with a computational time in the order of a minute.
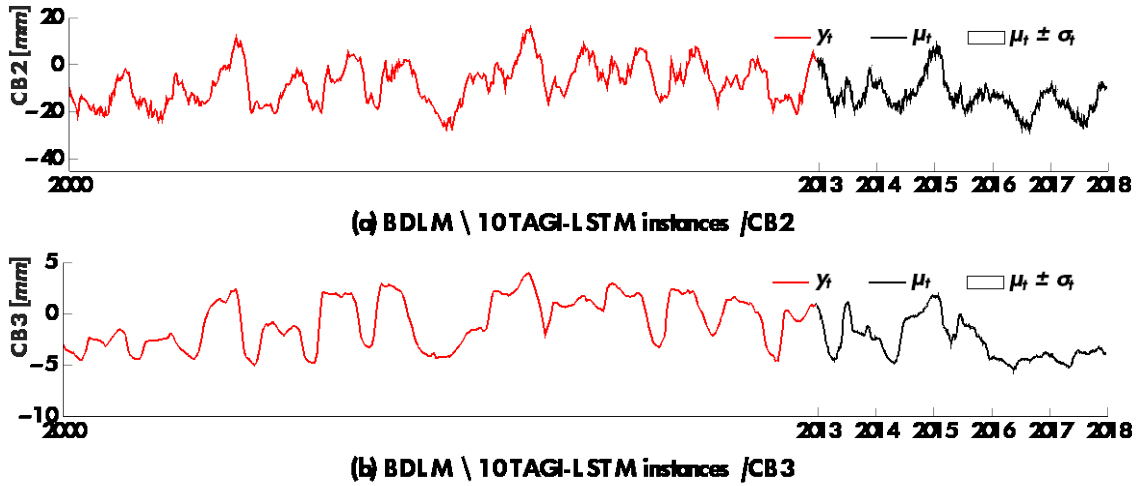
4.2 *Forecasting*

Figure 3. Forecast for the Gaussian mixture made form BDLM forecasts and 10 instances of TAGI-LSTM for both the CB2-3 sensors.

Figure 3 presents the forecasts for the period 2013--2018 obtained from the Gaussian mixture of the BDLM and ten TAGI-LSTM models.

4.3 *Model interpretation*

The model interpretation is made using the BDLM model only, as LSTM networks offer little help in understanding the nature of the dependencies between time series.

4.3.1 Dependencies and interaction between time-series

Figures 4 & 5 summarize the information that can be extracted from the BDLM model; (a) presents the relative importance of each component measured by the relative variance of each sub-component; (b) plot the non-linear relationships between the dam's response and the mean-centered water level as well as its long-term pattern as depicted in (d) with corresponding colors; (c) presents the periodic pattern extracted from the CB sensors that can include part of the temperature and water level effects; (d) presents the mean-centered water level as well as the long-term pattern extracted from it by BDLM; (e) presents the model residuals ($x^{\mathbf{AR}}$) i.e., the remaining part of the observation not attributed to observation errors not explained by the other components.

For the sensor CB2, we note in Figure 4a, the dominant relative importance of the mean-centered water level through the non-linear dependency $g(x_{\mathrm{WL}})$ depicted in Figure 4b (WL-NL), and secondly of the periodic pattern $x^{\mathbf{KR}}$ depicted in Figure 4c (CB-KR). The third most important contributor is the autoregressive component $x^{\mathbf{AR}}$ depicted in Figure 4e (CB-AR), which represents what cannot be explained by the model. Although the relative importance of other components is less than the residual term, they still matter because we are interested in detecting anomalies having small magnitudes. For example, an anomaly with a magnitude of 0.5 mm would still have a relative importance comparable to the one day moving average presented in Figure 4a (TB-MA1). Note for instance that the relative importance of the long-term pattern (see Figure 4d) within the water level through the non-linear dependency $g(x_{\mathrm{WL}}^{\mathbf{LT}})$ depicted in Figure 4b (WL$_{\mathrm{LT}}$-NL) is key in order to enable the detection of small anomalies as further detailed in Section 4.3.2.

Figure 4. Graphs illustrating the interpretation of the CB2 dataset that can be made from the BDLM components.

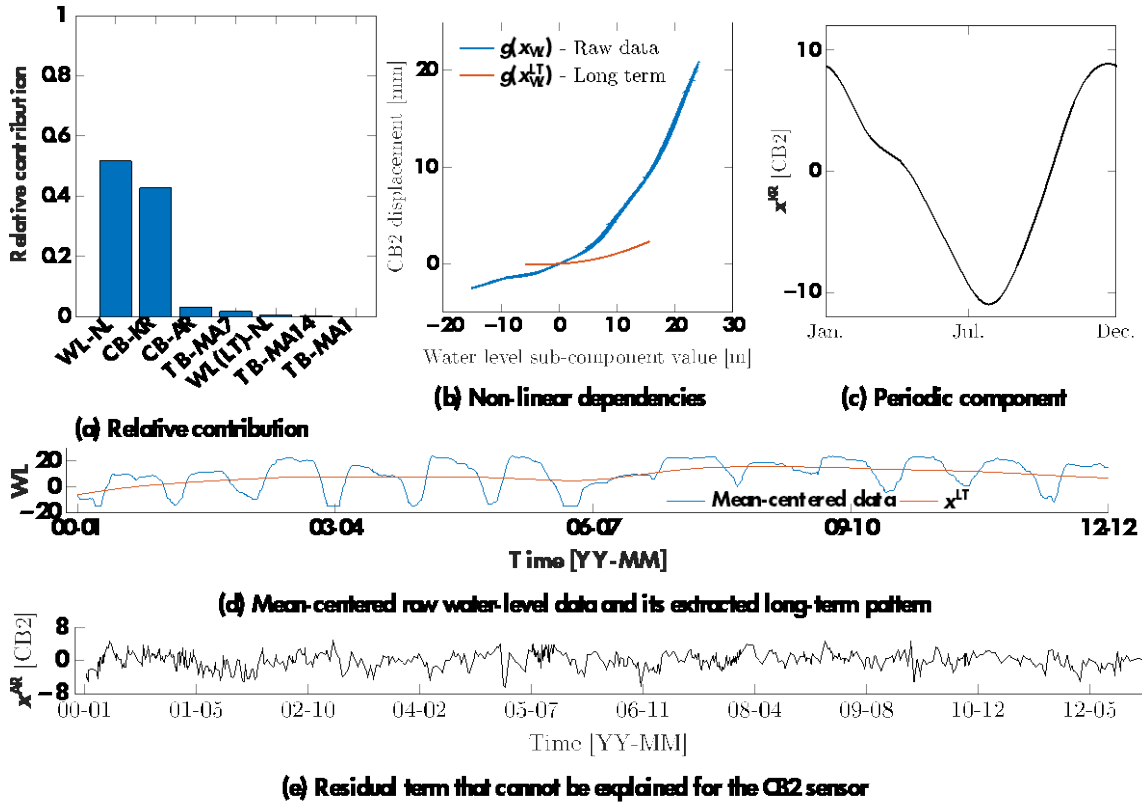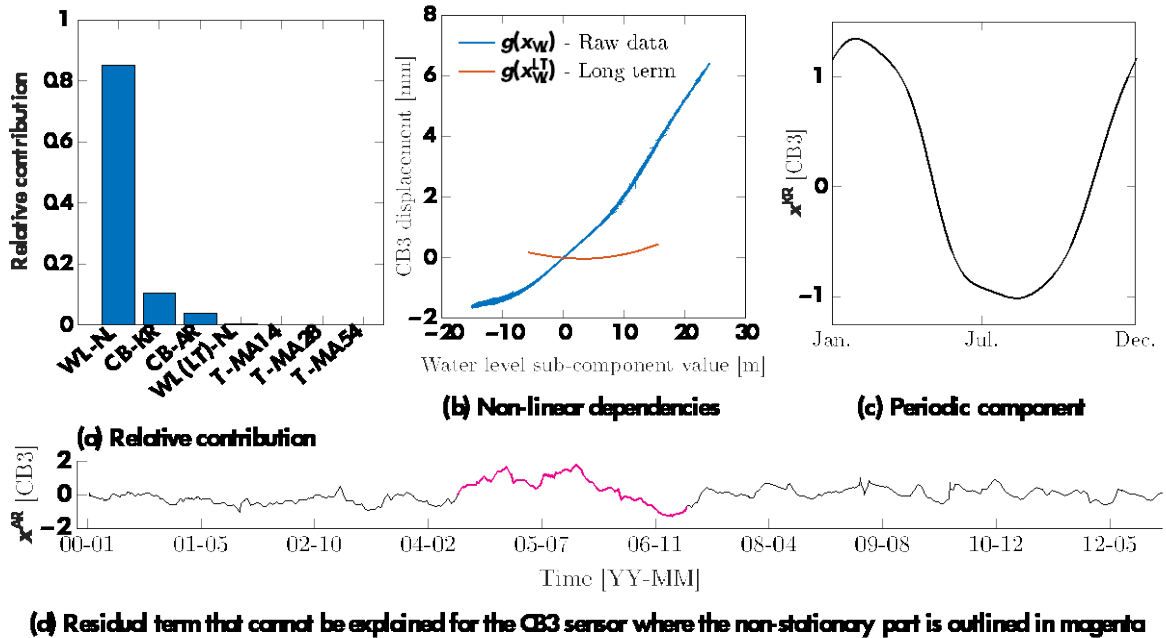Figure 5. Graph illustrating the interpretation of the CB2 dataset that can be made from the BDLM components.

For the sensor CB3, the contribution of the water level through the non-linear dependency $g(x_{\mathrm{WL}})$ depicted in Figure 5b is even more dominant than in the case of CB2. One particularity for CB3 is that the residual term corresponding to the autoregressive component in Figure 5d

presents a non-stationary pattern between February 2004 and 2007 as outlined in magenta. The presence of such a pattern indicates that the current components considered in our model for CB3 are missing a part of the dam's behavior. The next section will further investigate this non-stationarity by showing how using a regime-switching analysis would have been able to detect such anomalous occurrence in real time.

4.3.2 Anomaly detection using regime switching

As mentioned in Section 3.1, one key strength of BDLM, is its capacity to detect regime switches (Nguyen & Goulet, 2018a; Khazaeli et al., 2021). We performed such an analysis on the CB2/3 datasets while a first normal regime is modelled with a constant baseline through time, and a second abnormal regime is modelled with a constant-speed regime through time.

For the CB2 sensor, the black curve in Figure 6b presents the probability of anomaly identified using the switching Kalman filter (SKF). This probability close to zero across the dataset indicates that the dam's behaviour is stationary. We further confirm this conclusion by adding to the original data synthetic anomalies of magnitude $a_m = 0.5, 1, 2$mm building up over a duration of magnitude $a_d = 4$ years, as depicted in Figure 6a. The probability of anomaly identified by the SKF rises in all three cases where synthetic anomalies are added, thus correctly indicating their presence. In comparison, if we use an alarm-triggering threshold of 1 mm on the absolute difference between the predicted and measured values for the validation set presented in Figure 2a, we would on average, trigger more than 10 false alarms per year while no alarm should have been triggered. Figure 6c presents the result of this exercise repeated for alarm-triggering thresholds ranging from 0.5 up to 6 mm. Note that these anomaly magnitudes are all smaller than the amplitude of the residual term presented in Figure 4e. This shows that detecting anomalies based on the exceedance of threshold values is prone to false alarms and offers a poor anomaly detectability in comparison with the regime switching approach of Bayesian dynamic linear models. If one chooses a more robust criterion involving multiple successive crossings, the false alarm rate will indeed drop; Nevertheless, this strategy remains poorly suited for the detection of anomalies developing over the span of several years, as parametric models (e.g. HST, LSTM, SVM, etc.) will need to be retrained periodically in order to avoid drift, thus incorporating the changes due to the presence of an anomaly in the updated models.

(a) Schematic representation of synthetic anomalies added on the raw data to quantify anomaly detectability

(b) Probability of switching from a stationary to a non-stationary regime taken as a proxy for Pr(anomaly)

(c) Relation on alarm threshold and the number of false alarms
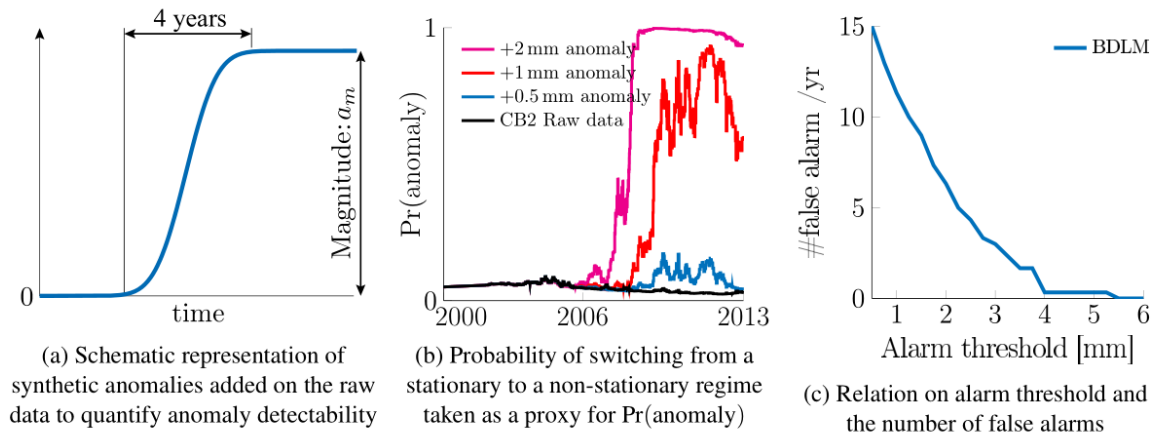
Figure 6. Comparison of the regime switching approach with a threshold-based one of the purpose of detecting anomalies while avoiding false alarms.

Figure 7b presents the same exercise applied to the CB3 sensor. In this case, the SKF detects a regime switch shortly before 2006 as indicated by the jump in the black curve. This regime change can be confirmed by looking at the residual term presented in Figure 5d, where a non-stationary pattern is visually observable between 2004 and 2007. As this pattern disappears after 2007 while the probability of regime switch return to 0 after 2006, we speculate that events other than those considered in our model have taken place during that period. We tested our capacity to detect anomalies on CB3 by adding synthetic anomalies as

depicted in Figure 7a, with magnitudes $a_m = 0.15, 0.25, 0.5$mm which are building up over a duration of $a_d = 4$ years. Note that the anomaly has been shifted after 2006 in order not to interfere with the actual anomaly present in the data. We can see in Figure 7b that synthetic anomalies with a magnitude low as 0.15 mm are detectable for this sensor.

(a) Schematic representation of synthetic anomalies added on the raw data to quantify anomaly detectability

(b) Probability of switching from a stationary to a non-stationary regime taken as a proxy for Pr(anomaly)
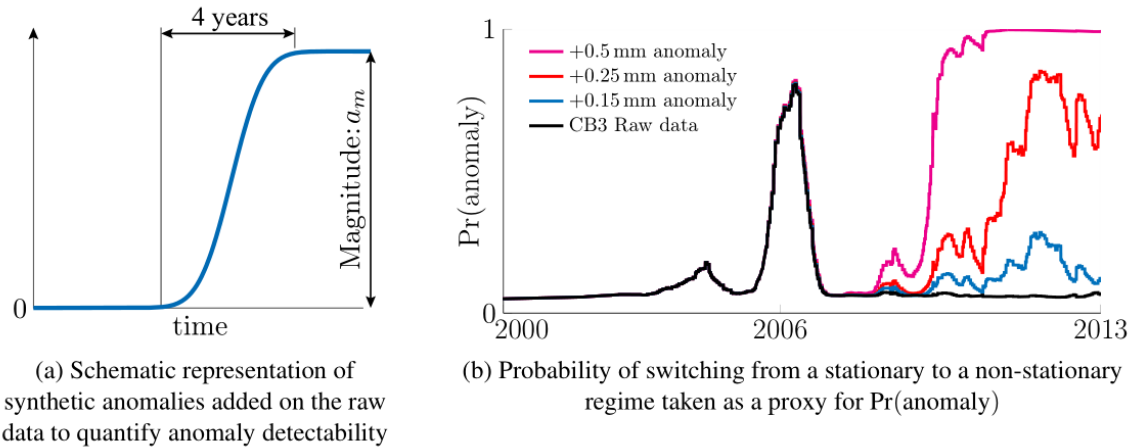
Figure 7. Regime switching analysis applied to the CB3 sensor for the raw data as well as additional synthetic anomalies.

5 DISCUSSION

The presence of a non-linear residual term for the sensor CB3 lead us to think that, in the context of this benchmark, the long-term predictive capacity for that sensor will be limited. In order to improve the model, it would be worth further investigating (1) the relationship between the anomaly detected on the sensor CB3 and the seepage and piezometric levels measured, (2) the possibility that the long-term effects of the water level on the sensors CB2/3 (see Figure 4d) may be related to creep/creep-relief effects (Bažant & Wu, 1974), and (3) following the results of this forecasting competition, if other submissions have identified features explaining the dam's behavior that were not considered here, these could be included in our BDLM model in order to further improve its forecasting accuracy and anomaly detectability.

Despite these limitations, as mentioned in Sections 3.1 & 4.3.2 the key aspect of our method is to enable the detection of anomalies based upon the probability of regime switch rather than on threshold crossing. This has enabled in Section 4.3.2 the detection of anomalies that are smaller than the residual terms for the CB2 and CB3 sensors. This shows that the anomaly detectability of our method can be decoupled from its long-term prediction capacity.

6 CONCLUSION

This paper presents the results of our submission to the ICOLD's dam prediction benchmark. We provide through our probabilistic ensembling method the explainability of BDLMs as well as the accuracy and ease of use of Bayesian LSTM. Although the benchmark focusses on prediction accuracy and threshold value definition for the purpose of anomaly detection, one should keep in mind that this way of envisioning anomaly detection is only one approach among many others. We showed in this paper that with our probabilistic regime switching method we expect to be able to detect anomalies of 0.5 mm for CB2 and 0.15 mm for CB3, where both can develop over the span of years.

ACKNOWLEDGEMENTS

REFERENCES

Bažant, Z. P. & Wu, S. (1974). "Rate-type creep law of aging concrete based on maxwell chain." *Matériaux et Construction*, 7(1), 45–60.

Gaudot, I., Nguyen, L. H., Khazaeli, S., & Goulet, J.-A. (2019). "OpenBDLM, an open-source software for structural health monitoring using Bayesian dynamic linear models." *13th Proceedings from the 13th International Conference on Applications of Statistics and Probability in Civil Engineering (ICASP)* (May).

Goodfellow, I., Bengio, Y., & Courville, A. (2016). *Deep learning*. MIT Press.

Goulet, J.-A. (2017). "Bayesian dynamic linear models for structural health monitoring." *Structural Control and Health Monitoring*, 24(12), 1545–2263.

Goulet, J.-A. (2020). "Chapter 12 - State-Space Models." *Probabilistic Machine Learning for Civil Engineers*, MIT press.

Goulet, J.-A. & Koo, K. (2018). "Empirical validation of Bayesian dynamic linear models in the context of structural health monitoring." *Journal of Bridge Engineering*, 23(2), 05017017.

Goulet, J.-A., Nguyen, L., & Amiri, S. (2021). "Tractable approximate gaussian inference for Bayesian neural networks." *Journal of Machine Learning Research*, 22(251), 1–23.

Kalman, R. E. (1960). "A new approach to linear filtering and prediction problems." *Transactions of the ASME–Journal of Basic Engineering*, 82(Series D), 35–45.

Khazaeli, S., Nguyen, L., & Goulet, J.-A. (2021). "Anomaly detection using state-space models and reinforcement learning." *Structural Control and Health Monitoring*, 28(6), e2720.

Nguyen, L. H., Gaudot, I., & Goulet, J.-A. (2019). "Uncertainty quantification for model parameters and hidden state variables in Bayesian dynamic linear models." *Structural Control and Health Monitoring*, 26(3), e2309 e2309 stc.2309.

Nguyen, L. H. & Goulet, J.-A. (2017). "Structural health monitoring with dependence on hidden non-harmonic covariates." *Submitted to Engineering Structures*.

Nguyen, L. H. & Goulet, J.-A. (2018a). "Anomaly detection with the switching Kalman filter for structural health monitoring." *Structural Control and Health Monitoring*, 25(4), e2136.

Nguyen, L. H. & Goulet, J.-A. (2018b). "Structural health monitoring with dependence on non-harmonic periodic hidden covariates." *Engineering Structures*, 166, 187 – 194.

Runnalls, A. R. (2007). "Kullback-Leibler approach to gaussian mixture reduction." *IEEE Transactions on Aerospace and Electronic Systems*, 43(3), 989–999.

Sagi, O. & Rokach, L. (2018). "Ensemble learning: A survey." *Wiley Interdisciplinary Reviews: Data Mining and Knowledge Discovery*, 8(4), e1249.

Salazar, F., Morán, R., Toledo, M., & Oñate, E. (2017). "Data-based models for the prediction of dam behaviour: a review and some methodological considerations." *Archives of computational methods in engineering*, 24(1), 1–21.

APPENDIX

A   BDLM MODEL STRUCTURE

The BDLM components used for modeling the independent patterns for CB2/3 are local level (LL), kernel regression (KR) and autoregressive (AR). The mean-centered water-level and its long-term pattern (Figure 4d) are modeled using an AR and a local trend (LT) component respectively. The two nonlinear patterns for CB2/3 that are nonlinearly dependent on these two time series are each modeled using a state-regression (SR) component. The moving averages of the temperature (TB) are modeled using AR components. The transition matrices for LL, LT, KR, and AR components (Goulet, 2020, 2017) are as follow:

$$\mathbf{A_t^{LL}} = 1, \mathbf{A_t^{LT}} = \begin{bmatrix} 1 & \Delta t \\ 0 & 1 \end{bmatrix}, \mathbf{A_t^{KR}} = \begin{bmatrix} 0 & \widetilde{k^{KR}}(t, t^{KR}) \\ \mathbf{0_{n \times 1}} & \mathbf{I_n} \end{bmatrix}, \mathbf{A_t^{AR}} = \phi^{AR} \tag{1}$$

where n represents the number of control points for kernel regression and Δt = 1day. The observation matrices for these components are given by

$$\mathbf{C_t^{LL}} = 1, \mathbf{C_t^{LT}} = \begin{bmatrix} 1 & 0 \end{bmatrix}, \mathbf{C_t^{KR}} = \begin{bmatrix} 1 & 0_{n \times 1} \end{bmatrix}, \mathbf{C_t^{AR}} = 1 \tag{2}$$

The process noise $\mathbf{Q_t}$ covariance matrices are

$$\mathbf{Q_t^{LL}} = (\sigma_w^{LL})^2, \mathbf{Q_t^{LT}} = (\sigma_w^{LT})^2 \begin{bmatrix} \frac{\Delta t^4}{4} & \frac{\Delta t^3}{2} \\ \frac{\Delta t^3}{2} & \Delta t^2 \end{bmatrix}, \mathbf{Q_t^{KR}} = \begin{bmatrix} (\sigma_0^{KR})^2 & \mathbf{0} \\ \mathbf{0} & (\sigma_1^{KR})^2 \cdot \mathbf{I_n} \end{bmatrix}, \mathbf{Q_t^{AR}} = (\sigma_w^{AR})^2, \tag{3}$$

The SR component includes $n = 20$ hidden states for the kernel values, $x^{SK} = \begin{bmatrix} x_1^{SK} & x_2^{SK} & \dots x_n^{SK} \end{bmatrix}^\mathsf{T}$; $n + 1$ hidden states for the regression coefficient that includes n hidden states of control-points, $x^{\phi^R} = \begin{bmatrix} x_1^{\phi^R} & x_2^{\phi^R} & \dots x_n^{\phi^R} \end{bmatrix}^\mathsf{T}$ and $x_0^{\phi^R}$ which is the hidden state of the predicted regression coefficient; hidden state for the nonlinear pattern for displacement, $x^{S,D} = \left(x_0^{\phi^R} \cdot x^{S,T} \right)$ where $x^{S,T}$ represents the covariate for modeling the nonlinear dependency, and n product terms, $x^{SKR} = \begin{bmatrix} x^{SKR,1} & x^{SKR,2} & \dots x^{SKR,n} \end{bmatrix}^\mathsf{T}$, where, $x^{SKR,i} = \left(x_i^{SK} \cdot x_i^{\phi^R} \right); \forall i = 1:n.$

The hidden states for the component can be grouped together as

$$x^{SR} = \left[(x^{SK})^\mathsf{T} \left(x^{\phi^R} \right)^\mathsf{T} x_0^{\phi^R} x^{S,D} (x^{SKR})^\mathsf{T} \right]^\mathsf{T}$$

The transition matrix for the SR component of size $3n + 2$ is formulated as

$$\mathbf{A_t^{SR}} = \begin{bmatrix} \mathbf{0_n} & \mathbf{0_{1 \times n}} & 0 & 0 & \mathbf{0_{1 \times n}} \\ \vdots & \mathbf{I_n} & 0 & 0 & \mathbf{0_{1 \times n}} \\ \vdots & \dots & 0 & 0 & \mathbf{1_{1 \times n}} \\ \vdots & \dots & \dots & 0 & \mathbf{0_{1 \times n}} \\ sym. & \dots & \dots & \dots & \mathbf{0_n} \end{bmatrix} \tag{4}$$

The observation matrix $\mathbf{C_t^{SR}}$ is given by

$$\mathbf{C_t^{SR}} = \begin{bmatrix} 0_{n \times 1}^\mathsf{T} & 0_{n \times 1}^\mathsf{T} & 0 & 1 & 0_{n \times 1}^\mathsf{T} \end{bmatrix}. \tag{5}$$

No process noise is considered for the **SR** component and is given by $\mathbf{Q_t^{SR}} = \mathbf{0_{3n+2}}.$

Using equations 1 & 4, the global transition matrix $\mathbf{A}_t$ is obtained by arranging the transition matrices block diagonally shown by

$$\mathbf{A}_t = \text{blockdiag}\left(\overbrace{[\mathbf{A}_t^{\mathbf{LL}}, \mathbf{A}_t^{\mathbf{KR}}, \mathbf{A}_t^{\mathbf{AR}}]}^{\text{CB2/3}}, \overbrace{[\mathbf{A}_t^{\mathbf{LT}}, \mathbf{A}_t^{\mathbf{SR_1}}]}^{\text{WL1}}, \overbrace{[\mathbf{A}_t^{\mathbf{AR}}, \mathbf{A}_t^{\mathbf{SR_2}}]}^{\text{WL2}}, \overbrace{[\mathbf{A}_t^{\mathbf{AR}}]}^{\text{T-MA1}}, \overbrace{[\mathbf{A}_t^{\mathbf{AR}}]}^{\text{T-MA7}}, \overbrace{[\mathbf{A}_t^{\mathbf{AR}}]}^{\text{T-MA14}}, \overbrace{[\mathbf{A}_t^{\mathbf{AR}}]}^{\text{T-MA28}}, \overbrace{[\mathbf{A}_t^{\mathbf{AR}}]}^{\text{T-MA54}}\right) \quad (6)$$

where WL1 and WL2 refers to the long-term pattern and the mean-centered raw water level, and the nonlinear dependencies are modeled using the SR_1 and SR_2 components. Using equations 2 & 5, the global observation matrix $\mathbf{C}_t$ is given by

$$\mathbf{C}_t = \text{blockdiag}\left(\overbrace{[\mathbf{C}_t^{\mathbf{LL}}, \mathbf{C}_t^{\mathbf{KR}}, \mathbf{C}_t^{\mathbf{AR}}]}^{\text{CB2/3}}, \overbrace{[\mathbf{C}_t^{\mathbf{LT}}, \mathbf{C}_t^{\mathbf{SR_1}}]}^{\text{WL1}}, \overbrace{[\mathbf{C}_t^{\mathbf{AR}}, \mathbf{C}_t^{\mathbf{SR_2}}]}^{\text{WL2}}, \overbrace{[\mathbf{C}_t^{\mathbf{AR}}]}^{\text{T-MA1}}, \overbrace{[\mathbf{C}_t^{\mathbf{AR}}]}^{\text{T-MA7}}, \overbrace{[\mathbf{C}_t^{\mathbf{AR}}]}^{\text{T-MA14}}, \overbrace{[\mathbf{C}_t^{\mathbf{AR}}]}^{\text{T-MA28}}, \overbrace{[\mathbf{C}_t^{\mathbf{AR}}]}^{\text{T-MA54}}\right) \quad (7)$$

The $\mathbf{Q}_t$ and the $\mathbf{R}_t$ matrices are

$$\mathbf{Q}_t = \text{blockdiag}\left(\overbrace{[\mathbf{Q}_t^{\mathbf{LL}}, \mathbf{Q}_t^{\mathbf{KR}}, \mathbf{Q}_t^{\mathbf{AR}}]}^{\text{CB2/3}}, \overbrace{[\mathbf{Q}_t^{\mathbf{LT}}, \mathbf{Q}_t^{\mathbf{SR_1}}]}^{\text{WL1}}, \overbrace{[\mathbf{Q}_t^{\mathbf{AR}}, \mathbf{Q}_t^{\mathbf{SR_2}}]}^{\text{WL2}}, \overbrace{[\mathbf{Q}_t^{\mathbf{AR}}]}^{\text{T-MA1}}, \overbrace{[\mathbf{Q}_t^{\mathbf{AR}}]}^{\text{T-MA7}}, \overbrace{[\mathbf{Q}_t^{\mathbf{AR}}]}^{\text{T-MA14}}, \overbrace{[\mathbf{Q}_t^{\mathbf{AR}}]}^{\text{T-MA28}}, \overbrace{[\mathbf{Q}_t^{\mathbf{AR}}]}^{\text{T-MA54}}\right) \quad (8)$$

$$\mathbf{R}_t = \text{blockdiag}\left(\overbrace{(\sigma_{v_1})^2}^{\text{CB2/3}}, \overbrace{(\sigma_{v_2})^2}^{\text{WL1}} \overbrace{(\sigma_{v_3})^2}^{\text{WL2}}, \overbrace{(\sigma_{v_4})^2}^{\text{T-MA1}}, \overbrace{(\sigma_{v_5})^2}^{\text{T-MA7}}, \overbrace{(\sigma_{v_6})^2}^{\text{T-MA14}}, \overbrace{(\sigma_{v_7})^2}^{\text{T-MA28}}, \overbrace{(\sigma_{v_8})^2}^{\text{T-MA54}}\right) \quad (9)$$

where σ_{v_i}, $\forall i = 1:8$ refers to the standard deviation of the observation noise for each of the time series.

B   LSTM MODEL STRUCTURE

We use two separate models which have the same architecture, but do not share the parameters to predict the displacements CB2 and CB3. The common network's architecture consists of one LSTM layer of 50 hidden units, and a dense layer with no activation function to combine the output of the LSTM layer. In order to take into account the lagging effect that the temperature and the reservoir's level may have on the displacement, we use a sequence of length M of covariates as inputs for the LSTM instead of using only the covariates at time *t* as

$$\boldsymbol{h_t} = g(\boldsymbol{h_{t-1}}, y_{t-L:t-1}, \boldsymbol{x_{t-M+1:t}}),$$

where $g(\cdot)$ is the function implemented by the LSTM, $\boldsymbol{h}$ are the hidden states, y is the displacement observation, $\boldsymbol{x}$ are covariates which are the reservoir's level and temperature TB, and $\mathbf{L}$ is the lookback period. During training when the data is missing, and during prediction when the data is not available, we replace y by the network's prediction, and $\boldsymbol{x}$ by $\mathbf{0}$. When using TAGI to perform Bayesian estimation for the LSTM network parameters, it is required to define an observation noise for each time series (Goulet et al., 2021). The standard deviation for this observation noise is a hyper-parameter which needs to be learnt from data. We perform a grid-search to find the best hyper-parameter values for each model as presented in Table 1. For each candidate value in the grids, we train our models with early-stopping on a subset of training data from 2000 to end of 2009 and report the log-likelihood for the validation period from 2010 to end of 2012. The values which maximize the log-likelihood of the validation set are chosen as the final hyper-parameter values.

Table 8: LSTM hyper-parameters.

Hyper-parameters	CB2	CB3	Grid
Observation noise's standard deviation	0.05	0.01	{0.01, 0.05, 0.1, 0.15}
L	35	14	{14, 35, 56, 70}
M	21	21	{7, 21, 35, 49, 70}

C   LOG-LIKELIHOOD AND WEIGHT

Table 9: Log-likelihood measured between 2012-2013 and weight by each model.

Model	CB2		CB3	
	Log-likelihood	w_i	Log-likelihood	w_i
BDLM	-63.89	0.506	-12.06	0.659
LSTM #1	-66.48	0.049	-46.96	0.017
LSTM #2	-66.53	0.049	-48.66	0.016
LSTM #3	-64.74	0.050	-11.64	0.068
LSTM #4	-64.98	0.050	-45.52	0.017
LSTM #5	-73.79	0.044	-35.36	0.022
LSTM #6	-65.14	0.050	-37.59	0.021
LSTM #7	-66.12	0.049	-24.71	0.032
LSTM #8	-62.40	0.052	-33.49	0.023
LSTM #9	-63.18	0.051	-28.68	0.028
LSTM #10	-62.51	0.052	-8.37	0.095

D   MEAN ABSOLUTE ERROR (MAE)

Table 3: MAE for the validation period between 2010-2013.

Model	CB2	CB3
Mixture	1.366	0.253
BDLM	1.312	0.248
LSTM #1	1.574	0.490
LSTM #2	2.109	0.537
LSTM #3	1.910	0.486
LSTM #4	2.008	0.534
LSTM #5	1.945	0.610
LSTM #6	1.833	0.566
LSTM #7	1.836	0.393
LSTM #8	1.705	0.524
LSTM #9	1.796	0.452
LSTM #10	1.869	0.462

DAM BEHAVIOUR PREDICTION USING LINEAR REGRESSION, NEURAL NETWORKS, AND FE MODELLING

Evgeniy Vitokhin
Vedeneev VNIIG, JSC, Saint Petersburg, Russia

Pavel Ivanov
Vedeneev VNIIG, JSC, Saint Petersburg, Russia

ABSTRACT: The paper presents statistical and finite-element prediction models for predicting CB2 and CB3 sensors data of an EDF arch concrete dam. Linear regression and neural networks were used to build the statistical models. The finite-element prediction model was built using Simulia Abaqus. Warning levels for the prediction was found and provided.

1 INTRODUCTION

In this paper we use statistical and calibrated finite element models to predict CB2 and CB3 sensors measurements of EDF dam.

2 STATISTICAL METHODS

2.1 *Theory*

First, we divide the entire dataset into training and test sets. The training set is used to define coefficients or weights of model. The test set is used to evaluate the accuracy of the model. In this paper, field data from 2000 to 2010 years used for training and data from 2011 to 2013 years used as test set.

For estimation of the model accuracy, we use mean absolute error MAE and NRMSE:

$$MAE = \frac{1}{n}\sum_{i=0}^{n-1}|y_i - \hat{y}_i| = \frac{1}{n}\sum_{i=0}^{n-1}|\varepsilon|, \quad NRMSE = \frac{\sqrt{\frac{1}{n}\sum_{i=0}^{n-1}|y_i - \hat{y}_i|^2}}{y_{max} - y_{min}}, \tag{1}$$

where y_i is the prediction, $\hat{y}_i$ – measured data.

Confidence intervals are calculated using the standard deviation:

$$\sigma = \frac{1}{n}\sum_{i=0}^{n-1}(\varepsilon_i - \bar{\varepsilon})^2, \qquad \bar{\varepsilon} = \frac{1}{n}\sum_{i=0}^{n-1}\varepsilon_i, \tag{2}$$

where ε_i – prediction error, $\bar{\varepsilon}$ – mean error.

The models considered in this paper use linear regression and a multilayer perceptron.

2.1.3 Linear regression

Linear regression is a model that assumes a linear dependence of the dependent variable on other (independent) variables or factors. This is a basic machine learning model that is widely applied in all fields of science.

With n observations, the dependent variable vector $\{y\}$ is written as follows:

$$\{y\}^T = \{y_1, y_2 \dots y_n\}. \tag{3}$$

If dependence on p factors is considered, then the matrix of independent variables $[X]$ is written as a rectangular matrix $n \times p + 1$:

$$[X] = \begin{bmatrix} \{x\}_1^T \\ \{x\}_2^T \\ \vdots \\ \{x\}_n^T \end{bmatrix} = \begin{bmatrix} 1 & x_{11} & \dots & x_{1p} \\ 1 & x_{21} & \dots & x_{2p} \\ \vdots & \vdots & \ddots & \vdots \\ 1 & x_{n1} & \dots & x_{np} \end{bmatrix}. \tag{4}$$

Each value of the dependent variable y_i corresponds to the vector of independent variables $\{x_i\}^T$. The first column is filled with ones, as the constant is considered a separate factor.

In the matrix form linear regression could be written as follows:

$$\{y\} = [X]\{\beta\} + \{\varepsilon\},$$
$$\{\beta\} = \begin{Bmatrix} \beta_1 \\ \beta_2 \\ \vdots \\ \beta_n \end{Bmatrix}, \ \{\varepsilon\} = \begin{Bmatrix} \varepsilon_1 \\ \varepsilon_2 \\ \vdots \\ \varepsilon_n \end{Bmatrix}, \tag{5}$$

where $\{\beta\}$ is vector of the coefficients, $\{\varepsilon\}$ is vector of model random errors (residuals between the calculated and observed parameters).

To make successful predictions we must obtain such coefficients $\{\beta\}$, which yield minimal error values $\{\varepsilon\}$. The error is usually minimized by least squares or gradient descent. When using the least squares method, the optimal coefficients $\{\beta\}$ are determined as follows:

$$\{\hat{\beta}\} = ([X]^T[X])^{-1}[X]^T\{y\}. \tag{6}$$

With a known optimal vector of coefficients $\{\hat{\beta}\}$, the predictive model takes the form:

$$\{\hat{y}\} = [X]\{\hat{\beta}\}, \tag{7}$$

where $\{\hat{y}\}$ is the prediction with known independent variables $[X]$. The prediction error is respectively defined as:

$$\{\varepsilon\} = \{y\} - \{\hat{y}\}. \tag{8}$$

One of the well-known disadvantages of linear regression is a large error in extrapolation. When the values of the independent variables are out of range in the training dataset, the predicted values often deviate significantly from the true (observed) values.

One approach to improve the ability of a linear model to generalize is to introduce regularization. Tikhonov's regularization method (ridge regression) introduces the parameter α into the formula for determining the optimal vector of coefficients $\{\hat{\beta}\}$.

$$\{\hat{\beta}_{ridge}\} = ([X]^T[X] + \alpha[I_p])^{-1}[X]^T\{y\}, \tag{9}$$

where $[I_p]$ is the identity matrix with dimension p.

Introducing parameter α leads to the fact that smaller values of the coefficients are encouraged. It leads to a smaller extrapolation error. Parameter α is a hyperparameter of the model, i.e. such a parameter that is not a factor, but directly affects the prediction. The selection of the best values of hyperparameters is carried out during cross-validation.

In this paper, we used linear regression using Tikhonov regularization and determining the values of the hyperparameter α using sliding cross-validation. An implementation by scikit-learn library Pedregosa, 2011 was used.

2.1.4 Hydrostatic-seasonal (HS) model

We use this model to predict CB3 sensor data. This model is the linear regression model, that takes to account upstream level, seasonality and time:

$$\hat{y} = \beta_0 + f_1(h) + f_2(s), \tag{10}$$

where β_0 is the free coefficient, $f_1(h)$ is the influence of the upstream level, $f_2(s)$ is the influence of seasonality.

In the original formulation, the influence of the upstream level was considered by a polynomial of the fourth degree:

$$f_1 = \beta_1 h + \beta_2 h^2 + \beta_3 h^3 + \beta_4 h^4. \tag{11}$$

The influence of seasonality was considered by the sum of trigonometric functions with a period of one year:

$$f_2 = \beta_5(\sin(s))^2 + \beta_6 \sin(s) + \beta_7 \cos(s) + \beta_8 \sin(s)\cos(s), \tag{12}$$

where s is calculated as the ratio of the number of the day in the year to the number of days in the year:

$$s = 2\pi \frac{number\ of\ the\ day}{number\ of\ days} \approx 2\pi \frac{number\ of\ the\ day}{365.25}. \tag{13}$$

The HS model assumes that the main contribution to the displacements of the dam is made by the upstream level. The second factor is temperature, the first harmonic of which is modeled using trigonometric functions f_2 with one year period. That is, one of the assumptions is the dependance of the concrete temperature to harmonic oscillations.

The simplicity of the formulation and the absence of a direct temperature factor make it possible to widely use the HS model on objects where the temperature is not measured, or where the temperature have a harmonic law. At the same time, with a sharp change in temperature, the accuracy of the forecast is significantly reduced.

Another advantage of this model is its ease of interpretation. However, if the upstream level strongly correlates with seasonality, then the model's ability to interpret data is significantly reduced, which at the same time does not affect the accuracy of the prediction.

2.1.1 Multilayer perceptron

This model was used for CB2 sensor data prediction. Multilayer Perceptron (MLP) is an artificial neural network architecture consisting of several layers with nodes (neurons). Each layer node is an activation function φ, which takes the value +1, and a vector of values obtained at the nodes of the previous layer:

$$\{x\} = \begin{Bmatrix} x_0 \\ x_1 \\ \vdots \\ x_n \end{Bmatrix} = \begin{Bmatrix} +1 \\ x_1 \\ \vdots \\ x_n \end{Bmatrix}, \tag{14}$$

and weight vector:

$$\{w_k\} = \begin{Bmatrix} w_{k0} \\ w_{k1} \\ \vdots \\ w_{kn} \end{Bmatrix} = \begin{Bmatrix} b_k \\ w_{k1} \\ \vdots \\ w_{kn} \end{Bmatrix}, \tag{15}$$

where b_k is a free coefficient, weight of the constant is +1. The value received by the node is calculated as follows:

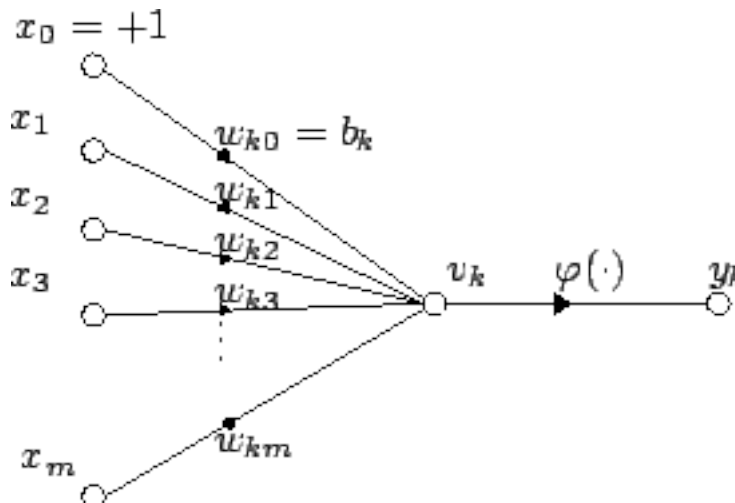$$y_k = \varphi(v_k), where \ v_k = \{x\}\{w_k\}^T = \sum_{i=1}^{n} w_i x_i. \tag{16}$$

Figure 1. Scheme of neural network node

The weight values for each node are determined during minimizing the residual function using the backpropagation method. Adam optimization is used with gradient descent rate $\lambda = 0.001$.

The first or input layer accepts pre-normalized field observation data with an identical mapping as an activation function. The next layers will use the Leaky ReLu function as an activation function:

$$LeakyReLu(v) = \max(0, v) + a\min(0, v) = \begin{cases} v & if\ v > 0 \\ av & if\ v \le 0 \end{cases}. \tag{17}$$

In this paper the Keras Chollet, 2015 library was used to implement multilayer perceptron.

2.2 *Transforming field data*

To build accurate predictive models, we need a large amount of input data. The more input data, the more accurate the predictive model. Therefore, we increase the number of input data available for training by using linear interpolation.

The air temperature and CB2 sensor data have a period of change of one year. To account for seasonality, we added trigonometric functions with a period of one year:

$$\sin(s)\ \text{и}\ \cos(s)\,, \text{где}\ s = 2\pi\frac{number\ of\ the\ day}{number\ of\ days} \approx 2\pi\frac{number\ of\ the\ day}{365.25}. \tag{18}$$

The air temperature sensor data has rapid changes of temperature from day to day. To improve predictions accuracy temperature time series was smoothed by moving average sum with window of 19 days.

From the measurements of the upstream level, it is evident that the reservoir is periodically completely empty. That is, values of the upstream level are less than 195 m, below the dam base elevation. These values do not affect the CB2 sensor data. We convert the upstream data to exclude data below the reservoir bottom at the upstream face of the dam:

$$UpstreamLevel = \begin{cases} h & if\ h > 195 \\ 0 & if\ h \le 195 \end{cases}, \tag{19}$$
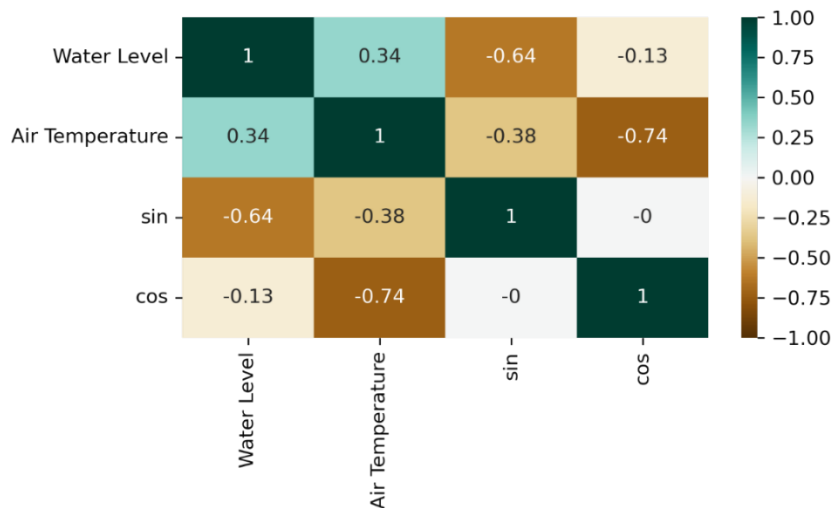
where h is initial upstream level.

Figure 2. Correlation matrix

Highly correlated data cannot be used together in linear regression. Analysis of the correlation matrix (see Fig. 2) shows that the input data used are not too strongly correlated, so they can be used for linear regression. At the same time, a sufficiently high degree of correlation of air temperature and upstream level with the sine and cosine functions confirms the assumption of harmonic variation of these values with a period of a year.

All input features are normalized by removing the mean and scaling to unit variance derived from training set.

2.3 *Results*

Hydrostatic-seasonal (HS) model, used for CB3 sensor data prediction, is implemented as follows:

$$\hat{y} = \beta_0 + \beta_1 UL + \beta_2 UL^2 + \beta_3 UL^3 + \beta_4 UL^4 + \beta_5(\sin(s))^2 + \beta_6 \sin(s) + \beta_7 \cos(s) + \beta_8 \sin(s)\cos(s), \tag{19}$$

where UL is upstream level according to (18).

This model yielded the best results for CB3. The model contains nine coefficients, which, when trained on the training dataset, take the values given in Table 1. The optimal value of the hyperparameter $\alpha \approx 4.72796$. The model prediction is shown in Figures 3 and 4. The distribution of errors is provided in Figure 5. For evaluating warning levels, we use $\pm 3\sigma$ intervals according to (2).

Table 1. Coefficients of HS model

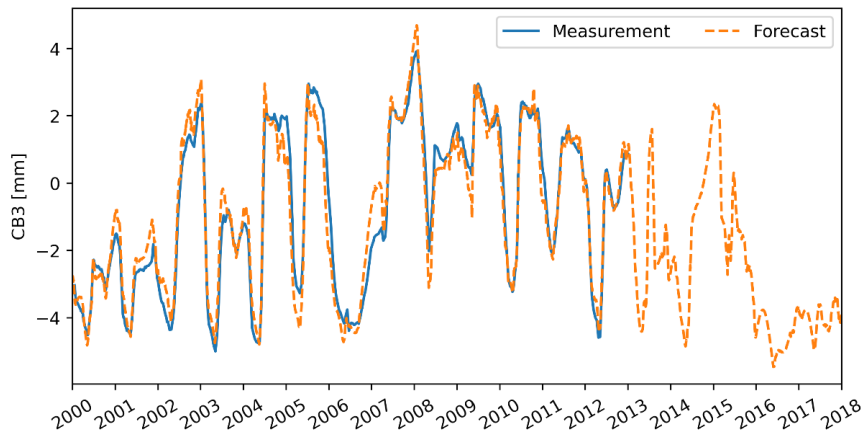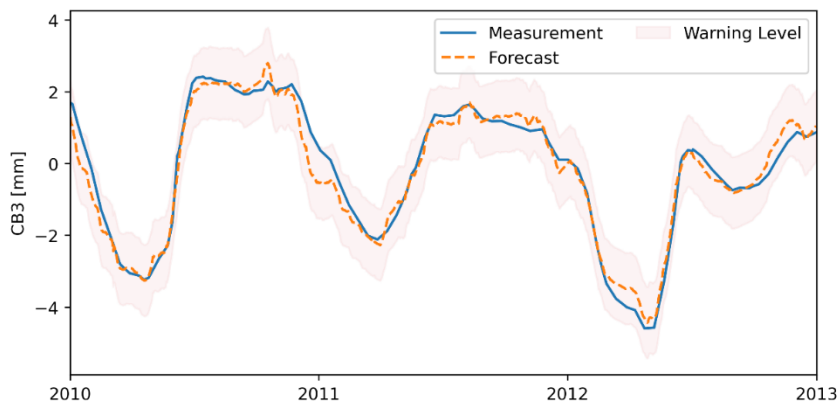| Coefficient	Value
β_0	-0.7563380357142856
β_1	0.35890753
β_2	1.84110614
β_3	1.1469593
β_4	-0.42977392
β_5	0.06657618
β_6	0.82528701
β_7	0.6129237
β_8	0.04377772

Figure 3. CB3 sensor data prediction

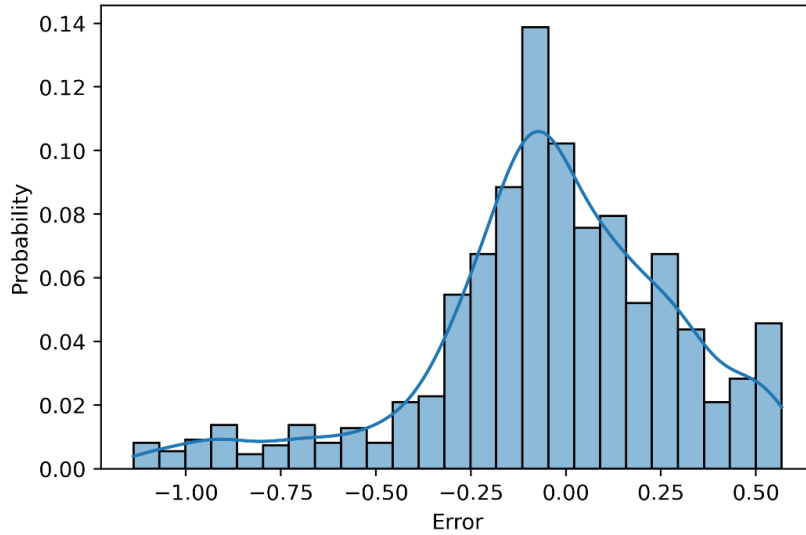Figure 4. CB3 sensor data prediction in a train range with warning levels

Figure 5. CB3 prediction error distribution in a train data set

The multilayer perceptron in this paper has the following architecture: four nodes in the input layer; two hidden layers with Leaky ReLu activation function and using batch normalization and dropout (factor 0.15) of 250 nodes each; output layer with one node and L1 regularization with factor 0.005. The model prediction is shown in Figures 6 and 7. The error distribution is provided in Figure 8.
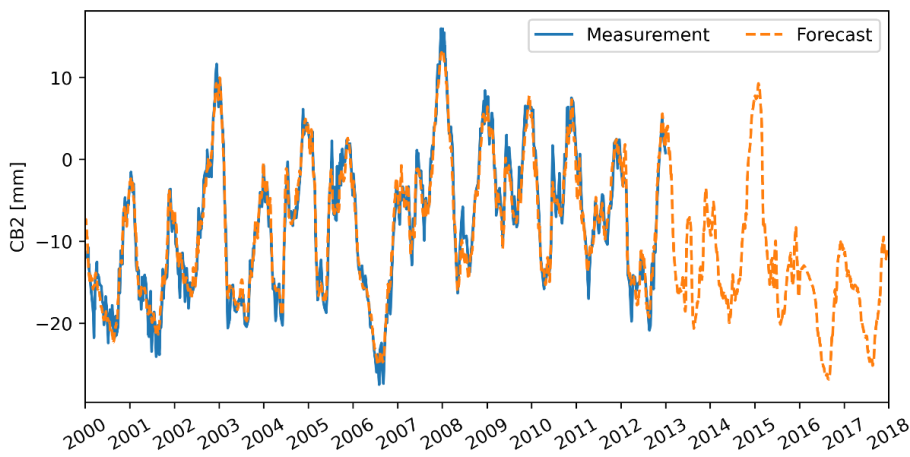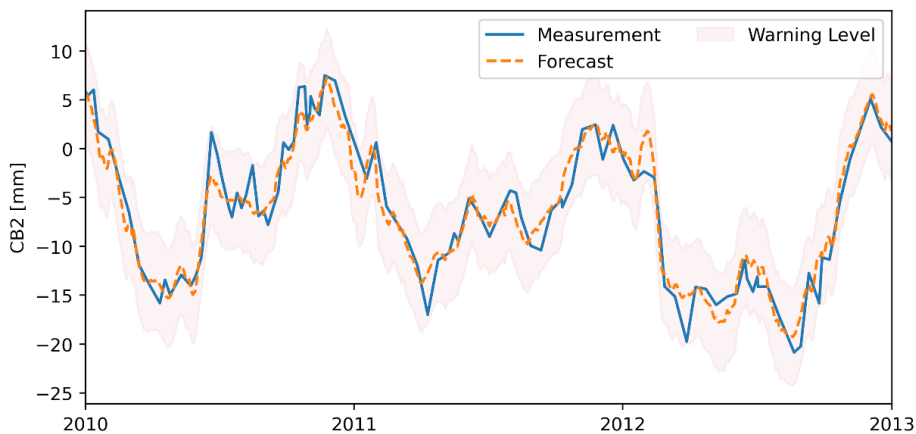

Figure 6. CB2 sensor data prediction

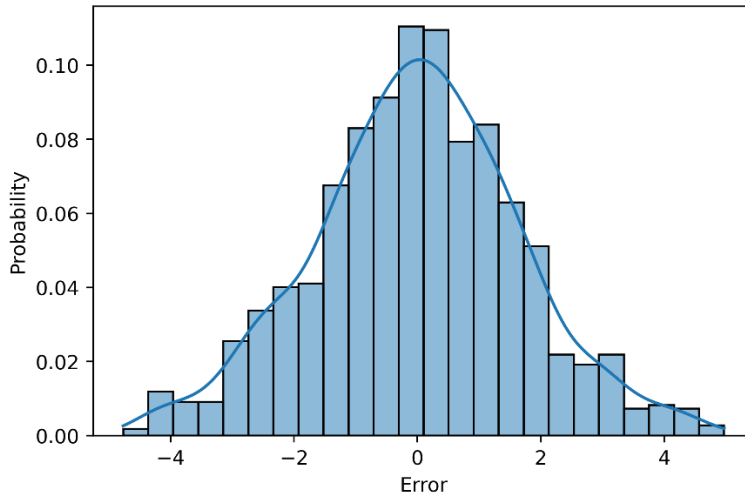Figure 7. CB2 sensor data prediction in a train range with warning levels

Figure 8. CB2 prediction error distribution in a train data set
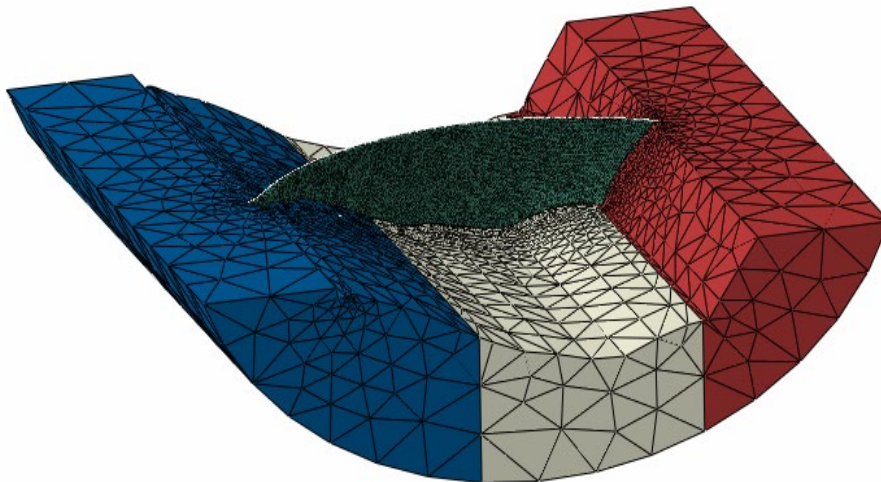
3 FINITE-ELEMENT MODELING

Figure 9. Finite-element model

   We use CAD model delivered by the formulators to create the finite-element model (see Fig. 9). The model was created using Simulia Abaqus 2021. The model of the dam remained unchanged, and the foundation model was modified so that the end surfaces were perpendicular to the lower semicircular surface (see Fig. 9). In addition, the base was divided into three parts to simulate the left and right bank, as well as the bottom part of the rock foundation. The properties of these areas were specified as transversal-isotropic, according to the case formulation. First-order C3D4 tetrahedrons were used to model the foundation (see Table 2). The dam was modeled as a linear-elastic isotropic body using second order C3D10 tetrahedrons. Total number of nodes are 261952, total number of elements are 215859.

Table 2. Finite-element mesh data

Region	Element type	Elements	Nodes
DAM	C3D10	168934	251428
ROCK	C3D4	46925	10524

Contact interaction between the dam bottom and the foundation was considered using tie-contact. The problem was solved in two stages. First, we solved the thermal conductivity problem with a variable upstream level, which was accounted by the user subroutine. The temperature field was found in increments of one day. Then the thermoelasticity problem was solved using the found temperature field. The hydrostatic pressure of the reservoir on the upstream face of the dam and the back pressure on the bottom of the dam were also considered using the user subroutine. The calculation was performed in one-week increments, and then the intermediate values were linearly interpolated for prediction. Calculated using finite-element model CB3 sensor data was modified:

$$\widehat{U}_{CB3\_195\_161} = U_{CB3\_195\_161} \cdot 4.5 - 3. \tag{20}$$

Calculated CB2 sensor data has no modification. Calculated CB2 and CB3 sensor data with warning intervals demonstrated on Figure 10 and 11 respectively.
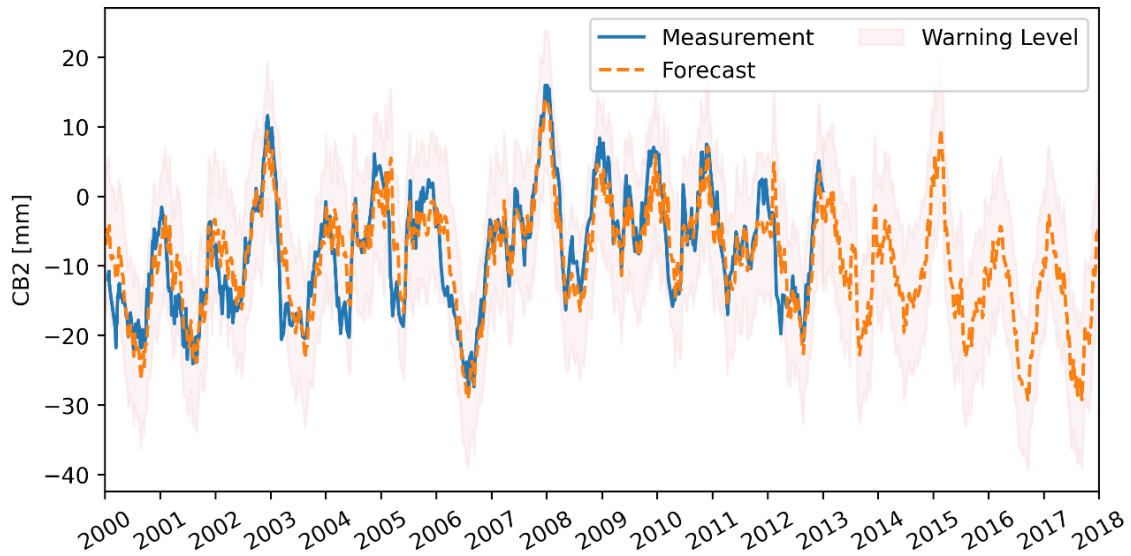

Figure 10. Calculated CB2 sensor data prediction with warning levels
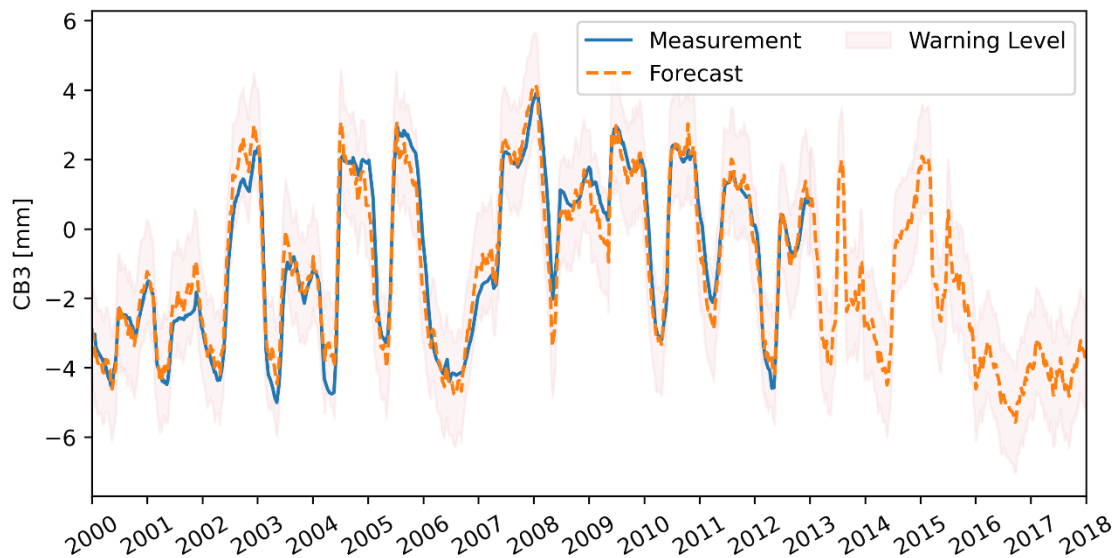
Figure 11. Calculated CB3 sensor data prediction with warning levels

4 CONCLUSION

In this paper we presented two types of prediction models: statistical and finite-element. In statistical models, the prediction of CB2 sensor data was built using a multilayer perceptron neural network. For prediction of CB3 sensor data linear regression was used. The finite-element model prediction was based on a calibrated linear-elastic model with a transversal-isotropic foundation. The accuracy of the prediction obtained with statistical models significantly exceeded the accuracy of the finite-element prediction.

REFERENCES

Scikit-learn: Machine Learning in Python, Pedregosa et al., JMLR 12, pp. 2825-2830, 2011.
Chollet, F., & others. (2015). Keras. GitHub. Retrieved from https://github.com/keras-team/keras

CORRELATION BASED PREDICTIONS OF ARCH DAM DISPLACEMENTS

Josh Corbett
US Army Corps of Engineers

Gabriela Lyvers
US Army Corps of Engineers

Steve Dominic
US Army Corps of Engineers

ABSTRACT: The 2022 ICOLD Benchmarking Workshop involves prediction of arch dam behavior based on recorded reservoir elevation, temperature, and rainfall. The US Army Corps of Engineers team utilized a simple correlation-based data analytics approach to develop predictions of the dam displacement. Dam displacement and cracking at the base of the dam were found to be strongly correlated with the reservoir elevation and air temperature. Displacement of the dam was also affected by cracking at the base, leading the team to utilize a two-stage correlation. The data analytics approach and finite element model led the team to conclude that there may be cracking of the dam or other issues associated with extreme drawdown of the reservoir.

1 INTRODUCTION

The goal of the benchmarking problem is to predict the short- and long-term behavior of the subject concrete arch dam based on relevant environmental data. The behavior of the dam is characterized by multiple sets of measured data including pendulum displacements, a crack opening displacement sensor, piezometers, and weirs to measure seepage flow rates. The problem formulation specifies that it is mandatory for participants to provide displacements during the calibration period (Case A) and provide both short-term (Case B) and long-term (Case C) displacement predictions. Performing predictions of all other data is optional. The two locations for the displacement measurements are for the central block and are shown in Figure 1 with the red circle. The location of the crack opening meter is shown in Figure 2. The team analyzed and predicted data for these three data sets only (both required data sets and one optional set). Measurements on the datasets was provided at 1.5-week intervals between 2000 and 2013 which are to be used as a calibration period. Both short term and long-term predictions are required for 6-months of 2013 and 2013-2017 respectively. For all predicted values, it is also requested that low and high warning levels be identified. These warning levels indicate that there may be a dam safety concern if the measured values fall outside of the warning level range.
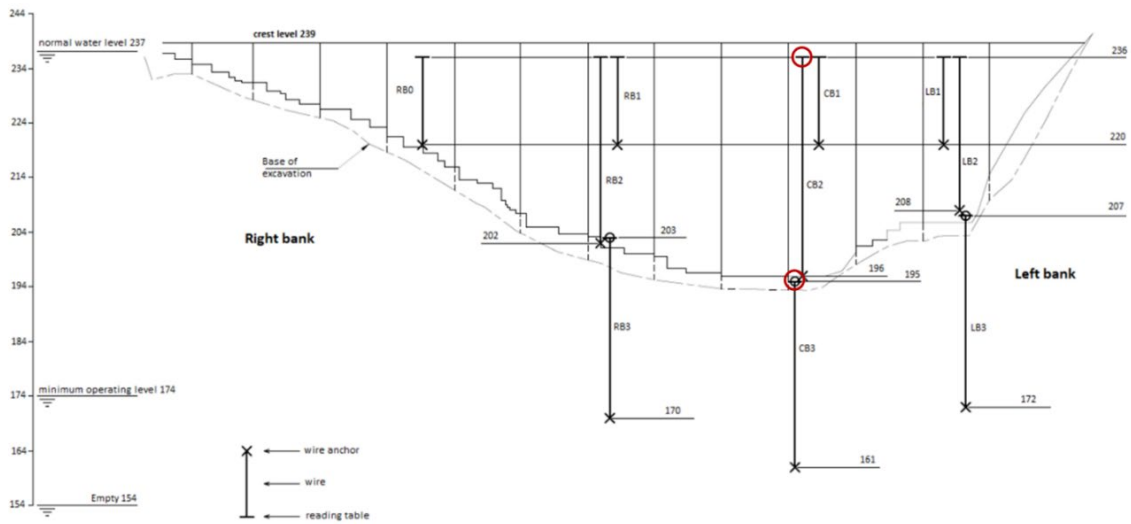

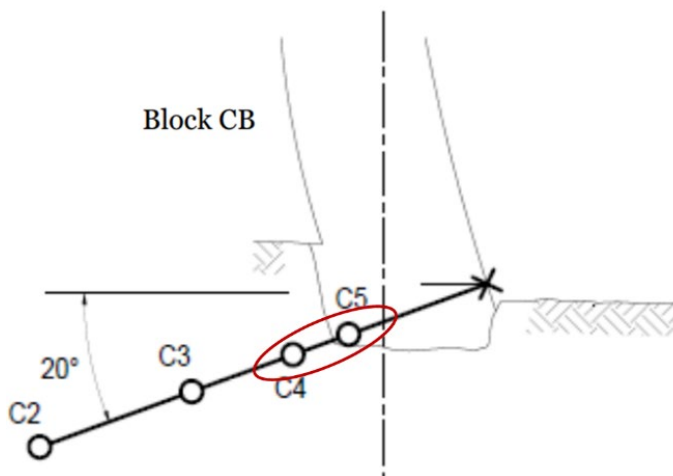Figure 1. Displacement Measurement Locations

Figure 2. Crack Gauge Location

2 DATA USED FOR CORRELATION

The environmental data provided consist of reservoir elevation, air temperature, and rainfall. All of the environmental data was provided at approximately daily measurement intervals for the full period of record including the prediction time periods (i.e. 2000-2017). Two ambient air temperature measurements were provided, referred to as T_a and T_b. T_a is recorded air temperatures from a nearby weather station 50 km from the dam at a different altitude than the dam. T_b is interpolated between weather stations to correspond to the dam site, including the altitude. Rainfall would be expected to effect seepage but has only a tangential effect on displacements and is therefore not used as a prediction variable. The displacement behavior of the dam is expected to be heavily dependent on reservoir level and temperature. While on first glance T_b would be expected to be superior to T_a, there is a closer correlation between T_a and displacement, possibly due to errors in the interpolation approach. Therefore T_a and water elevation are used to predict the displacement response.

3 EVALUATION OF FINITE ELEMENT MODEL

A finite element model of the dam was supplied with the data package. The USACE team is currently using LS-DYNA for finite element analysis. The provided model is built completely with tetrahedral elements, which gives poor results in LS-DYNA. A test model was run without a reservoir and there are substantial stress concentrations along the foundation contact due to the element type. The LS-DYNA model is therefore not used to make the final predictions. However, it was noticed that without a reservoir, the dam will tend to tilt upstream, putting the dam and abutments in tension. We should therefore expect crack opening displacements when the reservoir is very low.

4 DATA ANALYSIS APPROACH

A data analysis approach is used to perform the required predictions. The team used a simplistic method utilizing the correlation between water level and temperature to the displacement of the dam. The data is first sorted and processed to be most indicative of the performance. The data was subdivided and processed using the following approach:
1. The daily variations in air temperature do not immediately affect the displacement of the dam. It takes time to warm/cool enough of the dam mass to have a measurable effect on the structural response. Therefore, a two-week running average of the daily temperature is used, which provides the best fit to the data.
2. The effect of the water level on the dam displacement is based on the force that the water applies to the face of the dam. The water level is therefore converted to a pseudo force (referred to here as the head) by subtracting the empty water level elevation of 154 m from the measured water level at any given time and squaring the difference. Unlike temperature, the water level is expected to have a near immediate effect on the displacement, so daily measures values were used.
3. The crack opening gauge at the base of the dam indicates that the crack opens during high pools. The dam displacement response to head and temperature is different when the crack is closed, open a small amount, or open a large amount. To capture this effect, the data was subdivided into three subsets: Crack displacements of less than zero (i.e. the crack is in compression), crack displacements between zero and 1.85 mm and crack displacements greater than 1.85 mm. Based on the available data, using 1.85 mm as the crack displacement threshold value to discretize the data was found to return the highest correlation between displacement and temperature/water level.
4. Within each crack opening subset, the data was further divided into numerous discrete pool ranges, where the size of each pool range was set to be as fine as possible, while still leaving a reasonable number of data points across a range of temperatures. The minimum number of data points was in the highest pool range with 12 points spanning 8 to 21°C.

5. Within each sub dataset, the effect of crack opening and pool elevation are therefore held approximately constant, and the data is plotted against temperature. The displacement data was found to be approximately linearly related to temperature.

4.1 *Displacement correlation*

Based on the data processing approach presented above, the relationship between temperature and crest displacement for two arbitrarily chosen example pool ranges is shown in Figure 3. While the dam displacements vary in time, once the effects of temperature and reservoir level were removed, no strong pattern in time was detectable. Therefore, the prediction proceeds using only reservoir level and temperature.
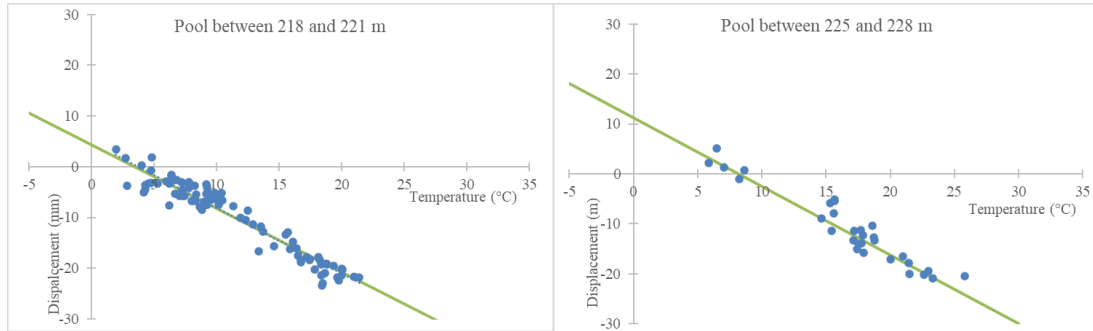

Figure 3. Crest displacement relationship to temperature with reservoir level held relatively constant

As the pool increases, both the slope and intercept of the temperature-displacement relationship also increase. The slope and intercept can be plotted, and a curve fit to these parameters as shown in Figure 4. This process is repeated for the three crack opening datasets. This results in a relationship between head on the dam and ambient temperature with displacement given in Equation (4). This process is repeated for both pendulum displacement (CB2 and CB3) gauges to determine the set of empirical constants for each. The empirical constants vary for the three crack opening ranges, therefore the crack opening must be predicted prior to using (4).
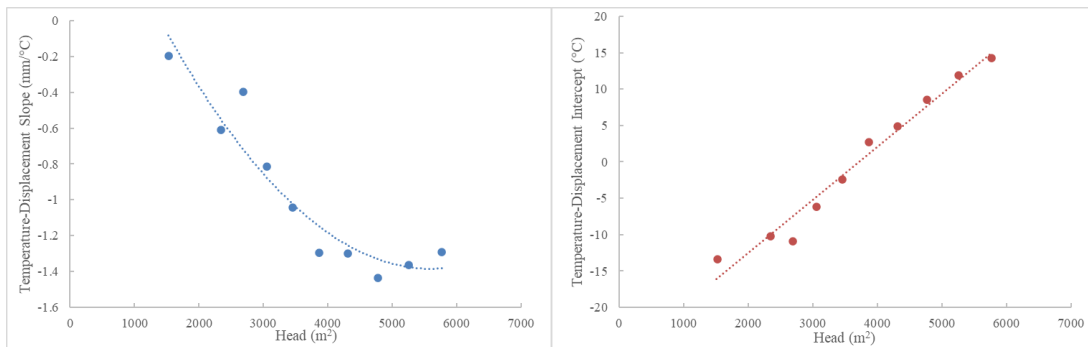

Figure 4. Slope and intercept of lines from Figure 3 as a function of head

$$\Delta = (c_1 H^2 + c_2 H + c_3)T + c_4 H + c_5 \qquad (4)$$

Where $c_{1\text{-}5}$ = empirical constants
Δ = Displacement (mm)
H = Head (m^2) = (pool elevation- reservoir bottom)^2
T = temperature (°C)

4.2 *Crack opening correlation*

The crack opening is primarily driven by the head on the dam, with some influence from the temperature. A curve is fit to the data for low (<7° C) and high (>20° C) temperatures, and intermediate curves are interpolated between these two temperature extremes as shown in Figure 5.
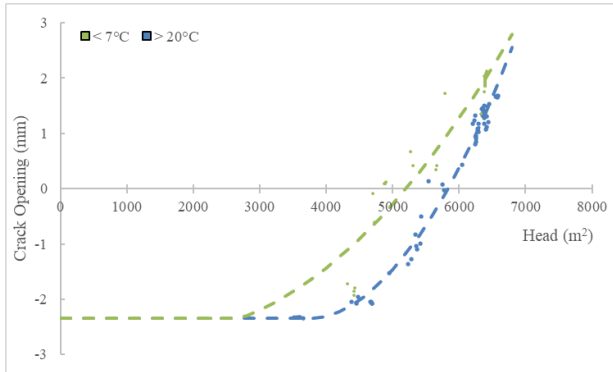

Figure 5. Head vs. crack opening relationship

4.3 *Crack opening prediction*

Using the relationship in Figure 5, the crack opening can be approximated for the full study period as shown in Figure 6 as the blue "Predicted" line. Also plotted are the measured values for comparison. The warning levels are also plotted. The warning levels for the crack opening are set such that approximately 90% of the data falls within the warning levels. The rationale for using the variability of the measured data is if the measured crack opening is outside of the historic expected variability, then there may be an issue with the dam. To more clearly see the three datasets, Figure 7 shows a close-up of Figure 6 spanning a portion of the calibration period and the prediction period. The predictions do not go below a value of -2.34 mm as this appears to be the limit of the gauge. This means there is also a warning level at -2.34 mm as this may indicate a problem with the dam and/or the gauge.
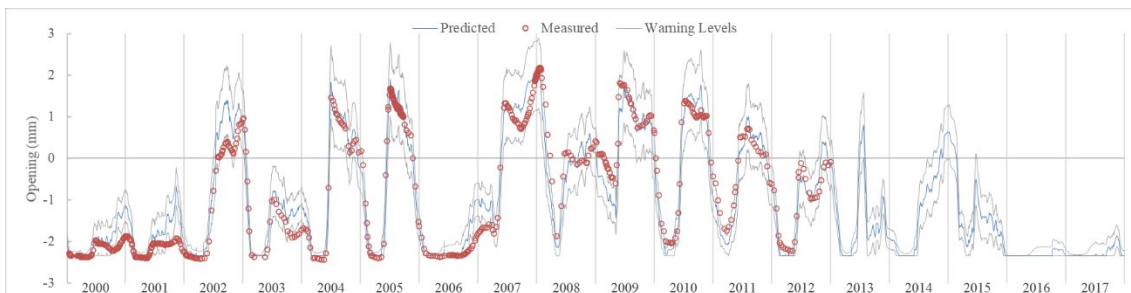

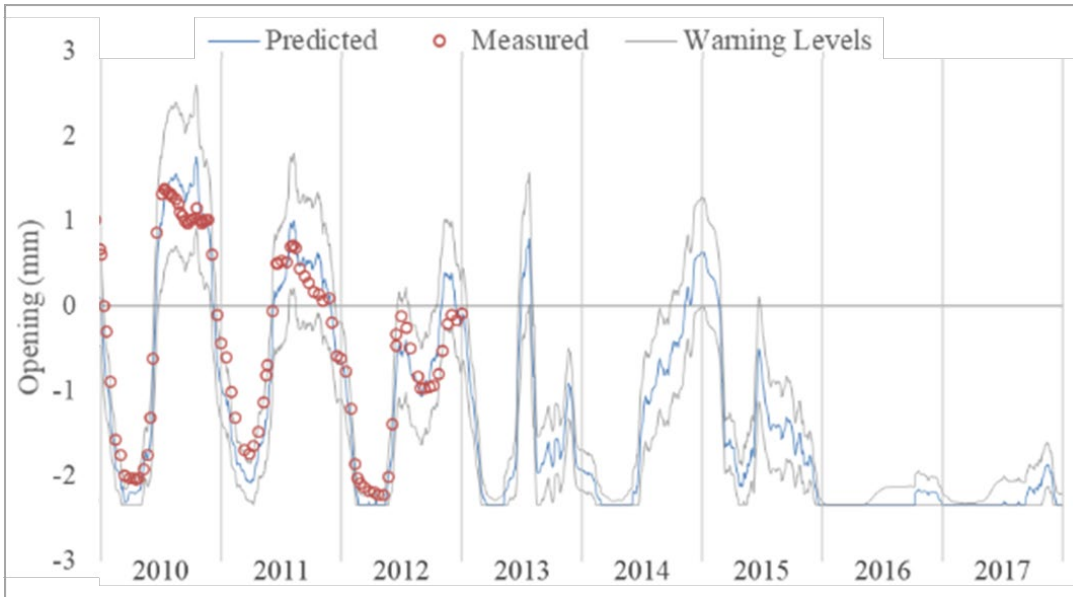Figure 6. Crack opening prediction (CB 4-5)

Figure 7. Closeup of Figure 6

4.4 *Displacement prediction*

Utilizing the calculated crack opening, the pendulum displacements can be calculated with Equation (4). The predicted, measured, and warning level displacements are shown in Figure 8 and Figure 10 The warning levels here are calculated similarly to the crack opening warning levels based on the expected variability at a given temperature/pool combination. However, there is a second consideration in the displacement warning levels based on the observation that at low pools the dam may go into tension. At extreme low pools the warning levels are shifted such that the predicted values fall outside of the warning level. This is identified in the data as the point where the measured displacements are least affected by temperature (i.e. pools where the temperature-displacement slope approaches zero). This can be seen for displacement at the crest in Figure 8 and Figure 9 during the extreme drawdown at the beginning of 2016. Through most of the record, the predicted (blue) line is between the upper and lower warning levels. However, at the beginning of 2016 the predicted values are below the lower warning limit, indicating there may be an issue with the dam at this time. The same effect can be seen for displacement at the base in Figure 10 and Figure 11.
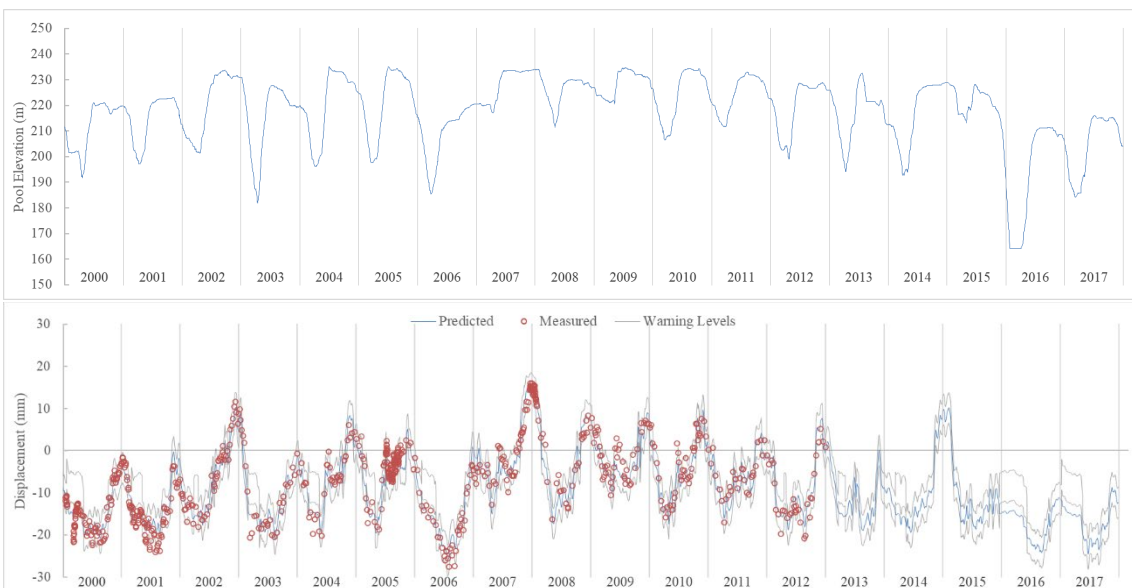

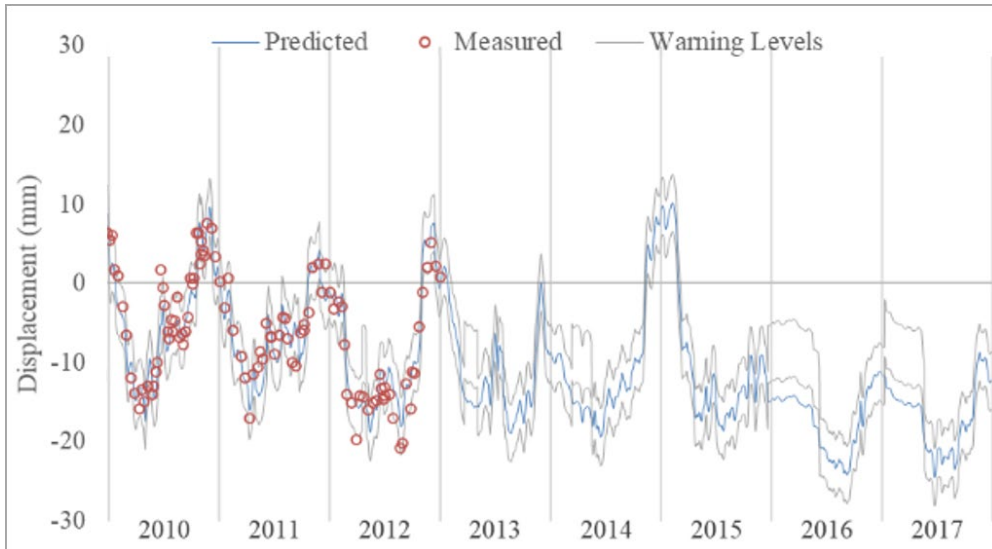Figure 8. Top: reservoir elevation, bottom: displacement at crest (CB2)
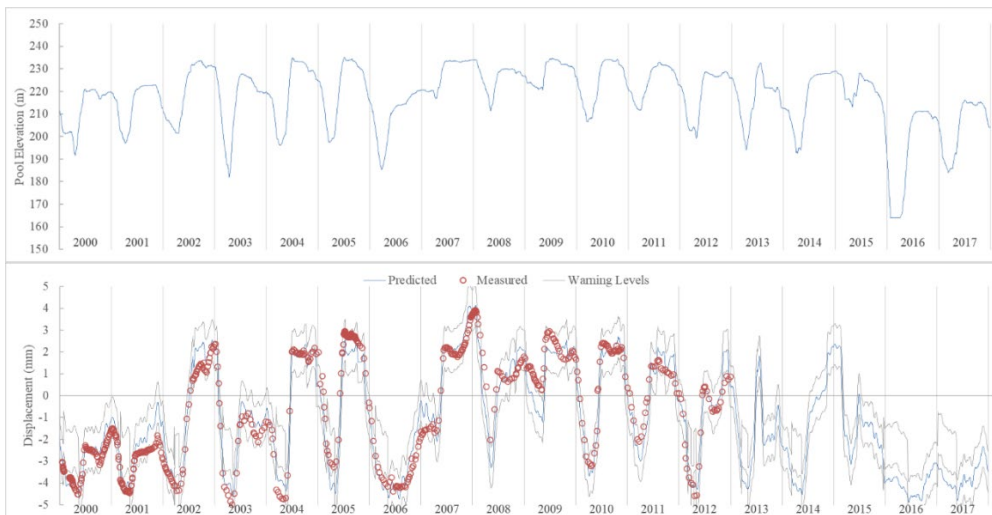
Figure 9. Closeup of bottom of Figure 8.

Figure 10. Displacement at base (CB3)
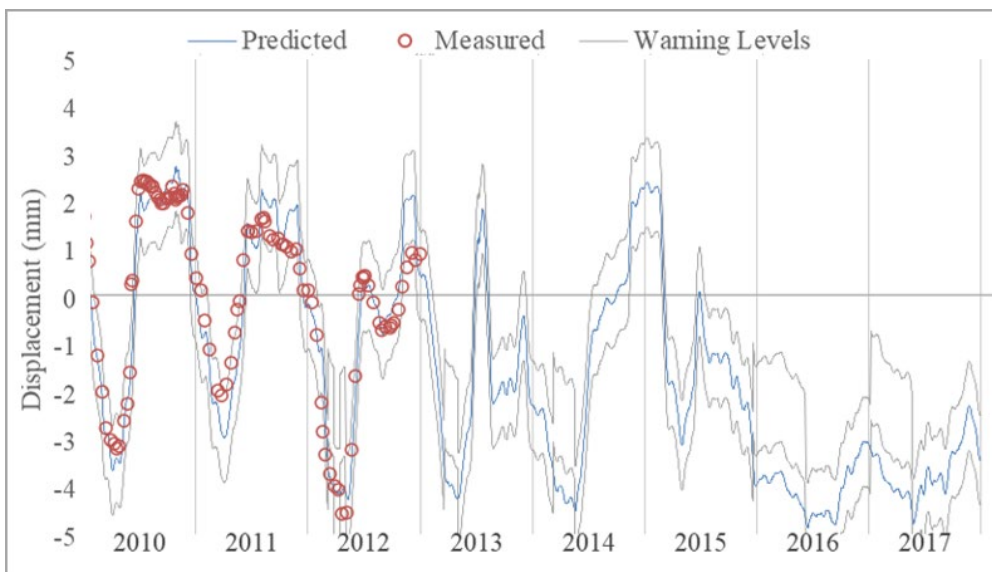
Figure 11. Closeup of Figure 10

5 CONCLUSIONS AND INTERPRETATION

The predicted displacements are considered reasonably close to the measured values given the simplicity of the model with only two predictor variables: water level and temperature. A closer prediction may have been obtained with additional data, however with additional dimensions a more complex data analysis approach may have been necessary. Furthermore, temperature data measured at the dam (rather than interpolated) would have likely resulted in a closer prediction.

In general, this type of model can be used to identify anomalous measurements which then must be investigated by other means. It is difficult to utilize this type of model to evaluate the dam behavior for loadings that have not been experienced at any time in the calibration period. The finite element model was used in a limited capacity to identify a potential issue that may result during periods of deep drawdowns. There are two periods in the past where the reservoir was low enough to cause concern during the calibration period: 2003 and 2006. Additional information from these events could be used to inform later drawdowns, such as in 2016. Without any further analysis, this model would predict cracking of the dam during the 2016 low water, but it is difficult to ascertain the degree of damage. Since the 2016 low water is lower than has previously been experienced, the predictions at this time may be worse than at higher pools, particularly if damage to the dam occurred, which could affect future response.

BEHAVIOUR PREDICTION OF A CONCRETE ARCH DAM: FINITE ELEMENT MODELLING AND MODELS OF SEPARATION OF EFFECTS

Nuno Monteiro Azevedo
LNEC, National Laboratory for Civil Engineering, Lisbon, Portugal

N. Schclar Leitão
LNEC, National Laboratory for Civil Engineering, Lisbon, Portugal

M. L. Braga Farinha
LNEC, National Laboratory for Civil Engineering, Lisbon, Portugal

E. Castilho
CEris, Instituto Superior Técnico, Universidade de Lisboa, Lisbon, Portugal

ABSTRACT: The double curvature arch dam, located in the south of France, proposed for the 16th International Benchmark Workshop on Numerical Analysis (theme A) was numerically studied using computational modules based on finite element method developed by the authors for dam analysis. The dam behavior was also assessed with regression based separation of effects models (SEM), following a hydrostatic-seasonal-temperature approach, taking also into consideration the predictions obtained with the finite element analysis that was carried out. Given that the developed numerical modules adopt preferentially 2nd order 20 node brick elements, a new numerical model of the dam and its foundation was built from the geometry files given by the organizing committee. The developed finite element model considered the contraction joints and the dam/foundation interface. A thermal analysis was initially carried out, using a transient analysis model, followed by several mechanical analyses including the gravity load, the hydrostatic pressure and the temperature variations resulting from the thermal analysis. Different nonlinear models were considered at the dam/foundation interface and at the contraction joints, and two different contact interface approaches were adopted, hard and soft contact approach. Results of the sequentially coupled thermal/mechanical numerical analyses are presented and discussed. Finally, the results of the regression based SEM predictions models are also compared, and the relevance of using the finite element model inputs in the SEM is discussed.

1 INTRODUCTION

The double curvature arch dam, located in the south of France, was numerically studied using computational modules based on finite element (FE) method developed by the authors for concrete dam analysis. The dam behavior was also assessed with regression based separation of effects prediction models (SEM) following a hydrostatic-seasonal-temperature approach, Wilm and Beaujoint (1967). In the adopted displacement prediction model, the results obtained with the finite element analysis that was carried out were incorporated in the SEM, Silva Gomes and Silva Matos (1985) and Rodrigues et al. (2021).

The thermal numerical analysis was carried out with the numerical module *PAT*, Schclar Leitão (2011) and Castilho et al. (2018) which adopts a transient analysis, including Dirichlet boundary conditions (concrete/water and foundation/water) and Robin boundary conditions (concrete/air and rock/air interfaces). The mechanical analysis was carried out with two different numerical models, the finite element module *Parmac3D*, Azevedo & Câmara (2015) which uses an explicit solution algorithm based on the central difference method and a dynamic relaxation algorithm for static convergence, and adopts a soft contact approach for the interface finite element models and a FE module, *PAVK*, Schclar Leitão (2021), that adopts a global matrix static solution approach using a Newton-Raphson algorithm for nonlinear analysis, following a hard contact approach with a high penalty stiffness value for the interface finite element elements.

Given that both mechanical numerical codes, *PAVK* and *Parmac3D*, use preferably 20-node 2nd order brick elements, a new finite element model of the dam and its foundation was built from the geometry files given by the organizing committee. The contraction joints and the dam/foundation interface were included in the developed model. Firstly, a thermal transient analysis was carried followed by the mechanical analysis, using sequential coupling. In the mechanical module *PAVK* a zero tensile strength behavior was adopted for both the contraction joints and for the dam-foundation interface. In the mechanical module *Parmac3D* a Mohr-Coulomb constitutive model with zero tensile strength and zero cohesion was assigned to the interface elements representing the contraction joints. For the dam-foundation interface a brittle Mohr-Coulomb model with a non-zero tensile and cohesion stress value was adopted. The authors have also developed computational models for the hydromechanical model of dam foundations, Farinha et al. (2022), but due to time constraints it was decided not to perform an analysis of this type for the prediction of piezometric heads and seepage flowrates.

Results of the coupled thermal/mechanical numerical analyses are presented and discussed. Finally, the results of the regression-based SEM models are also presented, and the relevance of using the FE model inputs in the adopted SEM is discussed.

2 FINITE ELEMENT MODEL

2.1 *Model description*

Figure 1 shows the numerical model that was used for both thermal and mechanical analyses. The dam is simulated by a group of finite element elastic blocks separated by joints, which represent vertical contraction joints. For the mechanical analysis, the arch dam was divided into 13 blocks separated by radial vertical contraction joints.

The dam body is discretized with 606 2nd order hexahedral finite elements, with 264 2nd order 8x8 node zero thickness interface elements to model the contraction joints, corresponding to a total of 6241 nodal points. The foundation is divided into three zones, left bank (Z1), bottom of the valley (Z2) and right bank (Z3), corresponding to a total of 1936 2nd order hexahedral finite elements and 12563 nodal points. The dam/foundation interface is discretized with 132 2nd order 8x8 node zero thickness interface elements. As shown in Figure 1, The dam comprises three layers of 20 node solid elements through its thickness.

a) 2nd order 20 node brick isoparametric elements representing the dam and its foundation (Z1 – Left bank, Z2 – Valley bottom and Z3 – Right bank)

b) 2nd order 8x8 node zero thickness interface finite elements representing the dam/foundation interface and the contraction joints.

c) Observation points – Pendulum CB2 and CB3, including the adopted radial direction and foundation extensometer C4-C5.
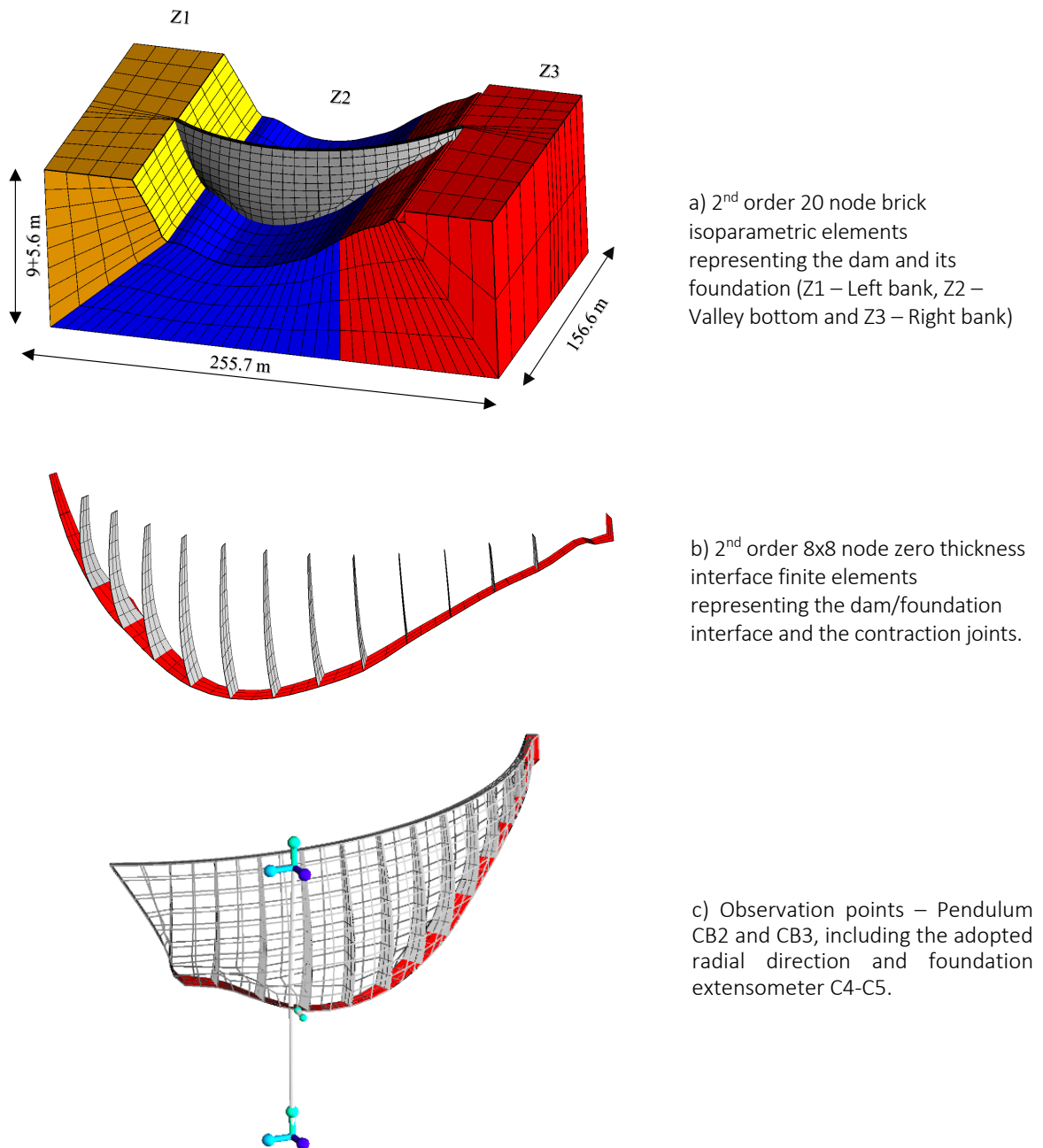
Figure 1. Numerical model for thermal and mechanical finite element analysis.

2.2 *Material properties and boundary conditions*

The material properties considered for both the thermal and the mechanical analyses follow closely the reference values defined in the benchmark. A thermal expansion of $1.0 \times 10^{-5}/C^{o}$ was adopted for concrete, which is the usual value adopted in Portugal for dam concrete, Schclar Leitão (2021). Several mechanical parametric studies were carried out using different Young modulus for the concrete dam and for the foundation, but it was decided to present only the results that adopted mechanical values close to the adopted in previous dam assessments, according to the benchmark organizers. In our point of view in order carry out a comprehensive numerical study it would be necessary to know the observed displacement field in more locations and to have more details regarding the dam concrete and its foundation. A linear elastic isotropic model was adopted for the foundation, given that the adopted mechanical modules do not have the ability to model an orthotropic material.

Table 1 and Table 2 present, respectively, the adopted material properties for the volume finite elements and for the interface finite elements, module Parmac3D. In the mechanical module *PAVK*, a hard contact approach was adopted with a high penalty value of 2200 GPa/m for the joint interface normal and shear stiffness.

In the mechanical module (*Parmac3D*) a Mohr-Coulomb constitutive model with zero tensile strength and zero cohesion with a friction angle of 45º was assigned to the interface elements representing the contraction joints. For the dam-foundation interface a brittle Mohr-Coulomb model with a non-zero tensile stress (2.0 MPa) and a nonzero cohesion stress (6.0 MPa) with a friction angle of 45º value was adopted.

Table 1. Material properties of the volume elements.

Material	Young's modulus E (GPa)	Poisson´s ratio ν (-)	Density ρ (kg/m3)
Concrete	22.0	0.20	2400
Foundation - left bank (Z1)	1.0	0.20	2700
Foundation - Valley bottom (Z2)	1.0	0.20	2700
Foundation - right bank (Z3)	10.0	0.20	2700

Table 2. Material properties of the joint elements – Module *Parmac3D*.

Interface	Normal stiffness k_n (GPa/m)	Shear stiffness k_s (GPa/m)
Concrete/Concrete	220.0	88.0
Concrete/Foundation (Z1)	10.0	4.0
Concrete/Foundation (Z2)	10.0	4.0
Concrete/Foundation (Z3)	100.0	40.0

In the mechanical analysis the nodal displacements at lateral boundaries of the foundation and at the base of the foundation were prevented in module *Parmac3D* simulations and in the *PAVK* simulations only the node displacements at the base of the foundation were prevented.

In the thermal analysis, all air-exposed boundaries were subjected to convection heat transfer boundary conditions, and, in the case of dam surfaces, solar radiation flux absorption boundary conditions were also applied. Specified water temperature boundary conditions were applied at the upstream nodes below the water. Adiabatic boundary conditions were applied at the lateral boundary of the rock mass foundation. Bottom nodes of the foundation were prescribed with a temperature of 4 °C.

In the convection boundary condition, the air temperature T_b was introduced as a table of discrete values and the given convection coefficient of 13 W/(m2 K) was used.

In the solar radiation boundary condition, the radiative model reported by Kumar et al (1997) was applied. To this aim, it was considered that the downstream face of the dam faces South West with its axes forming an angle of 37° with the South, a geographical location of 42.58ºN, 1.895ºE and an absorption coefficient of 0.65. Since the Kumar's model is a clear sky model, that is, under cloudless sky conditions, the beam irradiance was reduced by a factor of 0.30 each time that the rainfall was greater than 10 mm.

For the definition of the water temperature boundary, that is, the elements above or below the water, a discretization of the level of the reservoir in bands compatible with the mesh was adopted.

2.3 *Numerical analysis sequence*

The thermal analysis started in 1995 and a fully implicit solution procedure was used with a one hour time step. The thermal analysis allowed the definition of the thermal field in the concrete dam and foundation every forthnight from the 1st of January of 2000 to the 31st of December of 2017.

In the mechanical analyses that were carried out the gravity loading, the hydrostatic pressure and the thermal field were applied at each loading stage that represent a 15 days behaviour. In the nonlinear analysis, a dynamic relaxation algorithm using an explicit central difference scheme

was adopted at each load step in the *Parmac3D* module and a Newton Raphson algorithm was adopted in the *PAVK* computational module that adopts a global stiffness matrix static solution.

3 MODEL OF SEPARATION OF EFFECTS

3.1 *Model description*

A Separation of Effects Model (SEM) based on a hydrostatic-seasonal-time (HST) model, Wilm and Beaujoint (1967), was adopted for the prediction of the observed data (pendulum and foundation displacements, piezometric head and total seepage flowrate). As mentioned before, in the prediction of the displacement fields, the results obtained with the finite element analysis that was carried out were incorporated, Silva Gomes and Silva Matos (1985) and Rodrigues et al. (2021), namely the numerical displacement predicted at the points of observation due to the imposed temperature field assuming an elastic behaviour. The adoption of the FE elastic prediction due to the temperature field was found to lead to a better agreement between the SEM model prediction and the observed data. The incorporation of the FE predictions within a SEM model requires that a FE model is available and that the numerical results are constantly updated with the new water level and temperature values. The adopted SEM was based on the following functions:

$$\mathrm{Pr}\,edition\,(h,T,t) = \underbrace{f_1(h)}_{a_1 h + a_2 h^2 + a_3 h^3 + a_4 h^4 + a_5 h^5} + \underbrace{f_2(T)}_{\substack{a_6 \cos(s) + a_7 \sin(s) + a_8 \sin^2(s) + a_9 \cos(s)\sin(s) \\ or \\ a_6\,FE_{prediction}(T)}} + \underbrace{f_3(t)}_{a_{10}\log(1+t/300)} + k \tag{1}$$

The same SEM model was adopted for the long-term and for the short-term predictions using the provided data, namely the water level (h), and the monitored data throughout 13 years of observation (2000-2012).

3.2 *Warning levels*

The safety margin reference values were chosen according to the team members experience, mostly for pendulum displacements interpretation. The warning levels were chosen given the standard deviation of the difference between the predicted values, adopting a SEM model, versus the monitored data that was supplied by the benchmark organizers. An interval of +- 3 times the standard deviation was adopted in all sensors.

Observed values with a difference from the prediction values higher than 5 times the standard deviation should be immediately analyzed. It is important to assess the reason behind this difference, which can be due to equipment failure or due to a change in structural behavior that was not being included in the prediction model (damage due to swelling) or it can be an acceptable behaviour not represented by the model prediction.

In the analysis that was made for this dam and for the data that was received, it was found that a value of +- 3 times the standard deviation significantly reduces the days with warning levels along the 2000-2012 monitoring period. It was assumed that the monitored behaviour between 2000 to 2012 was a normal behaviour. To point out that an interval of +- 3 times the standard deviation is meaningful when the SEM predictions are in excellent agreement with the observed data, which as is later shown does not occur when analysing the seepage observed data, nevertheless a similar value was adopted.

4 MAIN RESULTS

### 4.1 *Finite element predictions*

Figure 2 compares the displacement field FE predictions from the 1st of January 2000 to the 31st of December 2012 with the pendulum observed data. It is shown that the *PAVK* elastic mechanical model predicts a response in close agreement with the *Parmac3D* mechanicals models (elastic and nonlinear). From the obtained numerical results it is clear that the different

support conditions adopted in each mechanical model do not have a meaningful influence on the predicted response. Nevertheless, the nonlinear response predicted with the *PAVK* module does lead to a slightly different response, which was expected as the nonlinear behaviour adopted in the dam/foundation interface is much more brittle (no tensile strength or cohesion for positive gap) than the model adopted in the PARMAC3D nonlinear mechanical model (maximum tensile strength and cohesion values up to failure).

The predicted pendulum numerical responses have a reasonable agreement with the observed data. Given the time constraints it was decided not to perform a parametric study in order to find the mechanical parameters that lead to a better agreement with the observed data. For this type of analysis, it is important to have more than one pendulum lines observations in order to proper calibrate the dam and the foundation elastic properties.

Regarding the foundation displacement sensor C4-C5, Figure 3, it is possible to observe that the *Parmaca3D* mechanical models, elastic and nonlinear, predict a numerical response closer to the observed data than the response predicted with the *PAVK* mechanical models. This is due to the fact that in the Parmac3D mechanical module a soft contact approach is adopted, and the dam/foundation interface has a much higher deformability, when compared to the *PAVK* module. A similar result would have been obtained with the *PAVK* module if a more discretized foundation was adopted closer to the dam/foundation interface with a lower Young's modulus. A soft contact approach is from the physical point of view less rigorous, but it has the advantage of allowing the interface to contribute to the overall displacement field, which sometimes can lead to a better numerical prediction with a less refined discretization when compared with mechanical modules that adopt a hard contact approach.
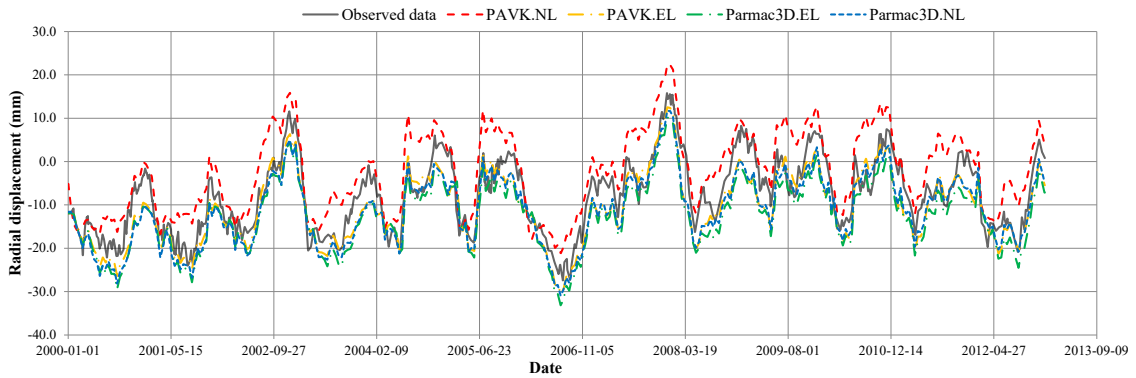
a) Pendulum CB2
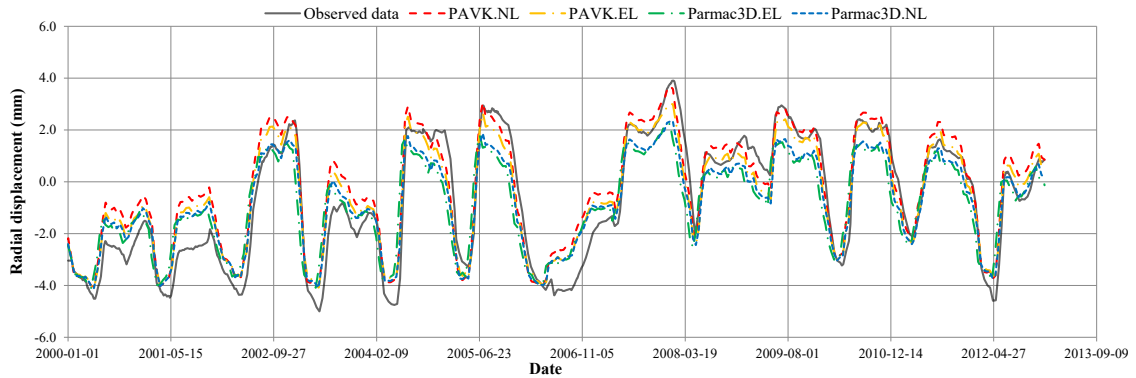
b) Pendulum CB3

Figure 2. Observed versus numerical pendulum displacement field time series – 1st of January 2000 to 31st of December 2012.
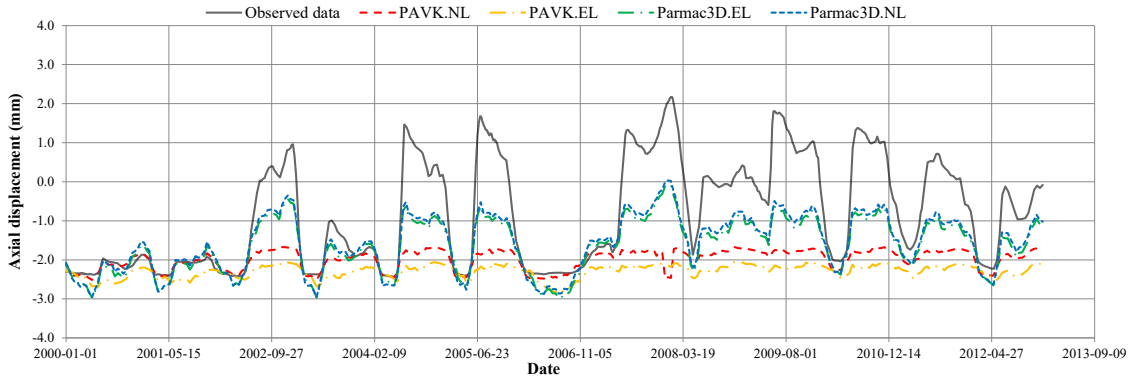
Figure 3. Observed versus numerical displacement field time series – Foundation displacement sensor C4-C5 – 1st of January 2000 to 31st of December 2012.

Figure 4 shows the damage at the dam/foundation joint interface integration points predicted with the *Parmac3D* module. Given the adopted brittle interface model, the damage is either 1, cracked integration point, or 0, which means that the integration point is still under an elastic behaviour. It can be seen that the *Parmac3D* nonlinear model predicts an extensive cracking at the dam/foundation in the vicinity of the right bank (foundation zone Z3). To further understand if this really occurred it would be important to analyse data collected in monitoring equipment installed in this area.

The presented finite element predictions clearly show that the thermal/mechanical coupled response in the linear regime can be performed with the available modules. Similar results have also been obtained within viscoelastic and damage regime. In our point of view the principal numerical focus should be in the development of models that also consider the hydromechanical response, Braga et al. (2022).
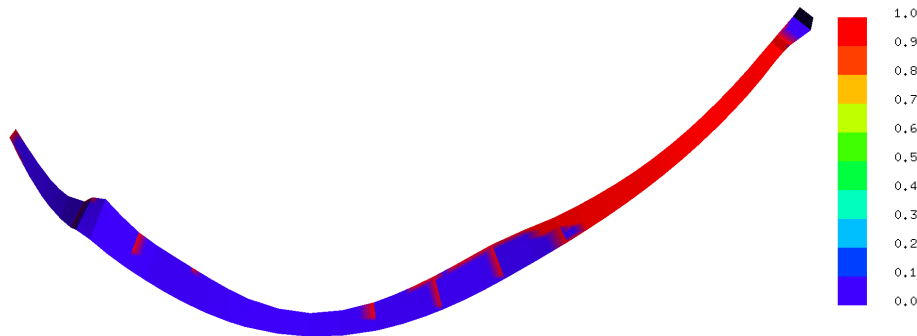

Figure 4. Damage distribution at the dam/foundation interface predicted with the mechanical module Parmac3D – Nonlinear model – 31st of December 2017.

4.2 *Separation of effects predictions*

Figure 5 shows the pendulum displacement field SEM calibration period and the SEM predictions from the 1st of January 2012 to the 31st of December 2017, following the usual HST approach (SEM.HST) and a hybrid approach adopting the FE analysis radial displacement field associated to the temperature field as the function representing the temperature effect ($f_2 (t)$). Figure 5 also shows the observed data from the 1st of January 2000 to the 31st of December 2012 adopted to calibrate the SEM model through a regression analysis. With the introduction of the FE predicted radial displacement the correlation coefficient was slightly increased from 0,93 to 0,95, as shown in Figure 5, where the SME.HST.FE slightly higher peaks are predicted when compared with the traditional SEM model.
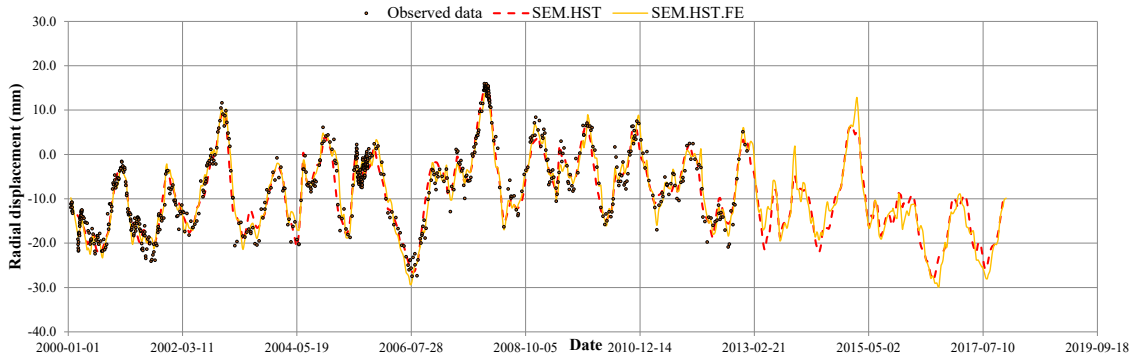
Figure 5. Observed versus SEM prediction pendulum CB2 displacement field time series – Calibration: 1st of January 2000 to 31st of December 2012 – Prediction: 1st of January 2013 to 31st of December 2017.

Figure 6 shows the radial displacement at pendulum CB2 SEM function associated to the water level influence (f1 (h)) and the FE radial displacement predictions adopting the module Parmac3D for both a linear and a nonlinear model. It can be seen that with the introduction of the FE predicted radial displacement, the water level influence slightly changes, being the SEM.HSM.FE predicted curve stiffer for water levels higher than 15 m, when compared to the response predicted with SEM.HSM.

Figure 6 also shows that the adopted FE model, linear and nonlinear, has a significant influence on the predicted response. The SEM water level prediction can be used to calibrate the FE material properties but a higher number of observed dam displacements and a better description of the dam foundation zoning and properties need to be made available in order to proper calibrate the FE model. with SEM.HSM.
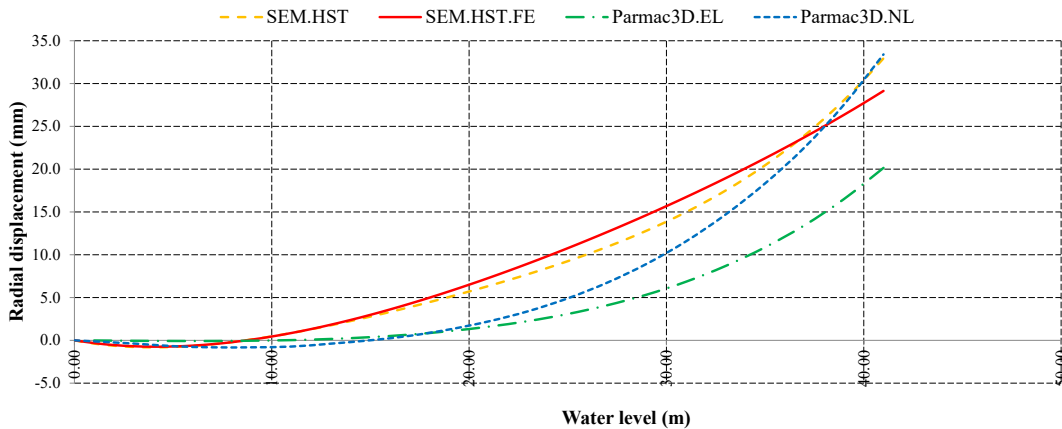

Figure 6. Pendulum CB2 radial displacement evolution with water level - SEM predictions versus FE predictions.

Figure 7 shows the total seepage flowrate SEM calibration period and the SEM predictions from the 1st of January 2012 to the 31st of December 2017, following the usual HST approach. For this type of data the lowest correlation coefficient of 0,50 showing that the adopted SEM model does not satisfactory explain the observed behaviour. Note that in the several attempts that were made the rainfall data and the derivative of the water level, Desideri (1985) were adopted in the SEM models but it was not possible to obtain a better correlation with the observed data. There is no perfect match between the rainfall peaks or 1st derivative peaks with the observed seepage values. Nevertheless, a similar SEM model has been shown to give a good agreement for seepage data, Farinha (2010), nevertheless for this better agreement it was important to separate the seepage values into two more than a zone and also to address the seepage origin. The difficulties in carrying out a successful SEM prediction show that the current SEM models for the interpretation of the hydraulic response need to be further improved in order to have better predictions.
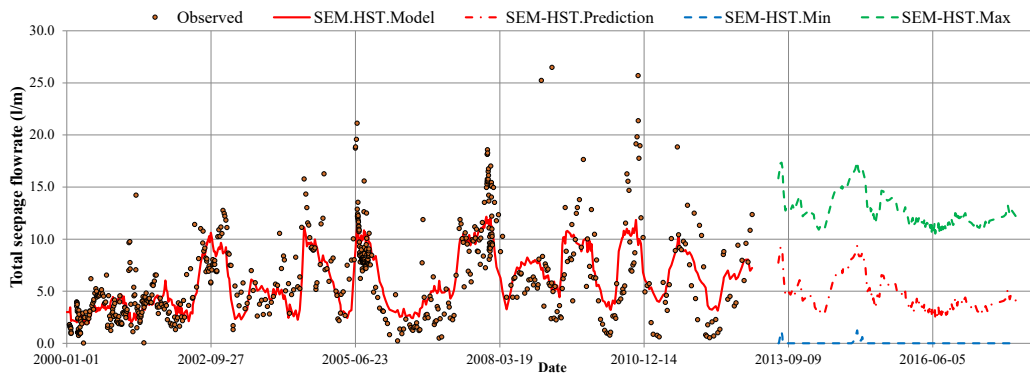
Figure 7. Observed versus SEM prediction total seepage flow rate time series – Calibration: 1st of January 2000 to 31st of December 2012 – Prediction: 1st of January 2013 to 31st of December 2017 – Including warning levels

5 CONCLUSIONS

The double curvature arch dam, located in the south of France, was numerically studied with thermal and mechanical computer codes purposely developed by the authors for dam analysis. The predicted displacement field numerical responses have a reasonable agreement with the monitored data. Due to time constraints, it was decided not to perform parametric studies in order to obtain an even better agreement. In previous studies where the research team has been involved it was found to be important to perform the parametric studies for more than one location of pendulum lines.

The difference between a soft contact approach and a hard contact approach for the interface elements was discussed. It was shown that even if a soft contact approach is not as physically correct as the hard contact approach, it can lead to a better overall agreement. Nevertheless, the results show that in the vicinity of the dam/foundation interface a more refined discretization with lower Young's modulus should be adopted in order to have a better agreement with the observed response at the dam foundation.

The presented finite element predictions clearly show that the thermal/mechanical coupled response in the linear regime can be performed with the available modules. Similar results have also been obtained within the viscoelastic and damage regime. In our point of view the principal numerical focus should be in the development of models that also consider the hydromechanical response.

The dam behavior was also assessed with separation of effects regression based prediction models following a hydrostatic-seasonal-temperature approach. During the displacement analysis it was found to be relevant to adopt in the SEM model the results obtained with the finite element analysis, namely the response obtained with an elastic model for the imposed temperature field. The prediction analysis that was performed also shows that the current SEM models for the interpretation of the hydraulic response need to be improved in order to have better predictions.

ACKNOWLEDGEMENTS

REFERENCES

Farinha, M.L.B. 2010. Hydromechanical behaviour of concrete dam foundations. In situ tests and numerical modelling. *Phd. Thesis, IST, Lisbon, Portugal*.

Farinha, M.L.B., Monteiro Azevedo, N., Schclar Leitão, N,.; Rocha de Almeida, J., Oliveira, S. 2022. Sliding Stability Assessment of Concrete Dams Using a 3D Discontinuum Hydromechanical Model Following a Discrete Crack Approach. *Geotechnics 2* :133-157.

Castilho,E., Schclar, N., Tiago, C., Braga Farinha, M.L. 2018. FEA model for the simulation of the hydration process and temperature evolution during the concreting of an arch dam, *Engineering Structures*, 174: 165-177.

Desideri, A. 1985. Modeli statistici previsionali delle misure piezometriche nella diga di Oroville. *ISMES G(550) qI8, no. 214*, Bergamo, Italy (in Italian).

Kumar, L., Skidmore, A.K., Knowles, E. 1997. Modelling topographic variation in solar radiation in a GIS environment. Int J Geogr Inf Sci, 11(5): 475-497

Monteiro Azevedo N., Câmara R. 2015. Dynamic analysis of concrete dams: fluid structure displacement based interaction models. *Dam Engineering* Vol. XXV (4): 113-132.

Rodrigues, M., Oliveira, S., Lima, N., Proença, J. 2021. Displacement Monitoring in Cabril Dam Using GNSS. *Dam Engineering*. Volume XXXI (3): 149-165.

Schclar Leitão, N. 2011. Environmental thermal actions – Thermal analysis of Alto Lindoso dam. In *Proceedings of the 6th International Conference on Dam Engineering*, Lisbon, Portugal.

Schclar Leitão, N. 2021. Study of the cracking process in an arch dam. In *Proceedings of the Congresso Nacional Reabilitar & Betão Estrutural 2020*, Lisbon, Portugal (in Portuguese).

Silva Gomes, A., Silva Matos, D. 1985. Quantitative analysis of dam monitoring results. State of the Art, applications and prospects. In *Quinzième Congrès des Grands Barrages,* Lausanne, Switzerland.

Willm, G., Beaujoint, N. 1967. Les méthodes de surveillance des barrages au service de la Production Hydraulique d'Életricité de France. Problèmes anciens et solutions nouvelles. In *IX Congress ICOLD. R.30 Q.34,* Istanbul, Turkey.

BEHAVIOUR PREDICTION OF A CONCRETE ARCH DAM FOR THE 2022 ICOLD BENCHMARK

Mirko Corigliano
Enel Green Power, Italy

Matteo Moscariello
Enel Green Power, Italy

Edoardo L'Aurora
Enel Green Power, Italy

Tiziano Pasqualato
Enel Green Power, Italy

ABSTRACT: The paper presents a study carried out to predict the response of some parameters measured on a concrete arch dam through statistical model, proposed as theme A in the frame of the 16th International Benchmark Workshop on Numerical Analysis of Dams. The prediction has been carried out using an ensemble model combining a linear regression model and a SARIMA model. The prediction has been performed for the displacement of two pendulums located at different levels, the opening of a crack on the foundation and a piezometric level.

1 INTRODUCTION

As part of the innovation and digitalization process of ENEL Green Power hydroelectric plants, the PresAGHO (Predictive System and Analytics for Global Hydro Operation) project was launched in September 2018, aimed at developing a predictive diagnostic process integrated into the maintenance process. In this context, starting from 2020 the project was extended to civil works, and the platform called "Dam Behavior" was developed with the aim of making available an integrated system for data quality analysis and structural measures processing for large dams, allowing predictive analysis and anomalies detection in the time series of the parameters. The algorithms used in "Dam Behavior" at the moment considers two models, one based on a multivariate analysis through a linear regression model, whereas the second is a SARIMA model. The two models are considered with different weights depending on the type of parameter analyzed, and its correlation with the cause parameters. The aims of the of the "Dam Behavior" platform is to perform anomaly detection using models which do not require a significant effort by the user in terms of model definition. For such reason, the models used consider a limited number of cause parameters and the required input are minimized. Consequently, this may result in a little less accurate model, nevertheless simple and reliable, that can be applied to a wide range of different parameters. To perform this "model generalization" in linear regression model, when the cause-and-effect parameters are not strongly correlated, it is necessary to preprocess the data applying a procedure of de-seasoning, which will be described in the section 3, to account for the seasonal effects.

To apply the procedure developed in the Enel "Dam Behavior" platform, to the prediction of the response of the double curvature arch dam proposed in the Theme A for the 2022 ICOLD International Benchmark Workshop on Numerical Analysis of Dams, an ensemble model will be defined combining, using a weighted average, the SARIMA and linear regression model. The weights are defined based on engineering judgement depending on the parameter considered. The algorithms have been implemented in Python environment. The typical interval of period considered in the "Dam Behavior" platform is of a yearly seasonal cycle, backwards or forward with respect to the day of analysis depending if the interest is on anomaly detection, by comparing model and measures, or a true prediction if the interest is on the definition of threshold of the measures accounting for seasonal contribution (i.e., dynamic threshold). It is worth notice that a "true prediction" implies that the cause parameters (e.g., water level, temperature, etc.) are unknown, in this case the use of a univariate model, such SARIMA, may help to reduce the epistemic uncertainty.

The characteristics of the dam, the monitoring system and the available measurements are included in the paper of the formulator and will not be repeated in this paper for sake of brevity. The prediction has been performed for the radial displacement of two pendulums located at crest and foundation levels in the central block of the dam, the opening of a crack on the foundation and a piezometric level.

2 DESCRIPTION OF THE STATISTICAL MODEL

The prediction of the response of the arch dam parameters is performed through an ensemble model, obtained combining a linear regression model with a time series forecasting method using SARIMA algorithm. The two models are combined through a weighted average, whose weights are defined based on engineering judgement depending on the parameter considered as described below.

One of the algorithms used for the prediction of the dam parameters is the regression analysis, which represents a statistical approach to predict the values of one or more dependent variables Y (i.e., defined predicted or estimated, corresponding to the effect parameters) from a set of independent variables X (i.e., defined predictive, corresponding to the cause parameters). Linear regression is one of the basic algorithms of supervised machine learning techniques. A linear regression with multiple variables was used (i.e., multivariate linear regression). The estimated value ($\hat{Y}$) through a multivariate linear regression can be expressed by the relation:

$$\hat{Y} = \beta_o + \sum_{j=1}^{p} X_j \cdot \beta_j \tag{1}$$

The term linear refers to the sum of the model parameters (β_j), each of which is multiplied by a single predictive variable (X_j). By including the unit constant among the predictive variables (i.e., $X = [1, \ X_1, \ X_2, ..., X_p]$), equation (1) can be rewritten in matrix form:

$$\hat{Y} = X \ \cdot \beta \qquad\qquad (2)$$

The unknowns of the problem are constituted by the vector of the coefficients of the model ($\beta^T = [\beta_o, \ \beta_1, \ \beta_2, ..., \beta_p]$). There are different methods for the evaluation of the model parameters, the "fitting" of linear models is usually carried out by choosing the coefficients β that minimize the sum of the squared residuals (least squares method):

$$RSS(\beta) = \sum_{i=1}^{N}\left(y_i - x_i \ \cdot \beta\right)^2 \qquad\qquad (3)$$

One of the predictive parameters is the time, which is considered linearly and is properly normalized so that in the training period of the model it varies in an interval between 0 and 1. The predictive parameter always considered in the regression is the water level, moreover depending on the available data other parameters can be eventually considered, as discussed in the in § 1.51. In order to improve the predictive capabilities of the model, additional characteristics are considered by means of suitable polynomial expansions. For example, if X_1 represents one of the predictive variables, the additional variables $X_2 = X_1^2$, $X_3 = X_1^3$, etc. can be considered.

The time series representing the dam response typically include seasonal effects characterized by annual cycles (however, for the most temperature-sensitive parameters, cycles of a shorter period, even daily, may also be present). The seasonal component can be conveniently represented by a harmonic model through a Fourier series:

$$s_t(t) = \sum_{n=1}^{N}\left[a_n \cdot cos\left(\frac{2\pi \cdot n \cdot t}{P}\right) + b_n \cdot sin\left(\frac{2\pi \cdot n \cdot t}{P}\right)\right] \qquad\qquad (4)$$

In which P is the period of the series, which for an annual seasonality is equal to 365.25 days, while N is the degree of the Fourier series. Expression (4) is a linear function of the coefficients a_n and b_n, the resulting linear system can be inverted to derive the coefficients of the Fourier series able to describe the seasonal contribution of the analysed time series. As part of the analysis of time series characterized by annual seasonal cycles, a value of N equal to 6 is to be considered sufficiently precise and furthermore allows no risk of "overfitting".

The quantification of the seasonal contribution can be used to perform an operation of "de-seasoning" of the considered time series, which is obtained by subtracting the seasonal contribution, obtained from the Fourier series described above, from the time series of the considered parameter. Linear regression is performed on the time series after de-seasoning, with the advantage of limiting the predictive variables to the normalized time and the basin level, including the required polynomial expansion, but excluding the temperature. After the regression, the seasonal contribution is added to the effect parameter to obtain the complete model. The operation of de-seasoning is typically required when the correlation between the effect parameter considered and the basin level is not very high, let say less than 0.85÷0.9. This procedure was developed and tested specifically within the "Dam Behavior" platform. Figure 1 shows as example the seasonal contribution of the water level.
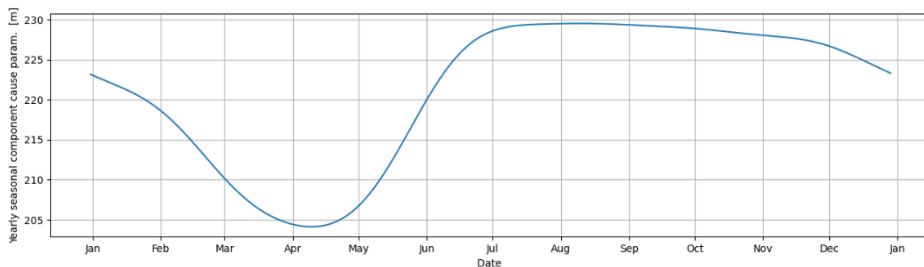

Figure 1. Seasonal contribution of the water level

The second algorithms used for the prediction is a Seasonal Autoregressive Integrated Moving Average (SARIMA) model, which is well known algorithm developed for univariate time series

forecasting with a seasonal component. For the mathematical details, the interested readers may refers to the wide technical literature on this topic. The SARIMA model tool is implemented in the statsmodels module of Python. Seasonal ARIMA models are usually denoted as ARIMA(p,d,q)(P,D,Q)m, where p is the order (number of time lags) of the autoregressive model (AR), d is the degree of differencing (the number of times the data have had past values subtracted) (I), and q is the order of the moving-average model (MA), m refers to the number of periods in each season, and the uppercase P,D,Q refer to the autoregressive, differencing, and moving average terms for the seasonal part of the ARIMA model (Hyndman & Athanasopoulos, 2018). SARIMA requires a set of data with constant frequency, for such reason the time series has been resample considering a weekly periodicity, furthermore to obtain the values in the desired timestamp a liner interpolation has been carried out.

The order of the SARIMA model has been set to (1,1,1) (0,1,1) with 52 periods in each season, the order has been maintained equal for each parameter analysed. They are selected based on an extensive analysis on the ENEL "Dam Behavior" platform because represents a good compromise between simplicity of the model and accuracy of the results. For the set of parameters considering in this work, the "autoarima" function has been used to obtain the best order of the SARIMA model, however the improvement of the fitting in negligible.

Despite the fact that the SARIMA is a univariate model, under particular conditions the use of SARIMA model provides a reliable alternative to the linear regression model and it is able to reduce the epistemic uncertainty. In order to identify the weight of the SARIMA algorithm in the ensemble model, two aspects are to be taken into account: the dependence of the water level and the duration of the period of prediction. Particularly, the use of SARIMA is more reliable when the effect parameters considered has Pearson correlation with basin level less than 0.85. Under such conditions, the response of the dam is affected by thermal effects, and it is characterized by a strong seasonal contribution, which can be properly captured by the SARIMA algorithm. This could be the case of the crest radial displacement of a concrete arch dam. Moreover, the use of SARIMA should be limited to the prediction not exceeding the yearly seasonal cycle, also in relation of the autoregressive nature of the algorithm which is more conditioned by the last part of the training period. It is worth notice that the limitation of the prediction period to not more than 20% of the length in the training period represents in general a good role for any kind of model, for such reason the 5-year prediction for the case C of this benchmark represents a challenging task.

Based on the previous consideration, the weights of the linear regression and SARIMA model used to define the ensemble model are defined based on engineering judgement. Particularly, when the effect parameters considered has Pearson correlation with basin level higher than 0.85, the weight of the SARIMA model is limited to less than 10%, in other conditions the weight of the SARIMA model can be larger. Such weight can be eventually differentiated under short- and long-term conditions, with lower weight in the last case. The selected weights will be discussed in § 38 in relation to the effect parameter considered.

The warning levels are evaluated considering 95% confidence intervals of the ensemble model. In relation to the Gaussian distribution of the residual, the 95% band of confidence are constructed considering 1.96 standard deviations of the mean. This choice can be considered a good balance, because avoid narrow thresholds, which may result in false anomalies, as well as wide ranges, which are not able of a prompt detection of unexpected behaviour, malfunctioning sensors, etc.

2.1 *Analysis of the available measurement and modelling assumptions*

The data used for the analysis are included in the excel file named 'ThemeA_data_fmt03.xlsx' pre-processed by the formulators, which includes all variables in one sheet with a common time vector in the format dd/mm/yyyy.

The first step to identify the key parameters to be included in the statistical model was the analysis of the correlation among the available parameters. Figure 2 shows the correlation matrix which allows to clearly identify that there is a set of parameters, such as the piezometric levels and the crack opening displacement that are strongly correlated with the water level, moreover also the radial displacement of the pendulum at the foundation has a high correlation with water level.
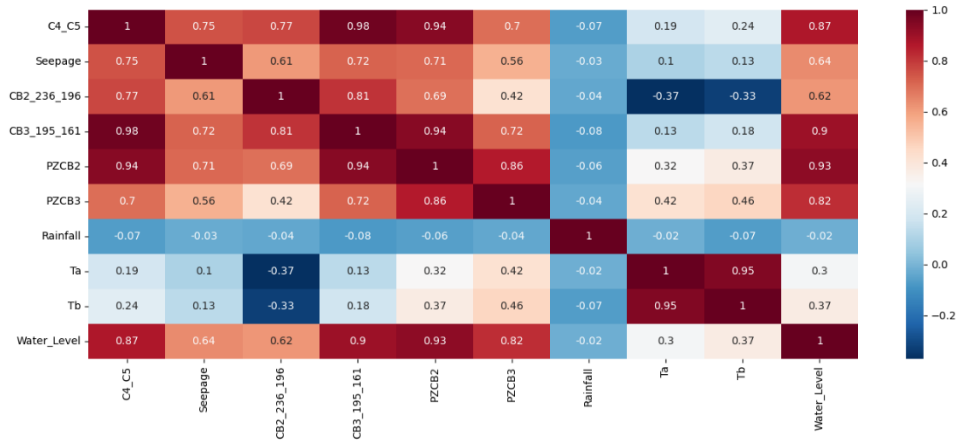
Figure 2. Correlation matrix between the available measures

The behaviour of a concrete arch dams is mainly governed by the ambient variation in temperature and water level. This can be inferred also by observing the moderate correlation between the radial displacement of the pendulum at the crest and water level. If the water level can be included in a statistical model directly in an easy way, accounting for the effects of the temperature is more complex, due also to the inertial characteristics of the dam. The thermal effects strongly affect the seasonal contribution of the response, especially for thermal sensitive parameters of a concrete dam, e.g. the crest radial displacement. For the Theme A of the benchmark two temperature time series has been provided (namely T_a and T_b). T_a measurements are carried out according to the standard of WMO (World Meteorological Organisation) and are located 50 km from the dam, however at a different altitude. T_b is calculated by interpolation from several air temperature measuring stations. The interpolation takes into account the altitude of the dam and is calculated on a mesh of 1 square kilometre. Both T_a and T_b are not measured at the location of the dam, for such reasons the statistical model considered for this work does not include the temperature as input parameter, because when required, the seasonal contribution is considered through the "de-seasoning" procedure described in the previous section.

Among the available cause parameters, the rainfall does not show a high level of correlation with any parameters and after a check to exclude specific influence on the interested parameters, it will not be considered in the analysis. Moreover, the measures came from a rain gauge located about 5 km from Dam, it is not able to capture local phenomenon which may eventually affect the response of the dam. For such reason is not used in the statistical model.

Summarizing, the cause parameters considered in all the effects parameters for linear regression is only the water level, and consequently the related input parameter considered is the degree of the polynomial expansion. Moreover, in the cases in which there is moderate correlation between the effect parameter considered and water level (i.e. Pearson correlation less than 0.85÷0.90), the linear regression is preceded by a "de-seasoning" procedure to account indirectly of the thermal effects induced by the seasonal cycle. Under such conditions the degree of the Fourier series is required.

The time series of the water level in the prediction period shows some interval in which the water level is below the toe of the dam, this aspect needs to be taken into account in the model for two reasons. The former of mathematical nature, it is related to the fact that only in few situations in the training period the water level goes below the foundation level, consequently the statistical model is not well constrained below that value. This means that using a polynomial expansion for the water level, in the prediction period below some level, the polynomial contribution is outside the calibration interval, that means extrapolation of the data which can lead to unrealistic results. Moreover, there is a physical aspect related to the fact that the dam is located on the top of a glacial threshold, and therefore when the water level is lower than 196 m, the whole upstream surface is exposed to ambient air temperature. Under such condition, the water level must not affect the response of the dam. To account for this aspect in the statistical model a modified water level is considered, which is obtained from the measured values but considering a constant value below a limit water level. This limit has been selected equal to 195 m, and it is considered the same for each parameter analysed.

The selected value corresponds to the position of some instruments such as the top of pendulum CB3, the head of the crack opening displacement sensor as well as of the piezometer PZCB2.

The period of calibration of the model may affect the goodness of fit in the training period and consequently is considered an input parameter of the model and it will be selected depending on the parameter considered.

The statistical models have been developed for the two radial displacements of the pendulums, at crest and foundation level, for the crack opening displacement named C4_C5, and for the piezometric level PZCB2. Conversely, the prediction model is not performed for the piezometric level PZBC3, because a leakage in the standpipe of piezometer was found in the past, and a cleaning of the drainage system was carried out. For such reason, the time series of piezometric level PZBC3 contains missing values in a certain interval of time and a change in the trend. Moreover, also the prediction model of the seepage is not performed.

3 MODELLING RESULTS

The Theme A is organised into three Cases, in accordance with the period of analysis:
- Calibration (Case A): 2000-2012.
- Short term prediction (Case B): January 2013 - June 2013
- Long term prediction (Case C): July 2013 - December 2017

The following sections describes the results of the statistical models for the parameters considered for the three cases listed above.

3.1 *Pendulum displacement - CB2_236_196*

The instrument named CB2_236_196 represents the radial displacement of the pendulum in the central block (CB) of the dam, between the altitudes 236 m (just under the crest Dam) and 196 m (toe of Dam). The unit of radial displacement is mm, and an increasing of the value indicates a movement of the highest point in the downstream direction.

The Pearson correlation between the radial displacement of the pendulum at the crest and the water level is equal to 0.62, as expected the correlation is not very high because the radial displacement of the crest of an arch dam is governed by the combination of both hydrostatic and thermal effects. For such reason, the linear regression is performed after the operation of the de-seasoning of the radial displacement and water level time series. The degree of the Fourier series of seasonal contribution is equal to 6, Figure 3 shows the yearly seasonal component obtained through equation (4), as well all the box plot with quartiles, whiskers bar with the 5÷95 percentiles and outliers. The prediction is performed separately for the short and long period, in the short period, the weight of SARIMA contribution in the ensemble model is assumed equal to 0.4 and the degree of polynomial expansion of the water level in the linear regression is equal to 3. Conversely for the long period the weight of SARIMA contribution in the ensemble model is limited to 0.1 and the degree of polynomial expansion of the water level in the linear regression is equal to 2. The training period considers 12 years of measures.
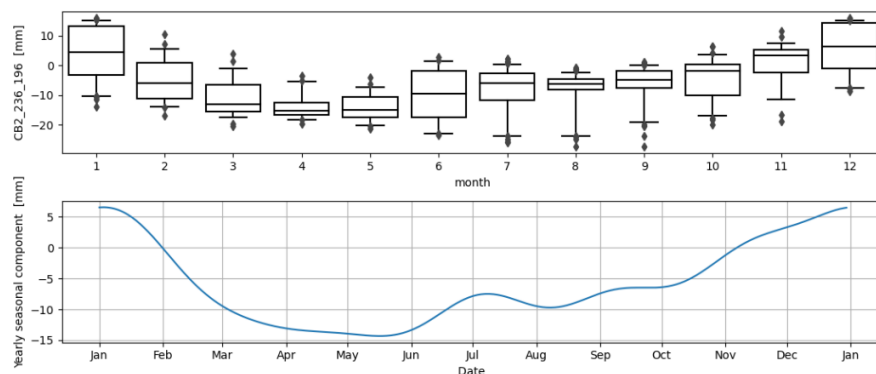

Figure 3. Seasonality of radial displacement of pendulum CB2_236_196 - High: Box plot with quartiles, whiskers bar with 5÷95 percentiles and outliers; Low: Yearly seasonal component obtained through Fourier series.

Table 1 summarizes the input data of the ensemble model as well as the goodness of fit parameters in the training period in terms of coefficient of determination (r^2) and normalized root mean square error (NRMSE). Figure 4 shows the calibration of the pendulum crest radial displacement model (Case A) with the comparison between model and measure, as well as the corresponding residual distribution. Figure 5 shows the water level and radial displacement of pendulum (CB2_236_196) in the short- and long-term prediction period (Case B and Case C).
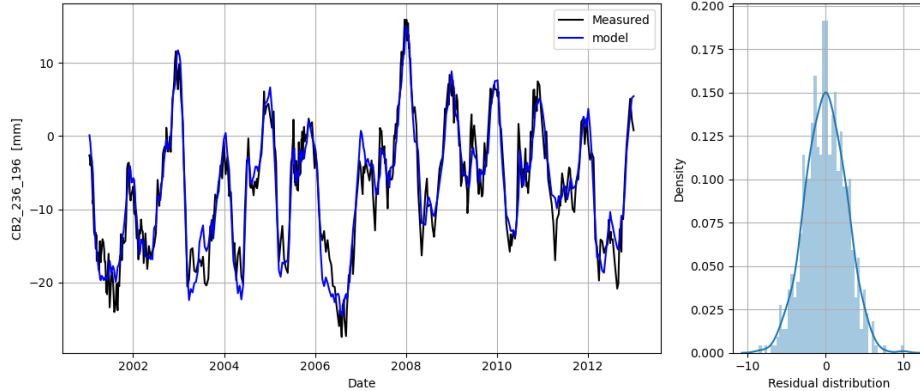

Figure 4. Case A – Calibration: radial displacement of pendulum CB2_236_196, comparison between model and measure and corresponding residual distribution.

Table 1. Parameter CB2_236_196: input data of the model and goodness of fit parameters in the training period.

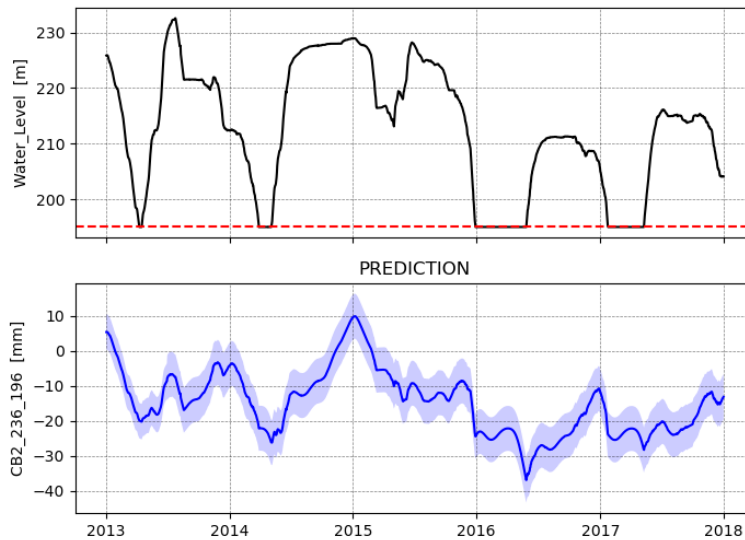| Prediction period	Training per. (year)	weights		De-seasoning / Fourier deg.	Pol. exp. deg.	r^2	NRMSE
		Lin. Regr.	SARIMA				
Short	12	0.6	0.4	Yes / 6	3	0.926	0.059
Long	12	0.9	0.1	Yes / 6	2	0.880	0.075

Figure 5. Case B and Case C, short- and long-term prediction: water level and radial displacement of pendulum CB2_236_196.

3.2 *Pendulum displacement - CB3_195_161*

The instrument named CB3_195_161 represents the radial displacement of the pendulum in the central block (CB) of the dam, between the altitudes 195 m (in the foundation) and 161 m. The unit of radial displacement is mm, and an increasing of the value indicates a movement of the highest point in the downstream direction.

The Pearson correlation between the radial displacement of the pendulum at the foundation and the water level is equal to 0.9, the correlation is rather high indication of the fact that the bottom part of the dam is not affected by the arch behavior of the dam as in the upper part, and the hydrostatic component are the predominant effects. For such reason it is not necessary to perform the operation of the de-seasoning. The linear regression is performed considering as only cause parameter the water level, with a degree of polynomial expansion equal to 3, the training period considers 10 years of measures. The ensemble model is obtained considering a weight equal to 0.9 for the linear regression model, whereas a weight of 0.1 is assumed for SARIMA contribution, the two weights are unchanged in short- and long-term prediction.

Table 2 summarizes the input data of the ensemble model as well as the goodness of fit parameters in the training period in terms of coefficient of determination (r^2) and normalized root mean square error (NRMSE). Figure 6 shows the calibration of the pendulum foundation radial displacement model (Case A) with the comparison between model and measure, as well as the corresponding residual distribution. Figure 7 shows the water level and radial displacement of pendulum (CB3_195_161) in the short- and long-term prediction period (Case B and Case C).
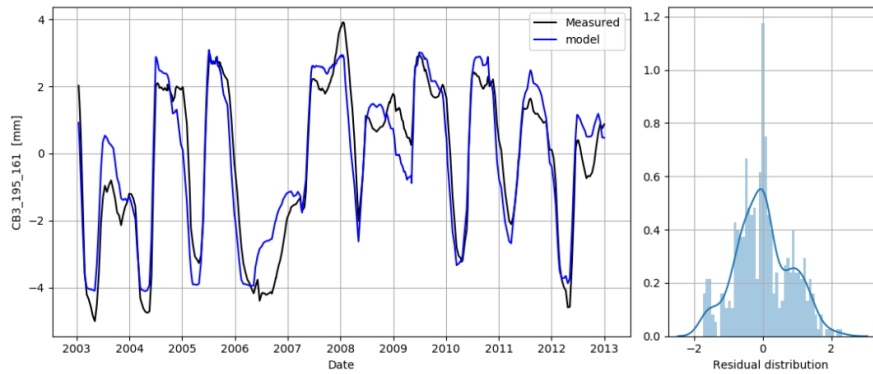

Figure 6. Case A – Calibration: radial displacement of pendulum CB3_195_161, comparison between model and measure and corresponding residual distribution.

Table 2. Parameter CB3_195_161: input data of the model and goodness of fit parameters in the training period.

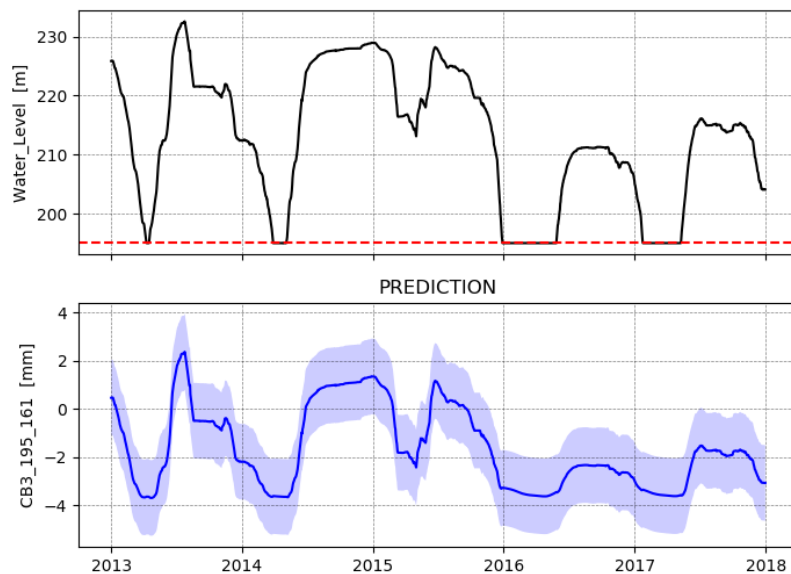| Parameter	Training per. (year)	weights Lin. Regr.	SARIMA	De-seasoning / Fourier deg.	Pol. exp. deg.	r^2	NRMSE
CB3_195_161	10	0.9	0.1	No / -	3	0.889	0.090

Figure 7. Case B and Case C, short- and long-term prediction: water level and radial displacement of pendulum CB3_195_161

3.3 *Crack opening - C4-C5*

The instrument named C4_C5 represents crack opening displacement at the rock-concrete interface, the sensor located in the central block (CB) of the dam measures the opening between C4 (in the foundation) and C5 (in the concrete, at the toe of the dam). The unit of crack opening displacement is mm, an increasing value of C4_C5 means that the distance between C4 and C5 is increasing, and therefore indicates a movement in the downstream direction.

The Pearson correlation between crack opening displacement at the rock-concrete interface and the water level is equal to 0.87, the correlation is rather high for such reason it is not necessary to perform the operation of the de-seasoning. The linear regression is performed considering as only cause parameter the water level, with a degree of polynomial expansion equal to 3, the training period considers 10 years of measures. The ensemble model is obtained considering a weight equal to 0.95 for the linear regression model, whereas a weight of 0.05 is assumed for SARIMA contribution, the two weights are unchanged in short- and long-term prediction.

Table 3 summarizes the input data of the ensemble model as well as the goodness of fit parameters in the training period in terms of coefficient of determination (r^2) and normalized root mean square error (NRMSE). Figure 8 shows the calibration of the crack opening displacement model (Case A) with the comparison between model and measure, as well as the corresponding residual distribution. Figure 9 shows the water level and crack opening displacement (C4_C5) in the short- and long-term prediction period (Case B and Case C).

Table 3. Parameter C4_C5: input data of the model and goodness of fit parameters in the training period.

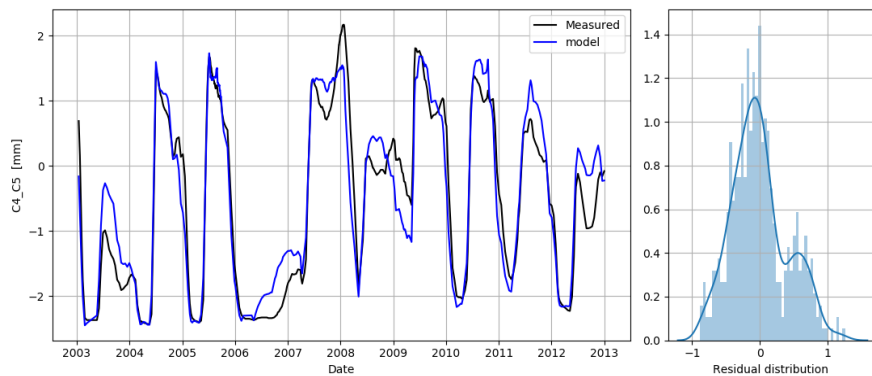| Parameter	Training per. (year)	weights		De-seasoning / Fourier deg.	Pol. exp. deg.	r^2	NRMSE
		Lin. Regr.	SARIMA				
C4_C5	10	0.95	0.05	No / -	3	0.920	0.089

Figure 8. Case A – Calibration: crack opening C4_C5, comparison between model and measure and corresponding residual distribution.
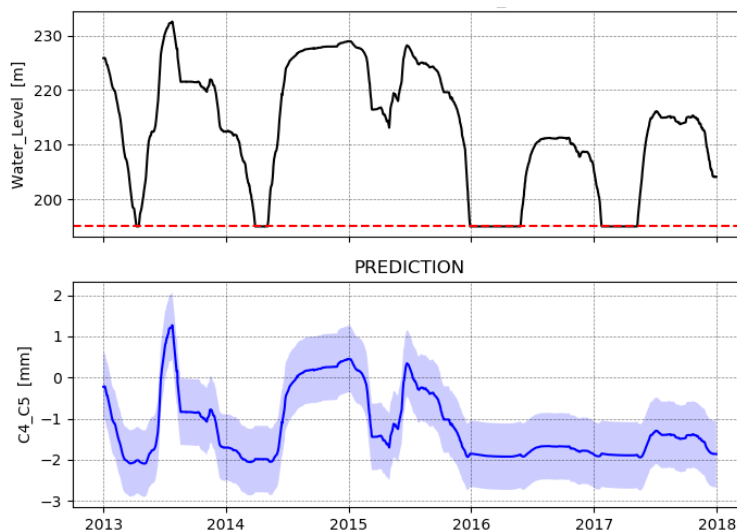

Figure 9. Case B and Case C, short- and long-term prediction: water level and crack opening C4_C5.

It is worth notice that the crack opening C4_C5 is strongly correlated with both the piezometric level PZCB2, as well as to the radial displacement of the pendulum at the foundation (CB3_195_161). The crack opening represents a good indication of the response of the rock mass at the foundation in terms of both deformability and hydraulic conductivity. For such reasons could be a good proxy to improve the statistical model the piezometric level PZCB2 and radial displacement of the pendulum at the foundation (CB3_195_161), unfortunately it is not available in the prediction period, otherwise it can be eventually used as additional cause parameter.

3.4 *Piezometric level - PZCB2*

The instrument named PZCB2 represents the piezometric level measured through a vibrating wire piezometer at the rock-concrete interface in the central block of the dam. The unit of piezometric levels is meter (m).

The Pearson correlation between the piezometric level PZCB2 and the water level is equal to 0.92, the correlation is rather high for such reason it is not necessary to perform the operation of the de-seasoning. The linear regression is performed considering as only cause parameter the water level, with a degree of polynomial expansion equal to 2, the training period considers 13 years of measures. The ensemble model is obtained considering a weight equal to 0.9 for the linear regression model, whereas a weight of 0.1 is assumed for SARIMA contribution, the two weights are unchanged in short- and long-term prediction.

Table 4 summarizes the input data of the ensemble model as well as the goodness of fit parameters in the training period in terms of coefficient of determination (r^2) and normalized root mean square error (NRMSE). Figure 10 shows the calibration of the piezometric level model (Case A) with the comparison between model and measure, as well as the corresponding residual distribution. Figure 11 shows the water level and piezometric level (PZCB2) in the short- and long-term prediction period (Case B and Case C).

Table 4. Parameter PZCB2: input data of the model and goodness of fit parameters in the training period.

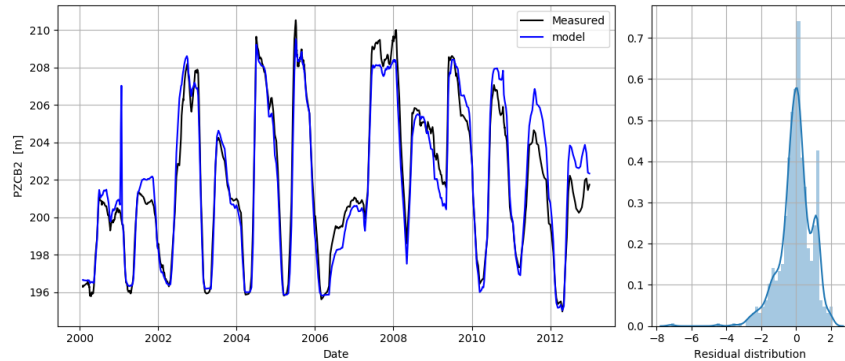| Parameter	Training per. (year)	weights Lin. Regr.	weights SARIMA	De-seasoning / Fourier deg.	Pol. exp. deg.	r^2	NRMSE
PZCB2	13	0.90	0.1	No / -	2	0.957	0.061

Figure 10. Case A – Calibration: Piezometric level PZCB2, comparison between model and measure and corresponding residual distribution.
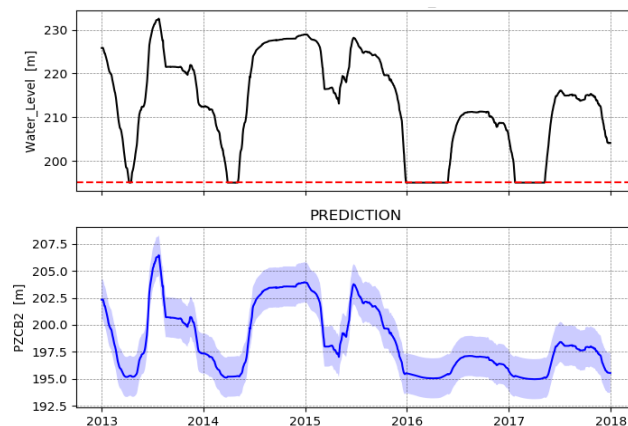

Figure 11. Case B and Case C, short- and long-term prediction: water level and Piezometric level PZCB2

REFERENCES

Hyndman, R.J. & Athanasopoulos, G. 2018. Forecasting: Principles and Practice. OTEXTS.

Taylor, S. J. & Letham, B. 2017. Forecasting at Scale. The American Statistician 72(1)

PREDICTION AND INTERPRETATION OF DAM RESPONSE WITH BOOSTED REGRESSION TREES

F. Salazar

CIMNE International Center for Numerical Methods in Engineering, Madrid, SPAIN
Universitat Politècnica de Catalunya, Barcelona, SPAIN

fsalazar@cimne.upc.edu

J. Irazábal

CIMNE International Center for Numerical Methods in Engineering, Madrid, SPAIN

D. J. Vicente

CIMNE International Center for Numerical Methods in Engineering, Madrid, SPAIN

ABSTRACT: Predictive models based on boosted regression trees were fitted for computing the response of an arch dam in terms of radial displacements, joint opening, piezometric levels and seepage as a function of time series of external variables: water level, air temperature, rainfall and time. A generic procedure was followed for all outputs, supported by two software tools developed by the authors. Warning levels were generated based on the residuals. The analysis of the models showed the effect of the main loads, the thermal inertia for radial displacements, and changes over time for piezometric levels due to the cleaning of the drainage system performed in 2008.

1 INTRODUCTION

This document describes the process followed in response to Theme A proposed in the frame of the 16th International Benchmark Workshop on Numerical Analysis of Dams organized by the International Commission on Large Dams (ICOLD). The text focuses on the methods and tools used. Details about the proposed problem can be consulted in the description of the Theme and are therefore omitted here. Both the predictions and the interpretation were generated by means of two software tools previously developed by the authors for data visualization and preprocess[1] and for fitting models based on machine learning (ML)[2].

2 METHODS

2.1 *Preprocessing*

Among the three versions of the starting data, we chose the file "ThemeA_data_fmt03.xlsx", which includes a common time vector for all variables and one record for each day in the period. For those variables with more than one value per day, the data set includes the mean. We checked such operation and the completeness of the time series. All preprocessing operations were performed using the free online tool "PREDATOR" developed by the authors 0.

We identified some missing values in the time series of water level, which were filled by linear interpolation (Figure 1). We verified that linear interpolation was reasonable, since the missing values were isolated. Time series for rainfall and temperatures featured no missing values. Since the entire upstream face of the dam is exposed for all values of water level below 196 m.a.s.l., we created a modified variable, in which all water levels lower than 196 are replaced by 196. It was called "modWL". Our approach includes generating derived variables:

- Moving averages of 7, 14, 30, 60 and 90 days for Water Level, modWL, T_a and T_b
- Cumulative sum of 7, 14, 30 and 60 days for rainfall.

This strategy allows for capturing delayed effects, such as the thermal inertia of concrete dams, as verified in previous works 0. Two additional variables are automatically created by PREDATOR: "Year" and "month". Only the first was used, to account for the time effect.

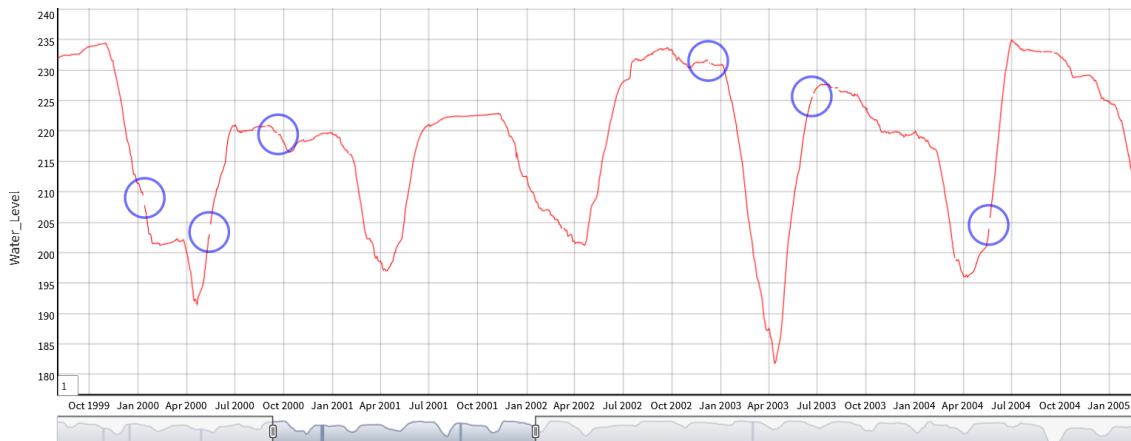Figure 1. Some of the missing values in the time series of Water_Level. They were all filled by linear interpolation with PREDATOR.

Since the records for the period 2013-2017 are not available for the output variables, the training data set includes the period 1/1/2000-31/12/12. We saved a data file with that period and a separated one to generate the predictions, which only includes the input variables.

2.2 *Model fitting*

2.2.1 *General approach*

Our predictive models make use of the algorithm "Boosted Regression Trees" (BRT from now on). It is an ensemble method, widely applied in different fields, whose theoretical fundamentals can be found in the literature (e.g. 0). We chose this algorithm on the basis of the conclusions of a previous comparative study among some of the most powerful ML algorithms 0, which were evaluated in terms of their accuracy for predicting dam behavior and their easiness of calibration and implementation. Further analysis showed its capability for identifying the effect of the loads on the response of the dam 0 and for detecting anomalies 0. The algorithm is implemented in a free online application for fitting models for dam prediction called SOLDIER 0.

BRT models are highly flexible, i.e., they deduce the underlying relation between inputs and response from the training data without the need for a detailed selection of input variables or parameter calibration. This implies that a common process can be followed for generating models for predicting outputs of different nature, as is the case (displacements, joint opening, piezometric levels and seepage). The addition of irrelevant inputs has a minor effect on the predictions of the model. Nonetheless, for this particular case, we included variable selection in the process, as described below.

The application used allows for easily modifying the training and test periods, the input variables and the BRT parameters: bag fraction, interaction depth, number of trees and shrinkage. Although their effect on the predictive model is moderate, we followed a calibration process for each output.

In addition to the prediction of dam behavior, the organizers also asked for warning thresholds. We chose to define them as a function of the model accuracy, as recommended by ICOLD 0. Therefore, a reliable estimate of the predictive accuracy is necessary for each model. BRTs always overfit to some extent, so computing model accuracy can be tricky. We chose fitting models using the period 2000-2010 and evaluating their accuracy on data for the most recent period (2011-2012). We verified that water level fluctuated along a relevant range in those last two years, which implies that the performance of the models for that period is sufficiently representative of their general prediction accuracy.

Fitting a BRT model for the size of the data sets used in the BW typically requires some seconds. However, the amount of possible combinations of input variables and model parameters is very high. The preprocessed input data includes 32 variables (original and derived variables), which means that the amount of possible combinations of inputs is 2^{32}-1=4.29x10^9. If each model took 10 seconds for training, considering one model for each set of inputs would require 1.98x10^5 days. Such process is therefore unfeasible. Instead, we followed a process for variable selection and model calibration that includes the following steps:

1. Interactively try options for each output using SOLDIER and visualize results. The options include both the input variables and the BRT parameters. In view of the results, make decisions to reduce the amount of possible combinations of inputs and model parameters to analyze.
2. Select a feasible set of combinations and perform random search model calibration.
3. Visually verify the candidate models –those with lower predictive error– back with SOLDIER

2.2.2 *Preliminary interactive exploration*

The first stage involved the following steps:

1. Fit a model with default training parameters, the period 1/1/2000-31/12/11 and all inputs: rainfall, temperature, water level –and their corresponding derived variables– and Year.
2. Interactively evaluate the effect of the model parameters: interaction depth, shrinkage and number of trees. The goodness of fit is evaluated by means of the mean absolute error (MAE).
3. Check the effect of the input variables with the relative influence and the partial dependence plots.
4. Check the residual distribution and evolution with time.

Figure 2 shows an example screenshot of the interface showing the mentioned information.

Figure 2. Interface of SOLDIER during model fitting. Target and input variable selection (top left), training period and model parameters (bottom left), accuracy measures for training and test (top right) and graphical representation of predictions, observations and residuals (bottom right)

As a result of this process, the overall options were narrowed and the following decisions were made:

- T_a and its derived variables were discarded, since T_b systematically resulted in higher relevance, i.e., stronger association with the responses.
- modWL and its moving averages were chosen instead of the raw Water_Level. In this case, the difference was moderate.
- Rainfall was neglected, since had negligible effect in all cases.

2.2.3 Random search calibration

This step was performed by means of ad-hoc scripts written in the R programming language. For each output, the same process was followed:

1. 100 combination of inputs were considered with the following criteria:
2. Time was taken as input in half of the models, and excluded in the others.
3. modWL and T_b_14 were always taken as inputs.
4. A random subset of the remaining inputs was taken to complete the input set.
5. For each set of inputs, all possible combinations of model parameters included in Table 1 were used, i.e., 36 versions of the model
6. As before, models were fitted over the period 2000-2010 and their performance was assessed for 2011-2012. MAE was computed both for the training and the test sets.
7. The models were evaluated on the basis of a score computed with Equation (1), and that with lower value was selected. With this criterion, when several models were obtained with similar precision in the test set, the one with the highest train error and therefore the lowest risk of overfitting was favored.

$$Score = MAE_{test} + (MAE_{test} - MAE_{train}) \tag{1}$$

Table 1. BRT Model parameters considered for each combination of inputs

Parameter	Values
Number of trees	1000, 2000, 3000
Shrinkage	0.01, 0.005, 0.002
Interaction depth	2, 3, 4, 5

2.2.4 Final model selection

The models selected in the previous step, i.e., those with lower score for every output, were again loaded in SOLDIER and verified: the accuracy for training and testing, the residual distribution and its evolution in time, and the importance of the variables.

In addition to the visual verification of model accuracy, this step allowed for checking that no spurious effects of any input variable were considered. We put special attention on the effect of time, which encompasses the information not recorded by the input variables available, and which is the input most prone to overfit. In particular, when the best model excluded time as input, the final check involved comparing the results with those obtained with a modified model adding "Year" to the input set.
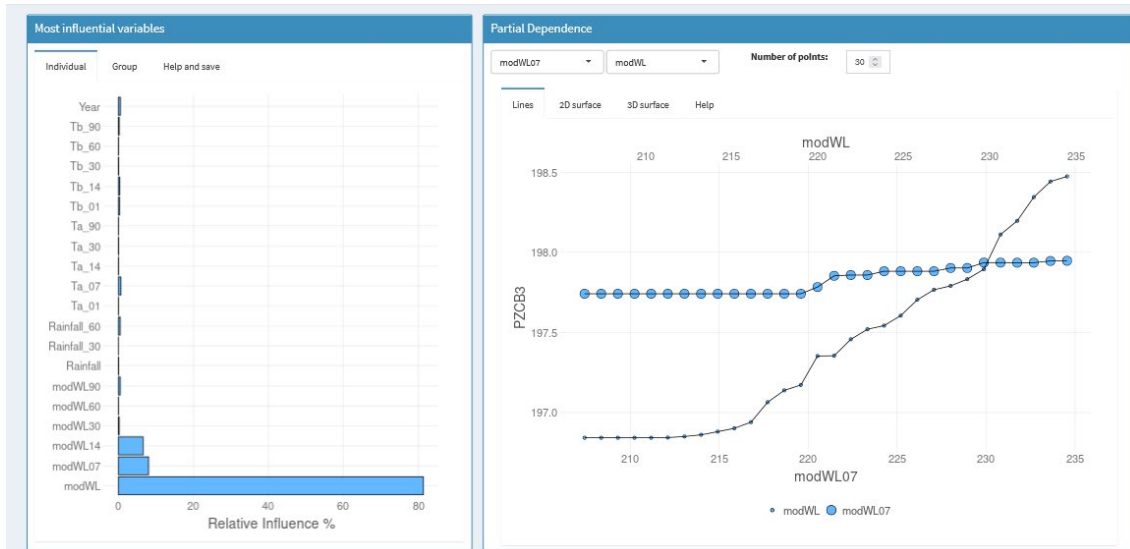

Figure 3. Interface of SOLDIER for model interpretation. Classification of inputs as a function of their relevance on the response (left) and partial effect of the most important inputs (right).

The final models were loaded back in R with another specific script, together with the test data for generating predictions. The density functions of the residuals were generated for years 2011 and 2012 to check normality. The main statistics of the residuals were computed: mean, median, standard deviation and quantiles for 0% and 100%. They were all plotted over the histograms of residuals. Although residuals followed distributions close to normal for many outputs, this was not the case for seepage. We finally decided to take the quantiles for computing the prediction intervals.

We also corrected the bias in predictions by adding the median of the residuals. As a result, predictions and warning thresholds were generated as described in Equations (2), (3) and (4).

$$Res = Obs - Pred \; \rightarrow Obs = Pred + Res \; \rightarrow Pred_{corr} = Pred + median(Res) \qquad (2)$$

$$Upp = \; Pred + Res_{q100} \qquad (3)$$

$$Low = \; Pred + Res_{q0} \qquad (4)$$

Where *Res* = residuals; *Obs* = Observations; *Pred* = Predictions; *Pred$_{corr}$* = corrected predictions; *Upp* = upper warning threshold; *Low* = lower warning threshold; *Res$_{q100}$* = Quantile 100 of residuals; *Res$_{q0}$* = Quantile 0 of residuals.

3 RESULTS AND DISCUSSION

Since the predictions are the main outcome of the analysis, and they will be evaluated by the organizers, only the most relevant aspects of model interpretation are described in this section for each output.

3.1 *Displacements*

3.1.1 CB2_236_196

The calibrated model included only three inputs: modWL, T_b_01 and T_b_14. The effect of the inputs on the displacement agrees with engineering knowledge, i.e., high water level and low temperature are associated with higher deformation in the downstream direction, and vice versa. The moving average of 14 days or air temperature has more influence than the daily temperature, which shows the thermal inertia of the dam.
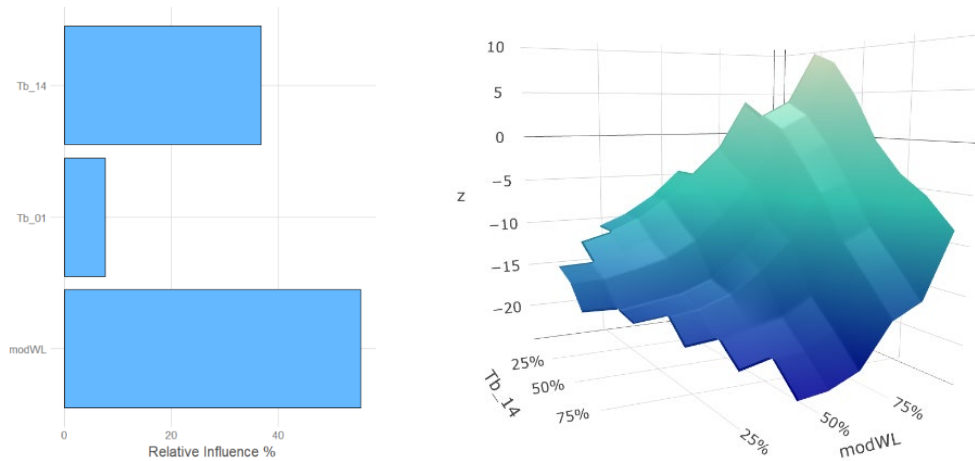

Figure 4. Left: relative influence of the selected inputs. Right: combined partial effect of hydrostatic load (modWL) and air temperature (T_b_14) on CB2_236_196

3.1.2 CB3_195_161

The final model for the displacement in the foundation is also based on three inputs, but T_b_60 is taken instead of T_b_01. Nonetheless, the effect of air temperature is much lower than before, as can be expected, since the foundation is less exposed to the variations in ambient temperature. As before, adding time as input resulted in similar accuracy.
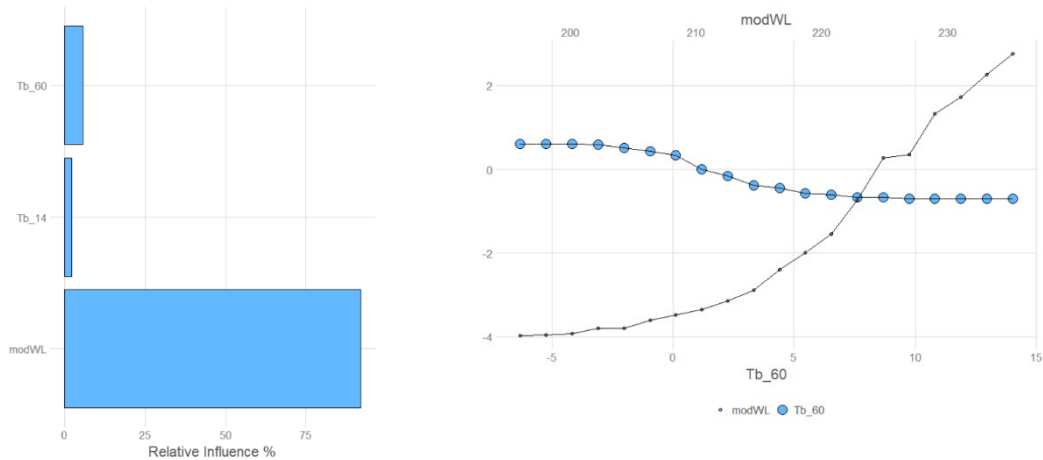

Figure 5. Left: relative influence of the selected inputs. Right: partial dependence of the displacements at the foundation on the water level (modWL) and air temperature (Tb_60).

3.2 *Joint opening*

The final set of inputs for joint opening includes several moving averages of both main loads. In particular, modWL, modWL60, modWL90, TB_07, TB_14, TB_30, TB_90. In this case, adding time as inputs led to lower accuracy for the test set (2011-2012), which means that induced overfitting.
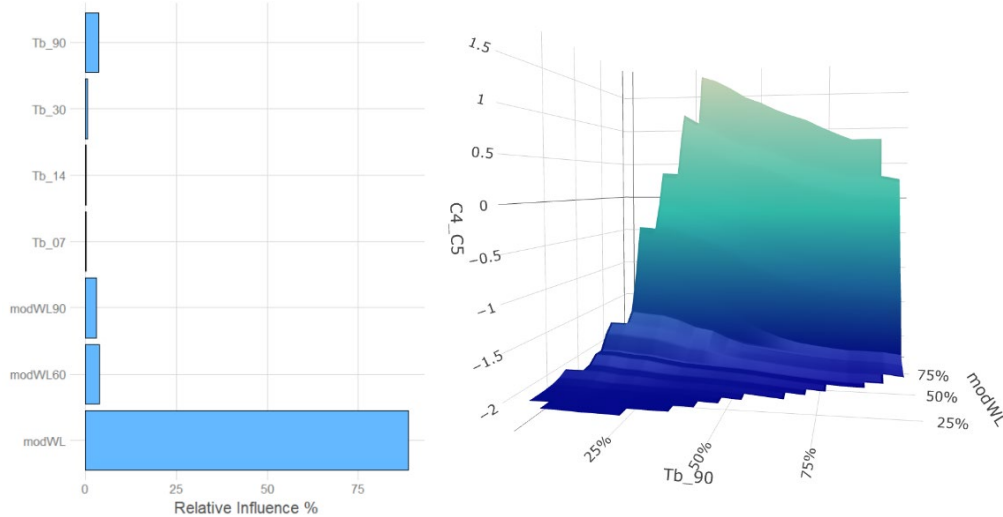

Figure 6. Left: relative influence of the selected inputs on joint opening. Instantaneous water level is by far the most important load. As for the air temperature, the effect increases with the period of the moving average. Right: combined effect of modWL and Tb_90 shows that the influence of air temperature is more important for high water level.

3.3 *Piezometric levels*

3.3.1 PZCB2

The calibration process resulted in a model including time as input for PZCB2. This implies that the algorithm identified an evolution on the dam response, i.e., for a given combination of water level and temperature, the piezometric level changed over time (Figure 7).
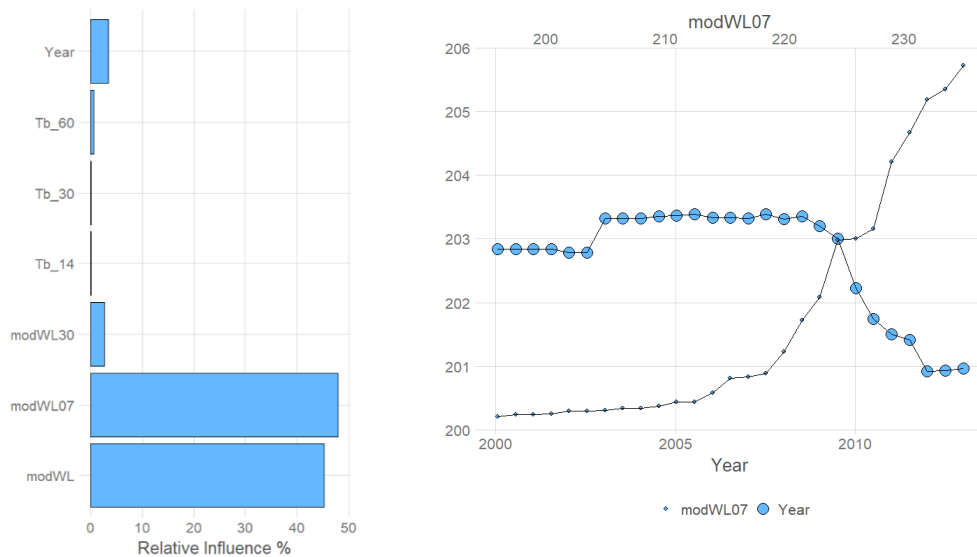

Figure 7. Left: relative influence of the selected inputs on PZCB2. Time (Year) has a relevant effect. Right: partial dependence on modWL and time. The algorithm identified a sharp decrease in PZCB2 on 2010 and stabilization in 2012.

This can be verified by exploring the time series of the measured data, included in Figure 11 in the Theme A description, as well as in the scatterplot in Figure 8.
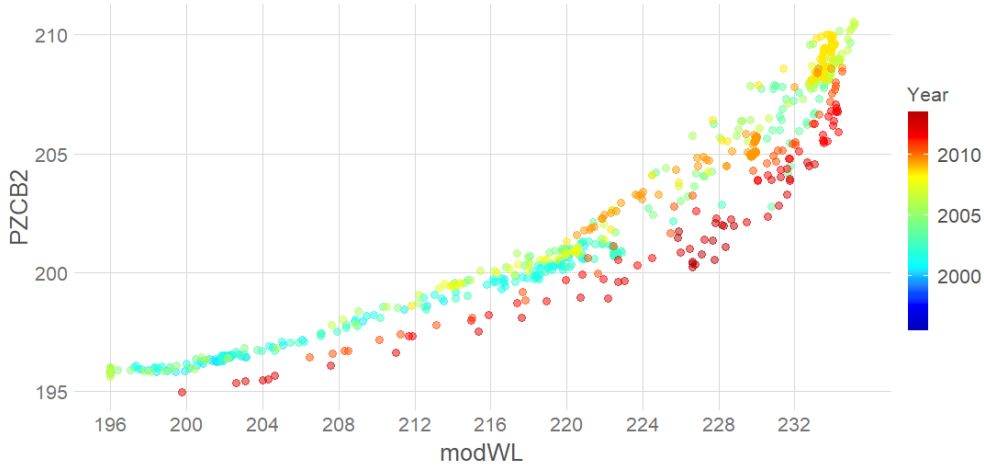

Figure 8. Scatterplot of PZCB2 as a function of water level, colored by time. Recent values are lower for a given hydrostatic load.

The final model included both modWL and modWL_07, being the latter even more influential. This may suggest some inertia in PZCB2 in response to changes in water level. However, we verified that changes in predictions were negligible after removing modWL_07. Therefore, the higher influence may be a spurious result due to the high similarity between both inputs.

3.3.2 PZCB3

The description of the Theme mentioned a change on PZCB3 in 2008, as well as a period with missing data. This change along time was also identified by the algorithm and "Year" was included in the input set resulting from the calibration process. The flexibility of BRTs allowed for using the same fitting process for this target, for which a clear change was known in advance. Indeed, the interpretation of the model (Figure 9 right) shows the mentioned change in 2008. Nonetheless, the algorithm also found another change in the last year of the period provided (2012), which is also observed in the exploratory plots (Figure 10).
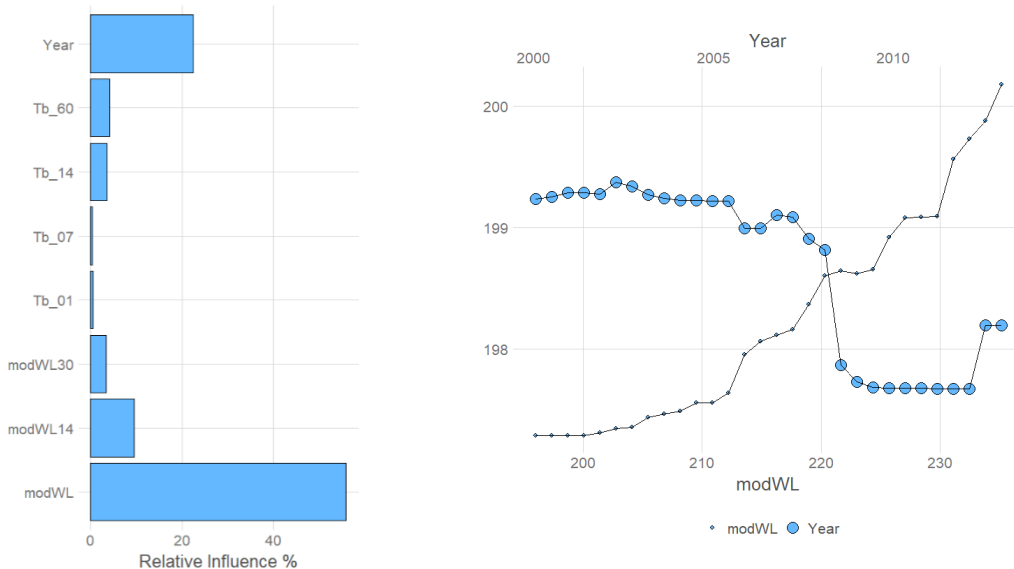

Figure 9. Left: relative influence of the selected inputs on PZCB3. Water level is the most important input, and its moving averages feature decreasing influence as the period increases. Time (Year) is considered as highly relevant. Right: partial dependence on the most relevant inputs. The effect of time shows the known change in 2008, but also a shift in 2012.
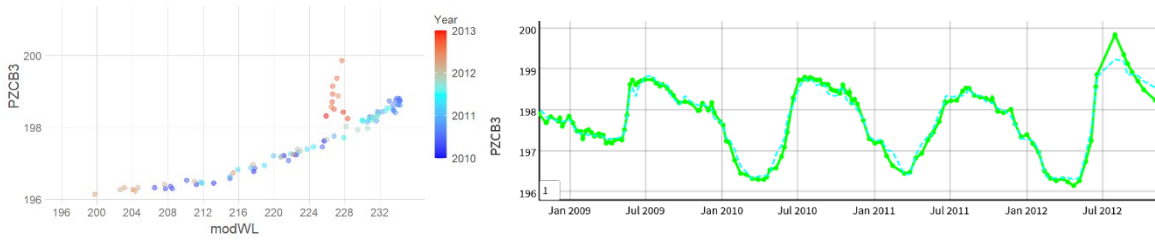
Figure 10. Verification of the abnormal records of PZCB3 in 2012 by exploration of the period 2010-2012. Left: scatterplot. Right: time series.

3.4 *Seepage*

Predictions of seepage were less accurate than those for the remaining targets. Although the MAE can be considered acceptable (around 2 l/sec), large errors occurred for high flows (Figure 11). Water level is clearly the more influential input. However, adding T_b consistently results in higher prediction accuracy. This may be due to some effect of temperature in joint opening and subsequently in higher leakage flows, but any conclusion is unreliable due to the low reading frequency.
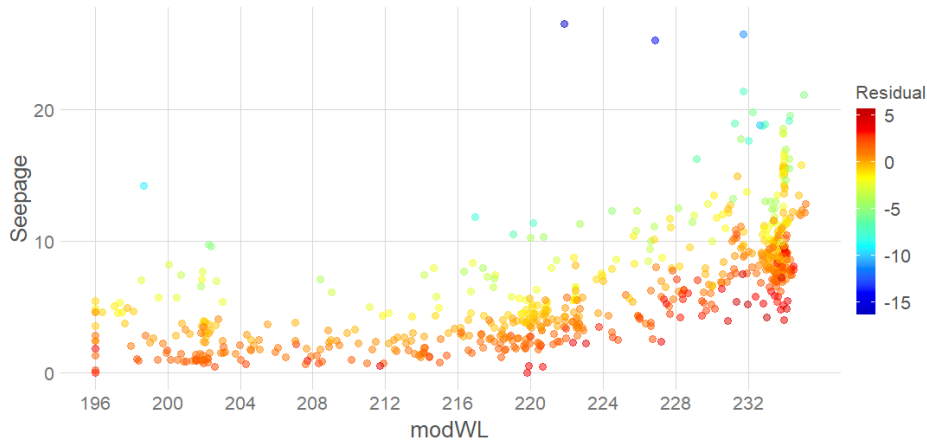
Figure 11. Scatterplot of Seepage as a function of water level, colored by residual (prediction error). Large errors are observed for some high flows.

Although the time series of seepage is noisier than the others, the formulators mentioned no anomalies for this variable. As a result, no record was discarded even though some look like outliers. For instance, in the period Dec/2008-Mar/2009, seepage gently decreases, apparently following the evolution of water level. However, two values higher than 25 l/sec are registered, clearly out of the overall trend (Figure 12).

Figure 12. Time series of seepage (red dots) and water level (green line) from Dec/2008 to Mar/2009. Two records of seepage seem to be out of the general trend.

4 CONCLUSIONS

Predictive models based on ML (BRTs) for response variables of different nature were generated and analyzed with a general process supported by two software tools. The flexibility of BRT models allowed for performing all posed tasks with minor changes. For piezometric 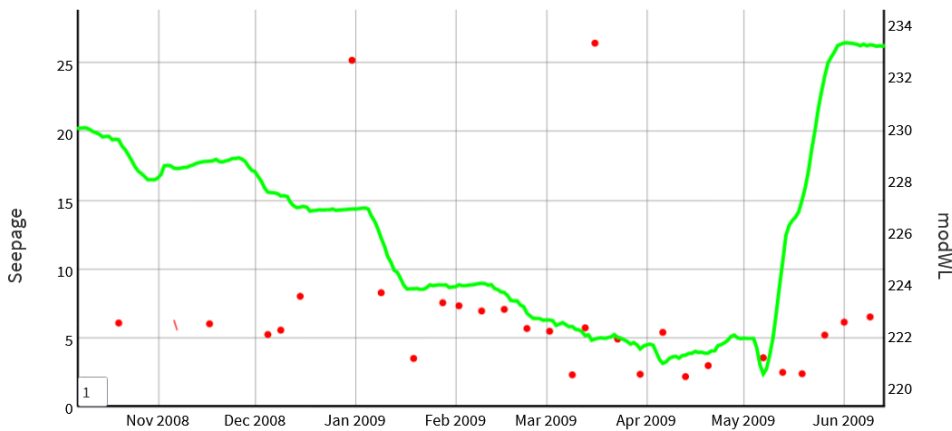levels, the entire available period was used without the need to include any modification to account for the known change in behavior in 2008 due to the cleaning performed on the drainage system. On the contrary, it was automatically identified by the model.

The interpretation of the models showed the effect of the main loads generally in accordance with engineering knowledge: high hydrostatic loads are associated to displacement in the downstream direction, high seepage, joint opening and piezometric levels; time effect and thermal inertia were identified for CB2_236_196.

We generated warning levels based on the quantiles of the residuals for the period 2011-2012. Although water level followed a similar pattern in those years to that observed in 2000-2009, such levels may not be useful for the entire prediction period because: a) water level was abnormally low in 2016 and 2017; b) we recommend updating the models every year to include additional information and possible changes in dam response. In any case, a record above the upper limit –or below the lower– should be taken as a warning for additional actions to make before issuing an alarm. These may include verification of related targets, increase of reading frequency and follow up of the evolution of the abnormal variable.

ACKNOWLEDGEMENTS

REFERENCES

[1] Salazar, F., Kohler, R., Conde, A., & Landstorfer, F. (2019, September). Interpretation of dam monitoring data combining visualisation tools and machine learning. Eberlaste Dam Case Study. In *ICOLD International Benchmark Workshop on Numerical Analysis of Dams, ICOLD-BW* (pp. 863-874). Springer, Cham.

[2] Salazar, F., Toledo, M. A., Oñate, E., & Morán, R. (2015). An empirical comparison of machine learning techniques for dam behaviour modelling. *Structural Safety*, *56*, 9-17.

[3] Salazar, F., Toledo, M. Á., Oñate, E., & Suárez, B. (2016). Interpretation of dam deformation and leakage with boosted regression trees. *Engineering Structures*, *119*, 230-251.

[4] Salazar, F., Toledo, M. Á., González, J. M., & Oñate, E. (2017). Early detection of anomalies in dam performance: A methodology based on boosted regression trees. *Structural Control and Health Monitoring*, *24*(11), e2012.

[5] ICOLD. (2018). *Dam Surveillance Guide* (Bulletin nº 158). CRC Press.

[6] Elith, J., Leathwick, J. R., & Hastie, T. (2008). A working guide to boosted regression trees. *Journal of animal ecology*, *77*(4), 802-813.

PREDICTION OF DAM BEHAVIOUR BASED ON MACHINE LEARNING METHODS

Miguel Á. Fernández-Centeno

ACIS Innovation+Engineering S.L. (ACIS2in), Parla, Madrid, Spain, 28983.
Universidad Politécnica de Madrid (UPM), ETS de Ingenieros de Caminos, Canales y Puertos; Madrid, Spain, 28040.

Patricia Alocén

ACIS Innovation+Engineering S.L. (ACIS2in), Parla, Madrid, Spain, 28983.
Universidad Politécnica de Madrid (UPM), ETS de Ingenieros de Caminos, Canales y Puertos; Madrid, Spain, 28040.

Miguel Á. Toledo

Universidad Politécnica de Madrid (UPM), ETS de Ingenieros de Caminos, Canales y Puertos; Madrid, Spain, 28040.

ABSTRACT: Prediction of dam behavior plays an important role in the field of dam safety as it can be used to establish warning levels and detect dam failure. Recently, Machine Learning techniques have been increasingly applied in this field due to their success in other areas. Our methodology is based on such techniques to predict different measurements of and arch dam's behavior and analyze the influence of external conditions. An initial exploratory analysis and the selection of the most important variables for prediction were made to reduce the dimension of the problem. Then, measurement of the degree of similarity between external factors in the available years was performed for classifying the years and detecting annual differences that may affect the training or prediction results. Several ML models were trained for each target variable and the most accurate was selected to make short- and long-term predictions and determine warning levels. The results reveal the main influence of water level in the behavior shown by most of the analyzed sensors. This influence is found stronger for different moving averages of this external variable, being specially surprising the long period of integration found for the prediction of the radial displacement in direct pendulum. Three groups of years in external conditions were also observed, with special differentiation for years 2016 and 2017 of the evaluation period. SVM, NN, and BRT turned out to be the most accurate methods and their errors were used to determine the warning levels.

1 INTRODUCTION

The practical problem to be solved in this research was denoted as Theme A and its main objective was to predict the behavior of a double curvature arch dam. The approach made was to use Machine Learning techniques to configure predictive models and perform the relevant analysis.

The application of these algorithms was carried out through the web App developed by ACIS2in specifically for the use of IA in dam safety.

Most of the algorithms used for this Workshop Benchmark were previously developed by ACSI2in in previous research projects and professional work.

The analysis of the external conditions that affect the dam and the training of Machine Learning models to make the short- and long-term predictions required were performed as well as the interpretation of the results obtained.

2 METHODOLOGY

2.1 *Exploratory analysis*

The research carried out in this workshop began with an exploratory analysis of the external factors and target variables. Their series and distributions were studied to understand their individual behavior, as well as the relationships between them.

To perform the individual analysis of the variables, time series, density, and boxplots grouped by the available years in the data set were plotted. The latter two were used to observe their mean, dispersion, and range. It was observed the difference between the behavior of the variables in each of the years through these graphs. The emphasis was placed on the study of water level, which, as discussed in the results section, has a crucial role in the prediction of the target variables.

Correlation and scatterplot graphs were used to analyze the relationship between target variables and external factors. The former shows values between -1 and 1 indicating the degree of linear relationship between them, while the latter shows the type of relationship they hold (linear, nonlinear, etc.).

2.2 *Synthetic variables*

The next step was to calculate synthetic variables related to the past of external factors. These variables play an important role in the training process, since the effect of external factors does not immediately affect the dam, but rather there is a delayed effect that will depend on the way these external factors evolve over time.

Three types of variables of different orders were calculated: moving averages (MM), aggregates (AG), and variation ratio (VEL).

Assuming we have a time series of variable $X \in (1 \text{ x } m)$, where t is the instance index at time t of variable X, the synthetic variables are computed as follows:

$$\text{X\_MM}_{t,k} = \frac{1}{k} \sum_{i=1}^{k} x_{t-i} ; \tag{1}$$

$$\text{X\_AG}_{t,k} = \sum_{i=1}^{k} x_{t-i} ; \tag{2}$$

$$\text{X\_VEL}_{t,k} = \frac{x_t - x_{t-k}}{k} ; \tag{3}$$

where k is the order of the synthetic variable.

Short- and long-term synthetic variables of orders 7, 15, 30, 30, 60, 90, 180, and 365 days were calculated regardless of the nature of each external factor and their expected influence on the target variables. This approach was selected with the goal of allowing ML algorithms to tell what is important to them in order to predict the behavior of the target variables. Among these variables, those of greatest importance in the prediction of the target variables were selected using our variable selection algorithm explained below.

2.3 *Variable Selection*

Variable selection arises due to the need to reduce the dimensions of the large data set generated after calculating the synthetic variables. Logically, all these variables are closely related to each other. Therefore, it is important to select only those that provide relevant information to the model to improve accuracy and reduce computational cost.

The outline of the selection algorithm is as follows:

1. Calculation of the degree of importance through Support Vector Machine (SVM).
2. Sort variables by importance degree in descending order.
3. Selection of certain numbers of variables: 10%, 20%, 30%, 50%, 60% and 80%.
4. Execute an SVM for each quantity in Step 3.
5. Selection of the variables that generate the most accurate model.

First, a simple model was trained using SVM to calculate the degree of importance of each variable. In our experience in other research, SVM takes less time to run and often gives the same results as other variable selection methods, such as ensembles of decision trees.

The next question to be answered was how many variables should be used to optimize the accuracy of the final model. The most accurate selection methods, such as leave-one-out, may become computationally expensive if the dimensions of the training set are large. Therefore, in our algorithm, different percentages of variables are selected in descending order of importance, and a simple model is trained with SVM for each of these quantities. Finally, the quantity that gives the smallest error is selected.

The variables resulting from this last step were used to train the final model to predict the target variable, where a grid search for the optimal hyperparameters and an estimation of the error was performed through cross-validation.

2.4 *Training and evaluation of models*

The model training stage consisted of the selection and training of models of different nature. Methods that are potentially accurate based on previous research experience were selected:

- Boosted Regression Trees (BRT).
- Random Forest (RF).
- Support Vector Machine (SVM).
- Neural Network (NN).
- Generalized Linear Regression (LM).
- Bayesian Neural Network (RRBB).
- Hydrostatic-Season-Time (HST).

Cross-validation was used to evaluate the models and estimate the optimal hyperparameters for each case. In this research, the folds match the years available in the dataset, which correspond to the dam cycles.

Therefore, the error measures used in this methodology are the RMSE of the CV ($RMSE_{cv}$) and the RMSE of validation ($RMSE_{val}$). The mathematical form of the RMSE is as follows:

$$RMSE = \sqrt{\sum_{i=1}^{m} \frac{(\hat{y}_i - y_i)^2}{m}};$$

(12)

where m is the total number of records in the data set, $\hat{y}$ the predicted values and y the actual values.

Considering that k years are available, we have an *RMSE* for each k years:

$$RMSE_{cv} = \frac{1}{k} \sum_{j=1}^{k} RMSE_j;$$

(13)

The measure $RMSE_{val}$ is simply the *RMSE* over the validation year, 2012 in this case.

The estimated error by averaging the error across folds ($RMSE_{cv}$) is more robust than the RMSE over the validation set (year 2012) since the latest correspond to the error for one particular year and the former averages the errors of the different years in the training set.

The optimal hyperparameters of each model were selected by searching the combination that gives the lowest error on average. For each combination, a model was created for each fold; then

the average *RMSE* committed across the folds was calculated and the combination with the lowest error was selected.

Accordingly, we obtained an estimated error for each of the seven trained models. The last step of this stage was to select the optimal model, which was the one with the lowest value of $RMSE_{cv}$.

2.5 *Warning levels*

Once the optimal models were selected for each target variable, the warning levels were generated.

The warning levels are defined as bands within which it is expected to find the measurements obtained from the monitoring system, so that outside of them the data are potentially anomalous and a more in-depth review of the situation must be carried out.

The boundaries of these bands were determined based on the estimated error of the prediction model for each component and application segment.

The formula used for establishing the warning levels is as follows:

$$U_{\pm} = \hat{y} \pm c\sigma_e; \tag{14}$$

where $\hat{y}$ is the predicted value, c is a confidence coefficient and σ_e the standard deviation of the error.
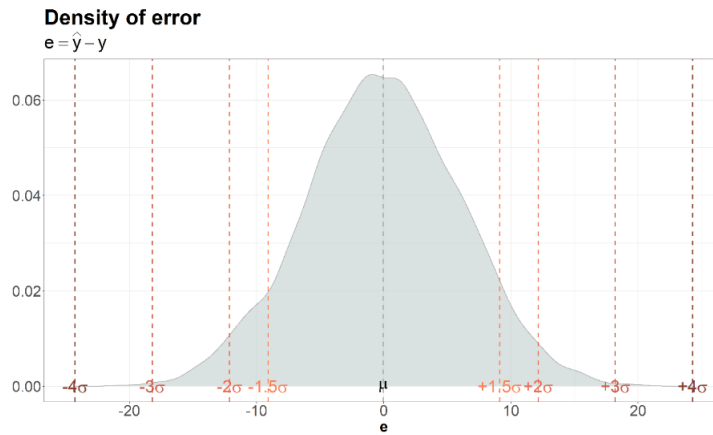

Figure 1. Example of error density with the mean and coefficient points multiplied by the error variance.

The selection of the value of the *c* coefficient should be done from a safe and practical O&M perspective. On the one hand, high values of *c* will provide a more relaxed warning levels that could miss relevant issues in the behavior. On the other hand, very low values of this coefficient will cause numerous warnings in non-anomalous situations.

The coefficient selected to establish the warning level was 2, since this interval approximately holds 95% of the real values.

3 RESULTS AND DISCUSSION

This chapter presents and discusses the results obtained by applying the methods previously presented. The subdivisions of the Methodology section are similarly implemented in this chapter for ease of understanding and to present the results in an orderly way.

3.1 *Exploratory analysis*

An exploratory analysis of external factors was carried out to determine their behavior and relationship with the target variables.

Figure 2 shows a cyclical behavior of the water level series. What is striking here is the pronounced water level drops observed in 2003, 2006, 2016 and 2017. After the decrease in

water level in 2006, its average in the following years is higher due to higher minimum values. They progressively decrease in average until the drop of 2016, which makes it an unusual year compared to the past.
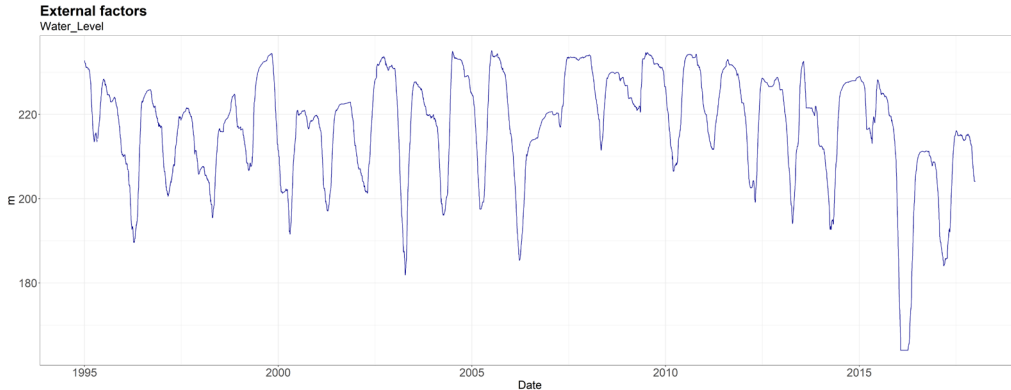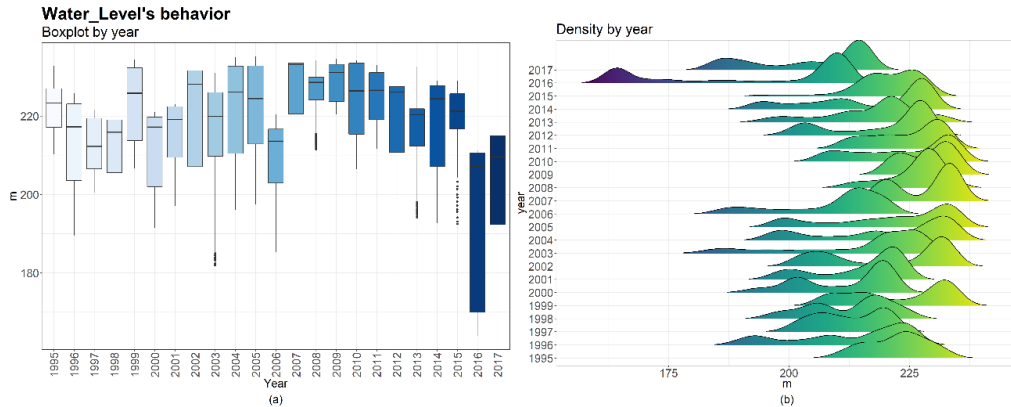

Figure 2. Water Level series over time

Figure 3. Boxplots (a) and density plots (b) of Water Level by years.

The plot (a) in Figure 3 shows what appears to be different behaviors of the water level according to the amplitude and the median value of the boxes: from 1995 to 2005, where the minimum values of water level are low; from 2007 to 2015, where these values are higher; and the atypical periods such as 2006, 2016 and 2017. The amplitudes of years from the first period mentioned are similar, although the values of the water level vary, especially those belonging to 2003, where a larger decrease is observed. This event makes the lower whisker longer and, accordingly, outliers appear. Year 2006 is significantly different from the years of the training set. The amplitude of its box is smaller compared with the preceding years, implying that the water level lays within a narrower range. From 2006 on, there is an increase in the water level, where we find higher medians and values that progressively decrease. Undoubtedly, the most atypical period is 2016-17, where the lowest values and medians are found.

These remarks are also seen in the density graph (Figure 3, b), where several averages are observed due to cyclical rises and drops in the water level. Most of the years have similar means, except 1996, 2003,2006, 2016 and 2017, which have lower mean of minimum values than the others. The most unique year also in this type of graph is 2016, where a particularly steeper water level drawdown is observed.

This behavior contrasts with the scarce temporal variation of temperatures, whose series show the usual cyclical behavior, and very similar means and medians over the years were observed.

Regarding the pendulum series, some changes can be identified, which might be related to the previously mentioned water level drops.

The variable most linearly correlated with both pendulums is the water level, with values 0.62 (CB_236_196) and 0.9 (CB3_195_161). Temperature, on the other hand, has a smaller linear relationship with both pendulums, finding its maximum at |-0.37| (CB_236_196).

3.2 *Synthetic variables*

Once the exploratory analysis was performed, the synthetic variables of the external factors were calculated to be used as inputs in the modeling training.
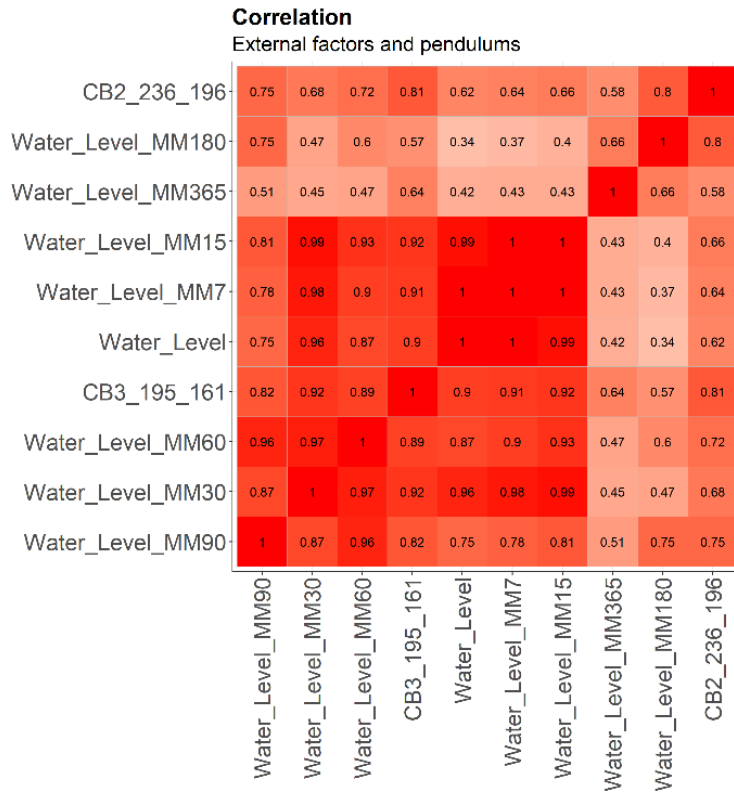
Figure 4. Correlation plot of Water Level moving averages and pendulums.

The correlation plot (Figure 4) shows that some of the moving averages of the water level are more correlated with both pendulums than the original variable.

The short-term moving averages of the reservoir level (MM15, MM30, etc.) are more correlated with CB3_195_161 than with the original variable, while, for CB_236_196, surprisingly, the most correlated variables are the very long-term averages (MM180, MM90, etc.).

The following images show the series of these variables and their relationship to the pendulums (Figure 5 and Figure 6).

Figure 5. Series of Water Level 15 and 180 order moving averages.

Figure 6. Scatterplot of the relationship between pendulums and moving averages 15 and 180 of the reservoir level by years: (a) CB_236_196 and (b) CB3_195_161.

Figure 6 shows a high degree of linear relationship between dam displacement of the dam and water level moving averages. Generally, points corresponding to the most current y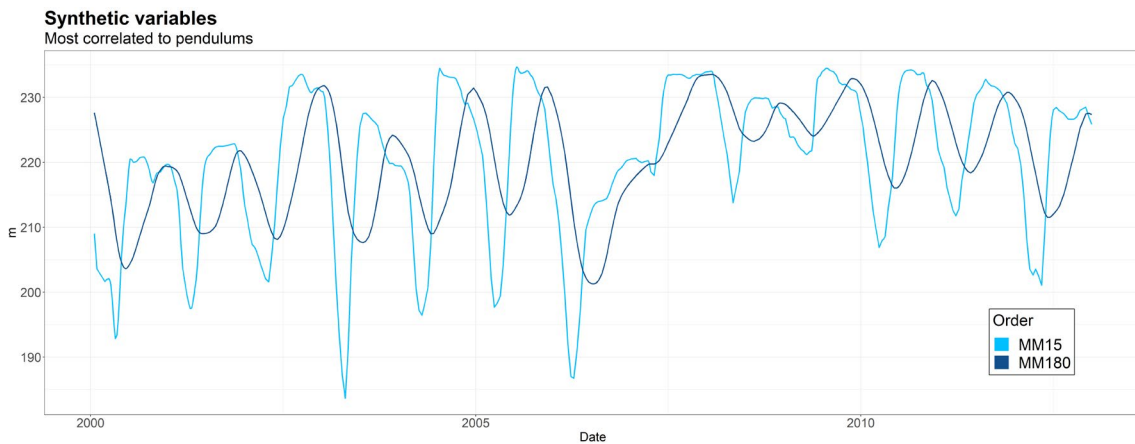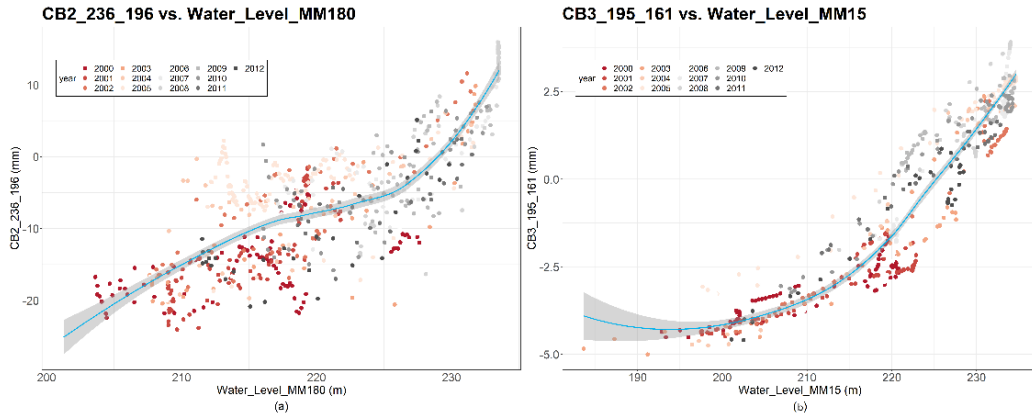ears, in gray, are concentrated in the upper right part of the graph, where the values of water level and displacement are higher. Those belonging to 2000 and 2001, in dark red, have lower values, whereas the rest are more dispersed. Given the greater dispersion in the upper pendulum compared to the water level, it would appear that it has a greater dependence on other variables than the lower pendulum in which this dispersion is smaller.

3.3   *Most important variables*

As mentioned in the Methodology section, the selection of the most important variables for each pendulum is important to increase predictive power and reduce the dimensions of the data set.

Logically, variables that have a high linear relationship will be important for the prediction of the target variable because many models tend to prefer this type of relationship for ease of modeling. This is the case with our variable selection algorithm that employs an SVM for the calculation of the importance degree.
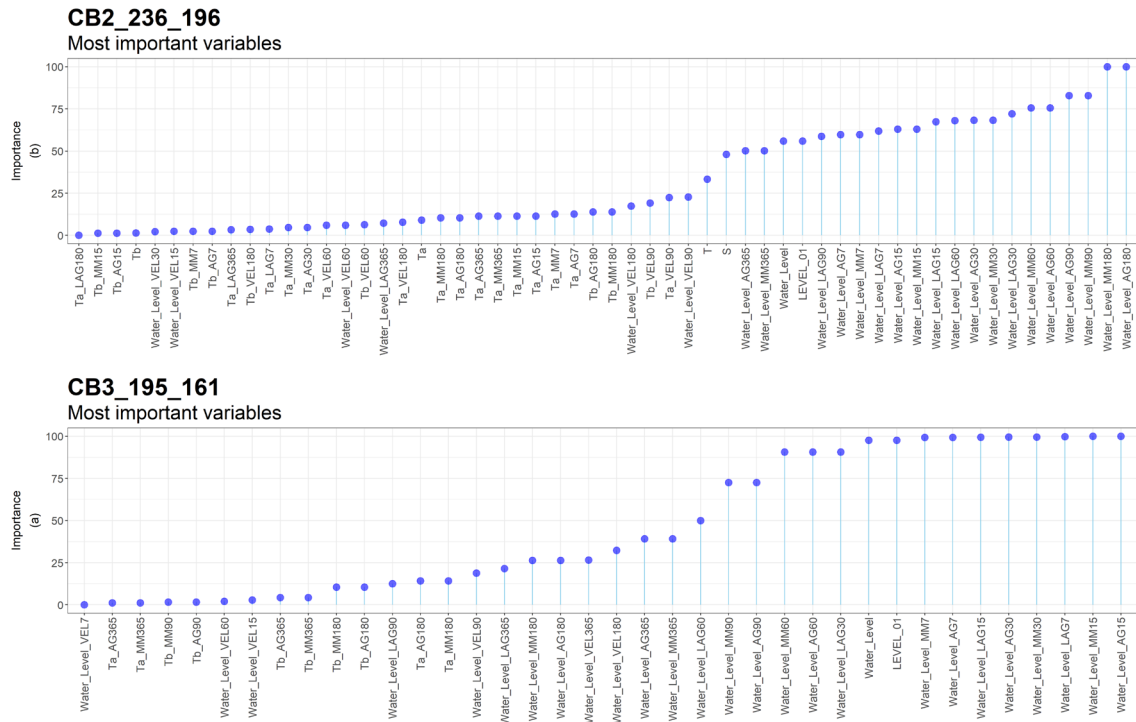

Figure 7. Most important variables of the model and their degree of importance (%).

The variables that top the list of importance for the CB_236_196 pendulum are the long-term synthetic variables (Figure 7). In contrast, in the case of CB3_195_161 the water level short-term variables occupy this position. Temperatures are not as important for the model, and time (T) and seasonality (S) are only ranked as important variables in the first pendulum.

It seems rare that the displacement of the direct pendulum due to water level depends more on longer term synthetic variables. Also, temperature-related part of the displacement, that it's supposed to be an important component in the physical sense, doesn't seem to have that relevance for the model.

On the other hand, it can be observed that direct correlation between direct pendulum radial movement and 180 days moving average of water level is greater than the direct correlation with other variables that should be more important from a dam behavior perspective. It would seem that the ML models used prefer more correlated variables for creating the prediction rules. Then, the question to be answered is if the importance of the variables obtained by traditional ML techniques provides a direct interpretation of the most relevant actions for the dam behavior explanation as it's commonly considered or if it requires further interpretation. If a direct interpretation could be considered, the only and uncertain interpretation found, considering our limited knowledge of this particular dam, is the existence of an upstream foundation deformation due to slow changes in pore pressure motivated by the variation in water level. The verisimilitude of this hypothesis should be subjected to further investigations.

3.4 *Similarity between years*

Since the training of the predictive models was to be made by yearly folds, the possibility of existence of groups of years depending on their external variables (including synthetic ones) was analyzed. The goal behind this approach is that, in the case that these groups could be found, more accurate prediction models may be trained over each one of them. This way, for new yearly data, a previous classification step would be to select the most similar group and then use the corresponding predictive model for improving the accuracy.

A dimension reduction of the most important variables of both pendulums was performed by Principal Components Analysis. Each pendulum has its own most important variables (Figure 7) and, therefore, their Principal Components will be different. This leads on differences in values or groupings from one pendulum to the other. The similarity measure used is summarized by calculating the Euclidean distance of the instances belonging to the test Fold to the centroids of the Principal Components of the training years.

The clusters resulting from running the kmeans algorithm (Figure 8) seem to coincide with the clusters that could apparently be formed by looking at the water level graphs (Figure 3). The rarest external conditions are found in 2016 and 2017, which form cluster 3.

The same groups are found for both pendulums, except for year 2002. It should be noted that the groups were made considering the centroids of 5 principal components, but to facilitate the explanation, they are represented in 2 dimensions. Hence, the actual cluster may not match what appears to be according to the graph (Figure 8).
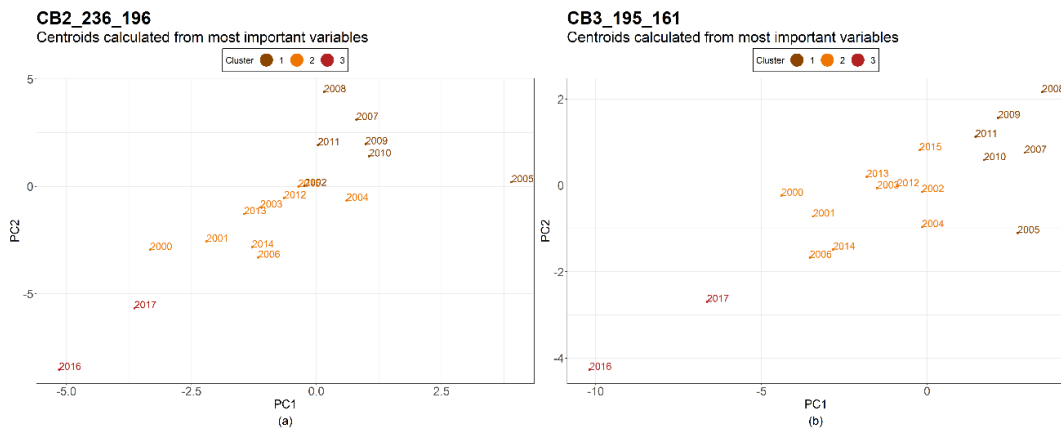

Figure 8. Centroids of the Principal Components of the years available in the dataset grouped by clusters generated through the kmeans algorithm.

Figure 8 only provides an idea of the years that are most similar to each other. To go into detail, the sum of the Euclidean distances from each observation in the data set to the centroids of the training years is shown in Figure 9.

Both series presented in Figure 9are very similar. The period of time from 2007 to 2011, approximately, stands out due to its smaller range of values. The explanation for this fact is that the Water Level variable, which has great importance for the models of both pendulums, takes values within a less disperse range. For this reason, the distance is smaller since there are more points within this range of values (Figure 2).

On the other hand, the largest distances are found in 2016 and 2017, which are the farthest periods from the rest of the centroids in the graph Figure 8.
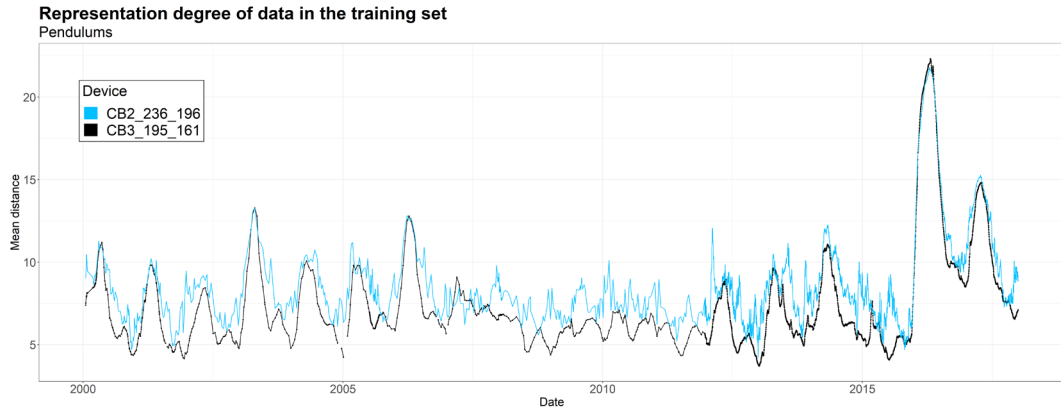
Figure 9. Series of the degree of representation, calculated as the Euclidean distance of the points of the different years to the centroids of the years used for training the models.

Figure 10 shows that, on average, the external conditions of 2016 and 2017 are the most different compared to other years. This is due to their low water level values. They are followed by the years 2006, 2003, and 2014, for both devices.
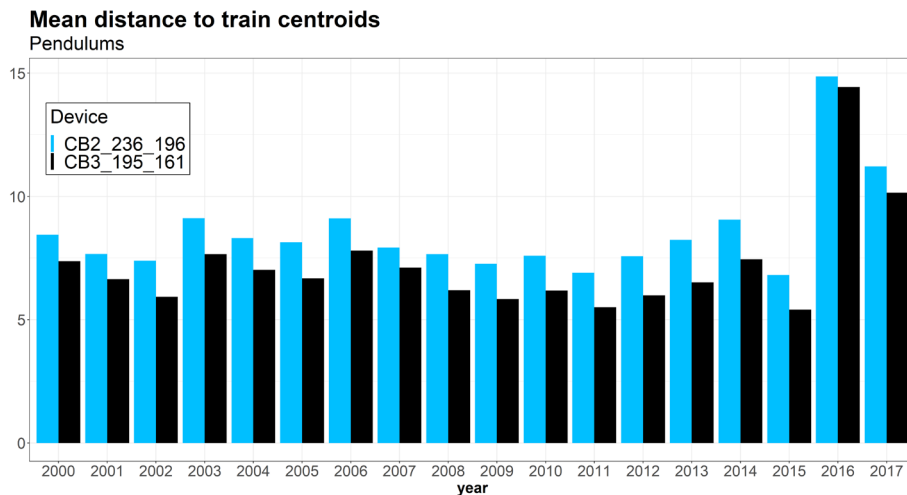
Figure 10. Mean Euclidean distance from the points of each year to the centroids of the training years.

Prediction models were trained for each cluster following the same yearly based CV process. Errors obtained in training and in the prediction of the validation year, once classified in the corresponding cluster, didn't show a sound improvement. It was finally decided to not use the clustered approach.

On the other hand, the results of this section indicate that the differences between the most important external conditions of each pendulum are related to low water levels and steep drawdowns. Given that 2016 and 2017 are revealed to be odd and since Machine Learning predictive models learn from data, a higher prediction error can be expected for those years.

3.5 *Models*

Among the results obtained when training the different models shown in Table 1, differences were found depending on the type of device. The SVM model was found to be the optimal model to predict the series of both pendulums; for the pore pressure measuring device, the best model was BRT, while for leakage and joint opening, the most accurate was NN.

Table 1. Results of the models for each device. $RMSE_{CV}$ is the estimated error during the Cross Validation process. $RMSE_{val}$ is the error made on the validation set (year 2012).

	Displacement (pendulums)				Joint opening		Pore pressure				Leakage	
Device:	CB2_236_196		CB3_195_161		C4_C5		PZCB2		PZCB3		Seepage	
Model	$RMSE_{CV}$	$RMSE_{val}$	$RMSE_{CV}$	$RMSE_{val}$	$RMSE_{CV}$	$RMSE_{val}$	$RMSE_{CV}$	$RMSE_{val}$	$RMSE_{CV}$	$RMSE_{val}$	$RMSE_{CV}$	$RMSE_{val}$
SVM	1.794	1.771	0.409	0.334	0.25	0.232	0.759	0.485	0.479	0.633	3.106	2.609
BRT	2.334	2.562	0.554	0.395	0.277	0.215	0.56	0.609	0.349	0.586	3.143	3.231
NN	4.165	7.136	0.893	0.441	0.189	0.107	1.102	0.907	0.926	2.114	3.054	2.821
RF	2.747	3.103	0.62	0.641	0.333	0.312	0.763	1.43	0.479	0.514	3.235	3.092
HST	2.869	4.099	0.594	0.622	0.305	0.353	1.029	1.526	0.724	1.291	3.113	2.632
RRBB	3.74	3.029	0.803	0.428	0.653	0.359	1.91	2.314	0.853	1.565	3.635	2.908
LM	3.642	2.862	0.686	0.465	0.623	0.354	1.853	2.288	0.77	1.255	3.514	2.727

It can be noticed that, in some cases, the validation error is lower with other models than those mentioned in the previous paragraph, as in the case of pore pressure and leakage devices. However, as explained in the Methodology section, the $RMSE_{CV}$ is a more robust estimator of the error because it uses more years in its calculation.

Figure 11 and Figure 12 show the results of the calibrated predictions during the CV and over the validation set of both pendulums. The series are significantly close to the actual values of the series. SVM seems to make a larger error in the high and low peaks of the years 2002, 2003, 2004 and 2005 in the case of the CB3_195_161 pendulum (Figure 11).

The short- and long-term predictions of both pendulums are also shown in these figures. The series corresponding to the CB3_195_161 pendulum appears to have a decreasing trend from approximately 2008 onwards, probably due to the trend of the water level during those years. From 2014 onward, the trend seems to disappear. The predictions for 2017 are within a narrower range than usual due to the large drop in the 2016 water level discussed in the exploratory analysis section that causes the 2017 water level to have low values (Figure 2). The same trend is observed in the series of predictions of the CB2_236_196 pendulum.
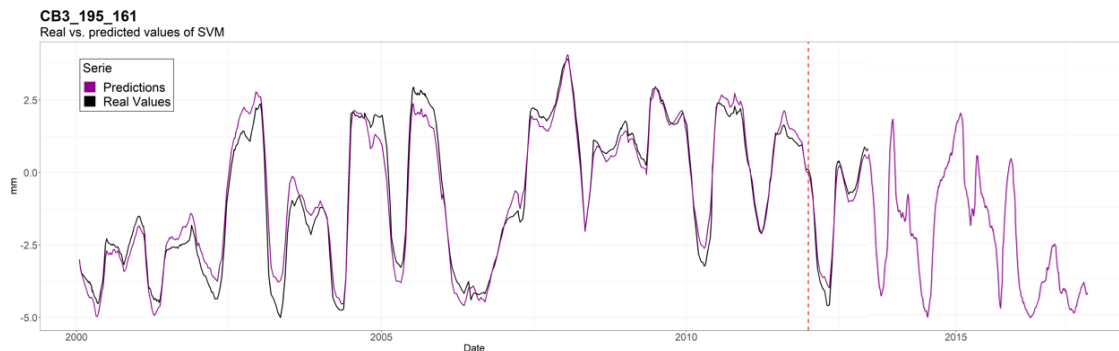

Figure 11. Series of real values of the CB3_195_161 pendulum and the predictions generated with the SVM model. The red dashed line separates the dates used to train the model and the validation set.

Figure 12. Series of real values of the CB2_236_196 pendulum and the predictions generated with the SVM model. The red dashed line separates the dates used to train the model and the validation set.
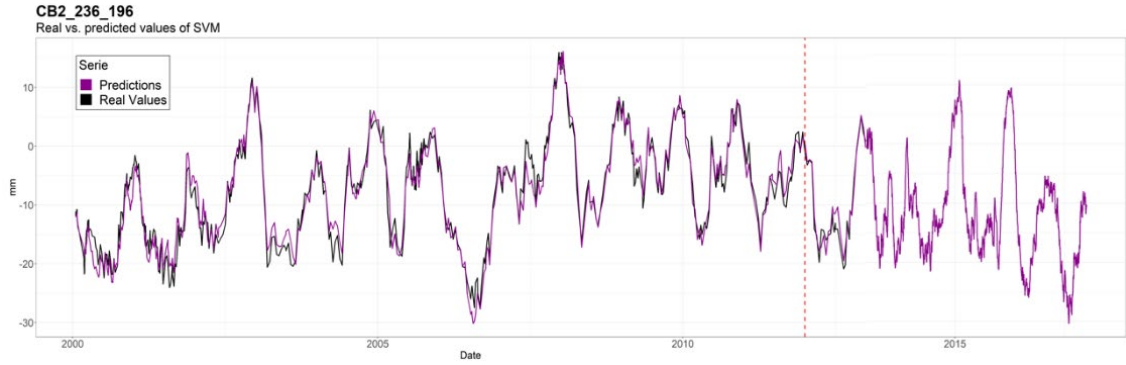
The outlier behavior of the water level in 2016 and 2017 makes it possible for the accuracy of the model to drop in those periods because that behavior has never been seen and the relationships between external conditions might not match those that the model has identified and configured.

3.6   *Warning Levels*

This section presents the results of the warning levels obtained by applying the formula explained in the Methodology chapter for each device.

Table 2. Table with the relevant information for the calculation of the warning levels of each target variable. Pto = c*σe.

	Displacement (pendulums)				Joint opening		Pore pressure				Leakage	
Device:	CB2_236_196		CB3_195_161		C4_C5		PZCB2		PZCB3		Seepage	
c	σ_e	Pto	σ_e	Pto	σ_e	Pto	σ_e	Pto	σ_e	Pto	σ_e	Pto
1.5		2.777		0.681		0.296		0.873		0.535		4.645
2	1.851	3.703	0.454	0.909	0.198	0.395	0.582	1.163	0.357	0.713	3.096	6.193
3		5.554		1.363		0.593		1.745		1.070		9.289
4		7.405		1.817		0.790		2.327		1.427		12.385

The coefficient selected to determine the warning levels is 2, so the band of each instance will be its predicted value plus 2 times the standard deviation of the error.
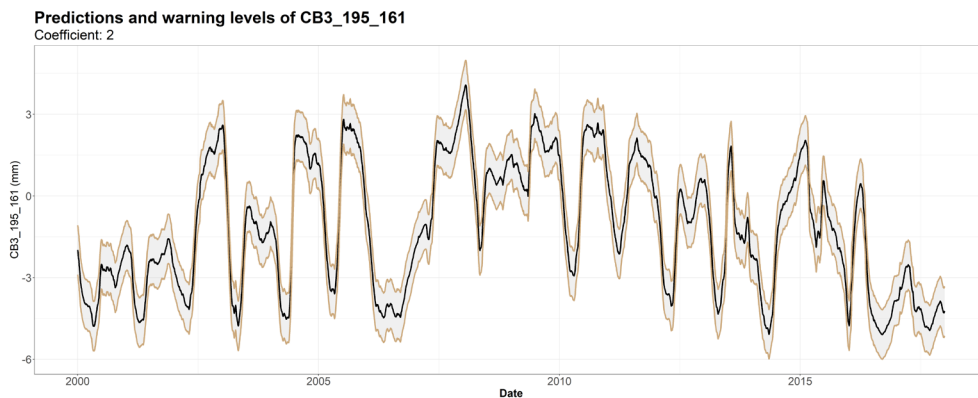

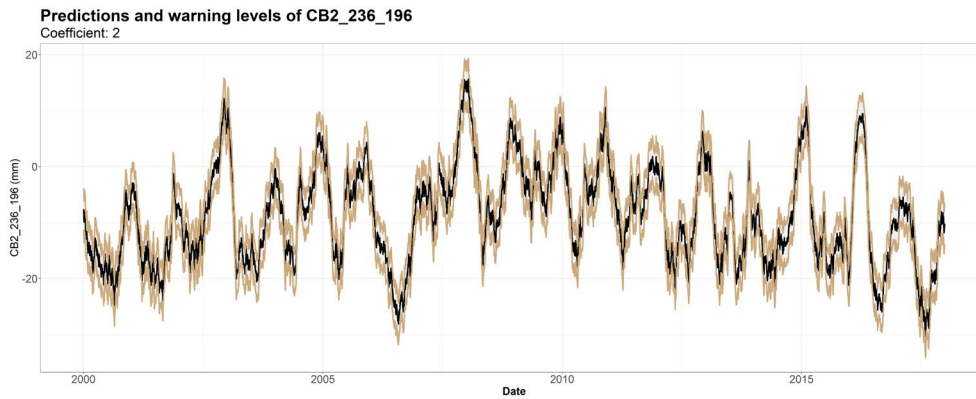Figure 13. Warning levels of the pendulum CB3_195_161 calculated with c = 2.

Figure 14. Warning levels of the pendulum CB2_236_196 calculated with c = 2.

4 CONCLUSSIONS

A ML approach has been made for developing predictive models to evaluate the monitoring data based on the external variables behavior. Relying on error estimates made through Blocked Cross-Validation, where each block was a different year, significantly accurate models have been achieved. Depending on the target variable, the most accurate algorithms have been SVM for dam displacements, NN in the case of leakage and joint opening, and BRT for pore pressure.

These models have been used for creating confidence bands, or warning levels, based on their predictions and the variance of the prediction error. The width of the band was established in two times this variance.

Taking into account that ML algorithms learn from the data used for their training, their predicting capabilities will depend on the similarity of the situations to be evaluated to those shown to the models during their learning process. The accuracy of a pure data-based model out of its training features space its hardly evaluable. Any data based (non-deterministic) model will have the same problem if it's fed with same training data. That is why an initial exploratory analysis of the features space was made.

This analysis revealed evident differences in the explanatory variables in 2016 and 2017 compared to the training period features space. Hence, the accuracy of the predictions made on this period will be probably lower than the one obtained for other periods with a more similar features space.

Considering the delay in the response of the dam to the variations of loads, synthetic variables were created based on the external conditions by temporal integration. These synthetic variables provide an accuracy improvement in predictions and an exploratory tool for dam behavior interpretation.

Regarding this interpretation of the dam behavior, the approach made was to let the models tell what they have found important to predict every particular variable and then make an interpretation of this information. For this purpose, a wide range of temporal integration of external variables were used for synthetic variables creation in order to ensure that relevant delayed effects were represented. Integration periods from 2 days to 365 days were used.

Short-term moving averages of water level seem to be the most relevant variables for inverted pendulum radial movements. This makes sense since thermal effect has usually less influence in the base of arch dams.

The most important variables obtained for the direct pendulum radial movements are, surprisingly, the very long-term moving averages of water level. It would have been expected to find thermal variables in the upper part of the ranking for this behavior. Trying to provide a physical interpretation, the only potential explanation found was an upstream foundation deformation motivated by slow changes in pore pressure due to variations in water level, but the verisimilitude of this hypothesis should be further studied.

BEHAVIOUR PREDICTION OF A CONCRETE ARCH DAM

Emanuele Catalano
Lombardi Engineering Ltd., Giubiasco, Switzerland

Riccardo Stucchi
Lombardi Engineering Ltd., Giubiasco, Switzerland

ABSTRACT: The paper presents a 3D numerical model that was conceived to predict the behaviour of a double curvature concrete arch dam. The model had the objective of reproducing the effective response of the dam to the hydrostatic load and to temperature loads. The calibration was performed on the base of monitoring data. The calibrated model was finally used to predict the short-term and long-term behaviour of the dam. This calculation exercise was proposed in the frame of the 16th International Benchmark Workshop on Numerical Analysis of Dams.

1 INTRODUCTION

The Theme A of the 16th International Benchmark Workshop on Numerical Analysis of Dams concerns the preparation of a behaviour model for a concrete arch dam. With the help of such models, engineers can evaluate the dam's performance, estimate the response of the dam for its actual loading conditions and define warning levels. The calibration and the prediction provided in the paper concerns the measurements of the pendulums and the crack opening.

A constitutive approach, preparing a 3D numerical model for reproducing the dam behaviour, is adopted at first. Also, the results that were obtained fitting the available monitoring data following a data-based approach are presented and commented in the light of comparison with the results that were obtained following the constitutive approach.

The dam is owned by Electricité de France (EDF) and it is located in the south of France at an altitude of approximately 2000 m asl. The name of the dam was kept undisclosed. The height of the dam is 45 m, the crest and base thickness is 2 m and 6 m, respectively. The crest has a radius of 110 m and a length of 166 m.

The dam is equipped with a comprehensive monitoring system, including pendulums, crack opening, displacement sensors, piezometers and seepage measurements. Monitoring data have regularly been acquired since the first impoundment. The monitoring data made available by the formulators are shown in Appendix, referring to the period from 1995 to 2017. The monitoring data to be predicted with the model refer to the period 2000-2012. As highlighted in the provided documents, all altitudes refer to a common value which is an arbitrary value, and not the sea level. It should be noted that when water level is lower than 196 m asl, there is only water in a lake located upstream and below the heel of the dam.

The air temperature is not measured at the location of the dam, and, as far as the authors know, the dam is not equipped with thermometers. Two time series of daily air temperature were available: T_a, which is a time series of measurements located in the area of the dam, carried out according to the standard of WMO (World Meteorological Organisation) and located 50 km from the dam, however at a different altitude; T_b, which is calculated by interpolation from several air temperature measuring stations, taking into account the altitude of the dam and is calculated on a mesh of 1 square kilometre. Some comment on this information and how these temperatures are used to compute thermal loads for the dam are given in Section 3.2.1.

The dam is equipped with several pendulums, as illustrated in Figure 1. Only the measurements of pendulums on the Central Block (labelled CB2 and CB3) were made available by the formulators. CB2 is the radial displacement between the altitudes 236 m (just under the crest of the dam) and 196 m asl (toe of the dam). CB3 is the radial displacement in the foundation between the altitudes 195 m asl and 161 m asl.

A crack opening displacement sensor is located at the rock-concrete interface of the Central Block (CB). The sensor measures the opening between C4 (in the foundation) and C5 (in the concrete, at the toe of the dam). The location of the crack opening sensor and of the piezometers is illustrated in Figure 1.
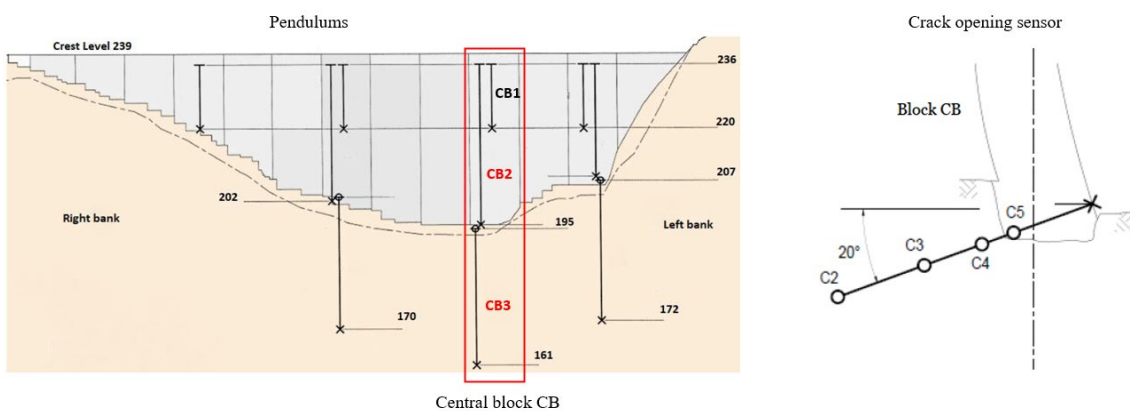

Figure 1. Monitoring equipment – pendulums and crack opening displacement sensor.

2 DATA TREATMENT AND COMMENTS

In Figure 2 pendulum and crack opening measurements are plotted as a function of the water level. It can be seen how the displacements vary over large ranges for each given water level, especially for the pendulum measurement CB2 and the crack opening. This must be related to the effect of the temperature on the displacements, which apparently has a strong influence on the dam response. A crack opening of about 4mm is measured for the highest water levels.
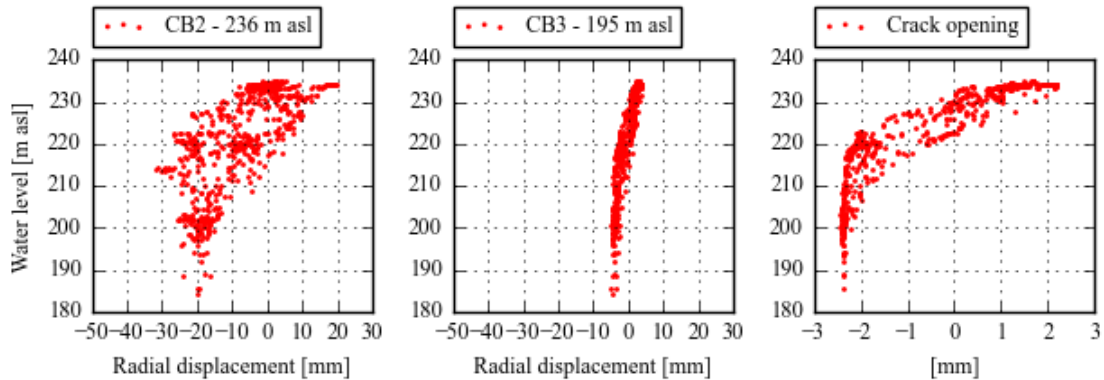

Figure 2. Pendulum and crack opening measurements as a function of the water level.

3 THE NUMERICAL MODEL

3.1 *The geometry*

The numerical model that was prepared is based on a three-dimensional explicit finite difference scheme. Material behaviour is simulated according to an elastic constitutive stress/strain law in response to the applied forces or boundary restraints. The software FLAC3D (Itasca Consulting Group, Inc., 2016) was employed for the simulations.

The geometry provided by the formulators has been processed to build a mesh that was suitable for the finite-difference model (FDM) that was prepared, as shown in Figure 3. The only significant difference with the mesh that was provided is that the dam is described as made of concrete blocks rather than a monolithic structure. This was done to properly simulate the dam construction considering the blocks as independent and not interacting between each other, thus fully neglecting the arch effect in this phase.
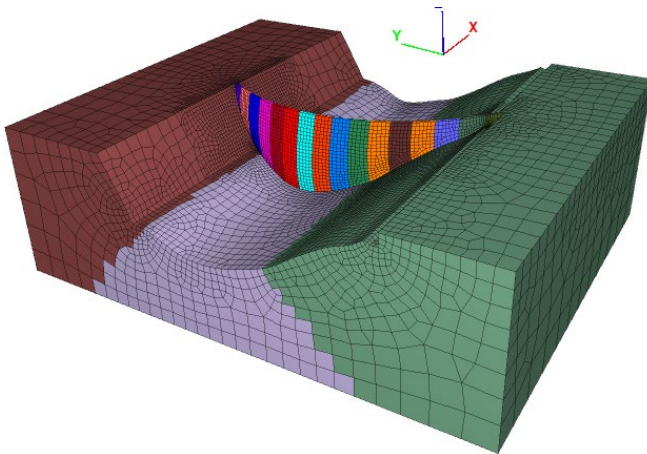

Figure 3. 3D view of the numerical FD model. Dam geometry described as made of concrete blocks. The rock foundation is described by three zones (left/right banks, valley floor) characterized by different mechanical properties (see Section 4.2).

No information was given on the construction phasing of the dam. The authors believed that given the age of the dam and the material of construction (traditional concrete), simulating the dam construction assuming independent blocks leads to a stress state close to the actual one. Having or not a realistic stress state at the end of construction does not impact in any way the elastic dam response to the loads. However, if one is interested in the stress state of the dam, to evaluate for example the possibility of onset of cracks, then having a consistent state of stress at the end of the construction phase is indispensable.

3.2 *Hydrostatic and thermal loads*

It was assumed that two effects have a dominant role on determining the behaviour of the dam: the effect of the hydrostatic load and the one of the thermal loads. Therefore, these two loadings only have been considered in the numerical model.

The hydrostatic load depends exclusively on the water level in the reservoir, and it was simulated by applying a mechanical normal stress to the dam upstream face. In this study the dam-foundation response is computed for five water levels in the reservoir, as represented in Figure 4, considering non-linear interfaces at the dam base and in correspondence of the vertical construction joints.
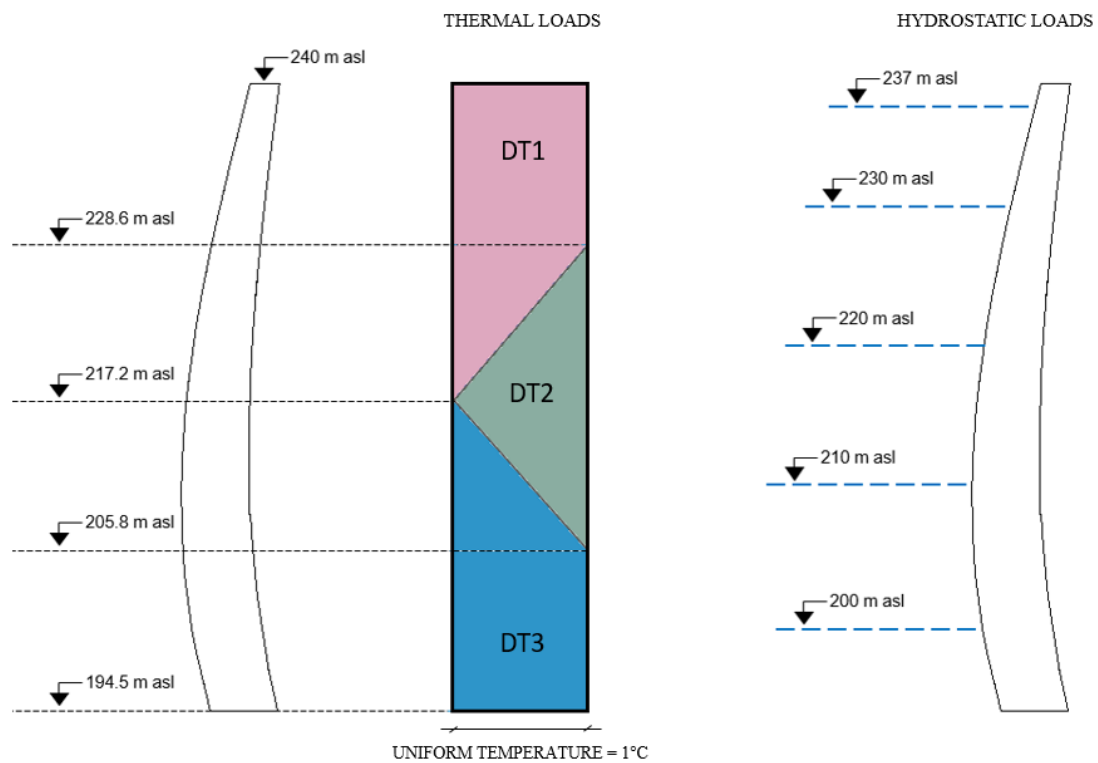
Figure 4. Thermal and hydrostatic loads.

Conversely, the dam response to the thermal loads is assumed to be elastic. The computation of thermal effects is therefore based on the superposition principle. The numerical model response to the thermal loads is computed for unit loads defined at various levels. Usually, the levels at which the unit loads are defined are related to the location of the dam thermometers. In the lack of such equipment, three different unit load patterns have been defined, as represented in Figure 4. Thermal loads are assumed to be constant towards the left/right abutments direction.

3.2.1 Definition of thermal loads

The thermal state within an arch dam is of primary importance for predicting its behaviour. In fact, the displacements of an arch dam are influenced also by the thermal elongation caused by temperature variations.

Although in most of the cases the temperature effects can be approximated by a seasonal effect which is repeated the same every year, in certain conditions (i.e., full and prolonged drawdown) the direct measurement of the concrete temperature by means of thermometers is necessary for correctly interpreting the dam behaviour. An extreme example is the case of the 250-300'000 m3 snow avalanche occurred in 1999 at the 67 m high Ferden arch dam (Switzerland), covering 35 m of the downstream face (Bianchi, 2000). In that case, the temperature measured by the thermometers installed in the dam body allowed to confirm the normal behaviour of the dam under such exceptional loading conditions, which had instead been questioned by the statistical interpretative model (Amberg, 2009).

Unfortunately, the examined dam is not equipped with thermometers in the dam body and the formulators provided only two time series of the air temperature (T_a, T_b). A comparison between the monthly averages of the two time series shows that T_a and T_b reproduce basically the same temperatures but with an offset of 8-9°C. Since T_b indicates temperatures which seems to be more compatible with the elevation of the dam (approximately 2000 m asl, according to the formulators), T_b is considered in the following for the definition of the thermal state.

The thermal state within the dam is evaluated by means of a transient thermal analysis. The thermal calculation is performed assuming 1D heat flow along the dam thickness. The thermal properties of the concrete are the following: conductivity: 2.0 W/mK, specific heat: 900 J/kgK, density: 2400 kg/m^3. Three calculation sections are considered at three different elevations: 205.8 m asl, 217.2 m asl, 228.6 m asl. Each section is characterised by a different concrete thickness: 5.2 m, 4.5m and 3.4 m, respectively.

The dam thickness is divided into 11 elements and the calculation procedure is based on a finite difference explicit method (see Amberg, 2003 for more details). Heat flow is assumed to occur by radiation and convection at the faces of the dam and by conduction within the dam.

The temperature boundary conditions at the upstream face depends on the upstream water level (see Figure 5): water temperature is considered in the case the water level is above the calculation section, air temperature is considered otherwise. In the first case a convective heat coefficient of 13 W/m^{2}K (concrete-air) is adopted, together with a surface emissivity equal to 0.7, while in the latter case a convective heat coefficient of 500 W/m^{2}K (concrete-water) is adopted, while the surface emissivity is assumed to be none.

The water temperature (T_w) is not directly measured, but it was derived from the air temperature by applying the following simplified approach suggested by the formulators:

$$T_w = \begin{cases} 0.7 \cdot T_b & if \ T_b > 0°C \\ 0 & otherwise \end{cases} \tag{1}$$

For the downstream face, being always exposed to air, the air temperature is considered as a boundary condition. The thermal calculation starts in 1995 and ends in 2017.

The results of the thermal calculation are shown in Figure 6in terms of average temperature along the dam thickness for the three considered elevations.
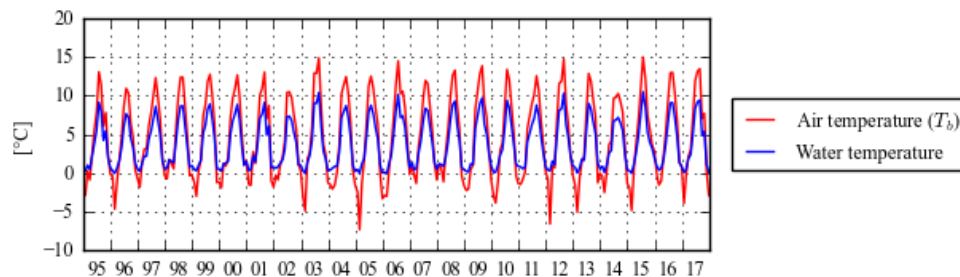

Figure 5. Air and water temperatures assumed in the thermal calculation (monthly averages).
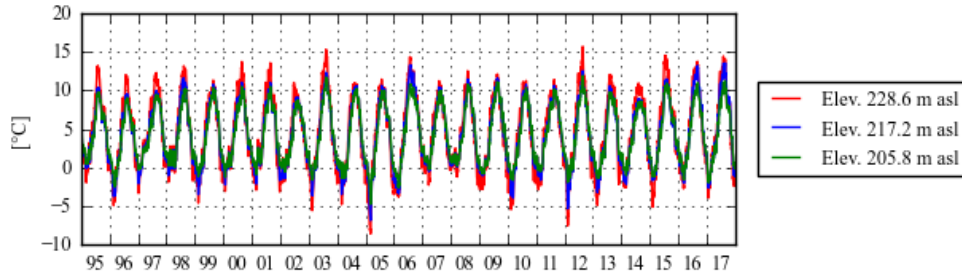
Figure 6. Concrete average temperature at the three elevations assumed in the thermal calculation.

4 MODEL CALIBRATION

4.1 *Procedure for model calibration*

A polynomial interpolation (4th degree) is performed on the displacements that are computed by the numerical model for each of the water levels that are represented in Figure 4. Computation of displacements for any water level is then possible.

The displacement $\delta_{W,i}$ induced by the hydrostatic load Q, at the measurement point i (i.e. measurement poinst of the pendulums), can be computed using the following expression:

$$\delta_{W,i} = a_i \cdot x + b_i \cdot x^2 + c_i \cdot x^3 + d_i \cdot x^4 \tag{2}$$

where:
- $x = \frac{Q - Q_{min}}{Q_{max} - Q_{min}}$ is the normalized level in the reservoir, with $Q_{min} = 160$ m asl and $Q_{max} = 237$ m asl.
- a_i, b_i, c_i, d_i are the coefficients of interpolation for the measurement point i (obtained from the results of the numerical model).

The displacement $\delta_{T,i}$ induced by thermal loads, at the measurement point i (i.e., measurement points of pendulums), can be computed using the following expression:

$$\delta_{T,i} = \sum m_{ij} \Delta T_j \tag{3}$$

where:
- m_{ij} is the displacement at the measurement point i for a unit load at level j (result of the numerical model);
- ΔT_j is the average concrete temperature at level j.

The procedure for model calibration consists in testing several scenarios in terms of material properties of the simulated materials, to reproduce at the best possible the observed behaviour of the dam (monitoring data). The effectiveness of the calibration is evaluated on the base of the difference between measurements and model predictions, expressed by the following equation:

$$\delta_{C,i} = \delta_{M,i} - \delta_{W,i} - \delta_{T,i} \tag{4}$$

Where:
- $\delta_{C,i}$ is the difference between the measured displacement at the measurement point i and the model prediction for the measurement point i;
- $\delta_{M,i}$ is the measured displacement at the measurement point i.

Equation 4 is calculated for each date in which the measurement $\delta_{M,i}$, the water load Q and the average concrete temperatures ΔT_j are available.

The internal software P0863 developed by Lombardi is used as a tool for model calibration. The software helps the user in the definition of a new numerical scenario in terms of material properties (concrete and rock stiffness, thermal expansion coefficient) that could better reproduce the effective dam behaviour.

4.2 *Material properties*

In the benchmark formulation, the following information were made available:
- The dam is made of concrete with cement dosage at 300 kg/m3. The average value of compressive strength is 34 MPa (after 90 days) with values varying from 22 MPa to 45 MPa;
- The foundation consists of laminated metamorphic slate with a high compressive strength. However, the anisotropy of foundation confers a higher deformability to the left bank.

The mechanical properties that were recommended by the formulators for the concrete and the rock foundation are summarized, the initial estimate for the numerical analyses and the result of the calibration are summarized in Table 1.

Table 1. Mechanical parameters of the modelled materials proposed in benchmark formulation, initial estimate for the numerical analyses and result of the calibration.

	Young's Modulus [GPa]		
	Formulator proposal	Initial estimate	Result of calibration
Concrete of the dam	22	22	24
Foundation right bank	Parallel: 15 Perpendicular: 10	12.5	3.5
Foundation (approximately bottom of the valley)	Parallel: 5 Perpendicular: 1	3	0.5
Foundation left bank	Parallel: 10 Perpendicular: 1	5	1.4

Some preliminary comment can be formulated on the proposed material properties, in the light of the information that was available from monitoring data. In this study, pendulums information is quietly poor, since only one measurement of dam displacements and one measurement of foundation displacements are provided. This information is given for the central block of the dam (see Figure 1). No other information was given about foundation behaviour (e. g. from extensometers). In this context, the introduction of an anisotropic behaviour for the rock foundation has been considered too complex without having enough information to verify the effectiveness of the adopted material properties. For this reason, average isotropic moduli have been defined for the rock foundation. Different values for left and right banks, and for the foundation at the bottom of the valley, are maintained, even though information from other pendulums located towards the left and the right abutment would have helped the interpretation of dam-foundation response to the loads.

The calibration process leads to a slightly increase of the concrete modulus to 24 GPa and a general decrease of the modulus of the rockmass (0.5 GPa at the bottom of the valley, 3.5 GPa at the right bank and 1.4 GPa at the left bank). Regarding the coefficient of thermal expansion, the obtained value is 1.4e-5 °C^{-1}, which is increased with respect to the value proposed by the formulators (0.7e-5 °C^{-1}).

4.3 *Results of the numerical FDM model*

The results of the numerical FDM model are shown in Figure 7, by comparing the predicted and measured dam displacement due to the hydrostatic loads. The measured value is obtained by removing from the measurement the displacement due to the thermal loads.

Two observations can be made. First, the dispersion of the measurement, although reduced, remains quite high. This means that the thermal state within the dam is not reproduced with accuracy. The lack of concrete temperature measurements has a negative impact on the reliability of the simulation of thermal behaviour of the dam.

Second, the behaviour predicted by the model does not fully match with the actual one, especially for the pendulum CB2: the dam seems to be more rigid for higher water levels and less rigid for lower water levels, with respect to the numerical model.
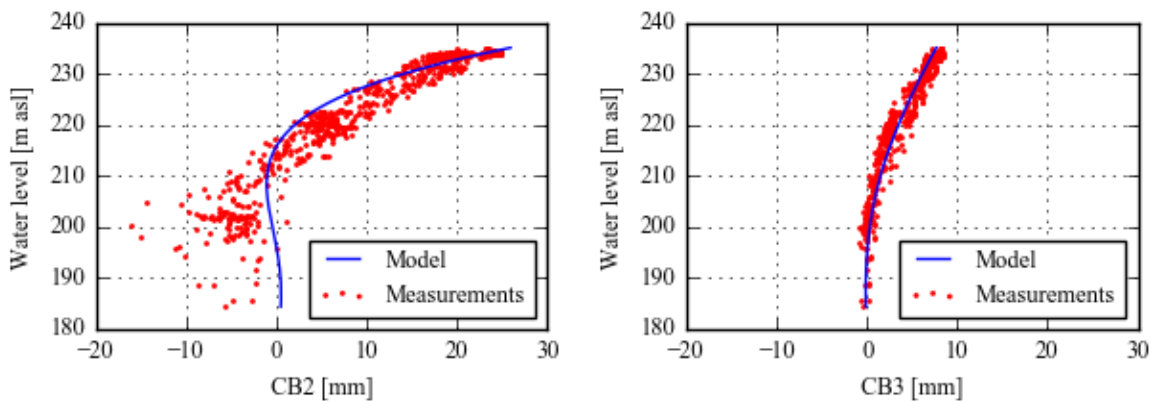

Figure 7. Pendulums – comparison of measurements and model results (note: the thermal effect is removed from the measurements).

Regarding the crack opening, Figure 8 shows a good agreement between the model and the measurements.
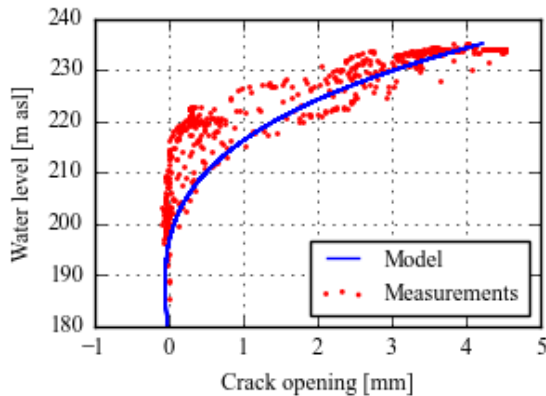
Figure 8. Crack opening – comparison of measurements and model results.

The behaviour of the pendulum CB2 could be explained with an opening of the vertical contraction joints in wintertime with a low reservoir level. Under these conditions the arch effect is reduced resulting in a more deformable structure than the monolithic one. With higher water levels, the joints are closing, restoring the full stiffness of the monolithic structure. This behaviour has been recognized in the past by the authors in other arch dams.

Because of the lack of information regarding the behaviour of the joints, hypothesis on the joint opening cannot be verified. Therefore, it was decided to reproduce the response of the dam to the hydrostatic loads by interpolating the measurements shown in Figure 7 with a polynomial function of 4th order.

In Figure 9 a comparison between the numerical model and the statistic interpolation is shown for the pendulums CB2 and CB3. It is evident that the polynomial interpolation better reproduce the actual behaviour of the dam.

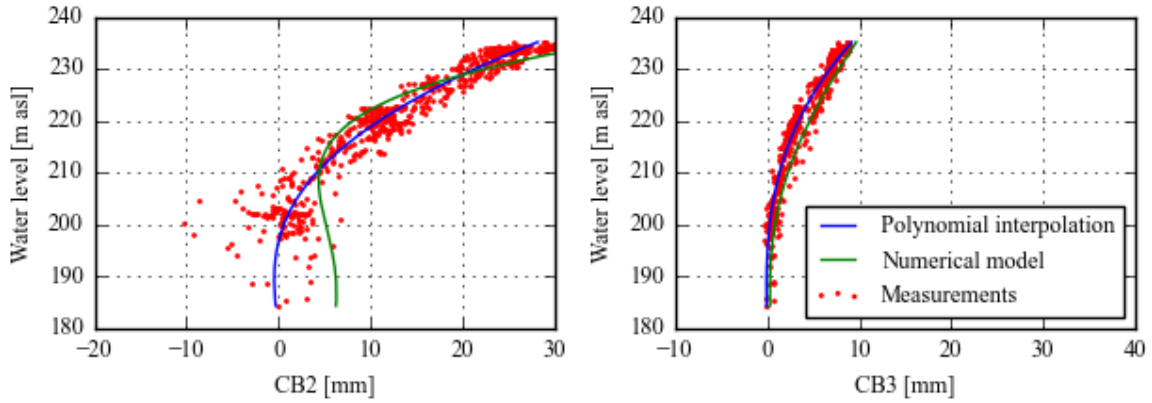Figure 9. Pendulums CB2 and CB3 – comparison of measurements and the results of the polynomial interpolation and the numerical model (note: the thermal effect is removed from the measurements).

4.4 *Interpretative model*

Based on the considerations presented above, the final model used for the prediction presented in the following is based on a hybrid model composed by:
- A constitutive model, i.e., based on the numerical model, for the prediction of the dam response to thermal loads and for the prediction of the crack opening;
- A data-based model, i.e., based on the polynomial interpolation, for the prediction of the dam response to hydrostatic loads.

The equations of the model used for the prediction of the behavior of the dam are listed hereafter. The set of equations 5 represents the model for the pendulum CB2, while the set of equations 6 is for the pendulum CB3 and the set of equations 7 is for the crack opening. In the equations, $\delta_{CAL,i}$ is the predicted displacement of the pendulum i (i = 2 for CB2, i = 3 for CB3) and the predicted crack opening (i = 4). The constants that appear in the equations minimize the average difference between measured displacements and calculated ones.

$$\delta_{W,2} = 15.655 \cdot x - 98.312 \cdot x^2 + 158.751 \cdot x^3 - 45.256 \cdot x^4$$
$$\delta_{T,2} = -1.413 \cdot \Delta T_{228} - 0.343 \cdot \Delta T_{217} + 0.284 \cdot \Delta T_{205} \tag{5}$$
$$\delta_{CAL,2} = \delta_{W,2} + \delta_{T,2} - 14.993$$

$$\delta_{W,3} = 3.028 \cdot x - 18.824 \cdot x^2 + 28.033 \cdot x^3 - 2.097 \cdot x^4$$
$$\delta_{T,3} = 0.031 \cdot \Delta T_{228} - 0.039 \cdot \Delta T_{217} - 0.162 \cdot \Delta T_{205} \tag{6}$$
$$\delta_{CAL,3} = \delta_{W,3} + \delta_{T,3} - 4.428$$

$$\delta_{W,4} = 1.225 \cdot x - 7.088 \cdot x^2 + 8.097 \cdot x^3 + 3.421 \cdot x^4$$
$$\delta_{CAL,4} = \delta_{W,4} - 3.172 \tag{7}$$

The measured and calculated displacements are shown in Figure 10, while their difference between is shown in Figure 11.

The correspondence between the measured and calculated displacements is considered satisfactory, given the available information. The standard deviation of the difference between the measured and calculated displacement is 2.3 mm for the pendulum CB2, 0.6 mm for the pendulum CB3 and 0.6 mm for the crack opening.

4.5 *Warning levels, short-term and long-term predictions*

The warning levels should be defined to identify anomalies in the dam behaviour. Assuming that the dam behaviour is regular in the calibration period, an excessive deviation from the model prediction should be considered as an anomaly. In the definition of what one should consider "excessive" the precision of the model in the calibration period must be accounted.

Therefore, it is proposed to define the warning levels as the envelope of the maximum differences between the measurements and the model predictions in the calibration period (2000-2012):
- for the pendulum CB2: ±6 mm with respect to the model prediction;
- for the pendulum CB3: ±3 mm with respect to the model prediction;

for the crack opening: ±2 mm with respect to the model prediction.
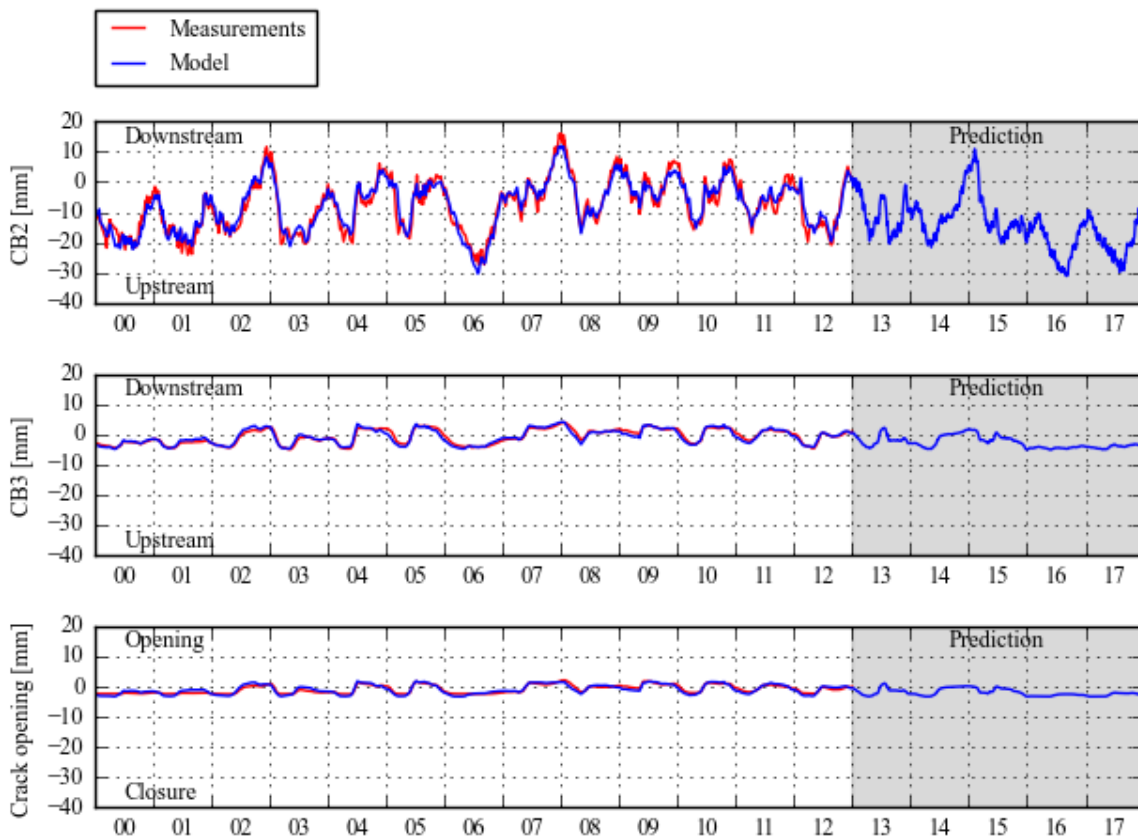
Figure 10. Pendulums and crack opening – comparison of measurements and model prediction.

An excessive deviation from the expected behaviour should not be necessarily interpreted as a safety concern for the dam. The warning levels, as defined on the next page, has the scope to highlight as soon as possible any anomaly in the dam behaviour or in the measurement instrumentation, in order to promptly analyse it and, if necessary, implement the appropriate corrective measures.

The figures on the next page also show the predictions of the model for the period 2013-2017, which is one of the tasks of the Benchmark. It worth mention that the period 2016-2017 is characterised by a low water level and the displacements of the pendulum CB3 are quite completely caused by the thermal loads.

Figure 11. Pendulums and crack opening – difference between the measurements and the model.

5 INTERPRETATION

The information gained from the monitoring measures, together with the results of the numerical model allow to point out some important aspects regarding the behaviour of the analysed dam.

The rock modulus obtained from the calibration process are quite low, in the order of 0.5-3.5 GPa, and significantly lower than those 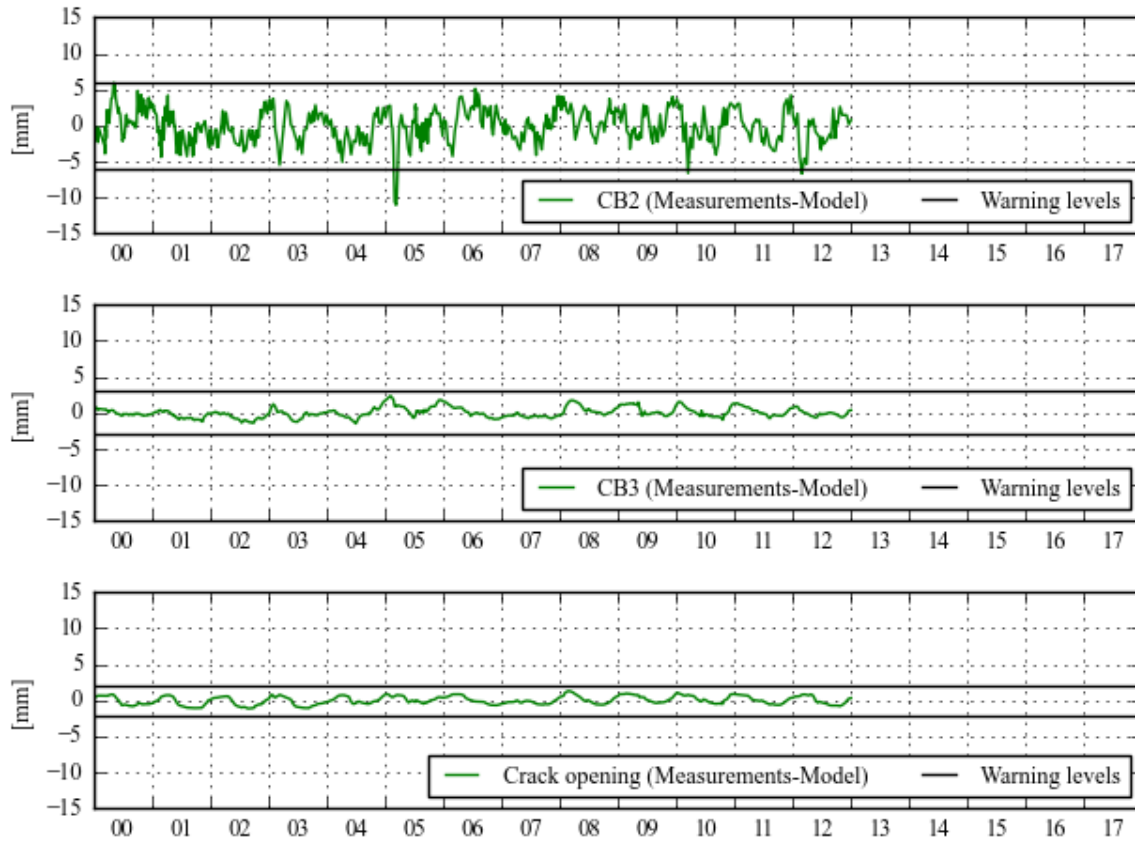proposed by the formulators (1-15 GPa). Although the obtained moduli allow to reproduce the displacements measured by the pendulum with a good agreement, drawing some conclusions regarding the actual stiffness of the rock mass is questionable. The reliability of the estimate is higher for the modulus of the central part of the valley (0.5 GPa), due to the presence of the pendulum CB3 which measure the response of the rock to the forces transmitted by the dam. However, the lack of information regarding the rock mass deformations in the left and right banks, makes the estimate less reliable.

The measurements of the pendulum CB2 has a high dispersion when plotted as a function of the water level (Figure 2). In fact, the range of variation of the displacement for a certain water level is of the same order of magnitude as the variation of the displacement due to the full reservoir. In this context, the lack of direct information regarding the thermal state within the dam (e.g., thermometers), leads to a reduced precision of the prediction of the model. The thermal analysis conducted to overcome this issue leads to a reduction of the measurement dispersion (Figure 7), which however remain quite high affecting the precision of the model.

The comparison between the measurements and the model shows that the dam behaviour is basically reversible, without any drift or irreversible displacements. Only a very modest delay between the measurements and the model is visible for the pendulum CB3, possibly indicating that the rock mass behaviour is affected by some viscous effect. Regarding the pendulum CB2, the numerical model results highlighted that the actual behaviour of the dam could be influenced

by an opening of the vertical contraction joints in wintertime with a low reservoir level, leading to a progressive activation of the arch effect as a function of the water level.

The numerical model is used also for estimating the maximum compressive stress in the arch for the load combination of maximum water level in summertime. It is remarked that the summertime condition is simulated in a simplified way by considering a temperature increase of 10°C for the whole dam. This value derives from assuming a reference temperature of 5°C and considering the maximum temperatures shown in Figure 7. The horizontal stresses in the direction of the arches are shown in Figure 12, while the vertical stresses are shown in Figure 13. The maximum compressive stresses are horizontal and located at the upstream face in the middle of the dam and reach 4 MPa, which is far below the compressive strength of the concrete (34 MPa as provided by the formulators).
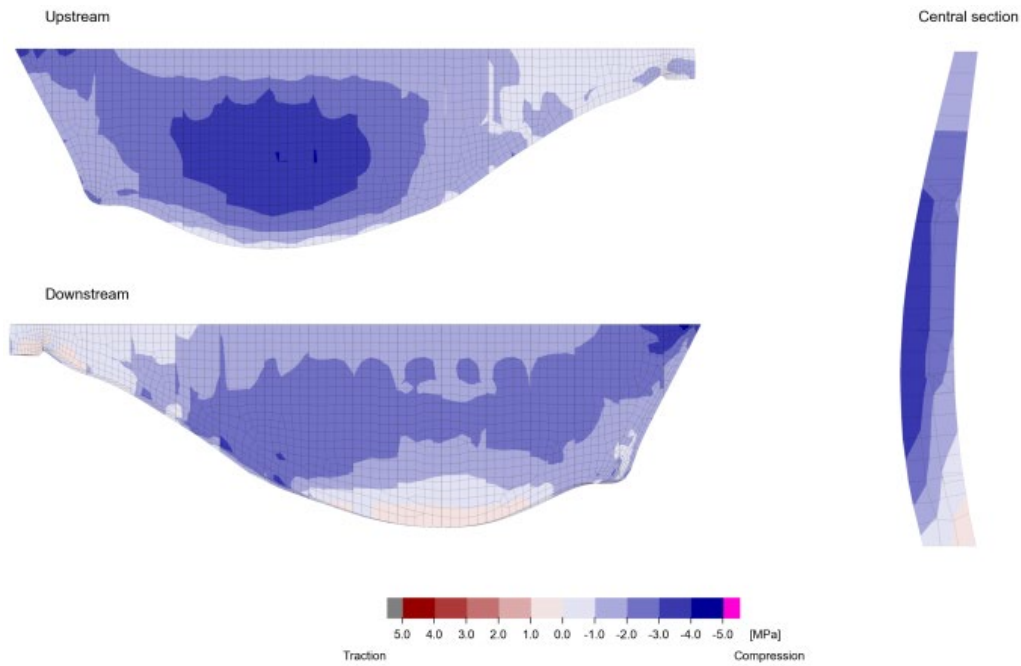

Figure 12. Horizontal stress in the direction of the arch for the condition of full water level and summer temperatures.
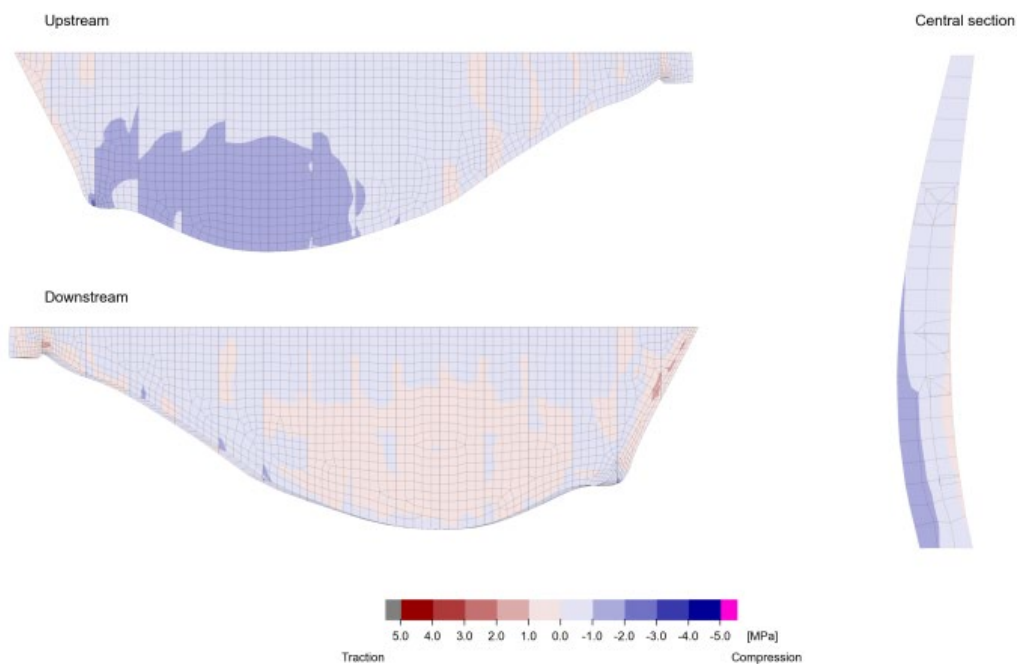

Figure 13. Vertical stress for the condition of full water level and summer temperatures.

6 CONCLUSIONS

The Theme A of the 16th International Benchmark Workshop on Numerical Analysis of Dams concerned the preparation of a behaviour model for a concrete arch dam.

The numerical model that was prepared is based on a three-dimensional explicit finite difference scheme. Material behaviour is simulated according to an elastic constitutive stress/strain law in response to the applied forces or boundary restraints.

The model had been calibrated to fit as best possible the measurements coming from monitoring equipment. However, some problems were encountered.

On one hand, the model was not able to capture properly the dam response to thermal loads. The reason for that could probably be related the poor available information on the thermal state of the dam over the calibration period.

On the other hand, measurements of dam displacements for low water levels indicate a deformability of the structure that the model was not able to capture. Dam response to the highest water levels is better reproduced by the model. Crack opening measurement from sensors near the base of the dam were also well reproduced. Some hypotheses have been formulated on this deviation between the measurements and the model results, such as the opening of vertical contraction joints in wintertime with low reservoir level. No information on joint opening was available, so this hypothesis could not be verified.

Finally, a data-based approach has been followed to interpolate the dam response to the hydrostatic load. The deterministic (constitutive numerical) approach was maintained in making predictions on thermal behaviour and crack opening. The result of the model can be considered satisfactory.

As engineers often involved in similar situations, we had a new opportunity to observe that following a constitutive approach when preparing dam behaviour models allows going in a deeper detail while interpretating dam's response. Calibrating a constitutive numerical model often brings to a better knowledge of dam's behaviour and of the characteristics of the materials. The data-based statistical approach is inherently valid as long as the *usual* conditions that characterize dam life are met again in the future (which is highly probable, though!). In case of *unusual* conditions, for which the information given by a model regarding dam safety are most valuable, the reliability of a statistical model could be lower.

REFERENCES

Amberg F., Thermal analysis of a RCC dam during construction. Proc. of the 7th Benchmark Workshop on Numerical Analysis of Dams, 2003.

Amberg F., Interpretative Models for Concrete Dam Displacements, ICOLD, 23rd Congress on Large Dams, Brasilia, 2009

Bianchi, M., Bremen, R., "Health Monitoring of Arch Dams – Recent Developments", International Workshop on The Present and Future in Health Monitoring, Bauhaus-University Weimar, Germany, 2000

Itasca Consulting Group, Inc. (2016) FLAC – Fast Lagrangian Analysis of Continua, Ver. 8.0. Minneapolis: Itasca.

APPENDIX – AVAILABLE MONITORING DATA
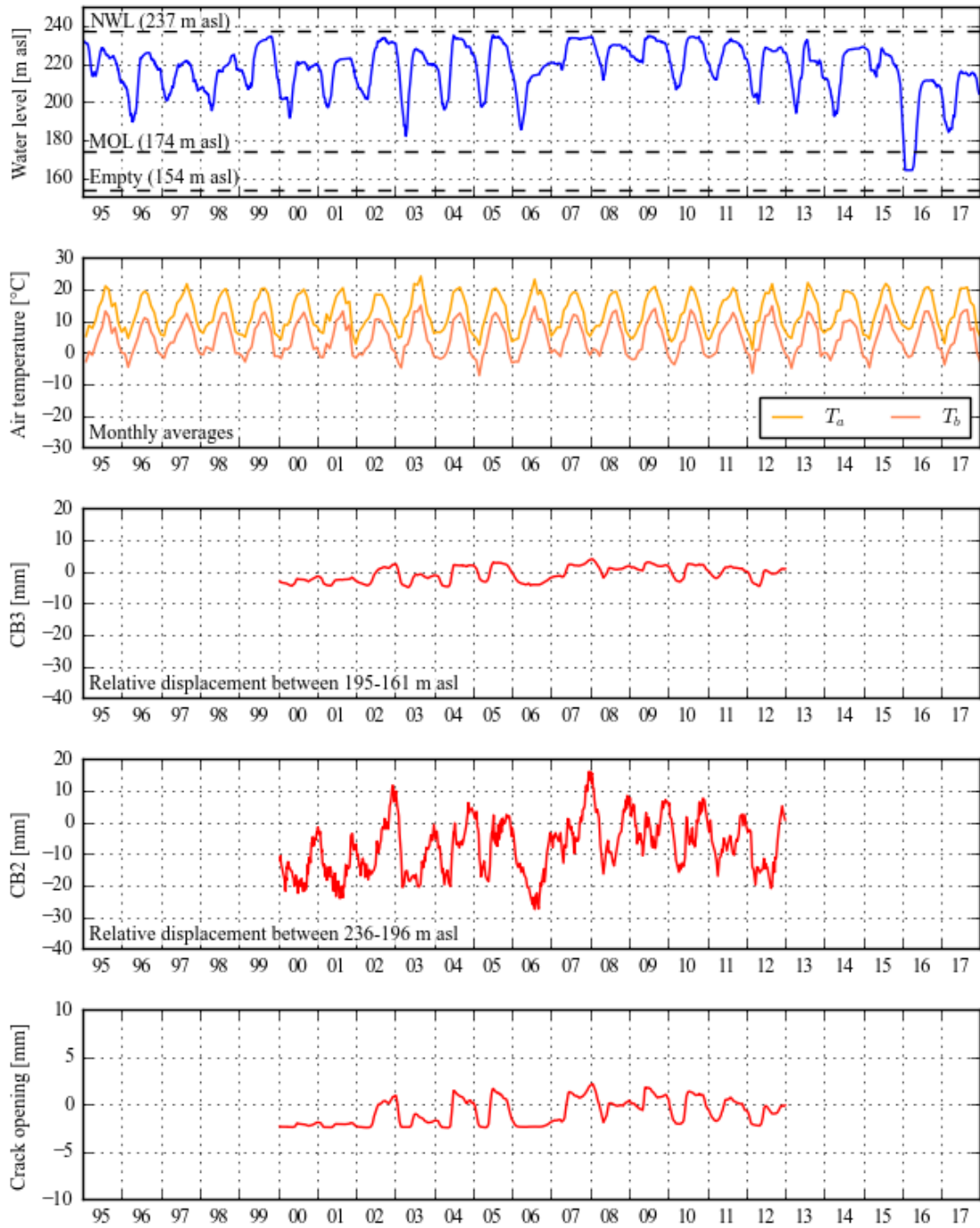
BEHAVIOUR PREDICTION OF A CONCRETE ARCH DAM IMPLEMENTED WITH AN HTT-FEM HYBRID MODEL

Alexandre Gomes

EDP, Gestão da Produção de Energia, SA. Generation Platform, Portugal

   alexandre.gomes@edp.com

João Cunha

EDP, Gestão da Produção de Energia, SA. Generation Platform, Portugal

   joaogomes.cunha@edp.com

José Paixão

EDP, Gestão da Produção de Energia, SA. Generation Platform, Portugal

   jose.paixao@edp.com

Marco Fernandes

EDP, Gestão da Produção de Energia, SA. Generation Platform, Portugal

   marco.fernandes@edp.com

ABSTRACT: The concrete arch dam proposed for the 16th International Benchmark Workshop on Numerical Analysis, theme A (Behaviour prediction of a concrete arch dam), was numerically analyzed with an HTT-FEM hybrid model using ANSYS software and computer codes purposely developed by the authors for arch dam analysis. A hydrostatic-thermal-time (HTT) model was used to determine the contribution of the hydrostatic load, the temperature variation and the time effect, to the observed measures. The predefined geometry delivered to the participants was directly imported in ANSYS and the mesh was developed using internal software capabilities. A sensitivity test was performed to obtain an adequate mesh discretization for the analysis. Structural analyses were performed for different water levels of the reservoir and for the thermal field in the observation dates, which was obtained by a transient thermal analysis. The computed displacements in this hybrid approach are the sum of the results obtained through the deterministic model for the hydrostatic pressure and the thermal action, with the time effect contribution obtained from the HTT model. The radial displacement prediction for both plumb lines is presented as well as their warning levels.

1 INTRODUCTION

This paper presents the methodology adopted for the analysis of "Theme A: Behaviour prediction of a concrete arch dam" proposed by the organization of the 16th ICOLD Benchmark workshop on numerical analysis.

After an exploratory data analysis phase, a conventional engineering approach was used, with the combination of an HTT and FEM models, allowing a more direct physical interpretation of the behaviour of the dam.

The concrete dam was numerically studied using ANSYS software and computer codes purposely developed by the authors for arch dam analysis, which have been used in the assessment of the behaviour of several operating arch dams.

This analysis methodology allowed the submission of the calibration and prediction results for the plumb lines displacements.

2 EXPLORATORY DATA ANALYSIS

The data exploration begun with a statistical synthesis, after visual inspection of the time series.

Table 1 presents the values of the parameters of the sinusoidal approximation, with an annual period, of the 2 daily air temperature series T (t) provided, $T_a(t)$ and $T_b(t)$, which were obtained by the least squares method

$$T(t) = T_M - T_A \,.\, \cos[2.\pi.(t - t_0)/365]$$

Table 1. Sinusoidal approximation parameters.

	Ta	Tb
Root mean square error (RMSE) [°C]	3.0	3.2
Greatest difference [°C]	7.6	8.0
Correlation coefficient	0.86	0.84
T_M=mean value [°C]	12.7	4.8
T_A=annual half-amplitude [°C]	7.4	7.1
T_0=initial phase [days]	22	27

The temperature series T_b has a larger number of negative values compared to T_a, and according to the formulators approach for the water temperature, the negative values will be deemed zero for the water temperature in the reservoir.

Afterwards, each behaviour data series (U(t)) was analyzed by a measured air temperature-based hydrostatic-thermal-time (HTT) model, which assumes that the elastic effects at time t of the variation of the hydrostatic load ($U_h(h(t)$) and of the biweekly mean air temperature, with a time shift t_T ($U_T(T(t-t_T))$), as well as the irreversible time effect ($U_t(t)$), are monotonic polynomials (4th degree for U_h and U_t, 3rd degree for U_T).

$$U(h, T, t) = U_h\,(h(t)) + \, U_T\,(T(t - t_T)) + \, Ut(t) + k$$

The statistical measures obtained were slightly better when assuming the daily air temperature series $T_b(t)$.

The most relevant time-dependent evolution was detected on piezometer PZCB2, with an effect of -3.3 m/decade.

The HTT model results are summarized in Table 2.

Table 2. HTT results.

		CB3_195_161	CB2_236_196	C4_C5	PZCB2	PZCB3	Seepage
	Number of records	698	703	675	705	670	672
	% discarded records	1	1	2	2	3	4
	tT [biweekly]	2	0	2	4	6	3
Statistical measures	RMSE	0.5	2.6	0.3	0.5	0.5	2.2
	Greatest difference	1.5	7.3	0.8	1.5	1.3	6.3
	Correlation coefficient	0.98	0.96	0.99	0.99	0.96	0.81
effects	Uh(h=235)-Uh(h=196)	8.2	27.6	4.5	15.0	5.0	9.7
	Annual seasonal effect	-1.9	-18.8	-0.9	-1.3	-0.4	-2.5
	Ut [decade]	0.4	1.3	0.4	-3.3	-1.9	-0.5

Subsequently, a brief implementation of Machine Learning algorithm, namely Gradient Boosting Regression and neural networks, was performed. The machine learning algorithms showed promising results regarding the interpretation of the hydraulic behaviour of the dam's foundation observation results: piezometers and seepage, which usually are of a harder approach with FEM models.

3 NUMERICAL MODEL

3.1 *Geometry and Mesh*

The geometry delivered to the participants (whole_dam.sat and whole_Rock.sat) was directly imported into ANSYS and the mesh was developed using internal software capabilities. A sensitivity test was performed by comparing the radial displacements on CB2, considering the water level in the reservoir at elevation 235.10 m, obtained in the finite element model (FEM) with four different mesh sizes. Table 3 shows the constitution of the different meshes considered.

Table 3. Mesh sensitivity test.

		MESH 00	MESH 01	MESH 02	MESH 03
DAM	Element Size (m)	1.5	3.0	6.0	10.0
	N.° Elements	55 233	7 575	1 394	654
	N.° Nodes	86 013	13 485	2 997	1 488
FOUNDATION	Element Size (m)	5	10	20	30
	N.° Elements	129 799	18 276	3 382	1 775
	N.° Nodes	185 808	27 997	5 212	3 153

The variation of the radial displacement on CB2 for the considered mesh sizes with reference to the radial displacement obtained with MESH 00 (Figure 1) shows that by adopting a less refined mesh the structure becomes stiffer, therefore, the downstream radial displacement is larger in more refined meshes. In this case, the refined Mesh 00 model (271 821 nodes) has a radial displacement of 19.18 mm, while MESH02 (8209 nodes) has a radial displacement of 18.49 mm. Taking into account the significant difference of the number of nodes between the two models, MESH 02 has 3% of the number of nodes of MESH 00, and the 0.69 mm difference between the displacements of the two models, MESH 02 was adopted in the analysis.
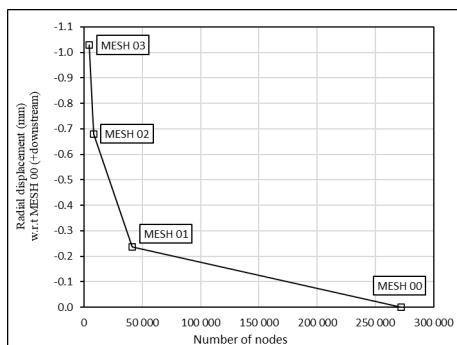

Figure1. Mesh sensibility analysis.

The finite element model adopted for both thermal and mechanical analyses was developed in ANSYS, using tetrahedral 10 node elements, Solid 187 for structural analysis and Solid 87 for thermal analysis. The model has 4776 elements, 1394 representing the dam body and 3382 representing the foundation. The adopted mesh and the coordinates reference is represented in Figure 2: the vertical axis z (+ descending w.r.t. the crest), the horizontal axis x is positive towards the left bank and the y axis is positive in the downstream direction.

Each nodal point has three degrees of freedom, in accordance with the displacement vector, and all the displacements were prevented in the lower face of the foundation block.
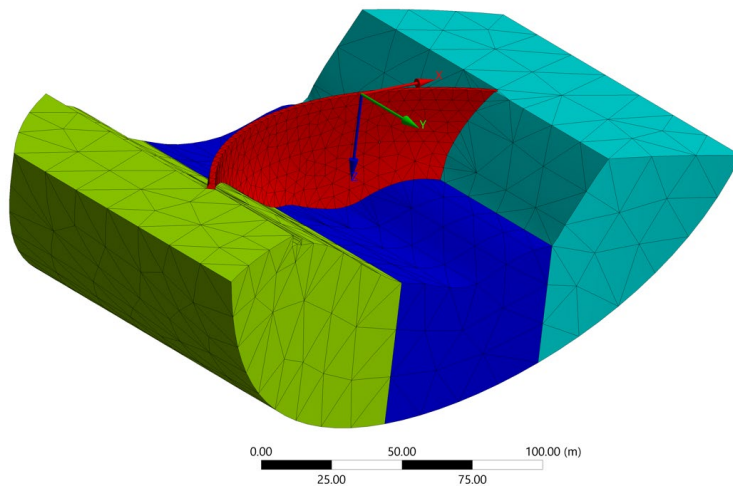

Figure 2. Numerical model.

To consider the different foundation materials three zones were adopted, separated by vertical planes parallel to XZ, allowing to differentiate the right and left banks and the center valley (Figure 2).

3.2 *FEM Analysis*

The dam structure and the foundation were assimilated as continuous and isotropic and a structural linear elastic behaviour was adopted.

Initially, the adopted materials properties were the ones presented by the organization that were updated by means of a calibration by comparison with the HTT model, namely by comparing the radial displacements obtained for the hydrostatic pressure applied to the upstream face of the dam on the FEM, with the same results obtained by the HTT. Figure 3 shows the comparison between the radial displacements results of the HTT (in red) and the FEM, considering three different values for the Young's Modulus of the dam and foundation materials.
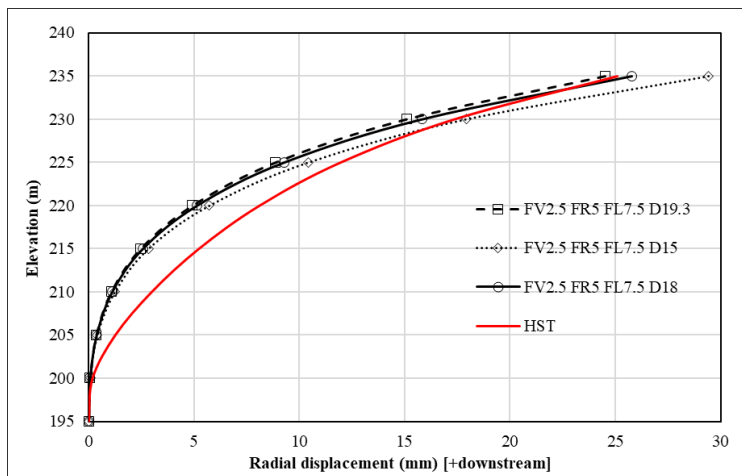

Figure 8. Calibration. FEM and HTT for hydrostatic pressure

Has it can be seen, the radial displacements closer to the crest of the dam have good agreement between models, however for lower elevations significant differences were obtained. The black full line plotted shows the best agreement between both models and the corresponding material properties are presented in Table 4.

Table 4. Material properties

	E (Gpa)	K W/(m · °C)	C J/(kg · °C)	α (°C^{-1})	v	R (kg/m^3)
Concrete	18.0	2	900			2400
Left Bank	5.0					
Center Valey	2.5	3	850	0.7 E-5	0.2	0
Right Bank	7.5					

3.3 *Analysis procedure*

A hybrid approach was implemented considering the displacements as a sum of the results obtained through the deterministic FEM model for the hydrostatic pressure and the seasonal temperature variation, with the time effect results obtained from the HTT model.

- The hydrostatic effect on the structure was estimated by applying the water pressure on the upstream face of the dam for 25 levels of the reservoir. For each observation date the hydrostatic effect was evaluated by interpolation along the results previously referred for the water level in that date.
- The thermal effect for each observation date was evaluated with the thermal field on the referred date. This field was previously evaluated by a transient thermal analysis with an incremental time of 1 day, between 01-01-1999 and 31-12-2017, assuming the air temperature series T_b for the air exposed dam surfaces and the water temperature on the submerged upstream face on that date, as proposed by the benchmark formulators.
- For the time effect in the period between 2000 and 2012 the HTT results were adopted (Figure 6).

3.4 *Calibration*

To obtain the best agreement between the computed and observed values a factor applied to the FEM response to the hydrostatic pressure (C_H) and another applied to the FEM response to the thermal action (C_T) were determined by minimizing the RMSE, in the period 2000 – 2012. In Table 5 are also presented the values of the concrete Young modulus and the coefficient of thermal expansion obtained by applying these factors to the initial values mentioned in 3.2. An alternative approach regarding the C_T coefficient would be to scale the values assumed for the air and water temperatures, as well as considering the solar radiation.

Table 5. Calibration factors

	C_H	C_T	RMSE (mm)	E (GPa)	α (°C^{-1})
CB2 236-196	1.1	1.3	2.7	17	0.9
CB3 195-161	2.5	3.1	0.5	7	2.2

The values obtained for CB2 are plausible; the values for CB3 may be affected by relevant local phenomena, such as the opening of the dam-foundation contact, which weren´t introduced in the developed FEM model.

Figure 4 and Figure 5 show the comparison between the radial displacements measured on the plumb lines CB2 and CB3, respectively, and the radial displacement obtained through the calibrated hybrid model.
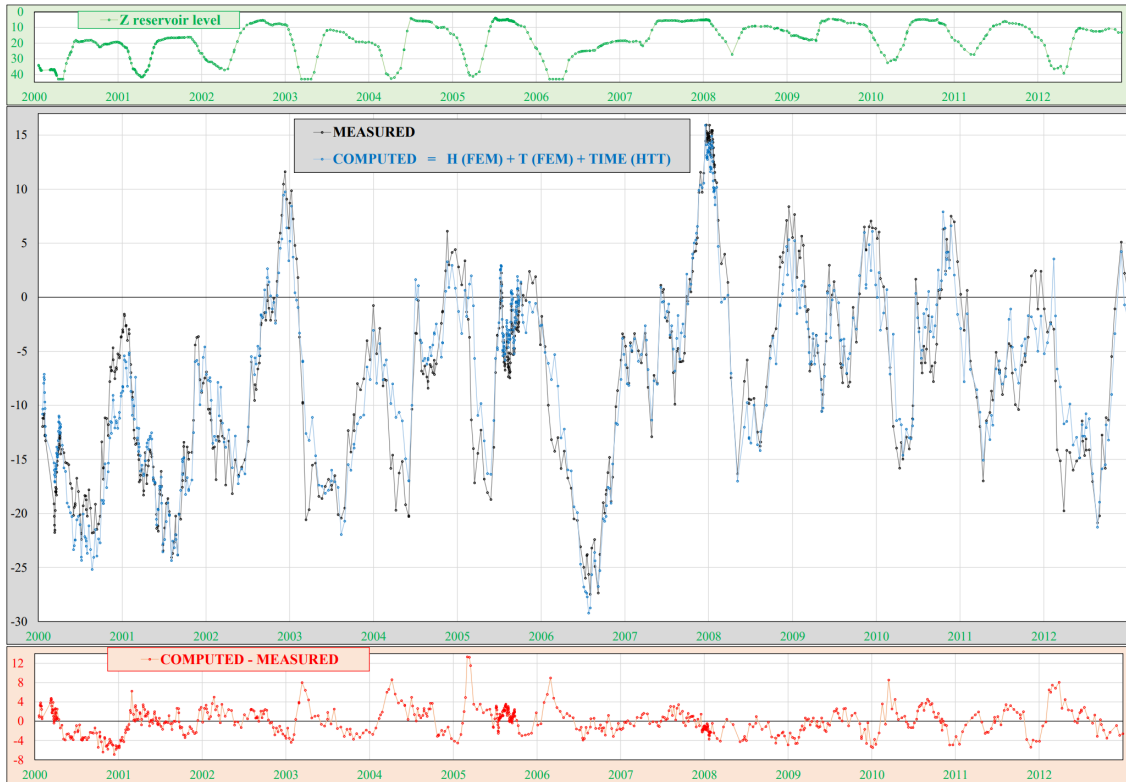
Figure 4. Radial displacement (+ downstream) CB2. Measured data and computed results.
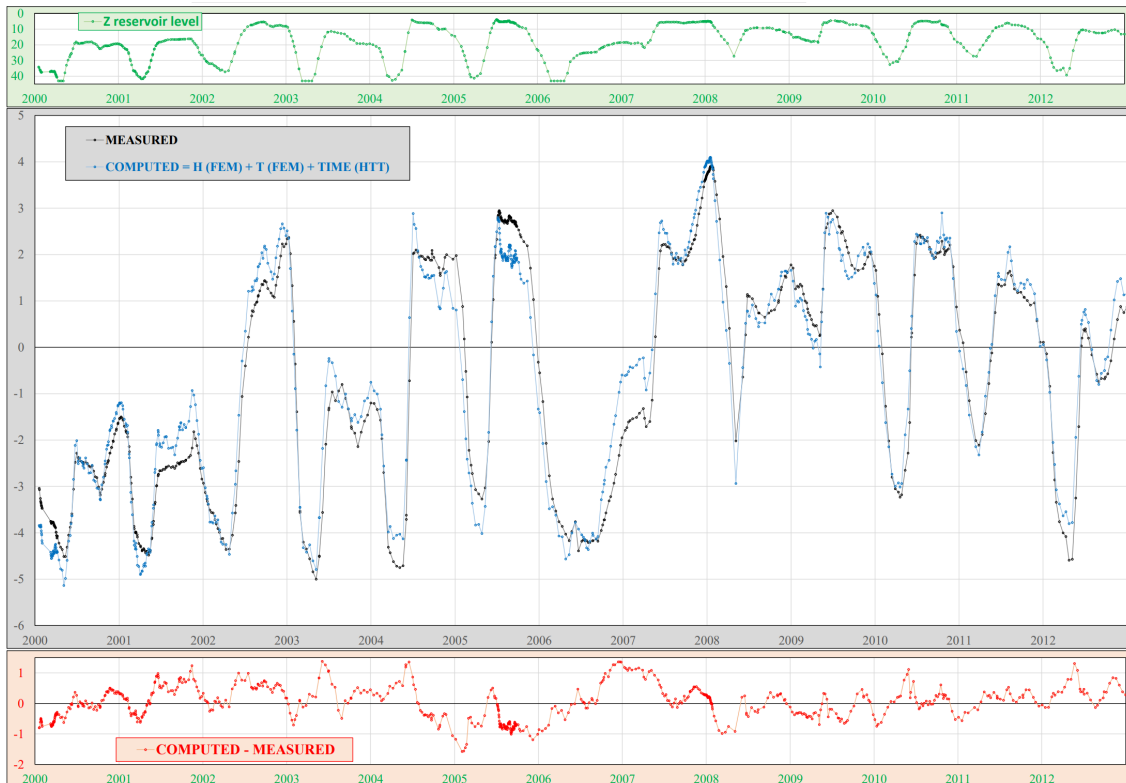

Figure 5. Radial displacement (+ downstream) CB3. Measured data and computed results.

Both figures show good fit. The results obtained for CB2 show small differences except for the water level decreasing events, namely in the beginning of 2005 when occurred the maximum difference of 13.3 mm. In this epoch also occurred the maximum difference for CB3 which is -1.6 mm.

3.5 *Predictions*

Following the calibration procedure, a prediction (for the period 2013 – 2017) of the radial displacements on both plumb lines was determined, using the same methodology, where the time effect for CB2 was assumed constant and equal to the value obtained at the end of 2012, and for CB3 it was assumed a linear evolution with time with the mean rate obtained between 2008 and 2012 (Figure 6).
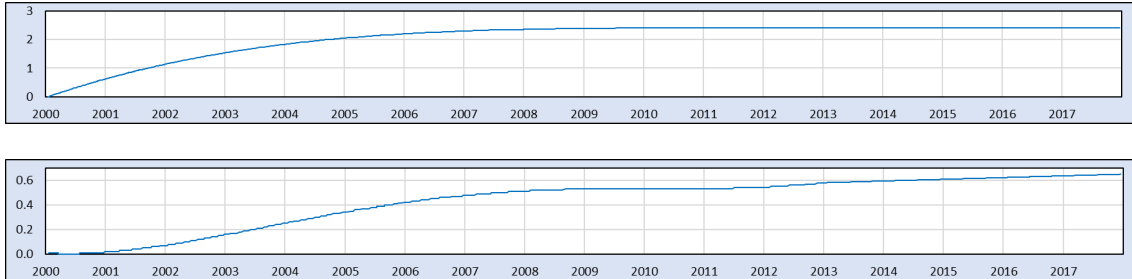

Figure 6. HTT time effect for CB2 (top) and CB3 (bottom).

The results plotted in Figure 7 show the radial displacements computed in the dates presented on the worksheets CB2_236_196 and CB3_195_161 of the file ThemeA_data_fmt01.xlsx delivered by the formulators, which were submitted as requested for scoring.

b) CB2   a) CB3
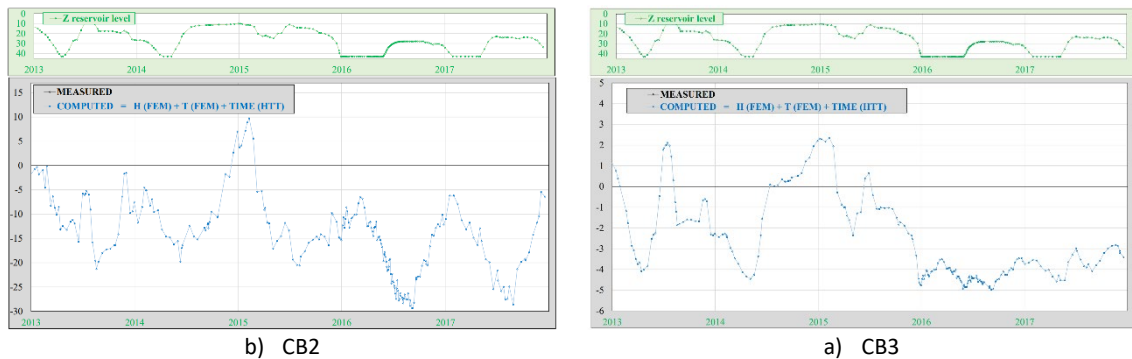
Figure 7. Radial displacement. Prediction 2013-2017.

4 WARNING LEVELS

The warning levels were defined by adding and subtracting the constant value of 3 * RMSE to the predicted values: ±7.5 mm and ±1.5 mm for CB2 and CB3, respectively.

5 CONCLUSION

The adopted methodology led to a reasonable fit between the computed and the measured results. Further developments could grant better results considering a more realistic time evolution of the temperature along the reservoir height. Furthermore, it should be relevant to consider the solar radiation and the joint opening of the dam/foundation contact. The structural analysis for the evolutionary thermal action could be fastened by a methodology where the computed thermal field would be approximated by interpolating a reduced number of key points, so that a unique structural analysis for each key point would be performed.

REFERENCES

Paixão, J. 2012. Shape optimization in the design of concrete arch dams - two case studies. *10th World congress on computational mechanics; São Paulo, 8-13 July 2012*.

Matos, D.S. 2007. Arch dam design of the Baixo Sabor upstream scheme. *5th International conference on dam engineering; Lisbon, 14-17 February 2007.*

Cunha, J. G. 2011. The monitoring and structural behaviour of Covão do Meio dam; *6TH International Conference on Dam Engineering, Lisbon, 15-17 February 2011.*

Leitão, N. S. 2015. *Analysis of the observed behaviour of Alto Ceira II dam during the first filling of the reservoir, Lisbon; 21-24 April.*

BEHAVIOUR PREDICTION OF A CONCRETE ARCH DAM COMBINING NN AND MLR MODELS – PROPOSAL FOR THE 16TH ICOLD BW

Juan Mata

Laboratório Nacional de Engenharia Civil, Portugal

jmata@lnec.pt

Carlos Serra

Laboratório Nacional de Engenharia Civil, Portugal

cserra@lnec.pt

ABSTRACT: The main purpose of assessment of dam condition, through the use of the information provided by the monitoring system, is achieved by having up-to-date knowledge of the dam. Early anomalous behaviour detection is expected in order to allow appropriate intervention to correct the situation or to avoid serious consequences. Once a dam is in its operation phase, the assessment of the dam's condition and the interpretation of the dam's behaviour are supported by data-based models, among others, in which the main goal is to predict the actual structural dam behaviour in order to detect a possible deviation from a considered normal pattern.

Within the scope of the 16th International Benchmark Workshop on Numerical Analysis of Dams, this paper presents a methodology for the prediction of different measurements based on the combination of the results from multiple linear regression and neural network models. The work discusses the advantages and applicability of the methodology to each type of dataset and the importance of engineering expertise and on site knowledge when using data-based models.

The obtained results show a good model performance for the training period being a valid option for dam engineering activities.

1 INTRODUCTION

For each concrete dam, different models can be used according to the purpose of the analysis, the existing knowledge about the actual structural behaviour and the quality of information available for the structural behaviour characterization. The selection of the conceptual model to represent the idealized dam behaviour must take into account: i) the purpose of the analysis (safety assessment, prediction of the structural response, interpretation of the recorded data from the monitoring system, or analysis of an accident or abnormal behaviour), ii) the ability to identify the key factors of the reservoir-dam-foundation system, and iii) the type, age and degree of deterioration of the dam and the available geological and geotechnical information, among others.

Dams are made of, and founded on, materials whose properties change with time. The establishment of the relation between causes and effects leading to the degradation of structural properties of the dam and appurtenant structures is key for the identification and characterization of the deterioration. During the dam's lifetime phases, the models are updated to take into account the observed dam behaviour through the monitoring systems. This is the case of traditional HST (hydrostatic, seasonal, time) and HTT (hydrostatic, temperature, time) models, whose parameters can be updated based on the measured dam response over time. In summary, the core of dam safety control is the establishment of multiple validations of the models, the measurements and the parameters which, by characterizing the structural behaviour, are able to elaborate and justify a judgment about structural safety. The main concern is to predict the actual structural dam behaviour in order to detect a possible anomaly.

Statistical models used to predict structural response are based on relationships between the loads and the structural response (SCD, 2003). These statistical models are based on the establishment of Multiple Linear Regression (MLR) models of monitoring data collected during the past history of the dam. In recent years, new data-based models based on Machine Learning (ML) methods have been adopted as a guaranty in redundancy to the traditional adopted models to describe the observed behaviour or, in some cases, to study a particular aspect of the dam behaviour (Perner & Obernhuber, 2010; Mata, 2011; Kao & Loh., 2011; Simon et al., 2013; Rancovic et al., 2014; Rico et al., 2014; Salazar et al., 2015, 2016; Li & Wang, 2019; Mata et al., 2021).

As referred to in the cited publications, the growing use of ML models is mainly restricted to scientific publications and academic examples. For this reason, this BW is an important milestone to disseminate the use of ML models by dam engineers. In general, model performance is important for model acceptance, but it is only the first step of the process. However, it is important to emphasize that model verification and validation, through engineering expertise, are a relevant part of the entire model development, since it establishes a relationship between the mathematical/numerical model and the structural behaviour. This topic is further discussed by Mata et al. (Mata et al., 2021).

The aim of Theme A in the 2022 ICOLD BW is to establish a prediction model for a dam. A double curvature arch dam is used as a case study. The participants are asked to build a model, calibrate it, and use it for long-term and short-term predictions using the provided data and by making their assumptions and choosing suitable approaches to solve the problem. The focus of the theme is on the following variables: radial displacement (two pendulums in the central block of the dam); crack opening displacement (sensor at the rock-concrete interface); piezometric levels (vibrating wire piezometers at the rock-concrete interface); and seepage (weir at the downstream toe of the dam).

For this BW, a methodology based on the combination of the results from multiple linear regression (MLR) and neural network (NN) models is presented for the prediction of the displacements observed, taking advantage of each of the methods. Care should be taken regarding model validity for the prediction period because the domain of the variables in the training period may not be the same as the ones observed in the predicted period. For the uplift pressures and for the seepage, a traditional HST approach based on multiple linear regression was adopted due to the drainage cleaning resulting in a short time training period (for potential ML models).

2 THE CASE STUDY

2.1 *Brief dam description*

In this benchmark problem, denoted as Theme A in the 2022 ICOLD BW, a double curvature arch dam, located in the south of France and owned by the EDF is used as a case study. The aim of the theme is to establish a prediction model for the dam for the following quantities: radial displacement, crack opening displacement, piezometric levels, and seepage.

The dam is located in the south of France. It is owned by EDF and was constructed between 1957 and 1960. It is a double curvature arch dam, which is asymmetric due to the shape of the valley. The dam consists of 13. The maximum dam height is 45 m and the total crest length is 166 m. The normal water level is 237 m and the crest level is 239 m.

The geometry, material properties, and loads have been defined and are delivered by the formulators. The monitoring data available is from 2000 to 2012, being the predicted set from 2013 to 2017. It was referred that the provided data has been pre-processed and can be directly used for the analysis, e.g. no further cleaning is necessary.

Furthermore, the data is provided without any modification of the actual time series and is measured with different frequencies. The main targets that should be predicted, including some relevant information (see also Figure 1), are the following: i) the radial displacement, CB2, between the altitudes 236 m (just under the crest) and 196 m (toe of the dam). The radial displacement, CB3, in the foundation between the altitudes 195 m and 161 m; ii) a crack opening displacement sensor is located at the rock-concrete interface of the Central Block (CB). The sensor measures the opening between C4 (in the foundation) and C5 (in the concrete, at the toe of the dam); iii) the piezometric levels PZCB2 and PZCB3, are located in block CB. In September 2008, cleaning of the drainage system was carried out; and iv) the flowrate was measured using a weir located in the gallery at the downstream toe of the dam. The measured total seepage is the total amount of water originating from different locations such as the surrounding rock, moisture transport in concrete, potential leakages in concrete cracks, and the drainage system.
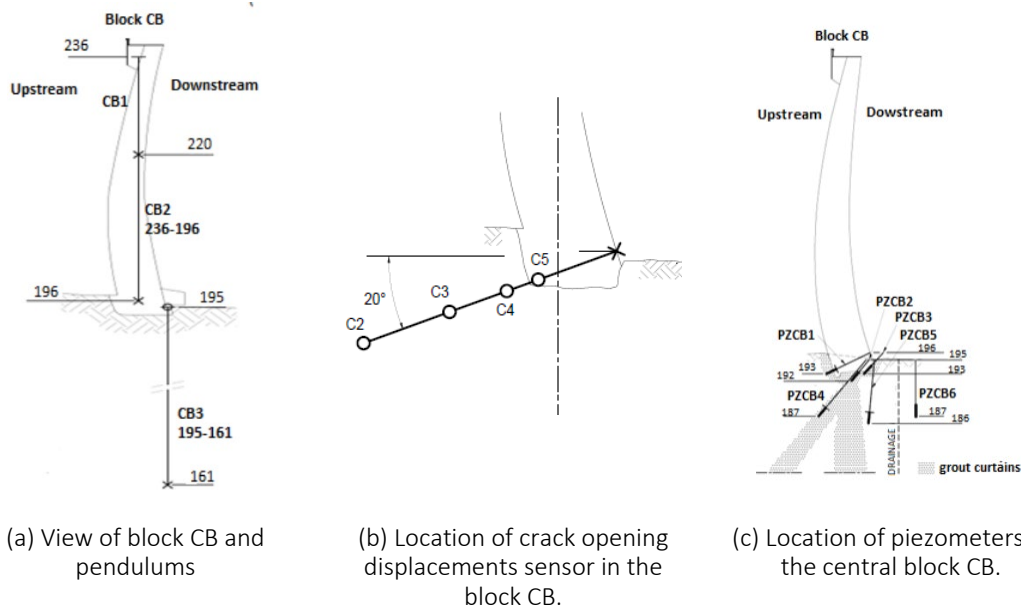

(a) View of block CB and pendulums

(b) Location of crack opening displacements sensor in the block CB.

(c) Location of piezometers in the central block CB.

Figure 1. Main aspects of the monitoring system of the dam.

2.2 *Data characterization*

The data analysed corresponds to a period between January 2000 and December 2017. The data between January 2000 and December 2012 was considered as the training period. Thus, the data obtained during the period between January 2013 and December 2017 was adopted as a predicted period. The evolution of the reservoir water level, radial displacements in the referred CB3 195-161 m and CB2 236-196 m, the opening displacements in C4-C5, the uplift pressure

measured in PZCB2 and PZCB3, and the seepage are presented in Figure 2, in which the black and blue dots represent, respectively, the measurements before and after cleaning the drainage system. Figures 3 and 4 present some examples of visual representation of the data as a function of the day of the year and the water level, respectively. The statistical characterization of the quantities is presented in Table 1.
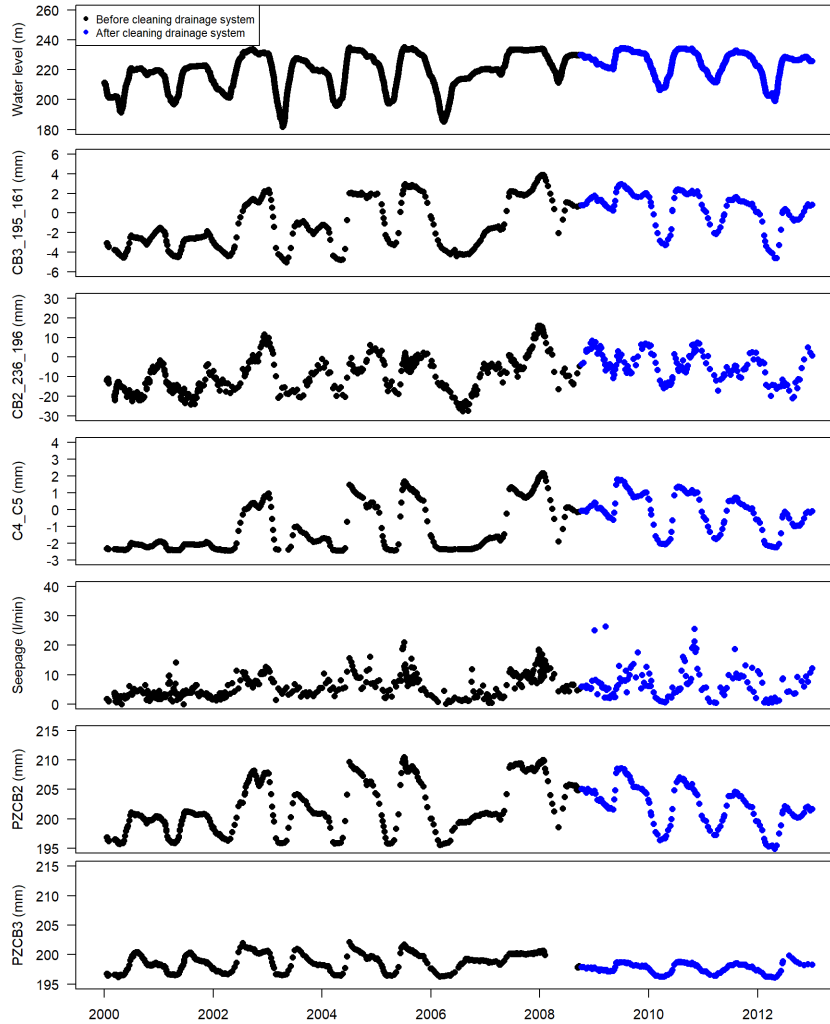

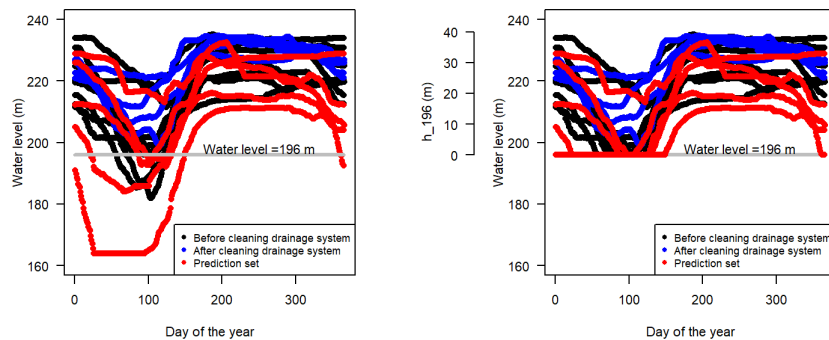Figure 2. Time series evolution of the main quantities under study.

Figure 3. Main visual characterization of the water level variation and the water height above the reference level 196.0m during the training period (before and after cleaning the drainage system) and for the predicted period.
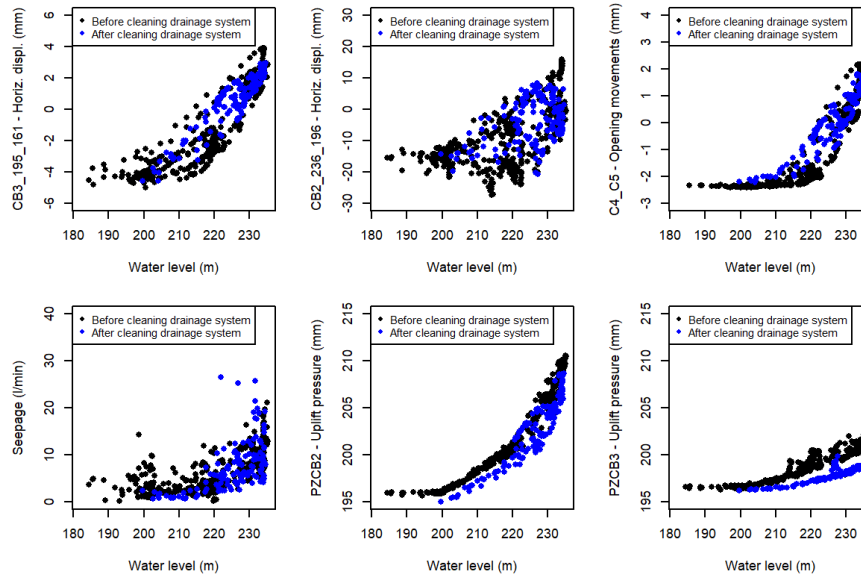
Figure 4. Main variation of the observed dam behaviour due to the water level variation.

Table 1. Statistical parameters of the main quantities under study.

Quantity	Training period					Predicted period				
	Numb. obs.	Mean	Min	Max	σ	Numb. obs.	Mean	Min	Max	σ
Water level (m)	4726	220.5	181.9	235.2	11.5	1826	210.5	164.0	232.6	16.3
h=h_196 (m)	4726	24.7	0.0	39.1	11.0	1826	17.0	0.0	36.6	11.1
Air temp. (tb) (ºC)	4726	4.6	-15.5	20.5	6.3	1826	4.7	-12.0	19.4	6.1
Air temp. (2 week mov. aver.) (ºC)	4726	4.6	-11.6	16.9	5.7	1826	4.7	-6.6	16.4	5.5
Air temp. (4 week mov. aver.) (ºC)	4726	4.6	-8.4	15.6	5.4	1826	4.7	-5.1	15.6	5.3
CB3-195-161m (mm)	681	-0.3	-5.0	3.9	2.7	-	-	-	-	-
CB2-236-196m (mm)	688	-6.8	-27.5	16.0	9.5	-	-	-	-	-
C4-C5 (mm)	662	-0.6	-2.4	2.2	1.6	-	-	-	-	-
PZCB2 (m)	171[*]	202.9	195.0	208.6	3.3	-	-	-	-	-
PZCB3 (m)	134[**]	197.9	196.3	198.8	0.7	-	-	-	-	-
Seepage (l/min)	143[*]	7.3	0.5	26.5	5.2	-	-	-	-	-

Note: [*] Data after the cleaning of the drainage system. [**] Data before 2012 and after the cleaning of the drainage system.

From the previous information (based on charts and descriptive statistics), it is possible to state that: i) there are some months, in the predicted period, where the values of the water levels were never observed before. This can mean that there is the possibility that a new combination of loads (temperature and water level) may lead to a new structural response; and ii) the cleaning of the drainage system leads to a change in the hydro-mechanic pattern observed in the PZCB3, PZCB2 and (but not so clear as expected) in the seepage.

3 METHODOLOGY

The main purpose of this BW challenge is to predict, as near as possible, the structural response for the training period and for the prediction period. This is a good exercise to test or validate new methods and disseminate new approaches. However, it is important to refer that this is not the ultimate goal that should motivate the development of any forecasting model. The knowledge and confidence on measurements, the capability of interpreting (by the end-users) the predicted values and correlating it with the main loads (or warning thresholds related to dam incidents or accidents scenarios) are some of additional aspects that must be taken into account, from the structural safety point of view.

Structural response of concrete dams in normal operation present good correlation with the main loads, a similar structural response being expected when subjected to the same set of loads (so, there is a pattern in the dam behaviour that is considered normal and that relates to an expected structural behaviour). However, when a time effect (that are irreversible and may be related to ageing or to some deterioration process) is observed in measurements, this time effect pattern should be characterized using some "rule" in order to be able to predict the influence of the time effect in the future observed behaviour.

The methodology proposed for this BW challenge is based on the combination of artificial neural network and multiple linear regression models for the construction of the (short-term and long-term) predictions, as presented in Figure 5.
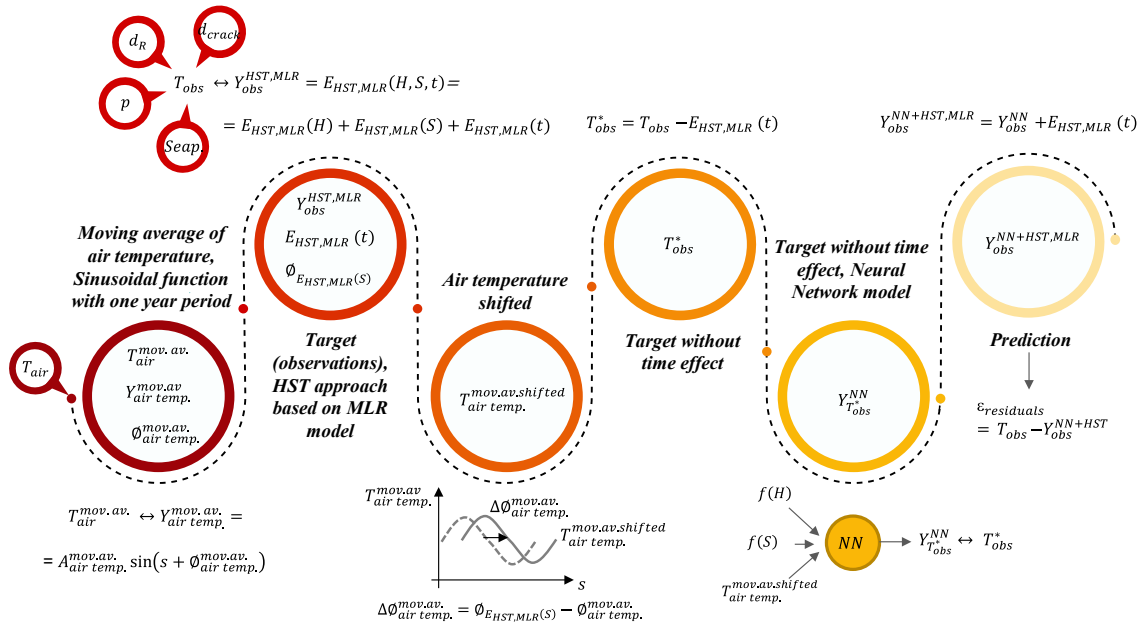

Figure 5. Proposed methodology based on combining NN and MLR models for short-term and long-term prediction.

The main steps of the proposed methodology can be described as follow:

Inputs (measurements):
- Organize air temperature, water level, structural response (observations). The rainfall was not directly considered in this study.

Step 0:
- Perform a descriptive statistical analysis. Paying special attention to the main domain of variables variation, potential outliers, possible patterns in quantity variations.

Step 1:
- Perform moving average of air temperature (4 and/or 2 weeks were adopted of time window for average);
- Perform linear regression to characterize the sinusoidal function ($Y_{air\ temp.}^{mov.\ av.}$) with one year period and the corresponding phase ($\emptyset_{air\ temp.}^{mov.av.}$) of the air temp. moving average;

Step 2:
- Perform HST approach through the adoption of multiple liner regression, as usual: $E_{HST,MLR}(H,S,t)=E_{HST,MLR}(H) + E_{HST,MLR}(S) + E_{HST,MLR}(t)$
- Define the suitable functions to represent the time effect, $E_{HST,MLR}(t)$, based on the dam engineer experience and the parameters indicators (such as p-value). In this study, due to the lack of historical context and on site inspections records, a simple linear function was used to represent time effect;
- Identify the phase of the structural wave of one year period ($\emptyset_{E_{HST,MLR}(S)}$) that represent the effect annual temperature variation;

Step 3:

- Shift the air temperature moving average values in order to present the same phase of the structural response, $\Delta\emptyset_{air\,temp.}^{mov.av.} = \emptyset_{E_{HST,MLR}(S)} - \emptyset_{air\,temp.}^{mov.av.}$

Step 4:

- Remove the time effect to the target value, obtaining $T_{obs}^* = T_{obs} - E_{HST,MLR}\ (t);$

Step 5:

- Perform NN model training and value prediction, $Y_{T_{obs}^*}^{NN}$, to estimate T_{obs}^*, considering as inputs terms to represent the water level variation (selected from h^4, h^3, h^2, h) and the temperature effect (sinusoidal function and shifted air temperature moving average were adopted).

Step 6:

- Calculation of the predicted value, $Y_{obs}^{NN+HST,MLR}$ as the sum of the predicted value obtained from the artificial neural network model added with the value of the time effect rule adopted, $Y_{obs}^{NN+HST,MLR} = Y_{obs}^{NN} + E_{HST,MLR}\ (t).$

The main advantages of the proposed methodology (combining NN and MLR methods) are that make use of the learning capability of the NN models (through a possible better characterization of the water level and temperature effects) and take advantage of the "fixed" term of the time effect adopted through the MLR model (being the expert on dam engineering able to "fix" the rate of evolution, for the time effect, that is expected (or accepted) – being able to identify early as possible deviations in the dam behaviour). The use of shifted values of the moving average (of 2 and/or 4 weeks) of the air temperature is expected to have a better prediction if the temperature effect is not well represented through a sinusoidal wave (which is often the case). However, one should be aware that the variations observed in the air temperatures measurements may lead to "noise" added to the model and may not compensate for the gains. The main disadvantage of the proposed methodology is that requires more effort than traditional HST models based on MLR method only and it is more sensible to the lack of data. It is important to refer that, as in any area of specialization, it is important that the development of data-based models for dam behaviour prediction should be performed by experts with a broad knowledge of dam engineering coupled with machine learning expertise.

One main condition for adopting the proposed data-based methodology is the need of data (both loads and response) representative of the dam behaviour, being the proposed methodology applied to the prediction of the horizontal displacements (CB3-195-161m and CB2-236-196m) and opening displacements in C4-C5 only. Due to the cleaning of the drainage system, the numbers of records available to characterize PZCB3, PZCB2 and seepage is limited. The authors opted to perform a traditional HST model for obtaining the predicted values. This option was also supported by the strong correlation observed in PZCB2 and PZCB3 with the water level (Figure 4). For seepage this option was adopted because it seems that there is not enough available data to reasonably characterize the complete pattern in the observed behaviour.

4 RESULTS AND DISCUSSION

4.1 *Prediction of the horizontal displacements and opening movements using the proposed methodology*

The proposed methodology, described previously, was adopted for the prediction of the horizontal displacements measured in the CB3-195-161m and the CB2-236-196m, and the opening movements measured in the C4-C5. The main results are summarized in Figures 6 to 11, and Table 2.
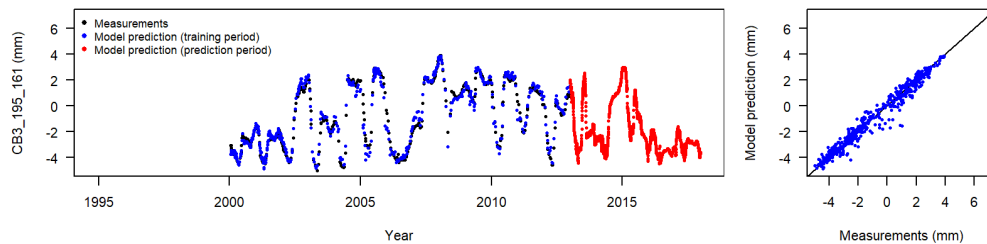

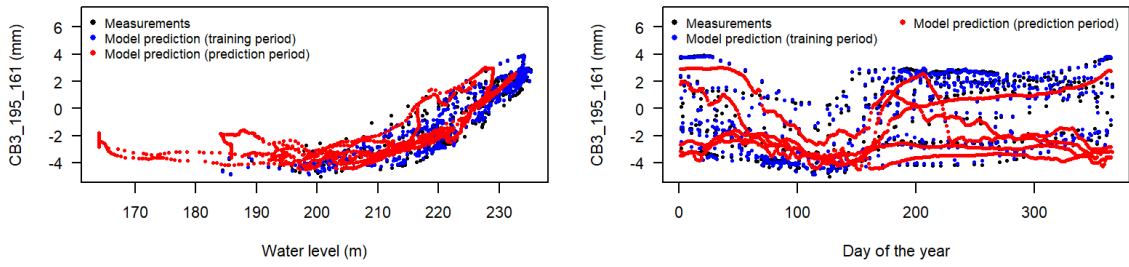Figure 6. CB3-195_161m – Measurements of the training period and predicted values along time

Figure 7. CB3-195_161m + Measurements of the training period and predicted values related to the water level variation and to the day of the year (associated to the temperature variation)
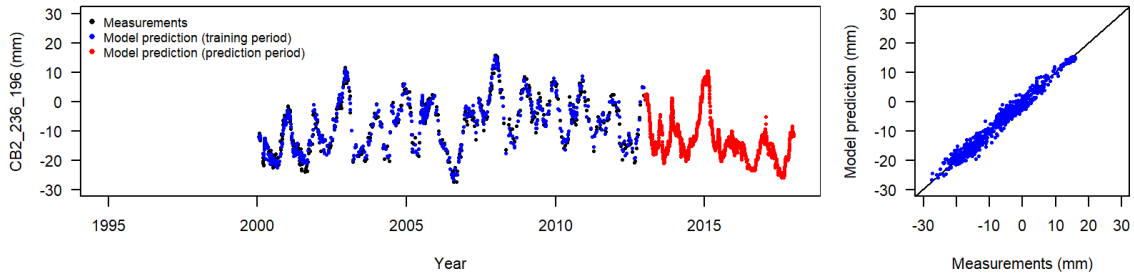

Figure 8. CB2-236-196m – Measurements of the training period and predicted values along time.

Figure 9. CB2-236-196m – Measurements of the training period and predicted values related to the water level variation and to the day of the year (associated to the temperature variation).

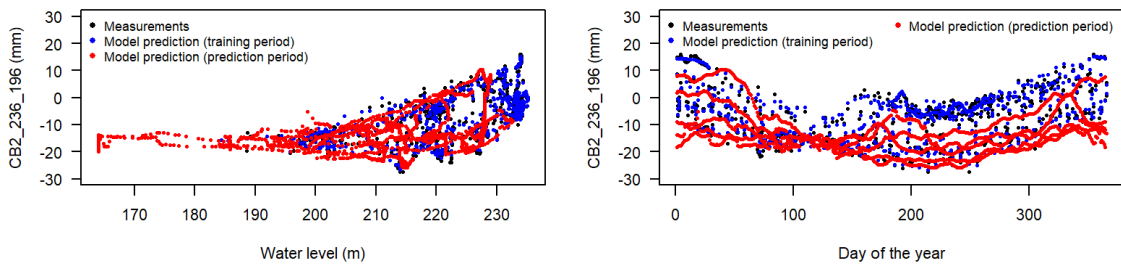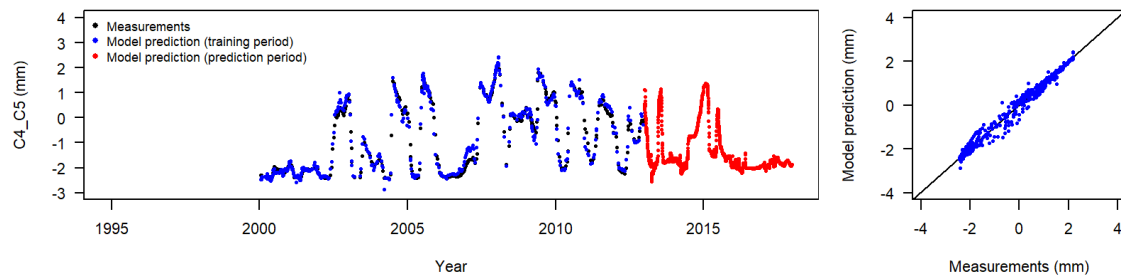Figure 10. C4-C5 – Measurements of the training period and predicted values along time.
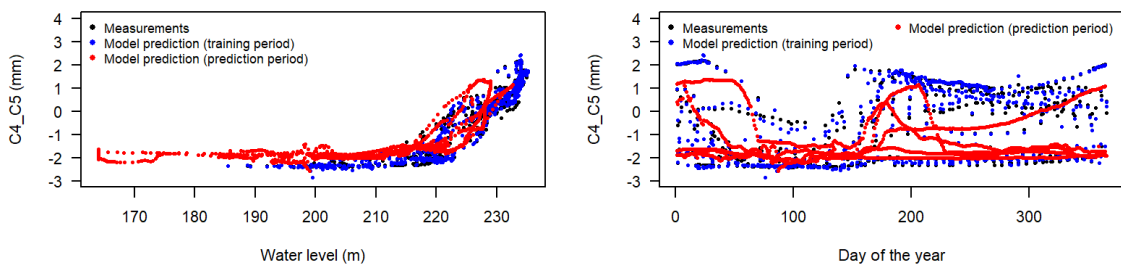

Figure 11. C4-C5 – Measurements of the training period and predicted values related to the water level variation and to the day of the year (associated to the temperature variation).

Table 2. Statistical parameters of the main model prediction related to the horizontal displacements and opening movements.

| | Training Period | | | | | | | Predicted period (2013-2017) | | | |
| | Model prediction | | | | Residuals | | | Model prediction | | | |
	Mean	Min	Max	σ	MAE	NRME	σ	Mean	Min	Max	σ
CB3-195-161m (mm)	-0.3	-4.9	3.9	2.7	0.3	0.0	0.4	-1.9	-4.5	3.0	1.9
CB2-236-196m (mm)	-6.7	-26.6	15.2	9.4	1.3	0.0	1.6	-13.5	-25.9	10.4	7.4
C4-C5 (mm)	-0.6	-2.9	2.4	1.6	0.1	0.0	0.2	-1.4	-2.6	1.4	0.9

4.2 *Prediction of the uplift and seepage using the traditional HST approach with MLR methods*

As previously described, for PZCB2, PZCB3, and seepage a traditional HST was adopted. This option was based due to the limited number of measurements (and corresponding time period) available and for PZCB2 and PZCB3 due to the fact that the expected behaviour seems to be well represented through the water level effect. Regarding the PZCB3, some kind of novelty in the behaviour pattern at the end of the training set was identified and these values were not considered for training. The main purpose is to identify early as possible potential novelties in the prediction set even though a worse performance of the model is expected. For seepage there are some uncertainties in the characterization of its pattern because there are some singular (or combination of) effect that may affect his pattern, depending on the exact placement of the drain (for example, rainfall). However, due to the limited number of measurements, a further analysis was not performed. The main results are summarized in Figures 13 to 18, and Table 3.

Figure 12. PZCB2 – Measurements of the training period and predicted values along time.

Figure 13. PZCB2 – Measurements of the training period and predicted values related to the water level variation and to the day of the year (associated to the temperature variation).
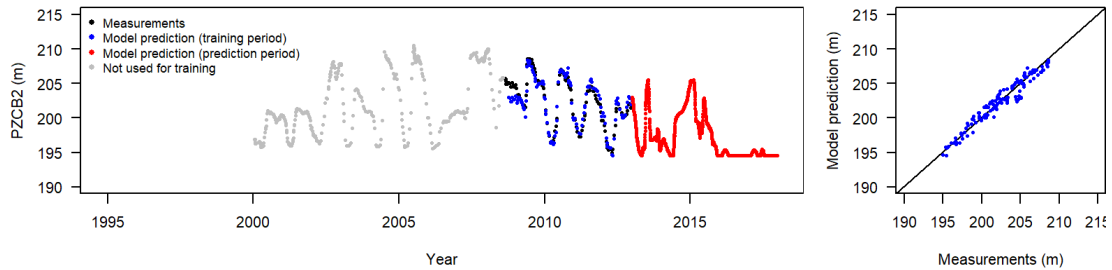

Figure 14. PZCB3 – Measurements of the training period and predicted values along time
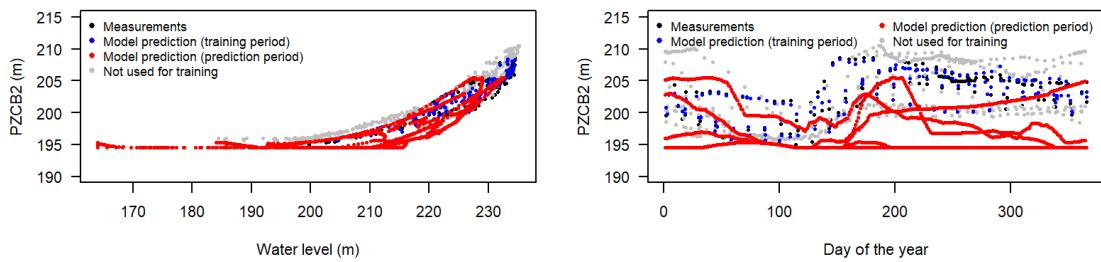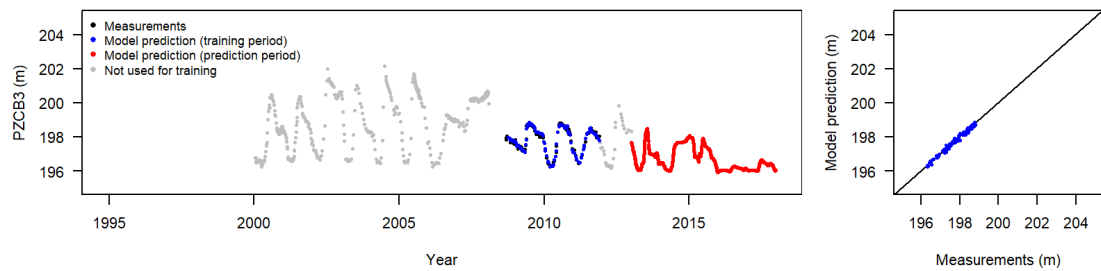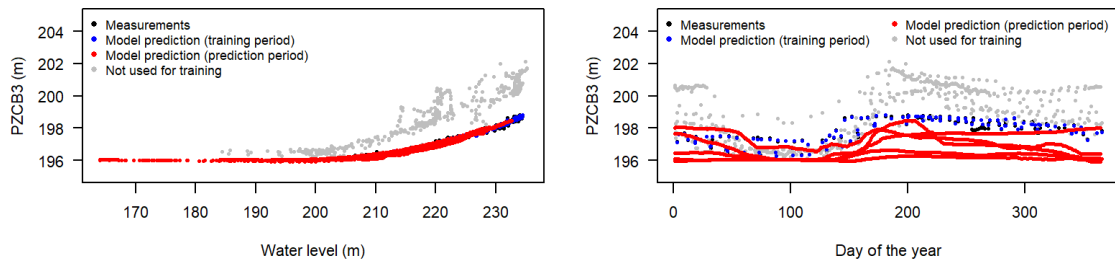
Figure 15. PZCB3 – Measurements of the training period and predicted values related to the water level variation and to the day of the year (associated to the temperature variation).
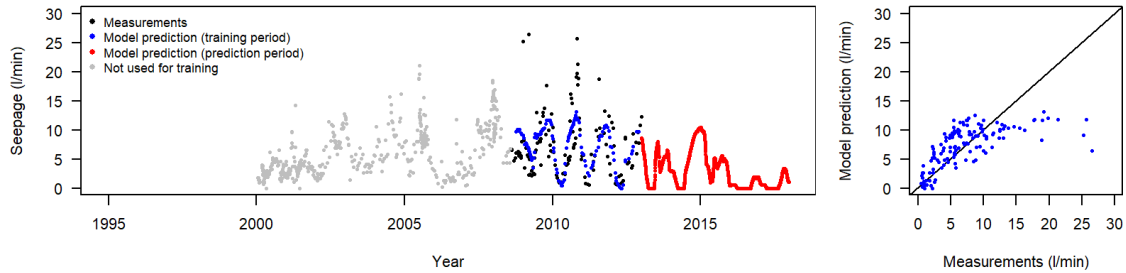

Figure 16. Seepage – Measurements of the training period and predicted values along time
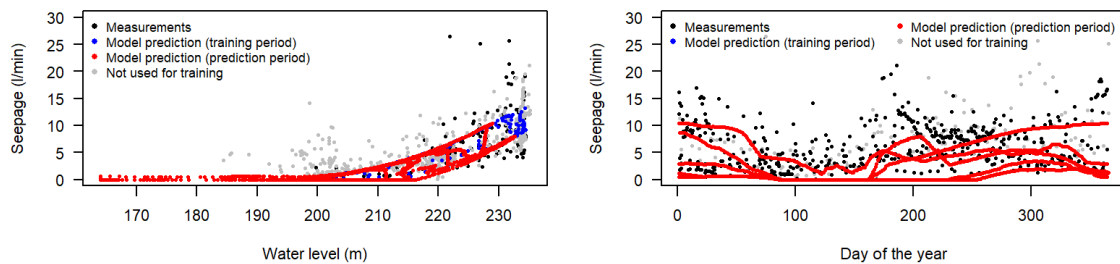
Figure 17. Seepage – Measurements of the training period and predicted values related to the water level variation and to the day of the year (associated to the temperature variation)

Table 3. Statistical parameters of the main model prediction related to the uplift pressures and seepage.

	Training Period							Predicted period (2013-2017)			
	Model prediction				Residuals			Model prediction			
	Mean	Min	Max	σ	MAE	NRME	σ	Mean	Min	Max	σ
PZCB2 (m)	202.6	194.6	208.4	3.3	0.6	0.0	0.8	197.1	194.5	205.5	3.2
PZCB3 (m)	197.7	196.1	198.8	0.7	0.2	0.0	0.3	196.7	195.9	198.5	0.7
Seepage (l/min)	7.4	0.0	13.2	3.4	2.8	0.0	4.0	2.9	0.0	10.4	3.0

5 FINAL CONSIDERATIONS

Once a dam is its operation phase, the assessment of the dam's condition and the interpretation of the dam's behaviour are also supported through the use of data-based models. However, the suitability and limitations of the models, the uncertainties or the incomplete knowledge about the loads, the dam's foundation, the material properties and geometrical definition of the dam are the reasons why (in normal operating scenarios) the real or measured dam behaviour may not match the expected behaviour. The development of new methodologies

based on ML can improve dam behaviour predictions and this BW is an important milestone to disseminate the use of ML models by dam engineers.

The authors propose a new methodology based on the combination of the results from multiple linear regression and neural network models in this Benchmark for the prediction of the horizontal displacements measured in pendulums and opening movements in crackmeters. The models presented good performance for the training period being a valid option for dam engineering activities. However, it is important to refer that additional care should be taken regarding model validity because the domain of the main loads within the training period may not be the same observed in the predicted period. A model may be valid for one set of experimental conditions and invalid for another. For the uplift pressure and for the seepage, a traditional HST approach based on multiple linear regression was adopted due to the short time training period, as a consequence of the drainage cleaning. Finally, the previous analysis of the main loads during the training set and the prediction set allows identifying that in the prediction set are a combinations of loads (temperature and water level) that never happened before. So, a decrease in the model performance is expected in order to identify these novelties in the dam behaviour.

REFERENCES

Kao, C. & Loh, C. 2011. Monitoring of long-term static deformation data of Fei-Tsui arch dam using artificial neural network-based approaches. Structural Control and Health Monitoring, 20(3):282-303

Li, M.; Wang, J. 2019. An Empirical Comparison of Multiple Linear Regression and Artificial Neural Network for Concrete Dam Deformation Modelling. Math. Probl. Eng.

Mata, J. 2011. Interpretation of concrete dam behaviour with artificial neural network and multiple linear regression models. Engineering Structures. Elsevier, 33(3):903-910.

Mata, J.; Salazar, F.; Barateiro, J.; Antunes, A. 2021. Validation of Machine Learning Models for Structural Dam Behaviour Interpretation and Prediction. Water, 13, 2717. doi.org/10.3390/w13192717

Perner, F. and Obernhuber, P. 2010. Analysis of arch dam deformations. Frontiers of Architecture and Civil Engineering in China, 4(1):102-108, 2010.

Rankovic, V.; Grujovic, N.; Divac, D.; Milivojevic, N. 2014. Predicting piezometric water level in dams via artificial neural networks. Neural Comput. Appl. 2014, 24, 1115–1121.

Rico, J.; Barateiro, J.; Mata, J.; Antunes, A.; Cardoso, E. 2019. Applying Advanced Data Analytics and Machine Learning to Enhance the Safety Control of Dams. In Machine Learning Paradigms: Applications of Learning and Analytics in Intelligent Systems 1; Tsihrintzis, G.A., Virvou, M., Sakkopoulos, E., Jain, L.C., Eds.; Springer International Publishing: Berlin/Heidelberg, Germany, pp. 315–350.

Salazar, F.; Toledo, M.A.; Oñate, E.; Morán, R. 2015. An empirical comparison of machine learning techniques for dam behaviour modelling. Structural Safety 2015, 56, 9–17.

Salazar, F.; Toledo, M.A.; Oñate, E.; Suárez, B. 2016. Interpretation of dam deformation and leakage with boosted regression trees. Eng. Struct. 2016, 119, 230–251.

Simon, A.; Royer, M.; Mauris, F.; Fabre, J. 2013. Analysis and Interpretation of Dam Measurements using Artificial Neural Networks. In Proceedings of the 9th ICOLD European Club Symposium, Venice, Italy, 10–12 April 2013.

Swiss Committee on Dams (SCD). Methods of analysis for the prediction and the verification of dam behaviour. 2003. In 21st Congress of the International Commission on Large Dams, Montreal, Switzerland.

A COUPLED STATISTICAL AND NUMERICAL APPROACH FOR THE ARCH DAM MONITORING

Chady El Moataz Billah
Artelia, Grenoble, France

Nicolas Ulrich
Artelia, Grenoble, France

Frédéric Andrian
Artelia, Grenoble, France

ABSTRACT: Monitoring is a major part of dam safety and surveillance provisions. Monitoring is a decision-making tool which allows a relatively detailed understanding of the behavior of the dam at a weekly timescale or even more frequently when required. In France, it is usual practice to calibrate the numerical model used for the stability analysis of arch dams by means of data from the monitoring system and use the mentioned numerical model for prediction of behavior and safety assessment. The aim of this paper is to present the results of different methods and assumptions used to process dam monitoring data for explaining the current behavior of an arch dam and predicting its future behavior. Two different methods are used: statistical analysis and numerical modelling. The monitoring data are used to set up HST (Hydrostatic, Season, and Time) and Thermal HST (HSTT) statistical models. Then a numerical thermo-hydro-mechanical model is performed to predict the arch dam's future behavior after being calibrated by means of the monitoring data. Then, a preliminary safety analysis of the dam with the numerical model is carried out by determining a few strength parameters allowing the dam to fulfill the current French Guidelines on stability analysis of arch dams.

1 INTRODUCTION

The aim of this paper is mainly to detail the used methods for filling up the excel files for reporting the results. The used assumptions are described, and some interpretations of the different analyses is made.

Two approaches are carried out: statistical methods and numerical models. Concerning statistical models, the three cases (calibration, short and long term predictions, and interpretation) have been carried out for all devices except for leakage device.

Warning levels are defined for each device based on usual practice.

Three different approaches are used in the current case study. The participants are requested to rank the ability of each of them in terms of best guess of the future behavior of the dam. In the point of view of the authors, the statistical models seem to be more accurate in predicting the future behavior of the current arch dam. Firstly, they are useful tools that allow complex phenomena involved in the raw data to be explained with a rather good confidence. Secondly, as long as the expected loadings (in a separate way) have already been submitted to the dam, statistical approaches are believed to be also of good accuracy to predict the future behavior under a specific load combination. On the other hand, numerical models must consider all the involved physical phenomena and related parameters in order to accurately simulate the behaviour of the real structure. In the current case, several assumptions are made for the missing data. Consequently, as only a few relevant data for the numerical analysis are available, the results are ranked at the third place. Regarding the statistical models, the HSTT method is judged better in this specific case. As the HSTT method has one more parameter to explain raw data and as the case study is a relatively thin arch, HSTT model is judged more accurate in this case where the concrete temperature can rapidly vary across the thickness of the dam. And finally, the data covers several years of dam operation, enhancing the ability of the statistical model to explain and predict the behavior. Therefore, HSTT models is ranked at the first place.

A reminder of the excel files content is given below

Table 1. Reminder of analysed data

Method	Device	Case A	Case B	Case C
HST models	CB2	Yes	Yes	Yes
	CB3	Yes	Yes	Yes
	C4_C5	Yes	Yes	Yes
	PZCB2	Yes	Yes	Yes
	PZCB3	Yes	Yes	Yes
	Leakage	No	No	No
HSTT models	CB2	Yes	Yes	Yes
	CB3	Yes	Yes	Yes
	C4_C5	Yes	Yes	Yes
	PZCB2	Yes	Yes	Yes
	PZCB3	Yes	Yes	Yes
	Leakage	No	No	No
Numerical models	CB2	No	Yes	Yes
	CB3	No	Yes	Yes
	C4_C5	No	No	No
	PZCB2	No	No	No
	PZCB3	No	No	No
	Leakage	No	No	No

2 DATA BASED MODELS

2.1 *HST method*

2.1.1 Description

HST Method is statistical model developed by EDF (Willm et al., 1967). The aim of this method is to explain dam monitoring data with three independent and additive effects. The first effect is the hydrostatic effect induced by the hydrostatic pressure of the water level in the reservoir. The second is the seasonal effect, it reflects such as a periodic behaviour of the dam regarding the period of the year. The last one is the time effect, which model the ageing behaviour of the dam or of a monitoring device over time. The hydrostatic and seasonal effect are supposed to be reversible whereas the time effect is considered as irreversible. These three effects are defined as follows:

$$f_{hydrostatic}(Z) = a_1 Z + a_2 Z^2 + a_3 Z^3 + a_4 Z^4 \tag{1}$$

$$f_{season}(S) = a_5(1 - \cos(S)) + a_6 \sin(S) + a_7 \sin^2(S) + a_8 \sin(S)\cos(S) \tag{2}$$

$$f_{aging}(\tau) = a_9 \tau + a_{10} \tau^2 + a_{11} e^{-\tau} \tag{3}$$

Z is the dimensionless water level in the reservoir defined by $Z = (Z\_PHE - h)/H\_br$. In this equation Z_{PHE} is the maximum water height in the reservoir (corresponding to the design flood), h is the current water level, and H_{br} is the dam's height above its foundation.

S is a radiant angle between 0 rad on the 1st January and 2π on the 31st December, S=$2\pi(d/365.25 - \lfloor d/365.25 \rfloor)$ with d the date of the day.

$\tau = t/T\_bt$ where t is the time of measurement expressed in years from a reference date, T_{bt} a constant expressed in years.

Coefficients $(a_i)_{i \in [\![0;11]\!]}$ are computed by least-square minimisation. Let Y be series of raw data and Ŷ be modelled data. The HST method models raw measurements and modelled data with

$$Y = a_0 + f_{hydrostatic}(Z) + f_{season}(S) + f_{aging}(\tau) + \varepsilon \tag{4}$$

$$\hat{Y} = Y - \varepsilon = a_0 + f_{hydrostatic}(Z) + f_{season}(S) + f_{aging}(\tau) \tag{5}$$

a_0 and ε are the constant and the residual error due to the linear regression.

An HST model is evaluated with the correlation coefficient R²=$\frac{\sum(\hat{y}_i - \bar{y})^2}{\sum(y_i - \bar{y})^2} \in [0; 1]$ and with the adjusted coefficient correlation $(R_a)^2 = 1 - \left(\frac{n-1}{n-p}\right)(1 - R^2)$. $\bar{y}$ is the mean of the sample Y, n is number of data and p the number explanatory variables. The clothier to 1 R_a^2 is, the better statistical model is adjusted.

2.1.2 Application to the case study

The same calibration period is used for pendulums CB2 and CB3 and crack opening C4_C5. They are calibrated between 19/01/2000 and 31/12/2012. Regarding piezometers, calibration periods are not identical. For both piezometers, the calibration considers the cleaning of the drainage system in February 2008. Consequently, the piezometer PZCB2 is calibrated between 20/09/2008 and 31/12/2012. Piezometer PZCB3 is calibrated between 01/01/2000 and 31/12/2012, but a drop in data is assumed to model the cleaning of the drainage system and to take into account the lack of data in early 2008. This drop is modelled on 10/09/2008.

Regarding the case C (long term predictions), a long period where the water level was below the lowest level experienced during the calibration period is noticed. In order not to misevaluate the hydrostatic function of HST method, the raw data are modified so as not to include any water level below that minimum value experienced during the calibration period, i.e., El. 185. When the water level values are lower than this elevation, this value is used as a replacement.

Finally, there isn't any successfully calibrated model for leakage. The best correlation coefficient reached about R²=0,5. This range of value is not high enough to result in an accurate HST model and to perform realistic monitoring analysis. Actually, leakage behavior is difficult to model with basic HST model. Indeed, leakage is subjected to strong non-linearities which is basically described by the law of Poiseuille, some threshold and/or cross-effects between thermal, mechanical and hydraulic effects (de Bigaut de Granrut, 2019).

The correlation factors of statistic models are given below.

Table 2. HST models correlation coefficients

	R^2	R_a^2
Pendulum CB2	0.9135	0.9130
Pendulum CB3	0.9646	0.9642
Crack opening C4_C5	0.9749	0.9747
Piezometer PZCB2	0.9925	0.9921
Piezometer PZCB3	0.9331	0.9326

2.2 *Thermal HST method (HSTT)*

2.2.1 Description

Thermal HSTmethod (HSTT) is an improvement of the classical HST method described in §2.1.1. It was developed by EDF after a heatwave in 2003 (Penot et al., 2009). HSTT considers one supplementary explanatory variable: air temperature. This new variable aims to explain raw data in which a high-frequency change in temperature occurs. Actually, the seasonal effect of the HST method explains only the low-frequency temperature changes, i.e., annual temperature changes. HSTT method allows the daily temperature changes to be considered.

This new variable called E_R and is added to the seasonal effect. The other effects of the HST method stay identical (eq. (1) and (3)). Thus, the seasonal effect from HSTT method is defined as follows:

$$f_{season}(S) = a_5(1 - \cos(S)) + a_6 \sin(S) + a_7 \sin^2(S) + a_8 \sin(S)\cos(S) + b_1 E_R \quad (6)$$

Coefficients $(a_i)_{i \in [\![0;11]\!]}$ and b_1 are computed by least-square minimisation.

Theoretically E_R is the impulse response to the unidirectional conduction equation

$$\frac{\partial \theta}{\partial t} = \frac{\lambda \rho}{c} \frac{\partial^2 \theta}{\partial x^2}$$

where the arch dam is assumed to be a finite medium of width L and only submitted to a temperature E at its extremities. (Penot et al., 2009)

In the modelling E_R is computed by

$$E_R(t + dt) = E(t + dt)\left(1 - \exp\left(-\frac{dt}{T_0}\right)\right) + \exp\left(-\frac{dt}{T_0}\right) E_R(t) \quad (7)$$

T_0 is the thermal response time of the dam and E represents deviations from the average temperature. It only represents deviations from the average temperature as the behaviour of the dam against the average temperature is modelled by the HST seasonal effect.

The average temperature is calculated from temperature data with linear regression. Let be θ_a the average temperature, modelled by

$$\theta_a = c_1 \cos(S) + c_2 \sin(S) + c_3 \cos(2S) + c_4 \sin(2S) \quad (8)$$

and thus, E is defined by $E = \theta - \theta_a$, θ is air temperature.

For each device, the thermal response time is calibrated with statistical optimisation but the value of T_0 is checked to ensure the physical consistency of this parameter which is supposed to represent the response time of the instrument to a thermal variation.

2.2.2 Application to the case study

The Hypotheses for HSTT method are the same as that of HST method. The same period of calibration between January 2000 and December 2012 is also used. PZCB2 is calibrated between 20/09/2008 and 31/12/2012 and PZCB3 is calibrated between 01/01/2012 and 31/12/2012 with a drop in the data on 10/09/2008. Regarding case C, the same hypothesis regarding minimum water level is made in order not to misevaluate hydrostatic effect.

The correlation factors of statistic models are given below which highlight the better correlation compared to the HST model.

Table 3. HSTT models correlation coefficients

	R^2	R_a^2	T_0 [days]
Pendulum CB2	0.9681	0.9677	5
Pendulum CB3	0.9690	0.9687	14
Crack opening C4_C5	0.9752	0.9749	10
Piezometer PZCB2	0.9936	0.9932	9
Piezometer PZCB3	0.9340	0.9334	9

2.3 *Warning levels*

Warning levels are defined on the corrected data from the calibration period. Corrected data are computed by subtracting reversible effects to the raw data.

$$Y_{corrected} = Y_{raw} - f_{hydrostatic}(Z) - f_{seasonnal}(S; E_r) \qquad (9)$$

Corrected data allows the dispersion of the data to be reduced and the analysis of the dam behaviour or monitoring devices to be facilitated. Warning levels are set to be equal to $\pm 2.5 \cdot \sigma_C$ in addition to the irreversible data modelled by HST/HSTT models. σ_C is the standard deviation of the corrected data during the calibration period and irreversible data are defined by

$$Y_{irreversible} = Y_{modelled} - f_{hydrostatic}(Z) - f_{seasonnal}(S; E_r) = a_0 + f_{aging}(\tau) \qquad (10)$$

Thus, warning levels are defined by

$$Upper\ Warning\ level\ = 2.5 \cdot \sigma_C + Y_{irreversible} = 2.5 \cdot \sigma_C + a_0 + f_{aging}(\tau) \qquad (11)$$

$$Lower\ Warning\ level\ = -2.5 \cdot \sigma_C + Y_{irreversible} = -2.5 \cdot \sigma_C + a_0 + f_{aging}(\tau) \qquad (12)$$

The value of $2.5 \cdot \sigma_C$ is based on ARTELIA's feedback in dam monitoring engineering. Based on experience, this value allows to not have too wide margins and not to have to narrow margins and to have significant alerts. Still, this is a preliminary initial value that may required to be gradually adjusted based on the corrected data after several years of monitoring analysis.

Figure 1. Examples of corrected data and warning levels

Warning levels help in distinguishing erroneous measurements from a rather unusual dam behaviour. Typically, in case of erroneous measurements, one device is usually out of its warning levels whereas in case of unusual dam behaviour, several devices usually exceed the thresholds. Still, the dam operator shall ensure that the only device with a peculiar measurement does not relate a local unusual behavior of the dam. Sometimes, when a device is regularly out of warning levels, this may require the warning levels to be adjusted.

In the case of the current case study, for examples between February and March 2005 three devices were out their warning levels (Figure 1). This may be explained the 2004/2005 winter which was colder than the mean winter, -15.5°C at 26/01/2005, combined with a high water level in the reservoir, at El. 230 m at the end of 2004.

3 NUMERICAL MODEL

For this benchmark workshop, the used numerical model is calibrated from statistical models and not directly from raw data.

3.1 *Geometry and meshing*

The numerical model is carried out with FLAC3D, an explicit finite difference calculation code. The used model involves a new meshing layout after slight changes in the provided geometry.

The mentioned changes include the consideration of the vertical joints between the cantilevers as based on ARTELIA's experience, such approach results in a more realistic modelling for arch dams (Mouy et al., 2019). The width and the position of the cantilevers are assessed from the few sketches from the formulation document but also from the original geometry files.

Moreover, the keying of the dam toe is deleted for geometrical convenience. On the other side, the dam / foundation interface is provided with numerical Shear keys so as to simulate the effect of the aforementioned keying.

The numerical model is made of 56000 linear elements distributed as follows:
- 16000 elements in the dam, mainly hexahedral. There are 6 elements across the thickness of the arch in order to accurately simulate bending and achieve a satisfactory resolution of analysis at the dam / foundation interface;
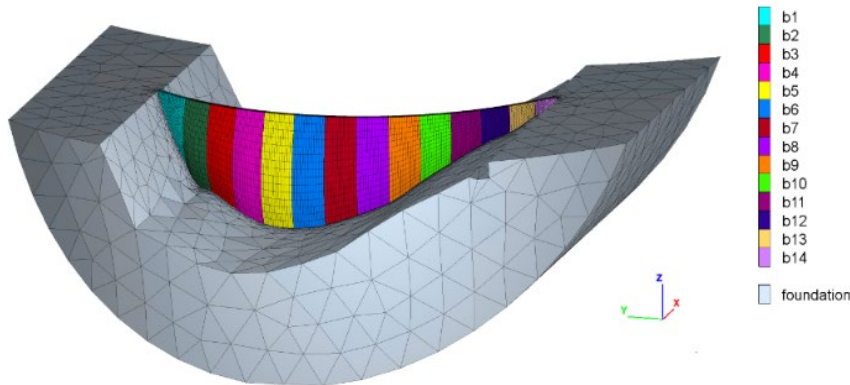- 40000 elements in the foundation, mainly tetrahedral.

Figure 2. Case study dam's block modelling

3.2 *Mechanical properties*

3.2.1 Foundation

As suggested in the formulation document, the foundation is divided into 3 different parts: left bank, right bank and bottom of valley. The Young's modulus of the bottom valley is calibrated using the pendulum CB3's HSTT model. The Young's modulus is determined from the simulation of hydrostatic effect and the thermal expansion coefficient from the simulation of seasonal effect.

The final model parameters are the results of many attempts of model calibration conducted considering both isotropic and anisotropic bedrock foundation. The best fitting is reached with the anisotropic plane presented in Figure 3.

The normal vector to the anisotropic plane is $\vec{n} = (1.25, 1, 0)$. The calibration is made by varying the reservoir level between 221.5 m and 237 m. The synthesis of calibration is given in the following table and shows a model base which is still slightly stiff with regards to hydrostatic effect:

Table 4. Young modulus of foundation Calibration

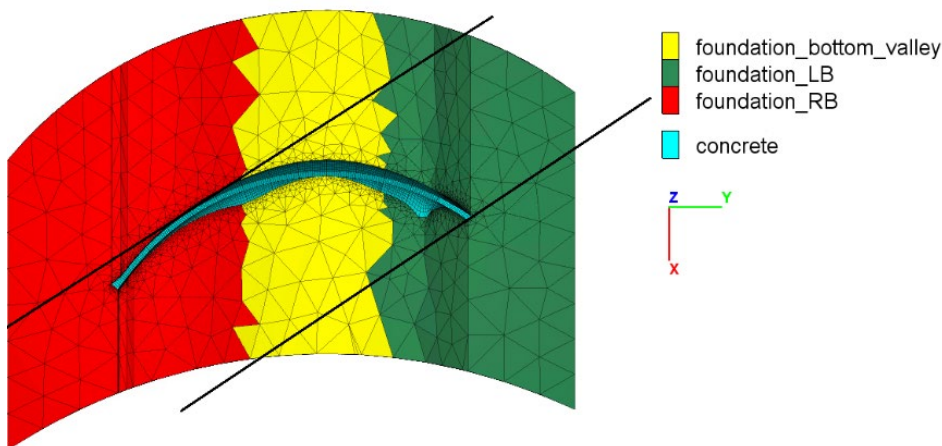| Radial displacement pendulum CB3 [mm]	Numerical anisotropic model		HSTT model	
	Computed hydrostatic effect [mm]	Computed seasonal effect [mm]	Target hydrostatic effect [mm]	Target seasonal effect [mm]
	4.34	2.52	5.88	2.52

Figure 3. The best fitting anisotropic plane for the foundation

The following table shows the selected material parameters in which the thermal conductivity and the specific heat capacity are usual values which are not assessed from the calibration process. One may notice the rather low Young's modulus normal to the anisotropic planes

Table 5. Foundation mechanical properties

	Left bank	Bottom of valley	Right bank
Young modulus in anisotropic plane $E_{\parallel}$ [GPa]	10.00	5.00	15.0
Young modulus normal to anisotropic plane $E_{\perp}$ [GPa]	0.300	0.300	3.00
Poisson ration	0.30	0.30	0.30
Density [kg/m3]	2700	2700	2700
Thermal conductivity [W/(m.K)]	3.00	3.00	3.00
Specific heat capacity [J/(kg.K)]	850	850	850
Coefficient of thermal expansion [K^{-1}]	$3.00 \cdot 10^{-6}$	$3.00 \cdot 10^{-6}$	$3.00 \cdot 10^{-6}$

3.2.2 Concrete

To calibrate concrete's Young's modulus, the same approach as the foundation's calibration is carried out. Hydrostatic effect from pendulum CB2's HSTT model is used to calibrate concrete Young's modulus. Seasonal effect from this HSTT model is also used to calibrate the coefficient of thermal expansion of the concrete.

The synthesis of calibration is given below:

Table 6. Young modulus and thermal coefficient of concrete Calibration

	Numerical anisotropic model		HSTT model	
Radial displacement pendulum CB2 [mm]	Computed hydrostatic effect [mm]	Computed seasonal effect [mm]	Target hydrostatic effect [mm]	Target seasonal effect [mm]
	22.89	23.50	22.34	20.97

The following table shows the selected material parameters in which the thermal conductivity and the specific heat capacity are again usual values which are not assessed from the calibration process:

Table 7. Concrete's mechanical properties

Young modulus [GPa]	35
Poisson ration	0.2
Density [kg/m^3]	2400
Thermal conductivity [W/(m.K)]	2
Specific heat capacity [J/(kg.K)]	900
Coefficient of thermal expansion [K^{-1}]	$8.5 \cdot 10^{-6}$

3.3 *Interfaces and joints*

The vertical joints of the dam are modelled and provided with numerical shear keys allowing the opening but not the sliding even under opened state.

To model the keying at the dam toe, the same numerical feature is also used. Note that because of this shear key and because of the elastic constitutive law, time effects cannot be considered in the prediction model.

3.4 *Loads*

Thermo-mechanical simulations have been carried out for prediction periods, thermal and mechanical loadings were updated for each days of predictions. The calculations involve the use of a thermo-hydro-mechanical simulation for which the features are described in the following. The calculation timestep (update in thermal and in mechanical loadings) is 1 day. As the

calibration is performed in a separate way, this stage consists only in predicting the future behavior.

3.4.1 Pore pressure, uplift and hydrostatic loading

The simulations are carried out in effective stress state: pore pressure acts as calculation variables in the same way as geotechnical analyses and influences total and effective mechanical stresses (without any backward coupling) with a Biot's coefficient which equals 1. Several pore pressure distributions are computed with flow calculation (Darcy's approach) for several water levels in reservoir. The foundation is assumed to be isotropic in terms of flow and neither the drainage system nor the grout curtain is considered. The calculated pore pressure contour matches with good accuracy to PZCB3, but not so much with PZCB2.

During the prediction calculations, the pore pressure distribution chosen for each day corresponds to the one that has the closest water level among the previously calculated distributions.

The full uplift propagates as external force in any opened region of the dam / foundation interface with an opening higher to 0.2mm as long as the region is in contact with the reservoir.

If the water level in the reservoir is very low (i.e., under dam's toe elevation), the pore pressure is set at the lowest level computed: 193.5 m.

Table 8. Hydraulic properties

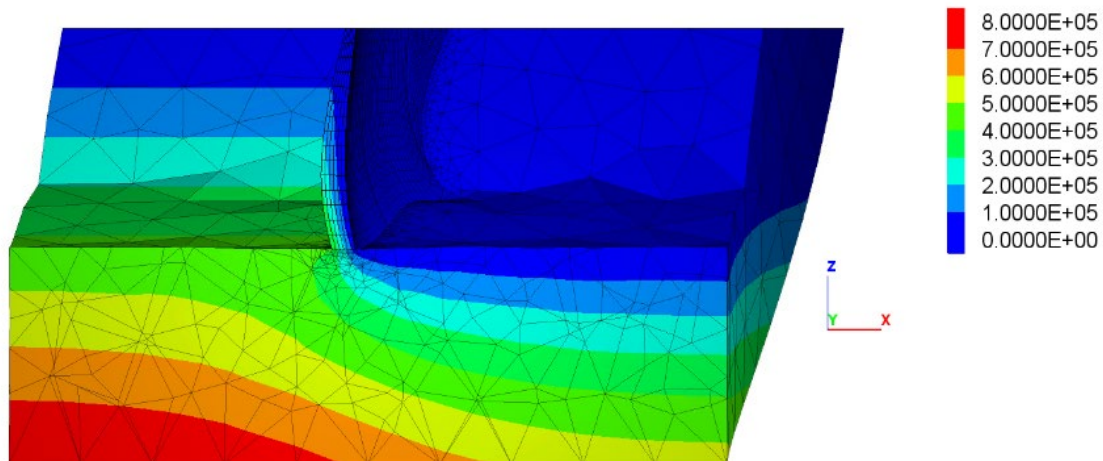|	Permeability m/s
Concrete	$1 \cdot 10^{-8}$
Foundation	$1 \cdot 10^{-7}$

Figure 4. Pore pressure distribution (Pa) corresponding to water level at El. 237 m

3.4.2 Thermal loadings

The temperature distribution in the dam and in the bedrock is determined from a transient thermal-only simulation with a timestep of 1 day and applied as thermal loading to the mechanical model. The thermal loadings are calculated from air and water temperature data with a few more assumptions based on ARTELIA's experience.

20 m under water surface, water temperature is assumed to be constant and equal to 4°C. Furthermore, across the 20 first meters under water surface, the temperature is assumed to vary linearly between 4°C and the air temperature.

The temperature of transverse joint grouting is considered to be the annual mean temperature between 2000 and 2012 and leads to 5°C. This uniform temperature distribution corresponds to zero thermal stress in the dam. The transient thermal analysis considers the variations of the water level in the reservoir.

The following table gives the thermal parameters related to heat exchange with air and water.:
Table 9. Thermal properties related to heat exchange with air and water

Convective heat coefficient air-concrete [W/(m²K)]	13
Convective heat coefficient air-rock [W/(m²K)]	13
Convective heat coefficient water-concrete [W/(m²K)]	500
Convective heat coefficient water-rock [W/(m²K)]	500

3.5 *Short and long term predictions*

The prediction simulations lead to the results presented in Figure 5 where also superimpose the HST and HSTT prediction curves. The numerical predictions for CB2 are in good agreement with that of HST and HSTT approaches except when the reservoir water level is below the modelled dam's toe. This denotes some poroelastic behavior of the bedrock justifying the use of the pore pressure as state variable but here not very accurate due to the lack of calibration data. The numerical predictions for CB3 are of lesser accuracy due to the stiffer model base compared to reality with regards to hydrostatic effects. Based on the authors experience in arch dam modelling, this case study is one of the very unusual cases where the model base is stiffer than reality. It is suspected that the orthotropy plane is somewhat different that the one modelled. Otherwise, the Young's modulus of the bedrock which would be able to simulate the real behavior of the dam would be too low to denote a bedrock suitable for constructing an arch dam. Moreover, the model is not able to consider the time effect which is rather low e in this case (0.03mm/year) and can then be neglected.
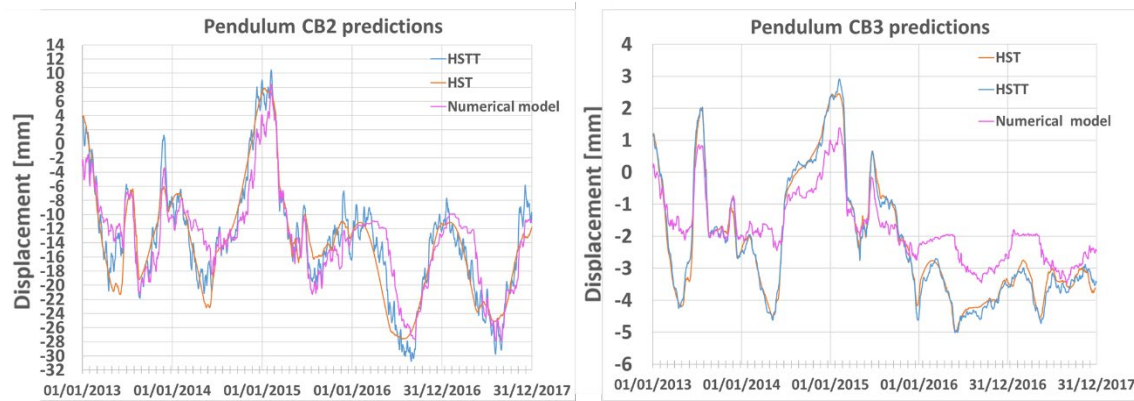

Figure 5. Pendulum predictions results – numerical, HST and HSTT approaches

4 SAFETY ANALYSES

The main advantage of numerical simulation compared to statistical approach is its ability to assess in a quantitative way the safety of the dam with regards to existing national or international guidelines. Consequently, it is considered less valuable to define warning levels based on the numerical simulation predictions. On the other hand, one can assess the safety margin of the dam for a defined load case with regards to a specific failure mode. The one analysed here as an example is the sliding along the dam / foundation interface.

With a maximum base width of 6 m and a maximum height above the bedrock of about 45 m, the case study is thin arch dam. With a straight distance between the abutment of about 158 m, the dam is built on a wide valley (relative to its height). This type of dam usually exhibits extended crack opening (or foundation extension) at their upstream toe when being impounded with full uplift/pore pressure propagating toward the downstream part. Such behavior is exacerbated by winter thermal loading with the shear strength being strongly mobilized at the dam / foundation interface.

The monitoring data confirm this crack opening and the uplift/pore pressure propagation toward downstream. In the numerical model, this opening is localized at the dam / foundation interface with a maximum magnitude of about 3 mm at NWL without thermal loadings. This opening may actually be distributed over several discontinuities within the bedrock.
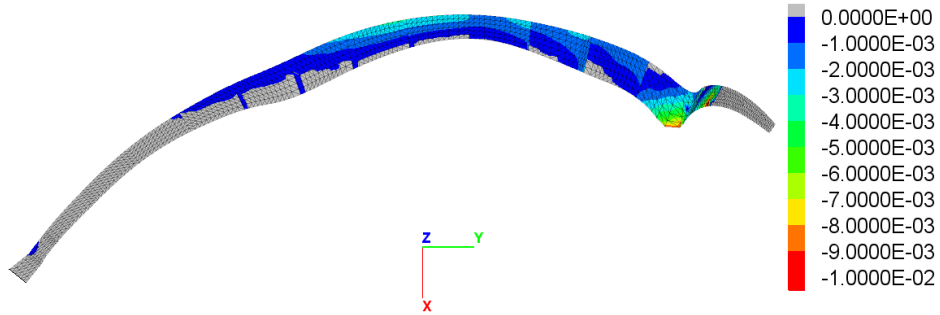
Figure 6. Cracks opening (m) at NWL

A first analysis consists in assessing the mobilized cohesion at the dam / foundation interface when considering a friction angle of 45°. Such cohesion denotes the contact roughness: the cohesion is mobilized even when the dam / foundation interface is in an open state. The maximum mobilized cohesion at the scale of one cantilever is about 800 kPa at NWL under winter thermal loading (Figure 7). This is in the higher range of encountered values for several arch dams studied so far (Robbe et al. 2022).
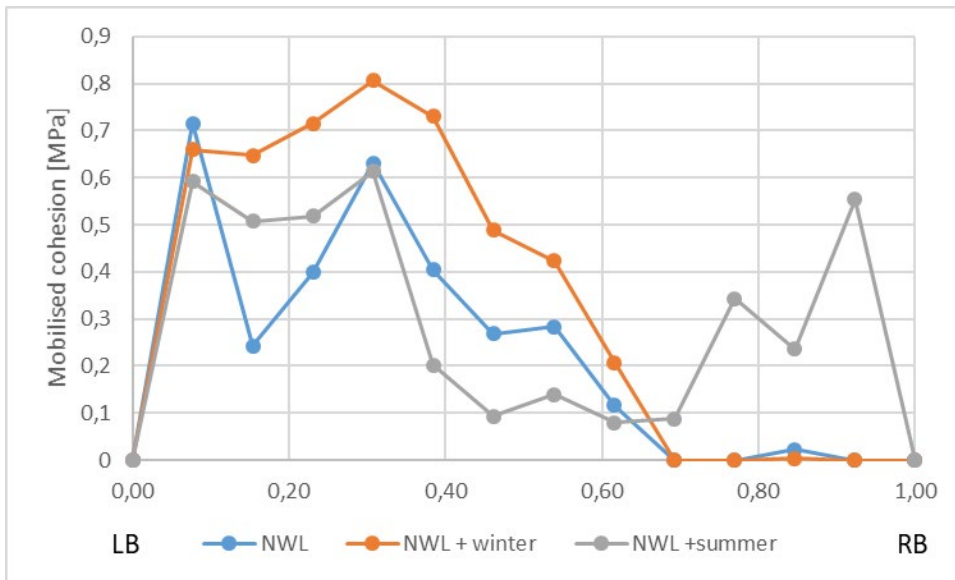

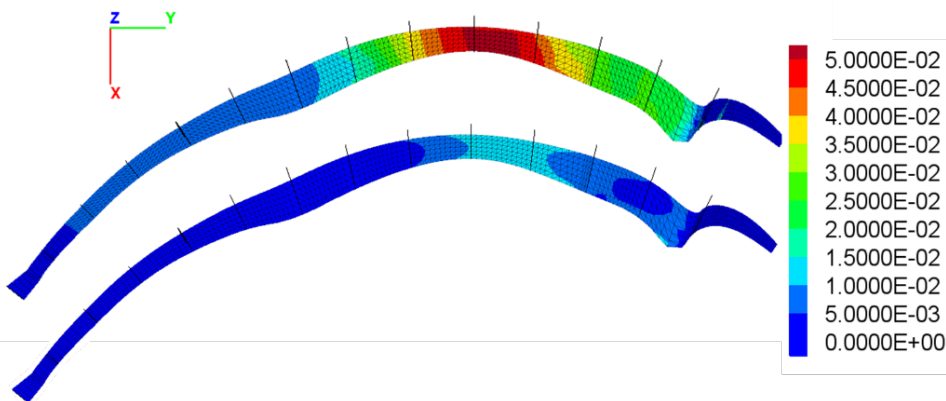Figure 7. Necessary cohesion to avoid the sliding of each block

Figure 8. Irreversible shear displacement (m) at rock concrete interface under normal conditions winter Upper interface's properties are c=0 kPa $\varphi = 45°$, Lower interface's properties are c=600 kPa and $\varphi = 45°$

Then a sensitivity analysis is carried out regarding the dam / foundation shear strength parameters. A first deterministic approach considers a friction angle of 45° without any cohesion (CFBR 2018, FERC 2018). With these assumptions generally used at design stage, a sliding up to 5 cm is calculated, without any failure mechanism being triggered (Figure 8). Such behaviour is not in line with the current French guidelines, though not specifically edited for newly designed dams. A second calculation considering 600kPa cohesion leads to about 1 cm sliding, at the limit of allowable value as per the current French guidelines. One may envisage that such cohesion can actually be mobilized at the dam / foundation interface through roughness or also deeper in the rock mass if there is not any unique localized crack. Moreover, the keying of the dam in the bedrock is also another reassuring aspect for this case study. But finally, it is also deemed possible that the calculated sliding displacements have gradually developed during several seasonal and drawdown cycles of the dam without jeopardizing its safety (Andrian et al. 2018).

5 CONCLUSIONS

The statistical HST and HSTT models are very often used in French arch dam engineering because they are simple, efficient and robust approaches based on the real behaviour of the dam. They can provide with rational explanation to raw and intricate data. They can be directly handed over to the dam operators in order to perform a regular check on the periodic behaviour of the dam based on the continuously collected data. On the other hand, the accuracy and the ability of the model to learn from the behaviour of the dam and to be able to explain or predict gradually increase with new data. However, based on the authors experience who are currently in charge of the monitoring analysis of more than 30 large dams, statistical approach is seldom used for predictions. Actually, they are not able to extrapolate data when the loadings are out of the range already experienced by the dam and hence unable to assess the safety of the dam in a clearly quantitative way.

On the other hand, numerical modelling is a rather complex tool which cannot be easily handed over to dam operators. In the authors experience, such tool is usually applied in a deterministic way at design stage with regards to the material parameters which are not directly related to safety. At the beginning, the strength parameters can be determined through tests but also by means of empirical approaches. Then the numerical model can be gradually calibrated by means of the regularly collected monitoring data. In the case of numerical models, the more physical phenomena are known and well modelled, the closer is the numerical model behaviour from the real behaviour of the dam. Through years, the gradual adjustments of such numerical model can turn the model into an actual digital twin of the dam which can more and more confidently be used predict the dam behaviour and to assess with a higher accuracy its safety.

The combination of statistical approaches on one hand and the gradually learning numerical model on the other hand is believed to become a higher range monitoring decision-making tool to be used by both the operator and the engineer in a tight collaboration.

REFERENCES

Willm G. and N. Beaujoint, 1967, The methods of dam supervision applied by the Service de la Production Hydraulique of Electricité de France. Old problems and new solutions. IXICOLD/CIGB, Q.34-R.30, Istanbul.

De Bigault de Granrut M., 2019, Analyse et interprétation de la pression d'eau en fondation des barrages-voûtes à partir des mesures d'auscultation. Université Grenoble Alpes

Penot I., Fabre J.-P., Daumas B., 2009, Analysis and modelling of the behaviour of civil engineering structures by taking into account air temperature: "Thermal H.S.T." Method. XXIII-ICOLD/CIGB, Q.91-R.60, Brasilia

Mouy V., Molin X., Anthiniac P., Roy M., Ulrich N. and Andrian F., 2019, Advantages and limits of cyclic calculations for the analysis of arch dams, Colloque CFBR, Chambéry.

Comité Français des Barrages et Réservoirs, Octobre 2018, Recommandations provisoires pour la justification des barrages-voûtes.

Federal Energy Regulatory Commission (FERC), March 2018, Engineering guidelines for the evaluation of hydropower projects, Chapter 11 – Arch dams.

Robbe E., Andrian F., Ulrich N., Jouy C., 2022, Shear at the concrete-rock contact of arch dams: feedback on existing dams, XXVII-ICOLD/CIGB, Q.104-RMarseille.

Andrian F., Roy M., Agresti P., Fournié Y., 2018, On the use of cyclic calculations as a support for the monitoring and surveillance of arch dams, Colloque CFBR, Chambéry.

BEHAVIOR PREDICTION OF A CONCRETE ARCH DAM: DATA-BASED MODELS USED BY THE FORMULATOR OF THE THEME A IN AN INDUSTRIAL CONTEXT

Alexandre Simon

EDF (Electricité de France)

ABSTRACT: This paper presents the data-based models used by the formulator of the theme A in order to analyze the monitoring data. The models proposed by the formulator are the models of reference for EDF, i.e., they are used in an industrial context. It does not mean that they should be considered as the reference or the best model for this benchmark.

The models applied for this benchmark are the following:

- Thermal HST for displacements
- A non-linear version of HST for crack opening displacements
- A physically based and non-linear version of HST for piezometers at the rock concrete interface
- Artificial Neural Networks for leakages

Regarding the short-term and long-term predictions, and since this paper is written by the formulator of the theme A who owns all monitoring measurements, it is stipulated that predicted values are provided without any knowledge of measurements during the prediction period. Predictions are provided for displacements, crack opening displacements, piezometers but not for leakages as Artificial Neural Network is not appropriated when it comes to extrapolating.

Simon

BEHAVIOR PREDICTION OF A CONCRETE ARCH DAM: DATA-BASED MODELS USED BY THE FORMULATOR OF THE THEME A
IN AN INDUSTRIAL CONTEXT

1 INTRODUCTION

Analyzing dam monitoring data (displacement, leaks, uplift, etc.) uses statistical analysis methods that have been developed to separate the different sources of variation in the measured phenomenon. Among these statistical methods multiple linear regression analysis using the HST (Hydrostatic-Season-Time, Ferry et al 1958, Willm et al. 1967) model has proved to be powerful and is widely used within EDF. Its main advantages are its robustness and its ease of interpretation and application. HST enables hydrostatic (due to hydrostatic load) and seasonal (due to thermal effects, for example) effects to be determined and to simply deduce the irreversible behavior of the structure.

Some limitations of HST have been identified: when explanatory variables (water level, season) are connected together, separating the effects is not accurate. In addition, the laws defining the explanatory functions (polynomials for water level) are given a priori and cannot always be modified to adapt to the real behavior of the dam (threshold effects among others).

To improve the shortcomings of HST in classical analysis, many explanatory models have been developed within EDF. All of them are derived from the HST classical formulation. Some of them are applied to the time series of monitoring data of this benchmark.

The models applied for this benchmark are the following:
- Thermal HST for displacements
- A non-linear version of HST for crack opening displacements
- A physically based and non-linear version of HST for piezometers at the rock concrete interface
- Artificial Neural Networks for leakages

The HST method for data correction is EDF's main method for analysing monitoring data (displacements, uplifts, leaks, etc.). The HST model assumes that raw measurements can be modelled by adding three states:
- An irreversible change in the phenomenon over time t, which may tend to decay (adaptation or consolidation), to increase (degradation) or to remain constant. The law f1 corresponding to this effect is as follows:

$$f_1(t) = b_1 e^{-t/t0} + b_2.t + b_3.t^2 + b_4.t^3 + b_5.t^4 \qquad (1)$$

It consists of two terms (negative exponential with the characteristic time t_0 representing the decay and a polynomial in time). Commonly the linear term is used.
- A reversible effect corresponding to the effect of the hydrostatic load *H*. The corresponding law f_2 is:

$$f_2(z) = b_6.z + b_7.z^2 + b_8.z^3 + b_9.z^4 \qquad (2)$$

Where

$$Z = (RN-H)/(RN-Rvide) \qquad (3)$$

with H the water level on the day of measurement, RN the normal operating water level and Rvide the water level when empty (When the dam is full z = 0).

A reversible seasonal influence including various cyclic phenomena (temperature, radiation, etc.). The seasonal law is a one-year periodic function. The season S is varying from an angle equal to 0° on 1 January and 360° on 31 December; then:

$$f_3(S) = b_{10}.\cos(S) + b_{11}.\sin(S) + b_{12}.\cos(2S) + b_{13}.\sin(2S) \qquad (4)$$

The coefficients bi (I varying from 0 to 13) are determined by minimizing the sum of square residues. The measurement X_i (displacement, uplift, etc.) at time t_i, for a water level z_i, at a season Si can be expressed as follows:

$$X_j = f_1(t_j) + f_2(z_j) + f_3(S_j) + b_0 + \varepsilon_j \qquad (5)$$

Simon

BEHAVIOR PREDICTION OF A CONCRETE ARCH DAM: DATA-BASED MODELS USED BY THE FORMULATOR OF THE THEME A
IN AN INDUSTRIAL CONTEXT

The term ε_j is the residue of the model, including the measurement errors and model imperfections. b_0 is the constant of linear regression. Thus, the measurements (M) "corrected" by the HST model are unaffected by the reversible effects ($f_2(z)$ and $f_3(S)$). Therefore, we note:

$$\text{Corrected Measurement }_i = X_i - f_2(z_i) - f_3(S_i) \tag{6}$$

The model makes a strong assumption: the reversible effects are independent (additive). The season (thermal effects) has the same effect on a full or an empty dam and vice versa. It is a shortcoming of HST.

The model enables data to be compared under identical seasonal (average season $f_3(S)=0$) and water level (full dam $f_2(z)=0$) conditions. This correction of measurement enables to highlight slow temporal effects or anomalies.

The article will briefly describe the method used to analyze each phenomenon and present main results and interpretation. Due to the brief size of this paper, a detailed description is only provided in the list of references.

2 METHODS, RESULTS AND INTERPRETATION

2.1 *Analysis of displacements*

Displacements are analyzed thanks to the **Thermal HST model** (Penot et al. 2009). This model is an improvement of HST by adding a term which accounts for the influence of the deviation from the season of air temperature. This term is also delayed from a characteristic time T0, which accounts for the thermal diffusivity of the dam (T0=8 days for pendulum CB2). Regarding the data of the benchmark, we use Ta for the air temperature as we observe from our own experience that using an air temperature according to the standard of WMO (World Meteorological Organization) is always better than using a temperature calculated by interpolation from several air temperature measuring stations. But this point needs to be confirmed by the benchmark. The figure 1 below presents the corrected measurement i.e. measurements that are removed from the reversible effects. They enable to highlight the irreversible trend, which is negligible in this case, except for the last two years. This upstream displacement for the last two years is not clearly understood, but it is perhaps due to the fact that the Thermal HST model is not well appropriated when the water level is low during a long time.
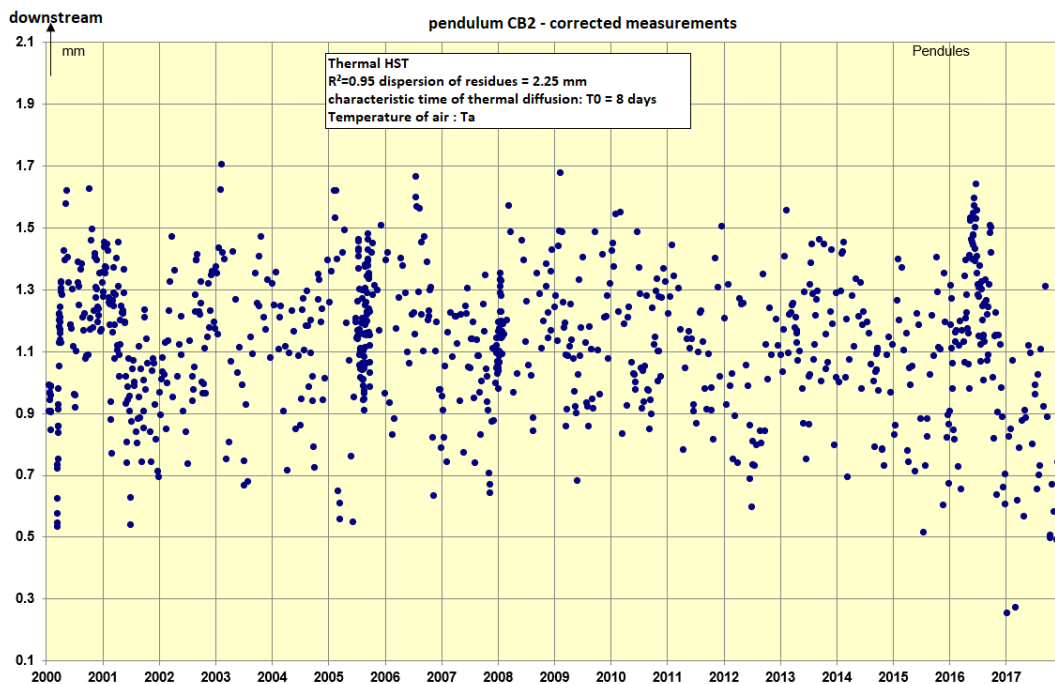

Figure 1. Corrected displacements for pendulum CB2.

Simon

BEHAVIOR PREDICTION OF A CONCRETE ARCH DAM: DATA-BASED MODELS USED BY THE FORMULATOR OF THE THEME A
IN AN INDUSTRIAL CONTEXT

Another interesting graph provided by the Thermal HST model is given on figure 2. The thermal displacements (seasonal plus deviation from the season) enable the dam owner to visualize the effect of cold waves and heatwaves.
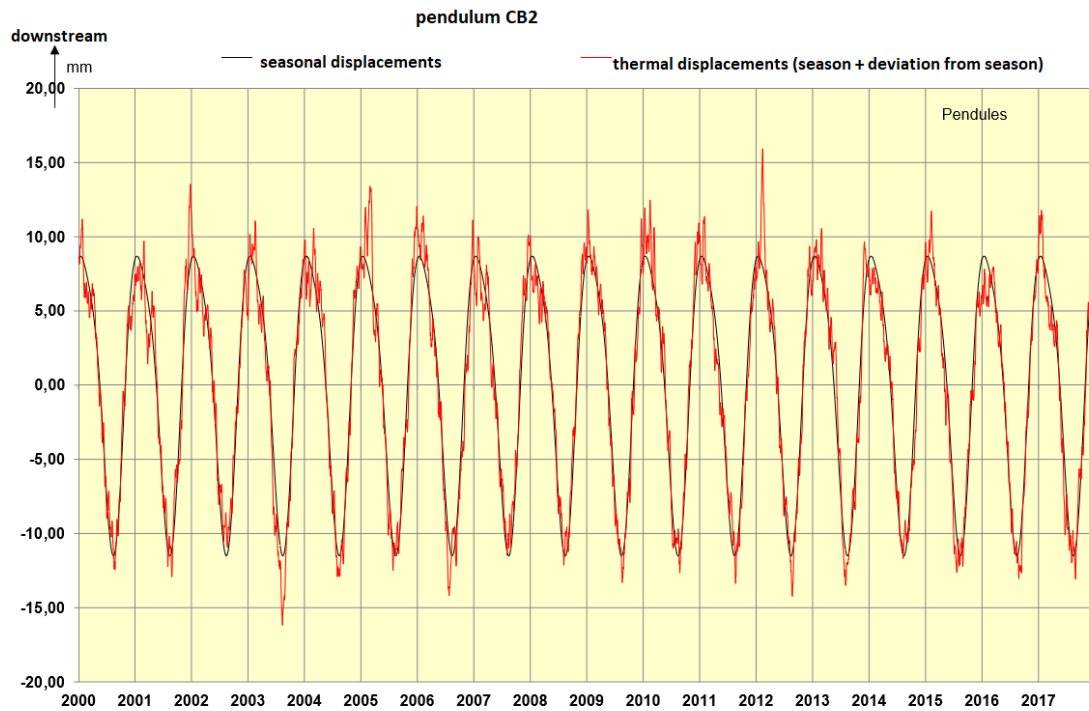

Figure 2. Thermal displacements (seasonal + deviation from the season) for pendulum CB2

Other effects such as hydrostatic effects and irreversible may also be displayed to interpret the dam behavior.

2.2 *Analysis of crack-opening displacements*

Time series of crack-opening displacements are characterized by a threshold which is obvious when observing the raw data. To overcome this issue, we build a non-linear version of HST model by using the hyperbolic tangent function. The general expression of this model is as follows:

$$X_j = a_0 + a_1 \tanh(a_2 + f_1(t_j) + f_2(z_j) + f_3(S_j) + \varepsilon_j \tag{7}$$

As this model is nonlinear, the multiple linear regression analysis cannot be used. To overcome this issue, we use the solver of Excel to determine the coefficient a_i and b_i. When interpreting the results of this model, one should keep in mind that the reversible effects are not unique and depend on the environmental conditions.

For example, Figure 3 shows the seasonal effect at different water levels. When water levels are low, the amplitude of the seasonal function is low as the crack is closed. Reciprocally, when water levels are high, the crack is open and consequently the seasonal function has a higher amplitude.

One other interesting thing to look at are the corrected measurements (see Figure 4). Times series exhibit a sudden irreversible increase in January 2008, which is probably caused by the historical value of crack opening displacement observed at the same date.

Among the drawback of this model, it should be noticed that the coefficient of correlation of this model is a little lower than the coefficient of correlation of the simple HST when considering the predicted period.

Simon

BEHAVIOR PREDICTION OF A CONCRETE ARCH DAM: DATA-BASED MODELS USED BY THE FORMULATOR OF THE THEME A
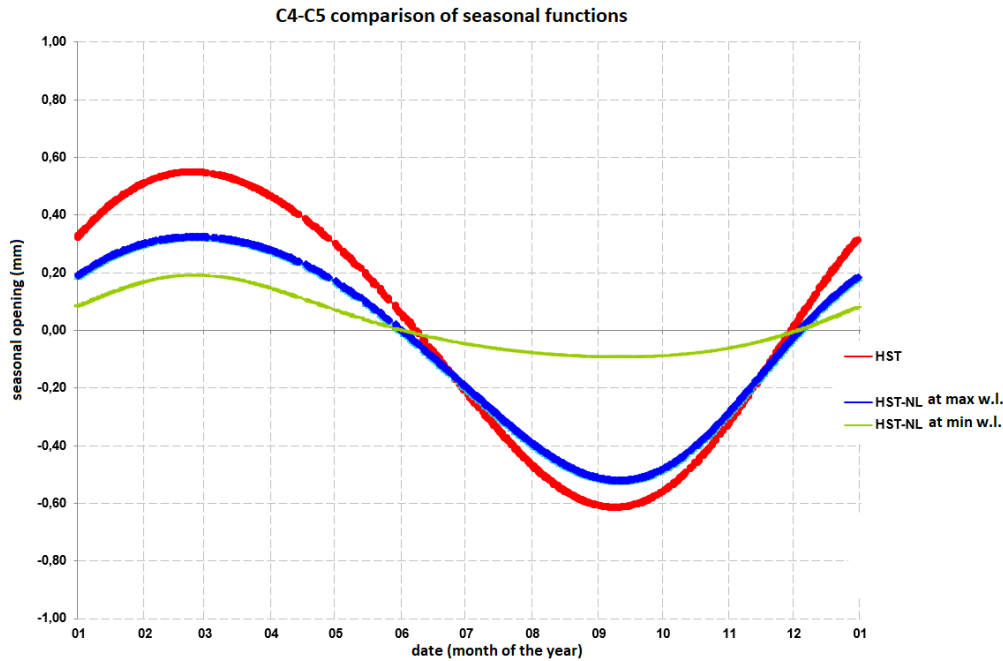IN AN INDUSTRIAL CONTEXT

Figure 3. Seasonal effect for the crack opening displacement C4-C5 at different water level
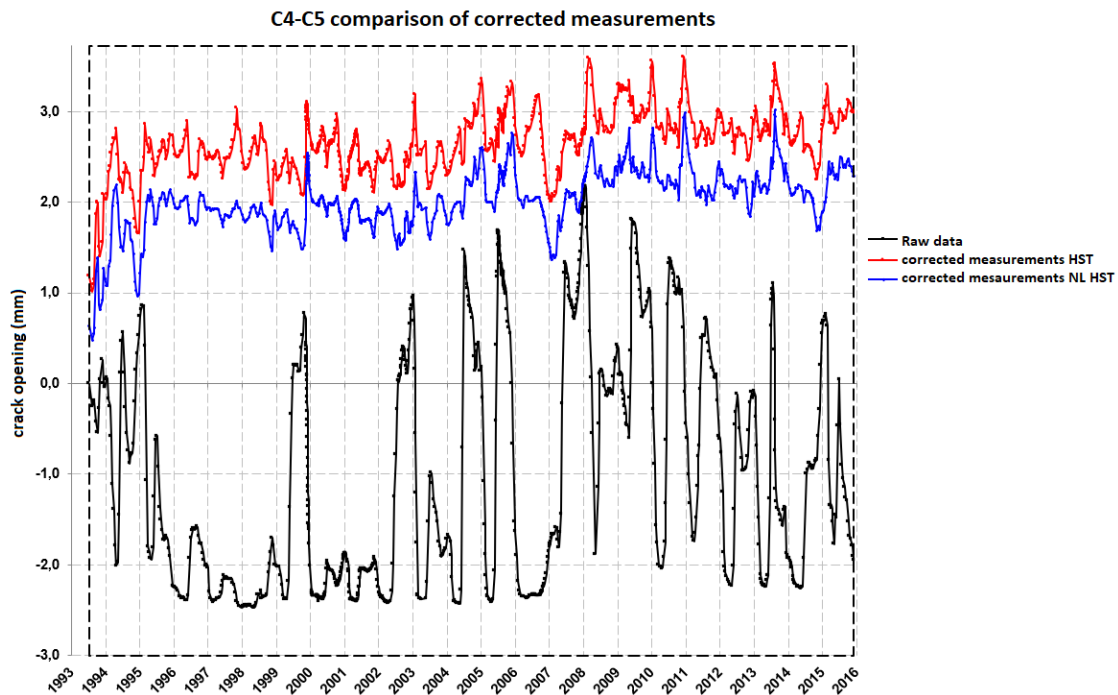

Figure 4. Corrected measurements of crack opening displacements C4-C4

2.3 *Analysis of pressure of water in the foundations*

When analyzing piezometric levels, we observe that the effects of the thermal and hydrostatic loads actually are interdependent. Indeed, for a given water level, the effect of the hydrostatic load differs from a thermal state to another. In winter, the low temperatures induce (for an arch dam) a thermal contraction of concrete which in turn induces a shifting of the arch in the downstream direction. This modifies the permeability at the interface by increasing it at the heel of the dam. The rock-concrete interface is said to be decompressed or open and allows the

Simon

BEHAVIOR PREDICTION OF A CONCRETE ARCH DAM: DATA-BASED MODELS USED BY THE FORMULATOR OF THE THEME A
IN AN INDUSTRIAL CONTEXT

hydrostatic load to propagate toward downstream. Uplift pressures in the rock-concrete interface thus increase. Reciprocally, in summer, the thermal expansion of concrete tends to close the interface and reduces its permeability, which limits the propagation of the hydrostatic load. Therefore, the effect of the hydrostatic load is modulated by the effect of the thermal state. Those two reversible effects are coupled. Some time-depending evolutions can also influence the permeability of the interface, such as clogging, or a loss of watertightness. From those reflections, one can infer that the effects of the different influencing loads (thermal state, hydrostatic load, time) are not merely additive, which invalidates the HST model. The model that is described in this article (De Granrut et al. 2019, De Granrut et al. 2018) aims at taking into consideration those couplings, by explicitly integrating them into a non-linear formulation.
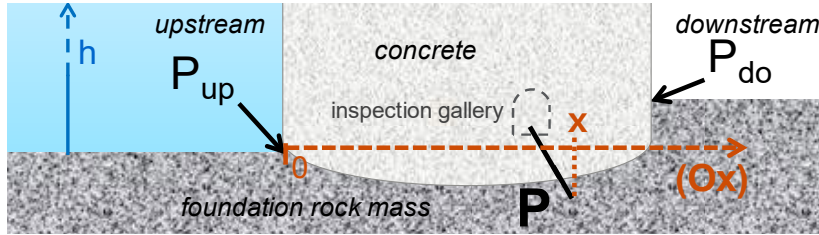
Figure 5. Representation of the rock-concrete interface, definition of the quantities of interest

Consider (fig. 5):
- $P(x)$ the piezometry measured by a piezometer situated at the contact, at a distance x from the upstream end of the heel. The notation is simplified to **P**;
- P_{do} the piezometry measured at the downstream end of the toe of the dam;
- $k(x)$ a dimensionless factor, written **k**;
- $H_{load} = h - P_{do}$ the hydrostatic load exerted by the water in the reservoir.

P is modelled as the sum of the downstream piezometry and a fraction of the hydrostatic load (8).

$$P = P_{do} + k \cdot H_{load} \tag{8}$$

k expresses the link between the head loss between the upstream end and the piezometer (as a fraction of H_{load}), and the measured piezometric level. If the permeability of the medium was homogeneous and isotropic, this link would be a proportional and constant link (Darcy law). However this is not the case, and the permeability of the foundation rock mass is actually influenced by the mechanical strains of the foundation, which are themselves a function of the mechanical stresses that affect the structure (dam plus foundation).

First, the effects of those mechanical stresses on the structure are modelled linearly, as the sum of a hydrostatic function, a thermal function and a temporal function. This choice was conditioned by the following observation: the vertical displacements (VD) being an image of the mechanical strain of the structure (*meca*).

$$VD \approx meca = f_1(S) + f_2(Z) + f_3(t) + \varepsilon_i \tag{9}$$

Where f_1, f_2 and f_3 are the same functions as in the HST model and ε_i is the modelling error.

Second, the effect of the global mechanical strains on the permeability, and thus on the piezometric levels, is not linear (10).

$$k = g_{non\ linear}(meca) \tag{10}$$

Where g is a function to be determined. Since the measurements are distributed following a hyperbolic tangent type function, the function $g_{non\ linear}$ was chosen as a hyperbolic tangent function.

Considering the expression of the relative trough Z, H_{load} can be expressed as a function of the water level in the reservoir h (11)

$$H_{load} = h_{norm} - Z \cdot (h_{norm} - h_{emp}) - P_{do} \tag{11}$$

Simon

BEHAVIOR PREDICTION OF A CONCRETE ARCH DAM: DATA-BASED MODELS USED BY THE FORMULATOR OF THE THEME A
IN AN INDUSTRIAL CONTEXT

Finally, for a monitored piezometric time series $P_{i \in \{1;N\}}$ containing N observations, the global model can be expressed as follows (12):

$$P_i = b_0 + [b_1 + b_2 \cdot tanh(a_0 + a_1 \cdot cosS_i + a_2 \cdot sinS_i + a_3 \cdot cos2S_i + a_4 \cdot sin2S_i + a_5 \cdot Z_i + a_6 \cdot Z_i^2 + a_7 \cdot Z_i^3 + a_8 \cdot Z_i^4 + a_9 \cdot t_i)] \cdot [h_{norm} - Z_i \cdot (h_{norm} - h_{emp}) - b_0] + \varepsilon_i ; \qquad i \in \{1;N\} \qquad (12)$$

This expression constitutes the regression model in which the coefficients b_0, $b_{1,...}$, $a_0,...,a_9$ are the regression coefficients. They are determined by nonlinear least squares fitting, using the Levenberg Marquardt algorithm, which iteratively minimizes the sum of squared residuals.

Once the 13 coefficients are optimised, the reversible effects (hydrostatic and thermal effects) can be computed by simulating the piezometric levels having either *Z* or *S* vary on its range, and the remaining variables being fixed to well-chosen baseline values.

The hydrostatic effect is interesting to plot as it reflects the aperture of the rock concrete interface (See Figure 6). In October, when the rock concrete interface is closed, the amplitude of the hydrostatic effect is low. Reciprocally, in April, when the entire dam is cold, the rock concrete interface is open and the amplitude of the irreversible effect is higher.
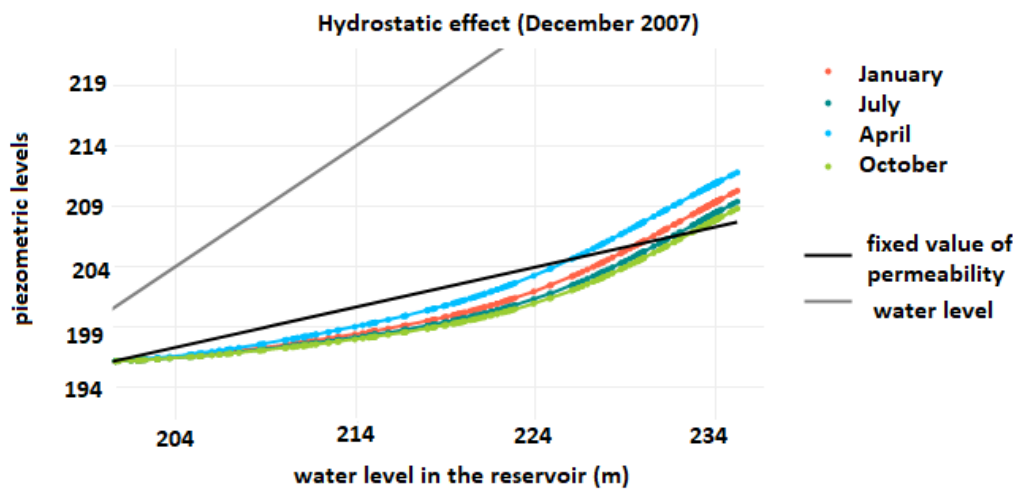

Figure 6. Hydrostatic effect for piezometric levels PZCB2

Thanks to the accuracy of the NL HST model, it is easier to detect any change in behavior when looking at the corrected measurements (see Figure 7). Time series of corrected measurements clearly shows a decrease after 2008, probably caused by the cleaning of the drainage system carried out at that date.
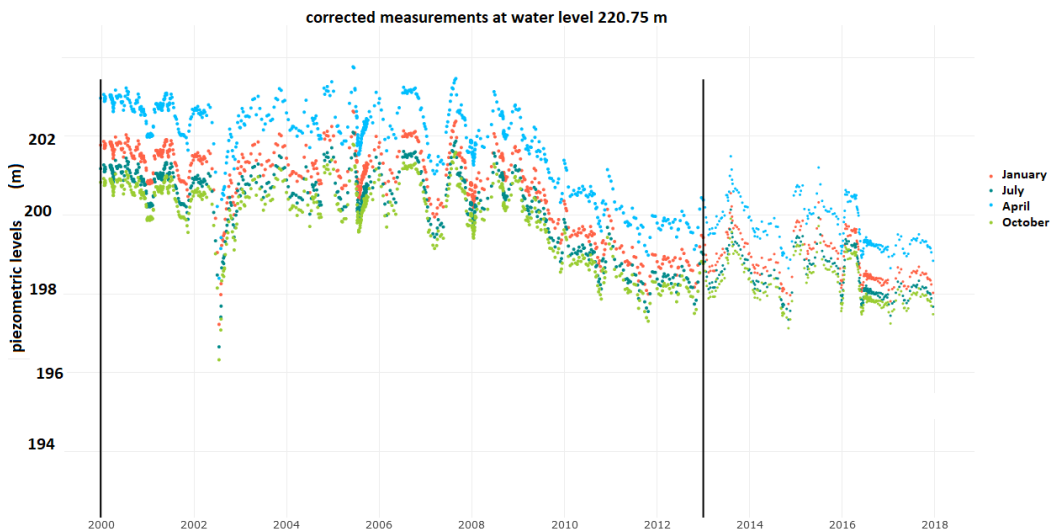

Figure 7. Irreversible effect (corrected measurements) for piezometric levels PZCB2

Simon

BEHAVIOR PREDICTION OF A CONCRETE ARCH DAM: DATA-BASED MODELS USED BY THE FORMULATOR OF THE THEME A
IN AN INDUSTRIAL CONTEXT

2.4 *Analysis of leakages*

In this article leakage are analyzed with a model based on Artificial Neural Networks. The architecture of the neural networks is given on the Figure 8. The explanatory variables (water level, season and time) are the same as the ones in the HST model. First tries using rainfall as explanatory variables were not conclusive.

The principle of Artificial Neural Networks and the main parameters used for that modelling are explained in Simon et al., 2013.
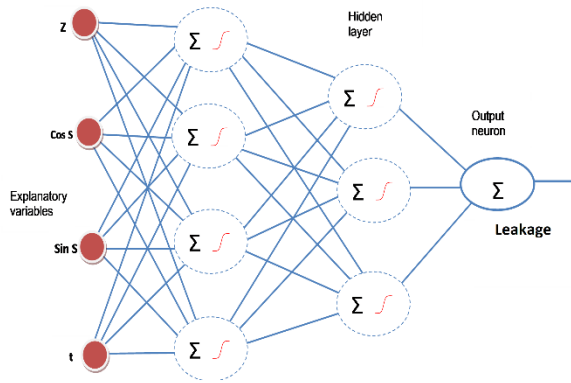
Figure 8: architecture of neural networks

The results show a coefficient of correlation of R^2_{ANN}=0.66 for the case A. This value is higher than the coefficient of correlation of the classical HST. R^2_{HST}=0.56. Since ANN has more parameters than the HST model, it is quite easy for ANN to improve the coefficient of correlation, especially when the initial coefficient we get with a multiple linear regression is low. However, when it comes to analyzing the reversible effects such as the hydrostatic and seasonal effect, it is not easy to interpret those sensitivity studies and understand why ANN has better performance than HST.
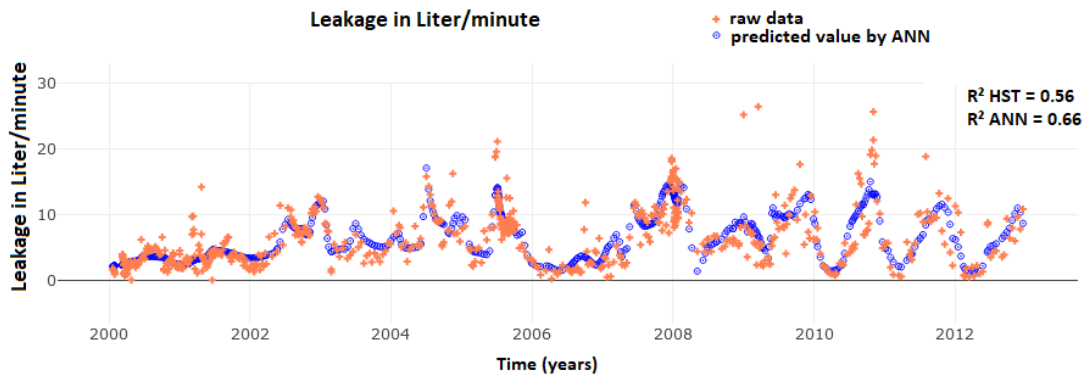

Figure 9. Prediction's performance of the Artificial Neural Networks

We did not try to carry out any short -term or long-term prediction with ANN as sensitivities studies did not reveal a high interpretability of the hydrostatic and seasonal effects. The modelling of leakages still remains a challenge for case B and C, and even for the calibration period A.

2.5 *Warning level*

Warning levels were defined by adding $\pm 2 \cdot \sigma$; σ is the standard deviation of the residuals of the models. This limit is commonly used in dam monitoring, and is rather restrictive, i.e. we assume we get a certain number of false alarms. If we use $\pm 2 \cdot \sigma$ and if residuals follow a gaussian distribution, we know that 5% of measurements will trigger the alarm.

Simon

BEHAVIOR PREDICTION OF A CONCRETE ARCH DAM: DATA-BASED MODELS USED BY THE FORMULATOR OF THE THEME A
IN AN INDUSTRIAL CONTEXT

3 CONCLUSION

The models proposed by the formulator are the models of reference for EDF, i.e., they are used in an industrial context. It does not mean that they should be considered as the reference or the best model for this benchmark.

Thermal HST is used for displacements and its main advantage is that it has a high interpretability of the thermal effects and that it is a relevant tool when predicting future measurements.

Crack opening displacements are analyzed with a nonlinear version of HST, which accounts for the threshold exhibited by measurements when crack is closed. This model calculates seasonal effects that are in accordance with the physical behavior, that is to say that the crack width does not evolve when it is closed at low water level. Reciprocally when the crack is open with high water level, the amplitude of the seasonal effect is at its maximum.

Piezometric levels are influenced by the crack at the upstream toe of the dam, that is why the nonlinear version of HST which is proposed in this article tries to overcome that issue by integrating a term which accounts for the crack-opening. As the crack-opening does not evolve linearly with external loads, the appropriate function for modelling that effect should be nonlinear. By doing so, the calculated effects reflect a higher permeability and consequently higher piezometric levels when the crack is open. This model also clearly highlights the irreversible effect which is not monotonous in this case.

Finally, leakages appear to be the most difficult phenomenon to model. Artificial Neural Networks give satisfactory numerical results, although hydrostatic and seasonal effects seem hardly interpretable. For this reason, we did not try to extrapolate for short-term (case B) and long-term (case C) predictions with that model.

REFERENCES

De Granrut M., 2019, Analyse et interprétation de la pression d'eau en fondation des barrages-voûtes à partir des mesures d'auscultation. Thèse de doctorat, Université Grenoble Alpes

De Granrut M., Simon A., Fabre J., Dias D., Letué F., 2018, Prediction of piezometric levels at the rock concrete interface considering the non linearity of permeability in the foundations, Foz do Iguaçu, Brazil, Dam World conference

Ferry, S. & Willm, G. 1958. Méthodes d'analyse et de surveillance des déplacements observés par le moyen de pendules dans les barrages. In VIth International Congress on Large Dams: 1179-1201. New-York. In French.

Penot I., Fabre J.-P., Daumas B., 2009, Analysis and modelling of the behaviour of civil engineering structures by taking into account air temperature: "Thermal H.S.T." Method. XXIII-ICOLD/CIGB, Q.91-R.60, Brasilia

Simon A., Royer M., Mauris F., and Fabre J., 2013, "Analysis and interpretation of dam measurements using artificial neural networks," European ICOLD.

Willm, G. & Beaujoint, N. 1967. Les méthodes de surveillance des barrages au service de la production hydraulique d'Électricité De France. In IXth International Congress on Large Dams: 529-550. Istanbul. In French.

BEHAVIOR PREDICTION OF A CONCRETE ARCH DAM

Stevcho Mitovski
Faculty of Civil Engineering, Ss. Cyril and Methodius University in Skopje, Skopje, North Macedonia

Gjorgji Kokalanov
Faculty of Civil Engineering, Ss. Cyril and Methodius University in Skopje, Skopje, North Macedonia

Ljupcho Petkovski
Faculty of Civil Engineering, Ss. Cyril and Methodius University in Skopje, Skopje, North Macedonia

Frosina Panovska
Faculty of Civil Engineering, Ss. Cyril and Methodius University in Skopje, Skopje, North Macedonia

Vasko Kokalanov
Faculty of Computer Science, Goce Delchev University, Stip, North Macedonia

ABSTRACT: The assessment of the structural stability and the behavior of the dam during construction and service period is of vital importance. In the paper are presented acknowledgments from the numerical analysis of concrete arch dam under static and hydraulic (seepage) action, by application of Finite Element models (code SOFiSTiK) and Neural Networks models (NeuralTools code). The aim of the task is to predict the dam behavior, that includes calibration (based on monitoring data) and prognosis stage (short-term and long-term) focusing on variables such as radial displacements, crack displacements, piezometric levels and seepage. Coupled thermo-mechanical analysis and seepage analysis in time domain were carried out the for calibration and prognosis stage of the specified variables, in case of FEM modelling. The conclusion from the both numerical experiments (FEM and Neural Networks) is that the dam behavior, with adopted geometry and material, is within the expected mode.

1 INTRODUCTION

The dams, having in consideration their importance, dimensions, complexity of the problems that should be solved during the process of designing and construction along with the environmental impact are lined up in the most complex engineering structures (Tanchev, 2014; Novak & all., 2007). The assessment of the structural stability and the behavior of the dam during construction, at full reservoir and during the service period is of paramount importance for such structures.

Static stability of concrete dams is confirmed with analysis (research) of the response of the structure (dam) under action of static loads (Mitovski & all, 2015, Mitovski & all, 2017a, Mitovski & all, 2017b]. In this paper are systemized acknowledgments from the linear and nonlinear static numerical analysis of concrete arch dam, obtained with application of Finite Element Method models (code SOFiSTiK) and Neural Networks models. Namely, here below will be illustrated output data from the numerical experiment for prediction behavior of the arch dam Dam EDF, located in France. The aim of the task is to predict the dam behavior, that includes calibration (based on monitoring data) and prognosis stage (short-term and long-term) focusing on variable such as radial displacements (two pendulums in central block of the dam), crack displacements (sensor at the rock-concrete interface), piezometric levels (vibrating wire piezometers at the rock-concrete interface) and seepage (weir at the downstream of the dam).

2 CASE STUDY

The analyzed dam is located in southern France, constructed in period 1957-1960. It is a case of double curvature arch dam, with asymmetric shape due to the valley formation (Fig. 1). The dam foundation is laminated metamorphic slate with high compressive strength, with present anisotropy in the left bank. The dam height above the foundation si H=45 m, with crest thickness of 2 m and base thickness of 6 m.
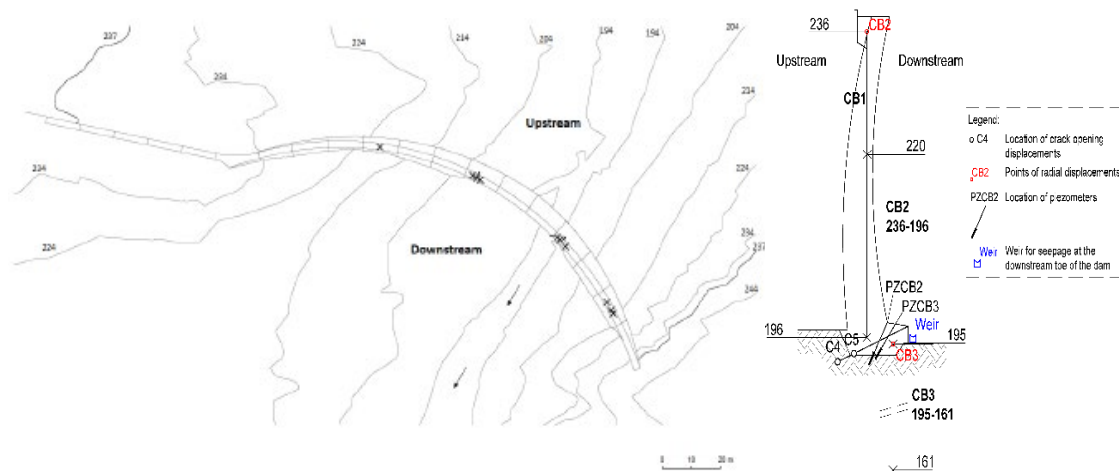

Figure 1. Layout of the dam (left) and central block section with display of monitoring instruments (right).

3 MODELLING OF THE DAM

3.1 *Numerical model of the dam*

The numerical analysis of Dam EDF is carried out by application of program SOFiSTiK, produced in Munich, Germany. The program is based on finite element method and has possibilities for complex modeling of the structures and simulation of their behavior. It also has possibility in the analysis to include certain specific phenomena, important for realistic simulation of dam's behavior, such as: discretization of the dam and foundation taking into account the irregular and complex geometry of the structure, simulation of stage construction, simulation of contact behavior by applying interface elements and etc. in order to assess the dam behavior and

evaluate its stability. The program SOFiSTiK in its library contains and various standards and constitutive laws (linear and non-linear) for structures analysis.

The numerical experiment includes following steps, typical for this type of analysis: (1) choice of material properties and constitutive laws (concrete and rock); (2) discretization of the dam and the rock foundation and (3) simulation of the dam behavior for the typical loading states (as required in the topic formulation).

3.1.1 Material properties

The linear material properties for the dam body (concrete) and the foundation (rock) are systematized in Table 1. The specified parameters are adopted according to Theme A formulation (Malm & all, 2021) as well and previous carried out analysis and reference literature (Desai & Gallagher, 1984, SOFiSTiK, 2022, EC 2, 1992, Mitovski, 2015, USBR, 1977).

Table 1. Material parameters.

Zone		dam body (concrete)	rock	Comment
γ_{spec}	kN/m³	24.0	27.0	Unite weight
k_s	m/s		2.0e-05	Permeability coefficient
v		0.350	0.450	Poisson coefficient
Alpha	1/C°	7.0E-06		Thermal expansion coefficient
E	GPa	22	3	Young's modulus of elasticity

Additionally, for carrying out of non-linear analysis of the dam in order to calibrate and predict the relative distance values at interface dam-foundation is applied non-linear constitutive law for concrete based on elasto-plastic material law Lade with non-associated flow rule from SOFiSTiK library of materials (Table 2).

Table 2. Non-linear material parameters for concrete.

Zone		dam body (concrete)	Comment
γ_{spec}	kN/m³	24.0	Unit weight
v		0.350	Poisson coefficient
Alpha	1/C°	7.0e-06	Thermal expansion coefficient
E	GPa	22	Young's modulus of elasticity
P3	kN/m²	2900	Uniaxial tensile strength
m		1	Parameter for curvature of the yield surface towards the hydrostatic axis
η		88162	Yield function
f_{cd}	kN/m²	33333	Compressive strength
ε_{tu}	‰	0.2	Tensile failure strength

3.1.2 Discretization of dam body and foundation by finite elements

Numerical analysis of the arch dam is carried out by spatial (3D) model, where the dam body and the foundation are modeled with volume elements, by full reproduction of the finite element model formulation data. A powerful and reliable finite element should be applied in case where an analysis of structure with complex geometry and behavior is required, having in consideration that the correctly calculated deformations and stresses are of primary significance for assessment of the dam stability. In this case, for discretization of the dam body and the rock foundation are applied finite element type bric, by 4 nodes, identical to C3D4 element from ABAQUS and kinematic constraints at the interface dam-rock foundation. Namely, the model is composed of dam body and rock foundation with constraints at the interface dam-foundation.

The spatial (3D) model has geometrical boundaries, limited to horizontal and vertical plane. In these planes are defined the boundary condition of the model (Figure 2). The curvature plane in the lowest zone of the model is adopted as non-deformable boundary condition (fixed displacements in XYZ direction), vertical planes perpendicular on X-axis are boundary condition

by applying fixed (zero) displacements in X-direction and vertical planes perpendicular on Y-axis are boundary condition by applying fixed (zero) displacements in Y-direction. The discretization is conveyed by including zones of various materials in the model – concrete and rock foundation. The dam is modeled as monolithic structure.
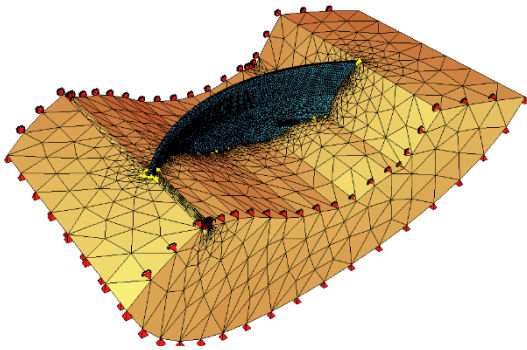

Figure 2: View of the numerical model, discretized with total of 186583 elements and 39419 nodes.

3.1.3 Dam loading scenarios for calibration and prognosis stage

The dam loading is directly correlated with the calibration and prognosis stage for the dam behavior. The numerical analysis is carried out by coupled thermo-mechanical model and hydraulic (seepage) model for analysis of the dam behavior in the calibration and prediction stage. The thermal effect of the dam is simulated by applying temperature loading of the dam body according to air temperature time series as uniform distribution within the volume (bric) elements. The assumption is that the temperature loading in the dam body is uniformly distributed in the various time steps and approximately in range of the air temperature. The temperature effect is coupled with the hydrostatic loading in accordance with the specified water levels from the reservoir for the identical time steps. The hydrostatic loading is applied at upstream face of the dam as spatial load in accordance with the water levels in the reservoir. The calibration process is carried out by combined choice of extreme (highest) values for the air temperature Ta, water levels in the reservoir WL and measured values for the variables records within the monitoring process. The method of adoption of the extreme values per dates for time series of pendulums CB2 means that are chosen maximal and minimal values from the recorded data. Namely, in such a way, by analogy are adopted records for the water levels and temperature, thus obtaining a representative number of load cases in order to assess the dam behavior, that are being run within the model.

Identical approach is applied and for the prognosis stage. Namely, for the short-term prognosis is carried out calculation of the dam response for all time steps from January-June, 2013 (total of 184), while for the long-term prognosis is applied also combined choice of extreme values for period July, 2013-December, 2017, regarding the water levels in the reservoir and temperature Ta, thus obtaining total a representative number of load cases for the various variables with aim to predict the dam's behavior, that are being run within the model. Static loading scenarios includes self-weight of the concrete arch dam and the rock foundation.

3.2 *Neural networks modelling of the dam*

Artificial neural networks are typical example of a modern interdisciplinary subject that helps solving various different engineering problems which could not be solved by the traditional modelling and statistical methods (I. Flood K. N., 1994). Neural networks are capable of collecting, memorizing, analyzing and processing large number of data gained from some experiments or numerical analyses. They are an illustration of sophisticated modelling technique that can be used for solving many complex problems. The trained neural network serves as an analytical tool for qualified prognoses of the results, for any input data which were not included in the learning process of the network. Their operation is reasonably simple and easy, yet correct and precise. The artificial neural networks, together with the fuzzy logic and genetic algorithms, belong to the group of symbolic methods of intelligent calculations and data processing that operate according to the principles of soft computing. Neural networks are developed as a result of the positive

features of a few different research directions: data processing, neuro-biology and physics (I. Flood K. N., 1994). Researches around the world showed that neural networks have an excellent success in prediction of data series and that is why they can be used for creating prognostic models that could solve different problems and tasks (I. Flood K. N., 1994; I. Flood C. P., 1996). For practical application of artificial neural networks, it is not necessary to use complex neuron models. Therefore, the developed models for artificial neurons only remind us to the structure of the biological ones and they have no pretension to copy their real condition (Flood, 1990). The artificial neuron receives the input signals and generates the output signals. Every data from the surrounding or an output from other neurons can be used as an input signal.

As follows, by applying Generalized Regression Neural Network (GRNN) specifically NeuralTools code from Palisade corporation, for data prediction in case of arch dam are shown. The data set used for training is basically values of the given measured data. In the training process, 70% of the data is used for training and 30% is used for validation. The variables are classified as independent or dependent, depending on their role in the prediction process. The dependent variable is the variable to be predicted. The independent variables are the "explanatory" variables used to predict the dependent variable. Cases where the dependent variable values are known are used to train and test a neural network.

The modeling by application of GRNN is based on the following variables: (1) water level in piezometer PZCB2 as dependent numeric value and water level in the reservoir as independent numeric value, (2) water level in piezometer PZCB3 as dependent numeric value and water level in the reservoir as independent numeric value, (3) seepage flow beneath the dam as dependent numeric value and water level in the reservoir as independent numeric value, (4) displacement in pendulum CB2 as dependent numeric value and water level and ambient temperature as independent numeric value, (5) displacement in pendulum CB3 as dependent numeric value and water level and ambient temperature as independent numeric value, and (6) crack opening in C4_C5 as dependent numeric value and water level and ambient temperature as independent numeric value.

4 CALIBRATION PROCESS OF THE DAM

The calibration process includes analysis of variables such as radial displacements (pendulums CB2 and CB3 in the central block of the dam), crack opening displacement (sensor C4-C5 at rock foundation interface), piezometric levels (PZCB2 and PZCB3 at rock-foundation interface) and seepage (weir at the downstream toe of the dam). The required calculated data are derived for corresponding nodes within the numerical model. The calibration process is carried out by comparison of the measured and calculated radial displacements at corresponding nodes for various variables of the FEM model respectively.

4.1 *Calibration of pendulums displacements time series*

By comparison of the radial displacements for pendulum CB2 by FEM analysis (Fig. 4) it can be noticed good matching of the data regarding the distribution and the values. The maximal measured values for pendulum CB2 range in interval from 15.95 mm to -27.48 mm, while the calculated values from 19.5 mm to -22.9 mm. The measured and calculated pendulums displacements time series are generally in correlation with the variation of the water level in the reservoir and air temperature. Namely, at higher water levels in the reservoir the displacements are in downstream direction (the hydrostatic pressure generates greater displacement then the temperature effect), while at lower water levels in the reservoir the displacements are in upstream direction, combined with the temperature effect that generates displacements in upstream direction.

By comparison of the radial displacements for pendulum CB2 by Neural Networks (NN) analysis (Fig. 6) it can be noticed good matching of the data regarding the distribution and the values. In case of radial displacements for pendulum CB3 by Neural Networks analysis (Fig. 5) it can be noticed excellent matching of the data regarding the distribution and the values. The interval of variation of the measured and calculated data for the displacements of pendulum CB2 is (-17.82÷19.41) mm, while the interval in case of pendulum CB3 is (-2.3÷2.3) mm. In analogy of the calculated data by FEM, and here the calculated displacements by Neural Networks models are

in correlation with the variation of the water level in the reservoir and air temperature (Fig. 6 and Fig. 7). Namely, at higher water levels in the reservoir the displacements are in downstream direction (the hydrostatic pressure generates greater displacement then the temperature effect), while at lower water levels in the reservoir the displacements are in upstream direction, by influence of the temperature effect that generates displacements in upstream direction.
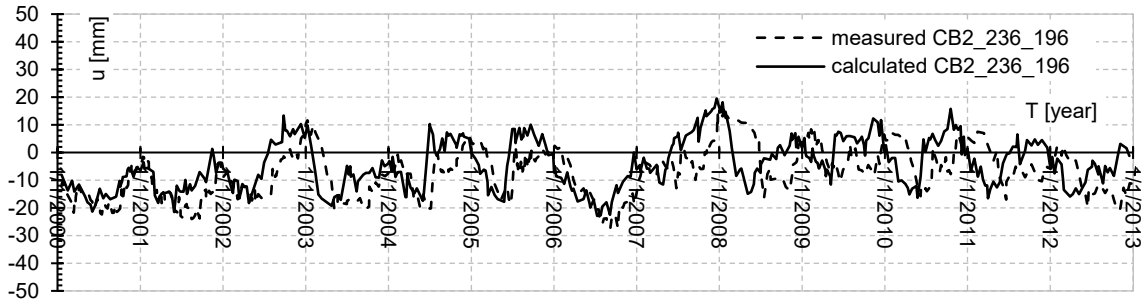
Figure 4. Display of measured and calculated time series of CB2 pendulums displacements for 2000-2012.
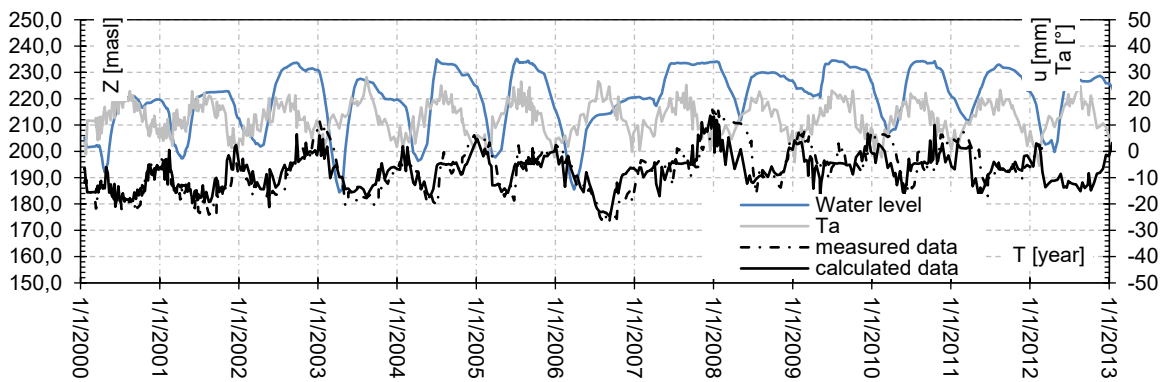
Figure 6. Display of measured and calculated time series of CB2 pendulums displacements for 2000-2012.
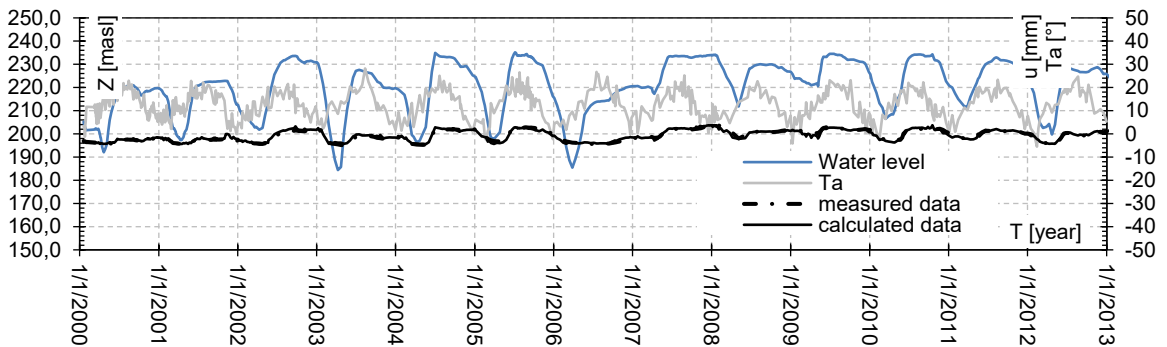
Figure 7. Display of measured and calculated time series of CB3 pendulums displacements for 2000-2012.

4.2 *Calibration of crack opening time series*

The calibration process for the crack opening displacements is carried out by numerical model with nonlinear constitutive law for concrete (Table 2). The calculated radial displacements as deduction of the radial displacements in the corresponding nodes are projected to sensor C4-C5 direction in order to obtain the variation values for the relative distance. On Fig. 8 are displayed calculated and measured relative distance for displacements in direction of the sensor C4-C5. It can be noticed that in general there is a similar distribution of the values for the calibration period, however there is a less good matching of the calculated and measured values. Namely, the calculated relative distance values are mainly lower them the measured values. The reason for such lower degree of matching of the values can be the stiff coupling condition at interface dam-foundation, modeled as kinematic constraint in the model. So a potential case to be investigated

is to model the contact dam-foundation by interface elements (with both linear and non-linear properties) combined with the variation of the stiffness properties of the rock (in central part and the banks) in order to improve the calibration process.

The measured and calculated values are mainly in reverse correlation with the water level in the reservoir apropos in period when the water level is low there is increase of the relative distance (positive values) while in period of higher water levels there is a decrease (negative values). Regarding the temperature, the displacement manifest more variable behavior apropos the applied temperature effect has lower influence the water level in the reservoir. The maximal measured relative distance values range in interval (2.17 ÷ -2.43) mm, while the calculated values vary in range (0.56 ÷ -0.65) mm.
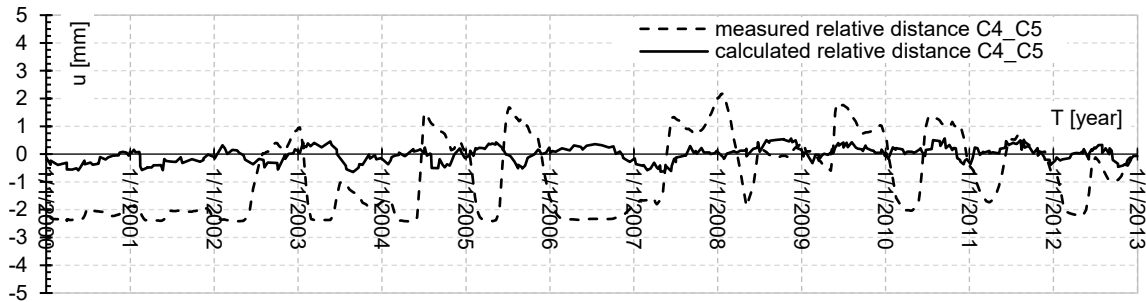
Figure 8. Display of calculated and measured time series of crack openings at sensor C4-C5 for 2000-2012.

On Fig. 9 are displayed calculated and measured data for the relative distance for displacements in direction of the sensor C4-C5 by applying Neural Networks model. An excellent matching for the distribution and the calculated values is obtained. This can be confirmed by the interval of variation of the measured and calculated data for the relative crack displacements of sensor C4-C5, in interval of (-1.8÷2.4) mm. In opposite of the calculated data by FEM for sensor C4-C5, here the calculated relative crack displacements by Neural Networks models are in correlation with the variation of the water level in the reservoir and air temperature (Fig. 9). Namely, at higher water levels in the reservoir there is decrease of the relative crack displacements (negative values), while at low water levels there is increase of the relative crack displacements (positive values).
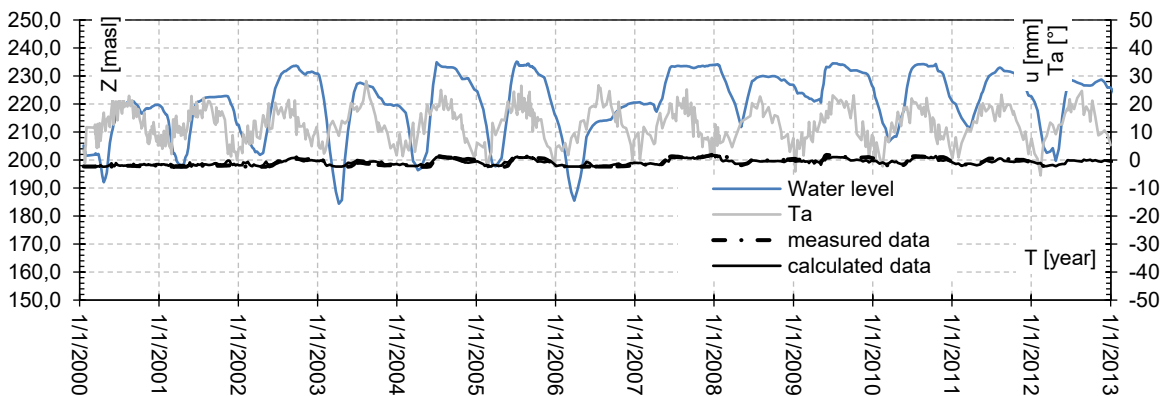
Figure 9. Display of calculated and measured time series of crack openings at sensor C4-C5 for 2000-2012.

4.3   *Calibration of piezometric levels and seepage time series*

The calibration process is carried out by plane (2D) numerical model for seepage analysis by modelling the foundation medium below the central block of the dam including running of load cases for full timeline period 2000-2012, and subsequent comparison of the measured and calculated piezometric levels at corresponding nodes for piezometers PZBC2 and PZBC3. The calculated piezometric levels are obtained by the values of the equipotential lines (H).

Numerical analysis of seepage flow in the foundation of the arch dam is carried out by plane (2D) model, where foundation with included grout curtain is modeled with plane elements. For

discretization of the dam body and the rock foundation is applied quadrilateral finite element, by 4 nodes. Namely, the model is composed of the rock foundation with included zone of grout curtain. The plane (2D) model has geometrical boundaries, limited to horizontal and vertical plane (Fig. 3), adopted according to the specified data [Malm & all, 2021]. The discretization is conveyed by including zones of various hydraulic parameters in the model – rock foundation and grout curtain, approximately modelling the rock foundation per 75m upstream and downstream of the dam.

However, the hydraulic properties for the material in the rock foundation were not available. So, the first step is to calibrate the value for the permeability coefficient k in accordance with the seepage values from the monitoring process for homogeneous rock foundation. The estimated permeability coefficient for laminated metamorphic slate ranges in interval $k=(10^{-7} \div 10^{-9})$m/s [Lianyang, 2016, Fell et all, 2015]. The permeability coefficient additionally is calibrated by the value of the full seepage flow directly below the dam, specified as measured values in weir at gallery located at the downstream toe of the dam. So, according to the available measuring data for water level at 232.0 m the average registered seepage flow is 8 l/min. From the registered reservoir water levels and seepage flow it can be noticed general correlation, however in some periods there is discrepancy in the measured values that could be indication that the seepage flow is caused by additional influences then the seepage process in the rock foundation. The seepage analysis was carried out for H=232.0 m as upstream boundary condition and H=0 m as downstream boundary condition, by applying Darcy flow rule adopting the rock foundation as heterogeneous flow medium, composed of rock material (laminated metamorphic slate) and two sections (vertical and inclined) of grout curtain, by assumed permeability coefficient in first iteration $k_{rf}=1\times10^{-7}$ m/s for the rock zone.

By the initial calibration calculation of the permeability coefficient for homogeneous rock foundation was obtained value of $k=2.89\times10^{-8}$ m/s, applied in the calculation for the full calibration and prognosis analysis of the piezometric levels and seepage. Due to the grout curtain in the rock foundation (heterogeneous zone), additional calibration were carried out, in order to match the measured seepage flow $Q_m=8$ l/min and thus obtaining value of permeability coefficient for the rock foundation $k_{rf}=12.5\times10^{-8}$ m/s and permeability coefficient for the grout curtain $k_{gc}=2.5\times10^{-8}$ m/s, used as input parameters for the seepage calibration and prognosis stage.

By comparison of the calculated and measure seepage values (Fig. 10) it can be noticed good matching of the registered and calculated seepage flow data regarding the distribution and the values. Also, there is good matching apropos correlation of the registered reservoir water levels and registered and calculated seepage flow. The measured peak values of the seepage flow occur are approximately at normal water level so this may be indication for additional leakage occurrences that affect the seepage process. The measured seepage flow varies in interval (0.01÷ 26.5) l/min, while the calculated values in interval (0.001 ÷ 18) l/min. However, the occurred peak values of the seepage flow (especially in 2009) required additional explanation and research due to the very high values at approximately constant water level in the reservoir. Namely, they could occur due to another reason such as seepage zone in the dam or zones in the rock foundation that have higher permeability than the presumed. Additional calibration should include modelling of eventual more permeable zones in the rock foundation and more precise calibration of the permeability coefficient of the grout curtain.
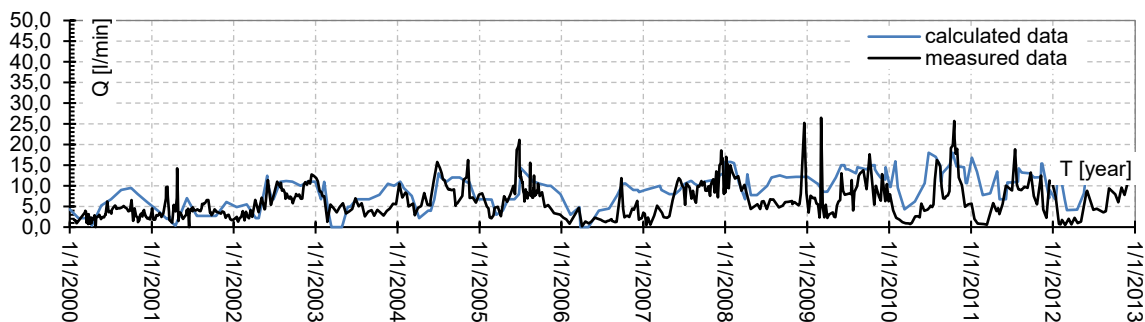

Figure 10. Display of measured and calculated seepage flow time series for period 2000-2012 by FEM.

By comparison of the piezometric levels for piezometers PZCB2, calculated by NN model (Fig. 11) it can be noticed excellent matching of the measured and calculated data regarding the distribution and the values. This can be confirmed by the interval of variation of the measured and calculated data for the piezometric levels for piezometer PZCB2, ranging in interval of (-3.6÷2.9) masl. The calculated piezometric levels by NN model, in analogy of the calculated values from the FEM model for seepage analysis, are in correlation with the reservoir water level.

By comparison of the measured and calculated seepage flow values, obtained by the NN model (Fig. 12), it can be noticed not so good matching of the data regarding the distribution and the values. The calculated values are in some period lower than the measured values while in some periods are higher. The maximal measured seepage flow varies in interval (0.01 ÷ 26.5) l/min, while the calculated values in interval (0.37 ÷ 11.9) l/min. The interval of variation of the measured and calculated data for the seepage flow is ranging in interval (-6.6÷21.6) l/min.
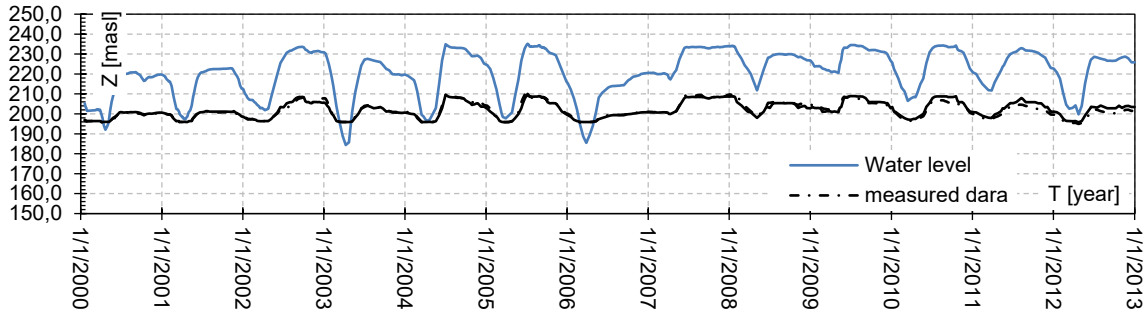
Figure 11. Display of measured and calculated piezometric levels for PZCB2 for period 2000-2012 by NN.
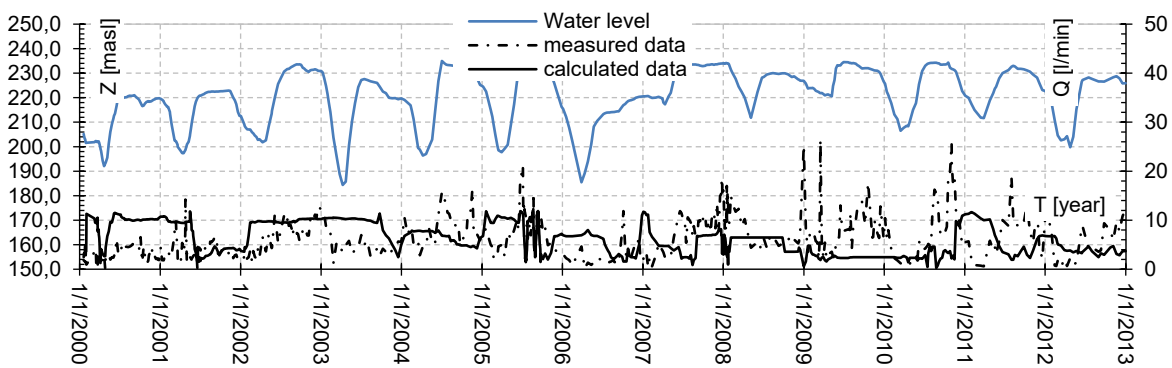
Figure 12. Display of measured and calculated seepage flow time series for period 2000-2012 by NN.

5 PREDICTION (PROGNOSIS) PROCESS OF THE DAM

5.1 *Prognosis of pendulums displacements time series*

The prognosis stage consists of short-term and long-term prediction of the specified variables. Namely, the short-term prediction includes period January, 2013-June, 2013, while the long-term prediction captures period July, 2013-December, 2017. The prognosis process is carried out by numerical model including running of full time steps for the time series within the short-term period. The prognosis process for the long-term behavior is carried out by numerical model including running of appropriate representative load cases for the time series.

The calculated displacements for pendulum CB2 (Fig. 13), calculated by FEM model, for the short-term prognosis are mainly in upstream direction, maximal value of -16.3 mm, while the maximal displacement in the downstream direction is 1.75 mm. The calculated displacements for pendulum CB3 for short-term period are mainly in downstream direction, with maximal value of 1.7 mm and maximal value of -0.3 mm in downstream direction. The calculated values for pendulum CB2 are in correlation with the water level apropos the lowering of the water level within the short-term period is dominant factor that enables modus for manifestation of the displacements in the upstream direction while the applied temperature effect has lower influence

on the displacements. In case of pendulum CB3 the lowered water level and temperature does not generate significant variation of the displacements values.

The calculated displacements for pendulum CB2 (Fig. 13), calculated by FEM model, for the long-term prognosis are also mainly in upstream direction, maximal value of -24.6 mm, while the maximal displacement in the downstream direction is 10.5 mm. The calculated displacements for pendulum CB3 for the long-term period are mainly in downstream direction, with maximal value of 2 mm and maximal value of -0.55 mm in downstream direction. The calculated values for pendulum CB2 are mainly in correlation with the water level apropos the lowered water level within the long-term period is contributing factor that enables modus for manifestation of the displacements in the upstream direction while the applied temperature effect has lower influence on the displacements. In case of pendulum CB3 the lowered water level and temperature does not generate significant variation of the displacements values.

The calculated displacements for pendulum CB3 (Fig. 14), calculated by NN, for the short-term prognosis are mainly in upstream direction, maximal value of -4.3 mm, while the maximal displacement in the downstream direction is 1.4 mm. The calculated values for pendulum CB3 are mainly in correlation with the water level apropos the lowering of the water level within the short-term period is dominant factor that enables modus for manifestation of the displacements in the upstream direction while the applied temperature effect has lower influence on the displacements. The calculated displacements for pendulum CB3 (Fig. 14), by NN model, for the long-term prognosis are also mainly in upstream direction, maximal value of -4.5 mm, while the maximal displacement in the downstream direction is 1.6 mm. The calculated values for pendulum CB3 are mainly in correlation with the water level apropos the lowered water level within the long-term period is contributing factor that enables modus for manifestation of the displacements in the upstream direction while the applied temperature effect has lower influence on the displacements. In case of pendulum CB3 the lowered water level and temperature does not generate significant variation of the displacements values.
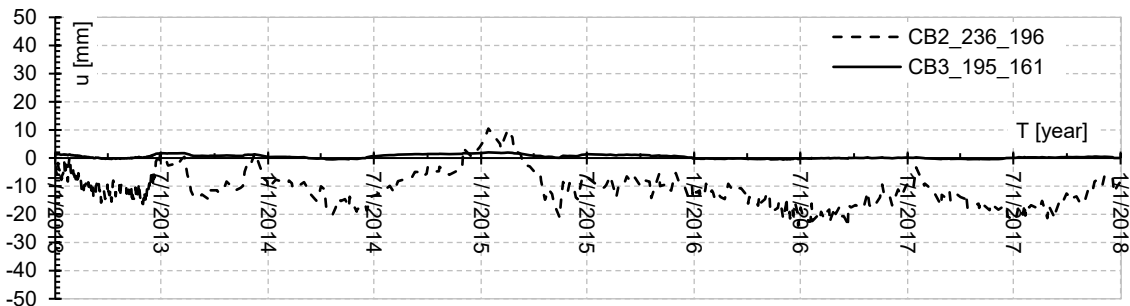

Figure 13. Display of calculated prognosis time series of pendulum CB2 and CB3 displacements for 2013-2017 by FEM.
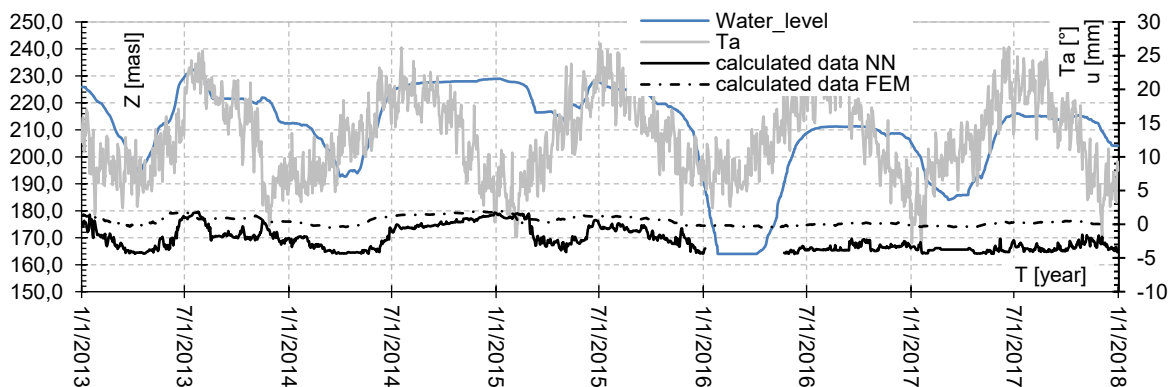

Figure 14. Display of calculated prognosis time series of pendulum CB3 displacements for period 2013-2017 by FEM and NN.

5.2 *Prognosis of crack opening time series*

The prognosis process is carried out by numerical model including running of full time steps for the time series within the short-term period. The prognosis process for the long-term behavior is carried out by numerical model including running of appropriate representative load cases for the time series. The calculated relative distance for the short-term prognosis at sensor C4-C5 are varying from increase (positive values) to decrease (negative) values (Fig. 15). The maximal calculated values are -0.5 mm and 0.3 mm respectively. The calculated values are in correlation with the water level apropos at higher water level the crack displacements are increasing while at lowered water level they are decreasing. Very similar case is also with the applied temperature effect apropos lowering of the temperature in the short-term period lowers the crack displacements. The calculated relative distance for the long-term prognosis at sensor C4-C5 are less varying from increase (positive values) and decrease (negative) values apropos mainly manifest decrease of the crack openings. The maximal calculated values are -0.72 mm and 0.56 mm respectively. The calculated values are in correlation with the water level apropos at longer period of higher water level the crack displacements are increasing while at lowered water level they are decreasing. Very similar case is also with the applied temperature effect apropos lowering of the temperature in the long-term period lowers the crack displacements.

The prognosis process is carried also out by Neural Networks model for the time series within the short-term and the long-term. The calculated relative distance for the short-term prognosis at sensor C4-C5, calculated by NN model, are varying mainly to decrease (negative) values (Fig. 16). The maximal calculated values are -2.5 mm and 0.1 mm respectively. The calculated values are in correlation with the water level apropos at higher water level the crack displacements are increasing while at lowered water level they are decreasing. Very similar case is also with the applied temperature effect apropos lowering of the temperature in the short-term period lowers the crack displacements. The calculated relative distance for the long-term prognosis at sensor C4-C5, by NN model, are also mainly decrease zone (negative) values apropos mainly manifest decrease of the crack openings. The maximal calculated values are -2.35 mm and 0.1 mm respectively. The calculated values are in correlation with the water level apropos at longer period of higher water level the crack displacements are increasing while at lowered water level they are decreasing. Very similar case is also with the applied temperature effect apropos lowering of the temperature in the long-term period lowers the crack displacements.
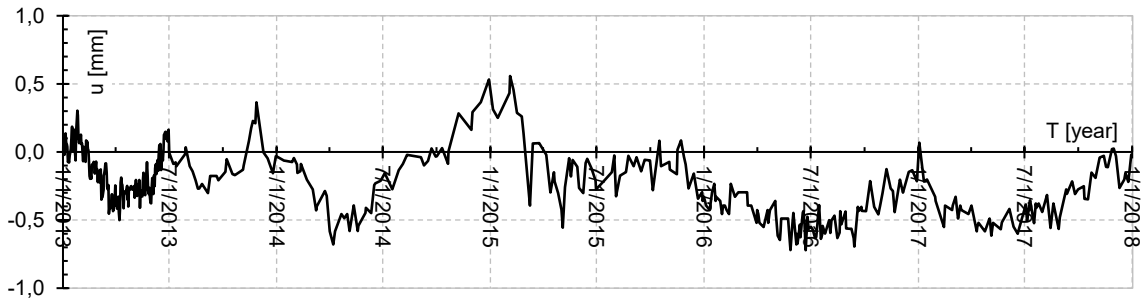

Figure 15. Prognosis calculated time series of C4-C5 relative distance for period 2013-2017 by FEM.
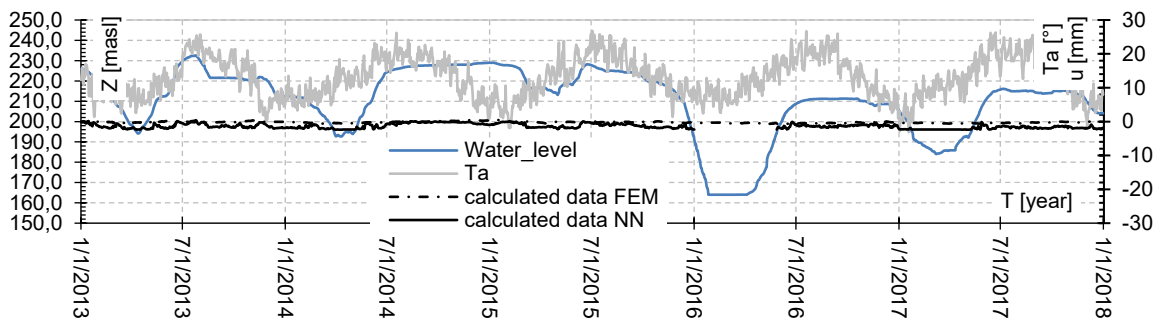

Figure 16. Prognosis calculated time series of C4-C5 relative distance for 2013-2017.

5.3 *Prognosis of piezometric levels time series*

The prognosis process for piezometric levels for PZCB2 is carried out by NN numerical model for seepage analysis. The calculated piezometric levels for piezometer PZCB2 for the short-term and long term prognosis, as expected, are varying in correlation with the water level in the reservoir (Fig. 17). The maximal and minimal calculated values for the piezometric levels are respectively 205.5 m and 195.5 m.
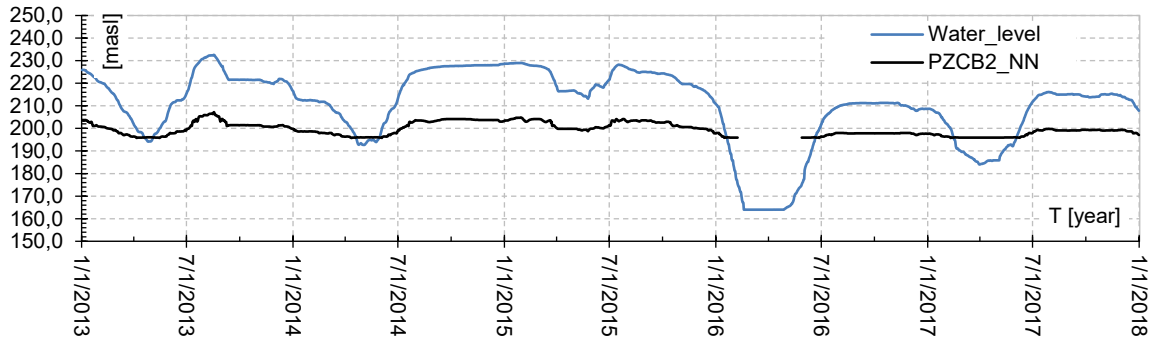

Figure 17. Prognosis calculated time series of piezometric levels for PZCB2 for 2013-2017 by NN model.

5.4 *Prognosis of seepage time series*

The calculated seepage flows for the short-term and long term prognosis, calculated by FEM model, as expected, are varying in correlation with the water level in the reservoir (Fig. 18). The maximal and minimal calculated values for the seepage flow are respectively 3.34 l/min m and 0.06 l/min. The calculated seepage flows for the short-term and long term prognosis, calculated by NN model, as expected, are varying in correlation with the water level in the reservoir (Fig. 19). The maximal and minimal calculated values for the seepage flow are respectively 11 l/min m and 0.1 l/min.
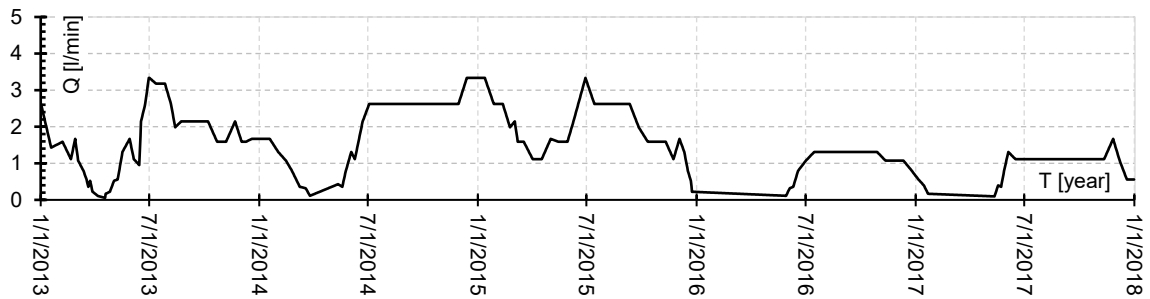
Figure 18. Prognosis calculated time series of seepage flow for Jan,2013-Dec,2017 by FEM model.
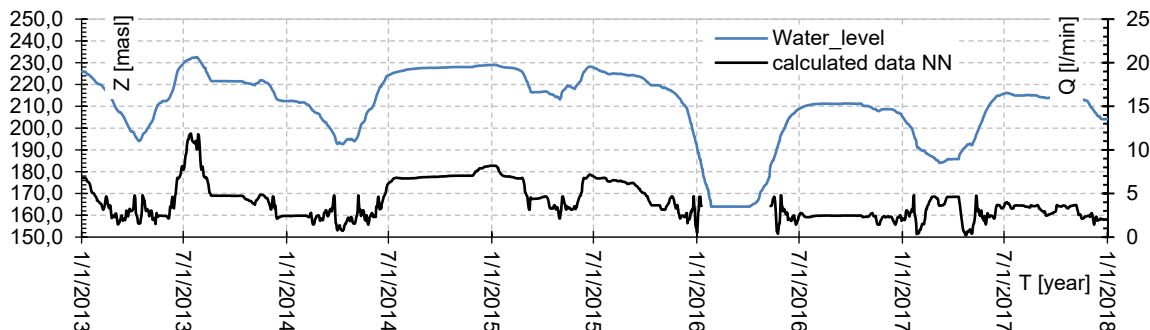
Figure 19. Prognosis calculated time series of seepage flow for Jan,2013-Dec,2017 by NN model.

6 CONCLUSIONS

The behavior of the dam during the service period for variation of the water levels in the reservoir and temperature effect was simulated by application of the Finite Element Method with spatial (3D) numerical model and Neural Networks model. The numerical analysis was carried out by taking in consideration the specified data for the numerical model (fully reproduced according to the formulation data) and variations of the water level in the reservoir and the air temperature, by applying coupled thermo-mechanical analysis of the dam in static conditions. The loading scenarios for calculation of the required variables were adopted according to the extreme values for the available monitoring records of the variables and records for reservoir water levels and air temperature by coupled thermo-mechanical analysis of the dam and hydraulic analysis of the seepage process.

The prediction of the behavior of the dam was analyzed in two stages – calibration and prognosis stage. From the carried out numerical experiment by FEM model for calibration and prediction of the behavior of the dam EDF, following conclusions and recommendations are derived:

(1) The calibration process of the measured and calculated radial displacements for pendulum CB2 provided good matching of the data regarding the distribution and the values. In case of pendulum CB3 a good matching of the data regarding the distribution and some less good matching od the data regarding the values is obtained.

(2) The calibration process for the relative distance C4-C5, in general, has a good matching of the distribution of the values, however there is a difference in the calculated and measured values (the calculated relative distance values are mainly lower them the measured). The measured and calculated values are mainly in reverse correlation with the water level in the reservoir apropos in period when the water level is low there is increase of the crack opening (positive values) while in period of higher water levels there is a decrease (negative values). Regarding the temperature, the displacements manifest less variable behavior apropos the applied temperature has lower influence on the displacements.

(3) By comparison of the calculated and measured piezometric levels for piezometers PZCB2 and PZCB3 as well and the seepage flow is obtained good matching of the records regarding the distribution and less good matching regarding the values.

(4) The calculated displacements for pendulum CB2 prognosis period are mainly in upstream direction, while the calculated displacements for pendulum CB3 are mainly in downstream direction. The calculated values for pendulum CB2 are mainly in correlation with the water level apropos the lowered water level while the applied temperature effect has lower influence on the displacements. In case of pendulum CB3 the lowered water level and temperature does not generate significant variation of the displacements values.

(5) The calculated relative distance for the prognosis period at sensor C4-C5 are varying from increase (positive values) to mainly decrease (negative) values. The calculated values are in correlation with the water level apropos at higher water level the crack displacements are increasing while at lowered water level they are decreasing. Very similar case is also with the applied temperature effect apropos lowering of the temperature in the short-term period lowers the relative distance C4-C5.

(6) The calculated piezometric levels for piezometer PZCB2, PZCB3 and seepage flow data for short and long term prognosis stage, are varying in correlation with the reservoir water level.

(7) Improved calibration should be carried out apropos the case to be analyzed is to model the contact dam-foundation by interface elements (by linear and non-linear properties) combined with the variation of the stiffness properties of the rock (in central part and the banks).

The prediction of the behavior of the dam was analyzed in two stages – calibration and prognosis stage. From the carried out numerical experiment by NN model for calibration and prediction of the behavior of the dam EDF, following conclusions and recommendations are derived:

(1) The calibration process of the measured and calculated radial displacements for pendulum CB2 provided relatively good matching of the data regarding the distribution and the values. In case of pendulum CB3 a very good matching of the data regarding the distribution and the values was obtained.

(2) The calibration process for the relative distance C4-C5,in general provided excellent matching of the distribution and the values. The calculated values are in correlation with the reservoir water level and the temperature.

(3) By comparison of the calculated and measured piezometric levels for piezometers PZCB2 and PZCB3 is obtained very good matching of the records regarding the distribution and the values. In case of the seepage flow less good matching of the data regarding the distribution and the values was obtained.

(4) The calculated displacements for pendulum CB2 and CB3 prognosis period are mainly in upstream direction. The calculated values for pendulum CB2 and CB3 are mainly in correlation with the water level apropos.

(5) The calculated relative distance for the prognosis period at sensor C4-C5 are varying mainly to decrease (negative) values of crack openings.

(6) The calculated piezometric levels for piezometer PZCB2 and PZCB3 and seepage flow for the short-term and long term prognosis, are varying in correlation with the water level in the reservoir.

(7) The overall behavior of the concrete arch dam, taking in consideration the findings from the calibration and the prognosis stage, is within the expected mode for such structure.

(8) According to the measured and calculated values for the variables by NN model, warning levels corridors are defined by applying criteria of 3×σ, where σ is standard deviation of absolute error, generated by the NeuralTools code.

(9) General conclusion can be drawn out for the analysis task that Neural Network model provided improved matching of the calculated vs measured data for all variables compared with the FEM model.

(10) The conclusion from the both numerical experiments (FEM and Neural Networks) is that the dam behavior, with adopted geometry and material, is within the expected mode.

REFERENCES

Flood, I. (1990). Simulating the construction process using neural networks. Proceedings of the 7th ISARC - International association for Automation and Robotics in Construction. Bristol.

Flood, I. C. P. (1996). Modeling construction processes using artificial neural networks. Automation in Construction, 4(4), 307-320.

Flood, I. K. N. (1994). Neural networks in civil engineering II: Systems and application. Computing in Civil Engineering.

Malm. R. & all, 2021. Theme A, Formulation, 16th International Benchmark Workshop on Numerical Analysis of Dams, Ljubljana, Slovenia.

Mitovski S., 2015a. PhD thesis, Static analysis of concrete dams by modeling of the structural joints, Ss Cyril and Methodius University in Skopje, Civil Engineering Faculty

Mitovski S., Dimov L., Petkovski L., 2017b. "Comparison of calculated and survey monitoring displacements for St. Petka dam", Scientific Journal of Civil Engineering (ISSN-1857-839X), Volume 6, Issue 2.

Mitovski S., Kokalanov G., Petkovski L., 2017a. Numerical analysis on St. Petka dam, 4th Congress on dams, Struga, N. Macedonia.

Mitovski S., Kokalanov G., Petkovski L., Tancev L. and Veleski G., 2017b. "Static and seismic analysis of an arch-gravity dam" 14th ICOLD International Benchmark Workshop on Numerical Analysis of Dams, Stockholm, Sweden.

Mitovski S., Petkovski L., Kokalanov G., 2015b. Safety evaluation of an arch dam by calibrating numerical models and monitoring data, SMAR2015 – Third Conference on Smart Monitoring, Assessment and Rehabilitation of Civil Structures, Antalya, Turkey.

Novak P. et all, 2007. "Hydraulic structures", Taylor & Francis Group, London.

P.V. Lade, 1984. Failure Criterion for Frictional Materials in Mechanics of Engineering Materials, Chap 20 (C.s.Desai,R.H.Gallagher ed.) Wiley & Sons.

Robbin Fell, Patrick MacGregor, David Stapledon, Graeme Bell, Mark Foster. (2015). Geotechnical engineering of dams. London, UK: CRC Press Taylor & Francis Group.

SOFiSTiK Manual, 2022.

Tanchev L., 2014. Dams and appurtenant hydraulic structures, Second edition, A.A. Balkema Publ., CRC press, Taylor & Francis Group plc, London, UK.

USBR, 1977. Design of arch dams,

Zhang Lianyang, 2016. Engineering properties of rocks, Elsevier Ge-Engineering Book Series, Series Editor John A. Hudson, Vol. 4.

DISPLACEMENTS PREDICTION OF AN ARCH DAM: LSTM VERSUS HST MODELS

Nathalie Rosin-Corre
Tractebel Engineering, Lyon/Gennevilliers, France

Christine Noret
Tractebel Engineering, Lyon/Gennevilliers, France

ABSTRACT: The readings of the upper and lower pendulums of the central block of an arch dam have been analysed for the 2000-2012 period in order to predict the deflections which occurred in the following years 2013-2017. Data-based models using Machine Learning methods have been preferred to structural analyses for this prediction because all conditions were optimal for their use (large experimental period, few non-cyclic delayed effects, no major non-linear behaviour expected).

Preliminary models for both time series based on the Hydrostatic-Seasonal-Time (HST) statistical method were prepared with CONDOR-C software, developed by Tractebel. These models showed that the deflections readings had no time drift. Then the model for the deflections measured by the upper pendulum between the crest and the toe has been enhanced by taking into account the air temperature using the Hydrostatic-Seasonal-Time-Temperature (HST-T) statistical method. Logically the model for the deflections measured by the lower pendulum between the toe and the foundation was not significantly enhanced.

Both time series have then been analyzed with models based on Machine Learning methods on a web platform developed by Tractebel. Whereas the models based on the Support Vector Regression and the Random Forest methods could not accurately follow the readings over the validation period, the models based on the Long Short-Term Memory method (Recurrent Neural Network) proved more efficient. They provided a prediction with an expected average accuracy of ± 2.5 mm for the readings of the upper pendulum and of ± 0.5 mm for the readings of the lower pendulum. The results compared well with HST/HSST models and were deemed more realistic when an extrapolation was needed.

1 INTRODUCTION

The objective of the present exercise is to predict the movements of an arch dam measured by pendulums CB2 and CB3 in the central block from 2013 to 2017, starting from observations accumulated during 2000-2012. For such purpose, two main methods are applicable: the structural, so-called 'deterministic' method, and the data-based one. Conditions prevailing for the subject are especially favourable to data-based analyses, since delayed effects are likely to be small. For this reason, the Authors decided to support their contribution upon data-based analyses.

Preliminary models for both time series based on the Hydrostatic-Seasonal-Time (HST) statistical method were prepared with CONDOR-C software, developed by Tractebel. These models showed that the deflections readings had no time drift. Then the model for the deflections of the upper pendulum (measured between the crest and the toe) has been enhanced by considering the air temperature. The model has been prepared with the Hydrostatic-Seasonal-Time-Temperature (HST-T) statistical method. Logically the model for the deflections measured by the lower pendulum (displacement between the toe and the foundation) was not significantly enhanced using the HST-T method.

The time series have then been analyzed with models based on Machine Learning methods on a web platform developed by Tractebel based on Support Vector Regression methods, Random Forest methods and Recurrent Neural Network methods whose results have been compared with those of HST/HST-T models.

2 PREPARATION OF THE DATA-BASED ANALYSIS

2.1 *Preparation of Databases*

Two databases have been prepared:
- One dedicated to Condor-C has been prepared including the main characteristics of the dam (crest level, height, date of impoundment) and with the readings extracted from the file ThemeA_data_fmt03.xlsx provided by the Formulator for the pendulums CB2 and CB3 in the central block of the dam.
- One dedicated to Tractebel Machine Learning Web Platform with the readings extracted from the file ThemeA_data_fmt03.xlsx provided by the Formulator with the special formatting required by the platform (cleaning of dates without water level or readings, time series for training and prediction on the last column of the Excel file). The characteristics of the dam have not been specified.

Statistical models have then been prepared with Condor-C for temperatures and water levels.

The attention has been called upon two special aspects which are discussed below. No abnormal reading or interpolated value (Tb temperatures) has been detected on these variables for the period 1995-2017.

2.2 *Seasonal variations of the reservoir level*

The reservoir level follows rather well a cyclic yearly variation (Figure 1), however the coupling with the season is imperfect with an explanation coefficient of only 0.25.

A rather good independence of hydrostatic ("H") and seasonal ("S") functions is therefore expected which is a favourable factor for the use of HST/HST-T models.

From 1995 to 2012 the reservoir has been operated between the normal water level and the minimum operating level, i.e. within the range 237 m – 174 m in the reference system given by the Formulator, and more precisely between 235.145 m and 181.89 m. This range is still valid from 2000 to 2012, a period when the deflections of the dam are known.

From 2013 to 2015 the reservoir levels have stayed within this range with yearly variations rather close to the ones known from 1995 to 2012.

The reservoir levels have been quite different in 2016 and 2017 as the reservoir was totally emptied in the first quarter of 2016 (down to 164 m) and as the yearly maximum reservoir levels stayed below those known before the full drawdown.
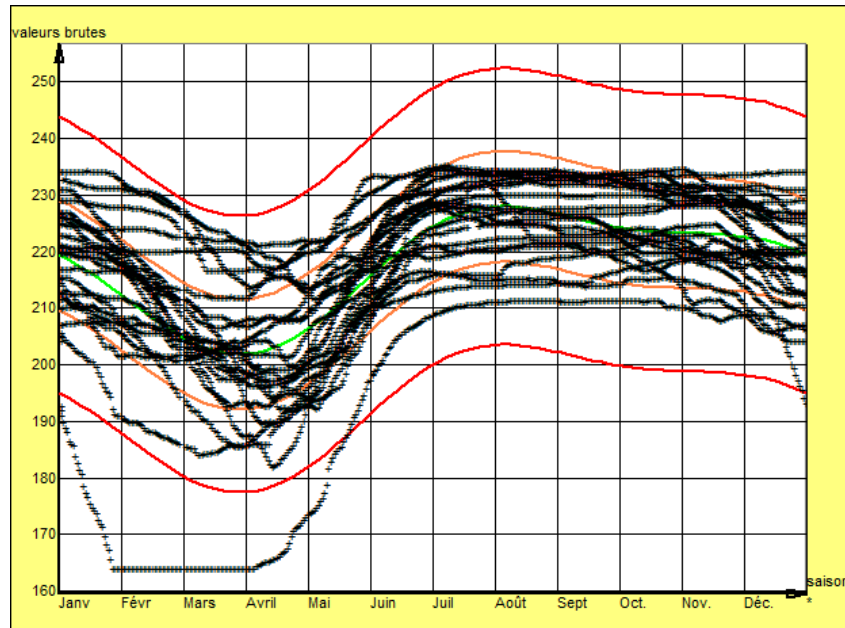
Figure 1. Yearly variations of reservoir level – 1995-2017.

2.3 *Seasonal variations of temperature values and selection of temperature time series*

The Formulator provided two time series of daily air temperatures from 1995 to 2017: Ta measured within 50 km from the dam but at a different altitude and Tb interpolated from several stations and reflecting the altitude of the dam.

Both time series show as expected similar seasonal variations with no time drift between them.

The standard deviation is roughly the same for both time series (respectively 6.24°c and 6.14°C) but the median value is lower for Tb (4.45°C for Tb compared to 12.60°C for Ta) as well as the minimum value (-15.5°C for Tb compared to -8.3°C for Ta) and the maximum value (20.5°C for Ta compared to 29.55°C for Tb). Tb values have been assumed to be more representative of the air temperature at the dam location and thus more likely to influence the pendulums readings variations and particularly the upper one.
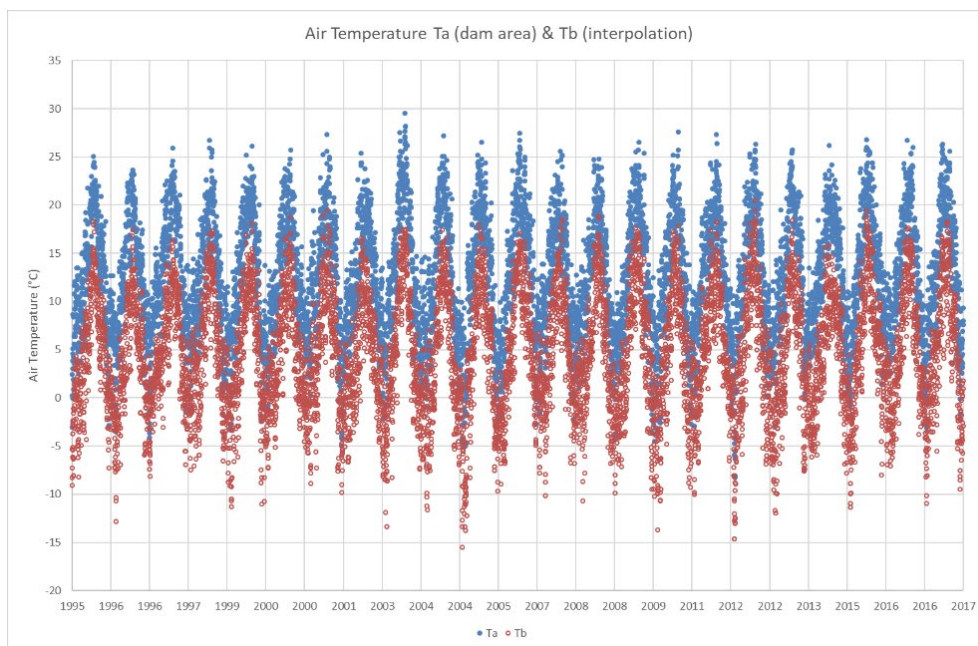
Figure 2. Variations of Air Temperature versus time – 1995-2017.

3 PREPARATION OF THE DATA-BASED MODELS

3.1 *HST and HST-T Models*

The HST models, classically used for the analysis of the monitoring data of dams, are multiple linear regression models which assume that the response of the dam is a sum of the responses to hydrostatic ("H") and thermal loadings ("S") (reversible effects) and in addition to time ("T") (irreversible effects). The HST method has been improved by considering the deviations of observed temperatures to seasonal variations with a time lag is called HST-T (Penot, 2009).

$$\text{Reading} = \text{constant} + f(Z) + f(S) + f(T) + f(\theta) + \varepsilon$$

The coefficients of the functions of Z, S, T and θ are determined by multiple linear regression.

Several models have been prepared successively for CB2 and CB3 readings, until reaching a prediction considered optimal. Results have been evaluated on the basis of the residual variation coefficient, which quantifies the average difference between the predicted values and the readings. All models are based on the observations available between 01/01/2000 and 31/12/2012, that is 689 observations for CB2 and 682 observations for CB3.

- For both CB2 and CB3 models the default model automatically calculated by the software has discarded insignificant functions and the time effect functions: time step function, time-drift function T and drift reduction function Exp.(-T).
- For CB2 model the software has kept three "H" functions (Z, Z², Z3) and all four seasonal "S" functions (SinS, 1-CosS, Sin²S and SinS × CosS). The residual standard deviation is 2.5 mm which corresponds to an explanation coefficient as high as 73.5 percent.
- For CB3 model the software has kept three "H" functions (Z, Z3, Z4) and all four seasonal "S" functions (SinS, CosS, Sin²S and SinS × CosS). The residual standard deviation is 0.5 mm which corresponds to an explanation coefficient as high as 80.7 percent.
- Since H functions are used to simulate the effect of hydrostatic pressure on the upstream face of the dam, we capped the water levels below the dam foundation to 194.

A second model has been prepared for CB2 and CB3 with the influence of the air temperature Tb with a thermal inertia. The "H" and "S" functions are the same (and the "T" functions are still discarded). The CB2 model shows a better adjustment with a higher explanation coefficient (78.4 percent). The influence of the hydrostatic effect is slightly lower and the seasonal effect is slightly higher. The CB3 model does not show any better adjustment as the displacements of the toe of the dam are not significantly influenced by the short-term variations of the air temperature.

- The main features of the CB2 model with Tb influence and CB3 model without Tb influence are provided below and illustrated by Figure 3 and Figure 4:
- The residual standard deviation is reduced to 2.0 mm for CB2 and is 0.5 mm for CB3,
- The corresponding explanation coefficients are higher than 70 percent, which is a good result: 78.4 percent for CB2 and 80.7 percent for CB3 (determination coefficients are respectively 95.3 percent and 96.3 percent),
- The influence of the seasonal effect is 20.7 mm for CB2, with the maximum at mid-August and the minimum at mid-January, and 2.6 mm for CB3, with the maximum at mid-August and the minimum at the end of February,
- The thermal inertia towards the air temperature calculated by Condor-C for CB2 model is 8.4 days,
- The influence of the hydrostatic effect when the water level varies from el. 235 to el. 194 (the correction function is no more valid below) is 27 mm for CB2 model and 9.1 mm for CB3 model.

Any attempt to obtain better adjustment of the models on readings over the 2000-2012 period have failed, which means that the models described above are the optimal ones for their kind. It has therefore been selected to carry out the prediction for the 2012-2017 period as a basis for comparison with the models based on Machine Learning methods.

	CB2	CB3		
Prediction (mm) =	+19.6777	+5.4456		Constant
	- 76.0574	- 21.48961	* Z	Hydrostatic functions
	+47.1672	+11.4479	* Z^2	Z = (237-water level) / 45
			* Z^3	
			* Z^4	
	- 8.4186	-0.7334	* [1-Cos(S)]	Seasonal functions
	+ 5.4527	+1.0514	* Sin(S)	S = 0 to 360 from 01/01 to 31/12
	- 1.0006	+0.2413	* Sin²(S)	
	- 3.5081	+0.3117	* Sin(S)*Cos(S)	
	+0.6493		*f(T°C)	Thermal correction, thermal inertia = 8.4 days (defined by software)

Figure 3. Formulation of the statistical HST/HST-T models for CB2 and CB3 pendulums
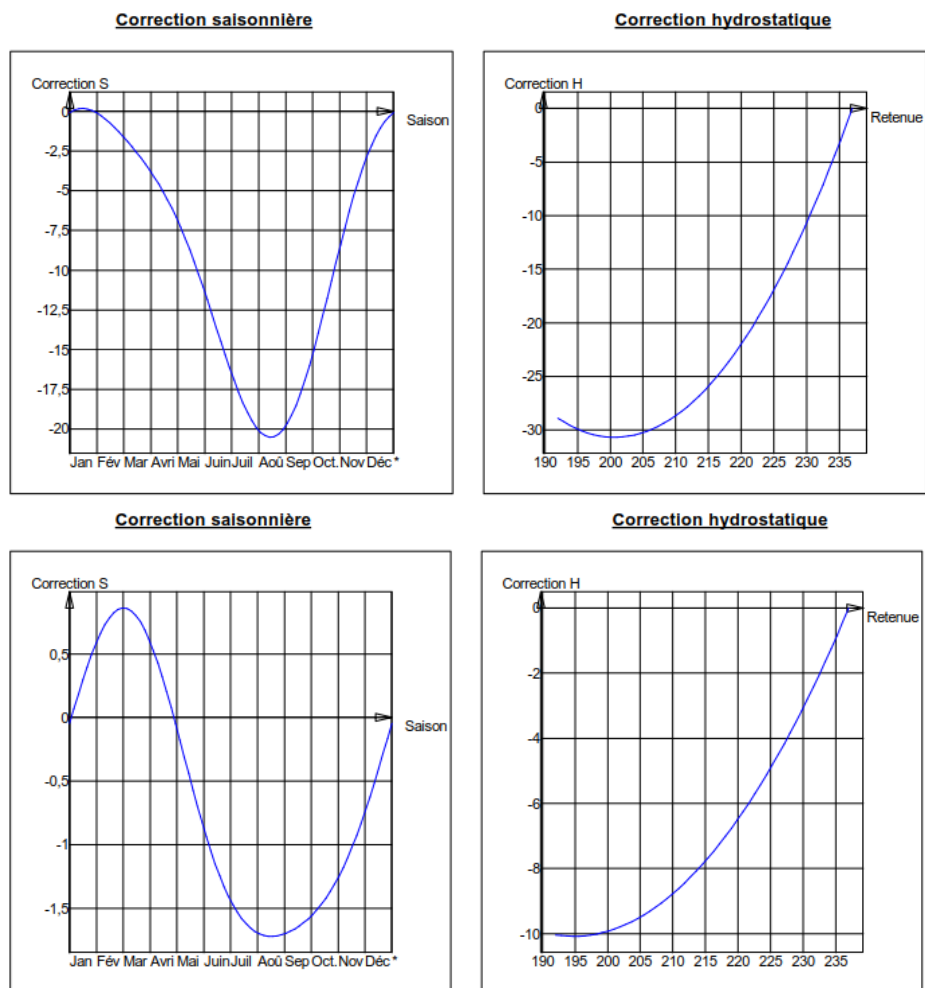
Figure 4. Left: Seasonal effect function; Right: hydrostatic effect function for CB2 model (Top) and CB3 model (Bottom)

3.2 *Models based on Machine Learning Models*

The Tractebel Machine Learning Web Platform has been developed to prepare and to run Support Vector Regression (SVR) models, Random Forest (RF) models and Recurrent Neural Networks (RNN) models. Scikit Learn, Tensor Flow, Keras and Plotly Python libraries have been used.

SVR methods (Vapnik, 1995) derive from Support Vector Machine (SVM) methods used for classification problems. RF methods (Breiman, 2001) are based on decision trees and segmentation functions. The reader will find a description of SVR and RF methods in (Veylon, 2021).

The Recurrent Neural Network method implemented in the platform is the Long Short-Term Memory (LSTM) method well fitted for time series (Hochreiter, Schmidhuber, 1997). As the other RNNs, LSTM has a chain-like structure with repeating modules of neural network but the repeating module is more complex. The core idea is to control the memory with gates letting or no information through as illustrated by Figure 5.
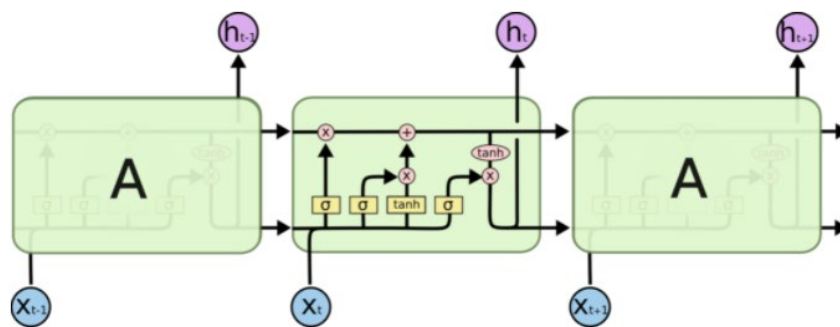
Figure 5. .Repeating module of LSTM (source: https://colah.github.io/posts/2015-08-Understanding-LSTMs)

The values given to the hyperparameters of the models have been chosen in the ranges generally proposed in the literature with a view to avoid over-fitting for the training period and to fit as much as possible the readings for the validation period. These values were as follows:

- SVR (Gaussian Kernel): C, regularization parameter penalizing the errors = 0.1; ε, tolerance margin on the regression error = 10.
- RF: number of trees = 100, number of variables randomly drawn at each branch = 2,
- LSTM: number of epochs, iterations during training = 30; batch-size, number of samples from the training dataset to work through before updating the internal model = 30; dropout percentage to avoid over-fitting = 30%. It has been checked that the number of epochs was sufficient to reach convergence.

The input variables used by the models are globally the same as those used for Condor-C models: "Z" functions: Z, Z^2, Z^3, Z^4; "S" functions: Cos S, SinS, Cos2S, Sin2S, 1-CosS; SinS, SinS $\times$ CosS; "T" functions: Exp(-T), T, T^2. As no time function has been used in the HST/HST-T models, some models including time functions have been tested but proved to be less fitted for the validation period than the models without time functions. The input variables used by the models have then been all the "Z" functions and all the "S" functions.

For the training and the validation process, 70% of the readings of CB2 (respectively CB3) from 2000 to 2010 are used for training. The 30% left are used for testing. The data are selected by random draw for each run of the model.

As the values calculated by the model differ for each random draw, the model has been run ten times successively to give ten (independent) series of calculated values which have been averaged to reduce the variance of the predictions.

The concept of correcting the data by subtracting the reversible hydrostatic and seasonal effects does not exist for these methods, contrary to the HST and HST-T methods, as the formulation is non-linear. The residual variation coefficients can thus not be assessed. The selection of the best-fitted model has been based on the determination coefficient on the

validation period. The data predicted from the model have been compared to the readings for the period 2011-2012, i.e. two full year of operation.

The SVR and RF models were not well fitted to the readings of the validation period. The determination coefficients for the validation period were around 60 percent. The LSTM models proved to be better fitted with determination coefficients on average 93.8 percent for CB2 model and 97 percent for CB3 model for the test period (30% of the readings from 2000 to 2010) and 82.9 percent for CB2 and 95.3 percent for CB3 for the validation period.

Figure 6 and Figure 7 show the main results of LSTM models for CB2 and CB3. The sign convention is: positive for downstream displacements of the upper part of pendulum (dam crest for CB2 and dam toe for CB3), negative for upstream displacements.

As LSTM models are not linear, the curves showing the influence of water level and season are drawn with the other parameters fixed at their median values (around 224 for reservoir level and July 1st for season).

The general trends are those expected: upstream displacement with increasing temperature and decreasing reservoir level with higher thermal and hydrostatic influence for the upper pendulum.

The influence of water level for and the influence of season has roughly the same shape for LSTM and HST/HST-T models for CB2 and CB3. The amplitude for seasonal influence is very similar for LSTM and HST/HST-T models. A smaller amplitude of the influence of water level is noted for LSTM models compared to HST/HST-T models: 21 mm compared to 27 mm for CB2 and 8.5 mm compared to 9.1 mm for CB3. The influence of the reservoir level for LSTM models is slightly smaller above 228.5 m for CB2 and 227.5 m for CB3 as shown by the small inflexion on the curves of Figure 6 and Figure 7.
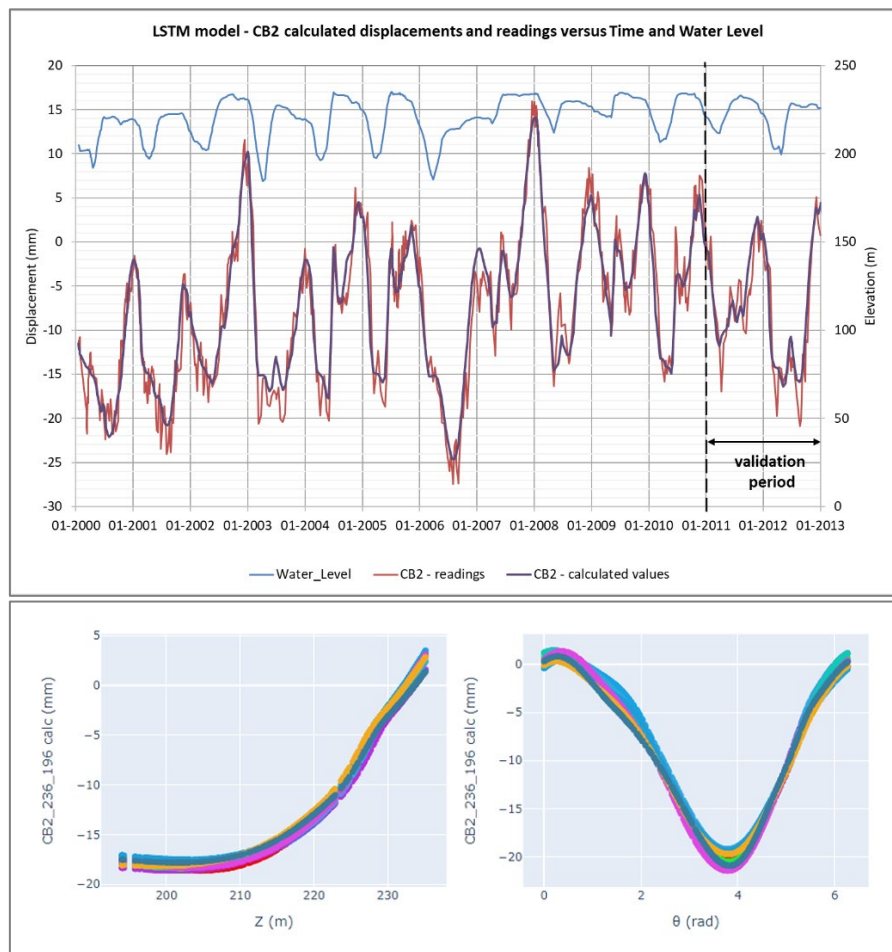
Figure 6. CB2 LSTM model –Top: calculated values versus Time and Water Level; Bottom: hydrostatic and seasonal effect function (θ: season angle)
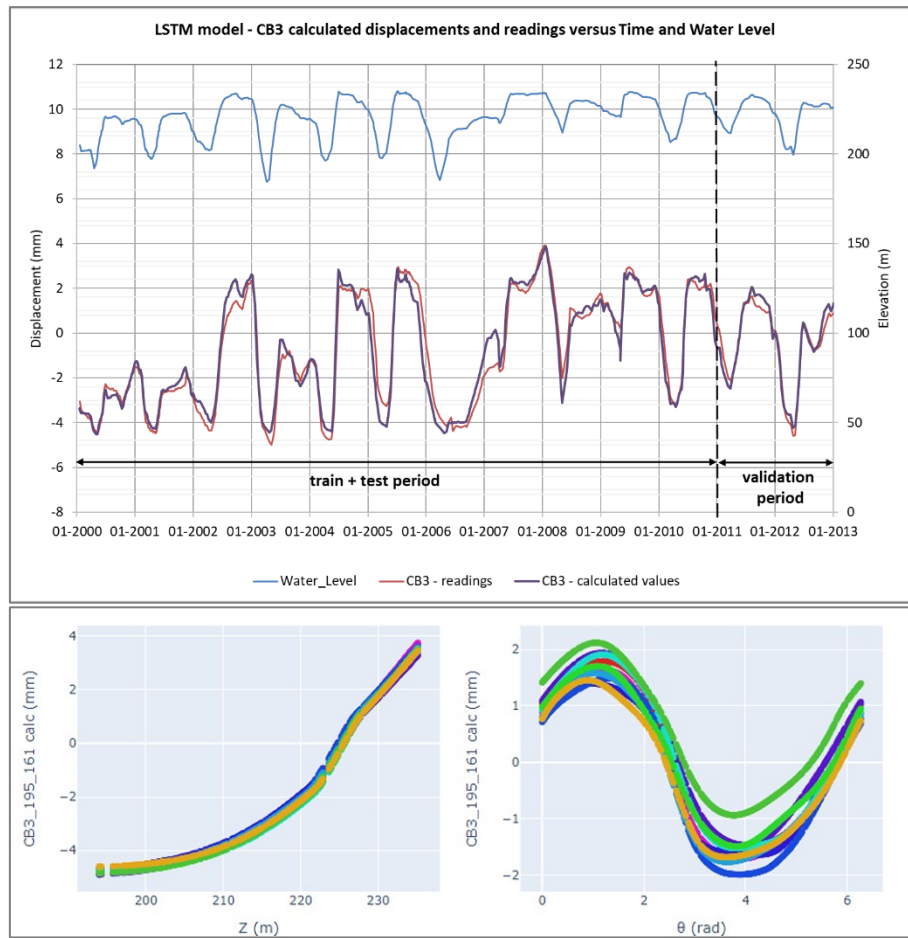
Figure 7. CB3 LSTM model – Top: calculated values versus Time and Water Level; Bottom: hydrostatic and seasonal effect function (θ: season angle)

4 RESULTS

The results for the LSTM models are provided under the shape of the predictive values for the first half-year of 2013 (short term prediction) and from beginning of July 2013 to end of December 2017 (long term prediction) as an Excel files provided to the Formulator for CB2 and CB3 LSTM models (average of 10 runs). The results for HST/HST-T models are provided for comparison.

Based on the standard deviation of the difference between readings and calculated values 2.35 mm for CB2 and 0.47 mm for CB3 the prediction with LSTM models is expected to have an average accuracy of ± 2.5 mm for CB2 and ± 0.5 mm for CB3. These values are very close to the values of the residual standard deviation obtained by HST/HST-T models: 2.05 mm for CB2 and 0.52 mm for CB3.

As shown on Figure 8 and Figure 9 the values predicted with LSTM models compare well to those predicted with HST/HST-T models from 2013 to 2015 when the reservoir level variations are within the range of 2000-2012 variations. This gives confidence in both models to provide good quality interpolation.

The main differences are found from 2016 to 2017 that is a period when the models need to extrapolate: the reservoir level has reached its historical minimum and remained below the dam toe from January to April 2016 and the yearly maximum levels for 2016 and 2017 are below those known for the 2000-2012 period, respectively around – 10 m and – 5 m to the lowest yearly maximum level of 2000.
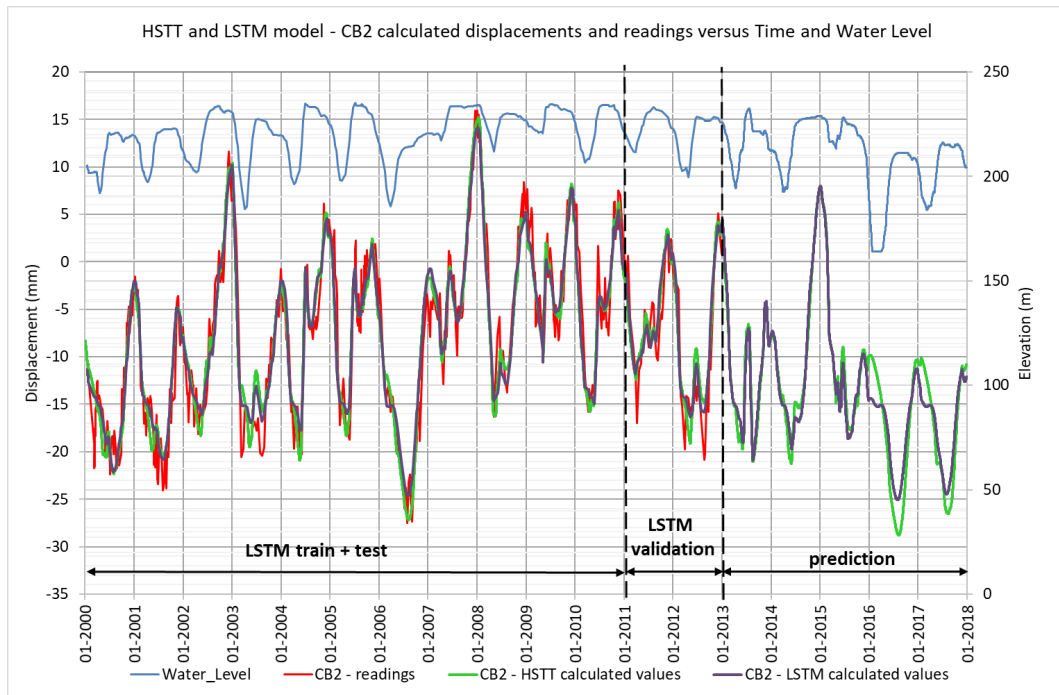
Figure 8. CB2 calculated values versus Time and Water Level (2000-2017)
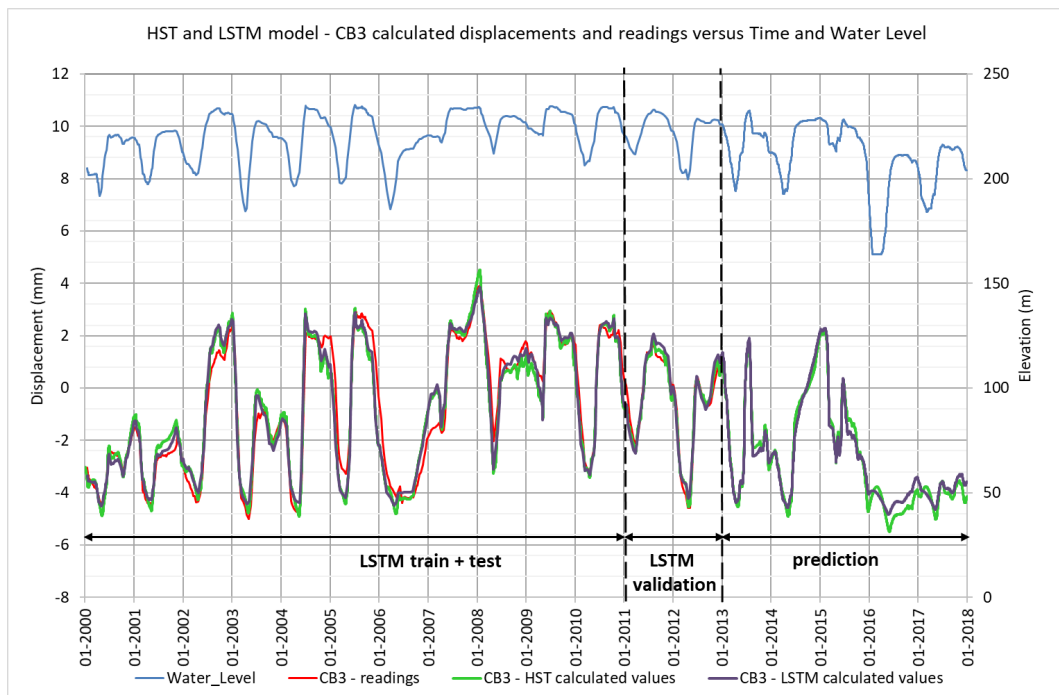
Figure 9. CB3 calculated values versus Time and Water Level (2000-2017)

- When the reservoir level remains below the dam toe in 2016 (winter):
  - CB2 HST-T model foresees a millimetric reversible downstream displacement and a position some 2.5 mm downstream the one reached in 2003 and 2006 with drawdown below the dam toe whereas the LSTM model levels off with a position similar to those reached in 2003 and 2006 which is more in line with expected behaviour.
  - CB3 HST model foresees a 1 mm reversible downstream displacement from the position reached in 2003 and 2006 whereas the LSTM model foresees almost no displacement and a position slightly downstream the ones predicted in the past which is more in line with expected behaviour.

—

- When the reservoir level reaches its 2016 and 2017 yearly maximum (summer):
  - Both CB2 models foresee an upstream displacement consistent with the predominance of thermal effects over hydrostatic effects. The most upstream position is reached in 2016 which seems rather consistent as the water level has been lower though the air temperature has been lower.
  - The position is the historical most upstream one with the HST-T model, more upstream than the one reached in 2006 with a reservoir 3 m higher with similar temperatures, whereas the LSTM model foresees an upstream position very similar to 2006 which is less realistic.
  - Both CB3 models foresee a 2016 downstream position below (upstream) the one reached in 2006 with lower reservoir level and a 2017 downstream position intermediate between the 2006 one and the 2000 one with higher reservoir level (+2 m) – which seems rather realistic.
  - When the reservoir level reaches its 2017 yearly minimum (winter), CB3 HST predictions level off before showing an upstream displacement and a position similar to the one reached in 2003 with roughly the similar reservoir and thermal conditions whereas CB3 LSTM model foresees a smoother upstream displacement similar to the one calculated for 2003 - which seems more realistic.

The predictions for CB2 and CB3 pendulums displacements with LSTM models seem globally more realistic than those with HST/HST-T models for the 2016-2017 period where an extrapolation is required.

Warning levels could be defined by analogy with the definition of warning levels of HST/HST-T models and assuming the readings follow a normal distribution as the calculated value ±2.5 x standard deviation of the difference between calculated values and readings for the period 2000-2012. This corresponds to ±5.9 mm around CB2 calculated values and ±1,2 mm around CB3 calculated values. These values compared well with the warning levels which could be defined for HST/HST-T models that is ±5.2 mm around CB2 calculated values and ±1.3 mm around CB3 calculated values.

In the opinion of the authors, these warning levels are not direct indicators of the safety of the dam. They only alert on the fact that the readings are out of a normality range. A reading exceeding the alert level should raise the attention of the person in charge of the monitoring data analysis. The reading should be repeated. If it is confirmed, following questions should be answered: is a change occurring in the behaviour of the dam? does this change affect the dam safety?

5 CONCLUSION

The exercise presented above showed that data-based models based on LSTM methods could be used for the prediction of monitoring data measurement.

For the case studied – displacements of an arch dam mainly influenced by the hydrostatic loading and the seasonal thermal condition – the results obtained with less input variables are very similar to those obtained with HST and even HST-T models and seem more realistic when an extrapolation is needed.

This conclusion needs however to be confirmed by the comparison of the prediction with the actual readings of 2013-2017 and by similar exercises with other time series.

Next steps considered for the development of the Machine Learning Web Platform are focused on improving the selection of hyperparameters of the models and including temperature time series in the input variables.

REFERENCES

Breiman L. (2001). Random Forests. In: Mach. Learn. 45.1 (2001), pp. 5–32. DOI: 10.3390/rs10060911
Hochreiter S, Schmidhuber J (1997). Long Short-Term Memory. In: Neural Computation, 1997 9(8):1735-80 DOI:10.1162/neco.1997.9.8.1735

Penot I. Fabre JP. and al. (2009). Analyse et modélisation du comportement des ouvrages de génie civil par la prise en compte des températures de l'air : Méthode H.S.T. Thermique, ICOLD 2009. Q. 91 – R. 60

Veylon G., Rosin-Corre N. et al. (2021), Analysis of Dam Monitoring Data by Machine Learning Methods, ICOLD 2021 Q. 106 – D. 2

DATA-DRIVEN & MODEL-BASED STRUCTURAL BEHAVIOUR PREDICTION OF A CONCRETE ARCH DAM

Irina Galliamova

Gruner Stucky Ltd, Renens, SWITZERLAND

   irina.galliamova @gruner.ch

Alban Kita

Gruner Stucky Ltd, Renens, SWITZERLAND

   alban.kita @gruner.ch

Anton Tzenkov

Gruner Stucky Ltd, Renens, SWITZERLAND

   anton.tzenkov@gruner.ch

ABSTRACT: This paper focuses on the benchmark problem Theme A ''Behaviour prediction of a concrete arch dam'' of the 16th International Benchmark Workshop on Numerical Analysis of Dams, Organized by ICOLD Committee on Computational Aspects of Analysis and Design of Dams. The calibration of the statistical regression HST model and the Finite Element model are presented, both capable to predict the behavior of the dam under examination in terms of radial displacements with respect to measurements of both pendulums. A training period of 13 years has been considered for the calibration, whereby temperature and water level data have been used as regressors. Two prediction periods have been considered for the prediction, namely short-term and long-term. On the one hand, a good agreement has been demonstrated between time series of measured and statistically estimated displacements, with very high determination coefficients. In particular, in the long-term period, the statistical model has been capable of estimating displacements which are compatible with the recent scenario of an exceptional drastic decrease of the measured water level. On the other hand, thermo-mechanical analyses have been carried out with FEM, whereby a staggered approach is adopted. In particular, the main steps include transient heat-flow analysis to define the dam-foundation system temperature states, and nonlinear structural analysis to determine displacements, strains, stresses, crack pattern, initiation and propagation. FEM has shown stress distribution and direction and zones subjected to cracks. These zones are mainly concentrated along the foundation of the dam, perpendicular to the rock surface. The observed crack pattern is rather typical and does not compromise the stability of the dam. While the statistical model demonstrates a higher accuracy for the predictions of radial displacements, the FE simulated opening of the joints in the upstream face of the dam potentially provides the reason of the exceptional lowering of the reservoir water level in the last two years of the monitoring period.

1 INTRODUCTION

The current analyses are performed following the requirements and using the data provided within the benchmark problem of Theme A ''*Behaviour prediction of a concrete arch dam*'' of the 16th International Benchmark Workshop on Numerical Analysis of Dams, Organized by ICOLD Committee on Computational Aspects of Analysis and Design of Dams.

The investigation aims to calibrate and predict the behavior of the dam based on the provided measurements. Namely, the radial displacements measured by dam pendulums are used as the parameter that describes the behavior of the dam and reservoir water level and ambient temperature (daily and seasonal variations) are the parameters governing dam behavior.

In order to achieve the objective, two approaches have been adopted:
- Statistical prediction, later called data-driven prediction;
- Finite element model, later mentioned as model-based prediction.

The 1st approach is a quick strategy to analyze the response of a dam, i.e. the so-called dependent variable that can be of static (displacement, tilting, crack opening/closing, settlement, etc) and dynamic (natural frequencies, mode shapes) nature. Based on the independent variables (or predictors or regressors), such as temperature, reservoir water level, ground water level, etc, a statistical model is calibrated over a sufficient first period of time (training period), to be finally used for predicting further developments of the response of the dam.

Among several predictive statistical models, whose scope is essentially to statistically reconstruct such measured data, the hydrostatic-seasonal-time (HST) model has been implemented in the present case. The HST model is the most used data-driven model for dams 0 and is particularly advantageous because it allows the decomposition of response time series in separate components (irreversible effects, hydrostatic and thermal variations).

The 2nd approach relies on finite element modeling for the prediction, which can be time-consuming and less straightforward method. It involves the assumptions regarding material properties, modeling of the weak zones, etc., that could be crucial in decision making. Moreover, this method, while carefully implemented, provides more details and insights to the behavior of the entire dam and particular elements. This method uses the time history of the measurements to define the current state of the dam and is able to predict further evolution, based on the applied load and material properties.

The obtained results have demonstrated that both models are capable to reproduce the provided measurements in the training period, and to predict in the prediction period. The HST statistical model has reached a smaller deviation from the measurements, while the numerical model requires more sophisticated adjustments in order to reach the same level of accuracy. Nevertheless, the results from the FEM have been exploited to further understand the behavior of the dam and suggest possible reasons for the observed operational sequences.

The paper is organized as follows. Section 2 illustrates the proposed statistical model and its validation. Section 3 presents the model-based approach. Sections 4 and 5 describe the calibration of the FEM model and the first results. Section 6 reports the result prediction from both data-driven and model-based approaches. Finally, Section 7 summarizes the main conclusions of the work.

2 DATA-DRIVEN STATISTICAL PREDICTION OF THE STATIC RESPONSE

2.1 *Methodology*

The dam response is driven predominantly by hydrostatic load (i.e. water level) and temperature (daily and seasonal variations). Several predictive statistical models (based on the monitoring data measured over a certain sufficiently time span) have been presented in the literature to statistically reconstruct such measured data. Among the relevant and recent ones, the most used data-driven model for dams is the *hydrostatic-seasonal-time* (HST) model. The HST model is particularly useful because it allows the statistical reconstruction/estimation of response time series and their decomposition in separate components, such as irreversible effects $f_1(t)$,

hydrostatic $f_2(w)$ and thermal $f_3(s)$ variations. The adopted component's equations can be reported as follows:

$$f_1(t) = a_1 + a_2 \cdot t + a_3 \cdot t^2$$

$$f_2(w) = a_4 \cdot w + a_5 \cdot (2 \cdot w^2 - 1) + a_6 \cdot (4 \cdot w^3 - 3 \cdot w) + a_7 \cdot (8 \cdot w^4 - 8 \cdot w^2 + 1)$$

$$f_3(s) = a_8 \cdot \sin(s) + a_9 \cdot cos(s) + a_{10} \cdot sin(2s) + a_{11} \cdot cos(2s)$$

Where t, w and s represent the normalized variables, computed as follows:

$$w = \frac{2 \cdot WL - NWL - MWL}{NWL - MWL} \qquad -1 \leq w \leq 1$$

$$s = day\ of\ year \cdot \frac{2\pi}{365.25} \qquad 0 \leq s \leq 2\pi$$

$$t = \frac{(actual\ date - first\ date)}{365.25} \quad 0 \leq t \leq total\ numer\ of\ years\ since\ 1st\ measure$$

WL refers to actual water level, NWL refers to normal water level and MWL refers to minimum water level. In the present case: NWL=237 m. and MWL=174 m.

2.2 *Validation of the statistical model*

The statistical regression analysis has been carried out by the *DamReg* software 0. A typical representation of the results is shown in Figure 2-1.
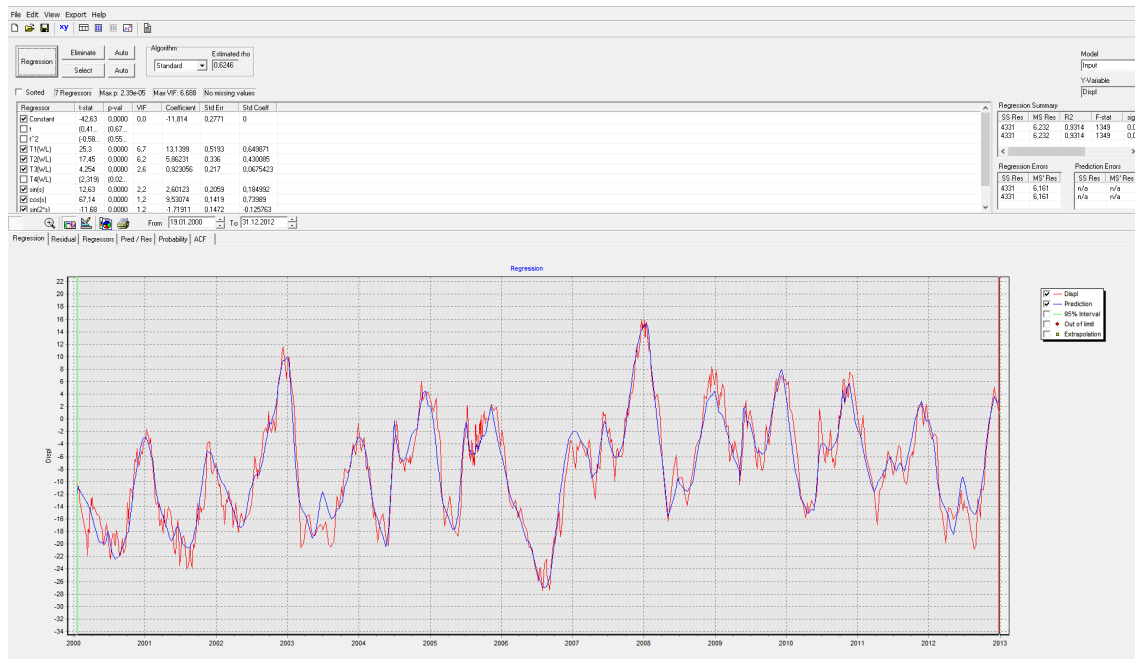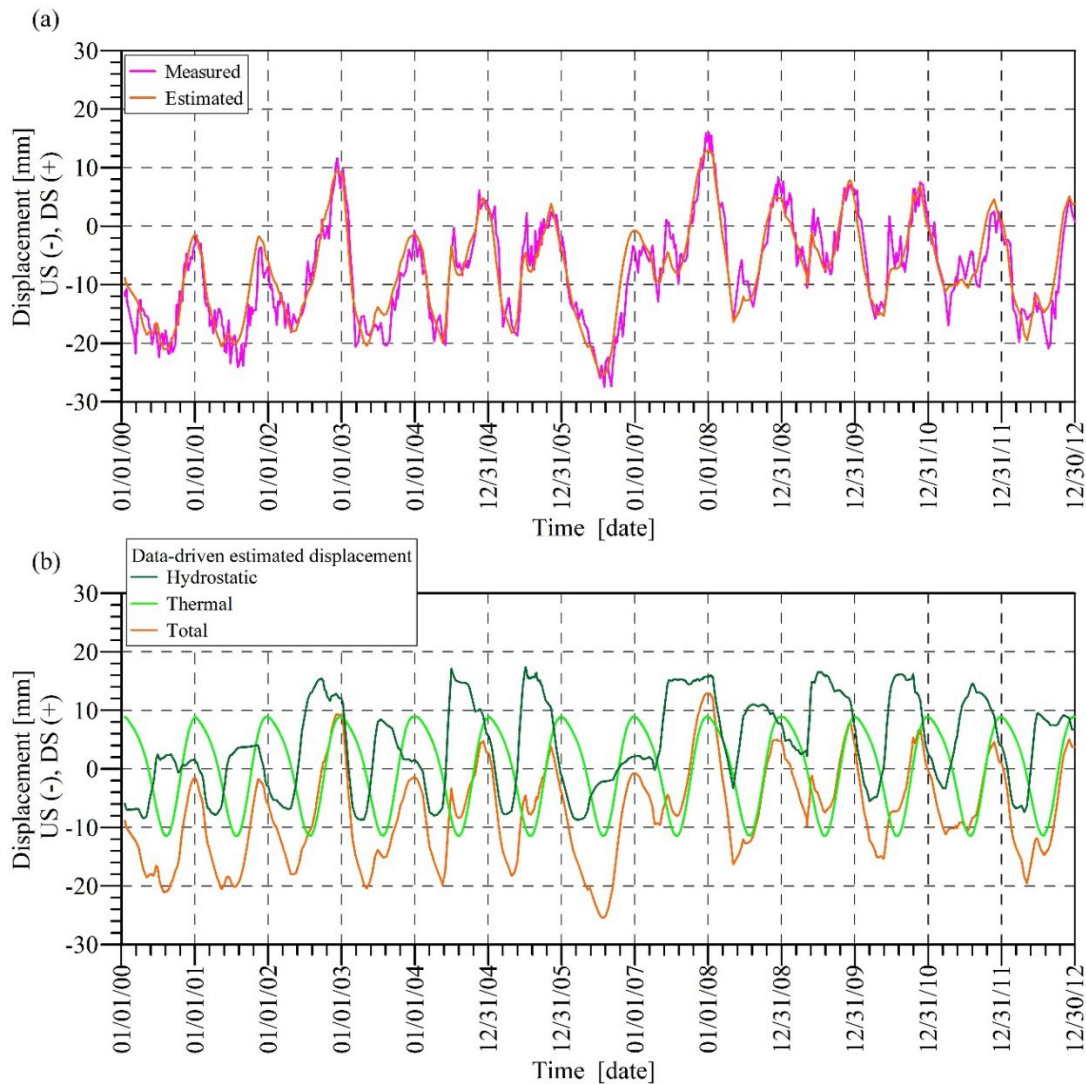

Figure 2-1. View of results from the DamReg software: time series of measured and statistically estimated displacements (CB2_236_196) in 13 years time window (10 regressors).

On the one hand, thirteen (13) years of water level and temperature time series have been exploited as input to the HST model defined within the software. On the other hand, data measured from both pendulums, CB2_236_196 and CB3_195_161, have been considered as the output variable. Ten (10) regressors have been defined according to the above equations (linear as well as polynomial powers, and sinusoidal/cosinusoidal). In particular, the 4th power of WL has been omitted because the regression coefficient is not significantly different from zero. Overall, the coefficient of determination resulted R^2=0.93. Figure 1-81 illustrates the time series of measured and statistically estimated displacements (CB2_236_196 pendulum) from January 1st 2000 to December 31st 2012.

Noteworthy to say, Figure 2-2 depicts an abnormal irreversible component (of the estimated displacements) both in trend and amplitude. In particular, it begins from zero, increases up to less than 2 mm, and returns to zero at the end of the period. On the basis of this consideration, the Authors conclude that introducing this component to the statistical model is irrelevant and not beneficial. Hence, for a more accurate prediction, it is omitted for the following validation.
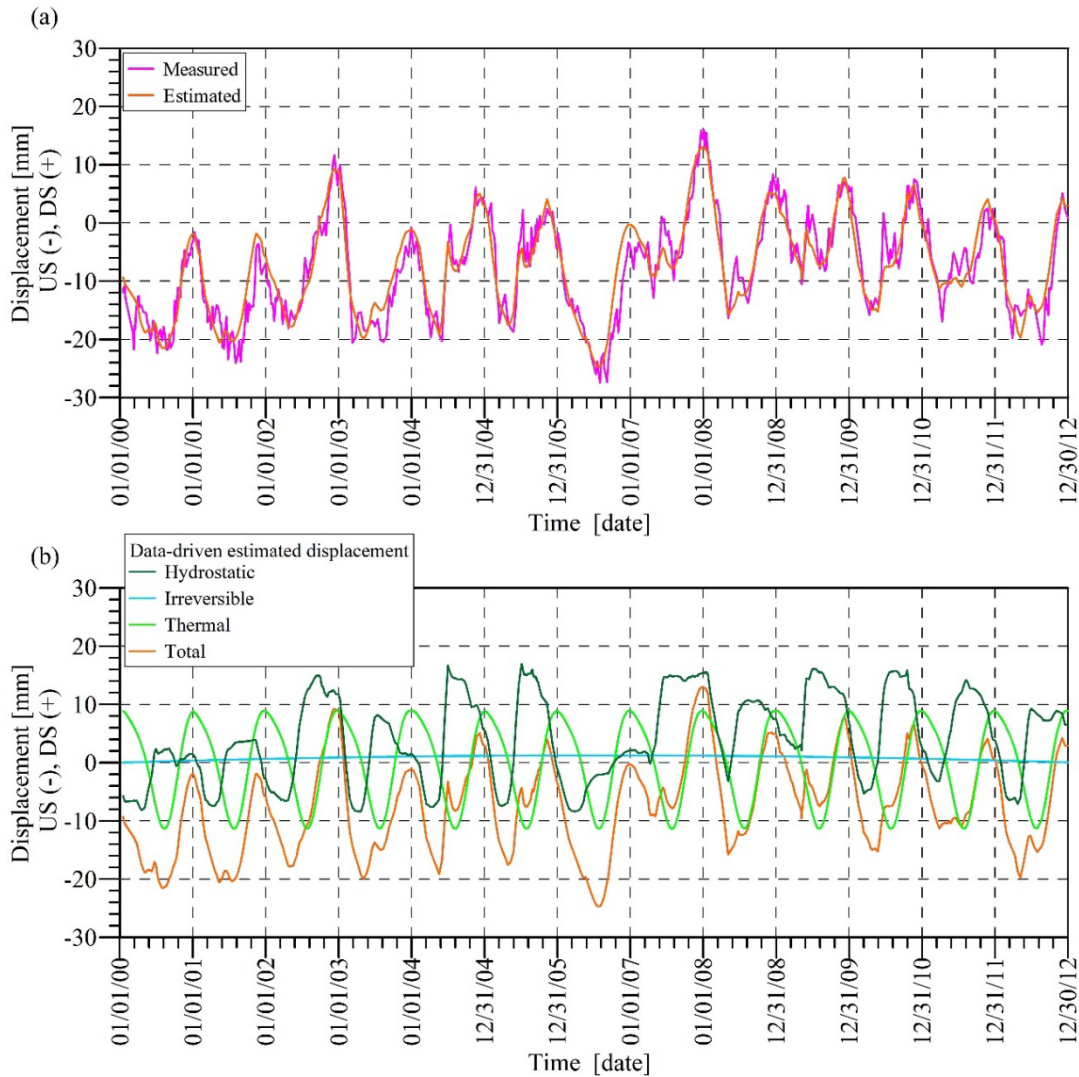
Figure 2-2. Time series of measured and statistically estimated displacements (CB2_236_196) in 13 years time window (10 regressors).

The statistical regression analysis has been carried out again by the software, this time by exploiting water level and temperature data only, for the same 13-year period. In this way, eight (8) regressors have been used ($a_2 \cdot t + a_3 \cdot t^2$ terms are not considered). In analogy to Figure 2-2, the time series of measured and statistically estimated displacements have been illustrated in Figure 2-3. The range spans from -30 mm to about 15 mm. Total values are presented in Figure 2-3, while time histories of each separate component (see HST model) of estimated displacements are presented in Figure 2-3b. From a visual investigation of the graph, it can be observed that the two separate components are out of phase between them, e.g. during summer the hydrostatic component has the most downstream displacements (15-20 mm), while the thermal component presents the less downstream displacements (highest values towards upstream, equal to -10 mm).

Overall, a good prediction can be visually observed in the case of the high pendulum CB2_236_196, whereas the coefficient of determination resulted R^2=0.932.
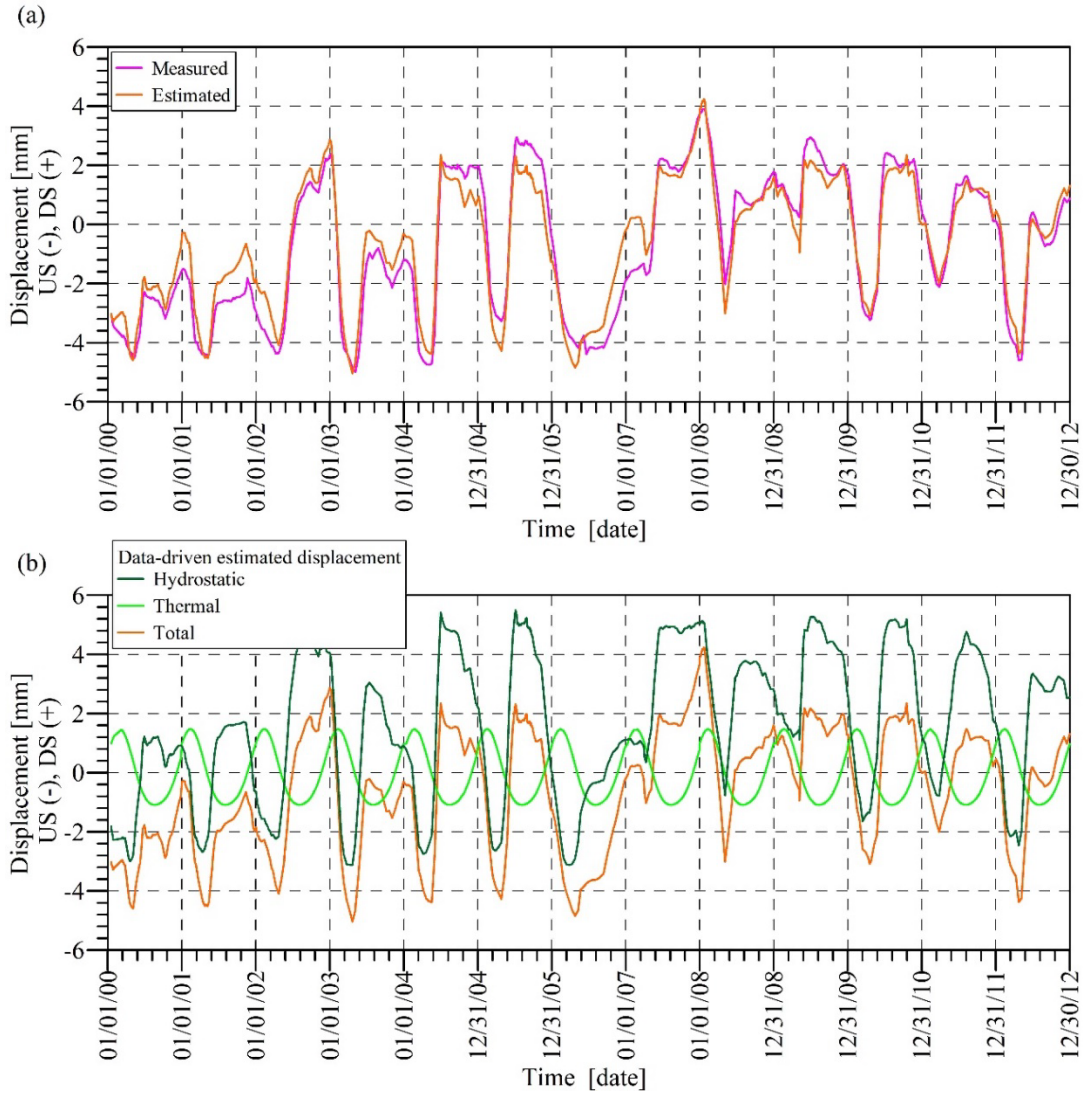
Figure 2-3. Time series of measured and statistically estimated displacements (CB2_236_196) in 13-years time window (8 regressors).

In analogy to the CB2_236_196, the statistical regression prediction has been carried out also in the case of the CB3_195_161 pendulum.

The same 13-year time series of measured water level and temperature data have been used as regressors (8) within the HST statistical model. Time series of measured and statistically estimated displacements have been comparatively illustrated in Figure 2-4 (January 1st 2000 to December 31st 2012). The range spans approximately from -6 mm to about 6 mm. The separate components (thermal and hydrostatic) of estimated displacements are presented in Figure 2-4b. On the one hand, a limited thermal component is observed (between − 2 and +2 mm). On the other hand, the higher amplitudes of the hydrostatic component with respect to the thermal one can be directly observed, demonstrating its predominant role for the low pendulum. This is because the top head of the low pendulum is located at the base of the dam, thus considering a much higher water head, and a region less subjected to high temperature variations.

The out of phase nature of the two separate components is confirmed also for the low pendulum CB3_195_161: during summer maximum values of the hydrostatic component (5 mm) and minimum values of the thermal component (-2 mm).

Overall, a good prediction can be visually observed in the case of the low pendulum CB3_195_161, whereas the coefficient of determination resulted R^2=0.964.

Figure 2-4. Time series of measured and statistically estimated displacements (CB3_195_161) in 13-years time window (8 regressors).

To better emphasize the accuracy of predictions for both pendulums, measured and statistically estimated displacements are plotted against each other as depicted in Figure 2-5, where the positioning along/around the diagonal is clearly visible.
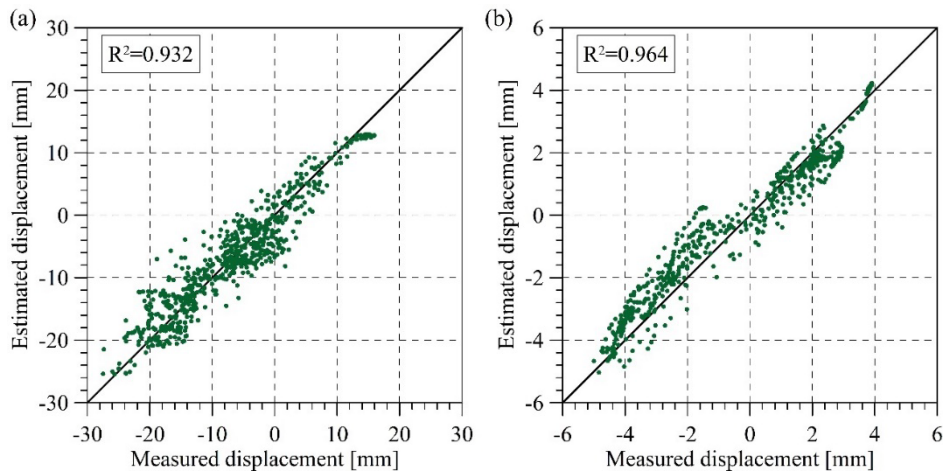
Figure 2-5. Measured versus statistically estimated displacements: (a) CB2_236_196, (b) CB3_195_161.

3 MODEL-BASED APPROACH

3.1 *Methodology*

In order to assess the current state of the dam and predict its further behavior thermo-mechanical analysis is adopted and includes self-weight, hydrostatic load due to reservoir water level and thermal load. The last two loads are time-dependent and based on the provided measurements.

For the thermo-mechanical analysis, a staggered approach is adopted. First, temperature distribution, based on the applied boundary conditions is calculated. Second, these temperature fields are applied as an external loading in the following structural analysis.

In particular, the staggered thermal-mechanical analysis performed consists of the following main steps:

- Transient heat-flow analysis to define the dam-foundation system temperature states;
- Nonlinear structural analysis to define the displacements, strains, stresses, crack initiation and propagation, crack pattern and crack width for a load combination involving the basic load cases (self-weight and hydrostatic pressure) and the temperature variations as defined in the previous analysis step.

3.2 *Transient heat-flow analysis*

The transient heat-flow analysis is performed by applying the entire sequence of the available temperature measurements starting from 1995. An initial condition of a uniform temperature distribution of 3°C is assumed for the dam-foundation system. However, considering that the period of interest starts 5 years later in 2000, the initial temperature assumption does not play a significant role.

Two analyses are performed with time-step equal to 2 days. Larger time step gives fair results for the temperature distribution, however, in order to improve the precision of the nonlinear structural analysis smaller time step is considered.

3.3 *Nonlinear structural analysis*

The main source of the nonlinearity is the nonlinear constitutive model associated with the concrete material.

The loading sequence on the dam-foundation system is numerically simulated in two main phases: self-weight; hydrostatic pressure; and temperature variations in time.

Self-weight of the dam is obtained by the staged construction. Afterwards, the time dependent load that includes the hydrostatic load and the thermal load defined by means of the transient heat-flow analysis are applied in time-steps of 2 days.

3.4 *Material parameters*

The following material parameters supplied by the formulators of Theme A are used:

Table 1: Material parameters

Material parameters	Units	Concrete
Modulus of elasticity	GPa	15.4
Poisson's ratio	-	0.2
Density	kg/m^3	2400
Thermal expansion	K^{-1}	10^{-5}
Thermal conductivity	W/(m*K)	2
Specific heat capacity	J/(kg*K)	900
Compressive strength	MPa	34
Tensile strength	MPa	2.0

The additional material parameters that are adopted to describe the nonlinear behavior of the concrete and the arch dam–rock foundation interface are given in the following.

3.5 *Concrete*

The total strain rotating crack model with linear tension softening curve defined in DIANA 0 is used to investigate the nonlinear effects in concrete. This material model requires input for Mode I fracture energy G_f^I. It is emphasised that the value of fracture energy of mass concrete used in dams is significantly higher than that of structural concrete, since in the former the fracture takes place mostly due to failure of the aggregates 0. In the same study, it is mentioned that the value of fracture energy is assumed equal to 280 N/m is considered reasonable. The compressive fracture energy is taken $G_c = 50\,000$ N/m.

| Linear tension softening, fracture energy based | Parabolic compressive behavior |
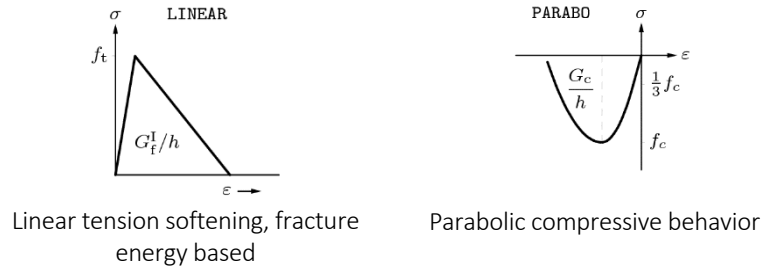
Figure 3-1. Total stain crack model

As far as the stiffness of the concrete is concerned the "sustained" modulus approach is introduced 0. It allows taking into account long-term behavior of the concrete such as creep, and slow thermal load application. Under these conditions, the reduction of the Young Modulus could reach 50%. In the current analysis, the reduction of 30% is implemented.

3.6 *Dam – rock foundation and joints interfaces*

A linear elastic interface is adopted in the dam-rock foundation connection. Based on the concrete and mass rock moduli of elasticity, interface linear stiffness moduli of $1.5E + 12$ N/m³ and $1.5E + 9$ N/m³ are specified for the normal and the tangential stiffness, respectively.

The joints between blocks are modeled by means of the linear elastic interfaces with the reduced stiffness in normal direction that equals to $1.35E + 9$ N/m³ and tangential stiffness remained equal to the stiffness of the concrete $1.54E + 9$ N/m³.

4 FEM MODEL AND BOUNDARY CONDITIONS

4.1 *3D FEM model*

The layout of the concrete arch dam and its abutments and foundation is shown in Figure 4-1.
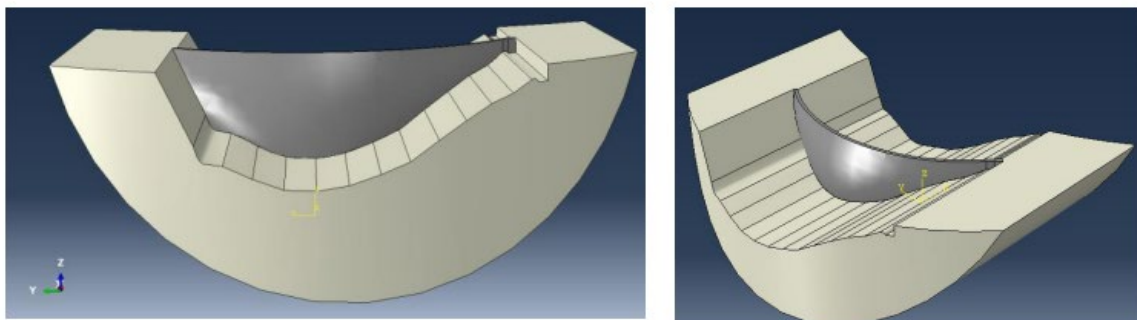
Figure 4-1. Illustration of the layout of the concrete arch dam and its abutments and foundation

Based on the provided geometry a FEM model of the dam-foundation system is constructed in DIANA FEA0. Solid element types with linear interpolation are used for mesh discretization. 2D boundary elements are used to apply heat flow boundary conditions with the external temperature.

The average element sizes of the dam and foundation are 3m and 40 m, respectively. The obtained model is presented in Figure 4-2.
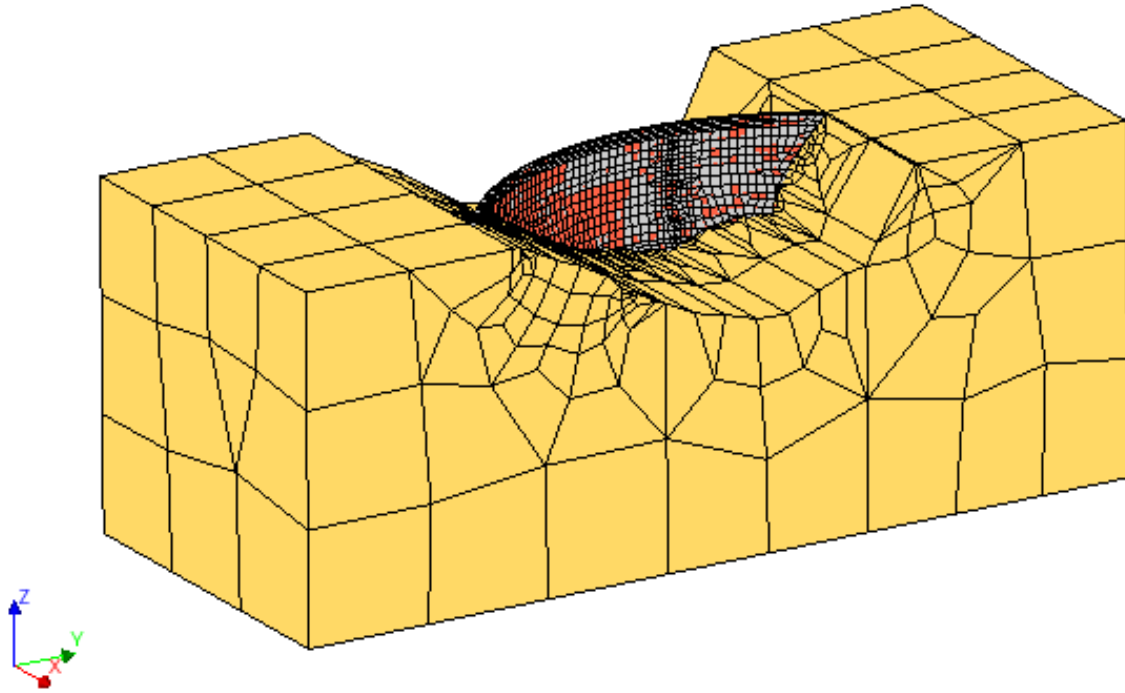
Figure 4-2. Finite element mesh of the dam with foundation

4.2 *Transient heat transfer analysis*

Time variable air temperature is applied as a boundary condition on the surface of the dam. It was considered that the time series Tb better approximates the ambient conditions.

The operational conditions do not allow to distinguish typical temperature zones of the US face: permanently underwater, transition (variable water level) and air temperature. Instead, the reservoir water level varies such that the entire height of the dam is exposed to the air temperature. Therefore, the following approach is adopted for better temperature approximation:

For the DS face, the air temperature is prescribed.

US face is divided by 2m height intervals. For each interval, the corresponding temperature is assigned depending on the reservoir water level varying in time. Namely, if the water level for a certain time is above the elevation of the interval, water temperature is assigned, otherwise, air temperature is prescribed. The proposed formulation of water temperature approximation is adopted in the analysis:

$$T_{water} = \begin{cases} 0.7 T_{air} & if\ T_{air} > 0\ C \\ 0 & otherwise \end{cases}$$

Zero flow condition is assumed for foundation surfaces.

4.3 *Nonlinear structural analysis*

Translational supports in the respective normal direction are specified as structural boundary conditions on the bottom and on the side surfaces of the foundation model.

Variational Water level load is considered on the US face of the dam and part of the foundation subjected to the hydrostatic load. The provided time series is employed in the analysis.

5 CALIBRATION OF FEM AND RESULTS

The results of the calibration are given for August 2006 and January 2008 as it is demonstrated in Figure 5-1. The reason behind this choice is that according to the provided measurements at these periods peak displacements in US and DS directions were observed.
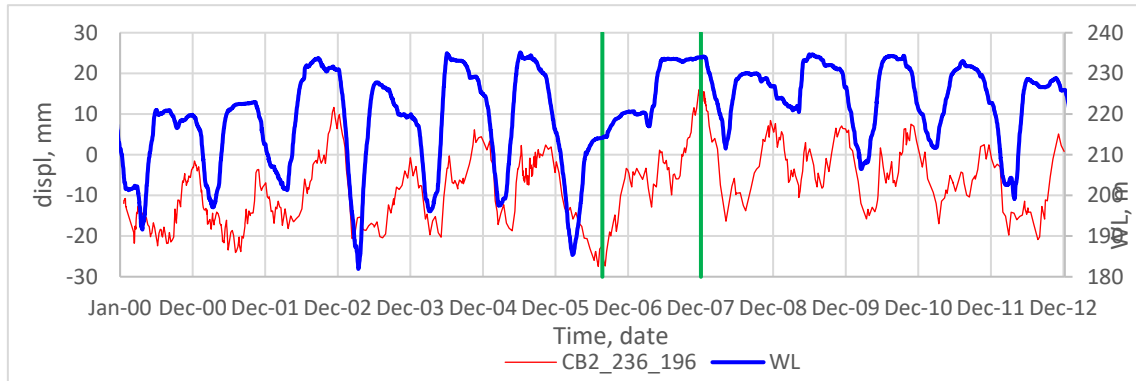
Figure 5-1. Radial displacements and reservoir Water Level measurements, the green line indicates time periods for data presentation

As far as the cross-section distributions are concerned it is given along the surface that corresponds to the position of the pendulums CB2, CB3.

The stress sign convention is such that a negative value means compression and positive one tension. For the displacements positive means movement in the downstream direction, negative towards upstream.

5.1 *Transient heat transfer analysis*

The calculated temperature distributions for the selected cross-section and time periods are shown in Figure 5-2. Additionally, temperature variation plot at the selected points of the dam body is given in Figure 5-3. These points are selected in the middle of the dam at different elevations, mainly to represent top, middle and bottom parts of the dam.

The plot shows that the biggest temperature amplitude is found in the top part of the dam and the lowest in the bottom, that corresponds to the expected behavior. Due to the fact, that the water in the reservoir isolates the dam from air temperature variations, in opposite, the top of the dam is not covered with the water and quickly reacts to the ambient changes. The average temperature amplitude inside the dam is found around 12 deg.

Aug - 2006   Jan - 2008
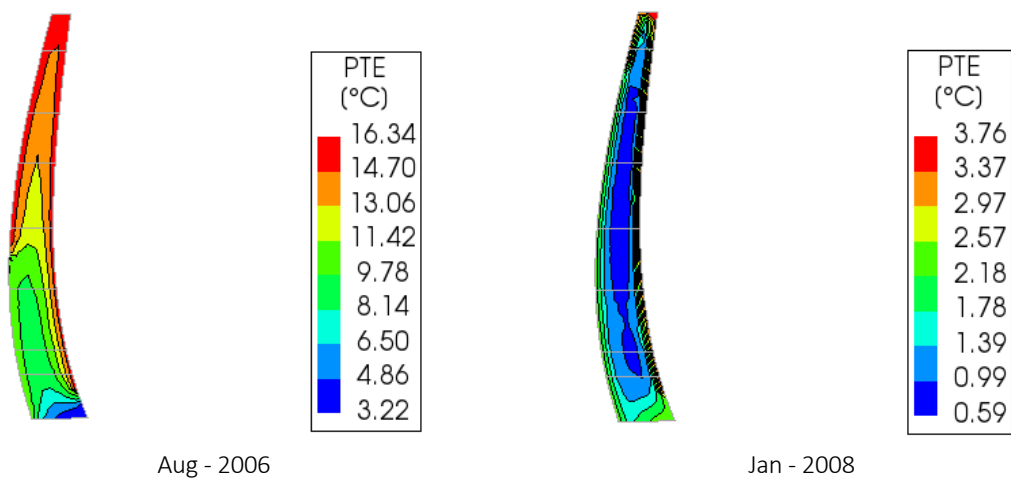
Figure 5-2. Temperature distributions for the considered periods of time
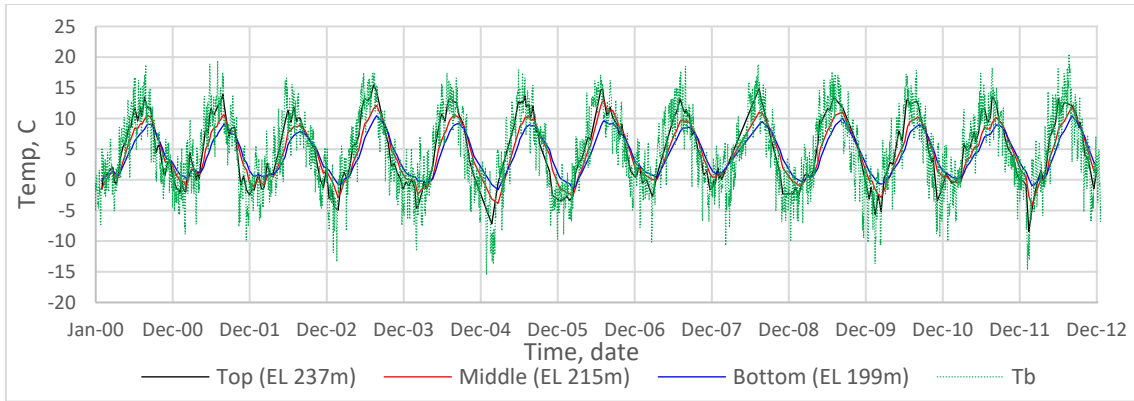
Figure 5-3 Temperature variation in the dam body at different elevations

5.2 *Nonlinear structural analysis*

In this section, the results obtained from a non-linear structural analysis with non-linear material properties of concrete are presented. It should be noted that the foundation remains elastic.

Radial displacements distribution is given in Figure 5-4 showing:

- expansion during warm period, that causes the movement in the upstream direction;
- shrinkage during cold period, creating deformation in the downstream direction.

It is noted that the overall seasonal amplitude is higher in the upstream direction than in downstream direction. Insight of the radial displacements of the dam along the height is given in Figure 5-5 where initial case includes self-weight of the dam and seasonal variations consists of a temperature and hydrostatic loads of the dam. Water load was not included in the initial conditions since it is not permanent through the year and almost empty during cold season.

Aug - 2006   Jan - 2008
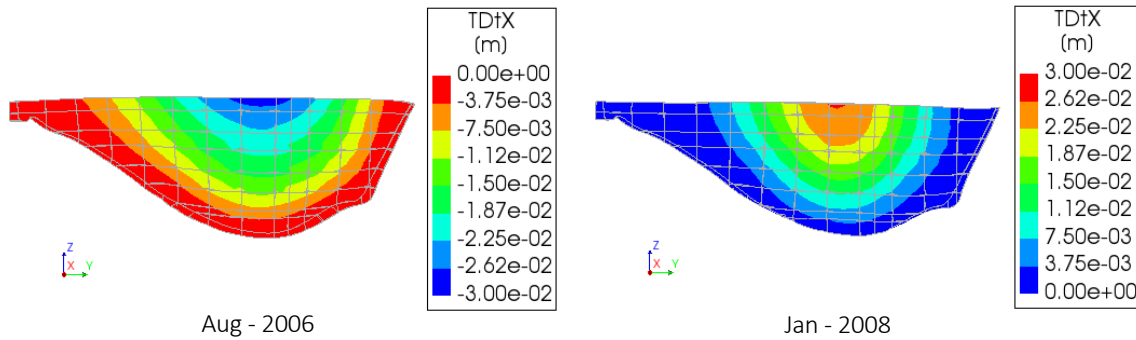
Figure 5-4. Radial displacements distribution during warm and cold periods
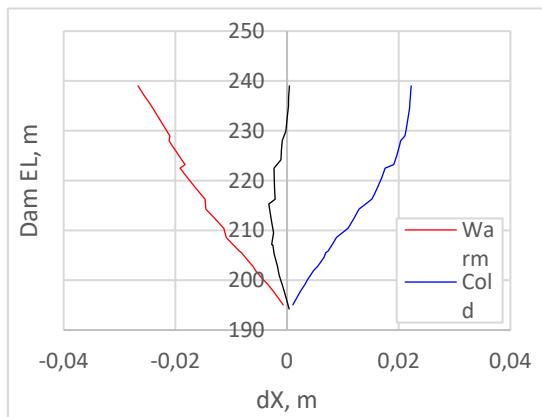
Figure 5-5. Radial displacements along the selected cross section

The obtained deformation pattern provokes certain stress distribution in the dam. Due to the low resistance to tension, the direction and intensity of maximum principal stress distribution is of interest while analyzing potential damages. Therefore, the stress distributions are given in Figure 5-6, Figure 5-7, followed by the observations:

- The tension zone in the foundation of the dam on the right bank is presented permanently. This artefact is explained by significant stiffness difference for the rock in the valley and right bank, that prevents continuous dam deformations.
- During warm period the tension zone is mainly concentrated in the dam foundation area due to the "pulling" effect of the expansion, eventually initiating the cracks perpendicular to foundation.
- Cold period produces tensile stress in vertical direction in the middle of the dam due to the bending in the downstream direction. Depending on the tensile strength of the concrete that is a potential zone of the horizontal cracks development. In the current analysis tensile stress equal to 2MPa is adopted and did not produce cracks in the downstream face.
- Cross section distributions show that the tensile stress remains rather superficial (around 0.5m) in downstream face of the dam.
- Upstream face of the dam remains under compression in vertical direction during the provided time.
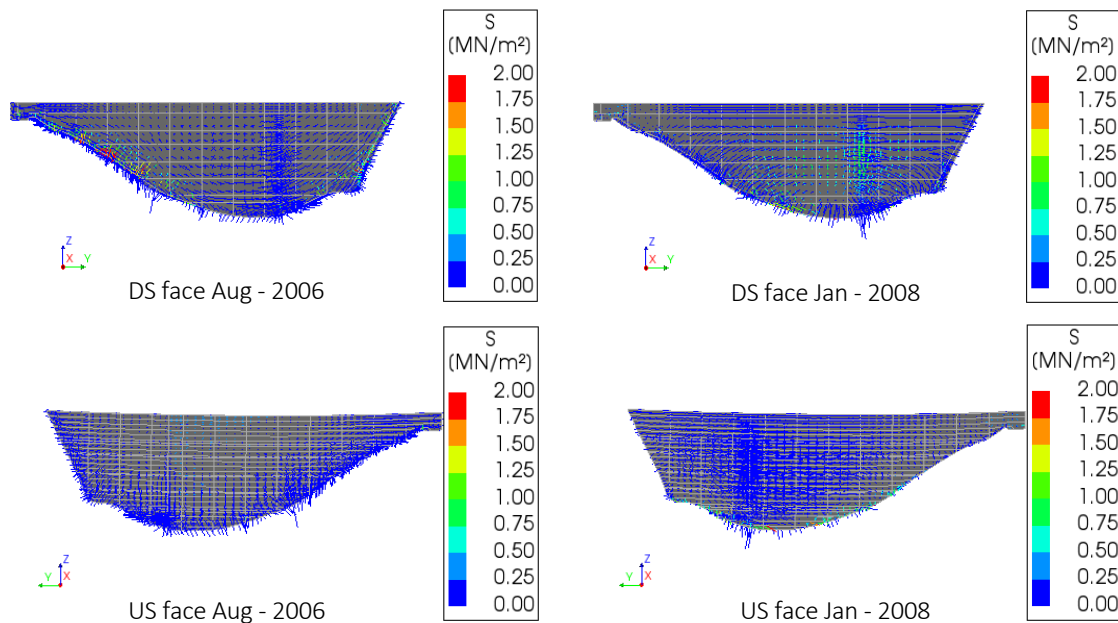
Figure 5-6. Stress directions during warm and cold periods
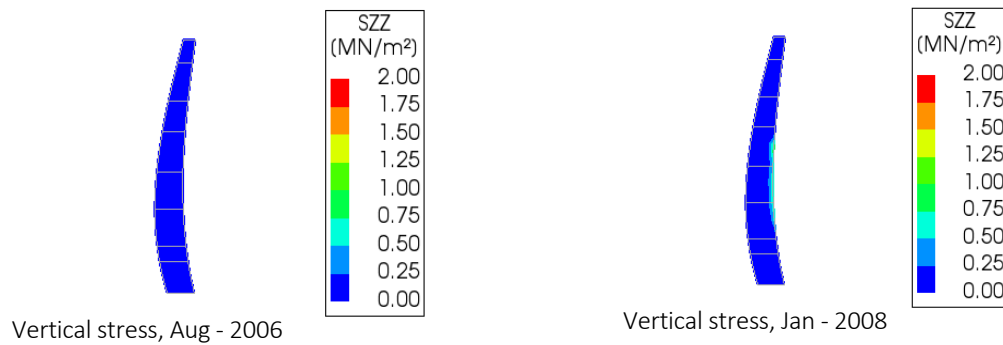
Figure 5-7. Vertical stress distributions for the warm and cold periods

Eventually, the cracks distribution is analyzed and given in Figure 5-8. The initial localization of the cracks applying self-weight and hydrostatic water pressure corresponding to WL 237 m is found in the connection of the dam with foundation.

Crack distributions at the end of the calibration period (end of 2012) shows the development of the damage in the dam blocks next to the right abutment and along the dam foundation is observed with time. First one is explained by the shape of the dam, these blocks have thinner height, therefore behave in a more rigid way, that eventually, could cause damages. The second one is a rather typical observation in the dam behaviour which is a result of the hydrostatic and temperature loads.
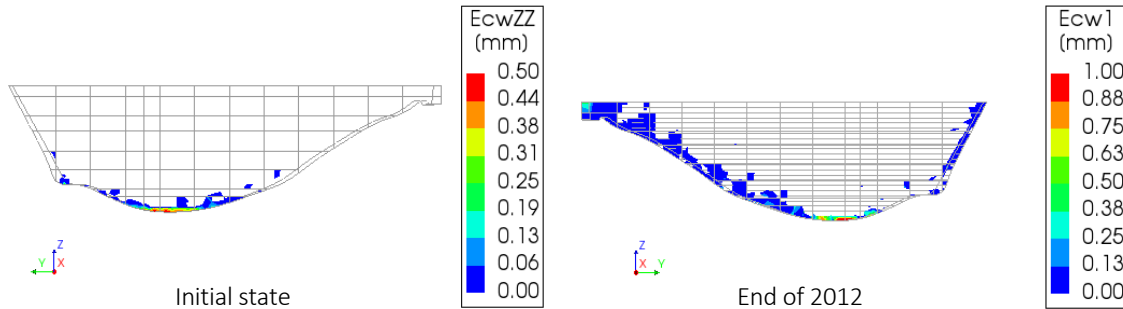
Figure 5-8. Cracks distribution

5.3 *Calibration from FEM*

FEM model results have been used to compare with the provided displacement measurements from two pendulums: bam body (CB_236_196) and dam foundation (CB_195_161) pendulums. The results for FEM are provided in Figure 5-9 and Figure 5-10 for the period of 13 years from 2000 to 2013.

FEM model is able to reproduce the displacement variations following the temperature and water level fluctuations. Similar to the provided measurements the dam tends to move in the upstream direction during warm season due to an expansion process. On the other side, the peak displacements towards downstream occur before the cold season when the reservoir water level reaches its maximum.

As far as the crest radial displacements are concerned fair correspondence between the measurements and calculated data is found. On the other hand, the model underestimates the displacement of the dam foundation in upstream direction. Furthermore, the crack opening measurements (C4_C5) brings the evidence for the movement of the dam. Therefore, it is suggested that the tensile stresses obtained in dam foundation is in reality partially compensated by the opening of the crack.
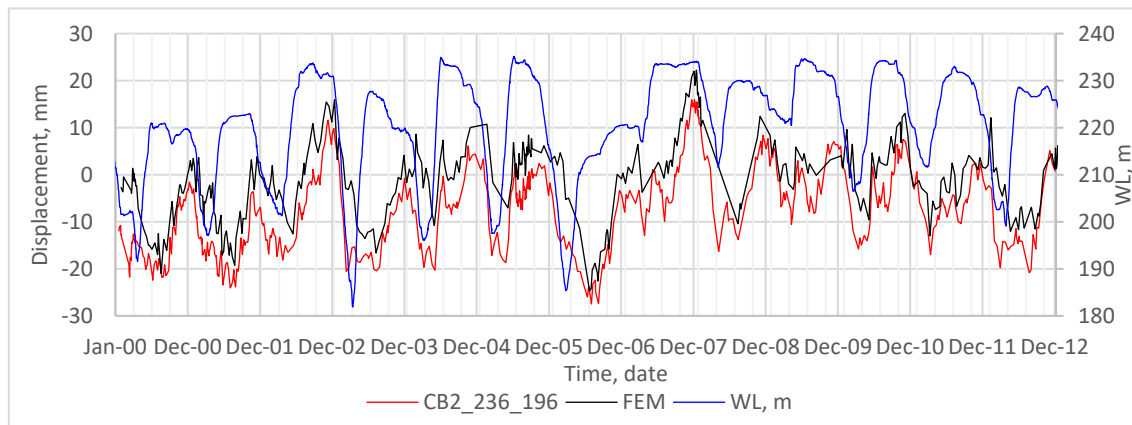
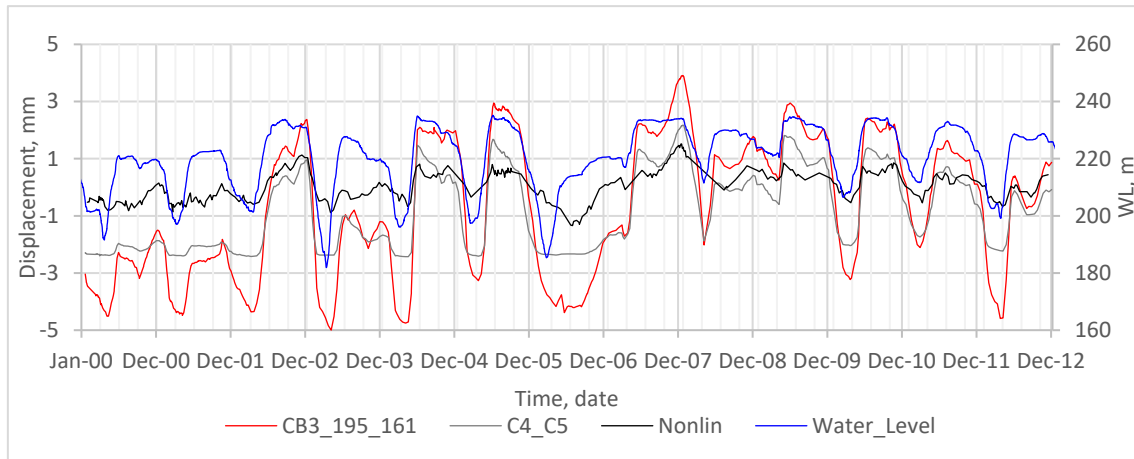Figure 5-9. Calibration of the dam body pendulum CB_236_196

Figure 5-10. Calibration of the low pendulum CB_195_161

6 PREDICTION FROM DATA-DRIVEN AND MODEL-BASED APPROACHES

6.1 *Data-driven prediction*

The 13-year time window has been used as a validation period of the statistical models, as described in the previous Section. In other words, it refers as *training period*, e.g. a sufficiently long period to model the variations of response displacements as driven from predictors or regressors (water level and temperature, in the present case). Therefore, these data have been used as regressors in the prediction period (from January 1st 2013 onwards) to statistically reconstruct displacements.

By a deep visual investigation of Figure 6-1 (CB2_236_196), observations can be derived about the two components of estimated displacements (due to water level and driven by temperature) during the training period (01/01/2000-31/12/2012) and the prediction period (01/01/2013-31/12/2017). Constant reference is dedicated to the measured water level.

During the training period:

- The temperature component of estimated displacements presents a regular trend, with oscillation in the range of approximately [-10, 10] mm. It decreases from winter towards summer, meaning that movements of the dam towards upstream are induced. Indeed, upstream displacements are maximum in summer due to material expansion (during spring a major sun exposure also), resulting in a closure of cracks in concrete and an overall increase of the stiffness.
- The water level component of estimated displacements has less regular trend if compared to the thermal one. The highest downstream displacements are observed in summer. Indeed, an increase of the water level (typically observed from spring to summer) produces movements of the dam towards downstream. In particular, during winter, a low water level (e.g. 31/12/2005) induces less downstream displacements (- 4 mm); a high water level (e.g. 31/12/2007) induces higher downstream displacements (13 mm).
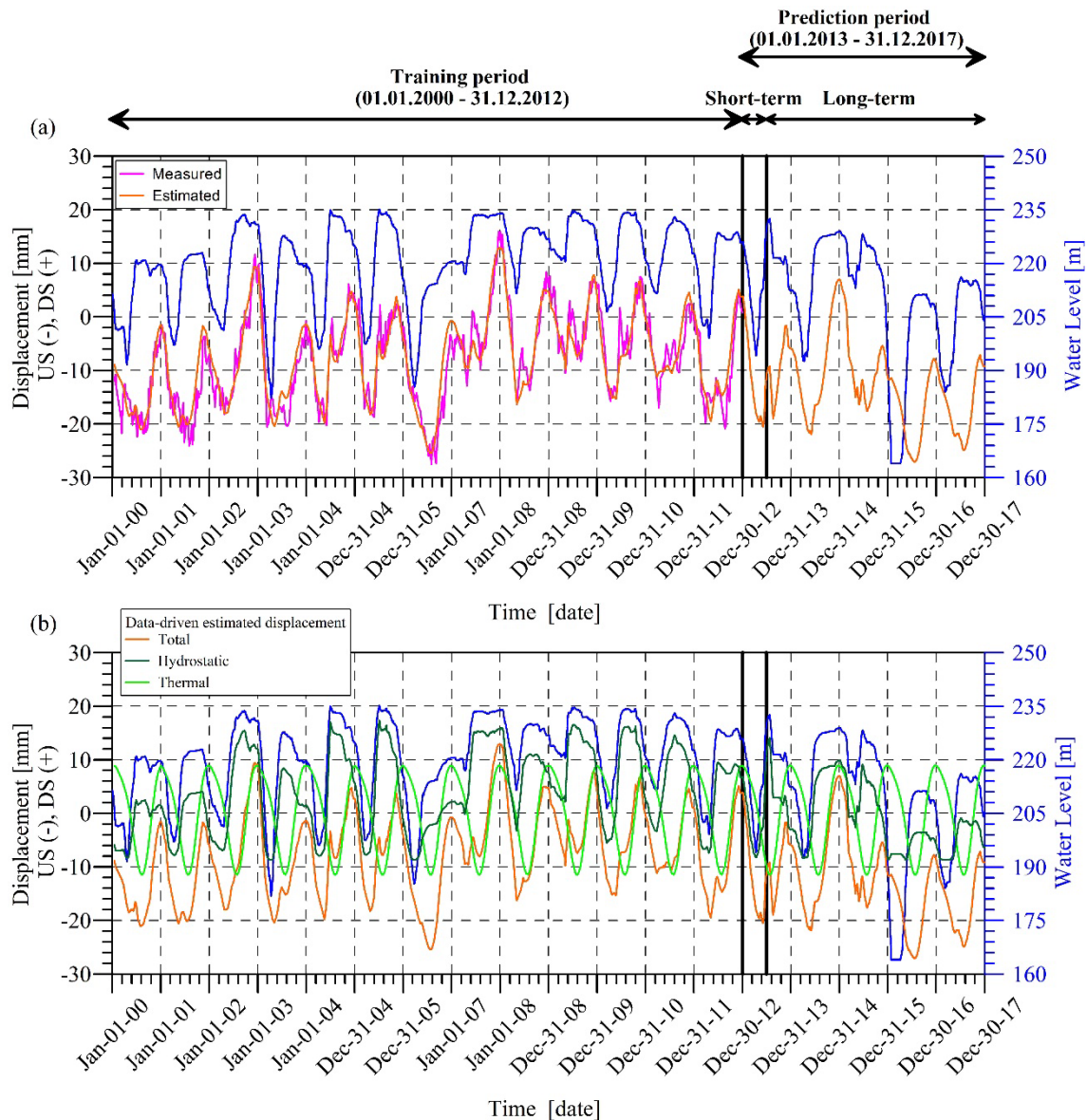
Figure 6-1. Statistical prediction of displacements (CB2_236_196) in the prediction period.

During the short-term prediction period (01/01/2013-30/06/2013):

- The same trend in terms of displacements during the training period can be essentially observed in the short-term prediction period. It has been noticed that measured maximum water level during summer in 2012 was lower (227 m) than during previous years (235 m), producing smaller amount of displacements towards downstream. Therefore, further reduction of the reservoir water level and changing to the warm season of 2013 mainly produce upstream movement and reaches its peak (-20mm) for the end of the short-term prediction period.

During the long-term prediction period (01/07/2013-31/12/2017):

- The regular trend of the temperature component is continuously confirmed.
- The minimum water level measured in spring-summer transition of 2015 is equal to 213.11 m (02/05/2015), lower with respect to previous similar periods.
- Following, an exceptional drastic decrease of the measured minimum water level is observed from autumn 2015 until 26/01/2016, reaching value of 164 m, which is lower than the minimum operating level (174 m). This abnormal decrease can be directly observed through the statistically estimated displacements due to water level that are very

low. The estimated total values of upstream displacements are the lowest values of all estimations, reaching approximately -27 mm and -25 mm (summers 2016 and 2017, respectively).

- On the other hand, after the drastic decrease abovementioned, the measured maximum water levels never went back to typical values about 230-235 m. Indeed, a decrease is observed in the summers of 2016 and 2017 (less than 215 m, if compared with typical levels of the training period, about 235), leading to less downstream estimated total displacements.
- It can be stated that the temperature-driven component of estimated displacements is predominant with respect to the water level component.
- Overall, in the long-term period, the statistical model has been capable to estimate displacements which are compatible with the abovementioned scenario, reaching very low values of -27 and – 25 mm, much smaller if compared to previous statistically estimated displacements.

For the sake of accuracy, the following Table summarizes three examples of measured as well as estimated displacements in correspondence to instants with similar water levels (during the long-term prediction period with reference to the training period).

Table 2. Comparatively investigation of measured and estimated displacements (CB2_236_196).

Water level	Measured	Estimated	Estimated
	Training period		Long-term prediction period
212.5 m	-6.9 mm (02/01/02)	-5.9 mm (02/01/02)	-6.0 mm (05/01/14)
197.4 m	-17.25 mm (17/04/03)	-17.97 mm (17/04/03)	-18.52 mm (20/04/13)
185.5 m	-15.84 mm (28/03/06)	-16.51 mm (28/03/06)	-16.05 mm (21/03/17)

Statistically estimated displacements (total and separate components) during the training and prediction periods have been illustrated in Figure 6-2 for the low pendulum (CB3_195_161). Based in these results, similar observations can be stated for predictions of displacements.

During the training period:

- The temperature component of estimated displacements presents a regular trend, with oscillation in the range of approximately [-2, +2] mm. It decreases from winter towards summer, meaning that movements of the dam towards upstream are induced.
- The water level component of estimated displacements has less regular trend if compared to the thermal one. The highest downstream displacements are observed in summer (5 mm), induced by an increase of the measured water level.
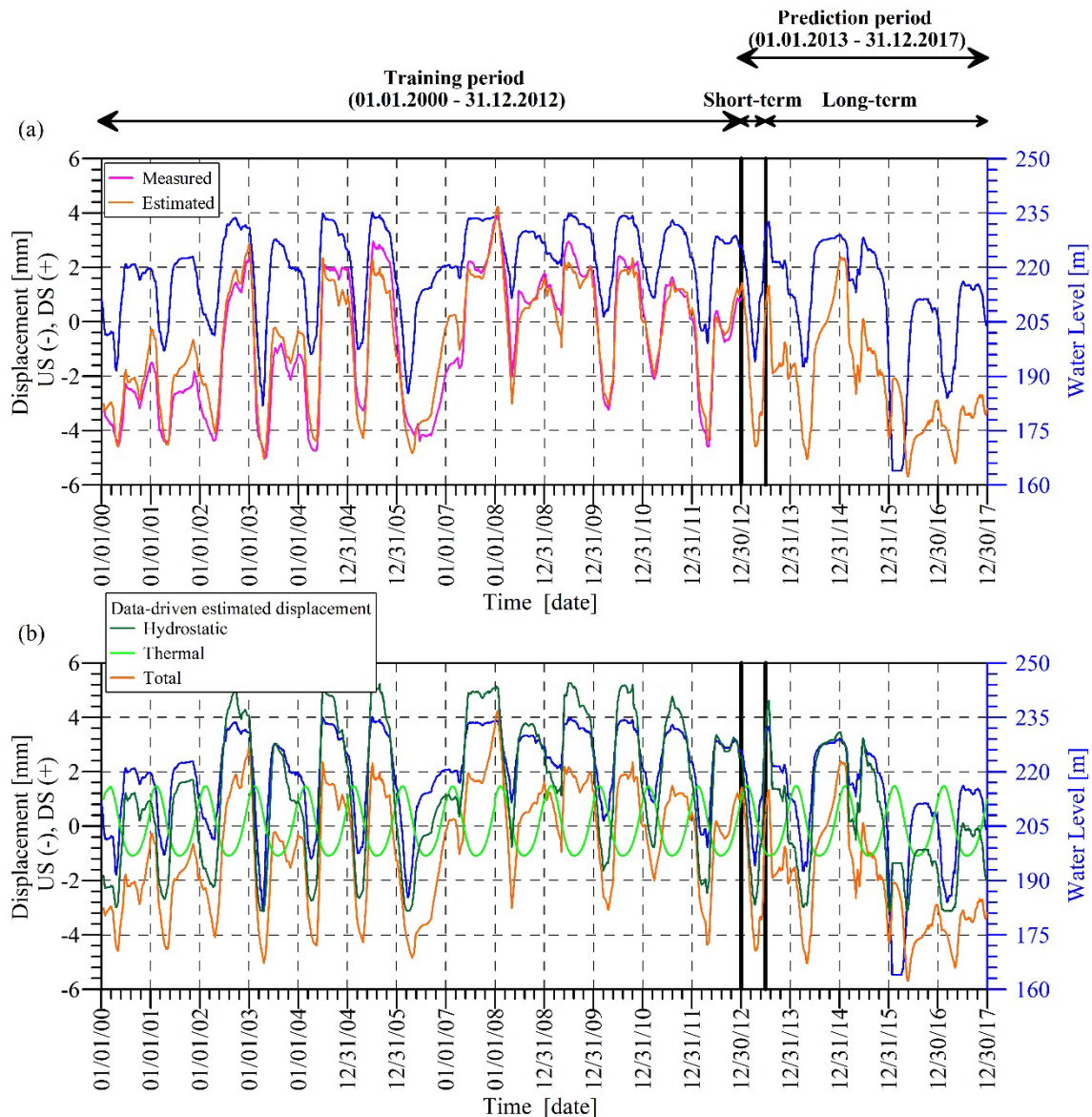- The water level component is predominant if compared to the thermal one.

Figure 6-2. Statistical prediction of displacements (CB3_195_161) in the prediction period.

During the short-term prediction period (01/01/2013-30/06/2013):
- The same trend in terms of displacements during the training period can be essentially observed in the short-term prediction period.

During the long-term prediction period (01/07/2013-31/12/2017):
- The regular trend of the temperature component is continuously confirmed.
- The exceptional drastic decrease of the measured minimum water level (from autumn 2015 until 26/01/2016) is directly mirrored through the statistically estimated displacements. The estimated total values of upstream displacements are the lowest values of all estimations, reaching approximately -6 mm and -5.5 mm (summers 2016 and 2017, respectively).
- With minimum water levels in the summers of 2016 and 2017, the temperature-driven component of estimated displacements is predominant with respect to the water level component.
- Overall, in the long-term period, the statistical model has been capable to estimate displacements which are compatible with the abovementioned scenario.

6.2 *Model-based prediction*

The model-based estimated displacements of both pendulums (obtained from the FE model) are presented in the present Section.

Figure 6-3 and Figure 6-4 illustrate the displacements of the high and low pendulum, respectively. They are plotted comparatively with the statistically estimated displacements. Model-based predictions seem to be closer to statistical predictions in the 1st case, in trend and amplitude.
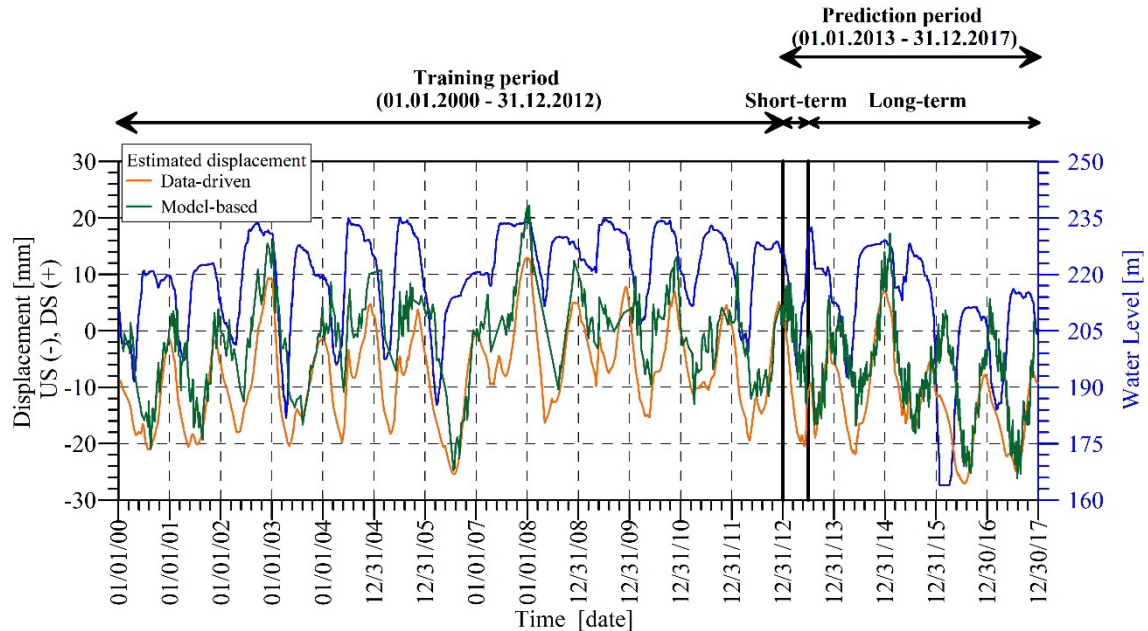
Figure 6-3. Data-driven and model-based predicted displacements (CB2_236_196).
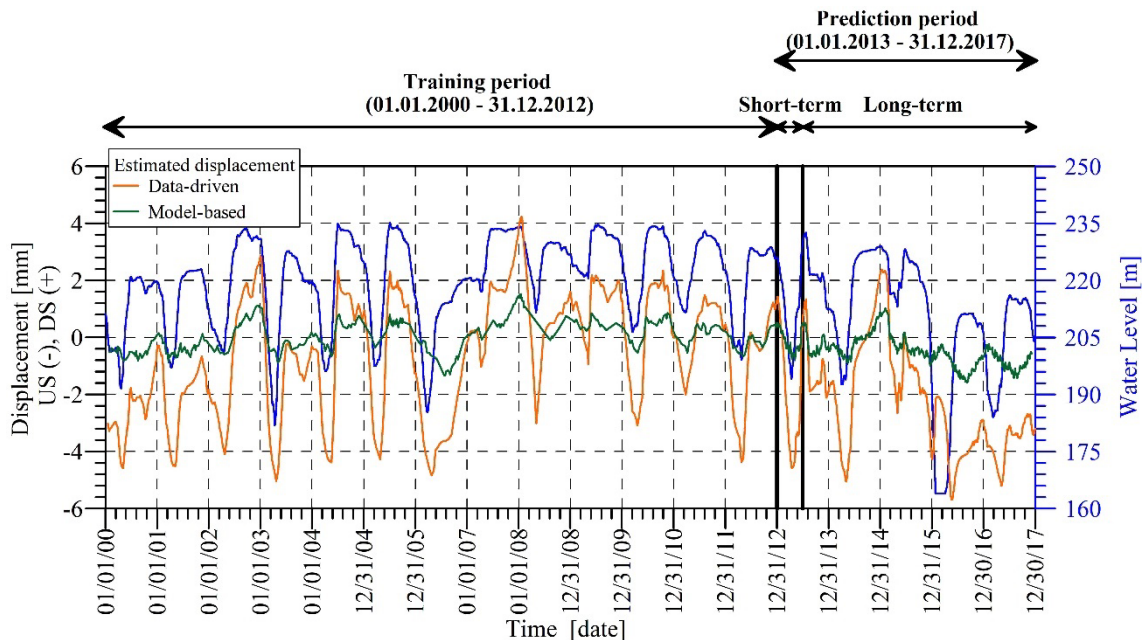
Figure 6-4. Data-driven and model-based predicted displacements (CB3_195_161).

6.3 *Discussion*

By analyzing the provided measurements data, possible explanation for the abnormal operation during the last two years of the prediction period (2016, 2017) has been suggested.

The typical seasonal operation cycle could be described as follows:

- Winter: water level decreases typically from December to January, depending on the year and reaches its minimum by the end of the winter.
- Spring: filling of the reservoir.
- Summer: continue filling of the reservoir, eventually reaching the maximum water level.
- Autumn: water level in the reservoir remains at its maximum level, either start to reduce approaching the beginning of the winter.

During these cycles the radial displacements fluctuate from upstream to downstream direction producing tension zones in the dam body. Typically, the dam leans upstream during warm period and shrinks in downstream direction during cold period 0. Such a behavior holds for quasi-constant water level, while hydrostatic pressure itself acts in the downstream direction.

As stated in the description document, the water level could drop below the heel of the dam leaving the upstream surface exposed to the ambient temperature and direct solar radiation. Already validated in the past 0, cracks are more likely to originate during cold season when the concrete contracts (shrinks), thus developing tensile stresses. On the one hand, horizontal cracks can potentially develop due to tensile stresses acting in the vertical direction. These cracks can be particularly dangerous for the operation, depending on their location, whether on the upstream or downstream zone of the dam. For instance, the development of cracks on the downstream face is considered less critical than damages of the upstream face. On the other hand, tensile stresses acting in the horizontal direction could be accommodated by the vertical contraction joints.

FE analysis demonstrates that there is a development of the horizontal tensile stresses in the upstream face of the dam, while vertical component remains in compression state. On the other side, it could be the case that accumulated tension in the contraction joints develop damages there, and with time it propagates deeper towards downstream. In the adopted finite element model, joints are modelled elastically, therefore, the obtained results could be used rather quantitative than qualitative. FE model results shows the joints that are more likely subjected to opening in the middle of the dam during cold period as illustrated in Figure 6-5.
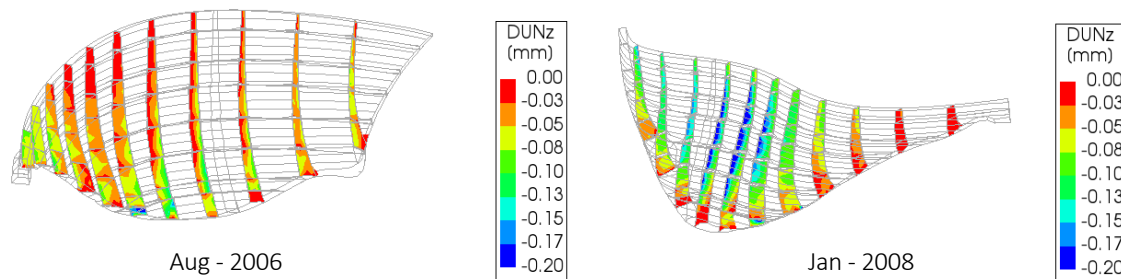

Figure 6-5. Indication of the contraction joints opening

In this context, it is suggested that the opening of the joints in the upstream face could be a possible reason of the exceptional lowering of the reservoir water level. For better prediction of the joints opening and its influence on the stability of the dam, more sophisticated material model (e.g. nonlinear elastic model, friction material model) should be used.

7 CONCLUSIONS

The present paper has focused on the benchmark problem Theme A ''*Behaviour prediction of a concrete arch dam*'' of the 16th International Benchmark Workshop on Numerical Analysis of Dams, Organized by ICOLD Committee on Computational Aspects of Analysis and Design of Dams.

The paper aimed at the calibration of a statistical regression model and a Finite Element model both capable to predict the expected future behavior of the dam under examination.

In particular, predictions have been provided for the radial displacements of both pendulums (CB_236_196, CB_195_161), by comparatively implementing both models. The obtained results have been investigated for the interpretation of dam's behavior.

A training period of 13 years (January 1st 2000 to December 31st 2012) has been considered for the calibration, whereby temperature and water level data have been used as regressors. Two prediction periods have been considered for the prediction, namely short-term (01/01/2013-30/06/2013) and long-term (01/07/2013-31/12/2017) periods.

The main results can be synthesized as follows.
- The hydrostatic-seasonal-time statistical model have estimated the two separate components of displacements (due to water level and temperature), while the irreversible effects not relevant. The out of phase nature of the two separate components has been observed for both pendulums.
- Overall, a good agreement has been demonstrated between time series of measured and statistically estimated displacements, with determination coefficients R^2 equal to 0.932 and 0.964 for high and low pendulum, respectively.
- In the long-term period, the statistical model has been capable estimating displacements which are compatible with the recent scenario of exceptional drastic decrease of the measured water level.
- FEM has shown stress distribution and direction and zones subjected to cracks. These zones are mainly concentrated along the foundation of the dam, perpendicular to the rock surface. The observed crack pattern is rather typical and does not compromise the stability of the dam.
- On the one hand, vertical stresses assessment indicated the tension zone on the downstream face of the dam. However, no cracks have been originated during computations, probably due to assumption of the relatively high tensile strength (2MPa). On the other hand, the upstream face remains under compression in vertical direction, which is crucial to prevent the horizontal cracks development.
- More detailed analysis revealed rather high horizontal tensile stresses on the upstream surface during cold periods of the year, when dam tends to shrink. Usually, these stresses are absorbed by contraction joints.
- Considering the low reservoir water level for the significant part of the cold period, originated tensile stresses could have provoked damages of the joints. It was suggested that the propagation of the damages could have caused lowering of the reservoir water level.

In can be concluded that, the opening of the joints in the upstream face of the dam could be a possible reason of the exceptional lowering of the reservoir water level in the last two years of the monitoring period.

More advanced modeling strategies, e.g. sophisticated material model (nonlinear elastic model, friction material model), could provide better insights and a more accurate prediction of the joints opening and its influence on the stability of the dam.

REFERENCES

[1] Malm, R., Hellgren, R., Ekström, T., and Fu, C. 14-th International Benchmark Workshop on Numerical Analysis of Dams, Theme A. ICOLD Committee on Computational Aspects of Analysis and Design of Dams, 2017.

[2] TNO DIANA (2017). DIANA User's Manual, Release 10.1. Delft, the Netherlands.

[3] ICOLD COMMITTEE ON CONCRETE DAMS THE PHYSICAL PROPERTIES OF HARDENED CONVENTIONAL CONCRETE IN DAMS, March 2008

[4] DamReg (2004). User Manual, Version 1.1, Benedikt Weber, Lennoxville, Québec, Canada. Federal Office for Water and Geology (FOWG), Bienne, Switzerland.

AAR affected dams

Theme B

EVALUATION AND PREDICTION OF THE BEHAVIOUR OF THE BEAUHARNOIS DAM

Description and Synthesis of Theme B

Formulators:

Simon-Nicolas Roth
Hydro-Québec, Montréal, Québec, Canada,

Benjamin Miquel
Hydro-Québec, Montréal, Québec, Canada,

1 INTRODUCTION

1.1 *Background*

The alkali-aggregate reaction (AAR) can cause serious concerns about the integrity of concrete structures. Moreover, the operation of hydraulic structures such as dams, power plants and spillways affected by this reaction can be compromised. To assess the integrity usability of these structures and to predict the long-term performance and the scale of the investments required to keep the structures in safe conditions, it may be necessary to use numerical models.

Due to the complexity of AAR, its multi-physical/multiscale nature and the constantly evolving research on this subject, there is currently no consensus on how to model AAR. The different modelling approaches were classified (Esposito & Hendriks, 2019) on the basis of their input parameters as: (1) models based on concrete expansion, (2) models based on internal pressure, (3) models based on the gel production and (4) models based on the ions diffusion-reaction mechanisms. Some of these approaches are limited to small-scale models whereas others can be extended to structural analyses.

These later models are generally not accessible to the general public in commercial software. Therefore, implementation of the complex physical equations required to properly model the AAR process (damage, reinforcements, moisture transport, thermal effects, chemical reaction, uplift pressures, etc.) is required by the engineering team.

From the dam owner point of view, it is not easy to take a decision involving a major investment on a structure whose sustainability may not be guaranteed by relying on numerical models whose verification and validation (V&V) process (Oberkampf & Roy, 2010) may not be carried out rigorously.

In a numerical model, the fundamental physics is coded using proper discretization (e. g. finite volume, finite difference, finite element, etc.) to predict the behaviour of a physical model. These models are used to reduce the time, cost, and risk associated with full-scale testing of products. In model V&V, verification and validation can be defined as (Oberkampf & Roy, 2010):

- Verification is the process of assessing software correctness and numerical accuracy of the solution to a given mathematical model
- Validation is the process of assessing the physical accuracy of a mathematical model based on comparisons between computational results and experimental data.

The validation process quantifies the credibility and predictive accuracy of a numerical model providing the decision maker with the information necessary for making high-consequence decisions. The fundamental elements that build credibility in computational results can be defined as (Oberkampf & Roy, 2010):

- quality of the analysts conducting the work
- quality of the physics modelling
- verification and validation activities
- uncertainty quantification and sensitivity analyses.

Engineers seeking to develop credible predictive models critically need model V&V guidelines and procedures. Organizations such as Society for Computer Simulation (Terminology for model credibility, 1979), US Department of Defense (Department of Defense, 2018), American Institute of Aeronautics and Astronautics (American Institute of Aeronautics and Astronautics, 1998), American Society of Mechanical Engineers (American Society of Mechanical Engineers, 2006), Los Alamos National Lab (M.C. Anderson et al, 2004) have published guidelines on model V&V.

To date, there were many difficulties to have a formal and systematic framework to validate numerical models able to model AAR-affected concrete structures. The assessment of numerical codes has been partially performed within the ICOLD International Benchmark Workshops on Numerical Analysis of Dams, where three benchmark cases were defined:

- 2011 - Valencia, Spain (Molin & Noret, 2011)
  Case: Kariba dam (arch dam)
  Exercise: Determining adequate swelling law and parameters which allow the best identification with both horizontal and vertical movements of the dam vs time.
  Number of participants: 9

- 2005 - Wuhan, China (Masarati, Mazzà, & Meghella, 2005)
  Case: Poglia dam (hollow gravity dam)
  Exercise: Structural behaviour of a large hollow gravity dam, with special reference to the ultimate strength against the hydrostatic load
  Number of participants: 2
- 2001 - Salzburg, Austria (Strutturale, 2001)
  Case: Pian Telessio dam (arch dam)
  Exercise: Forecast on stress-strain state generated by AAR
  Number of participants: -

The European project Integrity Assessment of Large Concrete Dams (NW-IALAD) also conducted a series of cases to help AAR numerical model V&V process. More recently RILEM Technical Committee 259-ISR (Saouma, 2020) released two sets of problems (first set at the material scale concrete specimens and the second, at the structural scale) with the objective of creating the first step towards the development of a formal approach recognized by the profession to achieve the V&V process to assess AAR numerical models.

This benchmark is proposed to enrich the database of validation cases at the structural scale. Due to the complexity of modelling such complex phenomena at a structural scale, it is our belief that dams affected by AAR for which rigorous monitoring and surveillance activities have been undertaken for many years should be used as validation benchmark to minimally confirm that a given model is able to estimate the observed behavior and damage.

1.2 *Objectives of the benchmark*

The objective of this benchmark is to perform modelling of a concrete power plant affected by AAR. The data necessary for the calibration of the model are provided and a prediction phase is proposed. Divided into four tasks, a step-by-step method is proposed to integrate the physics affecting the chemical reaction. Participants are invited to provide the displacements at certain topographic points, the resultant forces on given interfaces and to provide certain plots to qualitatively describe the cracking computed.

The phases of the studies are as follows:
- Calibration and prediction (50%): The formulators of the benchmark provide information necessary to perform the time-history studies of the structure, including geometry, details and arrangement of the reinforcement, finite element model, material characteristics, boundary conditions (displacements, thermal and hygral), static loading (self-weight and hydrostatic pressure due to reservoir loads). The participants are expected to analyze the data provided and the required results. They may introduce additional data, and refine the finite element mesh provided if required for the purposes of the envisaged analysis. It is underlined that the current benchmark problem concerns only the concrete body and excludes those related to the dam foundation.
- Results, evaluations and conclusions (30%): The expected results include the temporal displacements, the interface loads history and the structure stiffness change according to the progression of the alkali-aggregate reaction. A number of plots should be provided by the participants to identify the principal cracks. Cross sections are suggested to facilitate understanding and allow comparison with those of the other participants. It is also suggested that the participants comment and explain these results. It is recommended to define the possible failure mechanisms associated with the cracking computed. High emphasis should be given to the engineering interpretation and analysis of the obtained results in view of the dam's safety.
- A critical review of the numerical model (10%): A critical review of the numerical model employed within the context of the benchmark is requested. The participant may discuss the level of physics required to correctly predict the effect of the AAR.
- Proposals for stability and functionality analysis (10%): Participants are asked to give ideas on methods that could be used to evaluate the stability and functionality of the power plant based on computed damage, displacements, etc. Proposals and recommendations for further consideration are requested.

1.3 *Brief dam description*

The Beauharnois dam is located about 50 km west of the city of Montreal. The power station, with a total length of 1397 m, turbines the waters of the St. Lawrence River and includes 37 turbine-generator units, 36 of which are in service and two auxiliary units A and B out of service for a total installed power of 1903 MW.

The Beauharnois development includes a spillway, left and right bank gravity dams and approximately 50 km of dikes on the left and right banks of the Beauharnois Canal. This canal was built between 1929-1932 on the south side of the St-Lawrence River measuring 24.5 kilometres in length, with a minimum depth of 8 metres and a width of 182 metres. The canal was built to take advantage of the 24 metres drop between Lake St-Francis and Lake St-Louis. The Beauharnois development is part of the Beauharnois-Les Cèdres hydroelectric complex displayed in Figure 1.

Figure 9. Beauharnois-Les Cèdres hydroelectric complex

The construction of the Beauharnois power plant took place in three phases:
- the first phase (phase I) where the concreting of the groups took place in the period 1930-1932 with the commissioning of 14 groups (groups 1 to 14) between 1932 and 1948;
- 12 more groups (from 15 to 26) were put into service between 1950 and 1953 for the second phase (phase II);
- and finally during the third phase of construction (phase III), 10 groups (from 27 to 37) were put into service between 1959 and 1961.

Within the framework of a numerical benchmark, it is not realistic to model the entire power station with a length of 1397 m. Therefore, a single power unit with its two neighbouring units will be considered.
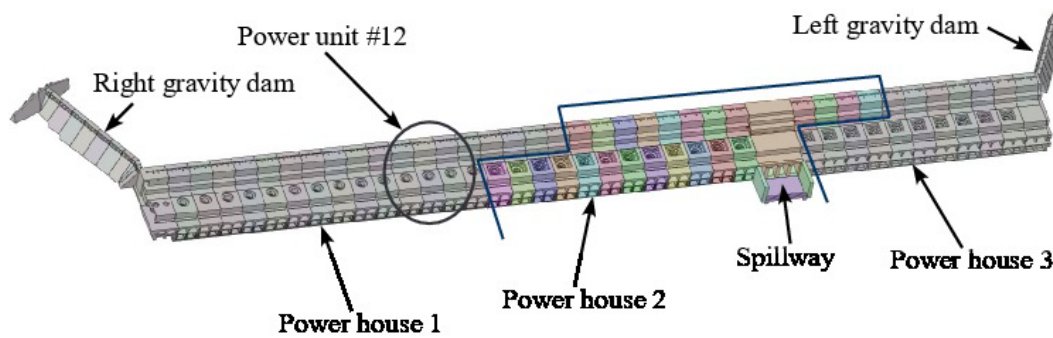
Figure 10. Beauharnois power plant

The power unit #12 (illustrated in Figure 2) was selected because it is reasonable, in the reduced numerical model, to assume symmetric boundary conditions as it is located far from the gravity dams and spillway sections which influence longitudinal displacements. In addition, this power unit has a more sophisticated auscultation system than other power units. Note that the topographic auscultation system was implemented in 1973, therefore the first 40 years of data was not recorded.

Several decades of investigations and interventions were made to mitigate the effect of AAR. These interventions have low effects on the displacements, therefore they will be ignored for this benchmark.

1.4 *Problem statement*

The benchmark proposes to calibrate the numerical model of power units #11 to #13 on the basis of the recorded data and to predict the displacements, damage, loads of the next 50 years with different levels of physics affecting the chemical reaction.

The formulators of the benchmark provide information necessary to perform the time-history studies of the structure, including geometry, details and arrangement of the reinforcement, finite element model, material characteristics, boundary conditions (displacements, thermal and hygral), static loading (self-weight and hydrostatic pressure due to reservoir loads).

Divided into four tasks (one mandatory and three optional), the participants are invited to provide the displacements at certain topographic points, the resultant forces on given interfaces and to provide certain plots to qualitatively describe the cracking computed.

1.5 *Deliverables*

The results provided by the participants will be both in paper format, but also the requested raw output data should be submitted to formulators by an Excel template file.

The paper should present the chosen solution method. The AAR model shall be described along with the method used to couple the physics with the chemical model. The process for performing the V&V of the AAR model should be presented in the document.

It is recommended to define and provide explanation for any additional parameters added to calibrate the model.

The items discussed in the phases of the studies (section 1.2) should be included in the paper. This includes the results, evaluations and conclusions. A section on a critical review of the numerical model is highly recommended. Finally, proposals for stability and functionality analysis shall be discussed.

2 NUMERICAL MODEL

2.1 *Coordinate system*

The coordinate system to be used by all participant is as follow:
- X direction: bank direction; positive towards right bank;
- Y direction: upstream/downstream direction; positive towards downstream;
- Z direction: vertical direction; positive towards elevation.

All information provided by this benchmark are in this coordinate system.

2.2 *Geometry*

The power unit #12 is part of the first phase of construction of the Beauharnois power station commissioned in 1932. Figure 3 shows a typical cross section of the first phase of construction. The water intake part has a height of approximately 21.5 m and includes the penstocks, the upstream gates and the busbar. The power plant is approximately 24 m high and includes the generator unit, the scroll case, the draft tube, the tailrace and the downstream gates. A cold joint separates the water intake part from the power plant.

2.3 *Mechanical boundary conditions*

The displacement boundary conditions applied to the model (displayed in Figure 4) are as follows:
- on the base of the foundation, a zero displacement in the 3 directions X, Y, Z is applied (Ux = Uy = Uz = 0);
- on the downstream part of the foundation, a zero displacement in Y is applied (Uy = 0);
- on the right bank and left bank boundaries of the foundation and the dam, the displacement in direction X is blocked (Ux = 0).
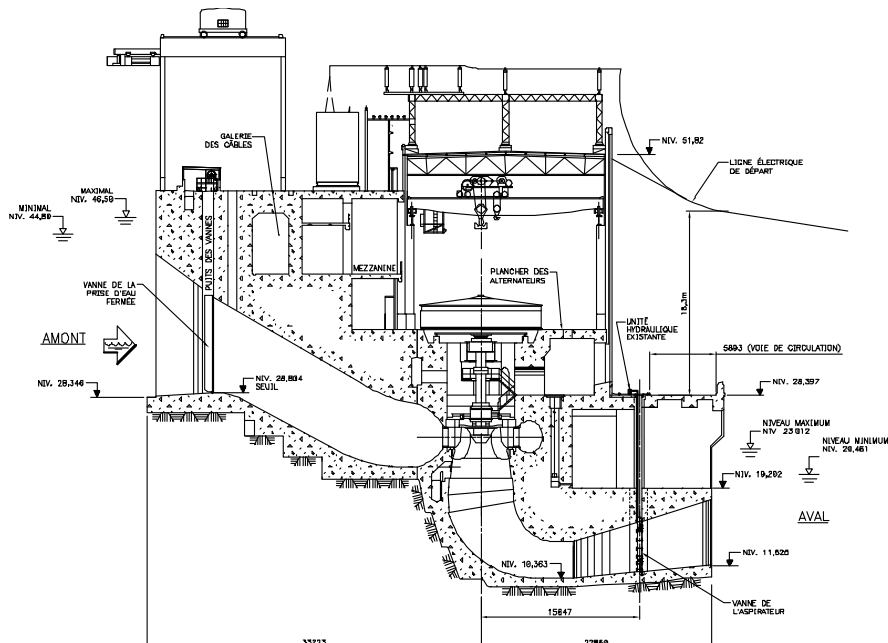
Figure 11. Cross section of power unit #12
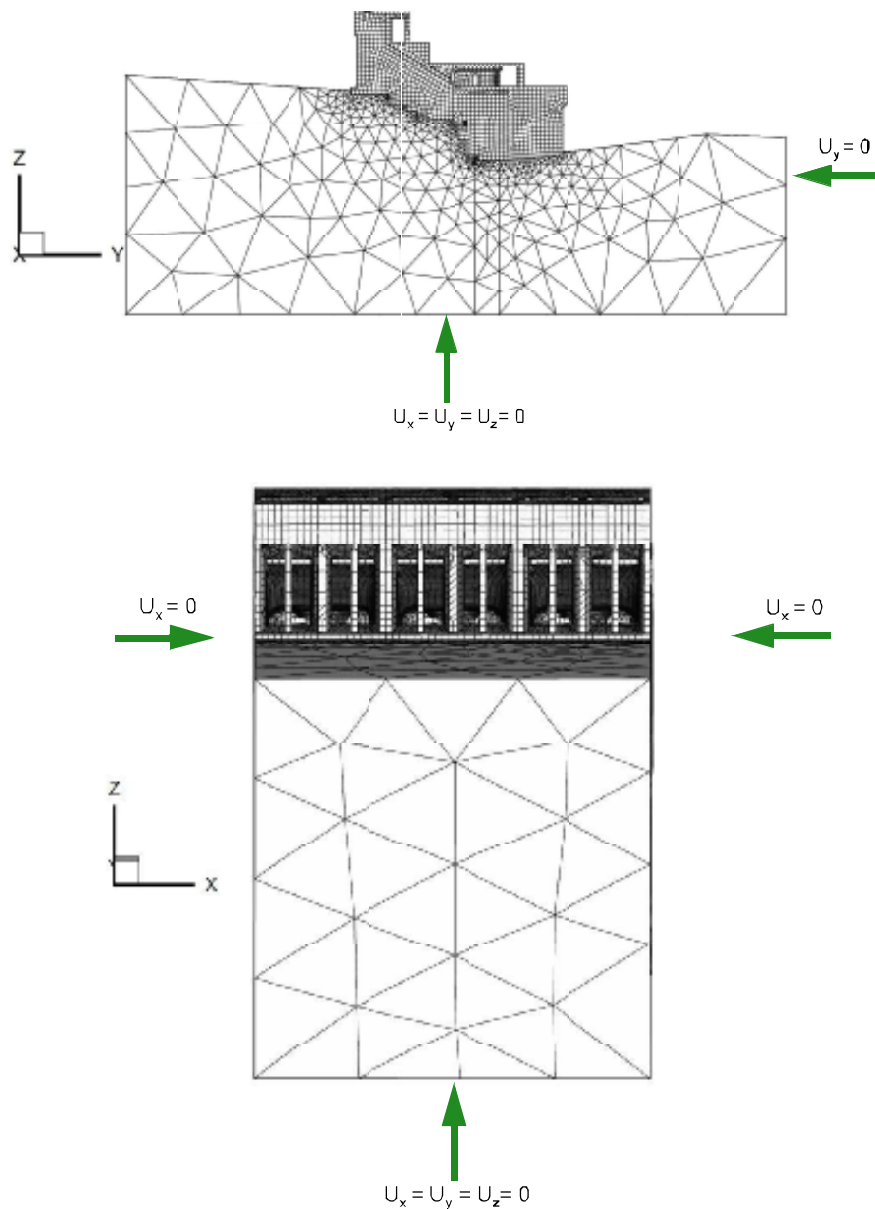
Figure 12 (a). Downstream and foundation boundary conditions, (b) Lateral and foundation boundary conditions

2.4   *Thermal boundary conditions*

Heat transfer analyzes are needed if the AAR kinetic model explicitly requires the temperature field. These allow to compute the temperature field within the dam. The temperature field can then be used as an input for mechanical analysis where the temperature of the concrete can greatly influence the kinetics of AAR.

It is recommended to use the same numerical model for heat transfer and for mechanical analysis. Heat transfer analyzes can be carried out in a transient regime over a sufficiently long period (by experience, about 6 years are required considering an initial nodal temperature value corresponding to the average outside temperature) to allow convergence (repetition of temperature variations year after year). The computed sixth year can be used repeatedly for mechanical analysis. However, any other method can be used.

The boundary conditions are defined in Figure 5 and the corresponding annual temperature distribution (colour code) is displayed in Figure 6. The excel file provided in the Temperature.xls package gives the numerical values displayed in the figure. The convective coefficient associated with each annual temperature distribution is given in Table 1.

No temperature must be applied at the concrete-rock interface, on the left and right banks, on the upstream, downstream and lower foundation limits ensuring free heat exchange. On the upper surface of the foundation located upstream and downstream of the power plant, the water temperature should be applied.
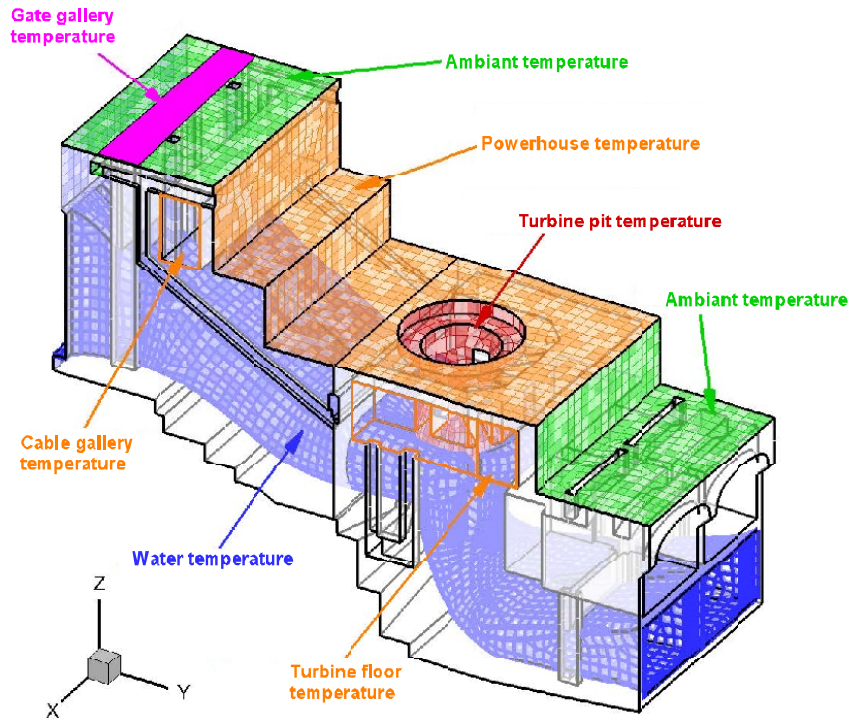
Figure 13. Thermal boundary conditions

Table 10 Temperature boundary conditions

Boundary name	Convection coefficient ($Wm^{-2}\ °C^{-1}$)
Ambient	24.7
Powerhouse/turbine floor	9.5
Water	696.0
Turbine pit	108.0
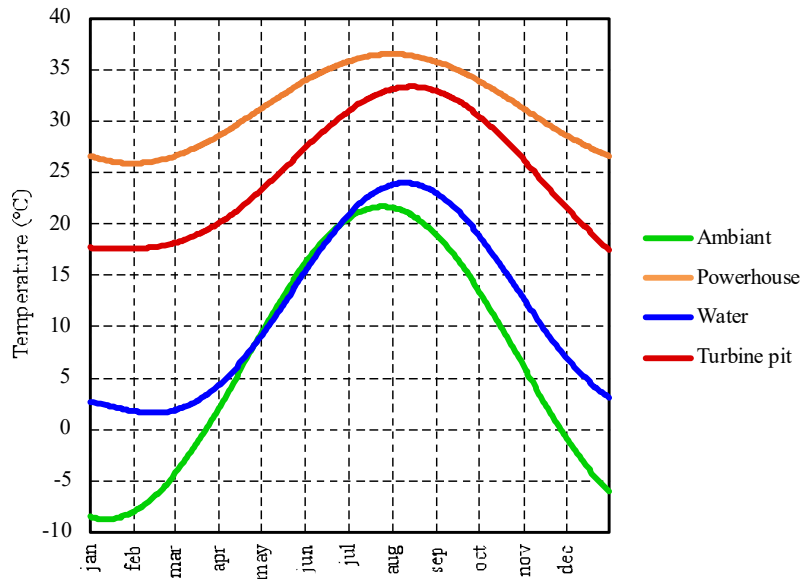
Figure 14. Yearly temperature variation

2.5 *Hygral boundary conditions*

In a concrete structure, the degree of initial saturation is close to 100% and is reduced by drying and desiccation. The drying modelling is generally based on a nonlinear diffusion equation governing the evolution of liquid water saturation. This equation is similar to a generalized Darcian flow in a transient state. The work of (Bear & Bachmat, 1990), (Mainguy, Coussy, & Eymard, 1999), (van Genuchten, 1980) and (V. Baroghel-Bouny et al., 1999) allow us to solve this equation formulated as a function of capillary pressure.

The boundary conditions are given in Figure 7 in terms of capillary pressure P_c and relative The capillary pressures given are based on the average temperature recorded near the boundary.
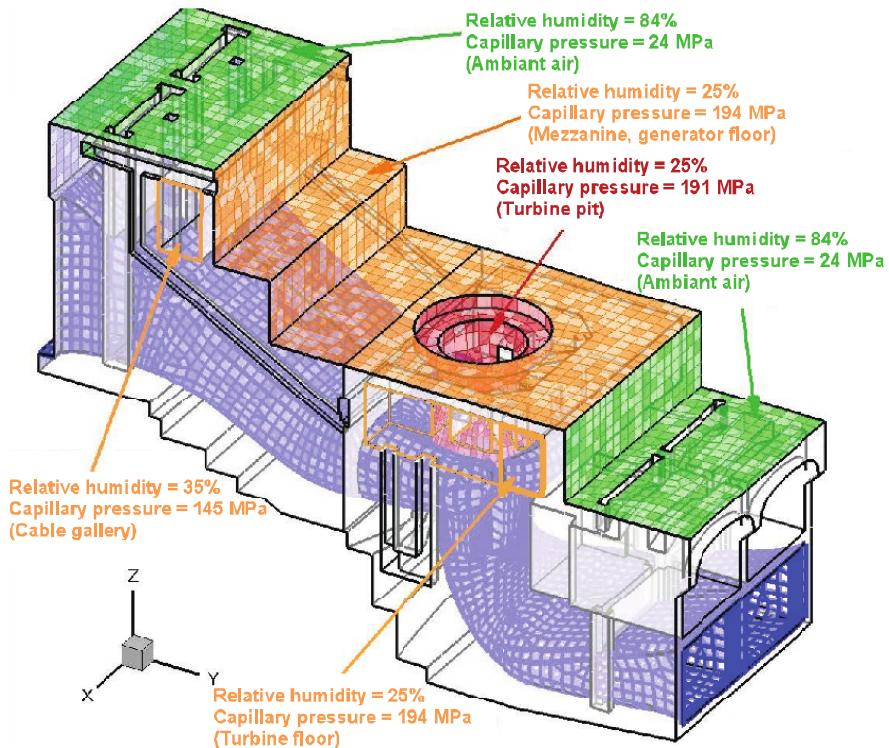
Figure 15. Hygral boundary conditions

2.6 *Concrete reinforcement*

Three different types of steel were used for the structural steel for the Beauharnois generating station:

- type HG for "Hard Grade";
- type SG for "Structural Grade";
- type IG for "Intermediate Grade".

Table 2 presents the steel properties for each grade.

Table 11. Reinforcement steel properties

Property	Tensile strength (F_y) (MPa)	Ultimate strength (F_u) (MPa)
Hard Grade	345	552
Structural Grade	228	397
Intermediate Grade	276	483

For groups 11, 12 and 13, rebars of 0.75 inch (19 mm), 1 inch (25.4 mm), 1.25 inch (31.75 mm) and 1.5 inch (38 mm) were used with square or round sections (given in Figure 8). The steel elastic modulus is 200 GPa. The participants are free to model the reinforcements using embedded, smeared or discrete formulations.
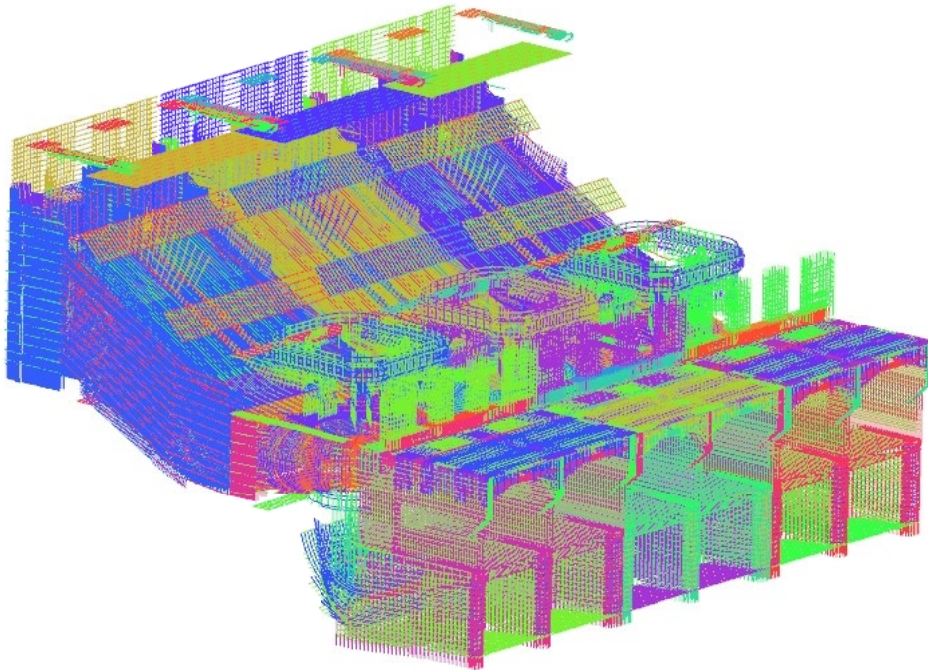
Figure 16. Concrete reinforcement

2.7 *Material properties*

The material properties used for the mechanical analyzes were determined in part using: empirical formulas from the literature, the characteristics of the concrete used during the different construction phases of the Beauharnois development and the multiple investigations and tests carried out over the years. Properties which could not be obtained from these sources were evaluated using sensitivity studies. The review of construction documentation, the concrete investigations and laboratory tests show that the same concrete was used in both intake and powerhouse structures. Therefore, participants should use identical chemical reaction properties for unconfined concrete at identical temperature and humidity in these two structures. Table 3

presents the material properties to be used for the numerical analysis while Table 4 gives the resistance parameters used for the material performance during nonlinear analyzes.

Table 12. Material properties

Property	Concrete	Foundation
Density (kg/m^3)	2365	0 (mechanical analysis)
		2627 (thermal analysis)
Poisson's ratio (v)	0.21	0.20
Instant modulus (GPa)	26	-
Deformation Modulus (GPa)	-	30
Specific heat (J/kg °C)	917	800
Coefficient of thermal expansion (°C^{-1})[1]	0	0
Thermal conductivity (W/m °C)	2.9	4.3
Reference temperature (°C)	10	4

Table 13. Concrete strength properties

Property	Value
Compressive strength (f'$_c$) (MPa)	30
Tensile strength (f$_t$) (MPa)	3
Fracture energy (G$_F$) (N/m)	350

The concrete hygral properties are defined in Table 5 and are related to the Mualem model for desorption. The foundation is considered fully saturated.

Table 14. Concrete hygral properties

Property	Value
Initial saturation	0.85
Parameter a (MPa)	18.6
Parameter m	0.44
Total porosity ϕ ($\frac{m^3}{m^3}$)	0.14
Absolute or intrinsic permeability k (m^2)	5.49×10^{-12}

3 REQUESTED ANALYZES

3.1 *Mechanical analyses*

The mechanical analyses are required to compute stresses and displacements in the dam. These time-dependent analyses may be performed as static or quasi-static depending on the preferences of the participant. The loads that should be considered in the analyses are:
- gravity loads;
- hydrostatic water pressure;
- induced load caused by the chemical reaction.

All mechanical analyzes are started on July 1, 1932 and the calibration period ends on January 1, 2017. The data available to calibrate the model does not cover the entire period. Therefore, to calibrate the model, it is suggested to shift the data to match the total displacement computed on the first day of acquisition. Finally, participants are free to define the time step of their choice.

---

[1] To simplify the analysis, the thermo-mechanical effects are not considered.

The temperature distributions obtained from the thermal analysis should be used as input to the analysis only to consider its influence on the chemical reaction. It is required to neglect the thermo-mechanical effects by setting the coefficient of thermal expansion $\alpha = 0$ for all materials as previously defined in Table 3.

3.1.1 Gravity loads

The gravity load for the concrete dam should be included in all analyses based on the densities given in Table 3. No gravity load or density should be considered for the foundation.

3.1.2 Hydrostatic water pressure

Hydrostatic water pressure should be included in all analyses. The upstream water level should be 46.10 m and the downstream water level should be 21.4 m. The penstocks, scroll case, draft tube and tailrace pressure is considered to vary linearly between the upstream and downstream level.

3.1.3 Induced load caused by the chemical reaction

All types of models, from the simplest to the most complex, can be used by the participants (thermal analogy, poroelasticity, multi-physics, chemo-mechanical, etc.). The considered model must be documented and presented in the paper.

3.2 *Other considerations*

In addition, all participants also have the possibility to include other specific aspects or assumptions that is believed to improve the analysis. The participants can use unbound interfaces between the power units and between the water intake part and the power unit. The type of physical coupling (one-way or two-way coupling) depends on the preferences of the participant. These can be documented and presented in the paper.

3.2.1 Creep and relaxation

The participants may choose to consider the effect of creep and relaxation in the analyses. Creep and relaxation have a significant influence on the state of stress due to induced AAR strains. A viscoelastic or viscoplastic rheological model can be introduced by the participants to convert swelling strain into realistic stress values. It is expected that the inclusion of creep and relaxation in the analyzes will reduce the damage, diffuse cracking, increase the crack openings and increase the displacements.

In the absence of creep tests which last several months or even years in order to obtain an asymptotic strain curve, it is recommended to use a creep modulus of 0.5 times the initial elastic modulus of concrete. This value comes from tests carried out on an American dam (Pirtz, 1968) and on cores extracted from another Hydro-Quebec owned dam.

3.3 *Linear task (mandatory)*

Prior to achieve the nonlinear tasks, the participants shall perform a static linear elastic analysis. Only the dead load and hydrostatic pressure shall be imposed. If the participants want to use unbound interfaces between the different power units and between the water intake part and the power unit, it is required to bound them for this analysis. In addition, no creep or relaxation shall be considered for this analysis.
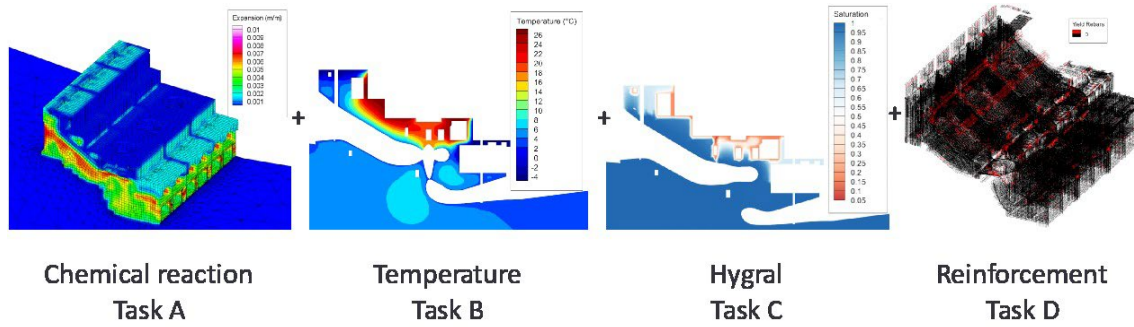
Figure 17. Tasks for theme B

3.4 *Nonlinear tasks*

Four tasks are proposed for this theme, with one mandatory (A) and the other three considered as optional (B, C, D). Figure 9 gives the proposed path to achieve the tasks. The participant can bypass a task, however it is recommended to integrate the physics in the proposed order. For example, if a model does not consider the effects of the concrete saturation on the chemical reaction, participants can integrate the physics of tasks A and B without considering that of task C when task D is performed. The tasks are described in the next sections.

3.5 *Task A: Baseline solution (mandatory)*

The baseline solution is considered to be the simplest of the four nonlinear tasks. The induced load caused by the chemical reaction is computed using a uniform and constant thermal field at 10 °C and the concrete must be considered to be fully saturated.

The calibration shall be carried out with the measured data and a prediction of 50 years up to January 1, 2067 is requested. Since the boundary conditions in the longitudinal direction (X component) is imposed and considered as zero, displacements in this direction shall not be compared to the measured data.

The instrumentation data available to calibrate the model does not start at the end of the construction period. The total displacement is therefore unknown. Thus, as the real displacement at the start of the acquisition period is not zero, the measured data must be translated for calibration. This translation value will be a function of the latency time imposed by the swelling model, on the variation of the concrete stiffness, on the state of damage, etc.

3.6 *Task B: Consideration of thermal effects (optional)*

The thermal effects are important on the latency time as well as on the rate of swelling. For a structure subject to a northern climate, areas exposed to ambient air should swell at rates lower than those found near power units. By carrying out a thermal study in transient mode (by a coupled or decoupled analysis), it is suggested to take the steps of the baseline analysis again, but by imposing the computed thermal field. Two methods can be used: (1) determine the mean nodal thermal field and impose it during the analysis (2) vary the thermal field as a function of time during the analysis. This analysis should be carried out by repeating the phases of calibration and prediction from rhe previous task.

3.7 *Task C: Consideration of hygral effects (optional)*

By taking the steps of the previous tasks, a sensitivity analysis of the results according to the distribution of the degree of saturation of the concrete should be carried out. By carrying out a nonlinear transient diffusion (by a coupled or decoupled analysis), it is suggested to take the steps of the previous tasks again, but by imposing the computed hygral field. Similarly to task B, two methods can be used: (1) determine the steady hygral field and impose it during the analysis (2) vary the hygral field as a function of time during the analysis. This analysis should be carried out by repeating the phases of calibration and prediction and optionally by integrating the physics of the previous tasks.

3.8 *Task D: Consideration of reinforcement (optional)*

The confinement effects caused by the presence of reinforcement have an influence on the rate of swelling, diffusion of cracks, reduction in cracks openings, etc. Task D therefore consists of taking into account the presence of reinforcement. This analysis should be carried out by repeating the phases of calibration and prediction and optionally by integrating the physics of the previous tasks.

3.9 *Summary of the tasks*

Table 6 gives a summary of the physic integration for each proposed tasks. The requested results are given in the next section.

Table 15. Physic integration

		Task	Dead load	Hydrostatic load	Thermal effects	Hygral effects	Reinforcement
Static	Linear	Initial	X	X	-	-	-
Time-History	Non-Linear	A	X	X	-	-	-
		B	X	X	X	-	-
		C	X	X	O	X	-
		D	X	X	O	O	X

X: Mandatory
O: Optional

4 REQUESTED RESULTS

4.1 *Topographic point location*

The location of the topographic point for model calibration and prediction period are illustrated in Figure 10 and located at these coordinates:
- Crest : monitoring point identified as 1250D160 (901.9829, 1194.1149, 48.9311);
- Turbine pit : monitoring point identified as 1295Q099 (893.4600, 1217.970000, 30.1341);
- Turbine floor : monitoring point identified as 1250U097 (902.3079, 1230.1218, 29.3903).
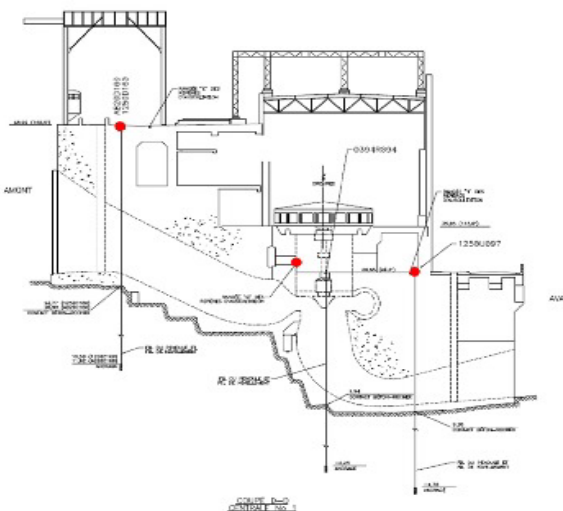
Figure 18. Topographic point and pendulum location (highlighted in red)

4.2 *Displacements*

For the topographic points given in section 4.1 the participants shall record the upstream/downstream (Y component) and vertical (Z component) in a table similar to Table 7 in the provided file.

Table 16. Results at topographic points

Topographic point	Y (mm)	Z (mm)
1250D160	X	X
1295Q099	NA	X
1250U097	X	X

4.3 *Displacements time histories*

The participants shall present the upstream/downstream (Y component) and vertical (Z component) time-history displacements for the entire result range (from July 1, 1932 up to January 1, 2067) in the provided file for the topographic points given in section 4.1.

4.4 *Resultant forces at the interface*

Participants shall output the resultant forces at different interfaces of power unit #12. The interfaces are displayed in Figure 11 and the results should be recorded in a table similar to the Table 8 provided in the provided file.

For comparison purposes, the resultant on one interface should ignore nodal forces located at the junction between two interfaces as follow:

- Intake 11/12 & 12/13: all nodal forces on this interface except those located at bedrock and intake/unit interface;
- Unit 11/12 & 12/13: all nodal forces on this interface except those located at bedrock and intake/unit interface;
- Intake/Unit: all nodal forces on this interface except those located at bedrock;
- Rock/Intake & Rock/Unit: all nodal forces on these interfaces.

Table 17. Results at the interfaces of power unit #12

Interface	X (MN)	Y (MN)	Z (MN)
Intake 11-12 (purple)	X	X	X
Intake 12-13 (cyan)	X	X	X
Intake/Unit (orange)	X	X	X
Unit 11-12 (brown)	X	X	X
Unit 12-13 (red)	X	X	X
Rock/intake (green)	X	X	X
Rock/unit (pink)	X	X	X
Sum left bank	X	X	X
Sum right bank	X	X	X
Sum rock-concrete	X	X	X

4.5 *Resultant forces at the interface time histories*

Participants shall present the time-history resultant forces at the seven proposed interfaces of power unit #12 for the entire result range (from July 1, 1932 up to January 1, 2067) in the provided file.

4.6 *Reservoir drawdown*
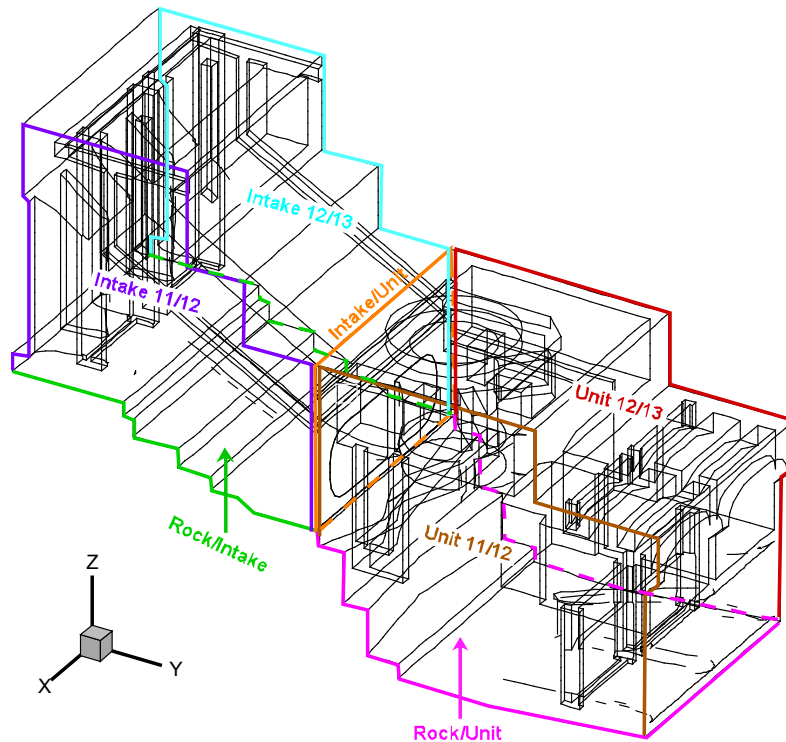
Figure 19. Illustration of the forces at the interfaces - power unit #12

As the stiffness of the dam changes according to the progression of the alkali-aggregate reaction, it is proposed to compare the upstream/downstream displacements at the crest of the dam (topographic point 1250L160) between two states. Sustained variation (including reversible creep) of a 5-meter water drawdown will allow comparison of the stiffness of the participants models after a swelling analysis over a defined period. For comparison purposes, this same variation in water level should be applied to a model not taking into account the alkali-aggregate reaction in order to compare with the initial stiffness of the dam. In summary, the following four steps are required:

- Define Y_1: steady analysis with an upstream water level of 46.10 m and a downstream level of 21.4 m;
- Define Y_2: reduction of the upstream level by 5 m (41.10 m);
- Define Y_3: transient swelling analysis until January 1, 2017 with a water level of 46.10 m upstream and a downstream level of 21.4 m;
- Define Y_4: reduction of the upstream level by 5 m (41.10 m).

To recover the effect of a reservoir drawdown level on the dam movements (step 2 and 4), it is recommended to continue the analysis for a period of 10 years by applying an instantaneous reduction in the water level on January 2, 2017. This period extension is carried out with the aim of recovering the displacements considering reversible and irreversible creep effects (if considered).

Figure 12 gives an example of the two analyses required to compute the stiffness change. Prior to AAR, the hydrostatic and body loads are applied on July 1, 1932. These loads are left constant until the displacement has reached an asymptotic value (creep). Thereafter the upstream water level is lowered by 5 m and creep recovery occurs until asymptotic value is reached. Both asymptotic values are recorded (values Y_1 and Y_2).

After the time-history analysis is performed between July 1, 1932 and January 1, 2017, the crest displacement is recorded (value Y_3). On January 2, 2017, the water is lowered by 5 m and the crest displacement is recorded after 121 days (value Y_4). The difference $\frac{Y_3}{Y_1}$ and $\frac{Y_4}{Y_2}$ gives respectively instantaneous and sustained stiffness variation.

4.7 *Qualitative results*

Another data that can be used in order to qualitatively compare the different models is to compare the computed cracks. Therefore, it is recommended that participants identify the principal cracks, comment and explain them through different plots. It is recommended to perform an interpretation of the cracks as well as the possible failure mechanisms associated with them. Since it is not trivial to analyze damage or plasticity plots by a member unfamiliar with the constitutive model used by the participants, this analysis phase must be carried out with rigour by the analysis team. Without being limited to the variables associated with damage/plasticity, cracks openings can be presented in order to facilitate understanding and allow comparison with those of the other participants. It is also suggested to provide thermal (summer/winter) and hygral (steady state) distribution at a cross section located at the centre of power unit #12. Examples are given in Figure 13, where cracks openings, reinforcement bars yielding, thermal and hygral distribution are displayed.
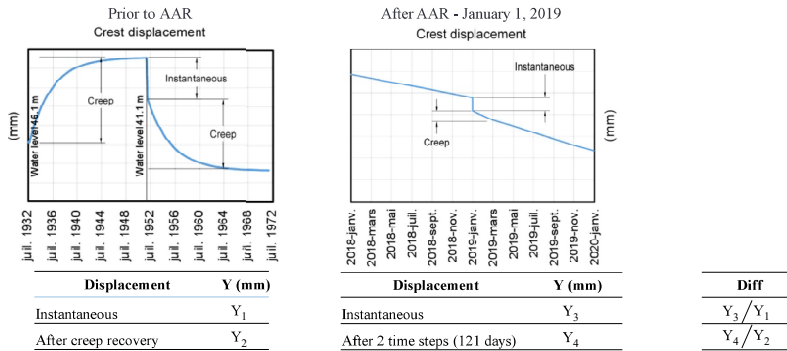
Figure 21 Effect of AAR on model stiffness (computation example)

(a)   (b)

(c)   (d)
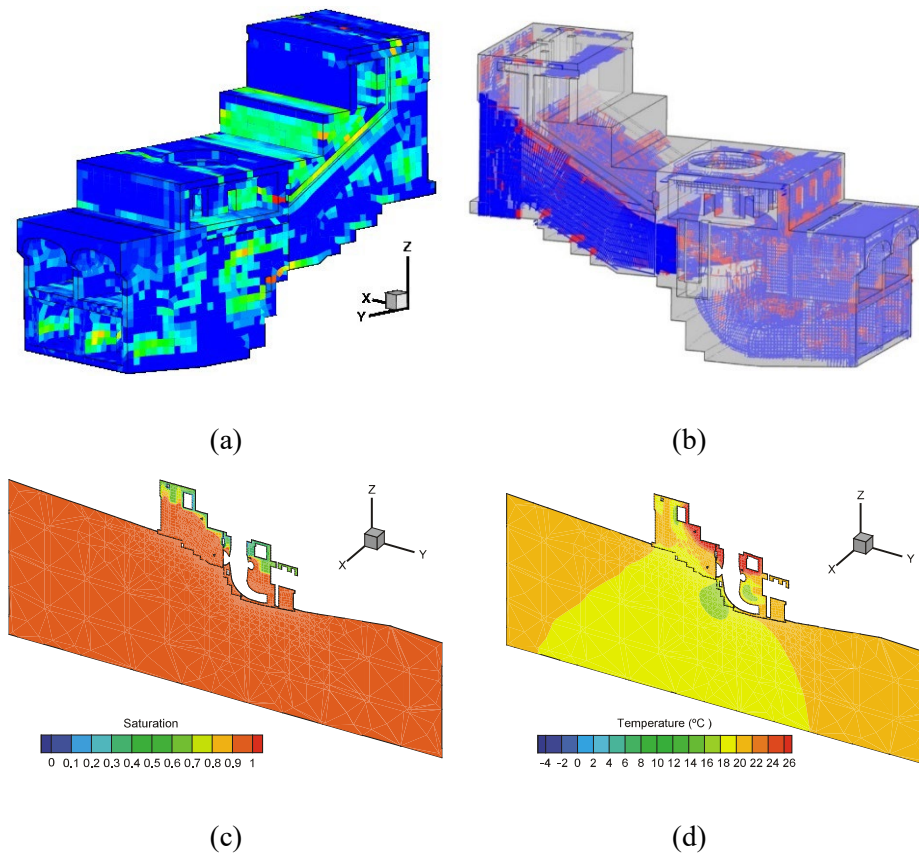
Figure 20. (a) Crack opening, (b) Reinforce-ment bars yielding, (c) Thermal distribution section cut (X=901.36 m), (d) Hygral distribution section cut (X=901.36 m)

4.8 *Summary of the requested results for each proposed task*

Table 9 gives a summary of the requested results for each proposed task.

Table 18. Requested results for each task

			Result description section					
		Task	4.2	4.3	4.4	4.5	4.6	4.7
Static	Linear	Initial	X	-	X	-	-	-
Time-History	Non-Linear	A	X[a]	X	X[a]	X	X	O[b]
		B	X[a]	X	X[a]	X	O	O[b]
		C	X[a]	X	X[a]	X	O	O[b]
		D	X[a]	X	X[a]	X	O	O[b]

X: Mandatory
O: Optional
[a] for January 1, 2017
[b] for January 1, 2017 and/or January 1, 2067

4.9 *List of supplied files: Model geometry*

The geometry of the three power units including the foundation is given in STEP and Parasolid file formats. These are provided to participants if, for the purposes of the envisaged analysis, a refinement of the provided finite element mesh is required.

```
Geometry
├── Geom-Complete.stp
└── Geom-Complete.x_t
```
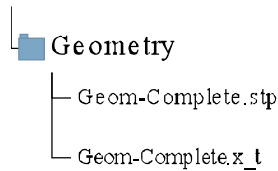
4.10 *Finite element mesh*

The mesh of the three power units was generated to reproduce the in-situ structure as accurately as possible. The model was not developed to assess the dam foundation. Thus, the foundation is formed by a mesh of coarse tetrahedral elements. Finally, the fineness of the mesh, with elements of approximately 1 m x 1 m x 1 m, was defined so that the computation time for a simulation period of 135 years, using a reasonable time step with an implicit finite element model, can be achieved within the range of one working day. Trilinear form of elements is provided; hence it is recommended to use enhanced strain (or incompatible mode) formulation. The mesh was generated favouring hexahedral elements, however, degenerated elements such as wedge, pyramidal and tetrahedral elements were also generated. The nodal definition of the elements are given in Figure 14.

(a) Hexahedral element

(b) Wedge element

(c) Pyramidal element

(d) Tetrahedral element
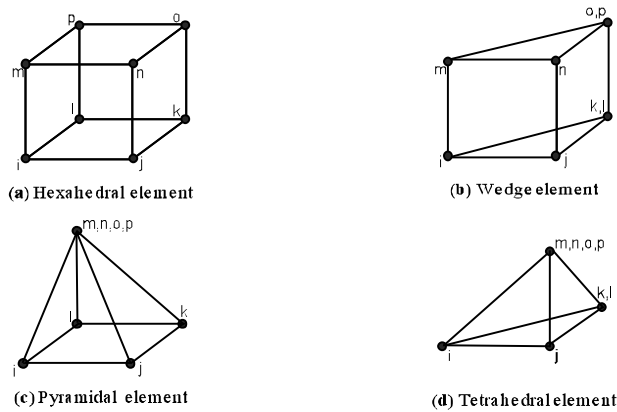
Figure 22. Element shape nodal definition

The finite element mesh includes a total of 271,164 elements and 114,674 nodes. It is required to link certain concrete components together at the interfaces using linear methods (constraint equations, multi-point constraints, bounded contacts, etc) or non-linear methods (contact elements with Mohr-Coulomb formulation, etc.). Taking into account that the nodes at the interfaces do not necessarily coincide, these links shall be applied to the interfaces between the intakes and the generator units and those in the transverse interfaces between the different power units. The interface mesh at the rock/concrete interface is made by making sure that the nodes coincide.

The mesh nodal boundaries, the nodal definitions and the elements topology are distributed in different files according to the following hierarchy:

- 📁 **Mesh**
  - 📁 **Interface**
    - 📁 **Group** {Group number}
      - 📁 **Intake**
        - P{Group number }_{Interface name}.txt
        - ...
      - 📁 **Powerhouse**
        - G{Group number }_{Interface name}.txt
        - ...
    - GDRAINAGE.txt
    - GDRAINROCHER.txt
    - MODELBANK_L.txt
    - MODELBANK_R.txt
    - MODELBASE.txt
    - MODELDOWNSTREAM.txt
    - MODELUPSTREAM.txt
    - RC_CONTACT.txt
    - WATERDOWNSTREAM.txt
    - WATERUPSTREAM.txt
  - Model.elem
  - Model.node
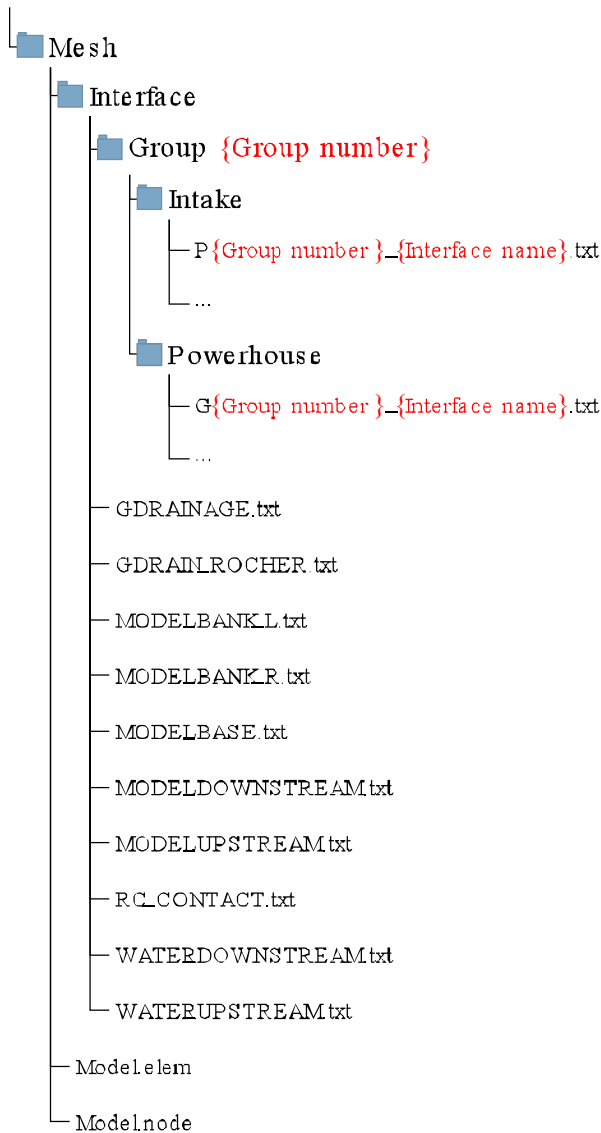
The mesh is separated in two files. The file Model.node contains the list of nodes and is defined as follows:

[Model.node]

Node number	X coordinate	Y coordinate	Z coordinate
1	922.9344482000	1244.778198000	11.54189873000
...	...	...	...

The file *Model.elem* contains the list of elements and is defined as follows:

[Model.elem]

i	j	k	l	m	n	o	p	Mesh group number
934	6003	933	933	24431	24431	24431	24431	1
…	…	…	…	…	…	…	…	…

The mesh group number corresponds to the different power-units geometry as defined in Table 10.

Table 19. Mesh group number

Number	Description
1	Foundation
2	Intake #11
3	Power unit #11
4	Intake #12
5	Power unit #12
6	Intake #13
7	Power unit #13

The files in the folder *Interface* with the extension *.txt* are the mesh nodal boundaries given in the form of a list of nodes. The name of the boundaries and their corresponding definition are displayed in Figure 15 and Figure 16.
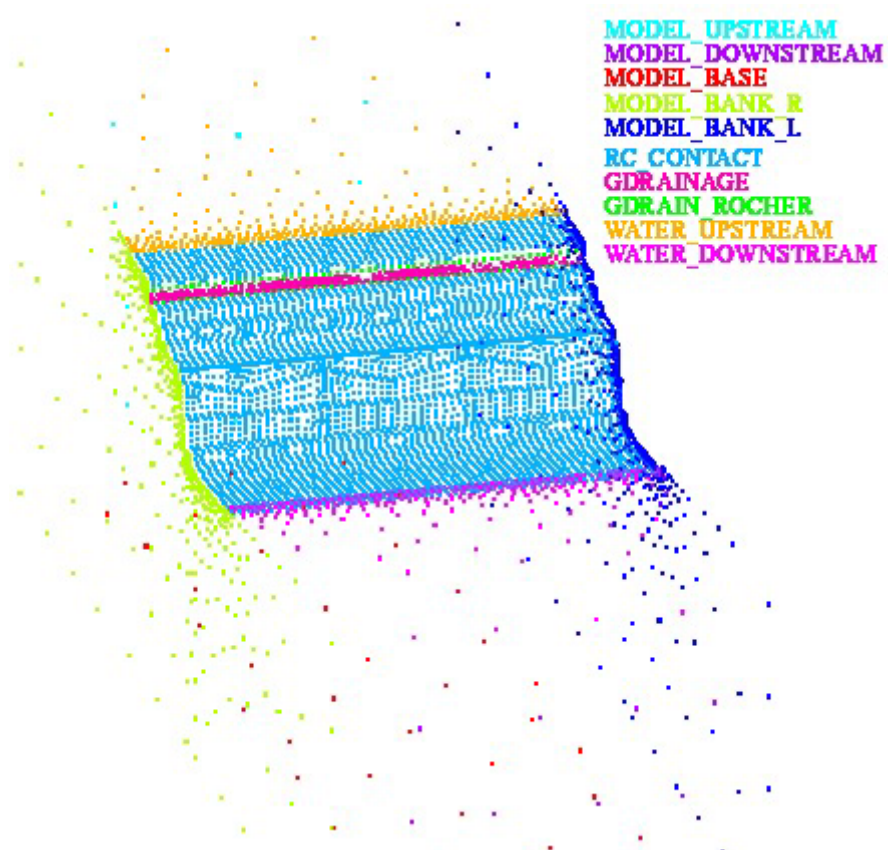
Figure 23. Nodal boundaries definitions

(a)

(b)

(c)

(d)
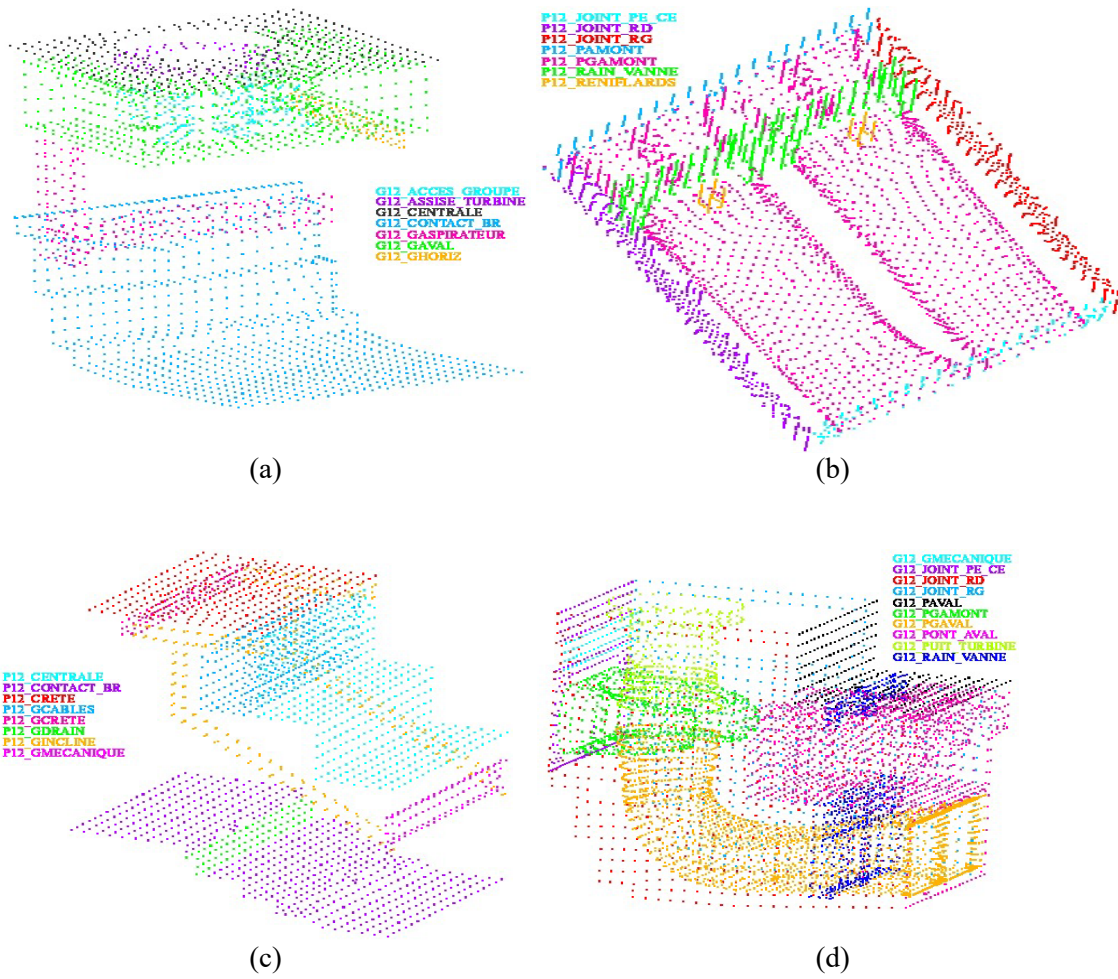
Figure 24. Nodal boundaries definitions (cont.)

4.11 *Concrete reinforcement*

For each power unit, the IGES CAD file containing the reinforcements represented by curves and lines is given with the following hierarchy:
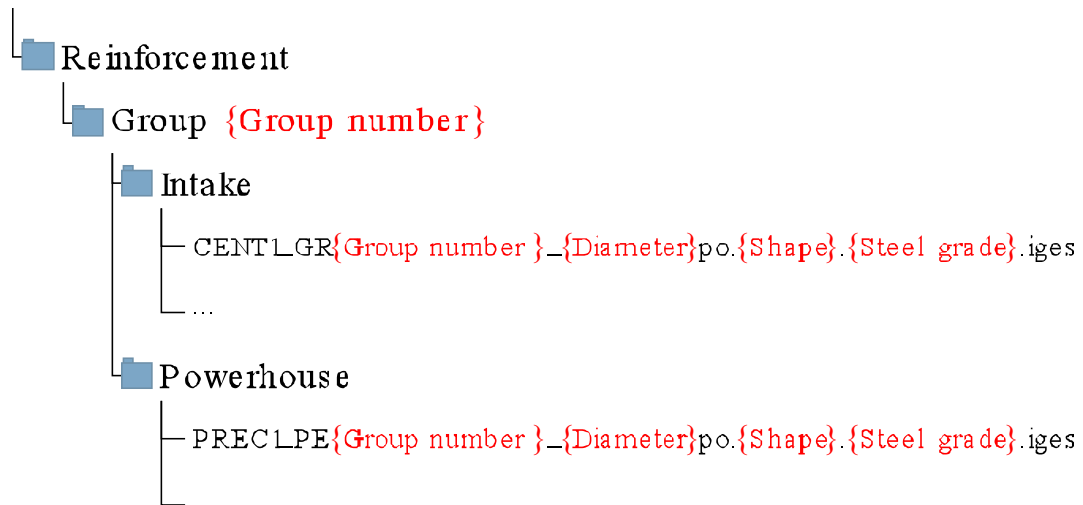
Where:
- {Group number} is the power unit number;
- {Diameter} is the bar diameter in inches;
- {Shape} is the bar shape (r:round, c:square);
- {Steel grade} is the steel grade (refer to section 2.6).

4.12 *Temperature boundary conditions data*

The temperature data for the four defined zones is given in the file *Temperature.xlsx*. They are given on a daily average temperature basis. It is assumed that these temperatures can be repeated each year.

```
└─ 📁 Data
      └─ Temperature.xlsx
```
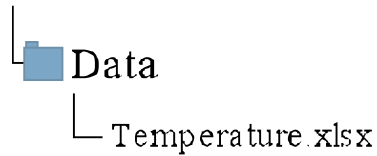
4.13 *Topographic data*

The available data for the monitoring points identified as 1250D160, 1295Q099, 1250U097 are given in the file *Topographic Displacements.xlsx*. The topographic auscultation system was implemented in 1973, therefore the first 40 years of data was not recorded. To calibrate the model, it is suggested to shift the data to match the total displacement computed on the first day of acquisition.

```
└─ 📁 Data
      └─ Topographic    Displacements.xlsx
```
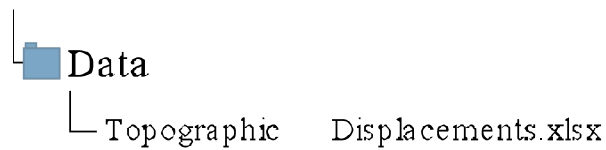
REFERENCES

American Institute of Aeronautics and Astronautics. (1998). *AIAA Guide for the Verification and Validation of Computational Fluid Dynamics Simulations.* AIAA G.: American Institute of Aeronautics and Astronautics. American Institute of Aeronautics and Astronautics.

American Society of Mechanical Engineers. (2006). *Guide for Verification and Validation in Computational Solid Mechanics.* ASME V&V. American Society of Mechanical Engineers.

Bear, J., & Bachmat, Y. (1990). *Introduction to modeling of transport phenomena in porous media.* Springer Dordrecht. doi:10.1007/978-94-009-1926-6

Department of Defense. (2018). *DoD Instruction 5000.61: Modeling and Simulation (MS) Verification.* Department of Defense.

Esposito, R., & Hendriks, M. (2019). Literature review of modelling approaches for ASR in concrete: a new perspective. *European Journal of Environmental and Civil Engineering*, 1311–1331. doi:10.1080/19648189.2017.1347068

M.C. Anderson et al. (2004). *Concepts of Model Verification and Validation.* Los Alamos National Laboratory.

Mainguy, M., Coussy, O., & Eymard, R. (1999). *Modélisation des transferts hydriques isothermes en milieu poreux: application au séchage des matériaux à base de ciment.* Études et recherches des Laboratoires des ponts et chaussées. Série Ouvrages d'art. Laboratoire central des ponts et chaussées.

Masarati, P., Mazzà, G., & Meghella, M. (2005). *Theme A: Evaluation of alkali-aggregate reaction effects on the behaviour of an Italian hollow gravity dam.* Wuhan, Hubei, P.R.China: VIII ICOLD Benchmark Workshop On Numerical Analysis Of Dams.

Molin, X., & Noret, C. (2011). *Theme A: Effect of concrete swelling on the equilibrium and displacements of an arch dam.* Valencia, Spain: XI ICOLD Benchmark Workshop On Numerical Analysis Of Dams,.

Oberkampf, W. L., & Roy, C. J. (2010). *Verification and Validation in Scientific Computing.* Cambridge University Press.

Pirtz, D. (1968). *Creep Characteristics of Mass Concrete for Dworshak Dam.* University of California: SESM Report. Structural Engineering Laboratory.

Saouma, V. (2020). *Diagnosis & Prognosis of AAR Affected Structures: State-of-the-Art Report of the RILEM Technical Committee 259-ISR.* RILEM State-of-the-Art Reports. Springer International Publishing.

Strutturale, E. -P. (2001). *Theme A: Evaluation of AAR effects on the structural behaviour of an arch dam: interpretation of the measured bahaviour and forecasting of the future trend.* Salzburg, Austria: VI ICOLD BenchmarkWorkshop On Numerical Analysis Of Dams.

Terminology for model credibility. (1979). SIMULATION 32.3. doi:10.1177/003754977903200304

V. Baroghel-Bouny et al. (1999). Characterization and identification of equilibrium and transfer moisture properties for ordinary and high-performance cementitious materials. *Cement and Concrete Research*, 1225–1238. doi:10.1016/S0008-8846(99)00102-7

van Genuchten, M. (1980). A Closed-form Equation for Predicting the Hydraulic Conductivity of Unsaturated Soils. *Soil Science Society of America Journal*, 892–898. doi:10.2136/sssaj1980.03615995004400050002x
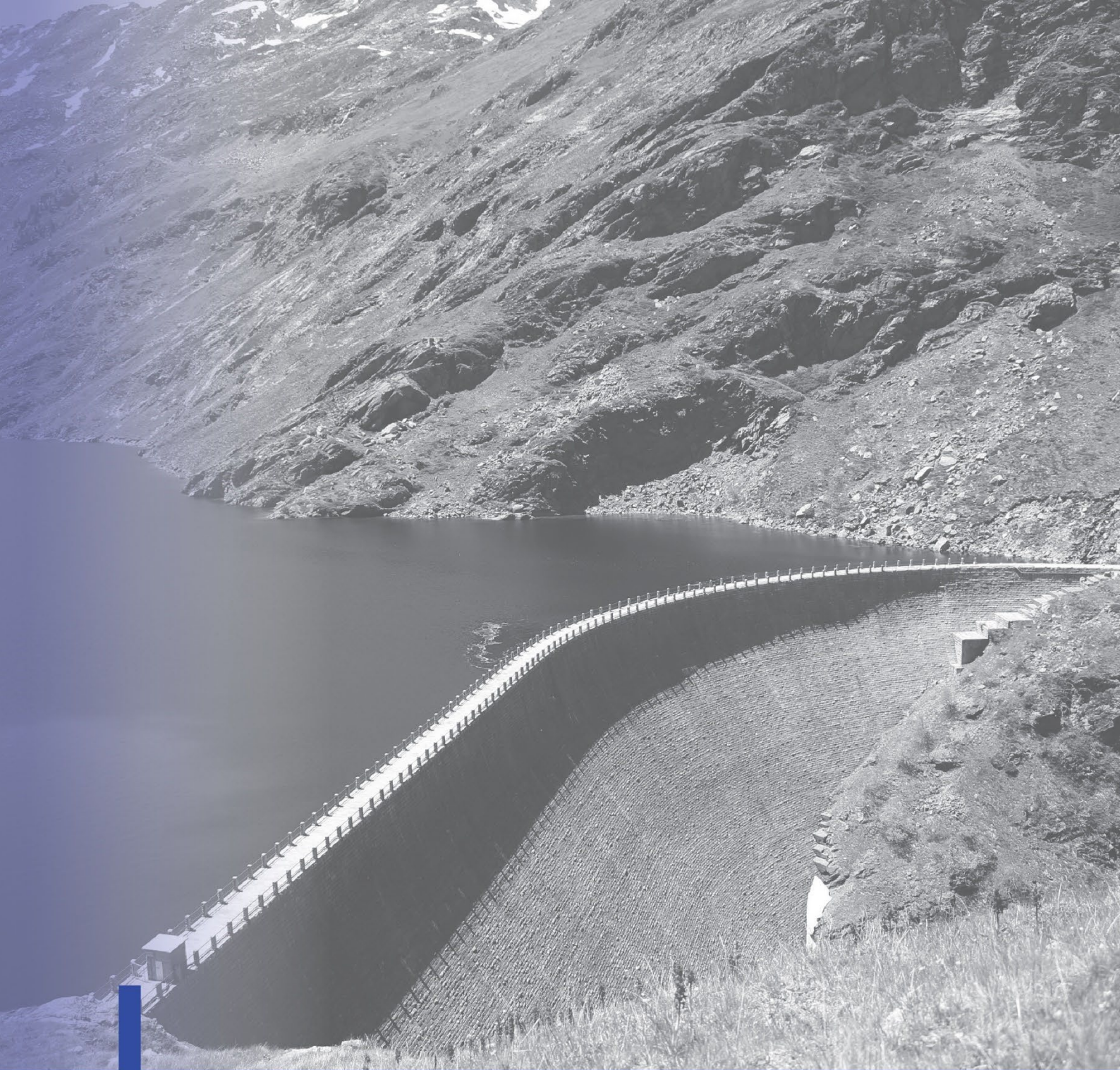
AAR affected dams

Recieved papers for Theme B

ASSESSMENT OF THE EXPANSION OF BEAUHARNOIS DAM

Luis Lacoma
Principia Consulting Engineers, Madrid, Spain

Javier Rodríguez
Principia Consulting Engineers, Madrid, Spain

Joaquín Martí
Principia Consulting Engineers, Madrid, Spain

Ana B. Martín
Iberdrola Generación, Madrid, Spain

Esperanza Menéndez
Eduardo Torroja Institute for Construction Sciences (IETCC), Madrid, Spain

ABSTRACT: The paper describes the contribution to the AAR benchmark of the Spanish team formed by Principia Consulting Engineers, Iberdrola Generación, and Eduardo Torroja Institute for Construction. The Beauharnois Generating Station is a large hydropower facility, with generating units spread out about a kilometre. The dam, constructed in 1932, is experiencing an expansion process caused by an AAR chemical reaction. Displacements measured at some points during the period 1973-2018 were provided by the organisers and were used to calibrate the expansion model using the general-purpose finite element program Abaqus. First, a thermal simulation was carried out to determine the periodic temperature oscillation during a representative year. The steady-state degree of saturation was also computed based on the available data. Then, mechanical models were constructed with different levels of approach. The expansion law was calibrated as a function of temperature, adopting an Arrhenius' law. The vertical displacements were used to determine an isotropic expansion rate, and the horizontal displacements to validate it. No creep was explicitly included in the models, and a crude plasticity model was defined for the concrete. The hygral conditions were assumed to eliminate the expansion when the saturation was lower than a certain threshold. The resulting displacement field appears to be reasonable for both the vertical and horizontal directions. Conservatively, the same expansion rate was assumed for the future time of interest.

1   INTRODUCTION

1.1   *Description of the dam*

The dam has an overall length of about 1400 m. Although the cross-section does not vary much along the length, the region being studied is specifically that of power unit #12 and the two adjacent units. A representative cross-section is shown in Figure 1.

Upstream from the dam the water levels may vary between 44.5 m and 46.5 m; those downstream vary between 20.461 m and 23.012 m. The calculations have been made with 46.1 m and 21.4 m, as suggested by the organisers.

The dam is made of reinforced concrete. The basic characteristics of the concrete are a compressive strength of 30 MPa, a Young's modulus of 26 GPa, and a Poisson's ratio of 0.21. The ground under the dam is rock, characterised by a Young's modulus of 30 GPa.

In the calculations described in the paper, the domain being studied, spanning the three units mentioned, is assumed to be bounded by symmetry planes on both sides.

1.2   *Problem statement*

For calibrating the models used in the analyses, the only information available consisted in histories of vertical displacements at three points and horizontal displacements at two of them; the locations of those points are marked on Figure 1. The displacements were obtained by topographic surveys conducted after 1973.
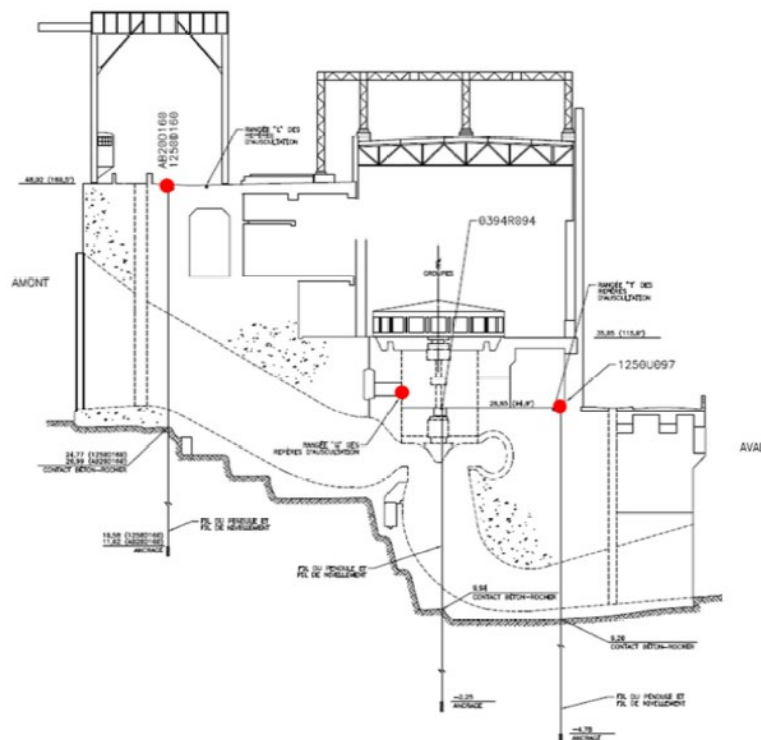
Figure 1. Representative section of a power unit

2   MODELLING APPROACH

2.1   *Geometry reconstruction*

It was found that neither the geometry nor the finite element mesh provided by the organisers were ideal for the calculations. The geometry had many undefined entities when importing it into Abaqus [5], and 20% of the mesh elements were of poor quality.

In this situation it was decided to reconstruct the geometry of the power unit with CATIA 3DEXPERIENCE [1]; the reconstructed geometry is shown in Figure 2. Also, tetrahedral meshes

were generated for dealing with the different problems; examples are shown in Figure 3 for the global mesh and Figure 4 for more detailed views of the intake and power units. First-order elements were used for the thermal and hygral calculations, while second-order elements were employed in the mechanical calculations.

2.2 *Methodology*

The calculations have proceeded in several steps. The first one consisted in performing thermal analyses in order to develop a stable thermal cycle along a standard year. The hygral calculations were conducted to determine the saturation conditions at each location.

Finally, the mechanical analyses were carried out, again in several steps. In a preliminary phase, calculations were performed for only the hydrostatic and gravity loads. Already with concrete expansion, the expansion was initially assumed to be uniform and homogeneous. Then, in a second phase, the influence of temperature was incorporated and, in the final one, both temperature and moisture conditions were taken into account. The mechanical analyses included both linear and non-linear calculations.
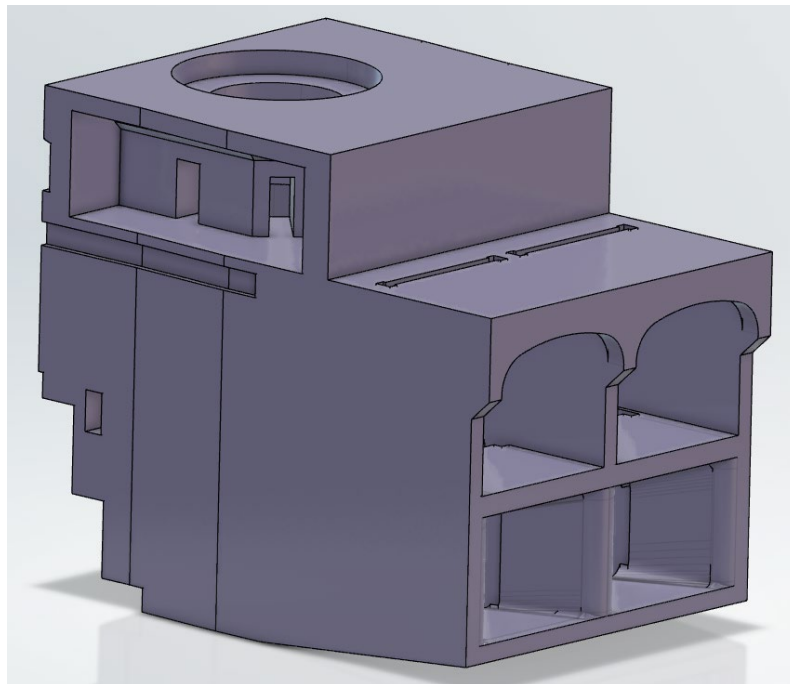
Figure 2. Reconstructed geometry

3 ENVIRONMENTAL SIMULATIONS

3.1 *Thermal analysis*

The object of the thermal analyses was to determine the evolution of the temperatures at each location during the year.

The mesh utilised in the thermal analyses included both the dam and the ground; it consisted of about 1.6 million nodes and 1.1 million first-order elements.

The analyses were performed with adiabatic boundary conditions at the ends and thermal exchanges across other surfaces with sinusoidally-varying ambient temperatures of the type (Figure 5):

$$T(d) = T_0 + A \cdot \cos(\omega d) + B \cdot \sin(\omega d), \cdot \text{where } \omega = 2\pi/365 \tag{1}$$

The analyses were conducted for a time span of 50 years to ensure a stable yearly temperature cycle at all locations. Figure 6 presents some results, namely the temperature distributions in January and July.
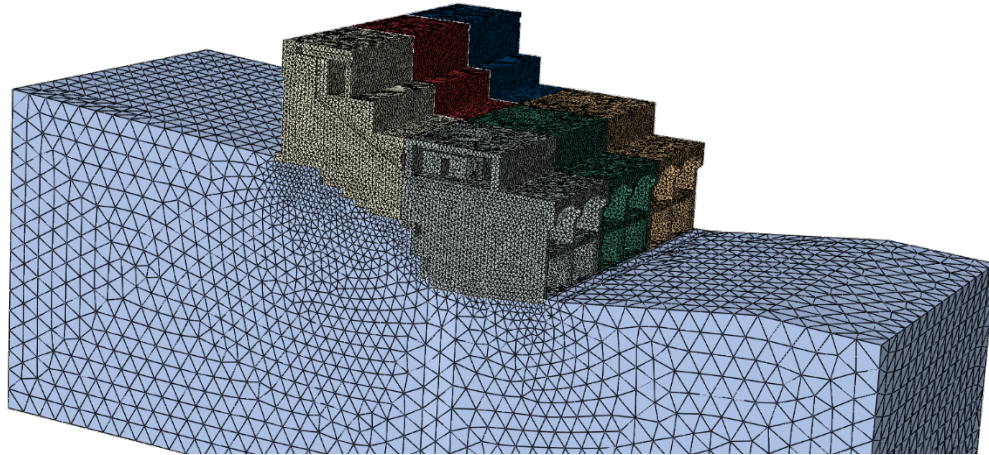
Figure 3. Representative finite element mesh
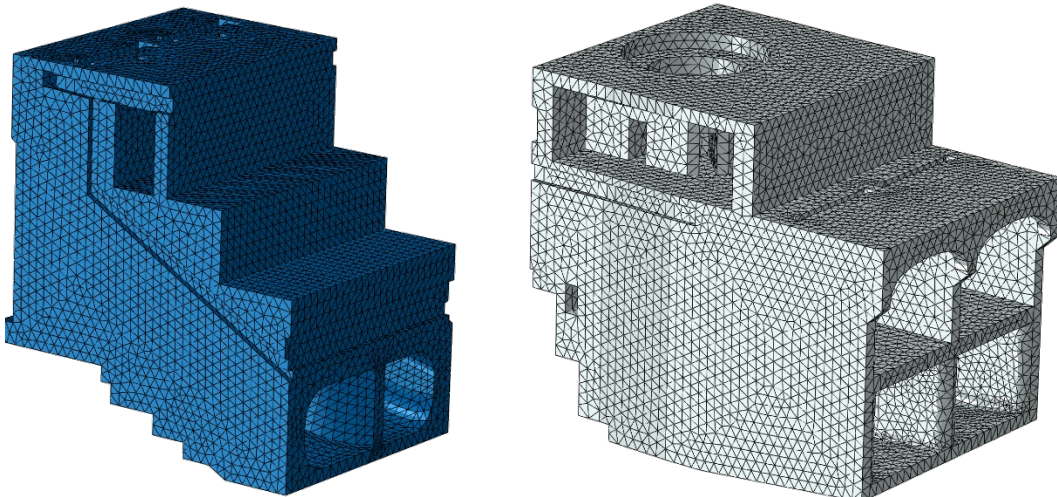
Figure 4. Detailed views of the intake and power-unit finite element meshes
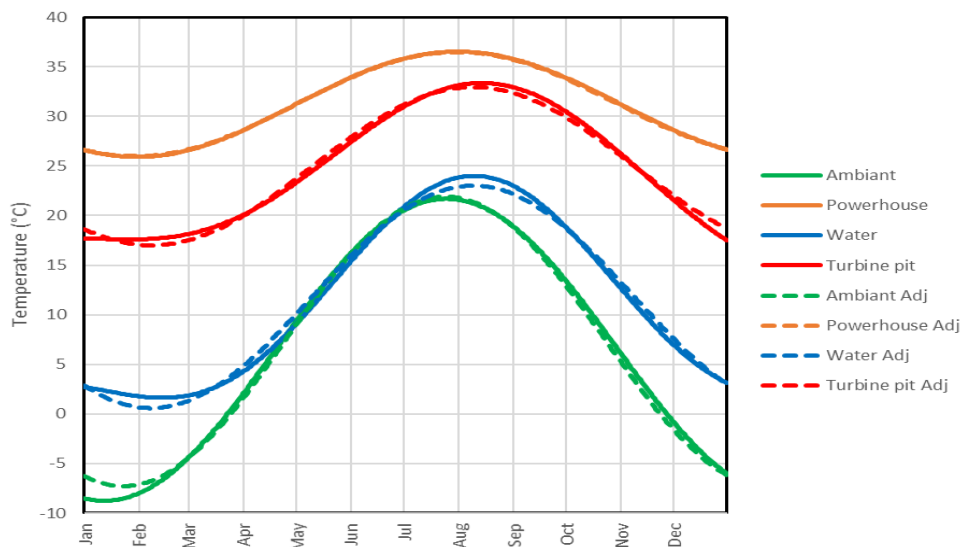
Figure 5. Harmonic fit of the season temperature for convection boundary conditions
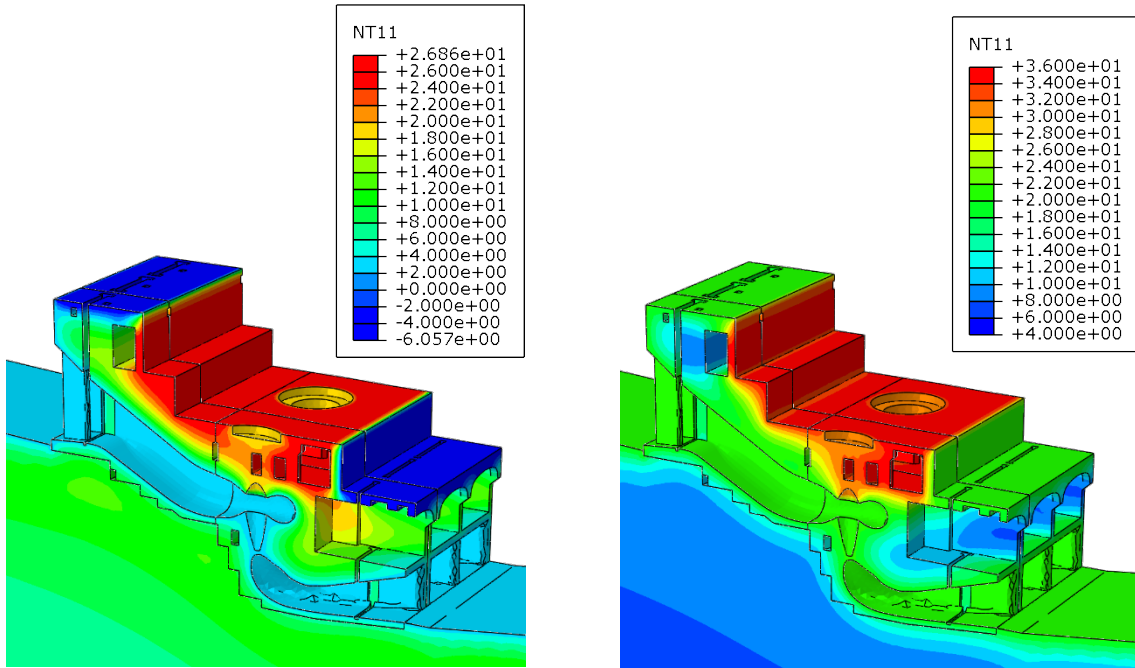
Figure 6. Temperature distribution in January (left) and July (right)

3.2 *Moisture analysis*

The mesh used for studying the moisture conditions is similar to that used in the thermal calculations, except that it only includes the body of the dam; first order elements are again used. The boundary conditions are specified in terms of pore pressures.

Capillary pressures arise when extracting particles to an unsaturated environment. The equivalent negative pressures (P_c) are approximated assuming that the ideal gas law applies, the process is isothermal, and, in equilibrium, the fraction of particles exchanged with the environment is a function of its relative humidity; more specifically, it is inversely proportional to the number of interactions between particles:

$$P_c = -\frac{\rho R T}{M} \ln h, \tag{1}$$

where ρ is the liquid density, *R* is the gas constant, *M* is the molar mass, *T* is the absolute temperature; and *h* is the relative humidity.

It is also assumed that the head loss is linear along the conduit across the dam. Concrete is characterised with its hydraulic conductivity and the capillary pressure law, both a function of the degree of saturation (Figure 7).

According to Mualem's model, as described in [2], the relative hydraulic conductivity (or permeability for Darcy's law) depends on the degree of saturation (Θ) and the tortuosity, the latter being a function of the pressure and the water content ($h(x)$):

$$K_r = \Theta^{1/2} \left[\int_0^\Theta \frac{1}{h(x)} \, \mathrm{d}x \Big/ \int_0^1 \frac{1}{h(x)} \, \mathrm{d}x \right]^2 \tag{2}$$

The phenomenological retention law is assumed to hold (with a logistic "S" shape)

$$\Theta = \left(\frac{1}{1+(\alpha h)^n} \right)^m \tag{3}$$

Conveniently $m = 1 - 1/n$ and the conductivity can be integrated explicitly, yielding

$$K_r = \Theta^{1/2} \left[1 - \left(1 - \Theta^{1/m} \right)^m \right]^2. \tag{4}$$

When the problem is analysed, using the previous hypotheses, the resulting distribution of the degree of saturation is that shown in Figure 8.
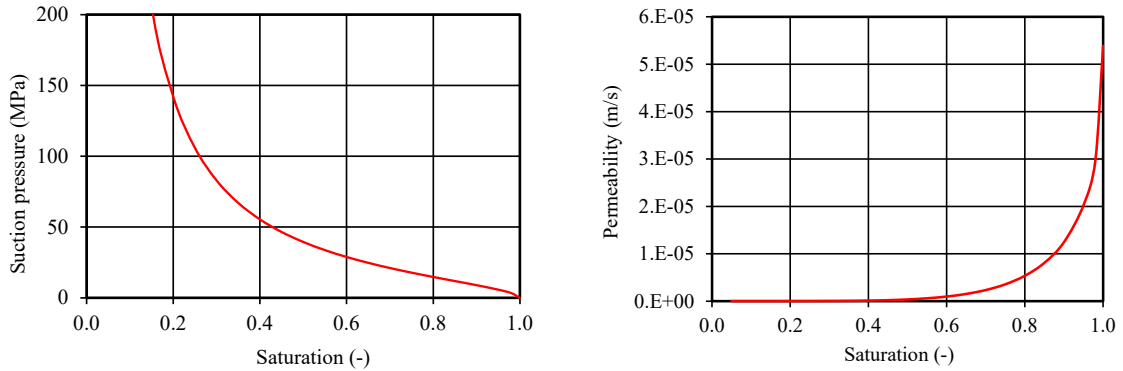
Figure 7. Suction pressure and permeability as a function of the degree of saturation
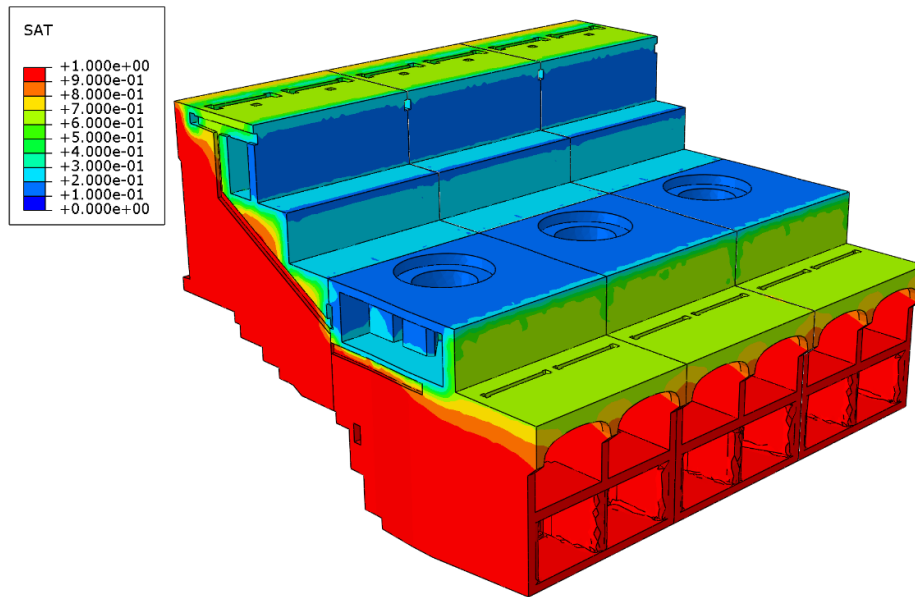
Figure 8. Distribution of the degree of saturation

4 MECHANICAL ANALYSIS

4.1 *Estimation of the expansion rate*

A first mechanical analysis was conducted to determine the displacements that would result from a given uniform expansion at the locations where its evolution was known. This was done using a mesh with about 740,000 second-order elements, 1.1 million nodes and 3.4 million dof's, provided with displacement boundary conditions.

The problem is linear, and a 0.1% uniform expansion was used. The annual displacement rate calculated for the homogeneous expansion is shown in Figure 9. The results allowed calibrating the expansion using the vertical displacement rates derived from the measurements: 0.984 mm/yr at the "Crest", 0.567 mm/yr at the "Turbine floor" and 0.479 mm/yr at the "Turbine pit". The estimated linear (not volumetric) expansion rate is $2.8 \cdot 10^{-3}$ %/year.

4.2 *Evolution of the expansion*

The chemical reaction is affected by temperature. Consistently, a steady-state, isotropic expansion model was established including the temperature dependence. The mechanical model did not incorporate creep, as it is difficult to separate from the expansion on the basis of the information available; also, as suggested by the benchmark organisers, thermal expansion was not considered in the calculations.

It was assumed that the annual rate of chemical expansion is a function of the yearly temperature cycle. The instantaneous rate was taken to be proportional to *exp(T/U)* with a factor *f*:

$$\dot{\varepsilon}_{\text{AAR}} = f \exp(T/U), \tag{5}$$

where *U* is an activation energy; the value given was 5400 K, taken from Larive [3] for the characteristic reaction time. The expansion tends to homogeneous as this value grows. An additional analysis was performed with 9400 K, given by Larive for the latency time, but the results were less satisfactory.

The simulation was carried out using the temperatures, updated every 15 days, in an Abaqus subroutine. The factor multiplying the exponential function was calibrated to achieve an annual expansion rate that coincides with the average rate recorded (written at the end of the previous section 4.1), and the result was *f* = 11.4 day^{-1}.

With the calibrated expansion model, the evolution was simulated for a period of 115 years (the total period of analysis required by the organisers is 2067 - 1932 = 135 year but no expansion is assumed during the first 20 years). The analysis times could be reduced by using in subsequent years information produced in the first year of expansion. The initial evolution of the dam is not well known, as the displacement records start in 1973, some 40 years after construction. A latency time of 20 years was assumed, based on the authors' experience on other dams.

A crude von Mises model was used to approximate some of the effects of plasticity. This should improve the accuracy of the reactions calculated between the various blocks and the foundation. The calculated distribution of the expansion rate appears in Figure 10. The reactions were calculated with an Abaqus tool that integrates the nodal forces.

4.3 *Effect of the degree of saturation*

To incorporate the effects of moisture, the strategy adopted consisted in eliminating the expansion when the degree of saturation is below 0.3. Figure 11, coming from a different project, shows representative stereomicroscopic images of the gel in concrete pores. In the images the porous are filled with a vitreous gel and surrounded by an aqueous gel; a value of 0.3 may be representative of the ratio of both volumes, and it is deemed reasonable as a threshold of the saturation degree to supress the macroscopic expansion. The factor multiplying the temperature-dependent exponential function (*f*) was still considered appropriate and was not recalibrated. The expansion distribution is also shown in Figure 10.

The comparison of the displacement histories, considering the effects of temperature and saturation, is provided in the next two figures: Figure 12 for the vertical displacements and Figure 13 for the horizontal ones. Notice that only the vertical displacements had been used for calibration purposes; also, since the origins are not known, the experimental curves were arbitrarily shifted for comparison purposes.
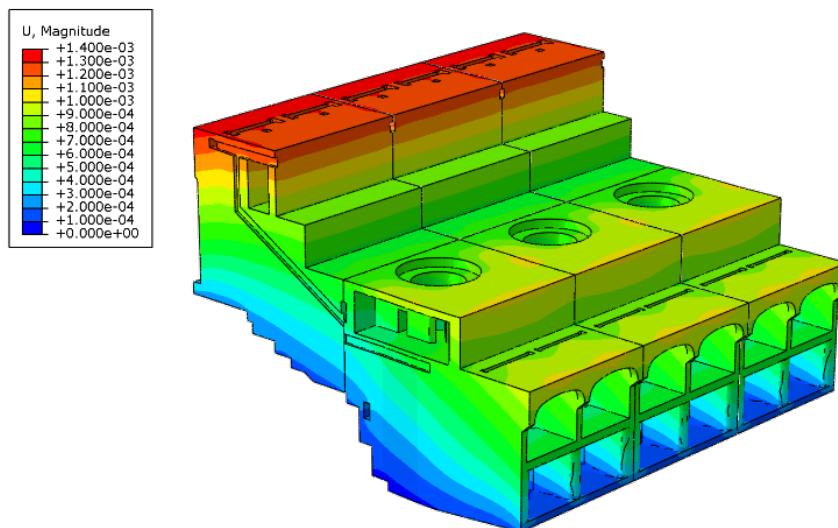

Figure 9. Annual displacement increment (m) for homogeneous expansion of 2.8·10-3 %/year
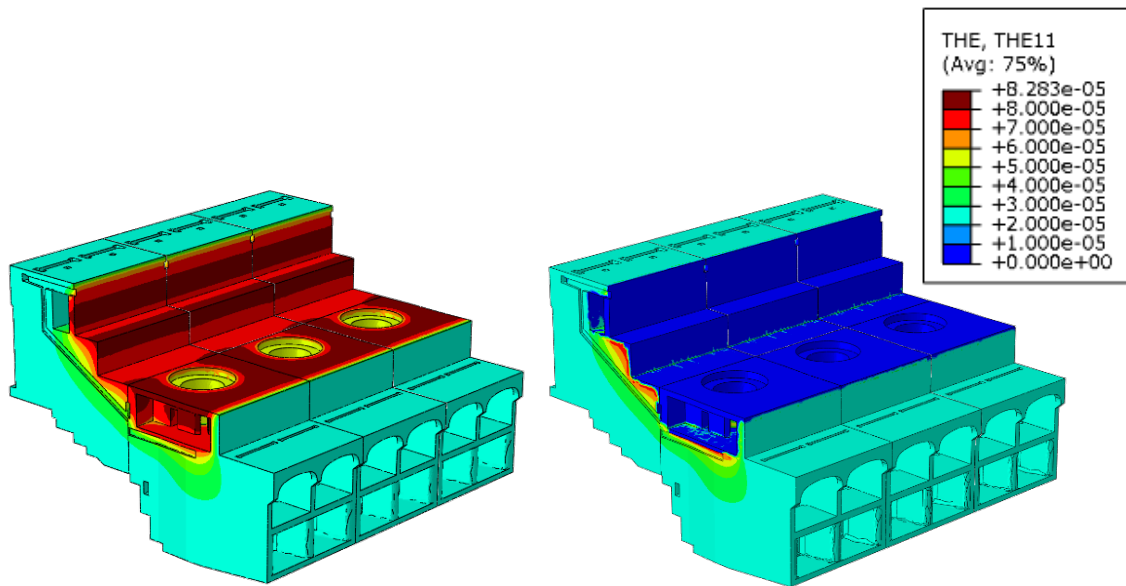
Figure 10. Distribution of the expansion rate without (left) and with dependence on the saturation degree

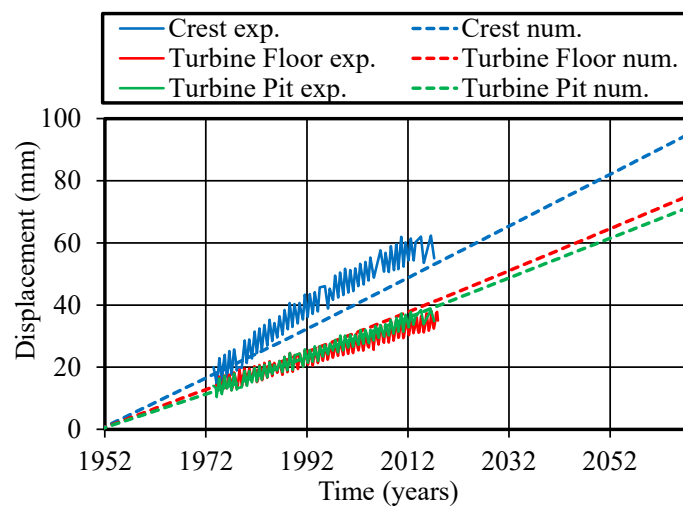Figure 11. Representative stereomicroscopic images

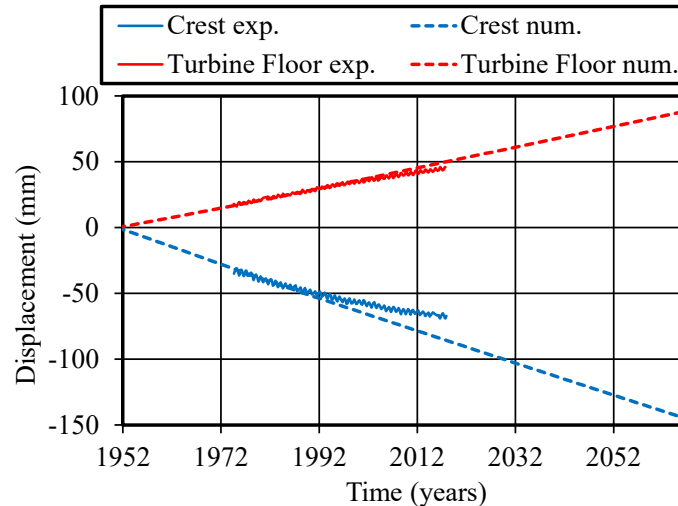Figure 12. Histories of vertical displacements of the control points (moisture dependent)

Figure 13. Histories of horizontal displacements of the control points (moisture dependent)

5 DISCUSSION AND CONCLUSIONS

State-of-the-art simulation tools have been used to analyse the state of a dam affected by chemical expansion. Additional experimental information, regarding both the material characterisation (e.g., according to [6]) and the structure, would be required for more conclusive results and to validate possible strategies and remedial measures; in any case, the exercise proposed by the organisers is deemed very useful for illustrating the different analysis methodologies.

With the available information, it is difficult to predict the future evolution of the expansion rate, which has been assumed to remain constant after a latency time following construction; this is typically a conservative assumption. The temperature dependence is introduced via an Arrhenius' law, using published activation energies of AAR.

Based only on displacement information, the creep and chemical effects cannot be decoupled. Conveniently, a viscoelastic model is not defined, and an effective expansion is calibrated.

There is no consensus about how to consider the effect of the degree of saturation; moreover, there are large uncertainties its value in concrete affected by AAR. Our approach consisted in simply supressing the expansion when the value is below 0.3; this threshold is considered reasonable, based on both micromechanics and sensitivity considerations.

The calibration was only based on the vertical displacements, but the computed horizontal displacement rates also turned out to be consistent with the data. A stress-dependent anisotropic expansion model could be assessed for improving the simulation.

It is possible to model the rebars, typically with truss elements embedded in the solid domain, characterised with a concrete inelastic model. But, in the context of the present exercise, this would not be expected to improve significantly the predictive capabilities of the model.

The rest of the information requested by the benchmark organisers has also been provided.

REFERENCES

[1] Dassault Systèmes. '3DEXPERIENCE User Assistance. 3D Modeling. Mechanical Design'. 2021.

[2] M. Th. van Genuchten 1980 'A Closed-form Equation for Predicting the Hydraulic Conductivity of Saturated Soils', In: Soil Science Society of America Journal. 44.5 (1980), pp. 892-898, doi: 10.2136/sssaj1980.03615995004400050002x

[3] C. Larive. 'Apports combinés de l'experimentation et de la modelélisation à la compréhension de l'alcali réaction et ses effets mécaniques'. Études et Recherches des LPC OA 28. Laboratoire Central des Ponts et Chaussées, Paris, France, 1998.

[4] S. N. Roth and B. Miquel. 'Theme B: AAR Affected Dam. Evaluation and Prediction of the Behaviour of the Beauharnois Dam'. In: 16th International Benchmark Workshop on Numerical Analysis of Dams, Ljubljana, Slovenia, 2022.

[5] SIMULIA. 'Abaqus Analysis User's Guide'. 2021.

[6] A. B. Martín, E. Menéndez and L. M. Lacoma. 'Nueva Metodología para la Predicción de la Expansión del Hormigón en Presas con RAA'. In: XI Spanish Conference on Large Dams, León, Spain, (2018), pp. 1-10.

EVALUATION AND PREDICTION OF THE BEHAVIOR OF THE BEAUHARNOIS DAM, USING FLAC3D

Davide Lamberti
Lombardi Engineering Ltd., Giubiasco, Switzerland

Emanuele Catalano
Lombardi Engineering Ltd., Giubiasco, Switzerland

Riccardo Stucchi
Lombardi Engineering Ltd., Giubiasco, Switzerland

ABSTRACT: The paper presents a study carried out to analyze the behavior of a concrete power station affected by AAR, the Beauharnois power plant. A step-by-step method is proposed to integrate the physics aspects affecting the swelling reaction, in particular: reaction kinetics, temperature field and degree of saturation. The calibration of the numerical model is performed on the basis of the displacement measurements that are available at three different measuring points. The calibrated model is furtherly used to provide a prediction of the future dam behavior in the next 50 years. This calculation exercise was proposed in the frame of the 16th International Benchmark Workshop on Numerical Analysis of Dams.

1 INTRODUCTION

The Theme B of the 16th International Benchmark Workshop on Numerical Analysis of Dams concerns the numerical modelling of the alkali-aggregate reaction (AAR) in the Beauharnois Dam (only the single power unit 12 with its two neighboring units will be considered, see Figure 1).

Due to the complexity of AAR, a step-by-step method is adopted, characterized by the progressive introduction of the different parameters influencing the swelling reaction: the development of the chemical reaction, the influence of temperature, and the influence of humidity. The objective of the analysis is to reproduce the observed behavior of the dam and to estimate the progress for the next 50 years.

The paper presents the main aspects of the numerical model that was prepared, the swelling model that was chosen to reproduce the behavior of the AAR reaction and its results. Some comments on the general behavior of the dam are also presented.
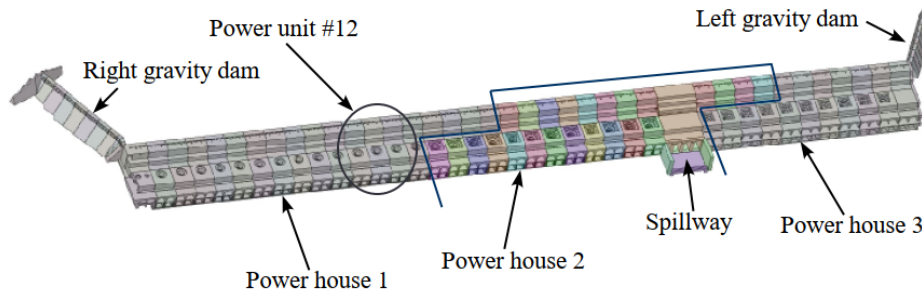
Figure 1. Beauharnois Dam, with position of the Power unit 12 (Benchmark formulation document, 2021).

2 AAR MODEL

The proposed AAR model includes four of the main known factors affecting the magnitude and spatial distribution of the AAR-induced concrete expansion: the reaction kinetics, the temperature effects, the dependency on the stress state and the influence of humidity.

The dependency of the structure stiffness on the progression of the alkali-aggregate reaction is not included in the model.

2.1 *Reaction kinetics*

The AAR expansion model adopted is based on the work of Capra & Bournazel 1998. This model assumes that AAR follows a first-order kinetic law, described by:

$$\frac{dA}{dt} = k \cdot (1 - A) \tag{1}$$

where A represents the percentage of alkali that have reacted and measures the advancement of the reaction varying between 0 and 1; k is the kinetic constant, i.e., the reaction velocity at time $t = 0$ (hence $A = 0$).

In addition, the model assumes that the chemical reaction and the concrete expansion are dissociated: the concrete expansion starts occurring only when the cracks, which are initially generated within the aggregates, also propagate in the cement paste. To dissociate the reaction and the expansion, a parameter A_0 is defined. When the reaction advance exceeds A_0, the macroscopically observable expansive phenomenon begins. The link between the AAR induced concrete expansion (ε_{AAR}) and the reaction advance (A) is therefore defined by the following bi-linear law (Figure 2).

$$\varepsilon_{AAR} = \begin{cases} 0 & se\ A < A_0 \\ \frac{A-A_0}{1-A_0} \cdot \varepsilon_\infty & se\ A > A_0 \end{cases} \tag{2}$$

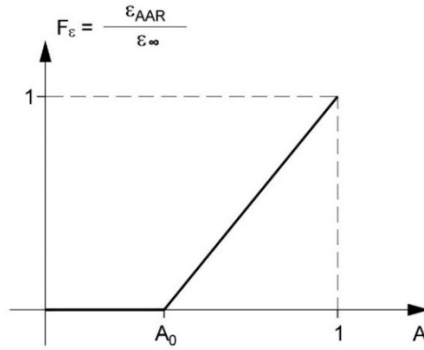where ε_∞ is the AAR induced concrete expansion at infinite time.

Figure 2. Relationship between normalized expansion ($\varepsilon_{AAR}/\varepsilon_\infty$) and reaction advancement (A).

2.2 *Temperature*

For all chemical reactions, temperature causes a change in the reaction velocity. In the considered model, the temperature influences the kinetic constant (k) of the chemical reaction according to the Arrhenius equation:

$$k = k_0 \cdot e^{\frac{E_a}{R} \cdot \left(\frac{1}{\theta_0} - \frac{1}{\theta}\right)} \tag{3}$$

where k_0 = reaction rate at the reference temperature θ_0; E_a = activation energy, a typical activation energy of 45 kJ/mol is used for the alkali-aggregate reaction (Gimal et al., 2010; Morenon et al., 2021); R = gas constant (8.31 J/mol/K); θ = temperature at which the reaction rate k is to be determined (temperatures are in Kelvin degrees).

According to Arrhenius' law, the relationship between temperature and reaction rate is nonlinear, characterized by a doubling of the reaction rate every 10°C for an activation energy E_a of 45 kJ/mol.

2.3 *Stress state*

It is known that the stress state within a concrete structure influences the AAR induced expansion. A compressive state of stress limits the expansion. To account for the effect of the stress state on the development of the reaction, reference is made to the formulation proposed by Saouma & Perotti, 2006. According to this approach, weights varying between 0 and 1 are assigned to each principal direction depending on the stress state. The higher the compression in a direction, the lower is the weight assigned to that direction. When the compression reaches a value of σ_u, the swelling in that direction is totally inhibited Figure 3 shows some examples of weight assignment.

In all possible combinations, the sum of the weights is always equal to 1, meaning that the expansion is redistributed in the three principal directions keeping the volumetric expansion constant, as shown in experimental studies by Multon & Toutlemonde, 2006.
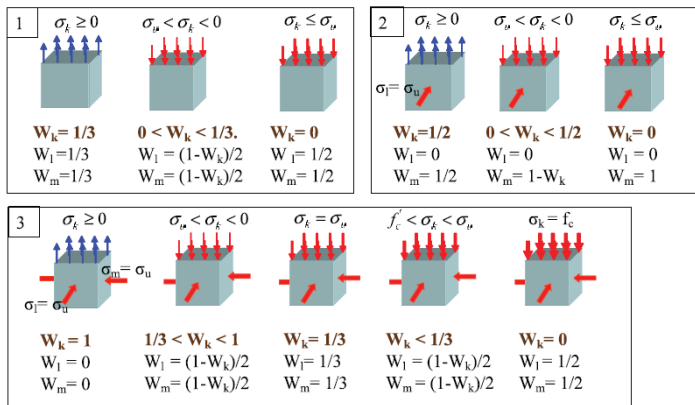
Figure 3. Weights for the redistribution of volumetric expansion (Saouma & Perotti 2006).

2.4 *Humidity*

Humidity plays an important role in determining the AAR. Since AAR needs water to occur, a low humidity hinders the development of the reaction. The most relevant parameter for considering the effect of the humidity on the AAR is the saturation ratio (S_r) inside the structure. The model proposed by Poyet et al., 2004 considers a coupling between the saturation ratio and the reaction kinetics by introducing two parameters:

$$\frac{dA}{dt} = k \cdot \alpha \cdot (\beta - A) \tag{4}$$

where α modifies the velocity of the reaction; and β modifies the maximum reaction advancement.

Based on several laboratory tests Poyet et al., 2004 conclude that the relationship between the two parameters and the saturation ratio is linear with $\alpha = \beta = S_r$.

3 MONITORING DATA

The construction of the dam took place in three phases between 1932 and 1961. The dam is equipped with a topographic auscultation system since 1973. Measurements of displacements in the y-direction (upstream-downstream, positive if towards downstream) and z-direction (vertical direction, positive if upwards) at three different points were available. The behavior of the dam in the first 40 years is not recorded. The measured values will therefore refer to relative and not to total displacements. The three points are defined according to their position: *Crest* at the top of the dam, *Turbine pit* located in the turbine chamber and *Turbine floor* located further downstream. The position of the three points is represented in Figure 4. The measured displacements that were available for model calibration are represented in Figure 5.

No other information was available, that could be useful in the interpretation of the behavior of the structure, such as laboratory tests, crack pattern in the structure, stress measurements, direct expansion measurement within the structure by means of extensometers.
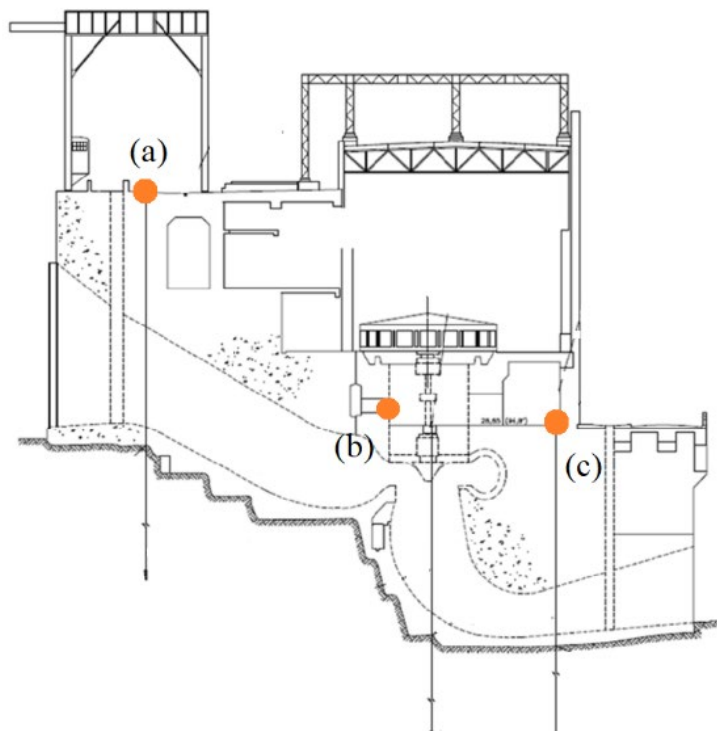
Figure 4. Position of the three points: Crest (a), Turbine pit (b) and Turbine floor (c) (Benchmark formulation document, 2021).
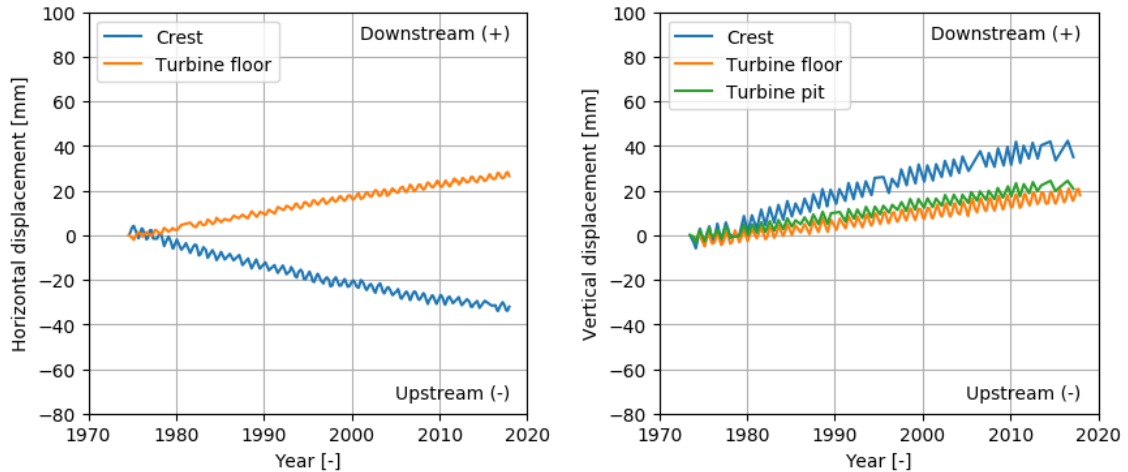
Figure 5. Topographic displacements for the three points (period 1974-2018).

4 NUMERICAL MODEL

4.1 *Geometry*

The numerical analyses proposed in this paper were carried out using FLAC3D vers. 7.0 (Itasca Consulting Group Inc. 2016), which implements the finite-difference method (FDM) and allows performing mechanical analyses in the linear and nonlinear domains. The model reproduces the geometry of three power units (11 to 13) including the foundation. The water intake part has a height of approximately 21.5 m and includes the penstocks, the upstream gates and the busbar. The power plant is approximately 24 m high and includes the generator unit, the scroll case, the draft tube, the tailrace and the downstream gates. A cold joint separates the water intake part from the power plant. The mesh (Figure 6) is composed mainly of hexahedral elements with a size of approximately 1 m for the dam body, while the foundation is formed by a coarser mesh with variable size from 1 to 20 m.
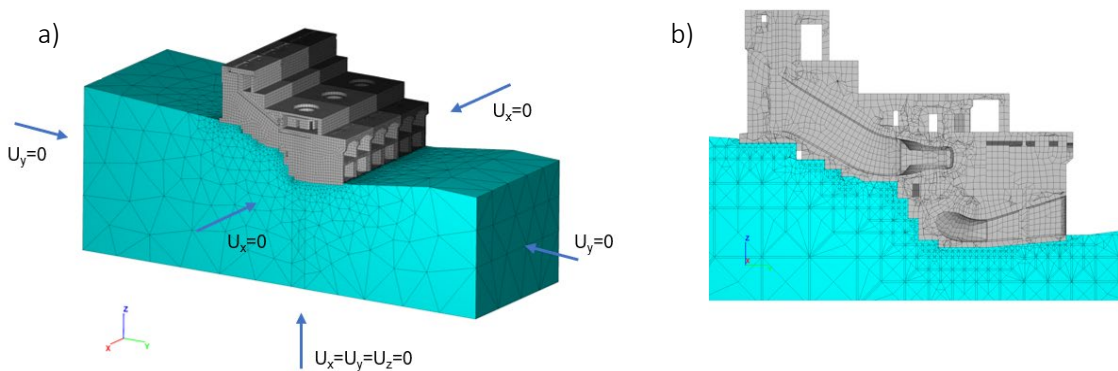
Figure 6. (a) Three-dimensional view of dam-rock system with displacement boundary conditions, (b) Finite element mesh of the Power unit 12, longitudinal section (y-z plane) (Benchmark formulation document, 2021).

4.2 *Interfaces*

The interfaces between the water intake part and the power plant, or between the different power units, have been modelled whit a non-linear behavior (except for static linear elastic analysis where the connection is bonded). The interfaces between the rock and the power unit have been kept bonded. Table 1 shows the main interface parameters introduced in the numerical model.

Table 1. Interfaces parameters.

Properties	Interfaces rock/concrete	Interfaces concrete/concrete
Shear stiffness [kPa/m]	1.0E+08	1.0E+08
Normal stiffness [kPa/m]	1.0E+08	1.0E+08
Cohesion [kPa]	elastic	3.0E+02
Tensile strength [kPa]	elastic	1.0E+01
Friction angle [°]	elastic	45

4.3 *Material properties*

Linear elastic behavior was assumed for the concrete and the foundation materials. Physical and mechanical properties are listed in Table 2. It is important to note that thermo-mechanical effects are not considered in the analysis, since a nil coefficient of thermal expansion is assumed.

All creep and relaxation influence on the stress state induced by AAR strains are neglected. Also, any computation of crack initiation was not performed. The presence of reinforcements within the structure is neglected.

Table 2. Material properties.

Properties	Concrete	Foundation
Density [t/m³]	2.36	2.62
Poisson's ratio [-]	0.21	0.20
Young Modulus [GPa]	26	-
Deformation Modulus [GPa)]	-	30
Specific heat [J/ kg °C]	917	800
Thermal conductivity [W/ m °C]	2.9	4.3
Coef. of thermal expansion [°C^{-1}]	0	0
Reference temperature [°C]	10	4

4.4 *Boundary conditions*

For determining the thermal state within the structure, the thermal boundary conditions shown in Figure 7 have been applied to the model. Temperatures at boundaries were available on a daily average basis, and it was assumed that these temperatures can be repeated each year. Hygral boundary conditions, necessary to calculate the saturation within the model, have been provided by the formulators in the form of capillary pressure and relative humidity as shown in Figure 8.
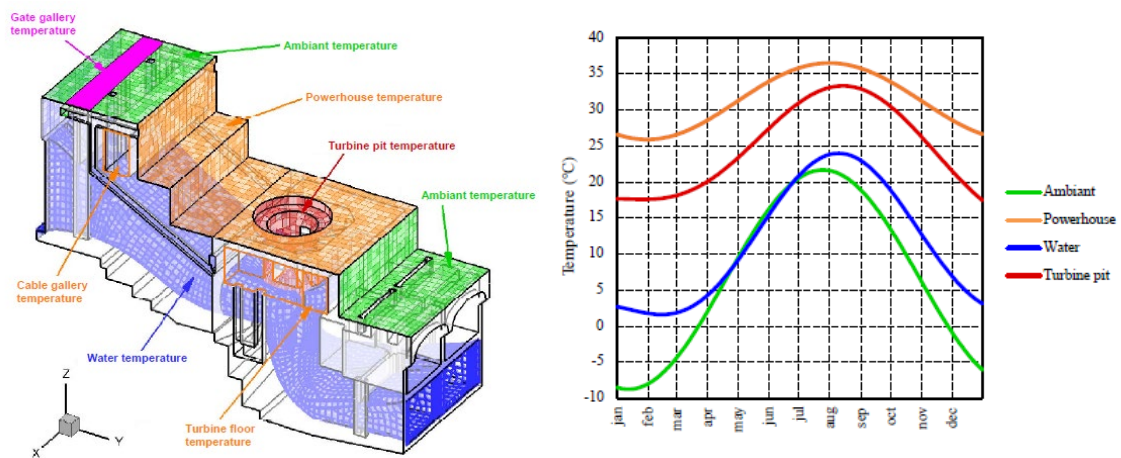
Figure 7. Thermal boundary conditions (Benchmark formulation document, 2021).
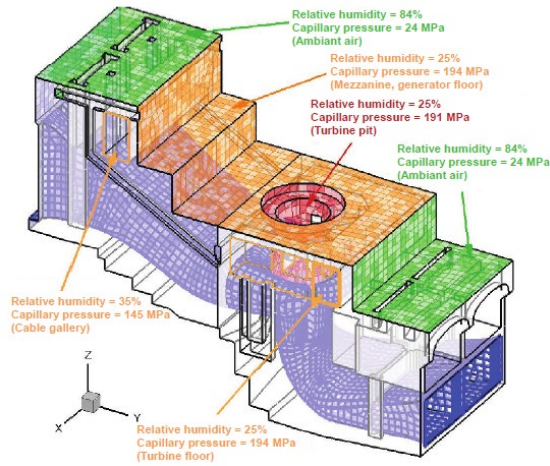
Figure 8. Hygral boundary conditions (Benchmark formulation document, 2021).

5 CALCULATION STEPS

5.1 *Introduction*

The simulation of the AAR effects in a structure is a complex task, because of the number of parameters influencing the swelling reaction. For this reason, a step-by-step procedure is implemented by progressively introducing each parameter of the model.

The steps listed in Table 3 are performed.

Table 3. Performed calculations.

Task	Stress redistribution	Thermal effects	Hygral effects
0 (calibration)	-	-	-
A	x	-	-
B	x	x	-
C	x	x	x

For the tasks A to C it is required to compute the stress field within the structure. The loading conditions considered in the analyses account for:
- Gravity loads;
- Hydrostatic water pressure. The hydrostatic load computation assumes an upstream water level at 46.10 m and a downstream water level at 21.4 m;
- Induced load caused by the concrete expansion.

In order to properly reproduce the effects of the seasonal temperature variation within one year, calculations are carried out with a 1-month timestep, starting in 1932 until 2017 (calibration period). The prediction of the model is computed until 2067 to consider a prediction period of 50 years.

5.2 *Task 0: First calibration of the AAR model*

In the lack of specific laboratory tests on concrete, a calibration of the numerical model has been performed to fit the field measurements. The two parameters that must be calibrated are:
- ε_∞ = AAR induced concrete expansion at infinite time
- k_0 = reaction rate at the reference temperature θ_0

The method of thermal analogy was used to estimate the initial parameters of the AAR model. This method consists in linking a thermal expansion to the volumetric deformation given by the swelling due to the alkali-aggregate reaction. Assuming an isotropic distribution of the expansion induced the AAR (no redistribution based on stress state), a constant temperature field equal to

the reference temperature (no thermal effects), and neglecting the hygral effects, a uniform expansion in the whole structure is obtained. Therefore, it is possible to calculate the dam elastic response in terms of displacements of the monitored points for a unitary expansion applied to the whole dam and then use this information to calibrate the model outside the numerical software.

The calibration of the model is performed by minimizing the difference between the measured displacements and the displacements obtained by the model in the calibration period (1974-2018).

5.3 *Task A: Constant temperature, fully saturated*

The effect of the chemical reaction is computed by adopting a constant and uniform temperature of 10 degrees (equal to the reference temperature, no thermal effects then). Also, the concrete is considered as completely saturated. The effect of the stress state is accounted for in this task.

5.4 *Task B: Introduction of thermal effects*

In a second stage of simulation, the effect of temperature on the development of the reaction is introduced.

Based on the temperature boundary conditions, which consist of daily temperature measurements over a year, a thermal conductivity analysis is performed. After 7 years all transient effects were found to be negligible. The thermal state in the dam is known at any moment during the year after this procedure.

However, for simplicity, the choice was made to compute an equivalent temperature for each point in the dam, to be kept constant over the entire period of simulation of the AAR reaction propagation. The equivalent temperature is defined as the temperature for which the total progress of the AAR reaction is the same as the one computed considering the daily variation of the temperature. The equivalent temperature was computed as the temperature that satisfy this condition over a period of 100 years. The final thermal field that was computed is represented in Figure 9. It is worth noting that the equivalent temperature is higher than the yearly average temperature, since the expansion increase due to the temperatures above the average exceeds the expansion reduction due to the temperatures below the average, because of the non-linearity of the expansion-temperature relationship.
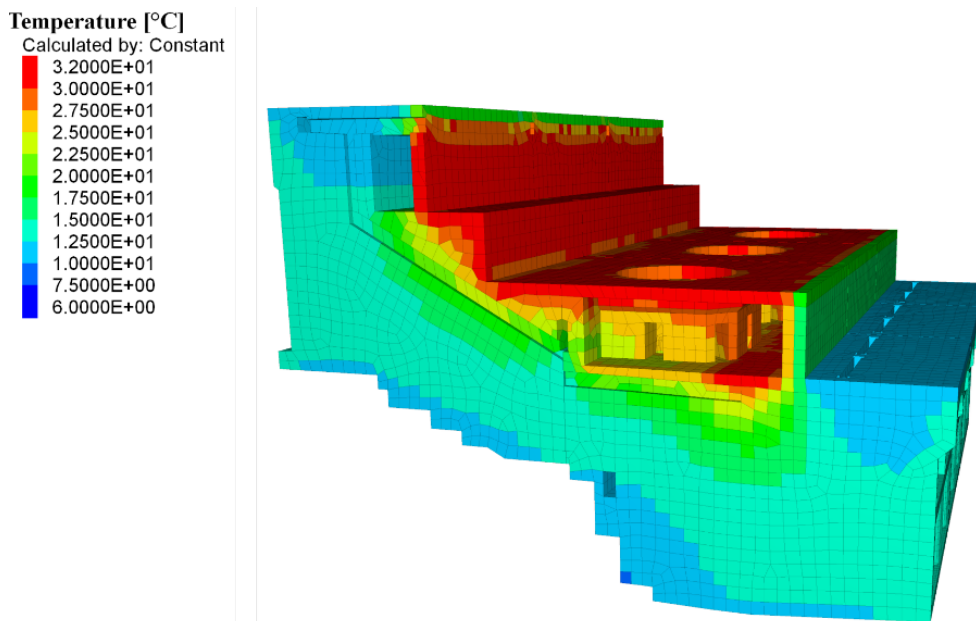

Figure 9. Equivalent temperature distribution used for calculation.

5.5 *Task C: Introduction of hygral effects*

The last case studied includes the effects generated by humidity. As described in section 7.29, humidity plays an important role in determining the AAR. Since AAR needs water to occur, a low humidity hinders the development of the reaction. The most relevant parameter for considering the effect of the humidity on the AAR is the saturation ratio (S_r) inside the structure.

To compute a saturation distribution inside the power plant, the software FEFLOW vers. 7.3 (Diersch 2014) was used, adopting the Mualem model (Van Genuchten 1980) with the following parameters: a = 18.6 MPa and m = 0.44.

The distribution of saturation that was computed (Figure 10) has been considered constant over the entire calculation period.
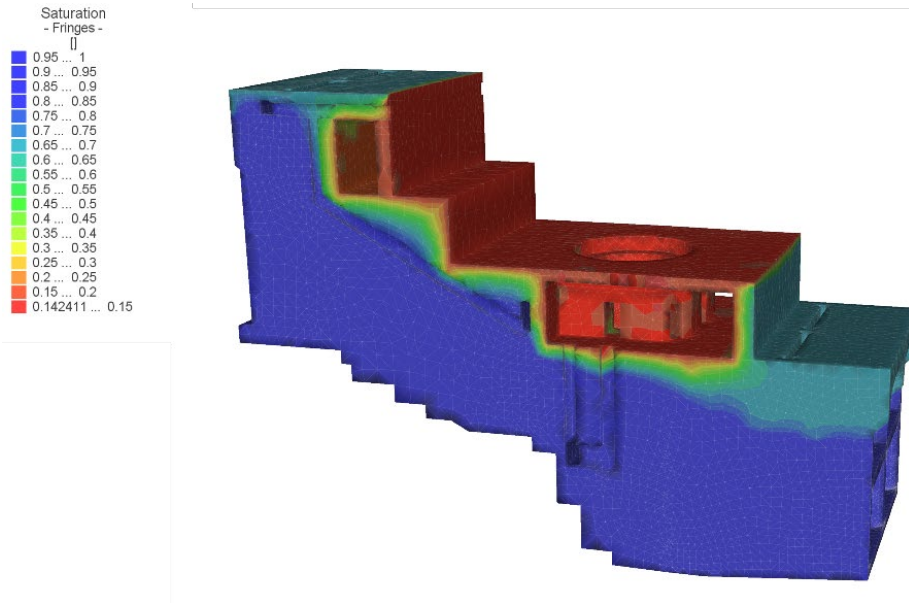
Figure 10. Saturation ratio (S_r) in the power unit 12.

6 RESULTS AND DISCUSSION

6.1 *Displacement induced by the AAR expansion*

The results of the model in terms of displacements of the monitored points, are shown in Figure 12 for the period 1940-2067. The calibrated set of parameters for the AAR model are listed in Table 4 for the four calibration steps. The parameter A_0 was not calibrated but was defined in order to reproduce a latency time, i.e., a period without concrete expansion after the chemical reaction start, of approximately 10-15 years.

The results obtained by considering only the reaction kinetics (Task 0) are remarkably satisfactory. The time evolution of the displacements is well reproduced for all the monitored points. A little overestimation is obtained for the horizontal displacement of the *Crest* and for the vertical displacement of the *Turbine Floor*, while a little overestimation is obtained for the vertical displacement of the *Crest* and for the horizontal displacement of the *Turbine Floor*. The concrete expansion at infinite time obtained by the calibration is 3900 μm/m, which seems to be plausible if compared with other structures (Amberg et al, 2013). The value is kept constant for the other tasks.

The introduction of the effect of the stress state (Task A) and of the temperature (Task B) produce minor changes in the predicted displacements, except for the vertical displacement of the Turbine Floor, which is overestimated by the model in the calibration period. This is supposed to be the result of the swelling redistribution due to the stress state. The concrete expansion in the x-direction is hindered by the presence of the adjacent blocks, leading to higher compressive stress in that direction that cause a redistribution of the expansion in the other less-compressed

directions. The same effect, though minor, is visible also in the predicted vertical displacements for the *Crest* and the *Turbine Pit*.

The best agreement between the measured displacements and the predicted ones is obtained with the introduction of the effect of the saturation (Task C). The displacements of all the points are correctly reproduced by the model, except the vertical displacement of the Turbine Floor. It has to be noted that the best result in the calibration process was obtained by neglecting the effect of the saturation ratio on the final advance of the reaction. Therefore, the parameter β has been taken equal to 1.

The good superposition of the curves for most of the points, indicates that, the proposed model provides a correct description of the AAR phenomenon. However, the increase of complexity in the model does not produce substantial improvements in the approximation of the curves. On the basis of the limited information available regarding the behavior of the dam, the introduction of other effects than the reaction kinetics seems not justifiable. A more comprehensive understanding of the behavior of the dam supported by stress measurements, crack pattern layout or direct measurement of the concrete expansion would be needed, in the opinion of the authors, to support the introduction of further elements and complexity in the model.

The prediction for the next 50 years, indicates that the displacement velocity would decrease in the future without, however, reaching a full stabilization phase in the next 50 years. This is compatible with field observations for other structures in which the full stabilization phase is not yet observed. The deceleration visible in the displacement is compatible with the reaction advance predicted by the model. Figure 11 shows, for the Task C, that the reaction advance in most of the dam has already reached in 2017 a level of more than 80-90 per cent, in particular in the regions with higher temperatures. The zones with a lower reaction advance are located in the less saturated zones.

Table 4. AAR model parameters.

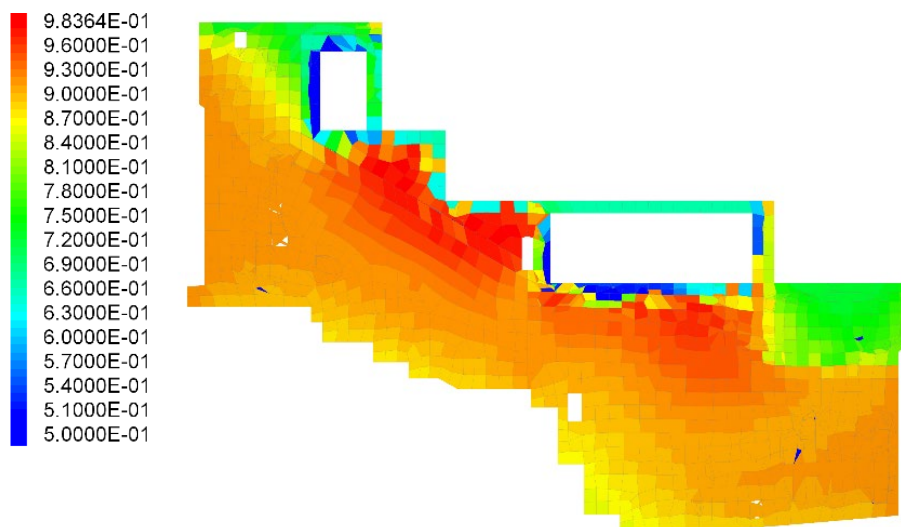| Parameters	Task 0	Task A	Task B	Task C
ε_∞ [μm/m]	3.9E+03	3.9E+03	3.9E+03	3.9E+03
k_0 [1/day]	4.1E-05	4.1E-05	4.1E-05	6.0E-05
θ_0 [°C]	10°C	10°C	10°C	10°C
E_a [kJ/mol]	-	-	45	45
A_0 [-]	2.0 E-02	2.0 E-02	2.0 E-02	2.0 E-02
α [-]	-	-	-	S_r
β [-]	-	-	-	1
σ_u [MPa]	-	10	10	10

Figure 11. Level of reaction (A) in 2017, which represent the advancement of the reaction.

6.2 *Stresses induced by the AAR expansion*

Concrete expansion produces stresses in the structure. The evolution of these stresses, computed over the surfaces represented in Figure 13, is presented in Figure 14 for the period 1937-2067. For the calculation of the average stresses, the resultants acting on the unit 12 are considered. For the Intake/Unit surface, the resultants acting on the Unit are considered. Figure 15 shows the resultant forces in 2067. Only the forces at the contact between the structure and the rock and in the Intake/Unit contact are shown. The sum of the vertical and horizontal forces at the concrete/rock interface, besides some imprecision due to some difficulties that were met while reading the forces acting on interfaces with the FLAC software, equilibrate vertically the structure weight and horizontally the hydrostatic force, respectively.

A relevant compressive stress develops in the X direction. The compressive stress in the X direction reaches 10 MPa in 2067, which is the value that inhibits the expansion according to the adopted model. A compression develops also in the Y direction, reaching approx. 8 MPa (approx.1150 MN) over the Intake/Unit interface, caused by the concrete expansion restrained by the rock foundation. The compressive force is transmitted to the rock by means of a sort of compressed arch, causing relatively high shear stresses in the concrete/rock interface of about 1.5-2.0 MPa (approx. 1500-1600 MN). The shear forces at the foundation are higher than the normal forces. Tensile stresses are computed over the Rock/Intake interface. The shear stresses arising at the concrete/rock interface are not a concern for the dam stability since they are self-equilibrating stresses. However, they could cause slippage and thus damage at the concrete/rock interface, reducing the capacity of the foundation to resist to the external forces (i.e., the reservoir force).
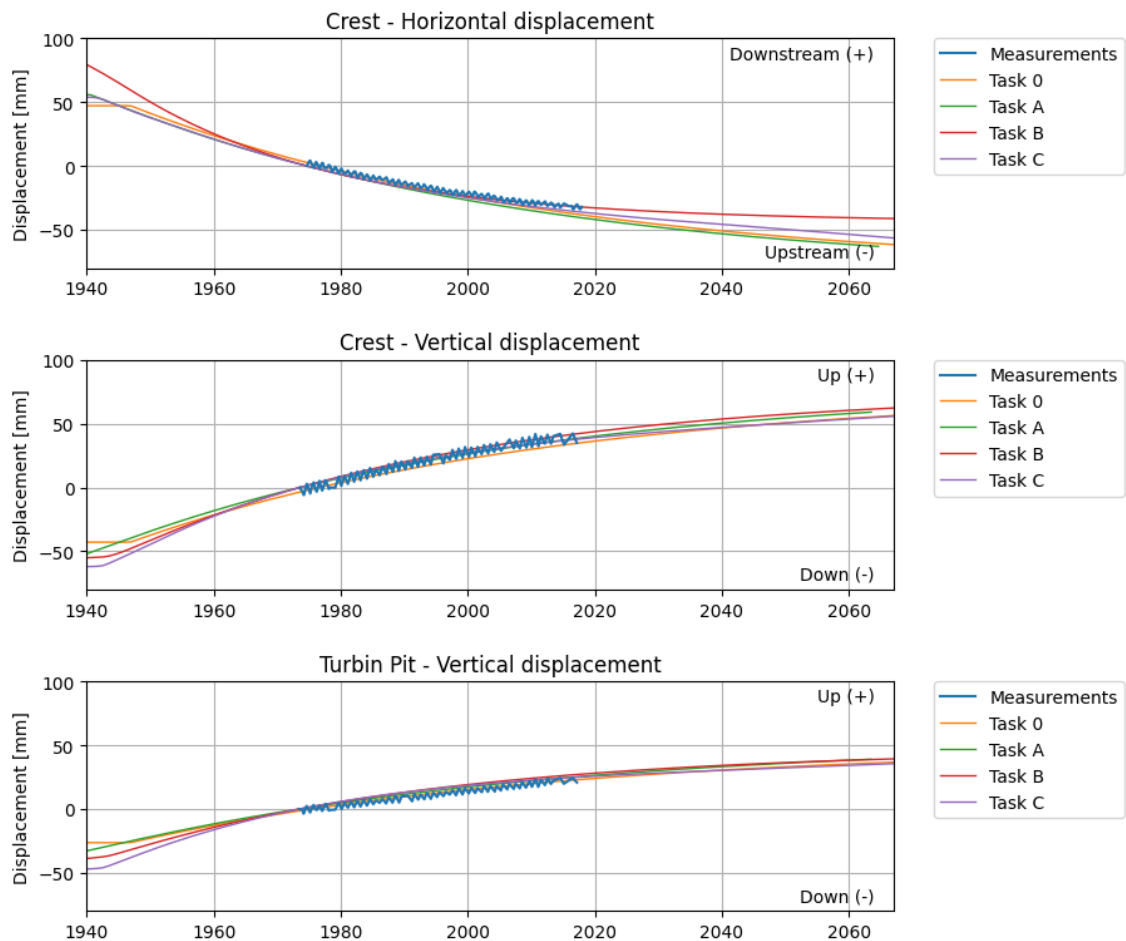
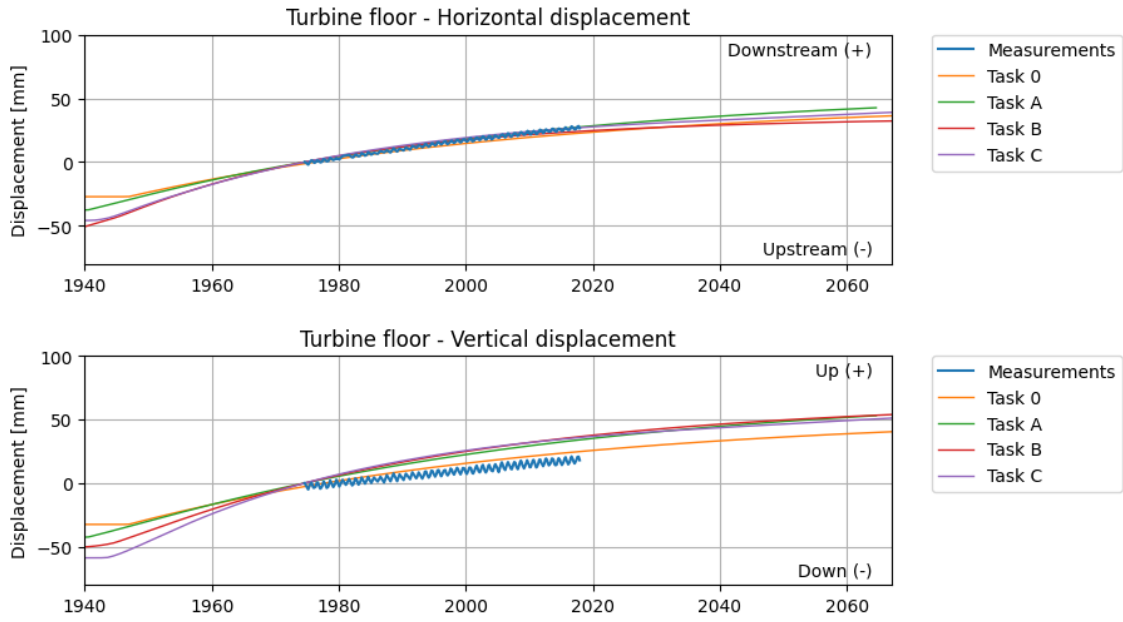Figure 12 (part 1). Time-history displacements for the three monitored points.

Figure 12 (part 2). Time-history displacements for the three monitored points.
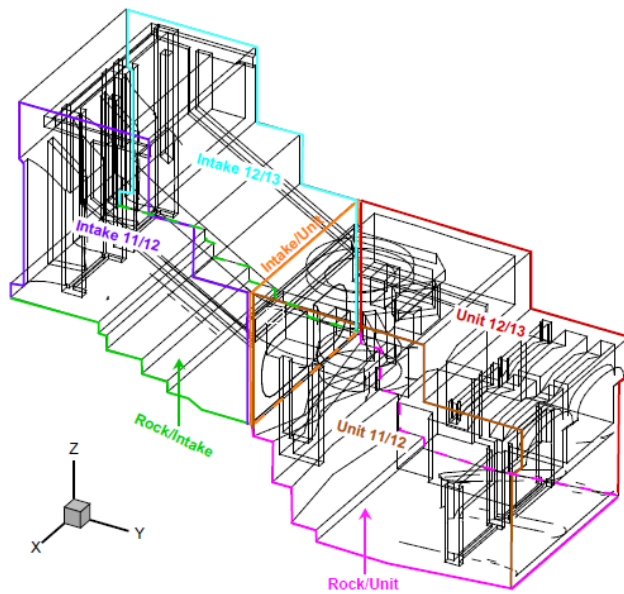

Figure 13. Definition of the surfaces in the model (Benchmark formulation document, 2021).
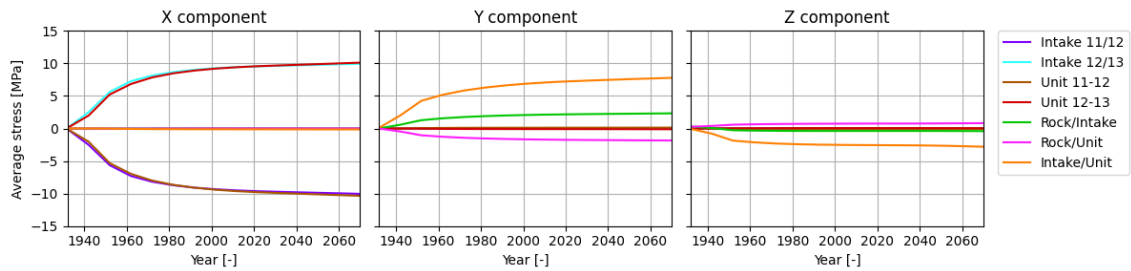

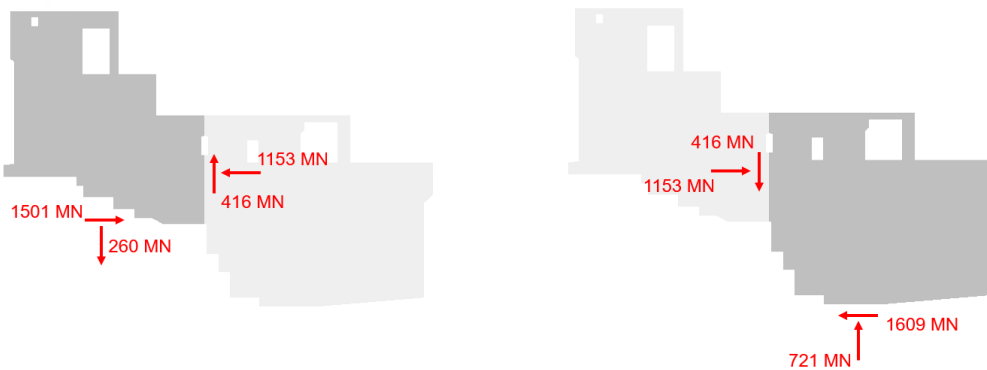Figure 14. Average stress in the interfaces for the Task C.

Figure 15. Resultant forces in 2067 for the Task C.

7 CONCLUSIONS

The behavior of the Beauharnois Dam affected by AAR is evaluated by means of a numerical model accounting for the effects of the reaction kinetics, of the temperature, of the stress state and of the humidity. This calculation exercise was proposed in the frame of the 16th International Benchmark Workshop on Numerical Analysis of Dams.

The model is calibrated on the measured displacement in 5 points in the dam in the period 1974-2018. A prediction for the next 50 years is also performed. The best agreement between the model and the measurements is obtained by including in the model all the above listed effects. However, a remarkable satisfactory result is also achieved by considering the reaction kinetics only. In other words, the addition of complexity in the model does not produce substantial improvements in the approximation of the actual behavior. A more comprehensive understanding of the actual behavior of the dam in terms of stress state (in situ stress test, crack pattern layout) and expansion distribution (by means of direct expansion measurements) would be needed, in the opinion of the authors, for supporting the introduction in a reliable way of further effects in the model.

Some general conclusions regarding the behavior of the dam can be drawn from the results of the model. A compressive stress state arises in the X direction, its magnitude being affected by the assumptions of the model, though. Also, in the upstream-downstream direction compressive stress develop, which are transferred to the rock foundation by relevant shear stresses, which could lead to slippages in the rock-concrete interface.

As stated before, these general considerations must be supported by further data for defining properly a possible rehabilitation work. According to the obtained dam behavior, a possible intervention can be the realization of vertical slot cuts between units (YZ plane) and between intakes and units (XZ plane) in order to relief the compressive stress in the X direction and in the Y direction, respectively.

REFERENCES

Amberg, F., Stucchi, R., Brizzo, N. 2013. The effect of temperature on the development of the Alkali Aggregate Reaction at the Pian Telessio dam. 9th ICOLD European Club Symposium, Venice

Benchmark formulation document, Roth S.-N., Miquel B., Theme B: AAR affected dam. Evaluation and prediction of the behavior of the Beauharnois dam, 16th International Benchmark Workshop on Numerical analysis of Dams, 2021.

Bérubé, M.-A., Frenette, J., Pedneault, A., Rivest, M. 2002. Laboratory assessment of the potential rate of ASR expansion of field concrete. Cement, Concrete and Aggregates, Vol. 24, n. 1, pp. 13-19

Capra B., Bournazel J.P. 1998. Modeling of induced mechanical effects of alkali-aggregate reactions. Cement and concrete Research, 2251-260.

Diersch H-J. 2014. FEFLOW, Finite Element Modeling of Flow, Mass and Heat Transport in Porous and Fractured Media, Springer-Verlag Berlin Heidelberg, Germany.

Grimal E., Sellier A., Multon S., La Pape Y., Bourdarot E. 2010. Concrete Concrete modelling for expertise of structures affected by alkali aggregate reaction. Cement and Concrete Research, 502–507.

Itasca Consulting Group, Inc. 2016. FLAC –Fast Lagrangian Analysis of Continua, Ver. 8.0. Minneapolis.

Morenon P., Sellier A., Multon S., Grimal E., Kolmayer P. 2021. Benchmark Study Results: EdF/LMDC. In: Saouma V.E. (eds) Diagnosis & Prognosis of AAR Affected Structures. RILEM State-of-the-Art Reports, vol 31. Springer.

Multon, S., Toutlemonde, F. 2006. Effect of applied stresses on alkali-silica reaction-induced expansions. Cement and Concrete Research 36 912-920.

Poyet, S., Sellier, A., Capra, B., Foray, G., Torrenti, J.-M., Cognon, H., Bourdarot, E. 2004. Modelling of Alkali-Silica Reaction in Cconcrete, Part 2: Influence of Water on ASR, Proc. Of the 12th Int. Conf. on Alkali-Aggregate Reaction in Concrete, Beijing, China.

2021. 16th International Benchmark Workshop on Numerical Analysis of Dams, Theme B, Evaluation, and prediction of the behavior of the Beauharnois dam. Ljubljana, Slovenia.

Saouma V., Perotti, L. 2006. Constitutive Model for Alkali-Aggregate Reactions. ACI Materials Journal 103(3) 194-202

M. Th. van Genuchten 1980 A closed-form equation for predicting the hydraulic conductivity of unsaturated soils. Soil Science Society of America Journal 44.5, pp.892–898.

Behaviour of the embankment dam

BEHAVIOUR OF THE EMBANKMENT DAM

Description and Synthesis of Theme C

Formulators:

Pavel Žvanut
Slovenian National Building and Civil Engineering Institute

Barbara Likar
Slovenian National Building and Civil Engineering Institute

Žiga Likar
Geoportal d.o.o.

Vanja Selan
Elea iC d.o.o

Mateja Klun
University of Ljubljana, Faculty of Civil and Geodetic Engineering

1 INTRODUCTION

In total, embankment dams represent over 80% of all dams built in the world (Wrachien, 2009). Additionally, most of the dams were built in previous decades. Unlike concrete dams, embankment dams can accommodate a wide variety of foundation conditions and construction materials are usually available close to the dam site. During the construction and commissioning, embankment dams are exposed to various loading conditions. Internal erosion is a common problem in embankment dams. For example, approximately 40% of all embankment dam failures have been attributed to soil instability due to uncontrolled seepage through the dam body or its sub-base (ICOLD Committee on Embankment Dams, 2017). Moreover, the dams were more or less built in the past, considering different safety, design and construction standards (United States Society on Dams, 2010). Additionally, we are often faced with a lack of data, and need to adopt different modelling assumptions to perform numerical analysis. The main purpose of this topic is to present a case from Slovenia. We prepared a case of an embankment dam with an interesting history and design. The dam is monitored, but there is still a lack of data that requires engineering judgement that can be described using various modelling approaches.

In this document you can find information on the dam and foundation, historical data, description of the provided data in separate files, the description of the tasks and subtasks, and the expected outcomes. In the theme, the geometry, material properties, and monitoring data are provided by the Formulators. Some aspects of the numerical modelling are intentionally not defined so that the participants could make their own assumptions and choose suitable approaches to solve the problem. In particular, the participants may select the analysis approach they think is appropriate for the case at hand. Thus, by comparing the different solutions, it will be possible to draw conclusions regarding how different assumptions and approaches affect the results.

In case the participants will express their interest in a technical visit to the dam, in the scope of the BW in Ljubljana, the visit can be organized (*in case the BW will be held in physical form and not in virtual form due to COVID-19 restrictions).

2 BASIC INFORMATION ABOUT THE DAM

The identity of the dam in this topic is confidential. The downstream view of the dam is shown in Figure 1. The following subchapters present the main features of the dam including its structure, material description, chronological description of construction and operation, detailed description of leakage, and available monitoring data.

The dam was built in 1989 for agricultural (irrigation) and flood protection purposes. The reservoir provides seasonal water storage, where excess rainwater is collected during the cold part of the year, when the inflows are high, while in the spring and summer months the water from the reservoir is mainly used for irrigation.

The dam site lies on an impermeable Eocene flysch. During the design phase, the geological conditions at the site were estimated as very good. However, this assessment was based on the performance of only basic geological and hydrological investigations. Moreover, excavations during construction revealed zones with permeable limestone deposits. To ensure lower permeability in the foundation, the permeable zones were grouted with a single-row grout curtain (cement-bentonite suspension), which was used to seal the permeable zones and reduce the permeability of the dam foundations. The depth of the grouting in the foundation is 68 m (the grouting reached the ground up to the elevation level 34 m asl). Grouting was done simultaneously with the dam construction, but the precise locations of the grouting are not known.

The construction of the dam lasted about a year and was completed in the late 1980s. The reservoir was fully impounded about 18 months after the completion of the construction works (details of the first impoundment are presented in the chapter *Loads*). After 20 years of operation, during regular maintenance, wet spot was noticed on the downstream slope of the dam (see 2.5). Rehabilitation works on the dam were finished in 2022 and the dam is now again fully operational.

3 DESIGN OF THE DAM

The main technical data of the dam are:
- Dam height above the foundation: 34.6 m
- Elevation of the dam crest: 102.00 m asl
- Elevation of the foundation: 67.40 m asl
- Crest width: 5 m
- Base width: 120 m
- Crest length: 174 m
- Elevation of the normal water level: 98.8 m asl

The dam under investigation is a zonal earthfill dam with a clay core. Typical cross-section of the dam is shown in Figure 2. The main zones in the dam structure are: (A) impermeable clay zone, (B) rockfill zone, (C) mix of limestone and sandstone blocks, (D) impermeable rock foundation, and (E) filter. On the upstream side of the filter, the dam consists of rockfill material (B). The upstream slope has an inclination of 1:1.5 and has intermediate berms. The core of the dam contains clay-silty materials, obtained mostly in the area of the reservoir. The impermeable core is protected with a two-layer filter (on upstream and downstream side). Figure 2 shows the cross-section of the dam, where we can see that the impermeable clay zone (A) and zone (C) are not divided vertically. The blocks of limestone and sandstone in zone (C) are sealed by the impermeable clay material, while the filter is installed at the boundary. The formulators are unfamiliar with the justifications for such design. The downstream slope has an inclination of 1:2. The embankment dam is 35.40 m high and 174 m long, while the width of the dam is 5.0 m at the crest and 120 m at the toe. The total projected volume of the reservoir is 8.0 hm^3 of water, of which 6.8 hm^3 (84.5% of the volume) is intended for irrigation, and the remaining 1.2 hm^3 (15.5% of the volume) for flood water retention.
.
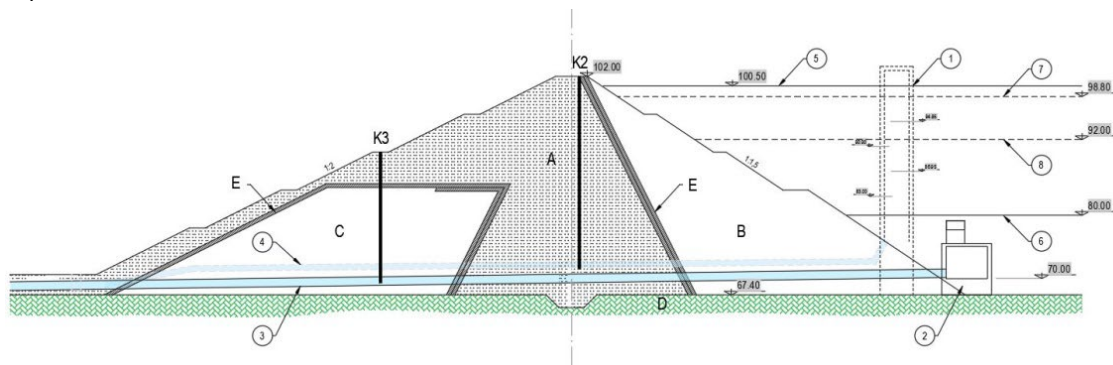
Dam structure:
(A) clayey-silty material
(B) rockfill material
(C) limestone and sandstone blocks
(D) impermeable rock base
(E) filter material

Reservoir levels:
(6)   Maximum reservoir level (100.5 m asl)
(7)   Minimum operating level (80.0 m asl)
(8)   Normal operating level (98.8 m asl)
(9)   Depleted operating level (92.0 m asl)

Hydrotechnical structures:
(1)   intake tower
(2)   intake structure
(3)   bottom outlets
(4)   irrigation pipeline

Crest elevation 102.00 m asl
Foundation elevation 67.40 m asl

Figure 25. Typical cross-section of the embankment dam.

In order to prevent breaching of the dam during extreme flood events, an emergency spillway is situated at the right abutment of the dam. The spillway is designed to evacuate a flood with a 1000-year return period. The bottom outlet with a capacity of 14 m^3/s consists of two steel pipes with a diameter of 120 cm, which are protected with a concrete cover. One of the pipes is used for abstraction of water for irrigation, while the other for emergency evacuation of water from the reservoir. Bottom outlet (number 3 on Figure 1) is regulated by a Howell-Bunger valve installed on the left downstream side of the dam, meaning that the pipes are filled with water even when the valves are closed. The RC intake structure for the bottom outlet is on Figure 1 marked with a number (2).

Additionally, the intake tower (number 1 on Figure 2) is equipped with 4 hydraulic gates that enabled abstraction of irrigation water at various elevations. The steel pipeline (number 4 on Figure 1) from the intake tower, which is protected with a concrete cover, has 100 cm in diameter and leads toward the outlet structure downstream of the dam. Since the leakage detection, this irrigation pipeline has been sealed and intake tower is no longer in operation. The disposition of the bottom outlet, the intake tower, the irrigation pipes and the bottom conduits is marked on the Figures 1 and 2.
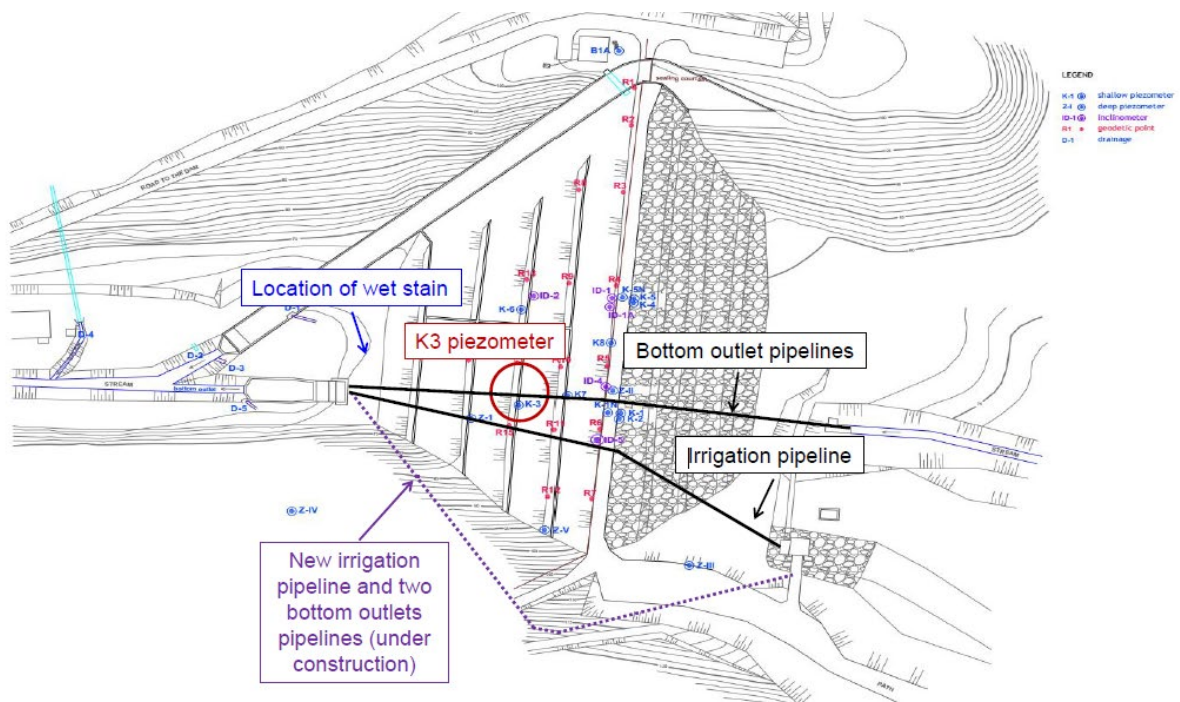
Figure 26. Plan view of the discussed dam.

3.1 *MATERIAL PROPERTIES*

3.1.1 Dam

The material properties are presented in Table 1.

Table 1. Material properties (w [%] – Soil moisture; γ [kN/m3] – Specific gravity; cu [kPa] – Undrained shear strength; c [kPa] – Effective cohesion; Eoed [MPa] – Oedometric modulus; E [MPa] – Elastic modulus; v [-] – Poisson coefficient; k [m/s] - Water permeability).

Zone	Description	w [%]	γ [kN/m³]	c_u [kPa]	ϕ [°]	c [kPa]	Eoed [MPa]	E [MPa]	v [-]	k [m/s]
A	Top layer of the dam (top 3 m from the crest) dolomite gravel mixed with silt or clay	13	21	/	36	36	15	/	0.4	10^{-6}
A	Clayey silt to silty clay	26	19.5	75	/	/	5	/	0.5	10^{-9}
B	Rockfill (limestone blocks)	/	24	/	38	/	50	/	0.3	10^{-3}
C	Blocks of limestone and sandstone	/	24	/	38	/	50	/	0.3	10^{-4}
D	Flysch	/	25	/	39	32	/	620	0.25	10^{-9}

Filter characteristics are unknown.

3.1.2 Foundation

Assume homogenous foundation, with the coefficient of water permeability: $k = 10^{-9}$ m/s.

3.2 *LOADS*

The following loads have to be considered: dead weight and hydrostatic pressure according to the reservoir water level. Water is considered to have a unit weight of 1000 kg/m³ and compression wave velocity of 1439 m/sec. Main reservoir levels are:
- Maximum reservoir level: 100.5 m asl
- Minimum operating level: 80.0 m asl
- Operational (normal) reservoir level: 98.8 m asl
- Lowered (emergency) reservoir level: 92.0 m asl

Additionally, reservoir levels for the period 1988–2020 are provided in an Excel spreadsheet.

First filling: First filling started about 12 months after the completion of construction works and lasted 722 days, with an average increment of 2.3 cm/day. The zero level of the reservoir was at 81.84 m asl and the final level of 98.34 m asl was reached at the end of the first impoundment. Time series of the first filling are provided as an input data.
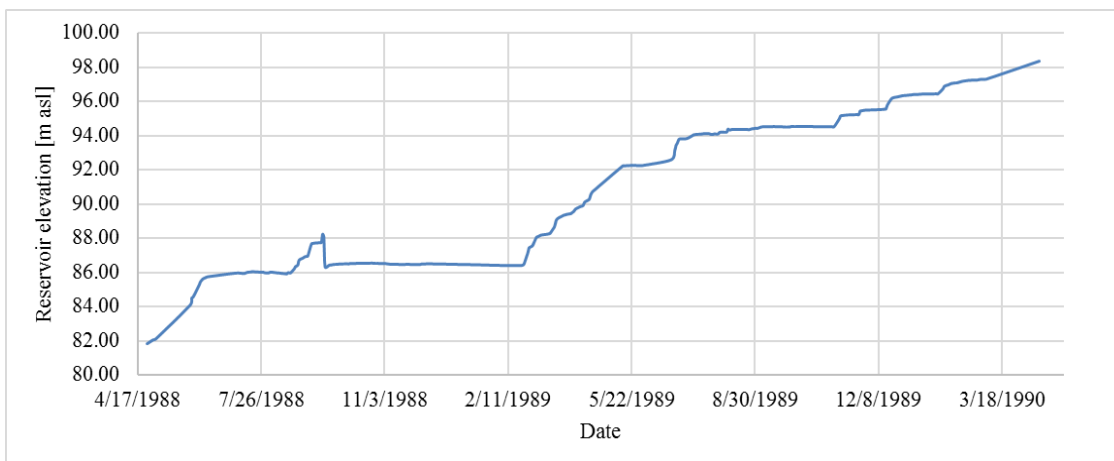
Figure 27. Time series of the first filling of the reservoir.

Filling of the reservoir after completion of the remediation work: When the reservoir will be impounded again, the following rules have to be considered: until the reservoir reaches the level of 90 m asl maximum daily rise of reservoir level may be 0.5 m/day, afterwards reservoir level can rise for only an additional 0.3 m/day until the final level of 98.8 m asl However, based on the hydrology data, the formulators estimate that an average rise of 5 cm per day should be considered by the participants who are solving theme C. Time series of the filling of the reservoir after remediation works are provided as an input data (see Fig. 4).
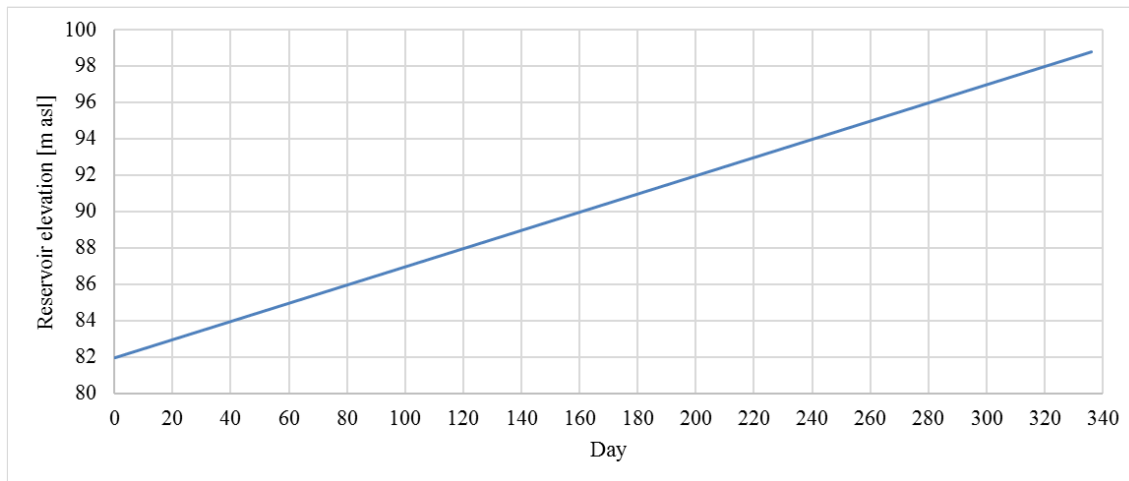
Figure 28. Filling of the reservoir after completion of the remediation works.

Seismic load: For the seismic analysis the participants were asked to consider horizontal peak acceleration of 0.3 g and vertical accelerations to be 0.67 of the horizontal.

3.3   *MONITORING*

The dam monitoring system was designed during the design phase. The basic monitoring system of the dam was already established during construction and immediately after the construction of the dam.   Regular technical monitoring consists of the following measurements and inspections:

- Deformation measurements (vertical and horizontal displacements, inclinations)
- Visual inspections (structural, geotechnical)
- Groundwater measurements (seepage in the dam body (i.e., drainage outflow, piezometric levels), seepage in the foundation of the dam and in the abutments, pore pressure in the clay core and in the foundations)
- Measurements of external loads on the dam (hydrostatic pressure, earthquake).

Geodetic measurements of vertical and horizontal displacements are performed once a year on 16 measuring points on the downstream slope of the dam: 7 points are located on the crest, 5 points on the fourth berm, 3 points on the third berm and one point on the second berm (see Figure 3). The vertical inclinometer casings were installed when the dam was already in operation, measurements are regularly performed on 4 inclinometers - 3 of them are installed on the crest of the dam and 1 is located on the upper berm.

3.4   *THE APPEARANCE OF THE WET ZONE*

On October 24, 2007, during a regular visual inspection of the dam, a wet zone was observed. The wet spot was located at the downstream toe of the dam in the central part, close to the axis of the dam (the location is shown on Figure 2). Moreover, the presence of surface water was observed at the downstream toe of the dam, between the stilling basin of the spillway channel and outlet structure of the bottom outlet. Furthermore, the extensive vegetation in the central part of the embankment dam indicated that the wet zone extended to the downstream slope of the dam above the wet spot. An emergency investigation revealed that the excess water on the downstream slope originated from the reservoir. It was suspected that the cause of the leakage was a damaged irrigation pipeline. After emptying the reservoir and inspecting the irrigation pipeline, this hypothesis was confirmed. Air bubbles were observed in several places under the silty layer deposited on the walls of the pipeline. The corrosion of the steel pipeline (the holes were a few cm to a few 10 cm in diameter) enabled seepage of water into the layer between the concrete cover and the steel pipe. Although the irrigation pipeline was emptied, the wet zone still existed. Therefore, the emergency investigations were also extended to the conduits of the bottom outlet pipeline, which can only be closed on the downstream side, so in the case of the damaged pipeline, the seepage into the dam body was possible. Detailed investigations revealed similar damage on the bottom outlet pipeline as in the previous case of the irrigation pipeline. Geotechnical investigations of the foundations (i.e., water permeability tests and coring) showed that there was only minimal (practically negligible) amount of seepage in the foundation layer under the dam, so piezometer levels showed no changes in the water level. In summary, the seepage was confined to the dam body in close proximity to both, the irrigation pipeline, and the bottom outlet pipeline.

3.5   *REMEDIATION WORKS*

In 2008, the reservoir level was lowered to a maximum of 93.6 m asl, and the irrigation pipeline was filled with the concrete. The space between the irrigation pipeline and the concrete cover was grouted with the cement grout. After this emergency remediation, the operating reservoir level was additionally lowered to a 92.0 m asl Operation of the reservoir is recorded in Excel file, where you can observe the reservoir drawdown. The reservoir operated in the lowered condition for more than 10 years.

During the time of the BW the reservoir was completely emptied, and remediation works were underway. During the works, the bottom outlet and irrigation pipes were be sealed with concrete filling. A new outlet building, and outlet tunnel were constructed in the left abutment and all the conduits in the dam body were permanently sealed. After all the above mentioned the works were completed, the reservoir water level was raised back to the original nominal level at 98.8 m asl

4 PROVIDED DATA

Participants are provided with the following data: geometry (.DWG file), reservoir levels, piezometric levels, projected reservoir levels for filling the reservoir after the remediation works, and geodetic measurements. The description of each data set can be found below:

- **Geometry**
  Data format: *.dwg
  Description: Three layers are provided: DAM GEOMETRY (cross-section), WATER LEVELS (maximal operating level: 100.5 m asl, minimal operating level: 80.0 m asl, normal operating level: 98.8 m asl and depleted operating level: 92.0 m asl) and BOTTOM OUTLETS. The geometry is positioned at the actual elevation.
- **Monitoring data – geodetic measurements**
  Data format: Excel spreadsheet
  Description: The data is stored on the Spreadsheets in the document:
  - Direction Z: settlements (settlements have a negative value)
  - Direction Y: displacement in the upstream-downstream direction; positive value "+" represents displacement in the upstream direction
  - Direction X: cross-valley displacement; "+" represents displacement toward the right bank side.
  - Units: [mm]
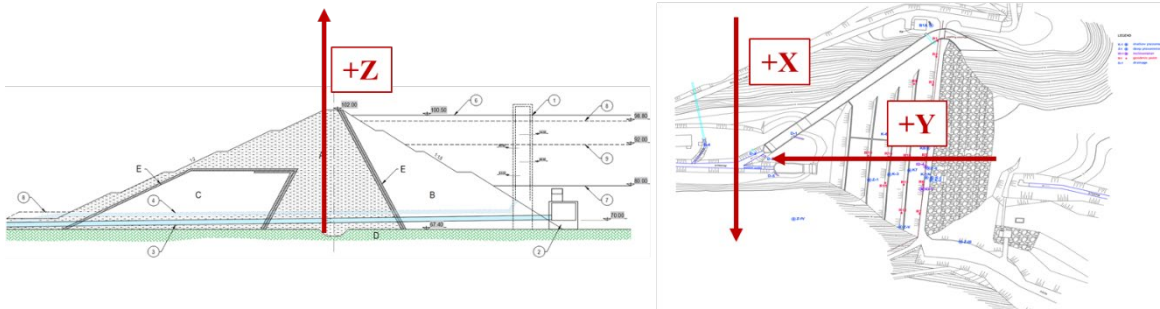
Figure 29. Positive directions in the coordinate system for geodetic measurements.

Positive directions are graphically presented on the Fig. 5.
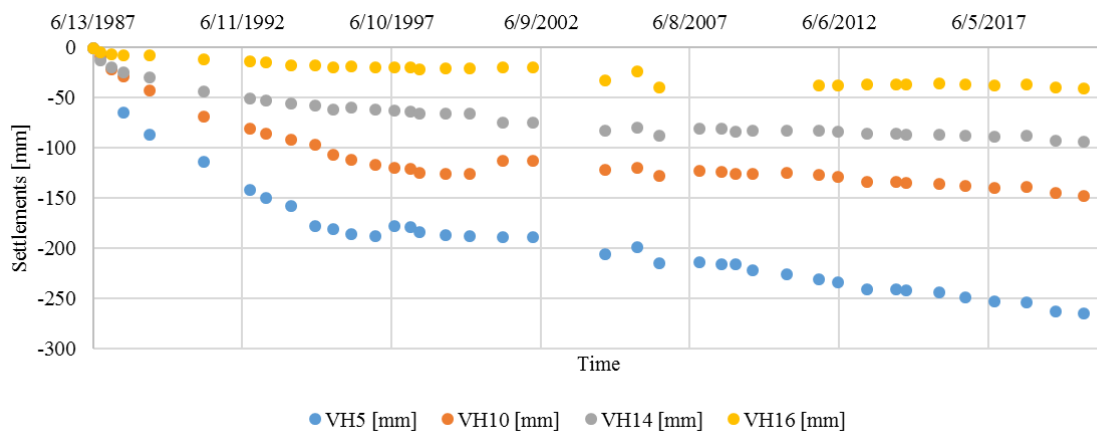
Figure 30. Time series of the measured settlements.

Locations of the geodetic points (VH5, VH10, VH14, and VH16) are marked on the Fig. 7.
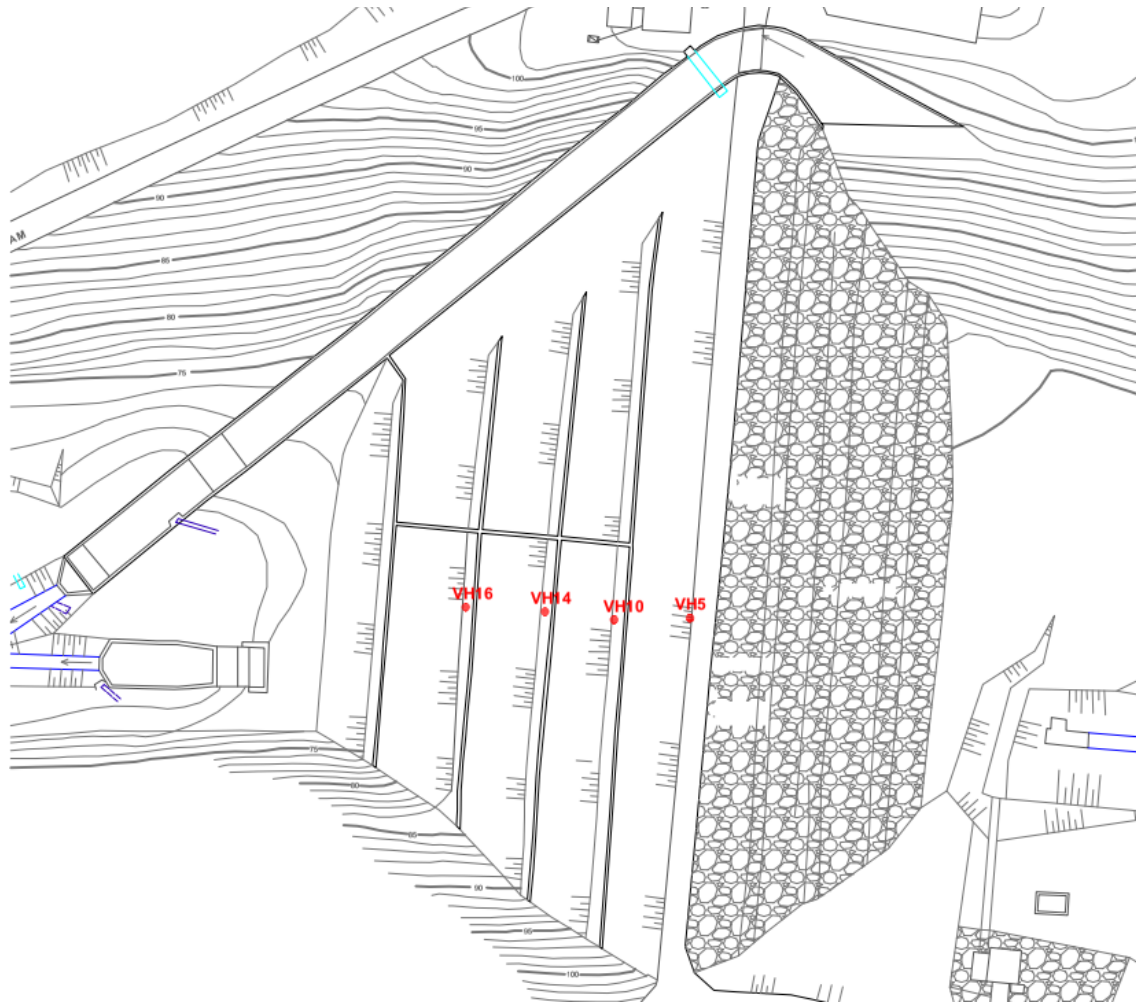
Figure 31. Locations of the geodetic points (VH5, VH10, VH14 and VH16).

- **Data: Piezometers**
  Data format: Excel spreadsheet
  Description: Raw data of the seepage level measured in piezometers. The data file contains piezometric water level in m asl The date format is mm/dd/yyyy. There are no empty cells in the data set. Data are for each piezometer is in a separate column. Measurements are taken manually and have an uneven frequency. Recorded data has been under some basic pre-processing but there may still be some faulty data in the data set.

Table 2. Piezometer lengths.

Piezometer	K2	K3
Length [m]	30.5	20.7
Elevation on the top [m asl]	102.30	91.50

Location of the piezometers is presented on Fig. 9 and 10.
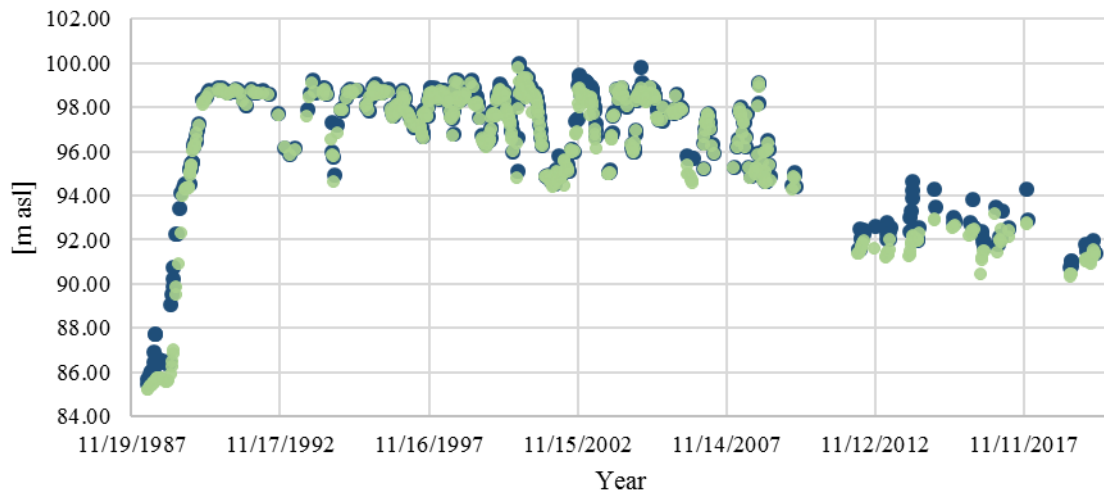
Figure 32. Time series of the piezometric levels of piezometers K2 and K3.
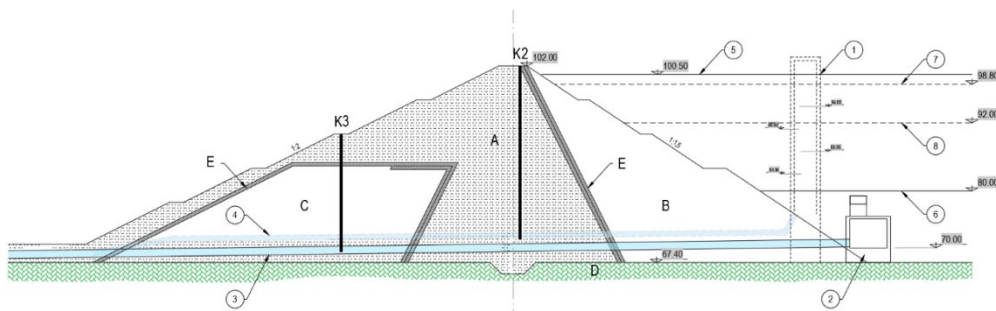
Figure 34. Location of the piezometers K2 and K3 in the plan view.
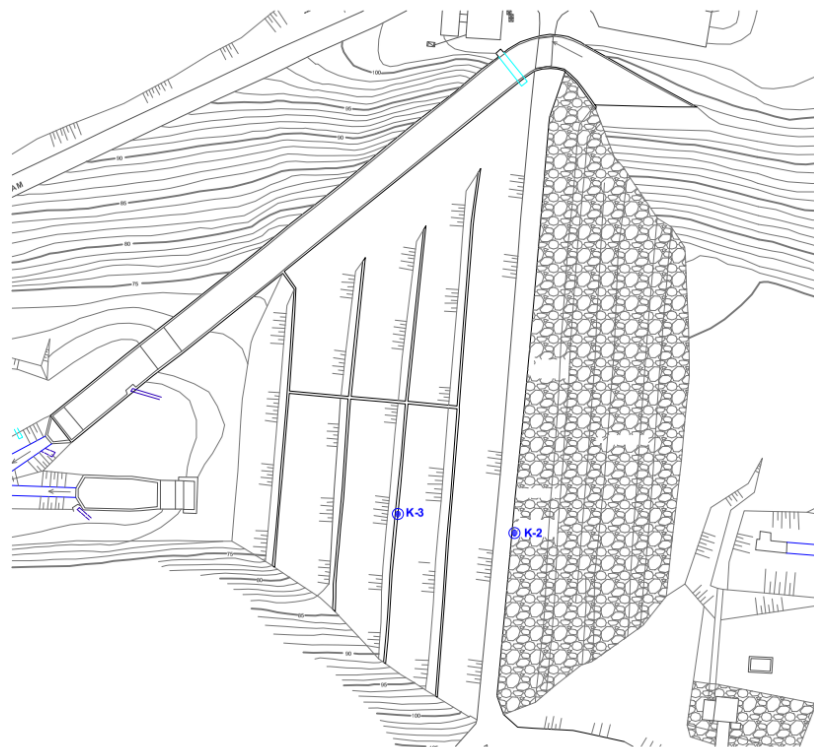
Figure 33. Location of the piezometers K2 and K3 in the cross-section.

- **Reservoir levels from 1988–2020**
  Description: The data of the reservoir levels are presented in the column and are presented as m above sea level. The date format is mm/dd/yyyy.
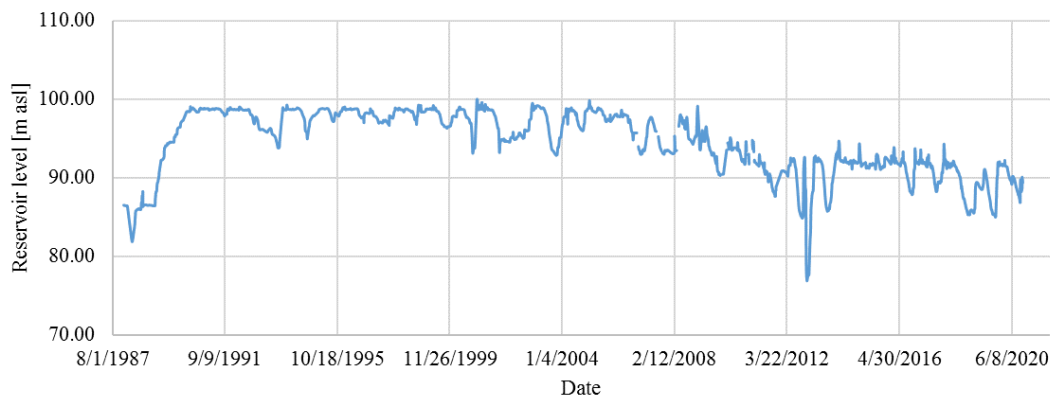
Figure 35. Changing the reservoir level over time.

- **Rising of the reservoir level**
  Description: The data of the reservoir levels are presented in the column and are presented as m asl (above sea level). The date format is mm/dd/yyyy.

5 SIGN CONVETION

To provide consistency among the results, the sign convention of the tension was POSITIVE « + » and for compression NEGATIVE « - ». The displacement in the downstream direction was POSITIVE « + » and in the upstream direction NEGATIVE « - ».

6 TASKS AND CASES

The embankment shape and geometry are very complex. The participants were asked to consider 2-D analyses as obligatory and 3-D analysis as optional. In the analysis, the consideration of the foundation layer is obligatory, and the material properties of the foundation layer are provided. During the geotechnical investigations it was estimated that the foundation is almost impermeable, some permeable zones were grouted and are now considered almost impermeable. The participants may decide of which constitutive laws and material models for the foundation rock will be used. For the ground, we asked the participants to assume the ground as homogenous. The participants were asked to describe their modelling assumptions in detail in the paper. The theme is divided in 4 cases which are presented in Table 3 and described in the chapters below. In the analysis, we assumed that all participants would use the same geometry, material properties, and basic loads. In case when participants decided to use different parameters, they were asked to explain their decision.

Table 3. Division of the tasks.

Case	Tasks
Case 1 (Mandatory, Optional)	**Task 1:** Construction of a 2D model. Calibrate the model using dam surveillance. Estimate the as-built characteristics of the dam. **Task 2:** Evaluate the initial state after the reservoir is filled to the nominal level. Estimate the dam condition before the detection of leakage. **Task 3 (Optional)**: Using calibrated data of 2D model, build a quasi-3D FE model (20 m wide section of the dam).
Case 2 (Mandatory, Optional)	**Task 1**: Consider the wet stain using 2D or quasi 3D model. **Task 2**: No action after the appearance of the wet stain.
Case 3 (Mandatory)	**Task 1**: Consider remedial works of the dam, consider long period of reservoir draw-down and its effect of the clay core. **Task 2**: Consider elevation of the reservoir back to nominal level according to the assumed filling times. Evaluate the safety of the dam under the final water level condition of the reservoir.
Case 4 (Optional)	**Task 1**: Seismic analysis.
Finalisation (Mandatory)	**Task 1**: Preparation of the technical paper. **Task 2**: Preparation of the presentation and presentation at the workshop.

* As an optional case the participants can build a full 3D model and perform the required analysis.

6.1 *DETAILED DESCRIPTIONS OF TASKS AND CASES*

6.1.1 *Case 1: Creation of a 2D model.*

In Case 1 a preparation of a 2D numerical model was considered (geometry in .dwg file). The participants were asked to prepare the model that captures and represents the initial operating conditions in the dam and foundation as realistically as possible. Soil characteristic data from the design phase and monitoring data of the operation of the dam before the leakage were provided in the data. Boundary conditions were defined and justified by the participant.

Task 1 (Mandatory)

While creating 2D model, the participants were asked to use the geometry from the references and soil data from design phase, and to consider suitable material properties for the dam and the foundation. The participants were provided with reservoir levels from 1988–2020, piezometric data, geometry (.DWG file), and geodetic measurements. Provided data should be used for creation and calibration of the numerical model. During the calibration process, any of the soil properties and constitutive laws could be modified, e.g., Mohr-Coulomb, Hardening Soil (i.e., back-analyses should be performed).

For the initial state analysis, the participants were asked to consider a fully constructed dam and empty reservoir, while the groundwater level is at the surface elevation. After performing the stability analysis of the dam, they were asked to estimate the as-built characteristics of the dam, settlements at the end of construction and before the first filling of the reservoir and provide for the critical sliding plane, deformation and stress state of the dam.

Task 2 (Mandatory)

In this task first filling of the reservoir was considered. The schedule of the filling of the reservoir was provided as the input data. The participants were asked to evaluate the data and include the process of the reservoir filling in the FE model, to describe the assumption on the inclusion of the reservoir in the FE model. In this scope of this task the consolidation process over the years was evaluated as well. The participants were provided with the data on reservoir and

piezometer fluctuations and asked to perform numerical analysis of the dam and evaluate stress and steady seepage state for representative situation until the year 2006. Additionally, they were asked to elaborate on any additional changes in the numerical model of the dam and to perform stability and seepage analysis of the dam.

Task 3 (Optional)

For this task participants ware ask to build a quasi-3D model using calibrated data from 2D model of the dam by adding thickness to the 2D dam section and assuming plane strain boundary condition on the lateral boundaries of the model. The thickness of the model should be 20 m.

6.1.2 Case 2: Appearance of the wet zone (2D and/or quasi 3D)

This case was devoted to the analysis of the wet zone. First, we asked the participants to elaborate on the reasons for the appearance of the wet stain and to explain modelling assumptions to consider this extraordinary event. Mandatory part of this task was to analyse the effect of the lowering of the reservoir.

Task 1 (Mandatory)

The participants were asked to consider the observed wet stain and different possibilities of occurrence. Moreover, to evaluate monitoring data and use the data in the model based on their engineering judgement. For the quasi-3D model, they were asked to consider the location of the wet zone to be in the centre of the segment and to perform stability and stage seepage analysis of the dam.

Task 2 (Optional)

In this task a scenario that after the appearance the wet stain was considered, the water level remained at the operational level of 98.8 m asl for 20 years. The participants were asked to perform stability and seepage analysis; to estimate the safety of the dam and to provide yearly safety assessment for 20 consecutive years.

6.1.3 Case 3: Remedial works (2D and/or quasi 3D)

This case was devoted to the analysis of the long-term drawdown of the reservoir and its effect on the dam body (i.e., clay core). As can be observed from the monitoring documentation the reservoir was operating at the lowered elevation for over 10 years. At the time of the workshop the reservoir was emptied, and after the completion of the remedial works the maximum reservoir level was then restored. In the analysis the participants considered the effect of long-term drawdown of the reservoir on the clay core and modify the FE model. In this task it was assumed that bottom outlet and irrigation pipelines have been permanently sealed.

Task 1 (Mandatory)

Participants were asked to analyse the long-term drawdown of the reservoir, to modify the material properties if they assumed material changes were needed, for example changes in core permeability. And finally, they were asked to perform steady seepage and stability analysis of the dam after a yearlong drawdown period (until the last record of the reservoir levels in 2020).

Task 2 (Mandatory)

The task was devoted to the analysis the future state of the dam, after the reservoir is again filled to the maximum level. The level in the reservoir should be gradually risen during the analysis (by following the filling timetable provided as an input by the formulators). The participants were asked to perform seepage and stability analysis of the dam.

6.1.4 Case 4: Seismic analysis (Optional)

In this task a basic seismic analysis of the dam, after the remediation works should be performed. The participants were asked to decide on to consider the mass of the foundation for the dynamic analysis or not. Water in the reservoir should be considered to have a unit weight of 1000 kg/m^3 and compression wave velocity of 1439 m/sec. The instruction was to perform linear

on non-linear dynamic analysis for various reservoir levels at the following elevation of the reservoir: empty, operational low, normal operational, maximum and to consider horizontal peak acceleration of 0.3g and vertical accelerations to be 0.67 of the horizontal. Moreover, the participants were asked to explain the consideration of the hydrodynamic effect in the reservoir, the reservoir length is 500 m, to estimate natural frequencies for dam-foundation-reservoir system, at the following elevation of the reservoir: empty, operational low, normal operational, maximum and to present the first 6 natural frequencies of the model and mode shapes.

7 SUBMISSION

The participants were asked to provide the following results to the formulators of the theme via the Excel template file:
- Properties of the model after the calibration
- Estimation of the as-built characteristics of the dam
- Deformation of the dam along the dam centre line in the cross-section (vertical and horizontal displacements)
- Safety factors for the upstream and downstream slope
- Prediction of the settlements
- Phreatic line
- Estimation of the time used to solve the tasks.

The formulators analyzed the data provided in the Excel spreadsheets and the papers prepared by the participants and provided synthesis of the results.

8 DESCRIPTION OF THE PARTICIPANTS TO THE THEME C

8.1 *Statistics*

In total, 5 teams participated in theme C from 5 countries: North Macedonia, Switzerland, Republic of Serbia, Canada, and Italy. 3 groups have already participated in previous BW, while 2 groups participated for the first time. The motivation to participate was in 40% to gain new experience and learn from others, in 40% to share expertise, and in 20% to test computational methods and compare the results with the results of the other teams. All teams have previous experience with modelling of embankment dams, in average 3 authors collaborated in a team that provided a contribution. By composition, 2 teams were from the university, the authors of 2 teams were from combined affiliations (university and dam owner), and one team was from a consultancy background.

The participants were asked to report how much time did they spent per author and per task, in average teams spent 43 days to solve the theme, and cases 1 and 2 were the ones that were the most time consuming. The theme consisted of mandatory and optional tasks, 4 cases with in total 8 tasks, in average 6 tasks were solved by each team and only one team solved all the tasks.
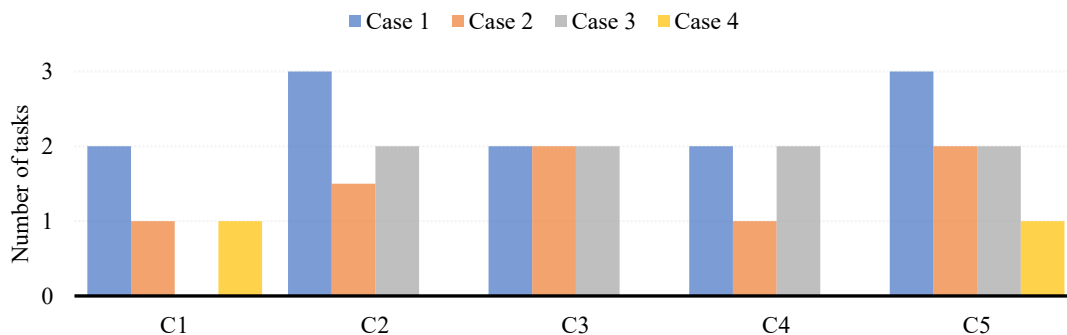

Figure 36. Number of tasks solved per participating teams.

To solve the tasks the participants used different software and constitutive models, all participants used commercially available software:

- Geo-slope
- Plaxis 3D
- Geo-studio 2015
- Abaqus
- Flac 2D and Flac 3D.

The following material models were considered:

- elastoplastic (variable E)
- elastoplastic (w/PWP change)
- Mohr-Coulomb
- HS (small).

The basic assumptions, the constitutive models, and the methods of analysis of the contributors are presented in their individual papers. Material characteristics of the dam zones were provided based on the design values and laboratory test performed on the built-in material in the dam. The table below summarizes the used material parameters in the modelling of the dam that were provided by the formulators. The red values in brackets are the variations of the material properties that were used by the participants in their models.

Table 4. Material properties.

Zone	Description	c_u [kPa]	φ [°]	c' [kPa]	E [MPa]*	ν [-]	k [m/s]
A (top 3 m)	Dolomite gravel mixed with silt and clay		36	36	9	0.4 (0.3-0.5)	10^{-6}
A	Clayey silt to silty clay	75 (70-150)	- (20 or 30)	0 (10 or 35)	2	0.5 (0.25-0.45)	10^{-9} (10^{-11}; 10^{-8})
B	Rockfill		38 (45)	0	37	0.3	10^{-3}
C	Blocks of limestone and sandstone		38	0	37	0.3 (0.28)	10^{-4}
D	Flysch		39	32	620	0.25 (0.3)	10^{-9}

9 EVALUATIONS OF THE RESULTS FROM THE CONTRIBUTORS TO THE THEME C

In this chapter a synthesis of the provided results is provided. The results are kept anonymized, while the contributions are marked with indexes C1-C5 in a random order. The comparisons of the results for stresses, displacements, and pore pressure for each analysis stage are prepared. Some of the analysis results are also compared with the measurements, which were not revealed to the participants in advance. Participants were provided with monitoring data, which enabled them to construct a finite element model, but some of the settlements were only revealed at the benchmark in April 2021.

9.1 *Initial state after building the dam (Case 1, Task 1)*

Comparisons of the initial stresses are presented on Fig. 14 and 15, where vertical and horizontal stresses with respect of the depth from the dam crest are presented. The results are displayed for a dam center line, as indicated with the red line on the Fig. 13.
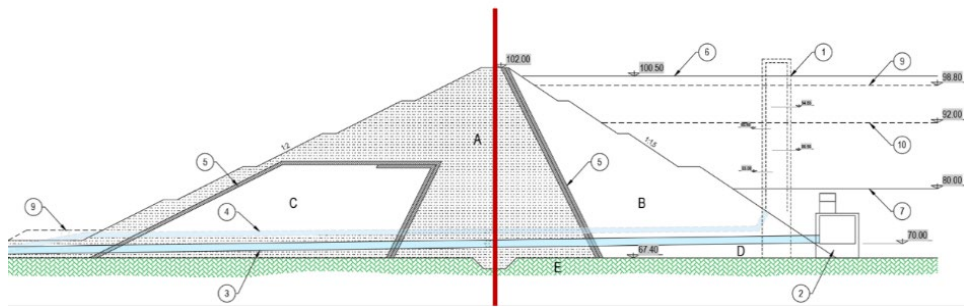
Figure 37. Center line of the dam.

The graphs on Fig. 14 and 15 show the comparison of the computed total stresses (vertical and horizontal). It can be seen from the graphs that the calculated initial stresses in the dam are more or less similar for all participants.
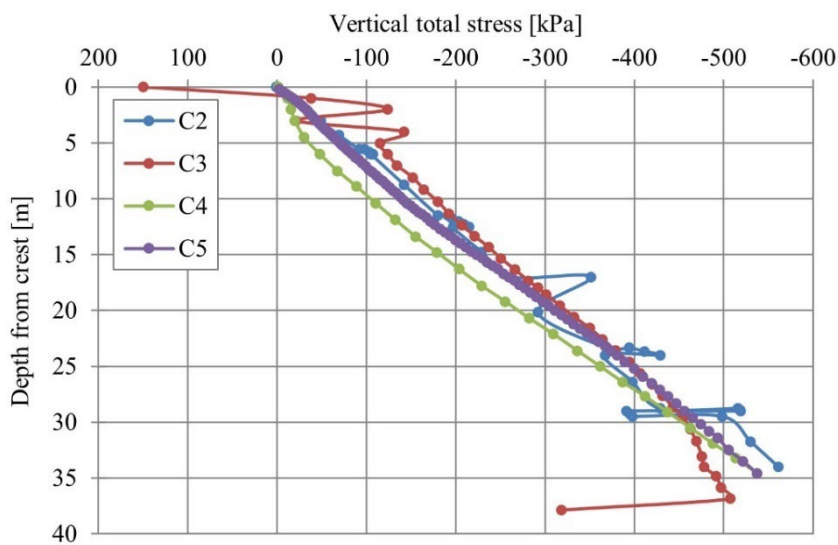

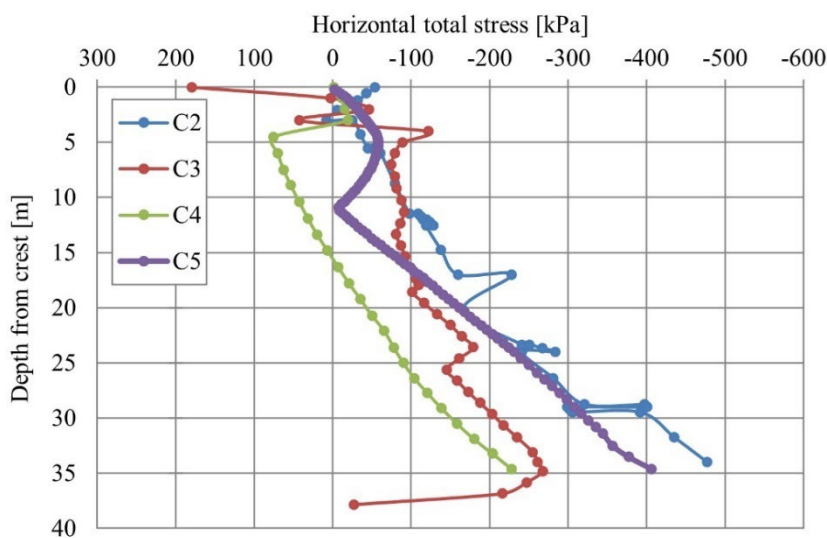Figure 38: Vertical total stresses - initial state.

Figure 39: Horizontal total stresses - initial state.

However, when the results for the settlements at the end of construction of the dam and before the first filling of the reservoir are compared, the substantial differences in the results are observed. The differences in initial vertical displacements are probably based on whether the displacements during the construction phase of the dam were included or excluded. Participants C2 and C4 probably included vertical displacement during construction, while participant C3 excluded those displacements. Unfortunately, the data about the settlements during the construction, and in the time of the first filling of the reservoir due to consolidation, were n[Pritegnite pozornost bralca z odličnim citatom iz dokumenta ali pa izkoristite ta prostor, da poudarite ključno točko. Če želite premakniti to polje z besedilom na katero koli drugo mesto na strani, ga preprosto povlecite.]

ot available. For the horizontal displacements it looks like that the participant C4 used different sign convention. So, the initial horizontal displacements could be between 20 and 30 cm in the downstream direction. Also in this case, the data of the horizontal displacements due to the construction and consolidation of the material before first filling of the reservoir, were not disposed.
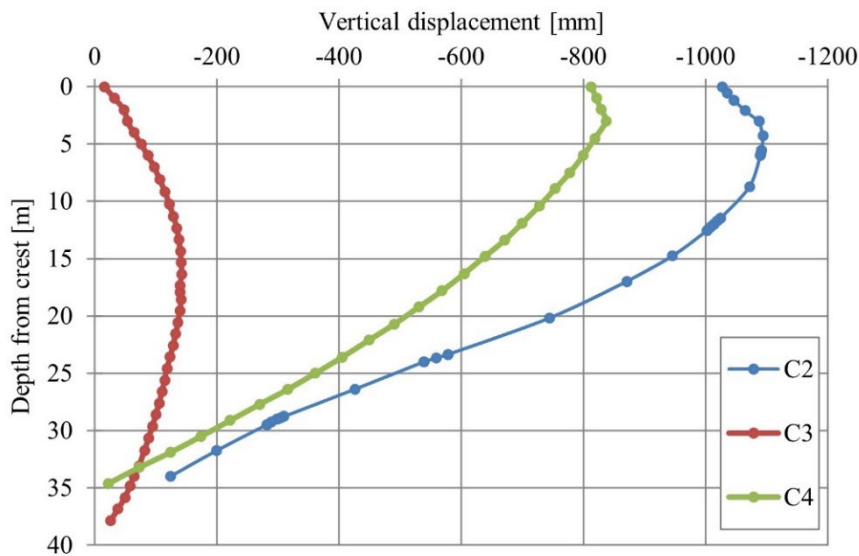
Figure 40. Vertical displacements - initial state.
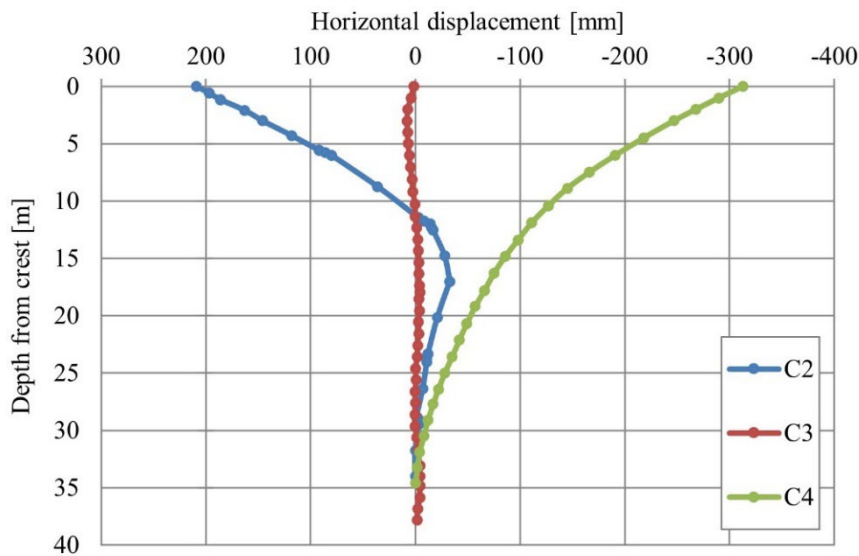
Figure 41. Horizontal displacements - initial state.

9.2 *First filling of the reservoir (Case 1, Task 2)*

For the first filling of the reservoir participants were provided with the data series from piezometers and reservoir head, and settlements measured on 4 locations on the dam after the construction until recently. The figures below present the obtained results, however, only 3 teams provided us with the requested results, and only their results were then analyzed. The computed vertical total stresses are for all 3 participants similar (see Fig. 18). However, when we compare the results for pore water pressure, the situation is not so unified. On Fig. 20 the results for the pore pressure are provided for the dam center line, and the provided results are the following. For the participants from the team C2 negative values of pore pressure start to develop at the depth 20 m depth below the crest level and then with the next 15 m of increasing depth develop to the 210 kPa, similarly for the team C3 negative pore pressure develops at the depth 25m below the crest and then with depth it gradually reaches the final value of -170 kPa. However, the model C4, provides different results, and this result also responds well to the measured values, the negative pore pressure develops in the dam at depth of 10 m under the crest level and then it gradually develops (in 25 m) to reach -210 kPa at the foundation level. However, we must note that, based on the results from monitoring, after the first filling of the reservoir the level of the ground water in the dam, behind the sealing curtain, was around 20-22 m below the crest level. Two examples of the pore pressure distribution in two different models are presented on Figures 21 and 22, by looking at the contour plot we can observe how the behavior of the dam is captured in the center line. Also it can be seen that in the center line the differences in pore pressure are maximal, through both embankments of the dam there can be observed comparable distribution of pore pressure in this two different calculations.
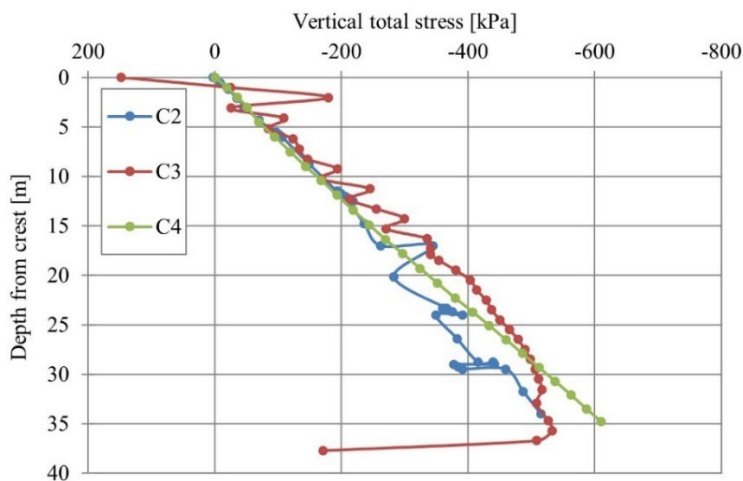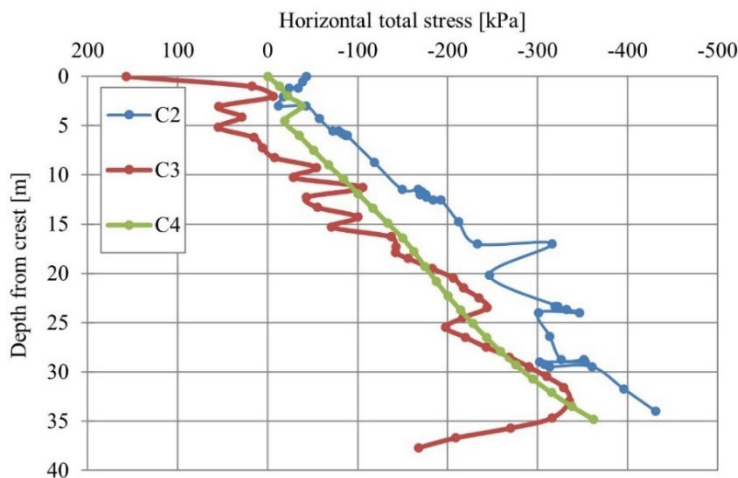

Figure 42. Vertical total stresses.

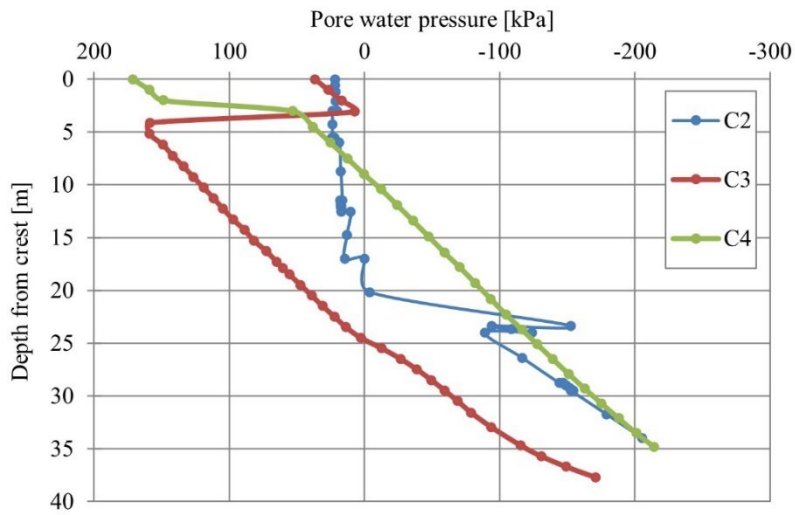Figure 43. Horizontal total stresses.

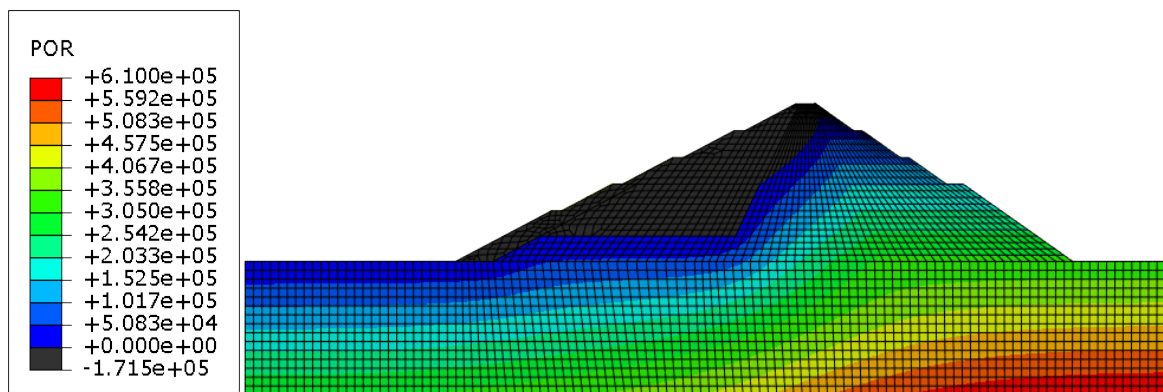Figure 44: Pore water pressures.
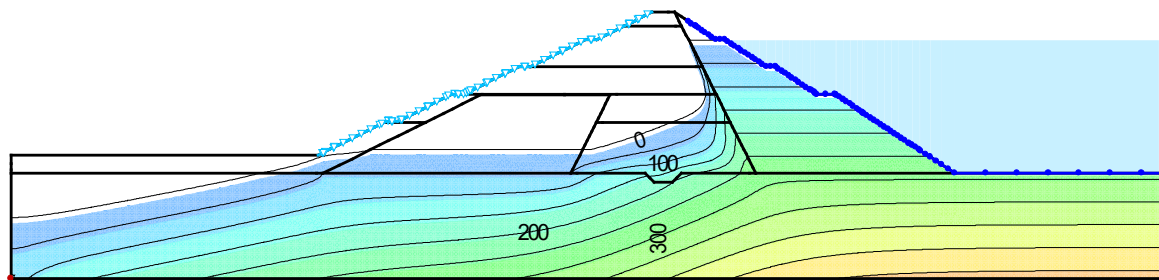

Figure 45: Contour plot – team C4.
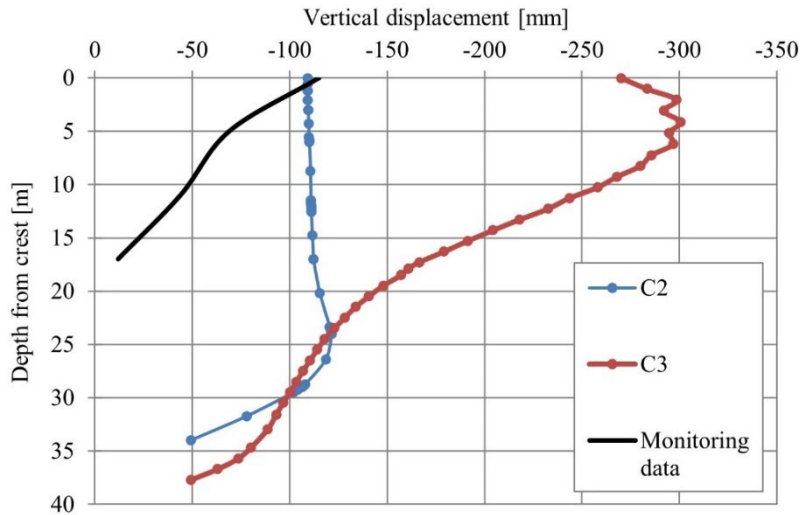

Figure 46: Contour plot – team C2.

Figure 47. Vertical displacements.

The vertical displacement results correspond well to the results of pore pressures. However, the displacement of the participant C2 are in better agreement with the real situation on the dam (comparison with measured data). Moreover, it should be noted that the measured data, which was also provided in the formulation data files, are obtained at the surface of the dam (on crest and berms) and not in the center line of the dam (where the data from the numerical is obtained from). When comparing the results for the vertical displacement, the situation is not so unified anymore. The data provided by the participants required additional post-processing, and again it should be assumed that some of the participants considered a different sign convention.
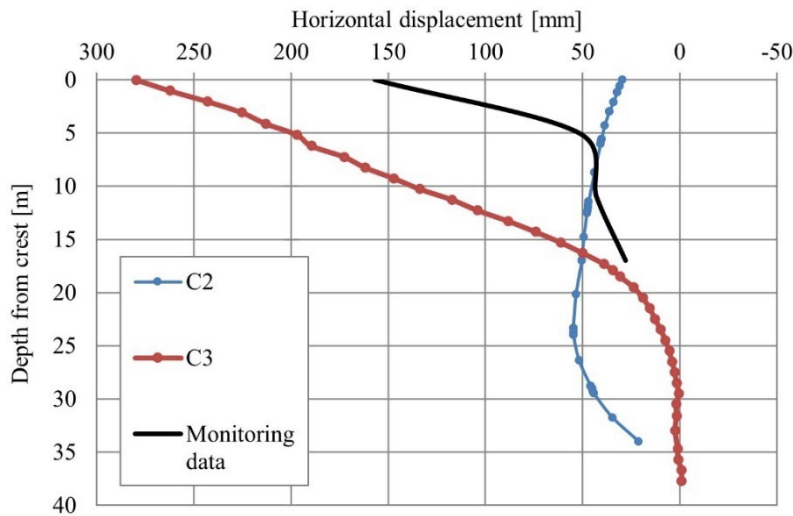
Figure 48. Horizontal displacements.

The computed horizontal displacements vary substantially between the participants. Moreover, it was realized again that some of the participants assumed a different sign convention, the positive direction was considered in the downstream direction, and changed the sign, where based on the paper and other results it was evident this is the case. It should be noted that the difference in the results on the crest displacement among the teams is substantial.

9.3 *Appearance of the wet stain (Case 2, Task 1)*

When comparing the stresses, the results of all 4 participants are similar (see Fig. 25 and 26). The differences appear when we review the results for pore pressures (Fig. 27), however it appears the reason is in the location of the limit line in the dam between the suction and negative pore pressures. While the participants C5 calculated that the whole dam is under negative pore pressures, the participants C4 calculated the limit line in the depth of 10 m under the crest level and the participants C2 and C3 in the depth of 20-25 m under the crest level. From the monitoring data the formulators believe that the participants C2 and C3 calculated a more credible situation.
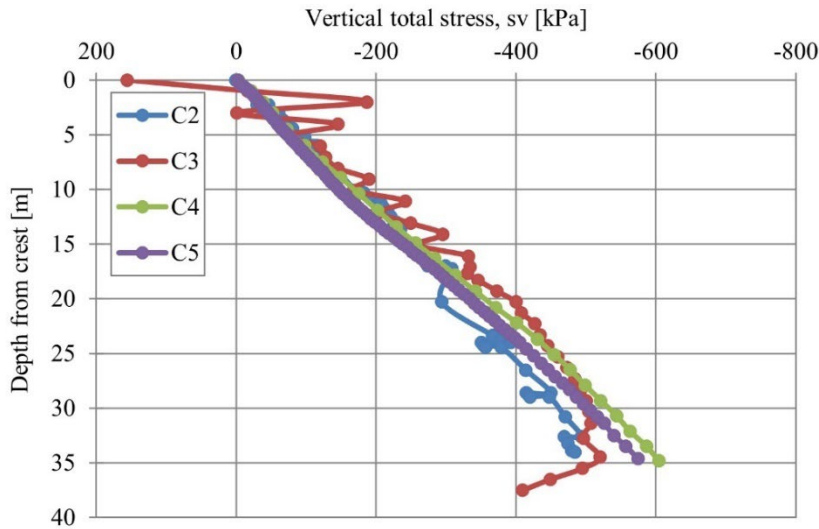
Figure 49. Total vertical stresses.
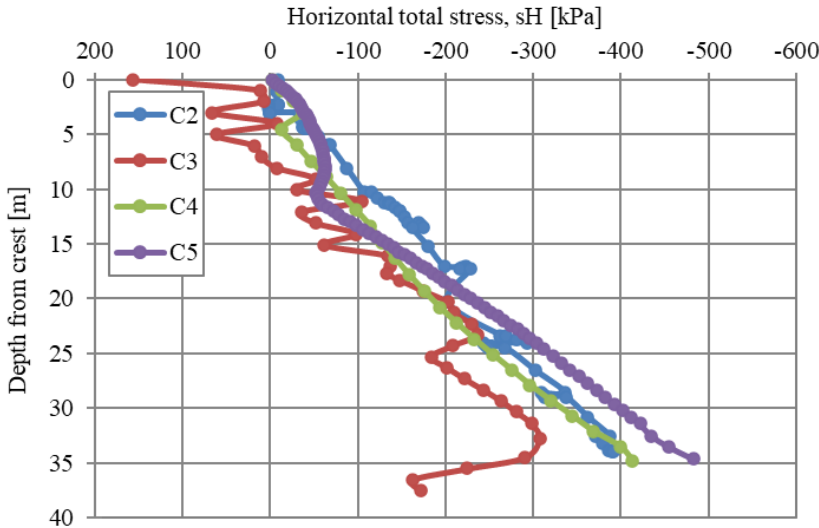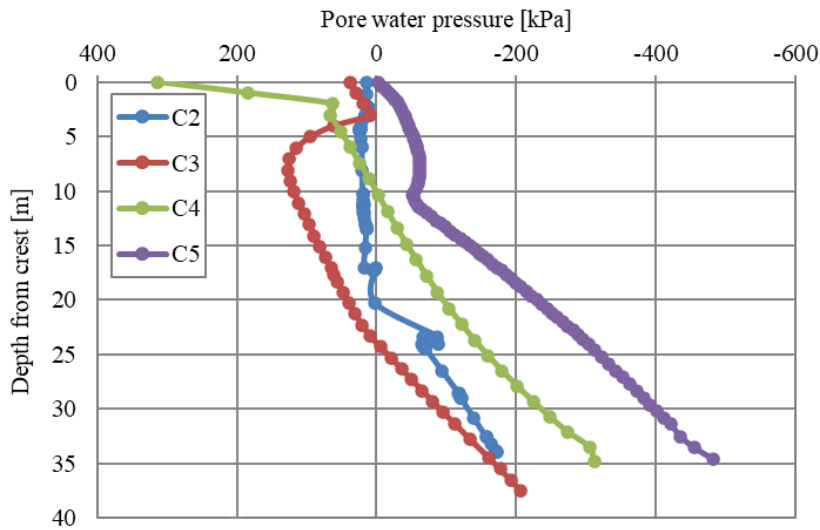
Figure 50. Total horizontal stresses.

Figure 51. Pore water pressures.

Similarly, when comparing the computed displacements for this Case, it can be expected that results can be quite different from participant to participant, since already the results for the pore pressures vary from one team to another. On Fig. 28 we can see the results for the vertical displacement, we can observe a substantial difference in the results, however, the opinion of the formulators is the following, the results of the team C2 only provided the results of the settlements for this Case, while for example team C3 provided the total settlements, therefore this figure is best interpreted if we look at it together with the Fig. 23. If we consider this fact we can observe that the results of the both teams are very similar.
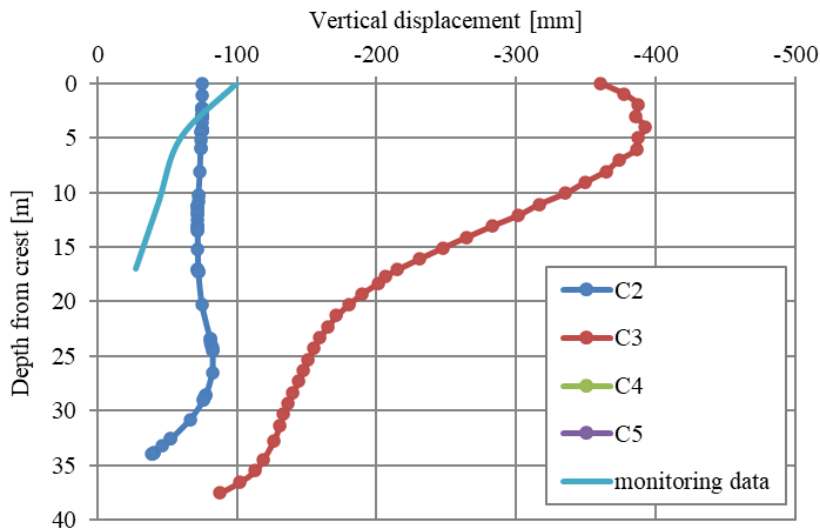

Figure 52. Vertical displacements.

The results for the displacements in the horizontal direction also vary, however we consider the total and relative values (in a similar manner as for vertical displacements), team C2 calculated small displacements in the downstream direction and if we look at the red dashed line on Fig. 29, where the relative values if the displacement for the team C3 are presented, we can see that there is about 10 cm of a difference in the calculated horizontal displacements between both teams at the crest level. If we compare the results with the monitored data, we can also observe that team C3 fits better the measured data than the other team.
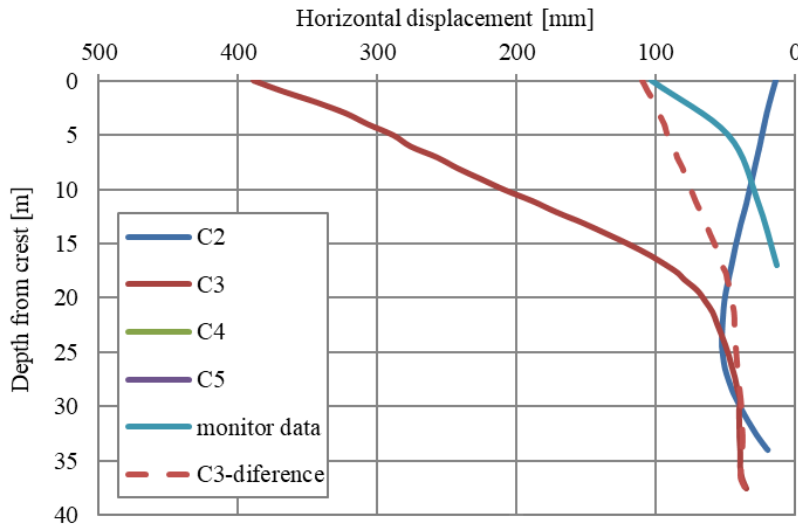

Figure 53. Horizontal displacements.

9.4 *Refilling the reservoir (Case 3, task 1)*

This case is devoted to the analysis of the dam after the reservoir is again filled to the maximum level. If we first observe the stresses, we received the results form 3 participating teams. Roughly we can conclude that their results are in the same magnitude and show similar behaviour of the dam (see Fig. 30 and 31). Immediately after refilling, we can observe suction in the first 10 to 20 m of the dam under the crest level and then lower. The computed pore water pressures are represented on Fig. 32 and reach up to the values between 150 and 270 kPa at the bottom of the dam. Vertical displacements are presented on Fig. 33.
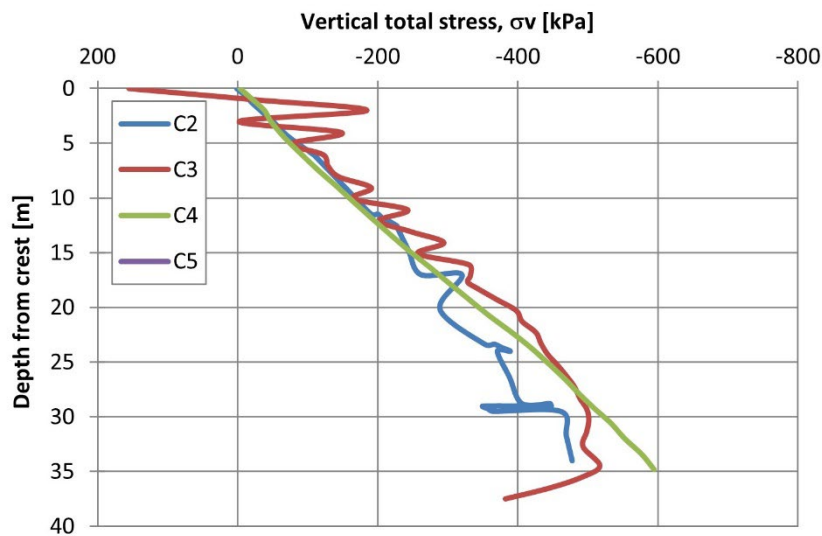

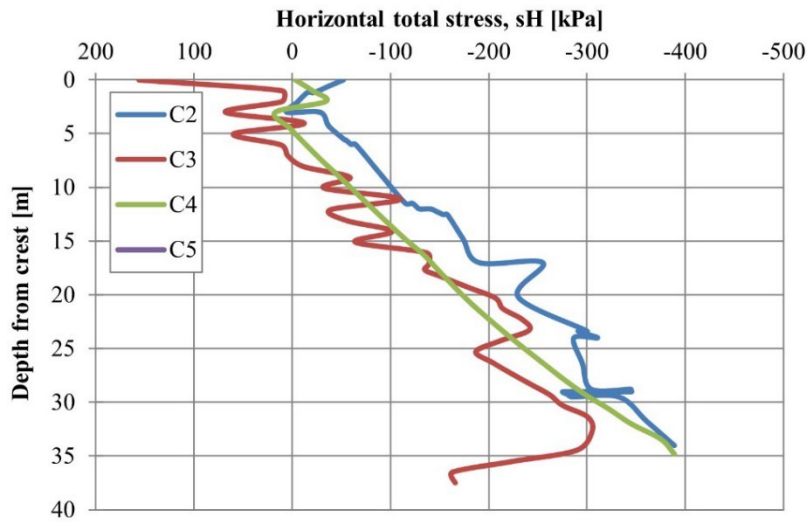Figure 54. Total vertical stresses.
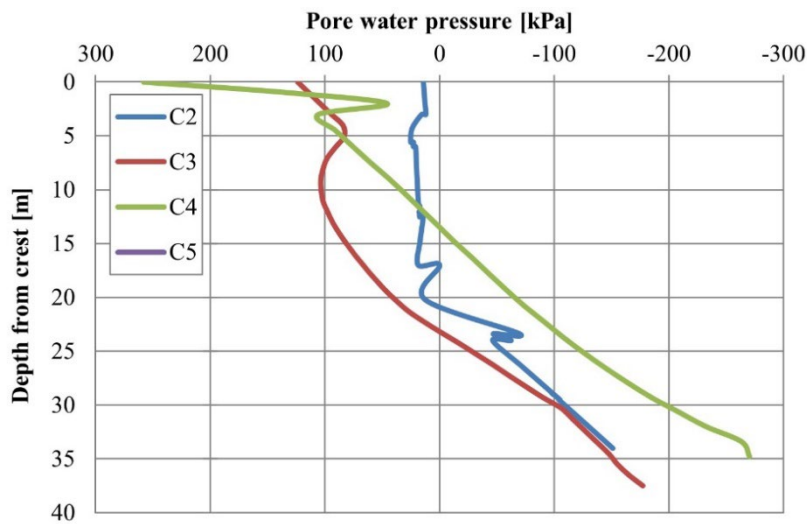
Figure 55. Total horizontal stresses.

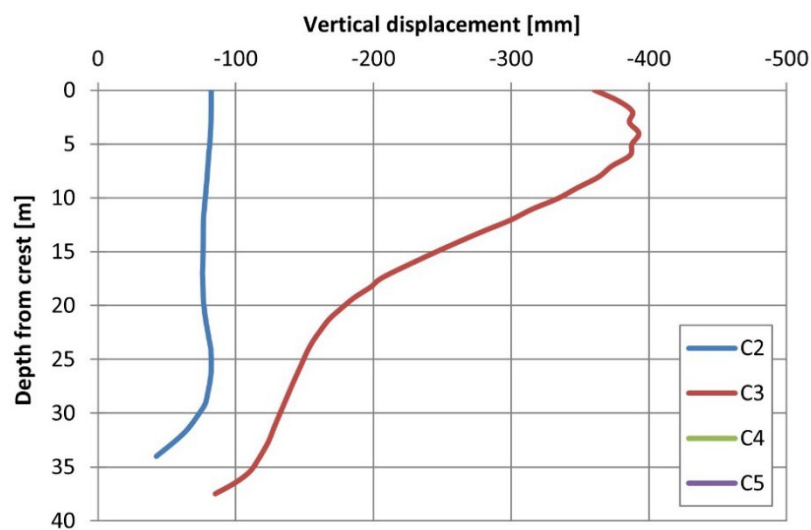Figure 56. Pore water pressures

Figure 57. Vertical displacements.

9.5 *Long term behavior of the dam after the filling of the reservoir (Case 3, task 2)*

The evaluation of the long-term behavior of the dam after the filling of the reservoir was done by 3 of the participating teams. Below we are summarizing their results for vertical and horizontal total stresses, for pore water pressures and for settlements in the vertical direction.
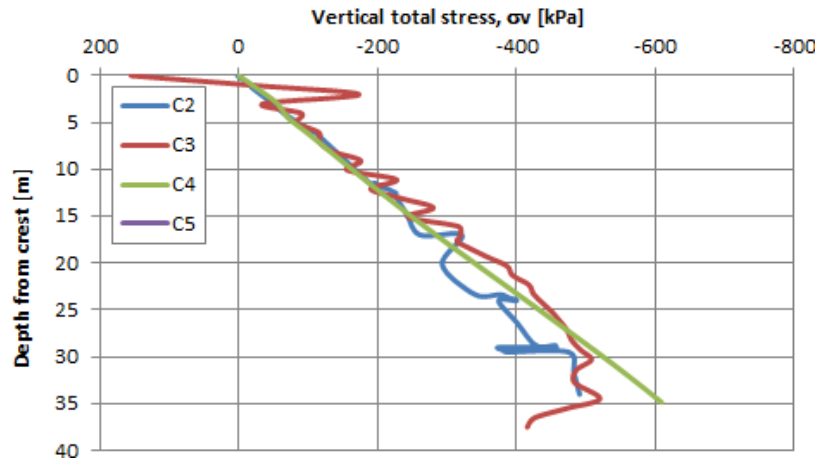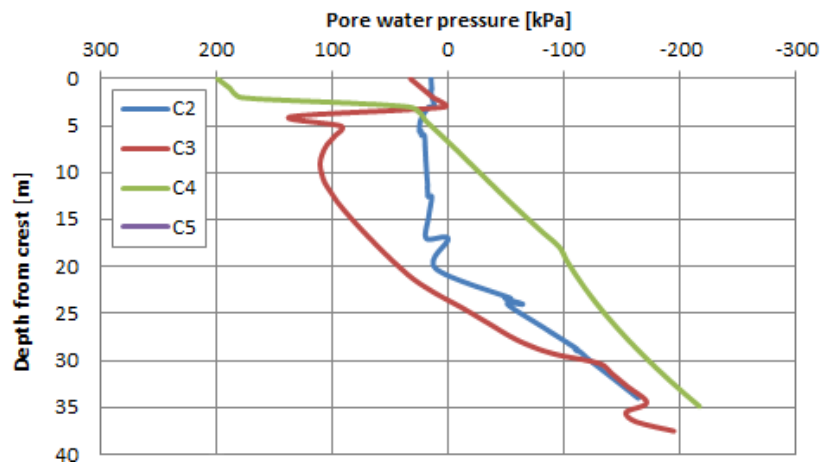
Figure 58. Total vertical stresses.

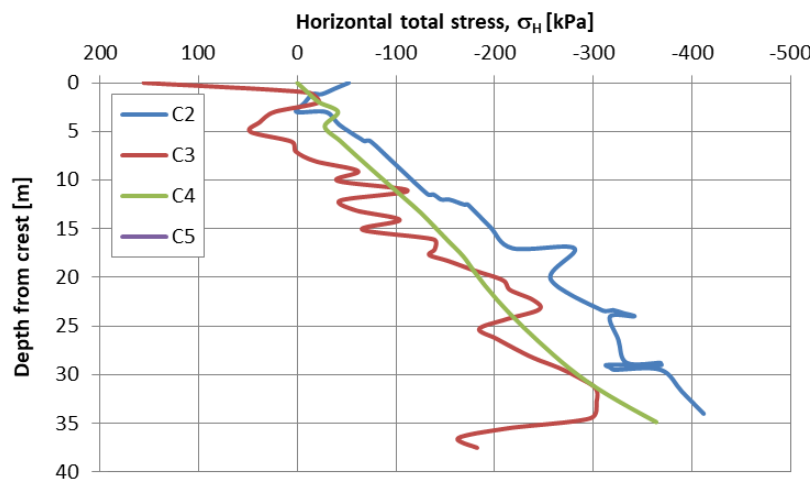Figure 59. Total horizontal stresses.

Figure 60. Pore water pressures.

Also, in the results of this task we observed, that the computed stresses for all 3 participants who submitted their results are comparable and show similar trend, while the results for the pore pressures are more variable. The results from C2 and C3 are comparable, the C4 calculated a lot higher values of pore pressure (about 50 kPa).
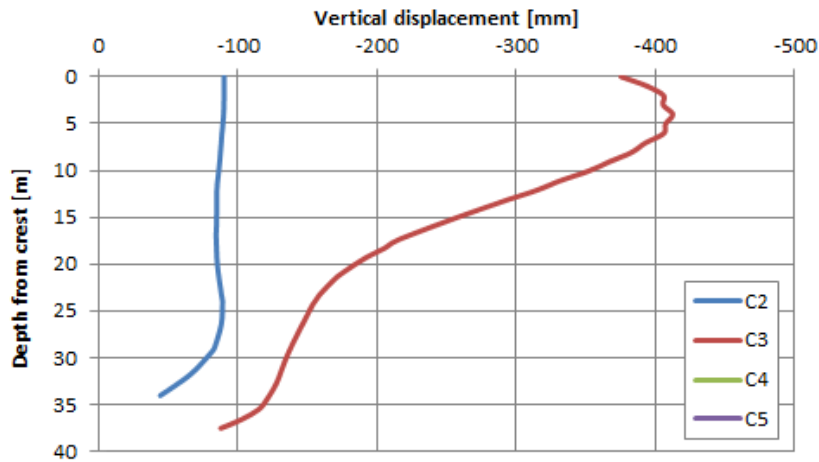

Figure 61. Vertical displacements.

The vertical settlements that will appear after refilling the reservoir reach values between 10 and 20 mm. The predicted settlement will be quite similar through the depth of the dam. For the horizontal displacement both participants, who submitted the results didn't predict large movements (less than 40 mm).

9.6 *Comparison of the measured data to the models*

We must note that some of the submitted models were good in matching the monitored parameters. Anyone interested in detail, we are suggesting reading the papers submitted by the participants. In this chapter we are only providing the general comparison on the vertical and horizontal displacements and pore pressures during the operation of the dam. We can observe that for the vertical and horizontal displacements teams C2 calculate lover values as the measured ones, while team C3 calculated larger settlements and displacements as observed in the monitoring. The results for the pore pressures are also very interesting, for example we can observe that the team C4 describes the actual pore pressures.
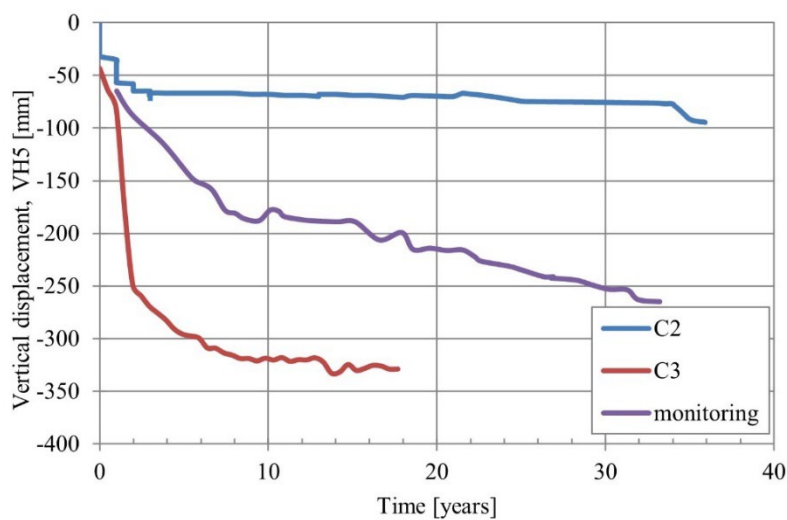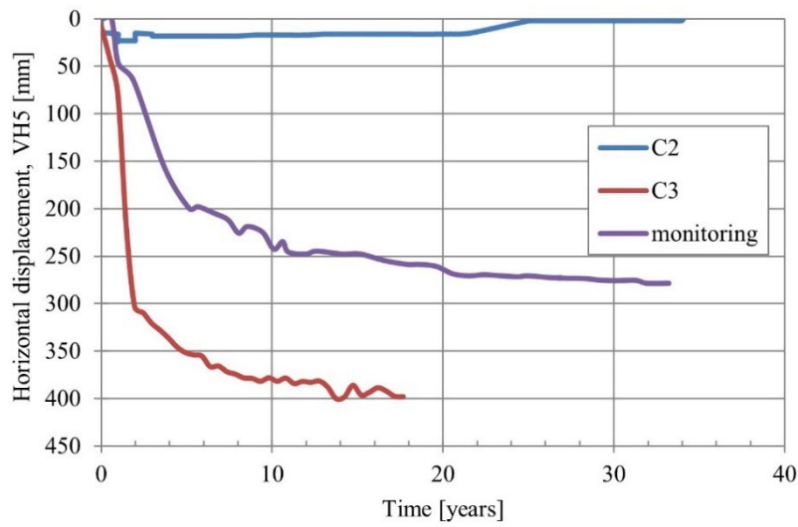

Figure 38. Vertical displacements at VH5.

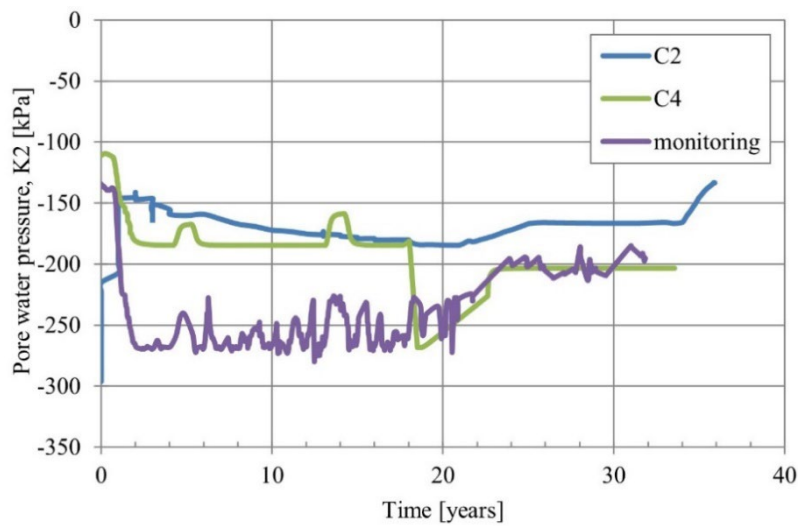Figure 62: Horizontal displacements at VH5.
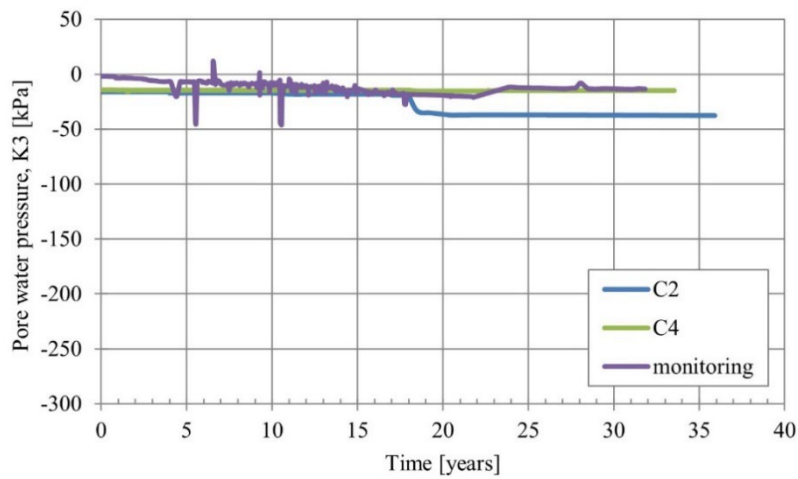

Figure 63: Pore pressures at K2.

Figure 41. Pores pressures at K3.

9.7 *Earthquakes*

Only two teams performed the seismic analysis, their results are very well presented in the submitted papers, here we provide only some general remarks. One of the teams estimated the strong earthquake horizontal displacement of 2,0 m and vertical settlements 1,2 m, and the other estimated the horizontal displacement to be at 0,8 m. Both teams concluded that strong earthquake may damage the dam, but it won't reflect in a sudden release from the water from the reservoir.

9.8 *Pore pressure distribution*

In this chapter we are only demonstrating the differences in the approaches of the participants to the theme C. For example, on the Figure below there are 6 models showing the pore water pressure, which we received form the 5 participating teams. We would like to emphasize that by using various software and modelling assumptions the pore pressure results will be very different from team to team and that this will then reflect also in the computed deformations. However, on a large scale all models show similar behavior and us (the formulators) are not so sure we were able to compare them fairly, however, we observed that some models reflected better the measured data on the dam, while we recommend the readers to read the papers sent by the participants, while a lot of information remains there for the cautious reader.
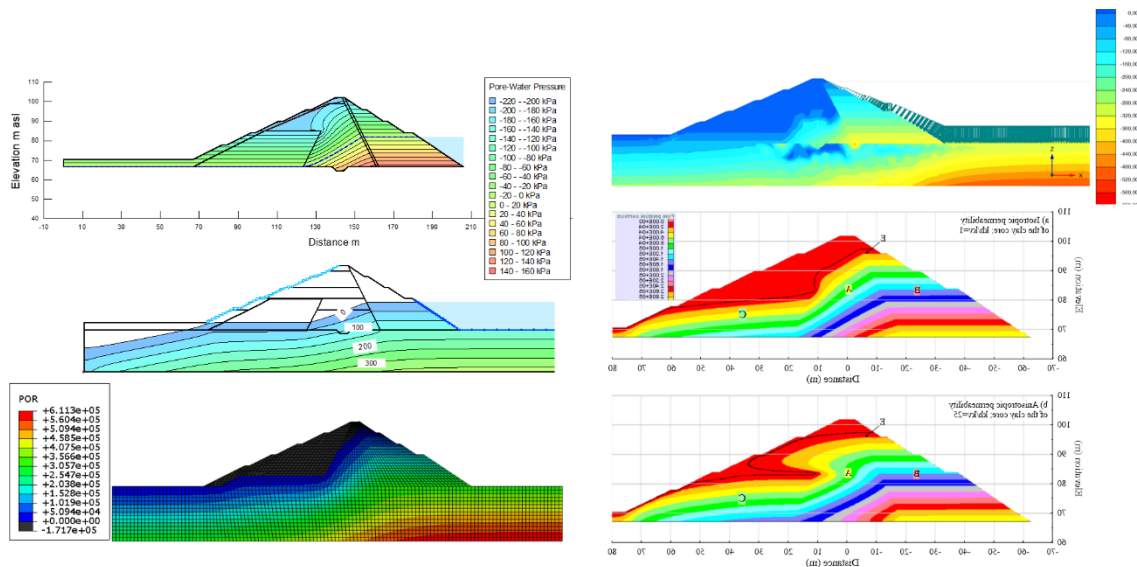
Figure 64. Pore pressure distribution for various models.

9.9 *Safety factors*

The participants were also asked to provide us with the safety factors. Below we are demonstrating their results for the safety factors at the first filling and after the refilling of the reservoir.
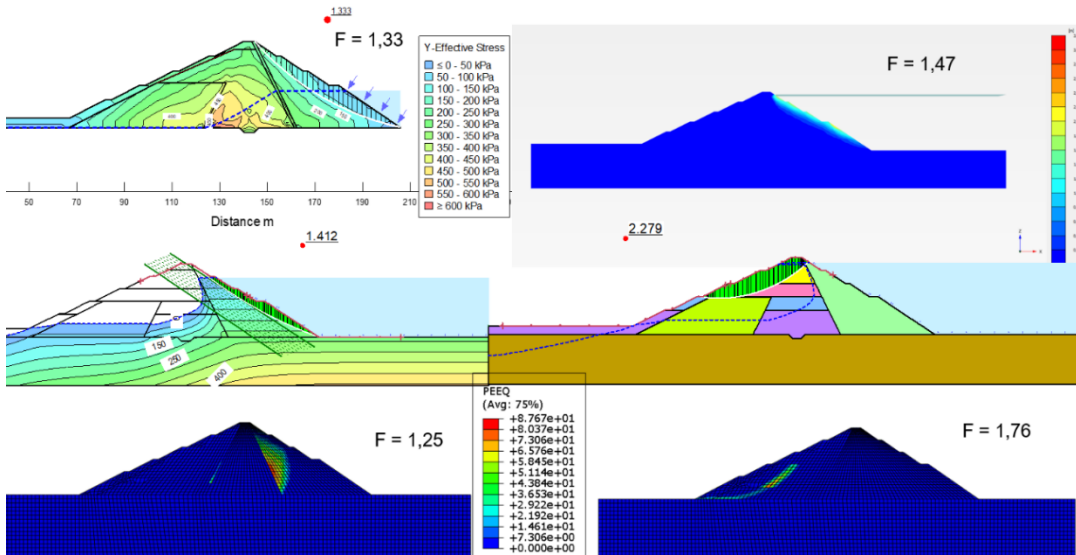
Figure 65. Safety factors after the first filling of the reservoir.
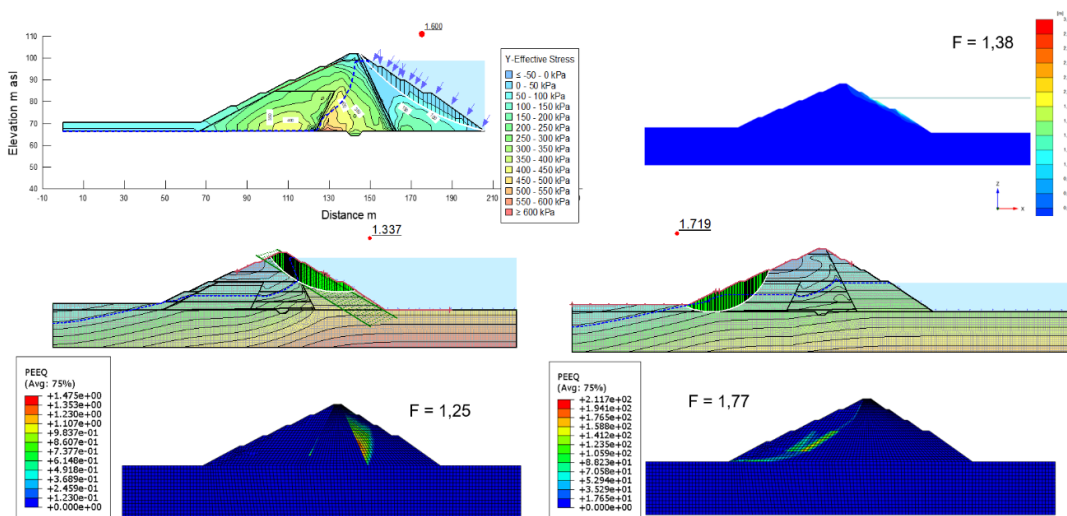
Figure 66. Safety factors after refilling of the reservoir and after long-term full accumulation.

Table 5. Comparison of the safety factors.

Team	Case 1		Case 2		Case 3	
	upstream	downstream	upstream	downstream	upstream	downstream
C1	1,33	> 2	1,37	> 2	1,60	> 2
C2	1,44	1,66	-	-	1,42	-
C3	1,42 (1,41)	2,19 (2,28)	1,42	2,28 (2,19)	1,20 (1,34)	1,79 (1,72)
C4	1,67 (1,25)	2,20 (1,76)	2,10	1,75	1,25	1,77
C5	-	-	-	-	-	-

For safety factors of the dam after the first filling and after remediation, all safety factors are above 1,25 for the upstream slope and for downstream slope we could say calculations show SF in range 1,7. In the design documentation we also found the design SF (see Fig. below), which is 1.7 in the downstream and 1.6 in the upstream, but in the upstream calculation it is visible that designer considered additional embankment which was not executed on the site.

$F_{upstream} = 1.6$

$F_{downstream} = 1.7$
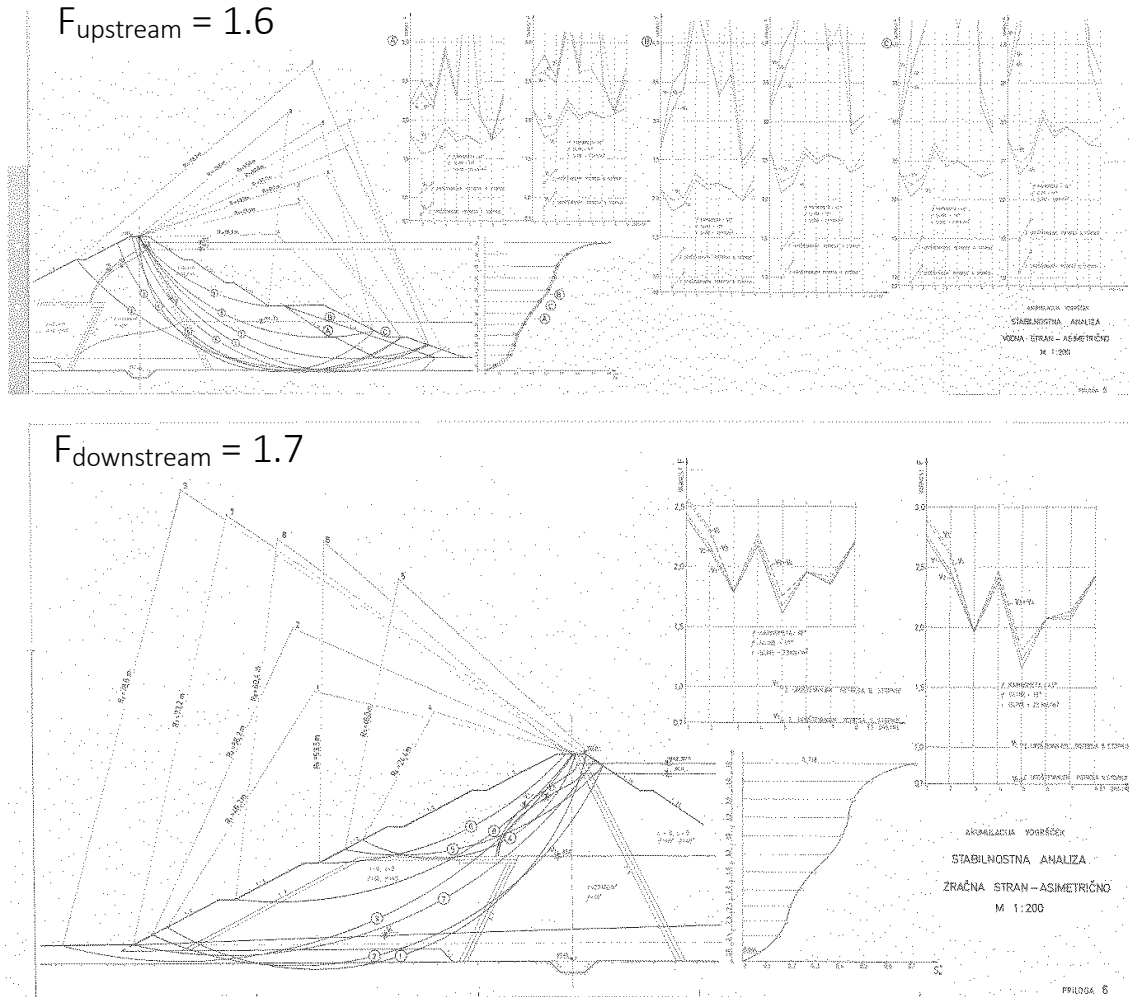
Figure 67. Safety factors from the original design.

10 CONCLUSIONS

The dam investigated as part of this theme was constructed in late 80s and very limited information is available about the construction. All available information was provided to the participants. As part of the safety measures, monitoring of the dam performance is performed regularly, so also some valuable results were provided to the participants, which were asked to perform the parameter fitting based on the monitoring results, since this method is often used to calibrate the model.

The results obtained were very scattered. One of the reasons for this may be in the fact that different material models were used. Especially the most precise models require large number of input parameters, so participants had to make assumptions that greatly affected the numerical model behaviour. Another important reason for such scattered results can be the fact that in the clay core with very low permeability open standpipe piezometers are installed. While they play

crucial role in the safety monitoring, the parameter fitting based on their results is very challenging task since they have quite large phase lag due to the volume of the piezometers.

Although no uniform picture about the dam behaviour, additionally to the monitoring results, can be obtained from the results of analyses, still an important lesson can be learned from this task. For the analysis of the embankment behaviour, a wide variety of very powerful computational models can be used, requiring a large list of input parameters which as a result provide colourful and very convincing results. Yet, the accuracy greatly depends on the input parameters and the engineering knowledge about the behaviour of the material used. Sometimes material models used require much greater number of input parameters that is obtained from the investigation. In such cases missing parameters are estimated based on the experience and engineering judgment. Despite taking great care in this process, this kind of parameter selection at the end of the day is just a good or bad guess. Therefore, although the parameters determined with investigation might be precise there is still enough space for making an error and consequently obtaining misleading results. Since the embankment dams are vulnerable structures with serious consequences in case of failure, all embankment dam designs shall undertake a revision and thorough discussion at all stages, i.e. investigation, design, construction and operation.

REFERENCES

ICOLD Committee on Embankment Dams. (2017). *ICOLD Bulletin 164 INTERNAL EROSION OF EXISTING DAMS , Levees and Dikes , and their Foundations*. Paris: ICOLD - CIGB.

United States Society on Dams. (2010). The aging of embankment dams, (May), 11 p.

Wrachien, D. De. (2009). Dam-break Problems, Solutions and Case Studies, (September), 334. https://doi.org/10.2495/978-1-84564-142-9/04

Behaviour of the embankment dam

BEHAVIOUR OF EARTH DAM DURING RESERVOIR FILLING AND EARTHQUAKE ACTION, DAM IN SLOVENIA

Ljupcho Petkovski
Faculty of Civil Engineering, Ss. Cyril and Methodius University in Skopje, North Macedonia

Stevcho Mitovski
Faculty of Civil Engineering, Ss. Cyril and Methodius University in Skopje, North Macedonia

Frosina Panovska
Faculty of Civil Engineering, Ss. Cyril and Methodius University in Skopje, North Macedonia

ABSTRACT: In the static analysis of the earth zoned dam in Slovenia, for the state of rapid filling of the reservoir and lowering of the level for remediation of the dam, up to the state of long-term maintenance at normal level, which is a pre-earthquake state, an elastoplastic model with variable modulus of elasticity was used, for the local materials in the dam body. The analysis was performed in drained conditions with effective stresses, using combined mechanical and seepage analysis in the time domain. Criterion for calibration of nonlinear elastic material parameters is the condition that the horizontal displacements in the dam crest, for the condition of the first filling of the reservoir, are approximately the same with the measured values, i.e. about -120 mm in the downstream direction. The key conclusion from the static analysis is that the embankment dam, with the adopted geometry and composition of materials, possesses satisfactory static stability. In the analysis of the dynamic response of the dam, a nonlinear model is applied (equivalent linear analysis with inelastic material parameters), where the local materials are approximated with a variable maximum shear modulus. Permanent displacements during seismic excitation are determined by dynamic deformation analysis, where from the difference of the effective stresses in two successive time steps, incremental forces are determined, which result in corresponding deformations. The dynamic analysis confirms the seismic resistance of the embankment dam in the action of a design earthquake with PGA of 0.30 g, i.e. there is no danger of rapid and uncontrolled reservoir emptying, because the crest settlements from dynamic inertial forces for the duration of the earthquake are 1.1 m, apropos are much lower than the height above the normal level in the reservoir till dam crest, which is 3.2 m.

1 MODEL OF THE DAM AND MATERIAL PARAMETERS FOR STRUCTURAL ANALYSIS

1.1 *Basic characteristics of the analyzed dam*

The representative cross-section, the parameters of the local materials for the embankment dam in Slovenia and the measured values from the dam monitoring are taken from the available data base [1]. The earth zoned dam with a clay core was built in 1985. It is founded on a rock foundation of Eocene flysch, which is practically waterproof and with high stiffness. The basic geometric characteristics of the dam and reservoir, Figure 1, are the following: crest elevation at 102.0 m.a.s.l., elevation of rock foundation 67.4 m.a.s.l., structural height 34.6 m, crest width 5.0 m, elevation at normal level 98.8 m.a.s.l. and elevation at minimum level 80.0 m.a.s.l.
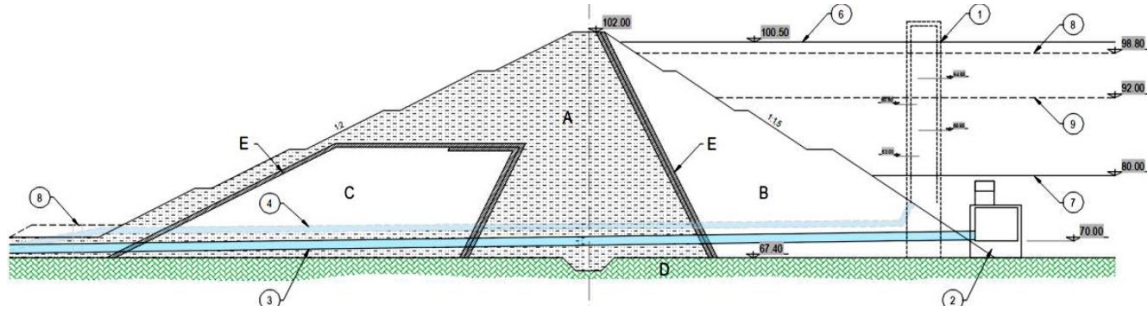

Figure 1. Representative cross-section of the earth dam.

1.2 *Basic geomechanical parameters of the materials*

The basic geomechanical parameters of the local materials are systematized in Table 1. The values from the available database are with a yellow background, and the other values are determined or assumed, according to the description of the materials.

Table 1. Material parameters.

Zone		A1	A2	B	C	D	Comment
dam structure		top of dam	core	upstream part	downstream part	bedrock	
material		gravel, silt	clayey silt	rockfill	rockfill and sand	Flysch	
γ_{spec}	kN/m^3	21.0	19.5	24.0	24.0	25.0	specific unit weight
γ_{dry}	kN/m^3	16.4	12.8	21.0	20.0	24.0	dry unit weight
n		0.219	0.344	0.125	0.167	0.040	void
e		0.280	0.523	0.143	0.200	0.042	void ratio
ω_{sat}	%	13.1	26.3	5.8	8.2	1.6	saturated wetness
$\omega < \omega_{sat}$	%	13.0	26.0	3.0	7.0	1.5	natural wetness
γ_{sat}	kN/m^3	18.5	16.2	22.2	21.6	24.4	saturated unit weight
γ	kN/m^3	18.5	16.1	21.6	21.4	24.4	natural unit weight
φ	o	36.0	0.0	38.0	38.0	39.0	angle if internal friction
c or cu	kN/m^2	36.0	75.0	0.0	0.0	32.0	cohesion
k_s	m/s	1.0E-06	1.00E-09	1.0E-03	1.0E-04	1.0E-09	coefficient of permeability - secondly

k_d	m/d	8.6E-02	8.6E-05	8.6E+01	8.6E+00	8.6E-05	coefficient of permeability - daily
$Ko(\phi)$		0.41	1.00	0.38	0.38	0.37	at-rest earth pressure coefficient
$\nu(Ko)$		0.29	0.50	0.28	0.28	0.27	Poisson coefficient
ν		0.35	0.45	0.30	0.30	0.25	Poisson coefficient
M_v	kN/m^2	15,000	5,000	50,000	50,000		modulus of compressibility
m_v		6.67E-05	2.00E-04	2.00E-05	2.00E-05		coefficient of compressibility
E	kN/m^2	9,346	1,318	37,143	37,143	620,000	Young's modulus of elasticity

1.3 *Mathematical model of the dam*

In the mathematical model for simulating the behavior of the earth dam during the filling of the reservoir and the earthquake action, Figure 2, four different local materials are provided in the body of the dam, while the rock foundation at the base below the dam is adopted as non-deformable zone (due to the large difference in the stiffness properties) and also waterproof (due to the low coefficient of permeability). The justification for such approximation is confirmed by comparing models with and without rock foundation, for the state of reservoir filling, whereby a negligible difference in the state of stresses and deformations in the dam body is ascertained. Therefore, in order to avoid the bulkiness of the numerical model and the possible negative impact in the numerical experiments, all further analyzes are conveyed with a mathematical model where the rock foundation is not included.
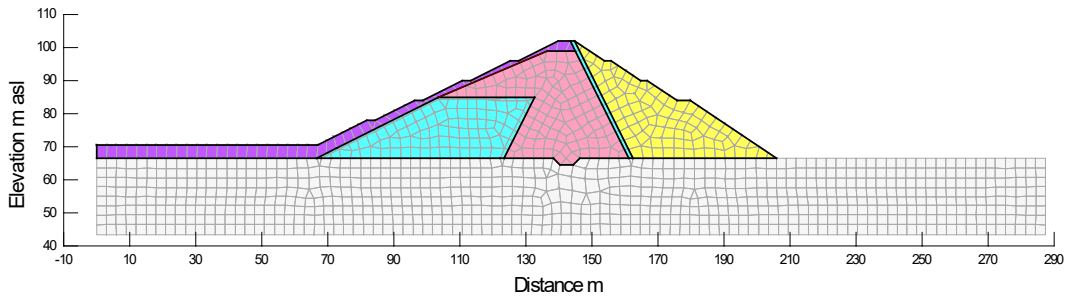

Figure 2. Mathematical model of the dam, discretized with 1,229 nodes и 1,147 elements.

2 SIMULATION OF DAM BEHAVIOR IN EXPOLOITATION PERIOD

2.1 *Stages of earth dam loading*

The behavior of the dam in the service period is simulated with a mathematical model in real time domain, appropriate to the measured values from the technical monitoring. This ensures that the initial load state in the current load state is taken over from the previous stress state. The analyzes were performed using the effective stresses, apropos by tracking the increase and dissipation of the pore pressure with a coupled mechanical and hydraulic response with non-steady seepage in drained conditions.

The loading stages of the earth dam are systematized in Table 2. The monitoring of the dam behavior is simulated in a period of 33.54 years, from the beginning of the first filling of the reservoir, until the state of long-term maintenance at a normal level.

Table 2. Stages of loading of the earth dam.

Stage No.	description	from		to		dZ	Dt	dZ/Dt	Dt
		m asl	yyyy-mm-dd	masl	yyyy-mm-dd	m	days	m/d	years
1	first filling	81.84	1988-04-25	98.34	1990-04-17	16.50	722	0.023	1.977
2	to normal level	98.34	1990-04-17	98.80	1990-04-27	0.46	10	0.046	0.027
3	normal level	98.80	1990-04-27	98.80	2008-01-01	0.00	6,458	0.000	17.681
4	to emergency level	98.80	2008-01-01	92.00	2008-05-17	-6.80	137	-0.050	0.375
5	emergency level	92.00	2008-05-17	92.00	2018-05-17	0.00	3,652	0.000	9.999
6	to remediation level	92.00	2018-05-17	82.00	2018-12-06	-10.00	203	-0.049	0.556
7	remediation level	82.00	2018-12-06	82.00	2019-12-06	0.00	365	0.000	0.999
8	to normal level	82.00	2018-12-06	98.80	2019-11-08	16.80	337	0.050	0.923
9	normal level	98.80	2019-11-08	98.80	2020-11-07	0.00	365	0.000	0.999
10	earthquake	98.80	2020-11-07	98.80			12,249		33.54

2.2 *Initial stress state prior to the first filling*

The data from the monitoring of the dam are given for the first filling of the reservoir from elevation 81.84 m. Therefore, the initial stress state is determined for steady seepage through the dam for water level elevation dam at 81.84 m.a.s.l., Figure 3, by application of Seep/W program [2]. For this state of seepage pore pressure, the distribution of effective stresses in the dam body is determined, Figure 4, by application of Sigma/W program [3]. The coefficient of slope stability of the upstream slope is calculated with the realized stresses by application of program Slope/W [4] and is F = 1.33, apropos it is greater than the required 1.3, for temporary load.
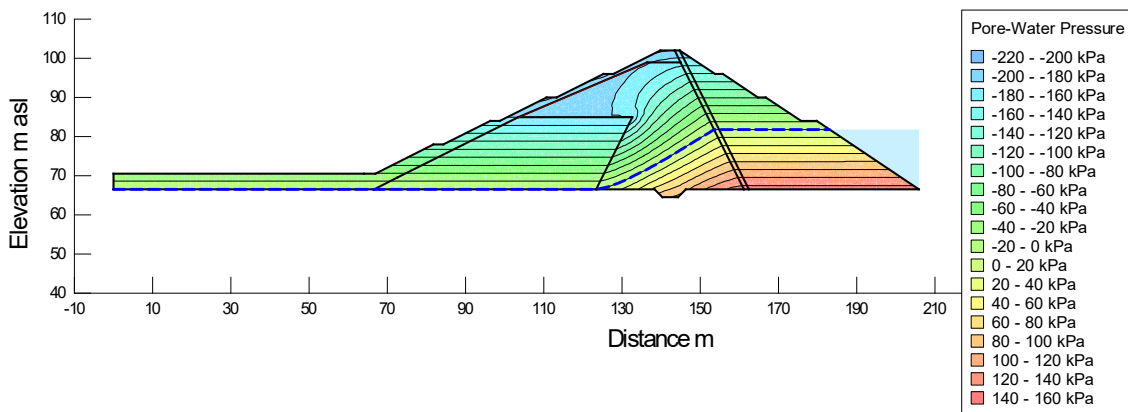

Figure 3. Initial state prior to the filling of the reservoir, distribution of pore pressure for steady seepage.
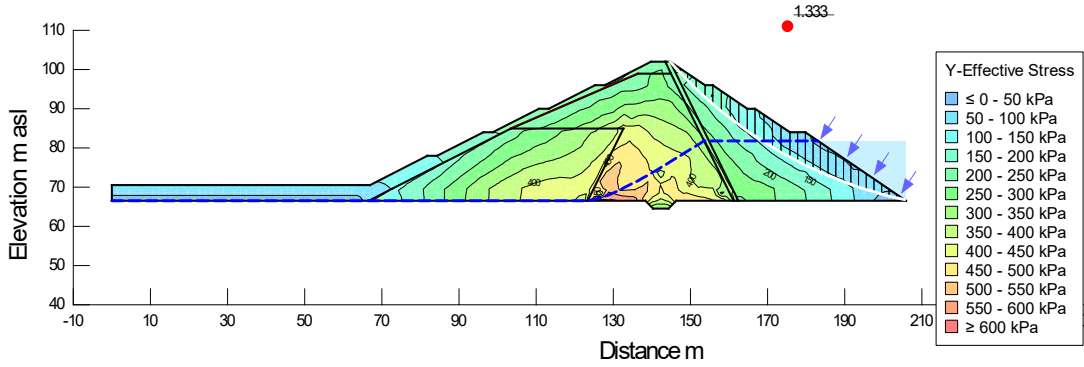
Figure 4. Initial state prior to the filling of the reservoir, distribution of vertical effective stress with coefficient of slope stability on the upstream slope F=1.33.

2.3 *First filling of the reservoir and calibration of nonlinear material parameters*

The first filling (or Stage 1) is simulated in 722 linear increments over a period of 722 days, according to the dynamics of the registered values from the technical monitoring, Figure 5.
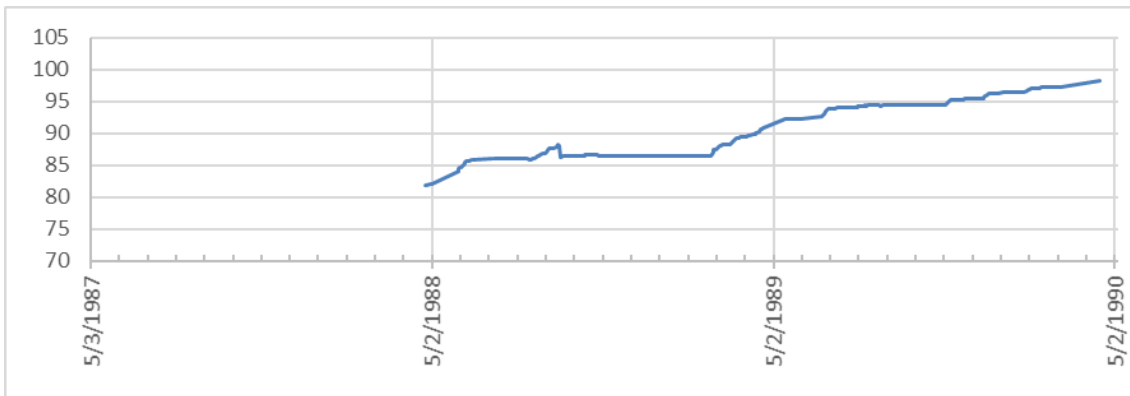
Figure 5. Dynamics of first filling of the reservoir, in m asl.

In the static analysis, for the local materials in the dam body, an elastoplastic model with variable modulus of elasticity E = E (σy '), Figure 6, with calibrated elastic parameters, is applied. Criterion for calibration is the condition that the horizontal displacements in the dam crest, for the state of the first filling of the reservoir, to be approximately same with the measured values, figure 7, i.e. about -120 mm in the downstream direction.

Figure 6. Calibrated values for variable elasticity modulus E=E(σy') for the local materials in the dam body.

Figure 7. Comparison of calculated and measured horizontal displacements in mm (- downstream direction), in the dam crest (measuring point V5) during the first filling of the reservoir.
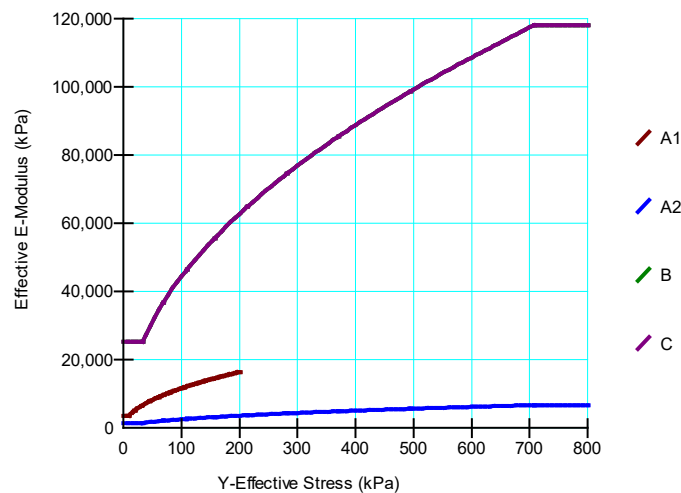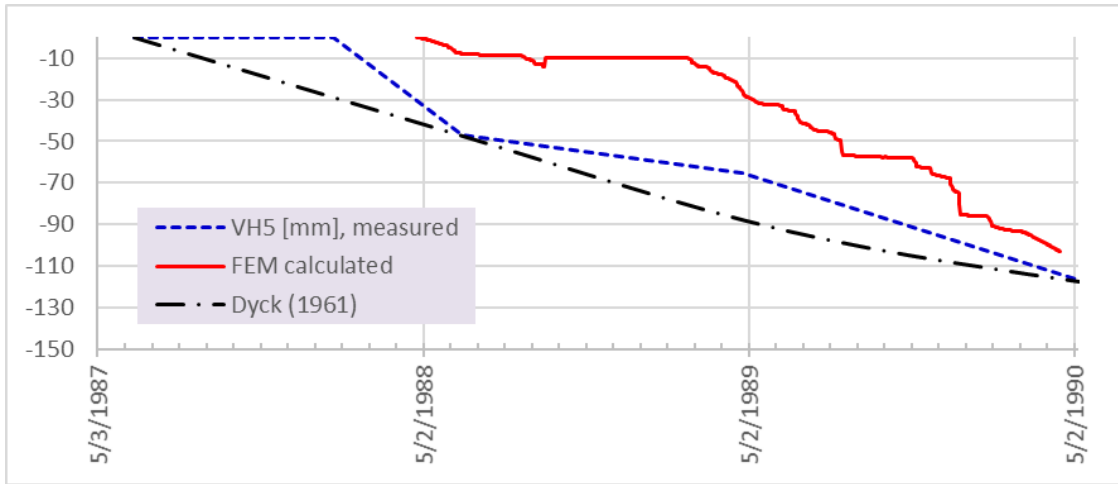
In all materials for construction of embankment dams, there is a dependence between stresses, deformations and time. That is, the materials show viscous behavior, and long-term loads on the viscous materials cause significant deformations called "creep" of the material. Figure 7 also shows the secondary horizontal displacements calculated by method of Dyck (1961). The following expression is used to calculate the secondary displacements at the embankment dams after the construction of the dam and the filling of the reservoir:

$$W = \frac{\varepsilon_t H}{100} \tag{1}$$

$$\varepsilon_t = \varepsilon_a + \alpha \ln t \tag{2}$$

Whereas, (W) is displacement in meters, (t) past period in years, (H) is height of dam above terrain, and coefficients (ε_o) and (α) depend on the type of dam and type of displacement.

Horizontal secondary displacements in the direction of the action of hydrostatic pressure are correlated with settlements caused by creep and, according to some authors, their value is about 50% of vertical displacements. Thus, if the mechanical response with the FEM and the empirical concept obtained horizontal displacements in the downstream direction of about 120 mm, the vertical settlement would be approximately 240 mm. For the values of the vertical rising in the crest obtained by the mechanical response with FEM of +150 mm, Figure 8, summed with the vertical creep settlement of -240 mm, we obtain approximately -90 mm, i.e. approximately to the measured settlement of around -100 mm.
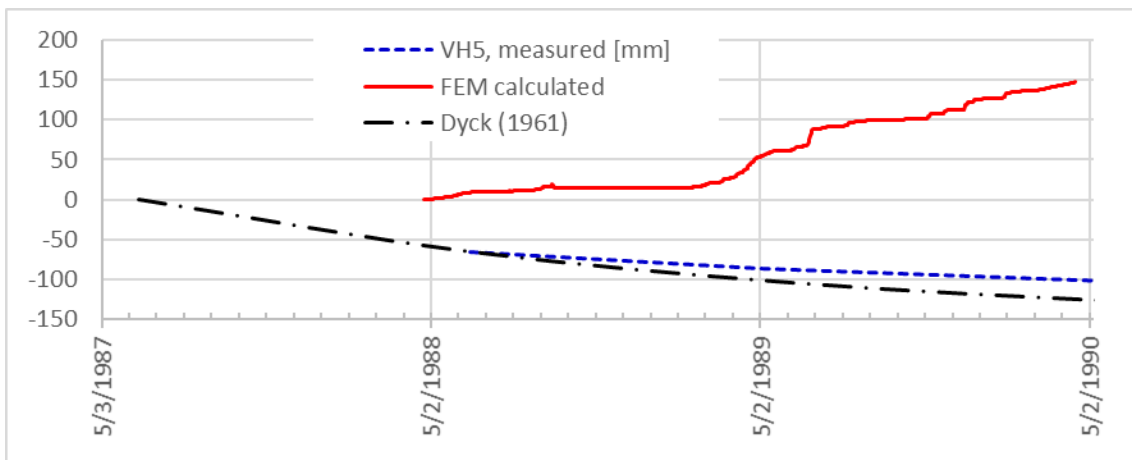

Figure 8. Comparison of calculated and measured vertical displacements in mm (+ elevation, - settlement), in the dam crest (measuring point V5) during the first charge of the reservoir.

2.4 *Variation of the water level in the reservoir*

The dam states during the variations of the water level in the reservoir from stage 2 to stage 9 (Table 2) are simulated in the time domain of the following numerical experiments:

- Stage 2, raising to normal level with 10 linear increments over a period of 10 days;
- Stage 3 maintenance of normal level with 60 exponential increments over a period of 6,458 days;
- Stage 4 lowering to emergency level with 20 linear increments in a period of 137 days;
- Stage 5 maintenance of emergency level with 30 exponential increments in a period of 3,652 days;
- Stage 6 lowering to remediation level with 30 linear increments over a period of 203 days;
- Stage 7 maintenance of remediation level with 15 exponential increments for a period of 365 days;
- Stage 8, raising to normal level with 30 linear increments over a period of 337 days and
- Stage 9 maintenance at a normal level with 15 exponential increments over a period of 365 days.

The comparison of the estimated (with FEM model and empirical) and the measured horizontal and vertical displacements in the dam crest are shown in Figures 9 and 10.
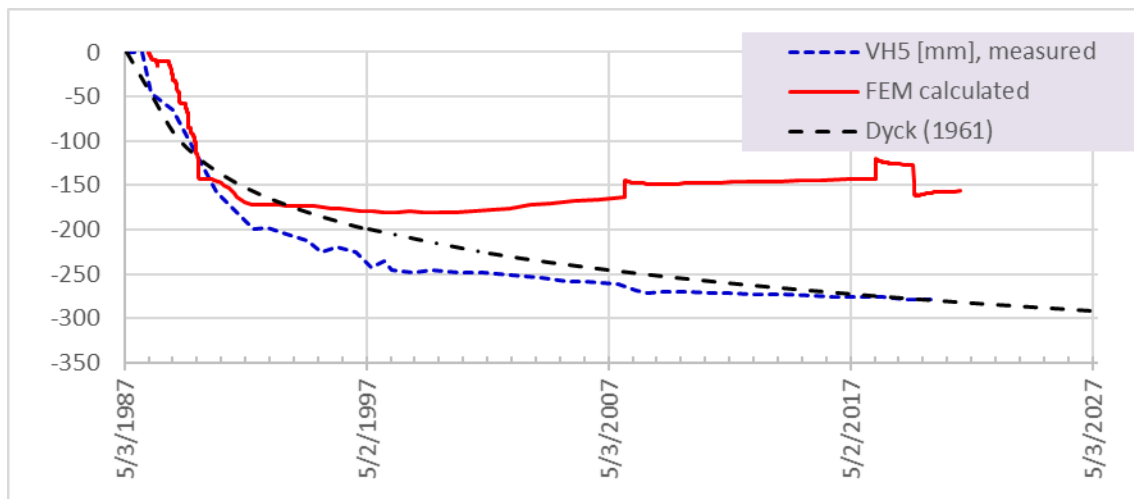

Figure 9. Comparison of calculated and measured horizontal displacements in mm (- downstream), in the dam crest (measuring point V5), during Stage 1 to Stage 9.
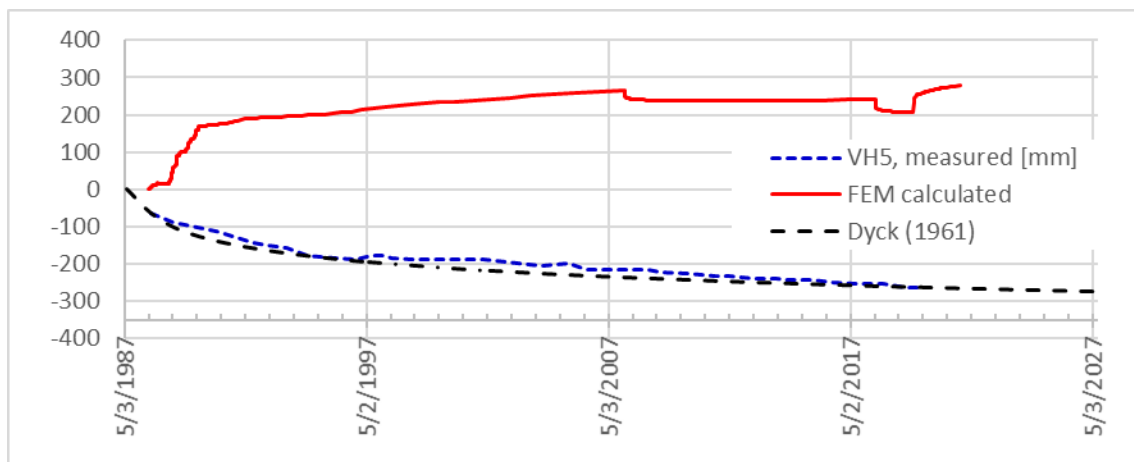
Figure 10. Comparison of calculated and measured vertical displacements in mm (+ elevation, - settlement), in the dam crest (measuring point V5), during Stage 1 to Stage 9.

By extrapolating the displacements in the crest until 2027, under the proper behavior of the dam, a horizontal downstream displacement of 300 mm and a settlement of approximately 300 mm can be treated.

The stress state in the final stage or stage 9, Figure 11, is the initial pre-earthquake state. The coefficient of slope stability of the upstream slope is calculated with the realized stresses with value of F = 1.6, i.e. it is greater than the required 1.5, for permanent load.
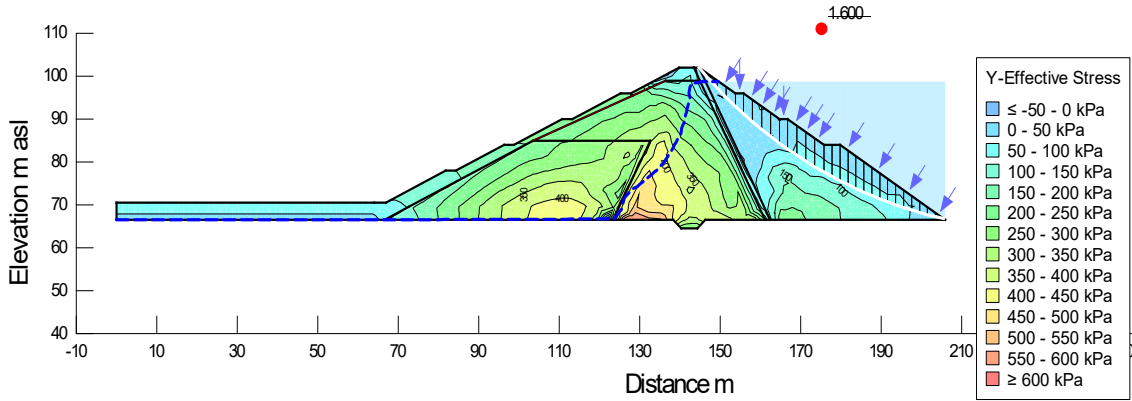
Figure 11. Initial state before earthquake action, distribution of vertical effective stresses, with coefficient of slope stability of the upstream slope F = 1.6.

3 DYNAMIC RESPONSE OF THE DAM

3.1 *Dynamic material parameters and model for permanent displacements*

In the dynamic analysis, a nonlinear model with variable maximum shear modulus is applied for the materials in the dam body, Figure 12. Dynamic analysis is performed with equivalent linear analysis (ELA) with inelastic dynamic parameters of local materials, Figures 13 and 14.
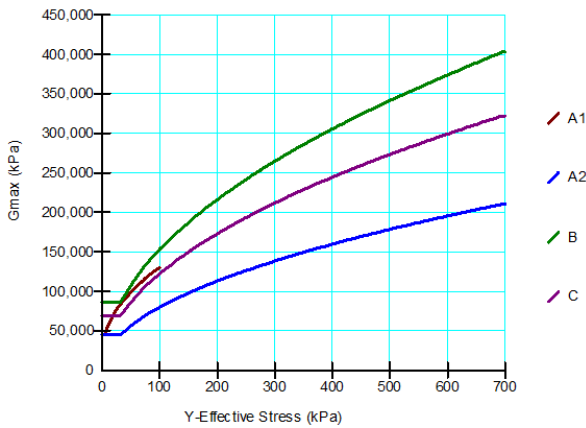
Figure 12. Variable maximum shear modulus G_{max} = G (σγ') for local materials in the dam body.
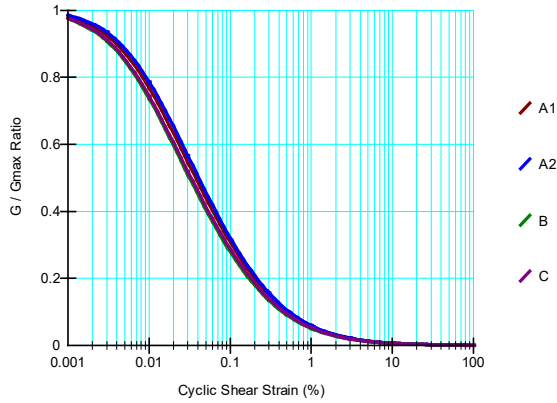
Figure 13. Reduction of the shear modulus with increase of tangential strains for local materials using an equivalent linear model.
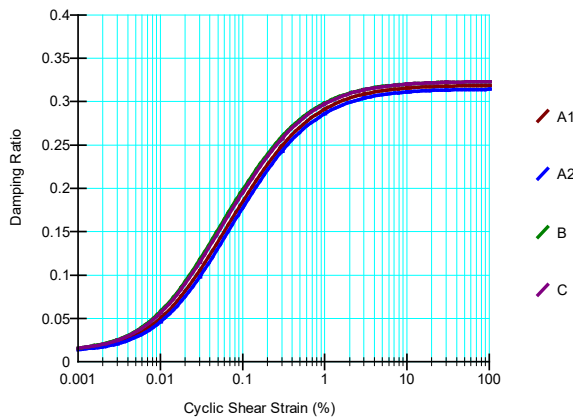
Figure 14. Increase in damping coefficient with increase in tangential strains for local materials using an equivalent linear model.

The approach applied in the present analysis for determination of the permanent deformations during the seismic excitation, for any node within the fill dam, is the method of "Dynamic Deformation Analysis" (DDA), which is successive non-linear redistribution of the stresses [2]. By such method, for geo-medium discretized by finite elements, are calculated deformations caused by forces in nodes, calculated by the incremental stresses in the elements. Thus, by application of non-linear model, for each time step of the dynamic response of the structure [6] is obtained new state of the total stresses and pore pressure. By the differences of the effective stresses in two successive time steps are obtained incremental forces, resulting in deformations, in accordance with the chosen constitutive law for dependence stress - strain. So, for each loading case during the dam's dynamic response are produced elastic and eventual plastic strains. If dynamic inertial forces cause plastic strains, then in the geo-medium will occur permanent deformations. The permanent displacements, at any point in the dam and at the end of the seismic excitation, are cumulative sum of the plastic deformations.

3.2 *Eigen periods of the dam*

To determine the eigen periods for a certain level of inelastic response of the embankment dam, a dynamic excitation of synthetic harmonic vibration with continuous change of frequencies was used, i.e. with evenly represented frequencies in the interval $f1 \div f2 = 0.4 \div 10.0$ [H1] = $2.5 \div 0.1$ [s]. This harmonic has a maximum amplitude $A_o = 0.001$ g, a total duration St = 12 [s], a time increment in the accelerometer dt = 0.01 [s], Figure 15. Spectra of excitation response and response, spectral acceleration Sa [g] for damping coefficient DR = 0.05, is given in Figure 16 for full reservoir. The dynamic response of the dam is determined using the Quake / W program [3].

sin=12s f=0,4-10Hz.acc
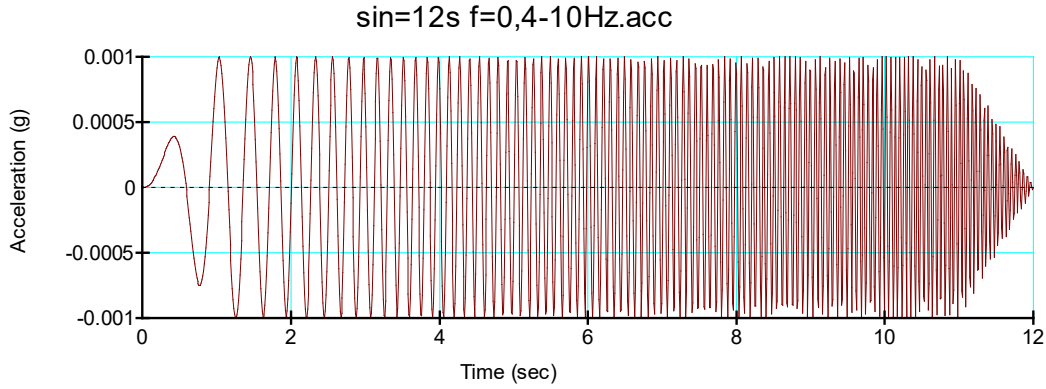
Figure 15. Time history of horizontal accelerations of harmonic vibration with evenly represented frequencies f1 ÷ f2 = 0.4 ÷ 10.0 [Hz], scaled with Ao = 0.001 g.
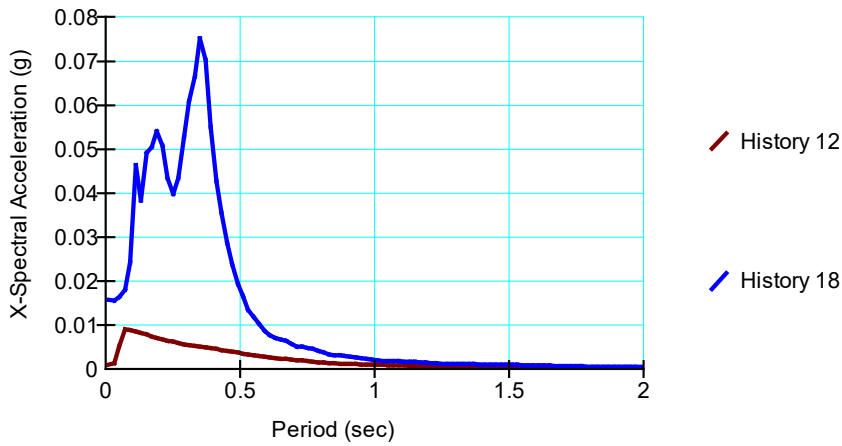
Figure 16. Response spectrum of absolute accelerations in the crest of the dam at full reservoir, caused by harmonic oscillation with low intensity PGA=0.001 g, with eigen periods T1=0.35 s, T2=0.19 s, T3=0.11 s.

3.3 *Seismology parameters of a strong earthquake*

As a basis for generating accelerogram for synthetic earthquake, design spectra are adopted - spectra of elastic response to normalized accelerations from design earthquakes. In the analysis, the design spectra according to the Eurocodes (Eurocode 8, 2003) were used, for type A base for horizontal and type 1 for vertical component. Accelerogram of the horizontal and vertical components of a strong earthquake are given in Figures 17 and 18.
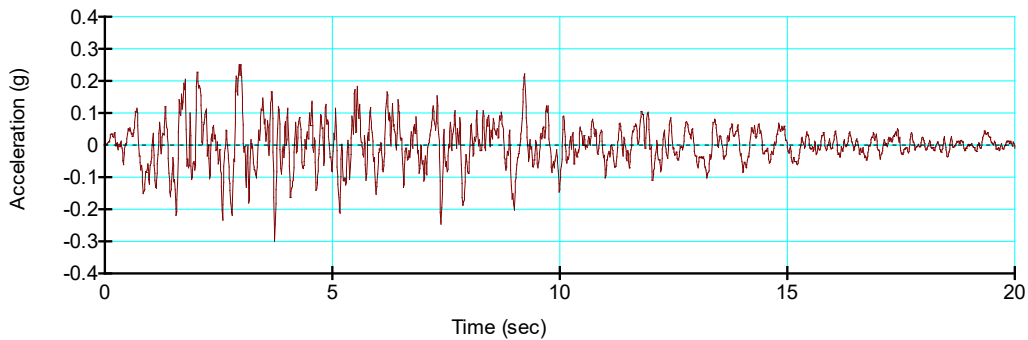
Figure 17. Time history of the horizontal excitation component in the rock foundation for a strong earthquake, PGAx = 0.3 g.
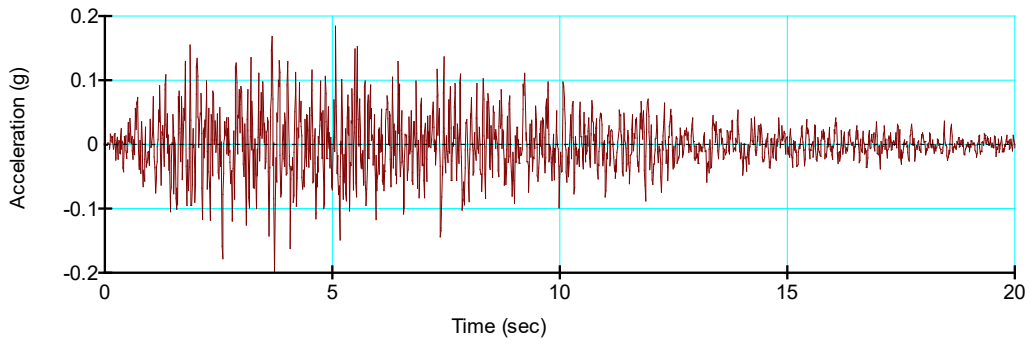
Figure 18. Time history of the vertical excitation component in a rock foundation for a strong earthquake, PGAy = 0.2 g.

3.4 *Dam response during a strong earthquake*

The horizontal accelerations in the dam crest at occurrence of a strong earthquake are given in Figure 19, and the response spectrum of the accelerations is given in Figure 20.
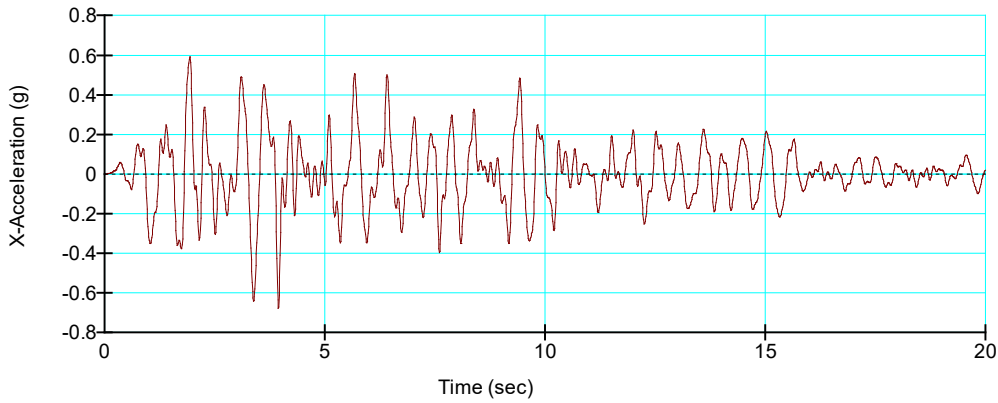
Figure 19. Time history of the horizontal component of the response in the crest of the dam with PCE = 0.671 g, under the action of a strong earthquake with PGA = 0.3 g.
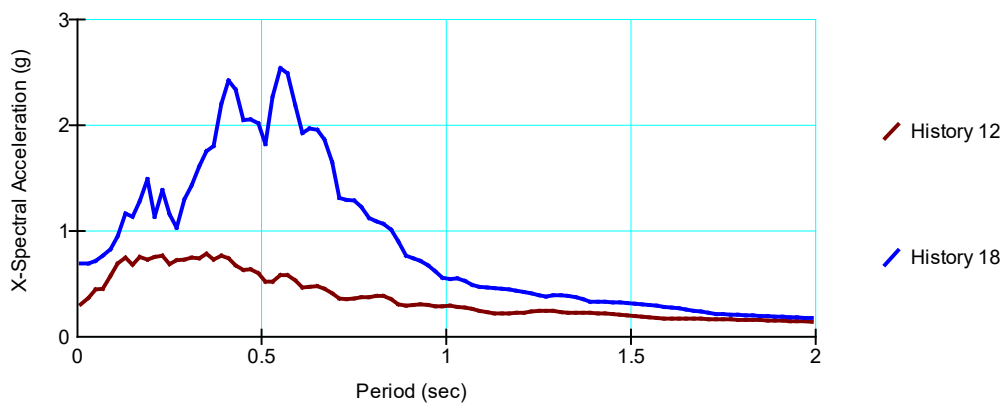
Figure 20. Response spectrum for the accelerations in the base and in the crest of the dam (with T1 = 0.55 s) during the action of a strong earthquake.

The relative displacements in the crest of the dam during the action of this earthquake are given in Figure 21.
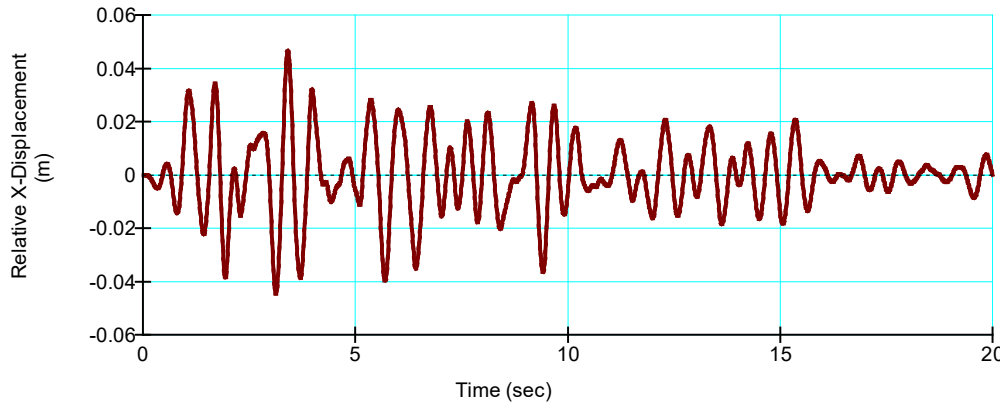
Figure 21. Time history of relative horizontal displacements in the dam crest during a strong earthquake.

The realization of the permanent horizontal and vertical displacements in the crest of the dam during the action of this earthquake are given in Figures 22 and 23, and after the action of the earthquake the permanent XY displacements in the body of the dam are given in Figure 24.
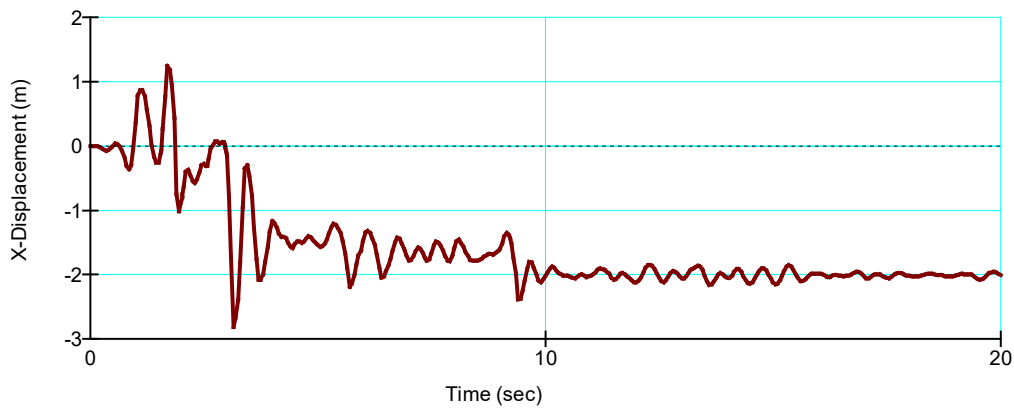
Figure 22. Permanent horizontal displacements in the dam crest (measuring point V5) during a strong earthquake.
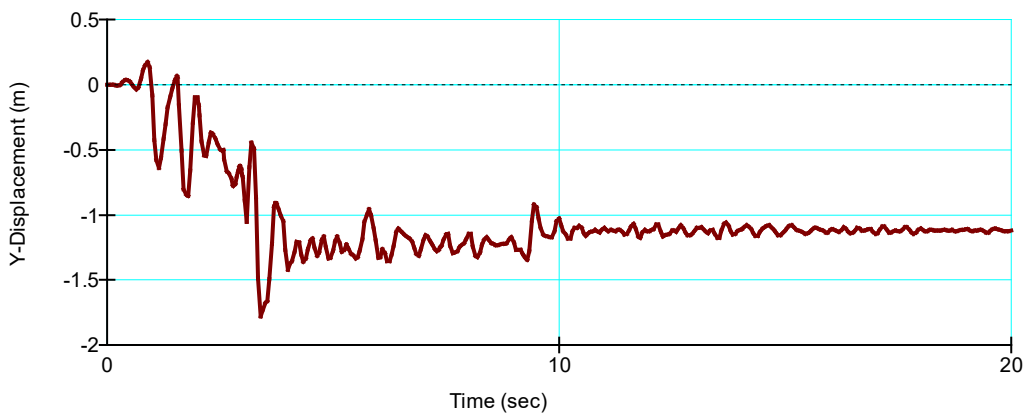
Figure 23. Permanent vertical displacements in the dam crest (measuring point V5) during a strong earthquake.
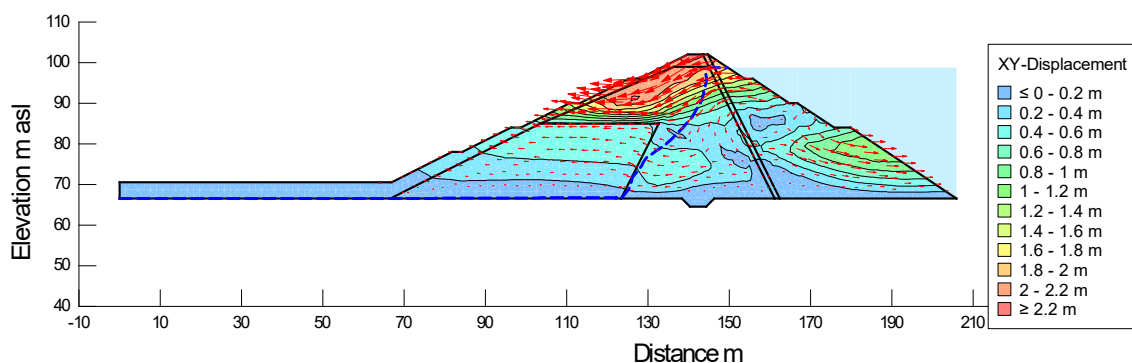
Figure 24. Permanent XY displacements in the dam after the action of a strong earthquake, XYmax=2.3 m.

4 CONCLUSION

The behavior of the dam during the filling of the reservoir, during the variation of the levels in the reservoir in the service period, and during the seismic excitation is simulated with only one model for structural analysis [6]. This ensures the transfer of the stress state in the analysis, as the initial state for each subsequent load case. The analyzes were performed using the effective stresses, i.e. by simulating of the increase and dissipation of the pore pressure in the drained conditions, with a coupled mechanical and hydraulic response with non-steady seepage.

In the static analysis, for the local materials in the body of the dam, an elastoplastic model with variable modulus of elasticity is applied, with calibrated elastic parameters. Criterion for calibration is the horizontal displacements in the crest of the dam, for the condition of the first filling of the reservoir, to be approximately the same with the measured values, i.e. about -120 mm in the downstream direction.

By extrapolating the displacements in the crest by 2027, under the proper behavior of the dam, a horizontal downstream displacement of 300 mm and a settlement of approximately 300 mm can be treated.

The stability of the dam is analyzed through the coefficient of slope stability (F) with the realized stresses, determined by the FEM model. The determination of coefficient F is performed only for the upstream slope, because with the adopted geometry and layout of the materials, it is obvious that the downstream slope has F>2 for any load case. For the initial condition before the first filling is obtained F = 1.33> 1.3, required for temporary load. For the state of full reservoir is obtained F = 1.6> 1.5, required for permanent load. For the condition of rapid drawdown of the level to remediation elevation (82.0 m.a.s.l.), by applying the Limit Equilibrium Method, a safety coefficient K_c = 1.373> 1.3, required for temporary load, is obtained. For this state, we emphasize that due to the high normal stresses (generated by the hydrostatic load during filling), the safety coefficient F calculated with the realized stresses is extremely higher. The key conclusion from the static analysis is that the embankment dam, with the adopted geometry and composition of the materials, possesses satisfactory static stability.

The dam's Eigen Periods are determined by the response spectrum when it is excited by harmonic vibration, with equal frequencies from 0.4 to 10.0 Hz, for the initial stress state at full reservoir. For low excitation intensity with PGA = 0.001 g, eigen periods T1 = 0.35 s, T2 = 0.19 s, T3 = 0.11 s are obtained. For higher excitation in a strong earthquake with PGA = 0.3 g the response of the embankment dam is nonlinear, the stiffness of the local materials decreases with the increased inelastic deformations, which causes an increase of the period of the eigen tone T1 = 0.55 s [7]. The values for the base tone (T1), determined in the analysis, match the measured values for dams exposed to strong earthquakes in Japan [8,9], which is the best confirmation of the correctness of the adopted dynamic material parameters for nonlinear dynamic analysis.

The values for Dynamic Amplification Factor, where DAF = PCA / PGA, where PGA - Peak Ground Acceleration (in the horizontal direction), and PCA e Peak Crest Acceleration in the horizontal direction) are: 0.671 / 0.3 = 2.24 for a strong earthquake. The response in the crest of the dam corresponds to the registered data on the degree of dynamic amplification of this type of

structures under the action of strong earthquakes, [10] and the time history of relative displacements are the key indicator for the correctness of the dynamic analysis.

The permanent settlements in the dam crest, caused by the dynamic inertial forces for the duration of the earthquake, determined by the method of Dynamic Deformation Analysis (DDA), is Y = - 1.1 m for a strong earthquake. Regardless of the fact that the subject analysis does not take into account the settlements from additional compaction and reduced stiffness of materials exposed to cyclic action, the total settlement cannot exceed the height of the dam crest (102 m.a.s.l.) to the normal level in the reservoir (98.8 m.a.s.l.).

The key conclusion from the dynamic analysis is that the embankment dam, with the adopted geometry and layout of the materials, has satisfactory seismic resistance. That is, there is no violation of the water resistance of the waterproof body (wide clay core), nor is there a danger of rapid and uncontrolled emptying of artificial lake, because the settlement during the design earthquake with PGA 0.3 g does not overcome the protective height of 3.2 m.

REFERENCES

[1] Zhvanut P., …., (2022). 16th International Benchmark Workshop on Numerical Analysis of Dams, Theme C, Ljupbljana, Slovenia

[2] Geo-Slope SEEP/W v8, (2017). "Seepage analysis", GEO-SLOPE International Ltd., Calgary, Alberta, Canada.

[3] Geo-Slope SIGMA/W v8, (2017). "Stress/deformation analysis", GEO-SLOPE International Ltd., Calgary, Alberta, Canada.

[4] Geo-Slope SLOPE/W v8, (2017). "Stability analysis"", GEO-SLOPE International Ltd., Calgary, Alberta, Canada.

[5] Geo-Slope QUAKE/W v8, (2017). "Dynamic Modeling", GEO-SLOPE International Ltd., Calgary, Alberta, Canada.

[6] Petkovski L., Tančev L., Mitovski S., (2007) "A CONTRIBUTION TO THE STANDARDISATION OF THE MODERN APPROACH TO ASSESSMENT OF STRUCTURAL SAFETY OF EMBANKMENT DAMS", 75th ICOLD Annual Meeting International Symposium "Dam Safety Management, Role of State, Private Companies and Public in Designing, Constructing and Operation of Large Dams", 24-29 June 2007, St.Petersbourg, Russia, Abstracts Proceedings p.66, CD-ROM

[7] Park D.S., (2018). Fundamental Period of Embankment Dams Based on Strong Motion Records, Topic Earthquakes - Embankments, USSD 38th Annual Meeting and Conference, A balancing Act: Dams, Levees and Ecosystems, April 3- May 4, 2018, Miami, Florida, USA, CD Proceedings

[8] Matsumoto N., …, (2005). "ANALYSIS OF STRONG MOTIONS RECORDED AT DAMS DURING EARTH-QUAKES", 73rd Annual Meeting of ICOLD, Tehran, IRAN, Paper No.: 094-W.

[9] Fry J.J., Matsumoto N., (2018). Validation of Dynamic Analyses of Dams and Their Equipment, CRC Press/Balkema, Tailor & Francis Group, London, New York, ISBN: 978-0-429-49116-0 (eBook)

[10] ICOLD, Bulletin 113, (1999). Seismic observation of dams - Guidelines and case studies

BEHAVIOUR OF THE EMBANKMENT DAM, THEME C OF THE 16TH INTERNATIONAL BENCHMARK WORKSHOP ON NUMERICAL ANALYSIS OF DAMS

Dr. Konstantinos Kassas
ETH Zurich, Institute for Geotechnics, Zurich, Switzerland

Prof. Dr. Ioannis Anastasopoulos
ETH Zurich, Institute for Geotechnics, Zurich, Switzerland

Stefan Ehlers
AFRY Switzerland Ltd., Zurich, Switzerland

ABSTRACT: The publication deals with an embankment dam located in Slovenia, which was constructed and impounded at the end of the 1980's. The dam is a zoned rockfill dam with a clay core, with a height of almost 35 m and crest elevation at 102 m asl (Fig. 1). The earthfill core extends to the downstream face in the upper part of the dam. The upstream and downstream dam shells mainly consist of rockfill. The dam is based on a mainly impermeable foundation, which was grouted as needed. An irrigation pipeline and two bottom outlet pipelines are leading through the embankment dam in its central part, close to the foundation. The pipelines corroded during the years and got leaky, leading to water infiltration from the reservoir into the dam body. A wet spot and surface water at the downstream dam face was noticed in 2007, after about 20 years of operation. As a consequence, the operating level of the reservoir was lowered in several steps and the irrigation pipe was sealed. Currently, the reservoir is completely empty and the bottom outlet pipes are getting sealed. This publication deals with the numerical modelling of the dam, covering the entire period from dam construction until today, including the pipe leakages and the remediation measures. A fully coupled 3D finite element (FE) model is developed and calibrated on the basis of monitoring data (geodetic settlement points and piezometers). The stability of the dam is calculated at various moments in time. A hypothetical scenario without reservoir lowering is also investigated, and a prognosis is made for reservoir refilling (envisaged for 2023). The analysis is a contribution to the 16th International Benchmark Workshop on Numerical Analysis of Dams.

Figure 1. Downstream and upstream face of the embankment dam.

1 INTRODUCTION

This publication is a contribution to the 16th International Benchmark Workshop on Numerical Analysis of Dams, which is organised by the ICOLD Committee A on "Computational Aspects of Analysis and Design of Dams". It covers Theme C "Behaviour of the Embankment Dam", formulated by the Slovenian National Building and Civil Engineering Institute, Geoportal d.o.o., Elea iC d.o.o. and the University of Ljubljana, Faculty of Civil and Geodetic Engineering (Žvanut et al., 2021). Theme C comprises 4 cases, each case consisting of 1 to 3 tasks.

2 BASIC INFORMATION ON THE DAM

2.1 *Purpose and operation*

The dam was built in the late 1980's for agricultural purposes (irrigation) and flood protection. Operated in a seasonal pattern (usually filled during winter times when the river discharges are high), the reservoir provides seasonal storage with a total volume of 8.0 million m^3. About 6.8 million m^3 or 84.5% of the reservoir volume is used for irrigation during the spring and summer months, while the remaining 1.2 million m^3 or 15.5% is reserved for flood water retention.

Dam design, geometry and material parameters

The dam has a height of almost 35 m with the crest elevation at 102 m asl, while the crest width is 5 m. Slope inclinations are 1V:2H upstream between four berms, and 1V:1.5H downstream between three berms. The normal reservoir operating level is at 98.8 m asl. The salient features and the main elevations of dam and reservoir are summarised in Table 1.

The dam is a zoned rockfill dam with clay core. A typical cross-section of the dam is shown in Fig. 2, while the provided material properties are summarized in Table 2. The earthfill core (zone A) extends to the downstream face in the upper part of the dam, entirely covering the downstream face. The upstream embankment dam body mainly consists of rockfill material (zone B). The lower part of the downstream embankment dam body consists of a mix of limestone and sandstone blocks. Two filter layers (zone E) are located between the earthfill core (zone A) and the rockfill zones B and C. No information regarding the filter material parameters is provided. The very top portion of the dam (i.e., the upper 3 m at the dam crest) consists of dolomite gravel mixed with silt or clay (also named zone A' in Table 2).

The dam is founded on Eocene flysch. The material was assumed to be impermeable, but during construction zones with permeable limestone deposits were encountered. The permeable zones were grouted with a single-row grout curtain down to an elevation of 34 m asl, resulting to a depth of 68 m.
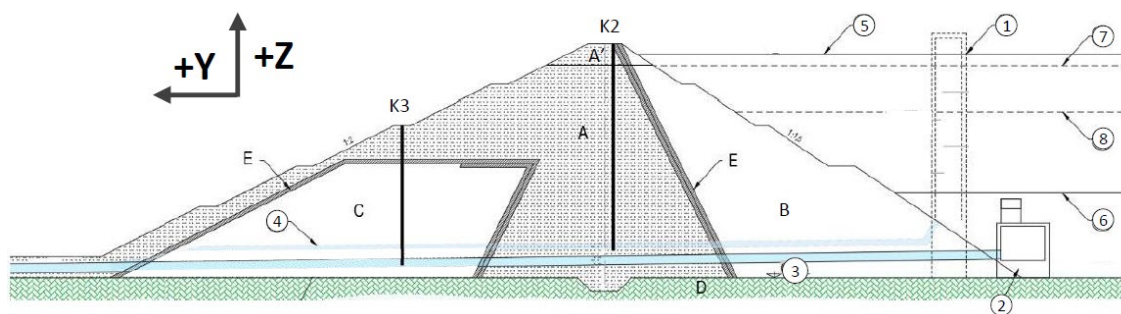

Figure 2. Typical cross-section of the dam with piezometers K2 and K3: (1) intake tower and (2) intake structure at the upstream dam toe, and (3) the two bottom outlet pipes and (4) the irrigation pipeline along the dam foundation.

Table 1. Main elevations and salient features of the dam.

Dam crest	102.0 m asl
(5) Maximal reservoir level	100.5 m asl
(7) Normal operating level	98.8 m asl
(8) Lowered operating level	92.0 m asl
(6) Minimal operating level	80.0 m asl
(3) Dam foundation	67.4 m asl
Dam height	34.6 m
Crest width	5 m
Base width	120 m
Crest length	174 m

Table 2. Material parameters provided by the theme formulators.

Zone	A	A'	B	C	D
Description	Clayey silt to silty clay	Top layer of the dam (top 3 m from the crest) dolomite gravel mixed with silt or clay	Rockfill (limestone blocks)	Blocks of limestone and sandstone	Flysch
w [%]	26	13	/	/	/
γ [kN/m^3]	19.5	21	24	24	25
c_u [kPa]	75	/	/	/	/
φ [°]	/	36	38	38	39
c [kPa]	/	36	/	/	32
E_{oed} [MPa]	5	15	50	50	/
E [MPa]	/	/	/	/	620
v [-]	0.5	0.4	0.3	0.3	0.25
k [m/s]	10^{-9}	10^{-6}	10^{-3}	10^{-4}	10^{-9}

2.2 *Appurtenant structures*

The bottom outlet consists of two steel pipes, each 1.2 m in diameter. The intake of the bottom outlet at the upstream dam toe and its alignment are shown in Figs. 2 and 3, respectively. Each of the bottom outlet pipes is regulated with a Howell-Bunger valve, located at the downstream dam toe. Thus, the pipes are always filled with water and are always under pressure. The bottom outlet pipes are protected with a concrete cover. In addition there is an intake tower at the upstream dam toe (Fig. 2), which serves for water withdrawal for irrigation purpose. The discharge through the irrigation pipe is controlled by the four hydraulic gates of the intake tower. The alignment of the steel pipeline is shown in Fig. 3. Designed to evacuate a design flood with a return period of 1,000 years, the emergency spillway is located at the right abutment.

3 OPERATION PERIOD

3.1 *Construction and first filling of the reservoir*

The dam was constructed in a period of about 1 year. No additional information is provided regarding the construction sequence and the specific timeline. First filling of the reservoir started in April 1988 at elevation 81.84 m asl. It was carried out with an average increment water level raise of 2.3 cm/day. After a period of about two years, the reservoir level reached about 98.5 m asl. The reservoir filling from the base (67.4 m asl) to the elevation of 81.84 m asl is not reported. In an effort to visualise and unify the time history of dam construction, its height and the recorded reservoir level, along with other milestones are illustrated in Fig. 4.

3.2   *Incident in 2007*

After about 20 years of operation, on the 27th of October 2007, a wet spot was noticed at the downstream toe in the central part of the dam (Fig. 3). Extensive vegetation on the central part of the embankment dam indicated that the humid zone extends to the downstream slope above the wet spot. Furthermore, surface water was observed at the downstream toe of the dam, between the stilling basin of the spillway and the outlet structure of the bottom outlet.

Investigations revealed that the water originated from the reservoir. The steel pipe of the irrigation pipeline was corroded, having holes ranging from a few centimetres to a few decimetres in diameter. The holes enable water to flow into the layer between the concrete cover and the steel pipe. Although the irrigation pipeline was emptied, the wet zone remained.

Further investigations revealed that the bottom outlet pipes had suffered similar damage than the irrigation pipeline, confirming that the seepage discharge at the downstream dam toe originated also from the two bottom outlet pipes.

Figure 3. (a) Layout plan of the dam with appurtenant structures; (b) location of the geodetic points VH5, VH10, VH14 and VH16; (c) location of the piezometers K2 and K3; and (d) location of the wet stain.

3.3   *Remediation works, lowering and refilling of the reservoir*

In 2008, the reservoir level was lowered to a maximum elevation of 93.6 m asl and the irrigation pipeline was filled with concrete (Fig. 4, I). The space between the irrigation pipeline and the concrete cover was grouted with cement. After this emergency remediation, the reservoir operational level was further lowered to elevation 92.0 m asl. The reservoir operated under the lowered condition for more than 10 years (Fig. 4, II). Reservoir levels are provided until 30.10.2020 (with a general resolution in the range of one to several days).

Currently the reservoir is completely emptied and remediation works are underway (Fig. 4, III). As part of the remediation, the bottom outlet pipes will be sealed with concrete filling. A new outlet building and outlet tunnel will be constructed in the left abutment. After the completion of the remediation works, the refilling of the reservoir from 82 m asl to 98.8 m asl is envisaged for 2023. The refilling is foreseen with a continuous reservoir level raise of 5 cm/day, corresponding to a filling period of 337 days (Fig. 4, IV).
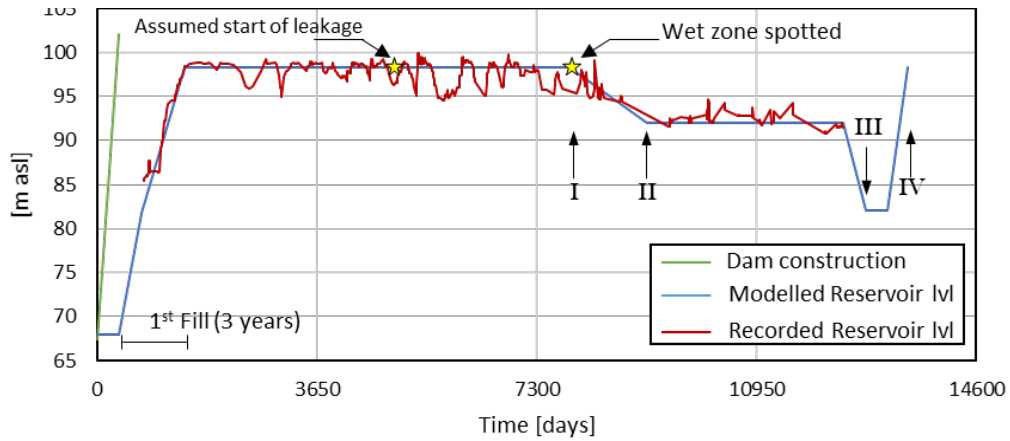
Figure 4. Dam height, recorded and modelled reservoir level.

3.4   *Monitoring instruments and provided monitoring data*

For dam surveillance, visual inspections are carried out in regular intervals. In addition, the behaviour of the dam is monitored with instruments. Displacements are recorded at Geodetic points VH5, VH10, VH14 and VH16 (Fig. 3). Furthermore, two piezometers record the piezometric head (Figs. 2, 3). The recorded displacements are illustrated in Fig. 5, while the sign convention can be found in Fig 2. The first day of dam construction is considered as time equal to zero. It is worth noting that in the horizontal direction, the dam is deformed towards the upstream shell (Fig. 5b).
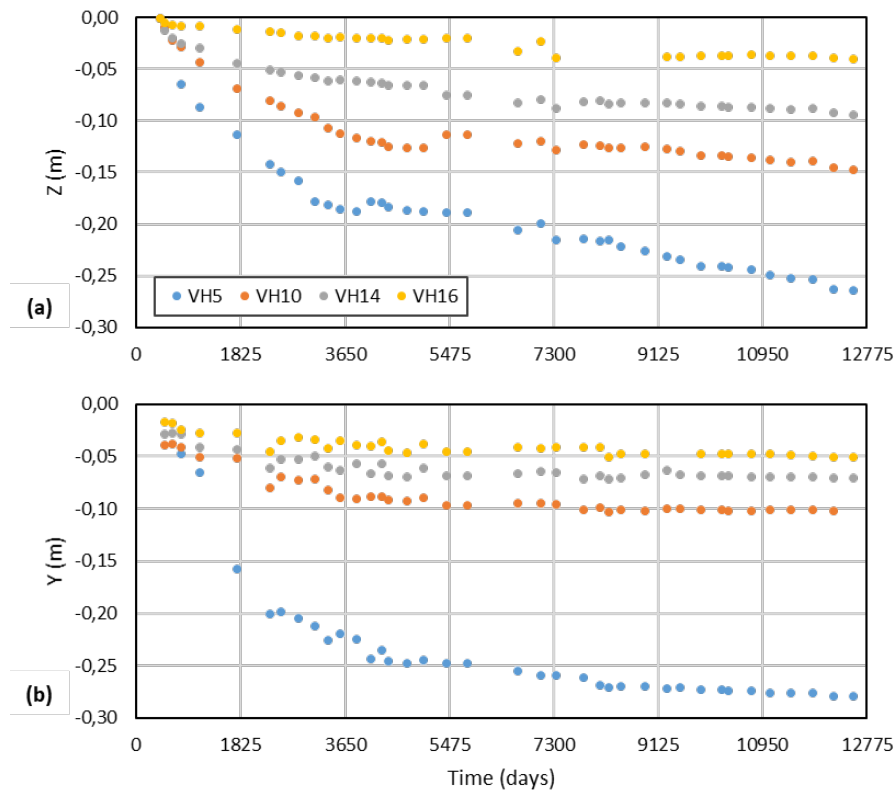
Figure 5. Monitoring data: (a) Settlement; and (b) horizontal displacement measured at the geodetic points VH5, VH10, VH14 and VH16.

4 NUMERICAL MODELLING

The problem is analyzed through coupled hydromechanical numerical analysis, employing the FE code PLAXIS3D, version 2017.1.0.0 (Plaxis, 2019). A 50 m slice of the dam is modelled, as shown in Fig. 6. Since the geometric characteristics and the material properties of the filter layers (E) are not provided, they are not considered in the numerical analysis. Nevertheless, their influence is not expected to affect significantly the results. Furthermore, the bottom outlet and irrigation pipelines and the related intake structures are also not modelled. The recorded variation of the reservoir level with time is considered as shown in Fig. 4. In the absence of detailed information regarding the construction sequence of the dam, its construction is modelled in 7 steps to get accurate stress conditions within the dam body. After each step, a consolidation analysis is conducted allowing for excess pore pressures dissipation. Overall, the construction is modelled to last 365 days, while the reservoir is considered empty.
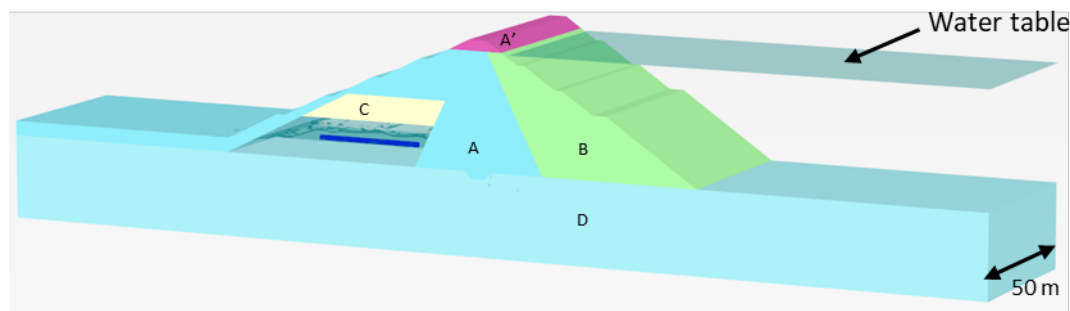
Figure 6. Outline of the numerical model.

4.1 *Constitutive models and material parameters*

The foundation layer is modelled with an elasto-plastic Mohr-Coulomb (MC) model. This is a simplification with negligible influence on the analyses results, as the stiffness of this layer is one order of magnitude larger than that of the dam zones.

For the dam zones, the Hardening Soil Small Strain Model was used (HS-small). The model realistically reproduces soil deformations, with a hyperbolic $\sigma - \varepsilon$ relation, accounting for the dependence of stiffness on confining stresses and loading history. Moreover, as the formulation of the HS-small model incorporates two hardening mechanisms, it is suitable for modelling both domination of shear plastic strains, which can be observed in granular soils and in over-consolidated cohesive soils, as well as domination of compressive plastic strains, which is typical for soft soils. However, the model cannot capture strain softening, which can be significant for the core material. Finally, the model accounts for the increased stiffness at small strain amplitude. More details on the model can be found in Schanz et al. (1999) and Brinkgreve et al. (2014).

Such constitutive models (as HS-small) can capture some of the key aspects of complex soil response, but require well-documented and reliable experimental data (preferably element tests) for model calibration. In the absence of such data (as is the case here), material parameters can only be estimated through back analysis, using the recorded displacements and pore pressures. However, this is not a trivial task, as the displacements are affected from both stiffness and strength parameters, and from the permeability. To that end, the given material parameters (Table 2) were adopted for the dam foundation and the rockfills, while the stiffness of the core material (Zone A) was estimated from back-analysis, based on the measured dam settlements during the first filling of the reservoir (Fig. 9). The estimated material parameters are shown in Table 3.

Based on the aforementioned lack of construction history and material behavior, the following results can be seen as a conceptual simplification of the problem, and not an accurate reproduction of the dam case history.

Table 3. Adopted material parameters of the numerical model.

Zone	A	A'	B	C	D
Model	HSsmall	HSsmall	HSsmall	HSsmall	MC
γ_{unsat} [kN/m³]	19,5	21	24	24	25
γ_{sat} [kN/m³]	20,9	21,9	24.9	24.9	25
φ [°]	20	36	38	38	39
ψ [°]	0	2	3	3	0
c [kPa]	35	36	1	1	32
E_{50}^{ref} [MPa]	6	15	50	50	
E_{oed}^{ref} [MPa]	5	15	50	50	
E_{ur}^{ref} [MPa]	12	30	100	100	
m [-]	1	0.5	0.5	0.5	
$\gamma_{0.7}$ [-]	2·10⁻⁴	2·10⁻⁴	2·10⁻⁴	2·10⁻⁴	
$G_{0.7}^{ref}$ [MPa]	24	30	100	100	
k [m/s]	10⁻⁹	10⁻⁶	10⁻³	10⁻⁴	10⁻⁹

4.2 *Initial state and stability analysis (0-365 days)*

As shown in the contours of maximum total displacement (u) at the end of the dam construction (365 days) of Figure 7a, the maximum u reached 1.2 m. The latter includes the consolidation settlement, originating from the dissipation of excess pore water pressures (p) (Fig. 7b) during the construction period, which is compensated by the addition of material required for the targeted dam height to be achieved. Figures 7b and 7c illustrate the critical failure planes corresponding to the minimum factor of safety (FS) for the upstream and the downstream faces, respectively.

Figure 7. (a) Total displacements (u) after the construction of the dam (365 days); (b) pore pressures (p) after the construction of the dam; (c) and (d) critical failure planes and factors of safety for the downstream and upstream faces, respectively.

4.3 *First fill of the reservoir (365 – 1460 days)*

The first filling of the reservoir was modelled according to the provided data (Fig. 4). For the period between days 365 and 730, for which no data was provided, it is assumed that the reservoir level was increasing with an average increment of 2.3 cm /day, similar to the recorded data (730-1460 days).

Figure 8a depicts the total displacement at the end of the first filling (1460th day / 4th year), due to the mechanical loading from the water pressure and the consolidation of the core material (zone A). Figure 8b illustrates the pore water pressures. It can be seen that the excess pore pressures at the base of the core have been dissipated.

The numerical model was calibrated on the basis of settlement measurements (geodetic points VH5, VH10, VH14 and VH16) during the 3 years of the first reservoir filling. The adequacy of the settlement calibration is illustrated in Fig. 9, which compares the calculated to the measured settlement (deformation in direction z). In general, the numerical prediction is reasonable for geodetic points VH5 and VH10, which correspond to the higher part of the dam. For geodetic points VH14 and VH16, which are located closer at the dam toe, above the stiff zone C (blocks of limestone and sandstone), the monitored deformations cannot be reproduced.

For all geodetic points, positive horizontal displacement towards the upstream shell of the dam was recorded, despite the direction of the mechanical loading from the reservoir, the shear stress direction and the stiffness asymmetry of the dam (upstream shell is stiffer than the downstream shell). The numerical model does not reproduce the horizontal displacements, which are calculated positive towards the downstream shell for all the cases.
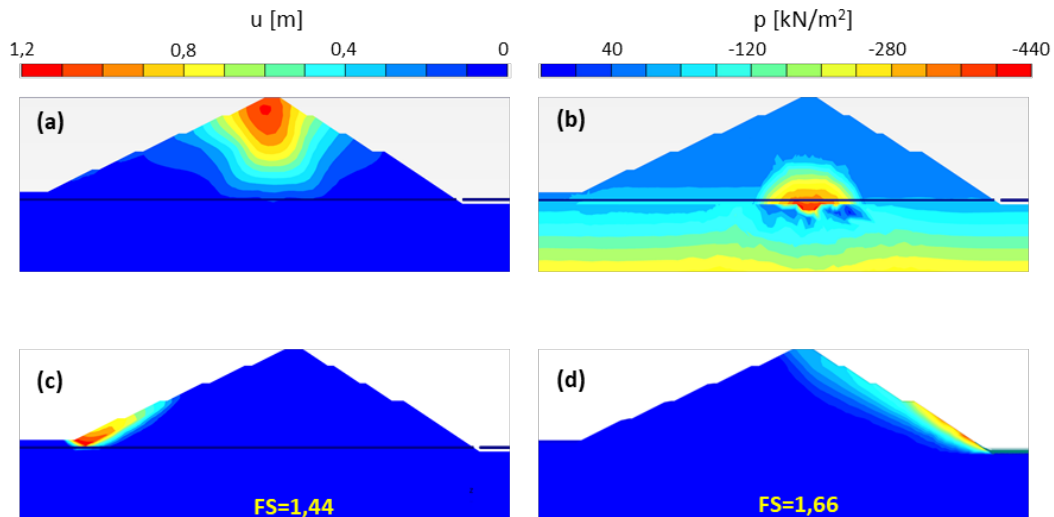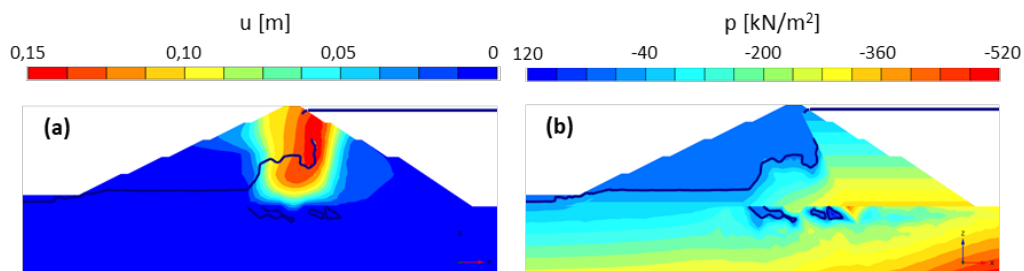

Figure 8. (a) Total displacements (u) after the construction of the dam (365 days); (b) pore pressures (p) after the construction of the dam.
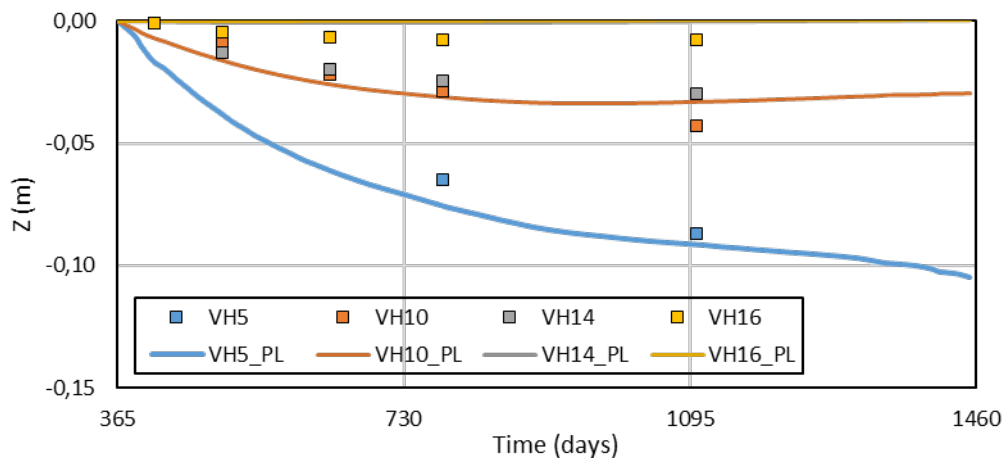
Figure 9. Model calibration: Numerically-predicted compared to measured settlement.

4.4 *The appearance of the wet zone (1461-7851 days)*

The wet spot is a result of pipeline leakage. In the numerical model, the leakage discharge is modelled as a constant discharge of water infiltrating from the well (leaking pipeline) into the dam body, illustrated in Fig. 6 with a blue line. The wet spot was observed on 24/10/2007 (7851th day). The time initiation of the leakage and the corresponding flow is unknown. To that end, it was assumed that the pipe leakage started on the 5000th day, while the water volume leaked per day (q) was in the range of 0.1 to 1.5 m^3/day.

Figure 10a compares the predicted piezometric head at K3 to the corresponding monitoring results (red line). The black line shows the piezometric head for $q = 0$ m^3/day. The piezometric head is under-predicted by 1 m, and the same applies to its evolution with time. To that end, the

calculation was repeated for a higher core permeability equal to k = 4·10⁻⁹ m/s (Fig. 10b). In this case, the piezometric head inclination is better predicted, indicating that the core permeability may actually be higher than the value considered.

The pipeline leakage leads to an increase of the piezometric head in the dam body (zone C). As expected, the increase is faster for higher water discharges. However, when the piezometric head reaches a critical height of 75 m (Fig. 10c,d), the failure mechanism on the downstream shell is triggered (Fig. 7c). Hence, in the hypothetical scenario where the reservoir level had not be lowered (remaining constant at 98.8 m asl elevation), the continuous water infiltration through the leakages in the pipelines would lead to a continuous increase of the phreatic line within the dam body, leading the dam to an unavoidable failure.
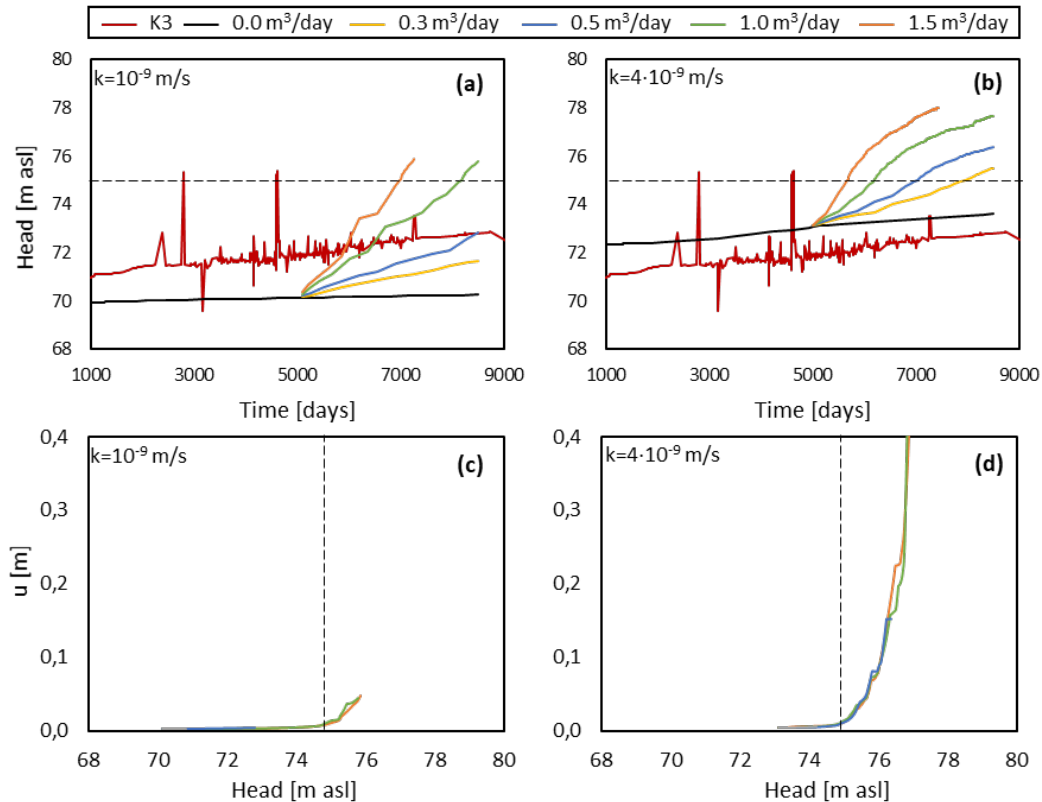
Figure 10. Monitored and calculated piezometric head at K3 for: (a) k = 10⁻⁹ m/s; and (b) k = 4 x 10⁻⁹ m/s. Predicted total displacement at VH18 versus calculated piezometric head at K3 for: (c) k =10⁻⁹ m/s; and (d) k = 4 x 10⁻⁹ m/s.

4.5 *Remedial works and future reservoir level to the maximum level (7852-13461 days)*

The reservoir level after the appearance of the wet zone is considered in accordance to Fig. 4. Seepage and stability analysis was carried out, assuming that the pipe leakage terminated after the filling of the irrigation pipe with concrete. The phreatic line within the dam body, along with the horizontal displacement, are illustrated in Fig. 11 for the time when: (I) the wet zone spotted; (II) the reservoir was lowered to 92 m asl; (III) the reservoir was lowered to 82 m asl; and (IV) the reservoir was refilled to the maximum level of 98.8 m asl.

Figure 12 illustrates the vertical profile of the calculated horizontal displacement (u_x) at the core when: (I) the wet zone was spotted; (II) the reservoir was lowered to 92 m asl; (III) the reservoir was lowered to 82 m asl; and (IV) after the final refill of the reservoir to the maximum level of 98.8 m asl. It is observed that with the depletion of the reservoir (I to III), the dam deforms towards the upstream shell (negative direction) and the direction of displacement becomes positive again (towards the downstream shell) with the final refill of the reservoir (IV).
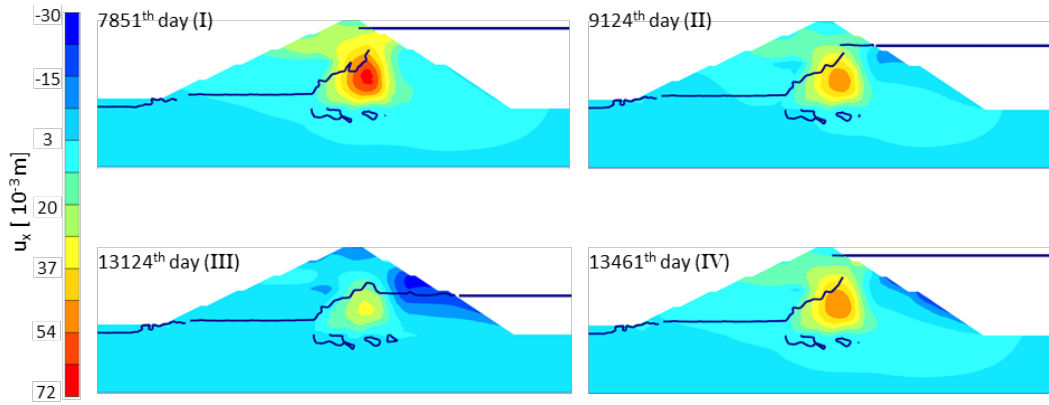
Figure 11. Calculated horizontal displacement (u_x) and phreatic line at the time when: (I) the wet zone spotted; (II) the reservoir was lowered to 92 m asl; (III) the reservoir was lowered to 82 m asl; and (IV) after the refill of the reservoir to the maximum level of 98.8 m asl.
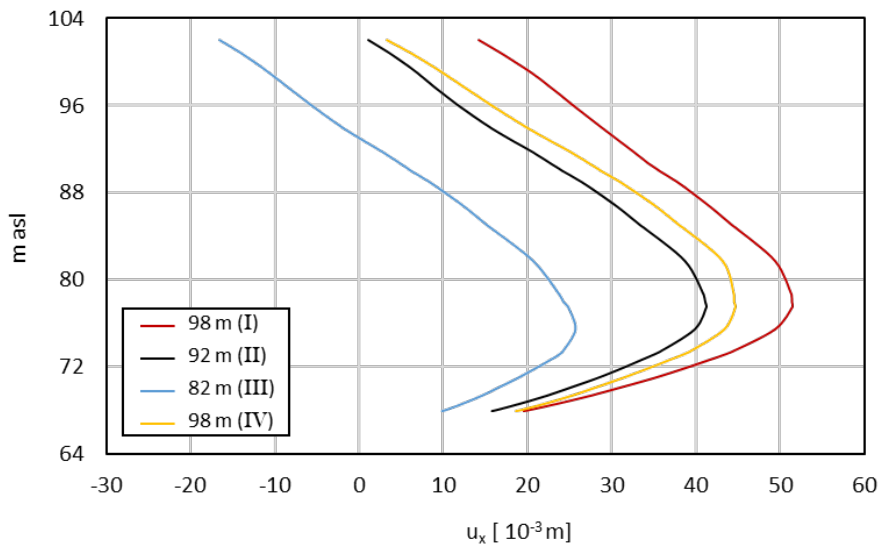
Figure 12. Vertical profile of the calculated horizontal displacement (u_x) at the core when: (I) the wet zone spotted; (II) the reservoir was lowered to 92 m asl; (III) the reservoir was lowered to 82 m asl; and (IV) after the refill of the reservoir to the maximum level of 98.8 m asl.

5 CONCLUSIONS

A 35 m high embankment dam located in Slovenia was considered. The dam is a zoned rockfill dam with a clay core and is based on a mainly impermeable foundation, which was grouted as needed. The irrigation pipeline and two bottom outlet pipelines, which are leading through the embankment dam in its central part corroded during the years and got leaky. In an emergency response, the operating level of the reservoir was lowered to allow for remediation work to take place; its refilling is planned in the future.

The behaviour of the dam throughout a period of 36 years is analysed employing a fully coupled hydromechanical numerical analysis. A 3D numerical model of the dam was developed in the finite element program PLAXIS3D and seepage and stability analyses were carried out. The dam soil zones were modelled with the Hardening Soil Small Strain Model, which can reproduce many of the key aspects of nonlinear soil response, but cannot capture soil softening. This is undeniably a limitation, but considering the lack of experimental data required for accurate model calibration, it is considered acceptable. In particular, considering the complexity of the problem, high quality information (experimental data, construction history, material information) is

necessary. In the absence of such data, model parameters were calibrated through back analysis of monitored deformation and pore pressure data. To that end, the presented results are considered a conceptual simplification of the problem, rather than an accurate reproduction of the dam case history.

REFERENCES

Brinkgreve, R.B.J., Bakker, K.J. and Bonnier, P.G. 2006. The relevance of small-strain stiffness in excavation and tunnelling projects. In: H.F. Schweiger (ed.) Numerical Methods in Geotechnical Engineering. Taylor & Francis. 133–139.

Plaxis (2019) Material models manual https://www.plaxis.com/support/?category=1100

Schanz T,Vermeer A, Bonnier P (1999) The hardening soil model: formulation and verification. In: Proceedings of beyond 2000 computational geotechnics 10 years PLAXIS, Rotterdam, The Netherlands, pp 281–296

Žvanut, P.; Likar, B.; Likar, Ž.; Selan, V. & Klun, M. 2021. 16th International Benchmark Workshop on Numerical Analysis of Dams, 5.-7. April 2022, organized by the ICOLD Committee on Computational Aspects of Analysis and Design of Dams. Theme C: Behaviour of the Embankment Dam. Ljubljana, Slovenia.

PREDICTION OF THE FUTURE BEHAVIOUR OF THE EXISTING DAM, BASED ON THE RESULTS OF AUSCULTATION MEASUREMENTS

Dajana Biorac

Enegroprojekt – Hidroinženjering Consulting Engineers Co, Belgrade, Republic of Serbia

ABSTRACT: In this paper, two-dimensional modeling of the existing dam was performed in order to determine the characteristics of the material from which the dam was built, as well as to assess the current state of the dam and to predict the behavior of the dam in the future. The material characteristics were adopted so that the benchmark movements and phreatic line in the dam body correspond to the measured in-situ values. The numerical analysis considered different situations during the operation of the dam and for each of them a stability assessment was provided.

Key words: dam, calibrated material properties, wet strain, slope stability.

1 INTRODUCTION

This paper presents numerical modeling of the behavior of the earth-fill dam, in which signs of wetting appeared on the downstream slope during operation.

Namely, it is a zoned earth-fill dam, whose cross section is displayed in Figure 1.

The dam was built in 1989 for agriculture purposes (irrigation) and flood protection. The dam is founded on an impermeable Eocene flysch. The construction lasted less than a year. The reservoir has been fully filled within about 18 (eighteen) months after construction completion. After 20 (twenty) years of operation, the wet spot was noticed on the dam's downstream slope during regular maintenance.

The main technical data of the dam are:
- Dam height above foundation: 34.6 m;
- Elevation of the dam crest: 102.00 m asl;
- Elevation of the foundation: 67.40 m asl;
- Crest width: 5 m;
- Base width: 120 m;
- Crest length: 174 m;
- Normal Water Level: 98.8 m asl.

2 NUMERICAL ANALYSIS

The basic monitoring system of the dam was established already during construction and immediately after the construction of the dam was completed. The results of auscultation measurements were used in numerical analysis for model calibration. After calibration, a prediction of the dam's future behavior was made.

All calculations were performed by the finite element method using the Geo-Studio 2018 software package, i.e., its programs: Slope / W (stability calculations), Seep / W (filtration calculations), Sigma / W (stress-strain analysis).

Numerical analysis was performed for the following cases, which will be described individually in the following chapters:
- case – Dam after construction
- case – First filling
- case – Occurrence of the wet spot
- case – Remedial works

Analyzes were performed on two-dimensional models.

Figure 1. Typical cross-section of the dam, gde je: A – clayey silt material; B – rockfill material; C – limestone and sandstone blocks; D – impermeable rock base; E – filter material; 1 – intake tower; 2 – intake structure; 3 – bottom outlets; 4 – irrigation pipeline; 6 – maximal reservoir level (100.5 m asl); 7 – minimal operating level (80.0 m asl); 8 – normal operating level (98.8 m asl); 9 – depleted operating level (92.0 m asl).

3 DAM AFTER CONSTRUCTION

In this part of the numerical analysis, the calibration of the material parameters, adopted by the design, was performed (Table 1) - so that the displacement values are obtained, which

correspond to the measured displacements of geodetic benchmarks immediately after the construction of the dam.

Table 1. Design material properties

Material	w	γ	cu	φ	c	Eoed	E	ν	k
	%	kN/m³	kPa	°	kPa	MPa	MPa	-	m/s
A'	13	21	-	36	36	15	-	0.4	10^{-6}
A	16	19.5	75	-	-	5	-	0.5	10^{-9}
B	-	24	-	38	-	50	-	0.3	10^{-3}
C	-	24	-	38	-	50	-	0.3	10^{-4}
D	-	25	-	39	32	-	620	0.25	10^{-9}

where w is soil moisture; γ – specific gravity; cu – undrained shear strength; φ – angle of internal friction; c – effective cohesion; Eoed – oedometric modulus; E – elastic modulus; ν – Poisson coefficient; k – permeability

In the numerical analysis, the construction of the dam was simulated in 37 steps in the program GeoStudio - Sigma / W (Figure 2). The "Coupled Stress / PWP" analysis was applied, which can be used to determine, in addition to the primary settlement, consolidation settlement as well.

The following boundary conditions were adopted (Figure 2):
1) the lower limit is a fix in the X and Y directions, 2) the left and right borders are a fix in the X direction, 3) the piezometric level is adopted on the terrain surface. The duration of one step t1 = 9 days was adopted, so that the total duration of the dam embankment is: t = 9 days · 37 steps = 333 days.

The parameters of the material, for which the displacements at the benchmarks closest to the in-situ displacements are obtained, are shown in Table 2.

Table 2. Calibrated material properties

Material	γ	cu	φ	c	E	ν	wc	M_v	k
	kN/m³	kPa	°	kPa	MPa	-	-	1/kPa	m/s
A1	21	-	36	36	25	0.35	0.10	$4 \cdot 10^{-5}$	$1 \cdot 10^{-6}$
A*	19.5	70	-	-	20	0.45	0.20	$5 \cdot 10^{-5}$	$2 \cdot 10^{-11}$
A2*	19.5	100	-	-	25	0.37	0.20	$4 \cdot 10^{-5}$	$2 \cdot 10^{-11}$
A3*	19.5	150	-	-	30	0.37	0.20	$3.33 \cdot 10^{-5}$	$2 \cdot 10^{-11}$
A4*	19.5	100	-	-	20	0.39	0.20	$5 \cdot 10^{-5}$	$2 \cdot 10^{-11}$
B	24	-	38	-	50	0.30	-	$2 \cdot 10^{-5}$	$1 \cdot 10^{-3}$
C	24	-	38	-	50	0.28	-	$2 \cdot 10^{-5}$	$1 \cdot 10^{-4}$
D	25	-	39	100	620	0.25	0.20	$1.6 \cdot 10^{-6}$	$1 \cdot 10^{-9}$

where γ - is specific gravity; cu – undrained shear strength; φ – angle of internal friction; c – effective cohesion; E – elastic modulus; ν – Poisson coefficient; wc – saturated volumetric water content; m_v – compressibility; k – permeability

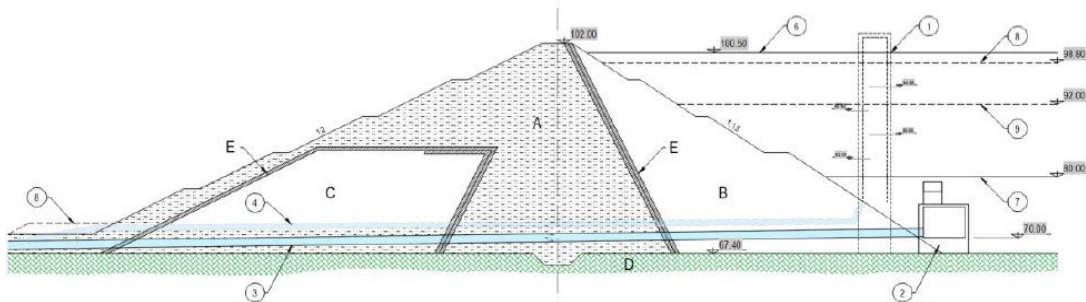*Zone A (clayey silt material) is divided on to subzones: A, A2, A3 i A4
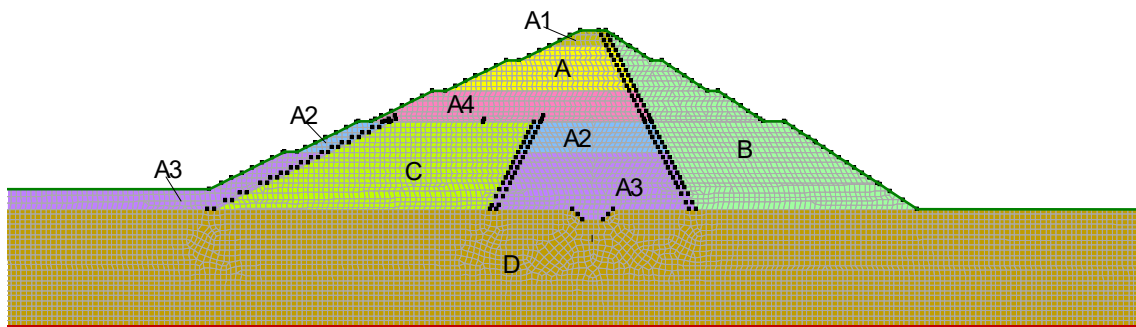
Figure 2. Calculation model, where: A – clayey silt material; B – rockfill material; C – limestone and sandstone blocks; D – impermeable rock base; E – filter material

The comparison of the results of numerical analysis with the values of the displacement of geodetic benchmarks at the end of the dam construction, is shown in Table 3.

Table 3. The displacements of the geodetic benchmarks (mm)*

Bench Mark	Numerical analysis		Readings in-situ 23-01-88	
	Y	Z	Y	Z
BM5	0	0	0	0
BM10	10.53	-22.76	-38	-22
BM14	25.61	-17.3	-28	-20
BM16	20.13	-8.86	-18	-7

* The convention is adopted in the table: Y displacements are horizontal displacements positive in the upstream-downstream direction; Z displacements are vertical displacements positive in the down-up direction.

The calculation of the stability of the slopes was performed by the finite element method, using the program GeoStudio-Slope / W. The minimum safety factors for the upstream and downstream slope, immediately after the completion of the dam construction are as follows:

Table 4. Dam stability after construction completion

Slope	FS
Upstream	1.416
Downstream	2.187

4 FIRST FILLING

The calculation model uses water level fluctuation, based on real measurements. To calibrate the values of the water permeability coefficients of the material in the composition of the dam, water level readings on piezometers K2 and K3 were observed. In Table 2, lower values of water permeability coefficients for clay material were adopted in relation to the projected values (Table 1).

Figure 3. Water level at piezometers K2 and K3 - results obtained by numerical analysis and values obtained by in-situ measurements

Water levels at piezometers K2 and K3, obtained by numerical analysis, align very well with measured values at piezometers K2 and K3.
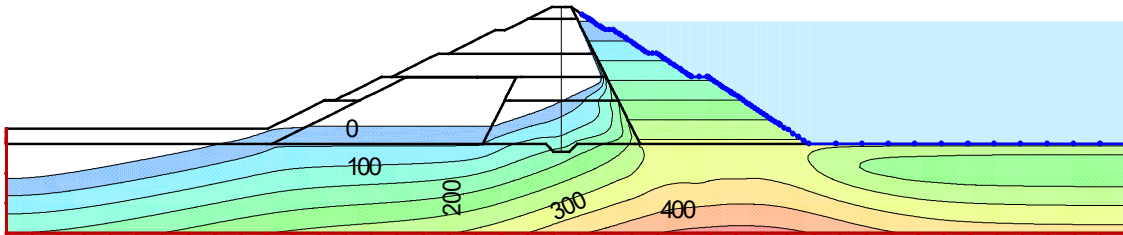
Figure 4. Piezometric line at the end of first filling

It can be noticed that piezometric line does not break through downstream slope plain at the end of first filling and that there is no significant change in dam stability in relation to "dam after construction" case.
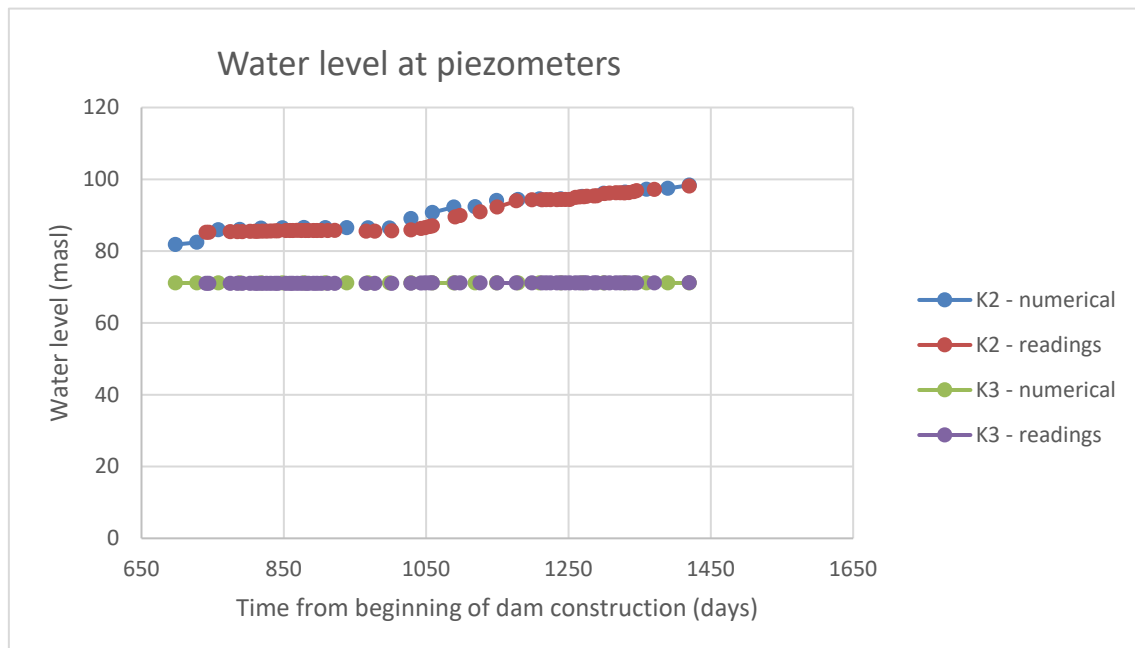
Table 5. Dam stability during first filling

Slope	FS
Upstream	1.376
Downstream	2.281

5 OCCURRENCE OF THE WET SPOT

After 20 (twenty) years of operation, the wet spot was noticed on the downstream slope of the dam during regular maintenance. The wet spot was located at the downstream toe of the dam in the central part, close to the axis of the dam. Extensive vegetation on the central part of the embankment dam indicated that the humid zone extends to the downstream slope of the dam above the wet spot. Emergency investigation revealed that excessive water on the downstream slope originates in the reservoir.

The change in the reservoir water level until the moment when the wet strain is noticed, is displayed in Figure 6.

The numerical model shown in Figure 2, displays correspondence of the real field conditions for the period after 20 years of operation, with the application of an upstream hydraulic boundary condition corresponding to real changes in the accumulation levels (Figure 6).

Therefore, without changes in material parameters and without changes of boundary conditions in relation to the ones used for the "dam after construction" case - the piezometric line does break through the downstream slope plain. This means that the dam had been built using such materials that the wet spot on the downstream slope plain is expected to appear, without any additional damages (pipe corrosion or internal erosion).
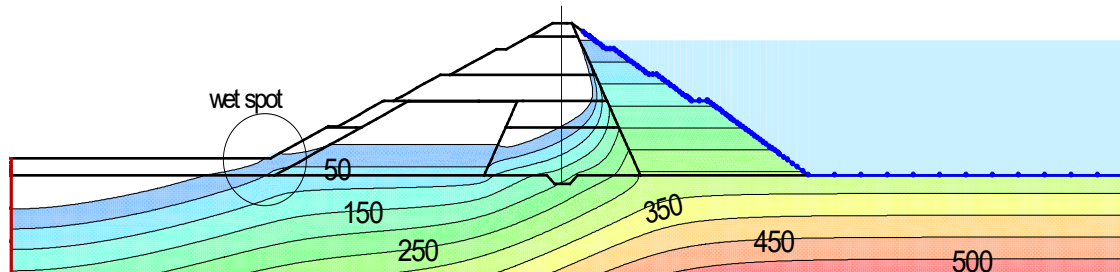
Figure 5. Piezometric line in the dam after 20 years of operation
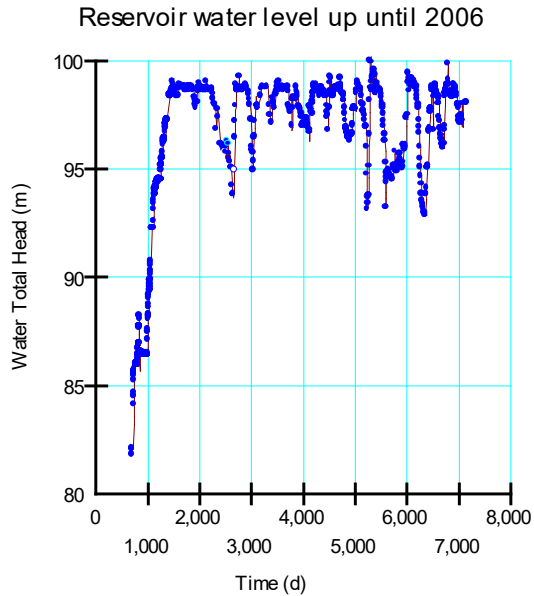
Figure 6. Reservoir water level up until occurrence of the wet spot

The minimum safety factor for the upstream and downstream slopes, for the period up to the wet strain occurrence, is shown in the following table 6.

Table 6. Dam stability up until the occurrence of the wet strain

Slope	FS
Upstream	1.41
Downstream	2.279

6 REMEDIAL WORKS

In 2008 the reservoir level was lowered to a maximum of 93.6 m asl and the irrigation pipeline was filled with the concrete. The space between the irrigation pipeline and the concrete cover was grouted with the cement grout. After this emergency remediation, the reservoir operational level was additionally lowered to a 92.0 m asl.

It is foreseen to fill all the pipes within the dam body, with concrete during the rehabilitation works, after which the reservoir water level would return to 98.8 m asl.

The value of the water permeability coefficient around the irrigation pipe was increased to k = 10^{-8} m/s in the numerical analysis. This assumption was introduced due to the possible change of the clayey material due to the lowering of the water level in the accumulation, as well as due to the migration of the clayey material particles through the corroded irrigation pipe.

In addition, due to the closure of the irrigation pipe with concrete, as well as due to the grouting of the zone around the pipe - the value of the water permeability coefficient in material C (limestone and sandstone blocks) was reduced to k = 10^{-8} m/s also in the zone around the pipe (Figure 7. and Table 7).

Figure 7. Construction model after remedial works

Table 7. Material properties after remedial works

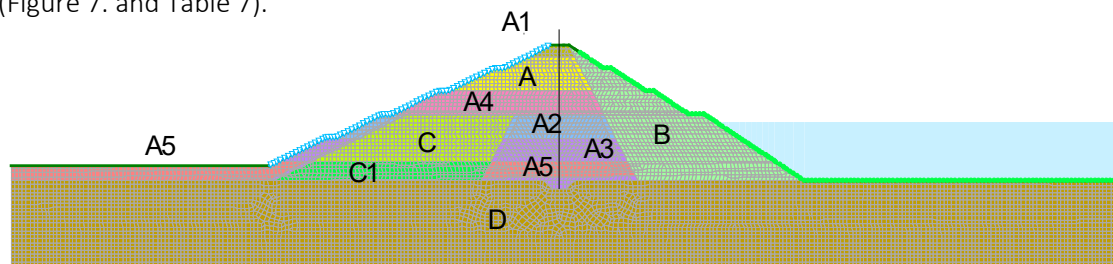| Material	γ	cu	φ	c	E	ν	wc	M_v	k
	kN/m^3	kPa	°	kPa	MPa	-	-	1/kPa	m/s
A1	21	-	36	36	25	0.35	0.10	$4 \cdot 10^{-5}$	$1 \cdot 10^{-6}$
A*	19.5	70	-	-	20	0.45	0.20	$5 \cdot 10^{-5}$	$2 \cdot 10^{-11}$
A2*	19.5	100	-	-	25	0.37	0.20	$4 \cdot 10^{-5}$	$2 \cdot 10^{-11}$
A3*	19.5	150	-	-	30	0.37	0.20	$3.33 \cdot 10^{-5}$	$2 \cdot 10^{-11}$
A4*	19.5	100	-	-	20	0.39	0.20	$5 \cdot 10^{-5}$	$2 \cdot 10^{-11}$
A5*	19.5	100	-	-	20	0.39	0.2	$5 \cdot 10^{-5}$	$\mathbf{1 \cdot 10^{-8}}$
B	24	-	38	-	50	0.30	-	$2 \cdot 10^{-5}$	$1 \cdot 10^{-3}$
C**	24	-	38	-	50	0.28	-	$2 \cdot 10^{-5}$	$1 \cdot 10^{-4}$
C1**	24	-	38	-	50	0.28	-	$2 \cdot 10^{-5}$	$\mathbf{1 \cdot 10^{-8}}$
D	25	-	39	100	620	0.25	0.20	$1.6 \cdot 10^{-6}$	$1 \cdot 10^{-9}$

where γ is specific gravity; cu – undrained shear strength; φ – angle of internal friction; c – effective cohesion; E – elastic modulus; ν – Poisson coefficient; wc – saturated volumetric water content; m_v – compressibility; k – permeability

*Zone A (clayey silt material) is divided on to subzones: A, A2, A3, A4 i A5

**Zone C (limestone and sandstone blocks) is divided on to subzones C i C1
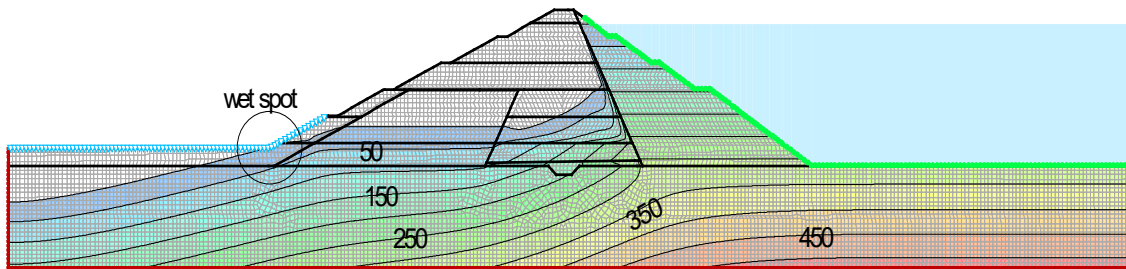
Figure 8. Piezometric line in the dam body after remedial works

The minimum stability factors for the upstream and downstream dam slope, after remedial works, are displayed in Table 8.

Table 8. Dam stability after remedial works

Slope	FS
Upstream	1.337
Downstream	1.719

7 CONCLUSION

This paper treats the two-dimensional modeling of the existing dam. The designed characteristics of the dam materials were calibrated based on the measured values of in-situ displacements.

The values of the vertical displacements, at the end of dam construction, are quite similar to the measured in-situ values at the places of reference, while there are significant deviations with the horizontal displacements. This anomaly can be explained by the limited accuracy of the 2D modeling of the objects with a three-axis stress state.

The water permeability coefficients of the dam materials were calibrated so that the water levels at the piezometers K2 and K3 correspond to the measured ones.

Numerical analysis treats the following cases during the exploitation of the dam:

1) Dam after construction, 2) First filling, 3) Occurrence of the wet spot, 4) Remedial works.

Slope safety factors for each case are displayed in Table 9.

Table 9. Dam stability for different calculation cases

Slope works	Dam after construction	First filling	Occurrence of the wet spot	Remedial
Uprstream	1.416	1.376	1.41	1.337
Downstream	2.187	2.281	2.279	1.719

Considering the conducted detailed numerical analysis, using the available data in regards to the movements of the benchmarks on the dam and in regards to the phreatic line levels in the dam body, it can be concluded that the wetting of the lower part of the downstream slope plain would occur even without the additional damages in the dam (pipe corrosion and the internal erosion). Therefore, by using the materials of certain characteristics in a manner it has been done on the subject dam, it is expected after 20 years of exploitation for the raised phreatic line level to occur on the lower part of the downstream slope. If internal erosion is not present, dam stability is not compromised (table 9), and phreatic line level could be lowered with the construction of the vertical drainage curtain, next to the lower part of the downstream slope.

Certainly, for the final verdict on the evaluation of the dam and effects of the applied measures, more results of the additional investigations are necessary: results of the laboratory tests of the samples from the dam body and foundations, installation and monitoring of the additional piezometers, acquiring data of vertical and horizontal movements inside the dam body, quantity and composition of the phreatic water on the springs downstream of the dam.

REFERENCES

Geo-Slope International Ltd, 2021. Stability Modeling with GeoStudio
Geo-Slope International Ltd, 2021. Stress-Strain Modeling with GeoStudio
Fell R., MacGregor P., Stapledon D., Bell G., 2005. Geotechnical Engineering of Dams
ICOLD B155, 2012. Guidelines for use of Numerical Models in Dam Engineering

SEEPAGE AND STABILITY ANALYSES OF A ZONED EARTH DAM SUBJECTED TO VARIABLE WATER HEADS: NUMERICAL SIMULATIONS WITH ABAQUS

Nicola Pontani

Department of Civil and Environmental Engineering, Politecnico di Milano, Milano, Italy

Chiara Rossignoli

Department of Civil and Environmental Engineering, Politecnico di Milano, Milano, Italy

Donatella Sterpi

Department of Civil and Environmental Engineering, Politecnico di Milano, Milano, Italy

Cristina Jommi

Department of Geoscience and Engineering, Delft University of Technology, Delft, The Netherlands
Department of Civil and Environmental Engineering, Politecnico di Milano, Milano, Italy

ABSTRACT: The behaviour of a zoned earthen dam is analysed by means of a finite element model implemented in Abaqus. The analysed dam was built in Slovenia at the end of the 1980s for irrigation and flood protection purposes. In 2007, detection of a wet stain on the downstream slope forced the drawdown of the reservoir to carry out remedial works. Transient fully coupled hydro-mechanical analyses under partially saturated conditions have been conducted to investigate the behaviour of the dam from its construction to present. Available in-situ measurements have been exploited to calibrate the model and to assess the reliability of the predictions. To address the effects of the wet stain and of the remedial works on the dam body, stability analyses have been performed at significant times. Future scenarios have been analysed, using provided information on the time schedule of the reservoir impounding after completion of the remedial works. The results show that the high pore water pressures measured inside the dam body may be explained by damage experienced by the irrigation pipelines and that remedial works are necessary to restore the dam functionality.

Pontani, Rossignoli, Sterpi, Jommi

SEEPAGE AND STABILITY ANALYSES OF A ZONED EARTH DAM SUBJECTED TO VARIABLE WATER HEADS:
NUMERICAL SIMULATIONS WITH ABAQUS

1 INTRODUCTION

Embankment dams represent over 80% of dams built in the world (Wrachien & Mambretti 2009) and approximately 40% of all embankment dam failures have been attributed to internal erosion due to uncontrolled seepage through the dam body (ICOLD 2017). During construction and operation, embankments are in a partial saturation condition, and they are subjected to various hydro-mechanical loads following from consolidation and from time variations of the reservoir water level. To properly account for all the aspects that contribute to the response of the system, coupled hydro-mechanical numerical analyses are necessary. The development of the numerical model should be supported by appropriate monitoring data. The comparison between numerical results and site observations will validate the approach and help in the calibration of the model for predictive purposes. The Formulators proposed the present benchmark to assess how different modelling assumptions and approaches could match the observations.

To simulate this benchmark, 2D finite element numerical analyses have been run with Abaqus 6.23 (Dassault Systèmes 2021). Fully coupled hydro-mechanical analyses in a three-phase porous media (Zienkiewicz et al. 1990) have been conducted to study the problem.

The focus has been on explaining the cause of a wet stain, detected on the downstream slope of the dam during regular maintenance in 2007, after twenty years of operation. Back analyses have been performed to calibrate the numerical model (case 1), where missing information was managed on engineering judgement. The comparison between numerical results and monitoring data at relevant time instants has allowed validating the model and has suggested including a defect in the pipe system (case 2). Eventually, the future state of the dam has been analysed when subjected to the given hydraulic load history (case 3).

2 MODEL DESCRIPTION

2.1 Geometry

The dam investigated in the benchmark is a zoned earth dam, with a clay core. Figure 1 shows the domain assumed for the analyses: the geometry of the dam has been defined based on the schematic 2D cross-section provided by the Formulators (Zvanut et al. 2022), while the dimensions of the foundation layer have been chosen as 245x30m. In the same figure, the finite element mesh considered in the analyses is shown. The numerical solution has been obtained using fully coupled pore pressure-displacement elements with reduced integration (CPE8RP).
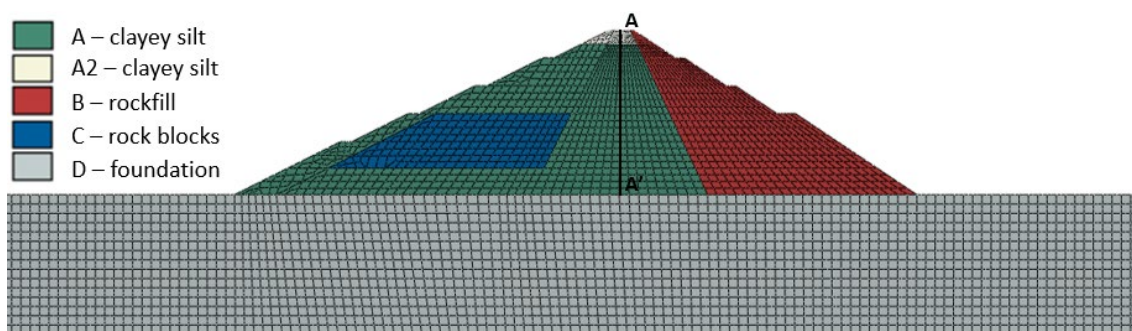
Figure 1. 2D geometry considered in the analyses. Different colours depict the 5 materials of the model. Section A-A' represents the central vertical axis of the dam, where significant quantities will be analysed in the following.

2.2 Material behaviour and properties

An elastic-perfectly plastic Mohr-Coulomb model has been used to model the behaviour of the different materials. Mechanical and hydraulic properties have been defined combining information provided by the Formulators with results of back-analyses. The values of the relevant

Pontani, Rossignoli, Sterpi, Jommi

SEEPAGE AND STABILITY ANALYSES OF A ZONED EARTH DAM SUBJECTED TO VARIABLE WATER HEADS:
NUMERICAL SIMULATIONS WITH ABAQUS

parameters adopted in the numerical simulations are listed in Table 1, where ρ_d is the dry density, c and ϕ are the shear strength parameters, ψ is the dilatancy angle, E is the Young modulus, ν is the Poisson ratio and k is the saturated hydraulic conductivity. The calibration stage has focused on the clay core material A. Drained values of shear strength parameters have been assumed starting from information on the nature and the state of the soil, while stiffness and hydraulic conductivity have been calibrated as described in the following paragraphs. To include the unsaturated response, water retention curves and hydraulic conductivity functions have been defined for fine and coarse materials, thus providing the relations between suction, degree of saturation and hydraulic conductivity, as shown in Figure 2. The choice of the specific relationships adopted in the analyses has been based on literature studies (Alonso et al. 2005, Caruso & Jommi 2005, Rossignoli & Sterpi 2021).

Table 1. Material properties after the calibration.

Zone	rd	c	f	ψ	E	n	k
	[kg/m3]	[kPa]	[°]	[°]	[MPa]	[-]	[m/s]
A	1578.0	10.0	30.0	20.0	11.0	0.30	10^{-8}
A2	1894.0	36.0	36.0	24.0	7.0	0.40	10^{-6}
B	2267.0	0.0	38.0	25.0	37.0	0.30	10^{-3}
C	2267.0	0.0	38.0	25.0	37.0	0.30	10^{-4}
D	2407.0	32.0	39.0	26.0	62.0	0.25	10^{-9}
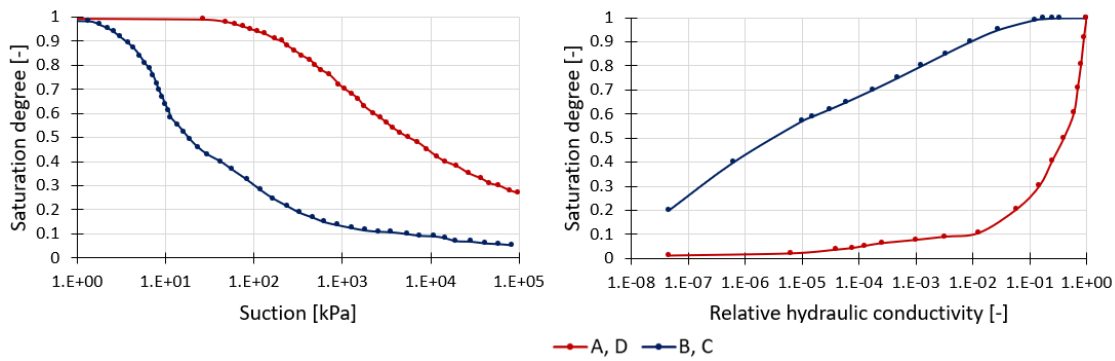
Figure 2. SWRCs (on the left) and permeability functions (on the right) assumed for fine materials (A and D, in red) and coarse ones (B and C, in blue).

2.3 *Time dependent seepage analyses*

The reservoir water level at the upstream side of the dam is modelled as a time-dependent boundary condition enforced on the pore-pressure field. The recorded water levels as well as the approximate time-history simulated in the analyses are represented in Figure 3.
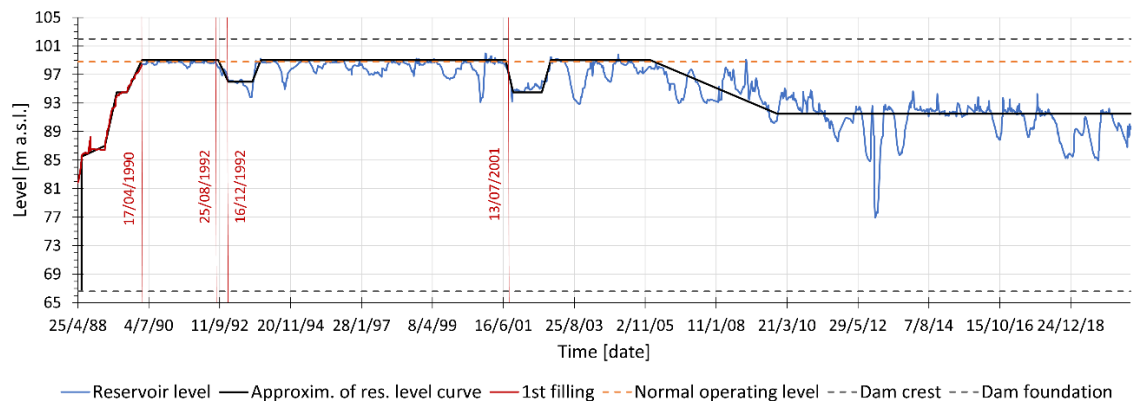
Figure 3. Time evolution of reservoir level from 1988 to 2020: recorded values (blue line) and approximate time-history simulated in the analyses (black line). Significant dates indicated with red lines refer to Case1-Task2.

Pontani, Rossignoli, Sterpi, Jommi

SEEPAGE AND STABILITY ANALYSES OF A ZONED EARTH DAM SUBJECTED TO VARIABLE WATER HEADS:
NUMERICAL SIMULATIONS WITH ABAQUS

2.4 *Stability analyses*

The stability of the system has been assessed according to the Shear Strength Reduction (SSR) method (Matsui & San 1992, Griffiths & Lane 1999), by reducing c and ϕ until failure occurs. The failure mechanism is identified by a localisation of shear strains. According to this method, the Safety Factor FS plays the role of a shear strength reduction ratio and is evaluated as:

$$FS = c/c_r = \tan\phi/\tan\phi_r \qquad (1)$$

where c_r and ϕ_r are the reduced shear strength parameters.

3 RESULTS AND DISCUSSIONS

3.1 *Case 1*

Case 1 simulates the construction of the dam, the first filling of the reservoir as well as its operating conditions before leakage is detected. Numerical results are compared with field monitoring data and the stability of the dam is checked at significant time instants.

3.1.1 Task 1: dam construction

At the beginning of the analysis, the water table coincides with the ground surface and the geostatic effective stress state is assigned to the foundation layer. The construction of the dam is reproduced by a gradual growth of the gravity loading, maintaining a constant level of the water table. Due to capillary rise, this condition leads to partial saturation of the dam body (Fig. 4). To obtain realistic settlements of the whole dam body, the stiffness of material A has been calibrated as E=11 MPa. The horizontal and vertical displacements along section A-A' at the end of the construction are reported in Figure 5a and 5b, respectively. According to the sign convention established by the Formulators, the horizontal displacements in the downstream direction are positive, while settlements are negative. The maximum settlement of about 0.80 m is observed slightly below the dam crest.

Stability of both the downstream and upstream slopes of the dam before the first filling of the reservoir is evaluated by means of the SSR method. The results show that the FS of the downstream slope is greater than the one of the upstream slope (Tab. 2). The reason lies on the fact that the downstream mechanism crosses materials with high cohesion and that the downstream slope has a lower inclination with respect to the upstream one. Figure 6 reports the contours of deviatoric plastic strains, which indicate the predicted failure surfaces in the two cases.
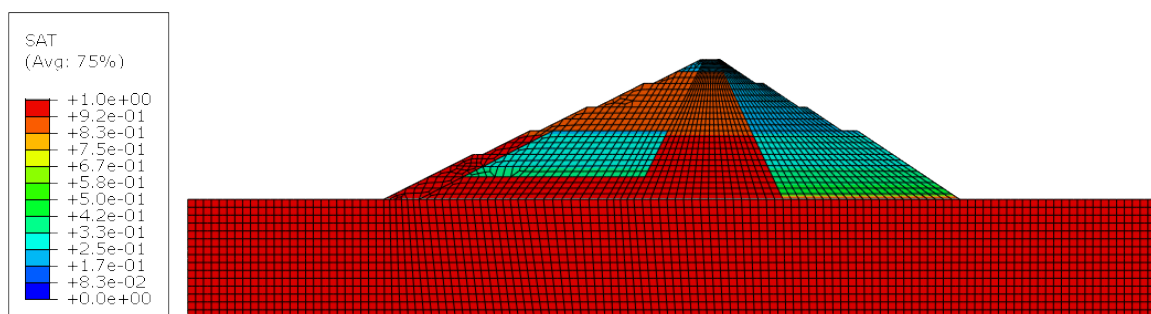

Figure 4. Contour of the degree of saturation at the end of the construction.

Pontani, Rossignoli, Sterpi, Jommi

SEEPAGE AND STABILITY ANALYSES OF A ZONED EARTH DAM SUBJECTED TO VARIABLE WATER HEADS:
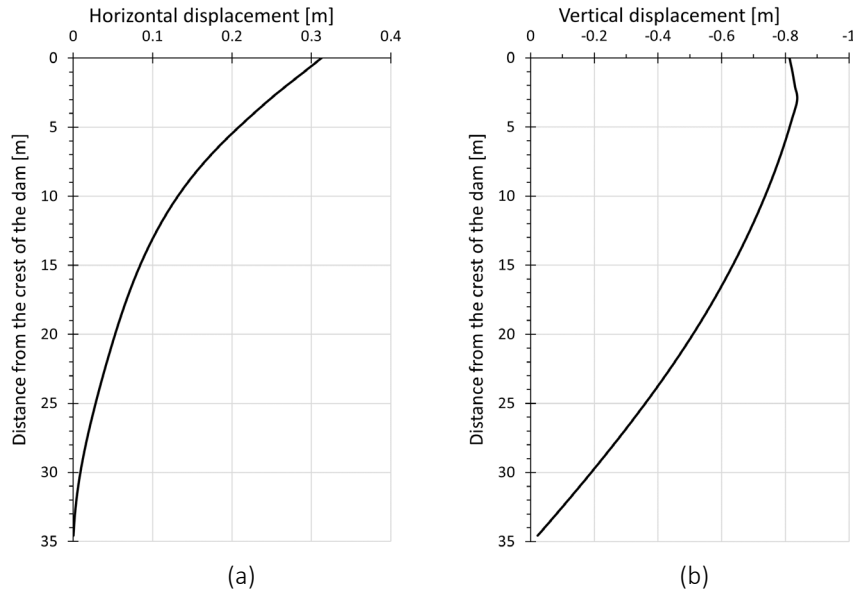NUMERICAL SIMULATIONS WITH ABAQUS

Figure 5. Horizontal (a) and vertical (b) displacement along direction A-A' at the end of the construction.
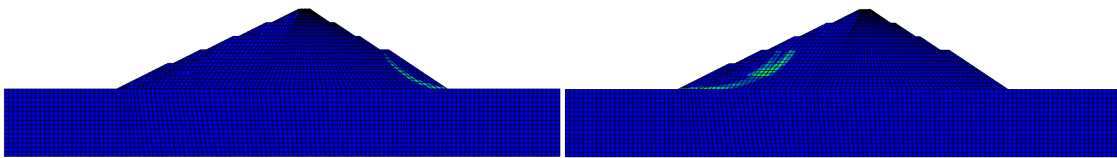

Figure 6. Contour of the plastic deviatoric strain showing the sliding surfaces at upstream (on the left) and downstream (on the right) slope.

3.1.2 Task 2: first filling and operating conditions

The simulation of the construction stage aims at reproducing the state of the dam before the filling of the reservoir, started on 25/04/1988 and lasted for 722 days. To simulate the initial conditions of the system, the water level is increased from the ground surface to the position indicated as the beginning of the filling, at around 82 m a.s.l. Since there is no information about the duration of this phase, a steady-state analysis is performed.

Starting from this situation, the water level in the reservoir is gradually raised, following the temporal evolution shown in Figure 3. Coupled hydro-mechanical analyses under transient conditions are performed, to predict the variations in time of the stress – strain state as well as the pore water pressure regime within the dam.

The temporal evolution of the pore pressure for two nodes is represented in Figure 7. These points are located at the base of the two piezometers, K2 and K3, whose data are reported as well. A free drainage condition was assigned to simulate the presence of drains between the clay core and the rockfill material, as shown in Figure 8. The calculated pore water pressures tend to reach values close to those recorded in piezometer K3. However, the numerical predictions underestimate the pore pressure in correspondence of the position of piezometer K2, although the same trend can be appreciated.

To better understand the source of the difference between the predicted and the observed pore pressure at K2, the latter is compared in Figure 7 with the pore pressure at the same depth corresponding to the current hydraulic head of the reservoir. It can be observed that the two almost coincide, suggesting that the loss in the hydraulic head between the reservoir and the section of the nucleus where the pore pressure is measured is negligible.

Notwithstanding this difference, the numerical model is able to respond appropriately to the enforced temporal variations in the boundary conditions, as shown over the two periods of decrease and increase of the water height in the reservoir reported in Figure 7. This means that

Pontani, Rossignoli, Sterpi, Jommi

SEEPAGE AND STABILITY ANALYSES OF A ZONED EARTH DAM SUBJECTED TO VARIABLE WATER HEADS:
NUMERICAL SIMULATIONS WITH ABAQUS

the assumptions made in terms of hydraulic properties in saturated and unsaturated conditions are satisfactory.

Figure 9 shows the increment of vertical displacements measured in the geodetic points and simulated through the numerical analyses starting from 06/06/1988. The measured displacements indicate that settlement occurred during the impounding of the reservoir, while the results of the numerical analyses show an opposite trend. This difference originates from the adopted constitutive model: in the numerical simulations the saturation process in the dam body caused by the increasing water level inside the reservoir induces an increase in pore water pressures and a consequent decrease of effective stresses, which results in swelling of the material. The result shows that the mechanical response of the dam over first impounding cannot be properly described using basic constitutive models, formulated enforcing the Bishop's effective stress definition (Lloret & Alonso 1985, Jommi 2000). The implementation of a more advanced model able to describe plastic collapse upon wetting is deemed mandatory to model the deformational response. Therefore, benchmarking the numerical results on settlements has been abandoned, and no further results are reported in this contribution.

The FS of the downstream and upstream slopes for the four representative situations indicated in Figure 3, are collected in Table 2. As a result of the new pore pressure distribution (Fig. 10) at the end of the first filling of the reservoir, i.e. 17/04/1990, the factors of safety of the downstream and upstream slope experience a decrease of 20% and 25% compared to the end of the construction, respectively. As reported in Table 2, a partial decrease of the water level in the reservoir, i.e. 16/12/1992, only affects the FS of the upstream slope, which increases, while the one of the downstream slope remains almost constant.
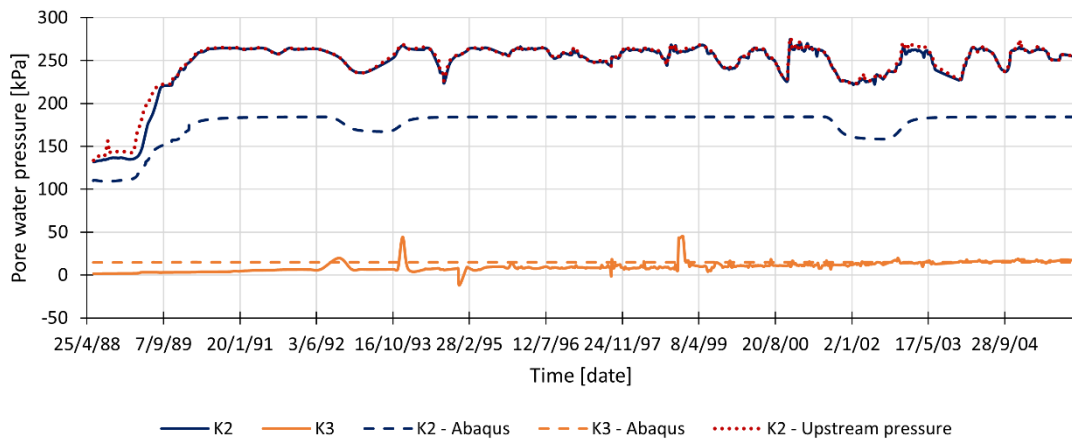

Figure 7. Comparison between pore water pressures measured at the base of piezometers K2 and K3 (solid lines) and results from the numerical analyses (dashed lines), from 25/04/1988 to 03/01/2006. The dotted red line represents the upstream pressure.
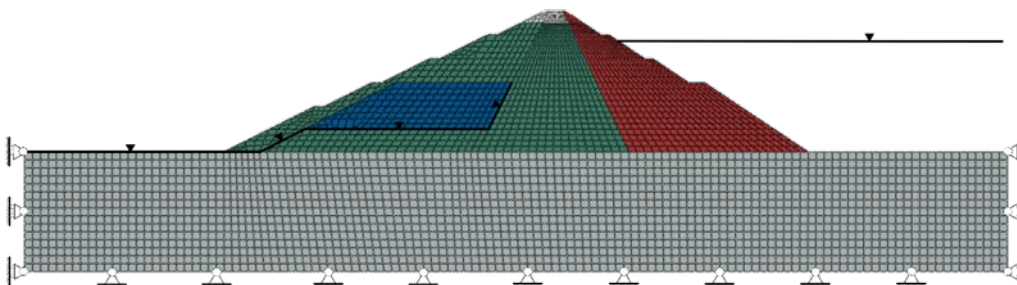

Figure 8. Mechanical and hydraulic conditions applied to simulate Case 1.

Pontani, Rossignoli, Sterpi, Jommi

SEEPAGE AND STABILITY ANALYSES OF A ZONED EARTH DAM SUBJECTED TO VARIABLE WATER HEADS:
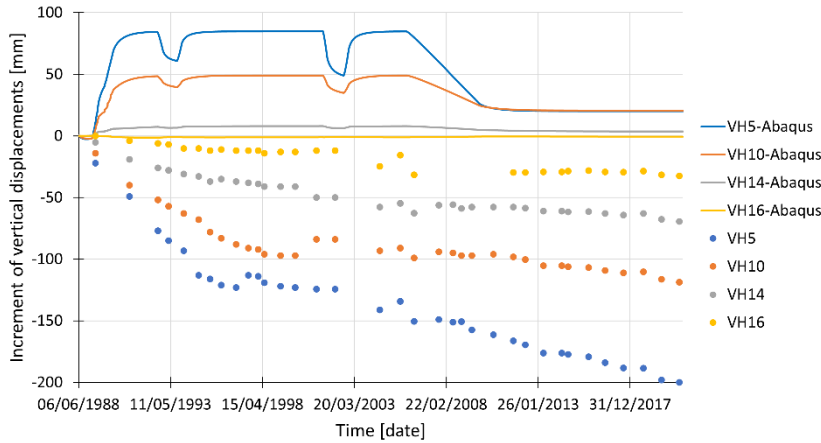NUMERICAL SIMULATIONS WITH ABAQUS

Figure 9. Comparison between the increment of vertical displacements measured in the geodetic points VH5, VH10, VH14 and VH16 (solid lines) and calculated from the numerical analyses (dashed lines) starting from 06/06/1988. Details about the position of the geodetic points are reported in the Formulation document.
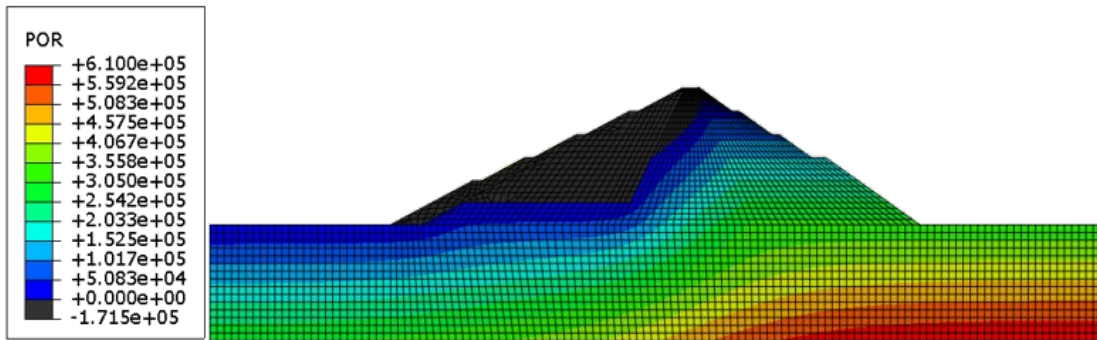

Figure 10. Contour map of pore water pressure inside the dam body and the foundation at the end of the first filling (i.e. 17/04/1990).

Table 2. Factor of Safety for the upstream and downstream slope of the dam for Case 1.

Time	upstream	downstream
As built	1.67	2.20
17/04/1990	1.25	1.76
25/08/1992	/	1.74
16/12/1992	1.48	1.77
13/07/2001	1.25	1.76

3.2 *Case 2 – Task 1: the appearance of the wet stain*

In Case 2 the attention is focused on the appearance of the wet stain, observed on October 24, 2007, at the downstream side of the dam. As already anticipated, the data recorded by the piezometers K2 and K3 (Figure 7), indicate the presence of pore water pressures higher than the ones numerically predicted under ordinary reservoir operation. This mismatch may be originated by localised water losses in the dam body, due to damage experienced by the pipes, well before the appearance of the wet stain. The relevant settlements experienced by the axis of the two pipelines over the construction period (Fig. 11) suggest that damage of the pipes might have originated from the high differential settlements undergone by the dam even before the first impoundment. To evaluate the consequences of this hypothesis, water sources were added at some nodes located along the axis of the pipelines, as shown in Figure 11. After some calibration, the nodes were assigned a specific discharge of 10^{-7} m/s each.

Pontani, Rossignoli, Sterpi, Jommi

SEEPAGE AND STABILITY ANALYSES OF A ZONED EARTH DAM SUBJECTED TO VARIABLE WATER HEADS:
NUMERICAL SIMULATIONS WITH ABAQUS

At the same time, the appearance of a wet stain downstream suggested that drainage at the toe should not be constrained. To allow free flow in the dam body without any a-priori restriction on the flow path, the previous downstream drainage was removed. At the face of the downstream slope a non-linear free outflow condition was assumed. The latter allows water to escape from the boundary when the water pressure is above the atmospheric one, otherwise keeping the boundary impervious. The same condition holds between the core and the rockfill C, in such a way that the drain can be easily modelled as an outflow surface.

The results in the period 25/04/1988 – 30/10/2020 are depicted in Figure 12, in terms of measured and predicted pore water pressures. The fluctuations measured by the piezometer K3 could be related to water management operations, which were disregarded in the numerical simulation. The comparison between the two time-histories confirms that the presence of additional water fluxes from the pipelines could be a comprehensive explanation for the high values of pore water pressures measured in the piezometer K2.

The stability of the system is evaluated after the wet stain was detected, i.e. 09/05/2008. Results are depicted in Figure 13 for both the downstream and the upstream slopes. The values of FS are reported in Table 3.
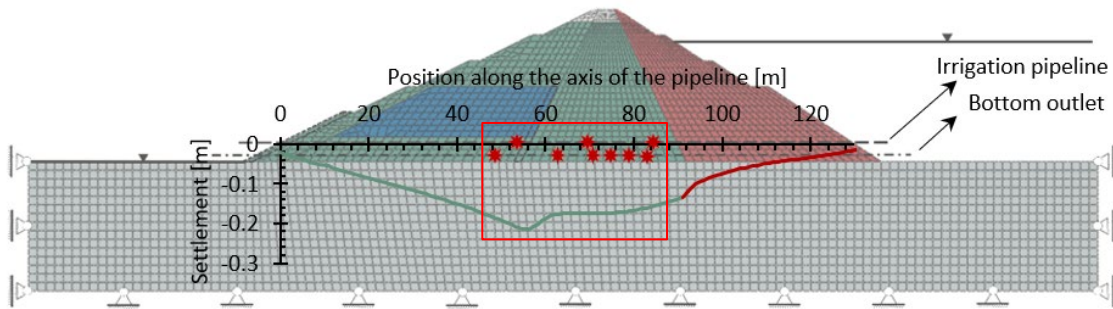
Figure 11. Settlements along the axis of the pipelines at the end of the construction. Different colours represent the different materials. The red marks indicate the nodes selected for the enforced flow of 10^{-7} m/s.
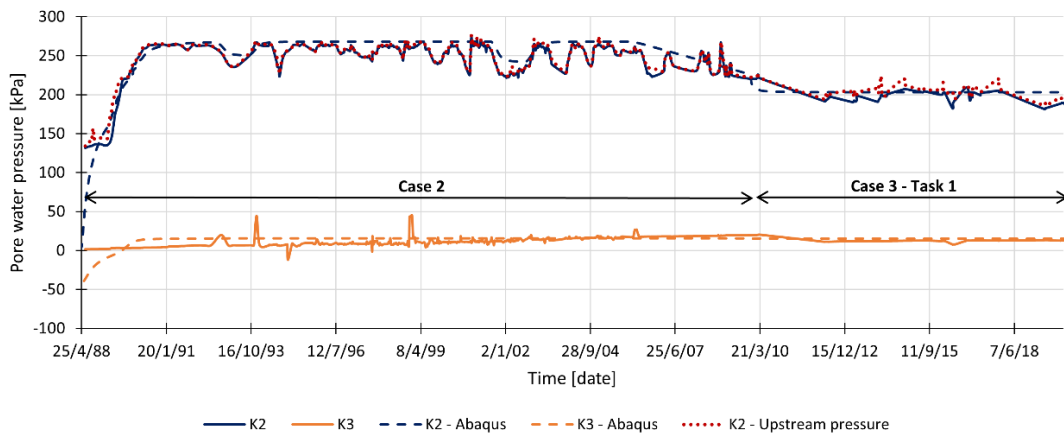
Figure 12. Comparison between pore water pressures measured at the base of piezometers K2 and K3 (solid lines) and results from the numerical analyses (dashed lines), from 25/04/1988 to 30/10/2020. The dotted red line represents the upstream pressure.

Figure 13. Contour of the plastic deviatoric strain showing the sliding surfaces at upstream (on the left) and downstream (on the right) slope after the detection of the wet stain (i.e. 09/05/2008).

Pontani, Rossignoli, Sterpi, Jommi

SEEPAGE AND STABILITY ANALYSES OF A ZONED EARTH DAM SUBJECTED TO VARIABLE WATER HEADS:
NUMERICAL SIMULATIONS WITH ABAQUS

Table 3. Factor of Safety for the upstream and the downstream slope of the dam for Case 2.

Time	upstream	downstream
09/05/2008	1.55	1.75

3.3 *Case 3*

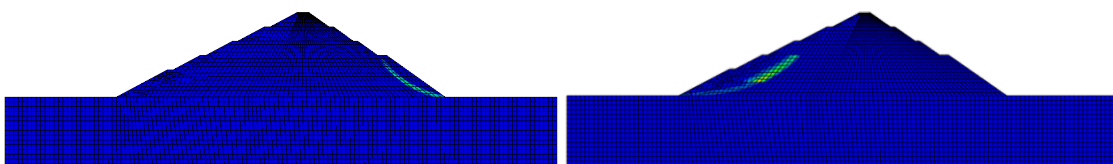Due to detection of the wet stain, in 2008 the reservoir level was decreased to a maximum level of 93.6 m a.s.l. and the irrigation pipeline was filled with concrete. The water level was lowered again to 92.0 m a.s.l. and the reservoir has operated under such conditions for more than 10 years. In Case 3, the drawdown of the reservoir as well as its re-filling after the remedial works are considered. Attention is devoted also to the effects of the drawdown on the hydraulic properties of the dam core.

3.3.1 Task 1: the long-term drawdown of the reservoir

The effect of the long term drawdown of the reservoir can be analysed referring to the data measured between 2010 and 2020, when the reservoir operated at a lowered elevation (Figure 12). Comparing the data measured in the piezometer K2 (solid blue line) with the values corresponding to the upstream pressure (dotted red line), no significant changes in the overall hydraulic response of the clay core have been identified. Therefore, no changes in the material properties have been considered in the definition of the numerical model. It is worth commenting that the difference between these two conditions is slightly higher than the one observed in the previous years (i.e. 1988-2008) since the sealing of the irrigation pipeline carried out in 2008 due to remedial works, led to a reduction of the additional discharge inside the dam body. To reproduce the hydraulic loads experienced on-site by the dam, sealing of the irrigation pipeline has been numerically modelled by removing the water sources along the axis of the irrigation pipeline. The comparison between monitoring data (solid lines) and numerical results (dashed lines) shows that the model is able to reproduce the hydraulic response of the system. At the end of the considered time-window, i.e. 30/10/2020, the stability of the dam is evaluated and the results are collected in Table 4.

3.3.2 Task 2: filling of the reservoir after the remedial work

After the completion of the remedial works, the reservoir will be impounded again; based on hydrology data the Formulators estimated that, considering an average rise of 5 cm/day, the normal operating level (i.e. 99 m a.s.l.) will be reached in 1 year (Zvanut et al. 2022). Figure 14 reports the estimated time series of the reservoir level after remedial works.

In the numerical simulations related to the analysis of the future state of the dam, to simulate the permanent sealing of both bottom outlet and irrigation pipelines resulting from remedial works, no additional water fluxes have been assigned in the domain and the seepage of water inside the dam body originates only from impoundment. Since the long-term drawdown of the reservoir could increase the permeability of the material, the hydraulic conductivity of the clay has been increased by one order of magnitude, according to experimental results obtained by Azizi et al. (2020). Particularly, to properly account for the effect of wetting-drying cycles on the hydraulic response of the clay core, only the hydraulic conductivity of the portion of the domain affected by impoundment and drawdown of the reservoir has been modified.

Figure 15 represents the variation in time of pore water pressures at the base of piezometers K2 and K3, as predicted by the numerical model. The pressures inside the clay core (dashed blue line) will be reduced compared to the upstream pressures (dotted red line), suggesting that the remedial works should be effective in reducing the high pore pressures inside the dam previously attributed to damage to the outlet pipelines.

The stability analyses performed at the end of the future filling of the reservoir (i.e. day 337) returns values of FS equal to those obtained in Case 1 (Tab. 4), for time instants characterised by the same hydraulic load (i.e. reservoir water level at 99 m a.s.l.). In fact, the change in the hydraulic conductivity of the material does not significantly affect the pore pressure distribution reached at the end of the re-filling process, as can be observed comparing Figure 10 and Figure 16.

Pontani, Rossignoli, Sterpi, Jommi

SEEPAGE AND STABILITY ANALYSES OF A ZONED EARTH DAM SUBJECTED TO VARIABLE WATER HEADS:
NUMERICAL SIMULATIONS WITH ABAQUS
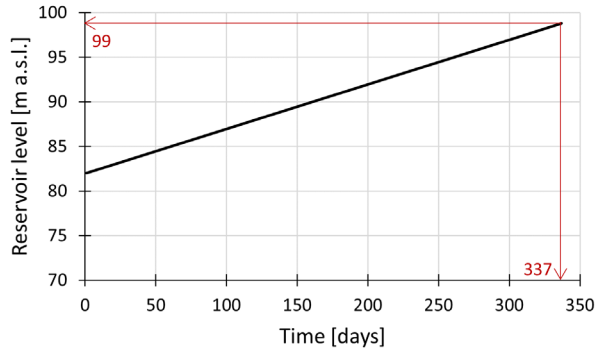
Figure 14. Filling of the reservoir after completion of the remedial works.
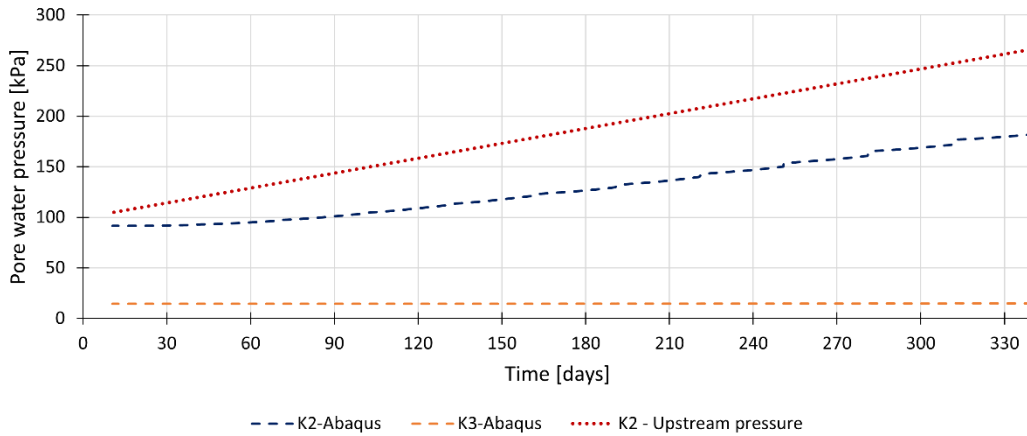
Figure 15. Predicted time-history of the pore pressure field at the base of piezometers K2 and K3 during the new re-filling of the reservoir. The dotted red line represents the upstream pressure.

Table 4. Factor of Safety for the upstream and downstream slope of the dam for Case 3.

Time	upstream	downstream
30/10/2020	1.64	1.75
Day 337	1.25	1.77

Figure 16. Contour map of pore water pressure inside the dam body and the foundation, at the end of the future filling of the reservoir (i.e. day 337).

Pontani, Rossignoli, Sterpi, Jommi

SEEPAGE AND STABILITY ANALYSES OF A ZONED EARTH DAM SUBJECTED TO VARIABLE WATER HEADS:
NUMERICAL SIMULATIONS WITH ABAQUS

4 CONCLUSIONS

In this work a finite element model is used to describe the behaviour of the zoned earth dam presented in the context of the proposed benchmark. Ordinary elastic perfectly plastic constitutive models in 2D transient consolidation analyses under conditions of partial satura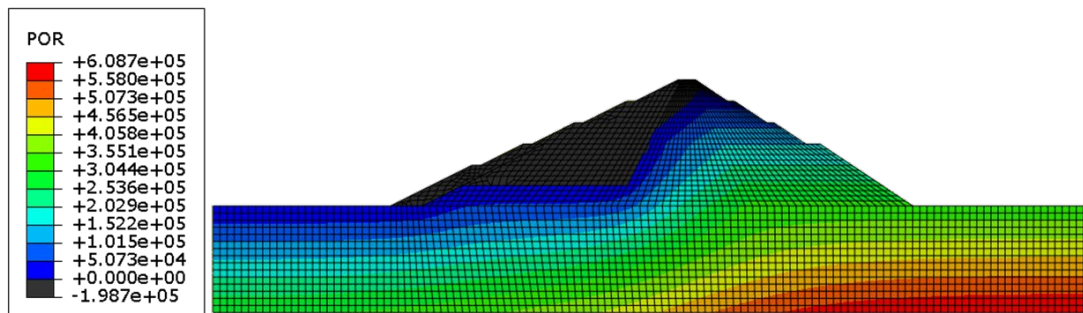tion prove to be able to describe some aspects of the problem, namely the seepage regime and the ultimate failure condition. However, an advanced mechanical modelling would be required to capture the complex time dependent stress-strain response in unsaturated conditions. In particular, the modelling of the material response under wetting and drying paths at constant total stress should be improved. The availability of field measurements must be emphasised, as they provide an essential contribution to the definition of the numerical model. Field measurements are essential not only in the calibration of hydraulic and mechanical properties of the materials, but also in the detection of an anomalous response of the system. The measurement of pore water pressure values higher than expected led to the conclusion that leaks have been taken place inside the dam body over years. The consequent additional water volumes may have led to a significant change in the pore water pressure distribution, resulting in a variation of the effective stress state. Consequently, the stability of the dam is directly affected, with a reduction of the safety factor calculated for the downstream slope. Furthermore, this is why the emergency measures put in place, such as the sealing of the original pipes, appear worthwhile.

Additional improvements in the numerical modelling could include the use of a 3D domain, to enhance the description of the contribution of the pipes inside the dam body. Finally, concentrated water flow along the interfaces of heterogeneous materials should be addressed, as it could result in internal erosion phenomena.

REFERENCES

Alonso, E.E., Olivella, S. & Pinyol, N.M. 2005. A review of Beliche Dam. *Géotechnique* 55(4): 267-285

Azizi, A., Musso, G. & Jommi, C. 2020. Effects of repeated hydraulic loads on microstructure and hydraulic behaviour of a compacted clayey silt. *Canadian Geotechnical Journal* 57: 100-114

Caruso, M. & Jommi, C. 2005. An evaluation of indirect methods for the estimation of hydraulic properties of unsaturated soils. *Eastern Mediterraneas University Press, Proc. Int. Conf. Problematic Soils, Famagusta, 25-27 May*

Dassault Systèmes 2021. Abaqus 6.23 Software Documentation. Dassault Systèmes Simulia Corp., Providence, RI, USA

Griffiths, D.V. & Lane, P.A. 1999. Slope stability analysis by finite elements. *Géotechnique* 49(3): 387-403

ICOLD Committee on Embankment Dams 2017. *ICOLD Bulletin 164 Internal erosion of existing dams, levees and dikes, and their foundations*. Paris

Jommi, C. 2000. Remarks on the constitutive modelling of unsaturated soils. A. Tarantino & C. Mancuso (eds), *Experimental evidence and theoretical approaches in unsaturated soils*: 139–153. Rotterdam: Balkema

Lloret, A. & Alonso, E.E. 1985. State surfaces for partially saturated soils. *Proc. 11th Int. Conf. Soil Mech. Fdn Engng, San Francisco*

Matsui, T. & San, K.C. 1992. Finite element slope stability analysis by shear strength reduction technique. *Soils and Foundations* 32(1): 59-70

Rossignoli, C. & Sterpi, D. 2021. Numerical prediction of the drying-wetting process in a river levee and floodplain. *Proc. 6th World Congress CSEE-21, Lisbon,* DOI: 10.11159/icgre21.lx.111

Wrachien, D. & Mambretti, S. 2009. *Dam-break problems, solutions and case studies*. Boston: WITpress

Zienkiewicz, O.C., Xie, Y.M., Schrefler, B.A., Ledesma, A. & Biĉaniĉ, N. 1990 Static and dynamic behaviour of soils: a rational approach to quantitative solutions. II. Semi-saturated problems. *Proc. Of the Royal Society of London. A Mathematical and Physical Sciences* 1877(429): 311-321

Zvanunt, P., Likar, B., Likar, Z., Selan, V., Klun, M. 2022. Theme C: Behaviour of the embankment dam, Formulation document. ICOLD 16th International Benchmark Workshop on numerical analysis of dams, 5-6 April 2022, Ljubljana, Slovenia.

BEHAVIOR OF THE SLOVENIA EMBANKMENT DAM

Daniel Verret
Hydro-Québec Production, Québec, Canada

Mourad Karray
Université de Sherbrooke, Québec, Canada

ABSTRACT: This article is about the C theme of the 16th International Benchmark Workshop on Numerical Analysis of Dams Ljubljana, Slovenia Organized by the ICOLD Committee on Computational Aspects of Analysis and Design of Dams. It consists in studying a zoned earthfill dam with a clay core located in Slovenia. The dam is 34,6 m height and its crest length is of 174 m which has exhibited atypical behavior after approximately 20 years of operation. The design of this structure, which incorporates pipes, suggested potential problems of internal erosion. The observations of erosion traces of the latter re-enforce this hypothesis. However, analysis of the downstream portion of the cross-section also shows a high potential of seepage on the downstream face of the dam, especially if the embankment fill has some anisotropic permeability. 2D and 3D numerical models have been built to study in more detail the behavior of this dam and its foundation. A series of works are proposed in the downstream area of the dam to add lines of defense to the design. At a minimum, the downstream filter should be raised to the top of the core with the objectives to lower the free water table in the upper downstream portion of the dam and to ensure a filtration capacity of this portion of the core which may have some permeability anisotropy. The dynamic analyses performed by simulating the Elazing Sivrice earthquake (24 January 2020) in Turkey adjusted to 0.3g indicates that the seismic stability would be ensured and no uncontrolled release of the reservoir is anticipated following an earthquake. However, it would be relevant to verify these conclusions with additional signals. After conducting laboratory tests to characterize the clay fill of the core and the creep model parameters, analysis of the creep process is recommended.

1 THEME C: DESCRIPTION

Embankment dams represent in total over 80% of the dams built in the world (Wrachien, 2009). Additionally, most dams were built in previous decades. Unlike concrete dams, embankment dams can accommodate a wide option of foundation conditions, construction material is usually available close to the dam location. During the construction and commissioning, embankment dams are subjected to various loading conditions. Internal erosion is a common issue in embankment dams. For example, approximately 40% of all embankment dam failures have been attributed to soil instability due to uncontrolled seepage through the dam body or its sub-base (ICOLD Committee on Embankment Dams, 2017). Moreover, the dams were less frequently built in the past considering different safety, design, and construction standards (United States Society on Dams, 2010). Additionally, we are often dealing with the lack of data and we need to adopt various modelling assumptions to perform numerical analysis.

For this workbench, a real case of a dam experimenting erosion problems is proposed. This dam is located in Slovenia. It was built in 1989 for agriculture purposes (irrigation) and flood protection. The construction of the dam ended in the late 1980s and it lasted roughly one year.

The reservoir provides seasonal storage of water, where the excessive rainwater is collected during the cold part of the year, when the inflow discharges are high; while in spring and summer months the reservoir water is used primarily for irrigation. The total projected volume of the reservoir is 8.0 million m^3 of water, of which 6.8 million m^3 (84.5% of the volume) is intended for irrigation, and 1.2 million m^3 (15.5% of the volume) for flood water retention.

Figure 1 shows a downstream view of the dam. A description of the dam and its foundation characteristics followed by the cross-section design and the observed problems are presented in section 2.
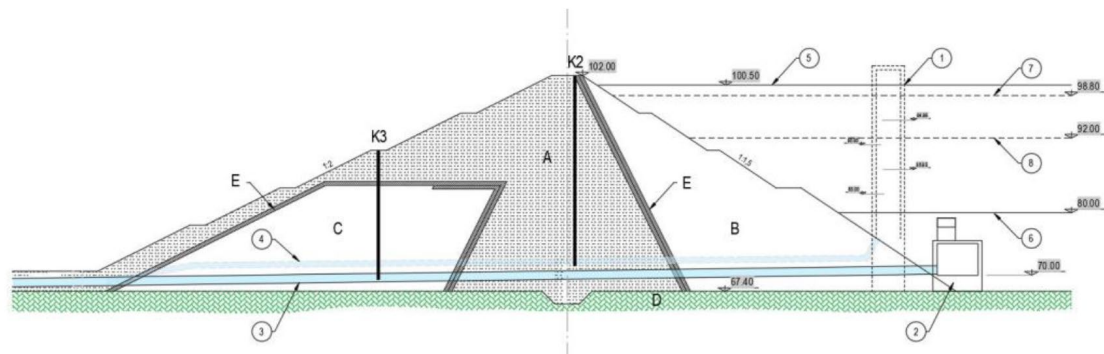

Figure 1. The downstream view of the dam.

2 DAM DESCRIPTION

Figures 2 and 3 illustrate the typical cross-section and plan view of the dam. This section first describes the geometric and geotechnical conditions of the dam and its foundation. Then the design is described, and its design feature are exposed.

Dam structure:
(A)   clayey silt material
(B)   rockfill material
(C)   limestone and sandstone blocks
(D)   impermeable rock base
(E)   filter material

Hydrotechnical structures:
(1)   intake tower
(2)   intake structure
(3)   bottom outlets
(4)   irrigation pipeline

Reservoir levels:
(6)   Maximal reservoir level (100.5 m a.s.l.)
(7)   Minimal operating level (80.0 m a.s.l.)
(8)   Normal operating level (98.8 m a.s.l.)
(9)   Depleted operating level (92.0 m a.s.l)

Crest elevation 102 m a.s.l
Foundation elevation 67.40 m a.s.l.

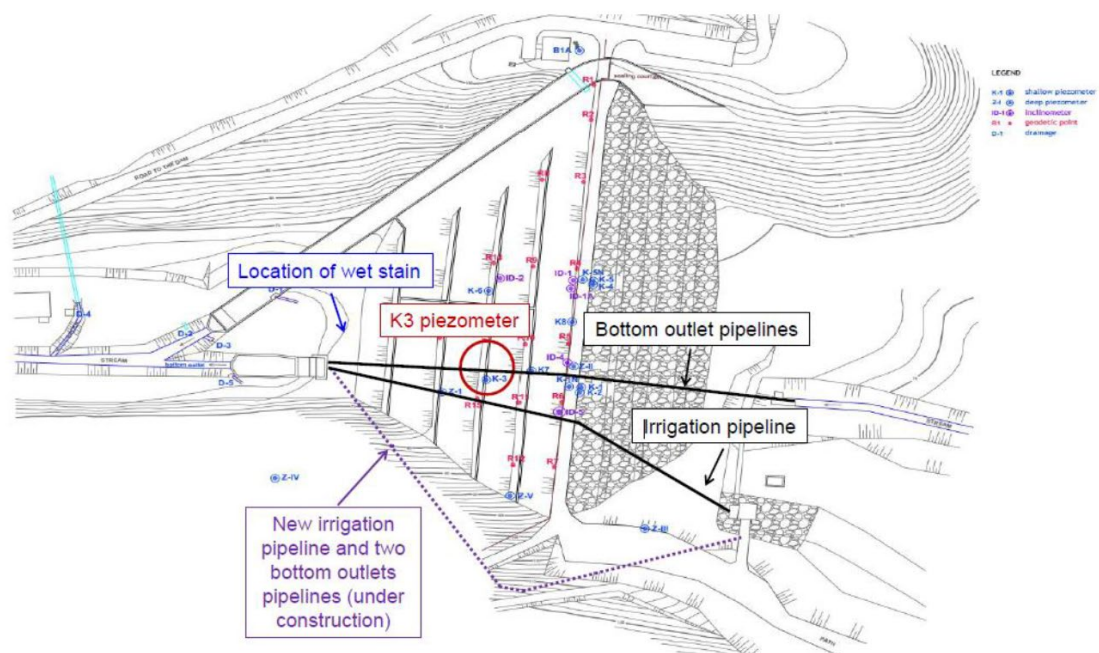Figure 2. Cross-section of the dam.

Figure 3. Plan view of the dam.

2.1   *Geometrical and geotechnical dam and foundation conditions*

The main technical data of the dam are:
- Dam height above foundation: 34.6 m;
- Elevation of the dam crest: 102.00 m asl;
- Elevation of the foundation: 67.40 m asl;
- Crest width: 5 m;
- Base width: 120 m;
- Crest length: 174 m;
- Normal Water Level: 98.8 m asl.

2.2 *Dam cross-section design and foundation treatment*

The dam under investigation is a zoned earthfill dam with a clay core. The cross-section of the dam is presented on Figure 2. The main zones in the dam structure are: (A) impermeable clay zone, (B) rockfill zone, (C) mix of limestone and sandstone blocks, (D) impermeable rock foundation, and (E) filter. On the upstream side of the filter, the dam consists of rockfill material (B). The downstream slope has a slope inclination of 2H:1V while on the upstream side the slope is steeper 1.5H:1V. For each of these external slopes, the dam concept includes intermediate berms. The core of the dam contains clay-silty fill materials, obtained mostly in the area of the reservoir. The impermeable core is protected with a two-layer filter (on upstream and downstream side). The blocks of limestone and sandstone in zone (C) are contained by the impermeable clay material, while filter is installed on the boundary.

The dam site is located on impermeable Eocene flysch. At the design stage the geological conditions at the site were estimated as very good. However, this assessment was based on the execution of only basic geological and hydrological investigations. Moreover, during the construction, the excavations revealed zones with permeable limestone deposits. To ensure the lower permeability in the foundation, permeable zones were grouted with a single-row of grout curtain (cement-bentonite suspension), which was used to seal the permeable zones and reduce the permeability of dam foundations. The depth of the grouting in the foundation reached 68 m (the grouting reached into the ground to the elevation level 34 m asl). Grouting was done simultaneously with the dam construction; precise locations of the grouting are not known.

2.3 *Design feature*

To prevent breaching of the dam during extreme flood events, an emergency spillway is situated at the right abutment of the dam. The spillway is designed to evacuate a flood with a 1000-year return period.

A bottom outlet with a capacity of 14 m^3/s crosses the dam at its base. It consists of two steel pipes, 120 cm in diameter, which are protected with a concrete cover. One of the pipes is used for abstraction of water for irrigation, while the second one is designed for emergency evacuation of water from the reservoir. Bottom outlet (number 3 on Figure 2) is regulated with Howell-Bunger valve installed on the left downstream side of the dam, meaning that the pipes are filled with water even when the valves are closed. The RC intake structure for the bottom outlet is on Figure 2 marked with a number (2).

Additionally, the intake tower (number 1 on Figure 2) is equipped with 4 hydraulic gates, that enabled abstraction of irrigation water at various elevations. The steel pipeline (number 4 on Figure 2) from the intake tower, which is protected with a concrete cover, has 100 cm in diameter, and leads toward the outtake structure downstream of the dam. Since the leakage detection, the irrigation pipeline has been sealed and the intake tower is no longer in operation. The disposition of the bottom outlet, the intake tower, the irrigation pipes and the bottom conduits is marked on the Figures 2 and 3.

3 OBSERVATION OF AN ATYPICAL BEHAVIOR

The construction of the dam ended in the late 1980s and it lasted roughly one year. The reservoir was fully impounded roughly 18 months after the completion of the construction work. The basic monitoring system of the dam was already established during construction and immediately after the construction of the dam was completed. After 20 years of operation, during regular maintenance wet spot was noticed on the downstream slope of the dam.

On October 24, 2007, during a regular inspection of the dam, a wet zone was observed. The wet spot was located at the downstream toe of the dam in the central part, close to the axis of the dam (the location is shown on Figure 3). Moreover, the presence of surface water was observed at the downstream toe of the dam, between the stilling basin of the spillway channel and outlet structure of the bottom outlet. Furthermore, the extensive vegetation on the central part of the embankment dam indicated that the humid zone extends to the downstream slope of the dam above the wet spot. Emergency investigation revealed that excessive water on the downstream slope originated from the reservoir. There was a suspicion that the damaged

irrigation pipeline is the cause for the seepage. After emptying the reservoir and the inspection of the irrigation pipeline, this hypothesis was confirmed. Under a silty layer deposited on the walls of the pipeline, air bubbles were observed in several places. The corrosion of the steel pipeline (holes were few cm to few 10 cm in diameter) enabled seepage of water into the layer between the concrete cover and the steel pipe. Even though the irrigation pipeline was emptied, the wet zone still existed. Therefore, the emergency investigations were also extended to the conduits of the bottom outlet pipeline, which can be closed only on the downstream side. In the case of the damaged pipeline, the seepage into the dam body was possible. The detailed investigations revealed similar damage on the bottom outlet pipeline as in the previous case of the irrigation pipeline. Geotechnical investigations of the foundation (i.e. water permeability tests and coring) showed that there was only minimal (practically negligible) amount of seepage in the foundation layer under the dam, so piezometer levels did not show any changes in the water level. In summary, the seepage was confined to the dam body in the proximity of both the irrigation and the bottom outlet pipelines.

4 REMEDIATION WORKS

Rehabilitation works are currently underway on the dam, the reservoir has been emptied and it is expected to become operational in 2023.

In 2008, the reservoir level was lowered to a maximum of 93.6 m asl and the irrigation pipeline was filled with the concrete. The space between the irrigation pipeline and the concrete cover was grouted with the cement grout. After this emergency remediation, the reservoir operational level was additionally lowered to a 92.0 m a.s.l. The reservoir operated under the lowered condition for more than 10 years.

Remediation works are underway. During the works, the bottom outlet and irrigation pipes will be sealed with concrete filling. New outlet building and outlet tunnel will be constructed in the left abutment, so all the conduits in the dam body will be permanently sealed. It is estimated that after the completion of the works, the reservoir eater level will be raised back to the initial nominal level at 98.8 m a. sl.

5 TECHNICAL ANALYSIS OF THE DAM DESIGN

5.1 *Cross-section of the dam*

This section presents an engineering analysis of the zoning of a Dam cross section.

The top of the draining zone of limestone and sandstone blocks (zone C) in the downstream shoulder is nearly 15 m lower than the normal operating level of the reservoir.

Filters (zone E), the most important area with the core, are very narrow. Any local deficiency in this zone translates into an increased risk to prevent internal erosion of the core. Above this drainage zone (zone C), in the downstream part of the dam, there is no filter and the embankment materials are of the same nature as the core (zone A).

Thus, there will be a drawdown of the free water table generated by the upper filter (zone E) and the draining fill (zone C), however, due to the impermeable nature of the clay fill (zone A) above these materials, the seepage flow at the top of the cross-section will tend towards the downstream face of the dam. This is of particular concern if the clay fill material (zone A) has some permeability anisotropy

Downstream of this drainage zone (zone C) and filter (zone E), the face of the dam is covered by a clay fill material (zone A) with the same permeability as the dam core. Normally, in dam design, we adopt free draining materials, respecting the filter criteria but increasingly permeable in the downstream region of a dam. The presence of a clay fill material (zone A) on the downstream face of the dam, downstream of the draining fill materials (zone C), favors an increase of the pore pressures on the downstream face of the dam.

Based on these design comments, the occurrence of humid zones on the downstream face of the dam was very predictable regardless of pipes passing through the dam body. With a clay fill material permeability of 1×10^{-9} m/s, and an anisotropy of 25 or a clay fill material permeability 25 times higher, the delay to observe humid zone on the downstream face of the dam following the

impoundment of the reservoir can be estimated to be about 20 years, which would be consistent with the observations described in section 3.

5.2 *Pipe crossing the dam*

The risks associated with piping through dams and dikes are also well documented in the international literature. According to this literature, nearly half of all embankment dam failures are caused by internal erosion of the embankment or its foundation. Approximately 30% of these failures are associated with pipes crossing embankment dams (Fell, R. & Foster, M., 1998). Therefore, this is an important issue for the safety of dams. The risks associated with pipes crossing dams are dependent on design and construction and increase as the pipes age. The issue is even more important when the latter are under pressure by a reservoir (FEMA, 2005).

Although it is preferable to avoid a design incorporating pipes in a dam, such a design when adopted requires a set of lines of defense to minimize the risk of internal erosion (FEMA, 2005). For example, installing a barrier around the pipe to lengthen the flow path is one of the measures generally recommended for this type of design. In this case, very little data is available to assess the design of these pipes crossing the dam. However, it appears that after only 20 years, some of the pipes were showing signs of corrosion. This exposes deficiencies in the design.

6 NUMERICAL MODELS

6.1 *2D model*

The two-dimensional explicit FD program FLAC (Itasca Consulting Group Inc., 2011) was employed to simulate the seepage flow and evaluate the static and dynamic performance of the dam. Figure 4 shows the basic characteristics (i.e., dimension, boundaries, and meshing) of the dam. Quiet lateral boundaries were set away from the region of interest so that reflected artificial waves were sufficiently damped and their influence on the dam response was minimized. To determine an adequate width for the model, preliminary seismic sensitivity analyses were carried out on slope models with different model widths. To ensure an accurate representation of the wave transmission with each model, the spatial discretization of the mesh followed the recommendations of Kuhlemeyer and Lysmer (1973), who stated that the spatial element size (Δl) must be smaller than approximately $\frac{1}{10}$ the wavelength associated with the highest frequency component (λ) of a given input wave. For instance, if $\Delta l \leq \lambda / 10$, $f_n = 2$ Hz, the shear wave velocity (Vs) = 200–350 m/s at the upper portion of the dam, and $\lambda = 100$ m. Therefore, for soil element of about 0.5 x 0.5m (Figure 4) the frequencies higher than 40 Hz should be considered with precaution.
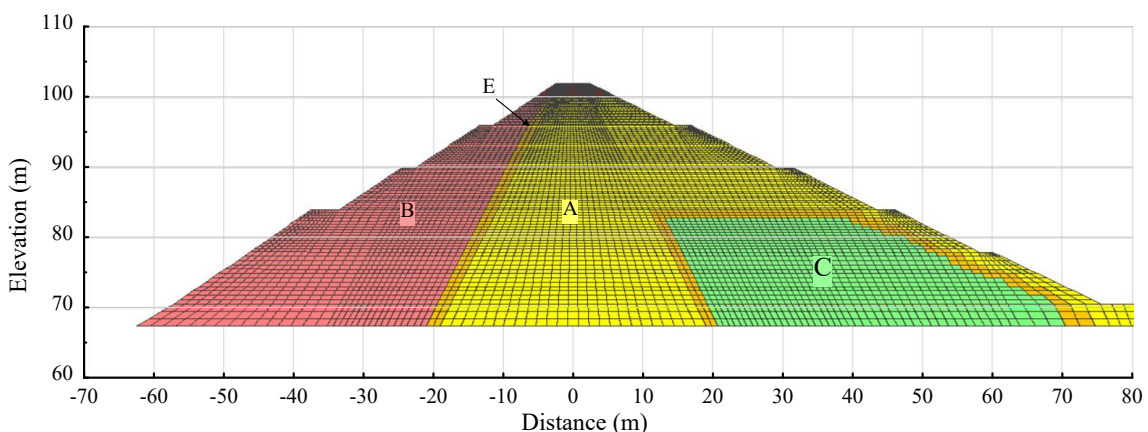

Figure 4. 2D FLAC numerical model

6.2 *3D model*

The three-dimensional explicit FD program FLAC3D (Itasca Consulting Group Inc., 2012) was employed to simulate the dynamic performance of the dam. Figures 5 and 6 shows cross-section and the isometric view of the dam and its valley (dimension, boundaries, and meshing). Some simplifications were introduced to the mesh without reducing the efficiency expected for the model. The entire dam leans against the bedrock, a level value of 67.5 m was assigned to the base of the bedrock; at this level, the valley width is 92 m. A symmetrical rock abutment inclination of 1.33H:1V was allocated to the entire dam footprint, which corresponds to the average slope of the bedrock abutment under the dam, as indicated in Figure 2. The crest length is simulated to 174 m.
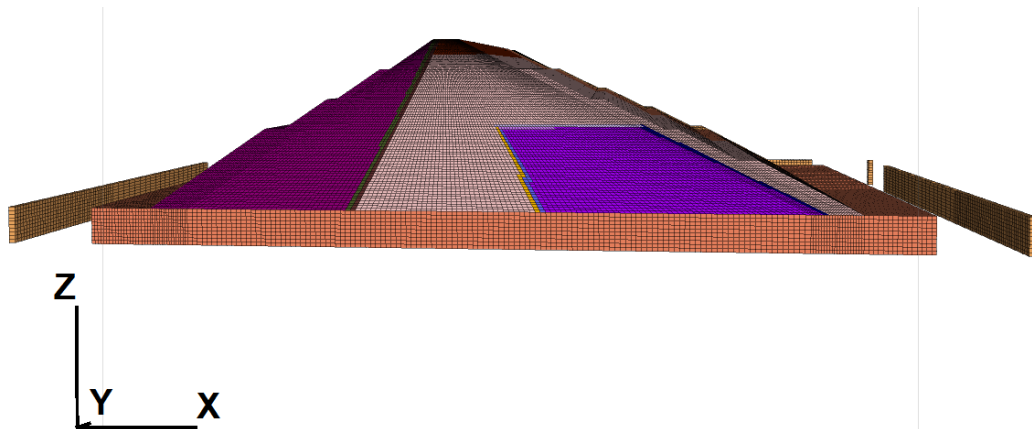

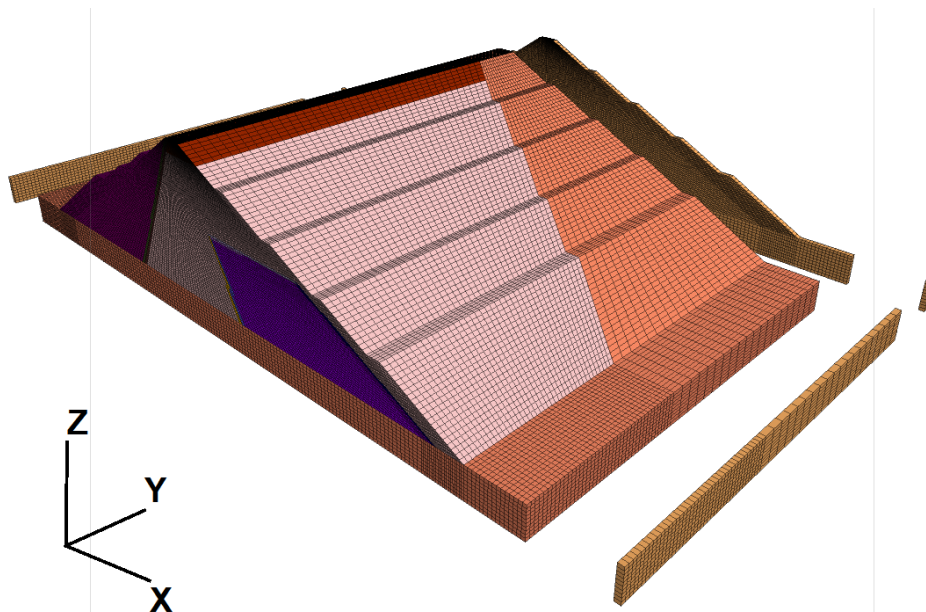Figure 5. 3D FLAC3D numerical model, Cross-section of the dam

Figure 5. 3D FLAC numerical model, Isometric view of the dam and its simplified valley

In terms of boundary conditions for static calculations, horizontal and vertical displacements equated to 0 for the bottom boundary of the mesh, whereas the horizontal displacements were valued to 0 for the lateral boundaries. In static analyses, fixed or elastic boundaries can be established realistically at some distance from the area of interest. However, in dynamic analyses, such boundary conditions reflect the outward propagating waves back into the model in use and do not provide the necessary energy radiation.

Given that the bedrock under the dam is rigid, free-field conditions were used at the lateral boundaries of the difference-finite mesh to reduce the model domain and consequently the

computational time. The seismic input was represented by external velocity input waves that propagate upward through the underlying material. The boundary conditions at the sides of each model accounted for the free-field motion that existed in the absence of a structure.

To ensure an accurate representation of the wave transmission with each model, the spatial discretization of the mesh followed the recommendations of Kuhlemeyer and Lysmer (1973), who stated that the spatial element size (Δl) must be smaller than approximately ¹⁄₁₀ the wavelength associated with the highest frequency component (λ) of a given input wave. For instance, if Δl ≤ λ / 10, fn = 2 Hz, the shear wave velocity (Vs) = 200–350 m/s at the upper portion of the dam, and λ = 100 m. Therefore, Δl was limited to 2 m although this limit is usually lower.

6.3 *Parameter used for modelling*

Table 1 resume the material properties proposed in the current benchwork for analysis and the shear wave velocity retained for each zone.

Note that the proposed oedometric modulus were not retained in the analyses because they are unrealistic in our opinion. Normalized shear wave velocities (V_{s1}) for soil were selected on the basis of laboratory tests performed on similar materials. Ibrahim et al. (2021) established relation between V_{s1} and the oedometric modulus, soil small-strain shear modulus, relative density, and particles shape for both granular and coherent soils. For the bedrock, the V_{s1} value was estimated based on its geological properties.

Notice that the friction angle of 38° for riprap also appears low, especially with a density of 24 kN/m³.

In this study, analyses were undertaken using elastoplastic models caped with Mohr–Coulomb criteria.

Table 1. Material properties

Zone	Description	w	γ	c_u	c'	φ'	υ	k	V_{s1}[*1]
		%	kN/m³	(kPa)	(kPa)	(°)		(m/s)	(m/s²)
A	Top layer of the dam (3m)	13	21	-		36	0.4	10-6	320
A	Clayey silt to silty clay	26	19.5	75		-	0.5	10-9	160
B	Rockfill (Limestone Blocks)	-	24	-	0	45[*2]	0.3	10-3	300
C	Blocks of limestone and sandstone	-	24	-	0	38	0.3	10-4	300
D	Flysch	-	25	-	0	39	-	10-9	800
E	Filter	-	19	-	0	35	0.3	10-4	260

*1 Normalized shear wave velocities (V_{s1}) for soil were selected on the basis of laboratory tests performed on similar materials (Ibrahim et al., 2021). For the bedrock, the value was estimated based on its geological properties.

*2 Proposed friction angle for the rockfill was 38°, this value is considered too low based on the nature of the materials described.

7 NUMERICAL RESULTS

7.1 *Seepage flow net analyses*

The seepage flow net was calculated simulating the reservoir at the normal operating level of 98.8 a.s. m.l. The permeabilities presented in Table 1 were programmed in the models. Figure 6 shows the seepage flow nets obtained with the 2D model for isotropic permeability conditions and with an anisotropic permeability of 25 for the core clay fill.

The results clearly expose the effect of a design without a downstream filter on the full height of the dam core. If the permeability of the clay fill is perfectly isotropic, pore pressures would be relatively well controlled in the upper portion of the dam by the filter (zone E) above the draining fill (zone C) in the lower downstream portion of the dam. However, the clay fill on the downstream face of the draining fill (zone C) and the filter (zone E) keeps the water table quite high on the lower third downstream face of the dam.

It is well documented that anisotropic permeability is inherent to the fill placement, particularly fills with a significant proportion of fine particles (silt and clay). Several factors can promote anisotropic permeability. Variability in material grading during dam construction, water content at the time of fill placement and compaction, variations in compaction energy, etc. are examples A seepage flow net analysis was performed by modeling an anisotropic permeability of 25 (Figure 6b). Results show that pore pressures are significantly higher in the upper portion of the dam and the free water table reaches the downstream face of the structure. These latter results are consistent with the site observations after 20 years of operation and the technical analysis of the dam design presented in Section 5.

The 2D model was modified to allow verification of the effect on the flow net if the downstream filter will be extended to the full height of the core while maintaining an anisotropic permeability of 25 for the entire dam clay core. Figure 7 shows the seepage flow net. Clearly, according to the state of the art, the effect of raising the downstream filter to the top of the dam clay core would provide a line of defense for the design of the dam. However, the clay fill placed on the downstream face of the draining fill (zone C) and the filter (zone E) still keeps the water table quite high on the lower third downstream face of the dam.
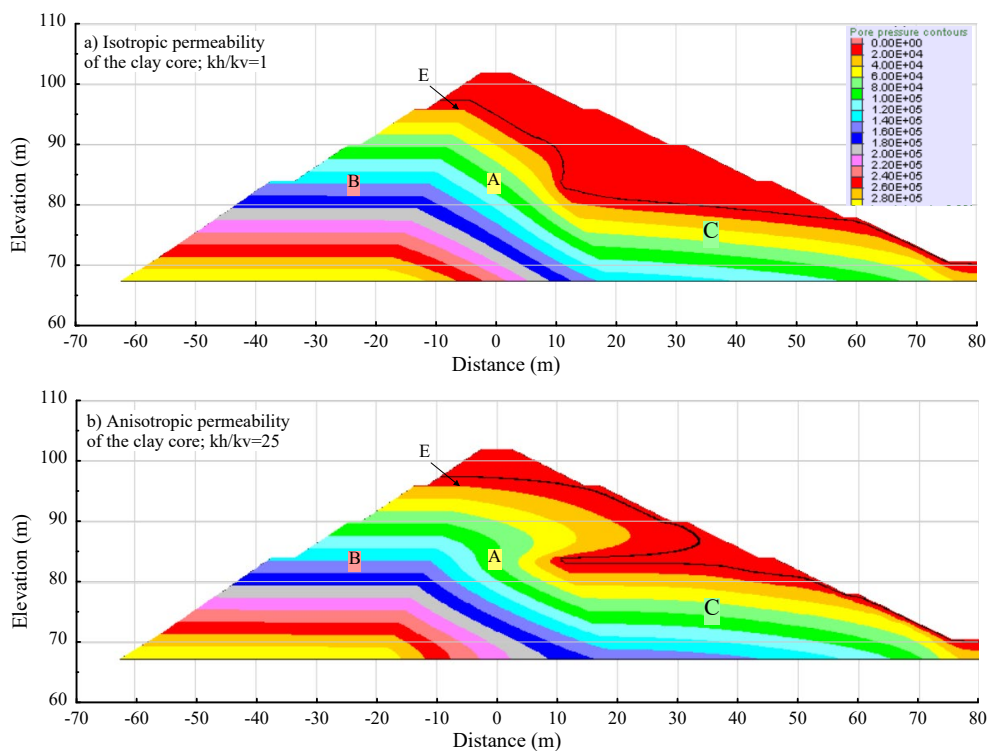

Figure 6. 2D seepage flow net of the dam, a) Isotropic permeability for the clay core and b) Anisotropic permeability of 25 for the clay core
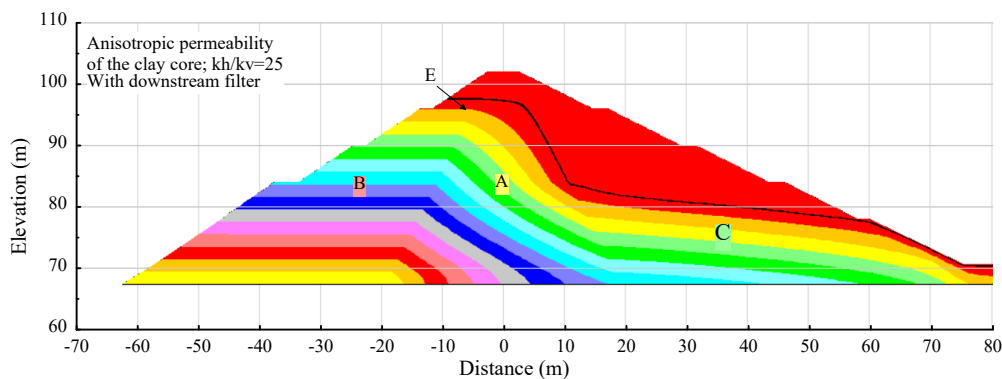

 Figure 7. 2D seepage flow net of the dam, Anisotropic permeability of 25 for the clay core and downstream filter extended to the full height of the core

7.2 *Static stability analyses*

Static stability analyses are carried out to confirm the factors of safety of the upstream and downstream slopes of the dam. Table 2 presented safety factor results. The upstream slope has a marginal stability resulting from the angle of friction of 38° and a density of 24 kN/m^3 for the rockfill combined with an external slope of 1.5H:1V. With a minimal friction angle of 45°, as expected, the safety factor is satisfactory.

Table 2. Static stability analysis: Safety Factor results

2D Model	Upstream	Downstream
Isotropic permeability for the clay core	1.9[1]	1.6[2]

[1] Retained friction angle of 45° for the rockfill

[2] The analysis was performed with the clay fill (zone A) undrained shear strength. Rigorously, the static stability should also be checked with the clay fill drained shear strength parameters (c' and φ') and thus compare the safety factors. The downstream slope has probably a marginal drained condition static slope stability with the actual design when considering the seepage flow net based on an anisotropic permeability of 25 for the clay fill core. However, the scenario with a downstream filter extended to the full height of the core will improve the safety factor.

7.3 *Dynamic analyses*

- Fundamental frequencies of vibration

A modal analysis was carried out to establish the fundamental frequencies of vibration of the dam. Table 3 gathers the vibration frequencies of the first three modes calculated with the 2D model in the transverse and in the vertical directions.

Table 3. Fundamental frequencies of vibration based on the 2D model

Direction	1st mode, f_0 (hz)	2nd mode, f_2 (hz)	3rd mode, f_3 (hz)
Transverse	2.1 hz	3.7	5.5
Vertical	3.3	4.8	6.8

The vibration modes were also determined with the FLAC3D model. Table 4 gathers the vibration frequencies of the first modes calculated with the Flac3D model in each 3 directions. With the FLAC3D model, frequencies are slightly higher due to a valley effect

Table 4. Fundamental frequencies of vibration based on the FLAC3D model

Direction	1st mode, f_0 (hz)
Transverse	2.9
Longitudinal	4.3
Vertical	6.8

- Dynamic response analyses

Dynamic analyses were performed with 2D and 3D numerical models. In order to more accurately represent the soil parameters and dam conditions in this study of the dynamic behavior, a specific stiffness value was assigned to each material along with individual values of normalized shear wave velocity (Vs1), the dependence of material reduction curves on the effective confining pressure was specified, and the flow network in the dam was applied to the reservoir thrust on the upstream side.

The constitutive model that was used is a non-linear model implemented in the FLAC and FLAC3D softwares (Itasca Consulting Group Inc. 2011 and 2012). During dynamic simulations, the shear modulus of the soils was reduced using the constitutive model "sig 4" curve-fitting built in the FLAC and FLAC3D software. Prior to conducting the dynamic analysis, the soil was modelled as an elastic material, initial in situ stresses were developed to simulate gravity, and the model strains and displacements were reset.

The damping value was calculated using the implemented "sig3" and "sig4" hysteretic damping function built in the FLAC and FLAC3D softwares. In many cases, seismic analyses require the incorporation of additional material damping to ensure stability of the numerical solution process at low strain levels. The predominant frequencies selected to adjust the Rayleigh damping in the models were the fn values of the dam. The limit of 0.2 % centered at 5 Hz was used for each zone except the top 3 m of zone A at the crest (adjusted to 0.4 %) to reduce the effect on the analysis duration. Rayleigh damping is related to stiffness-proportional damping because it dominates at higher angular frequencies.

The material response to dynamic cyclic loading is quantified by a shear modulus reduction curve (G/Gmax) and damping ratio curve (ε). Representative curves were selected for each fill material to provide an accurate representation of the wave attenuation and energy dissipation during dynamic loading. For a large structure, it is necessary to select depth-dependent curves to make the simulated energy dissipation more realistic by considering the high confining stress in the lower portion of the dam (Oztoprak and Bolton 2013; Yang et al. 2017). Based on experimental test results on similar soils at the laboratory of Université de Sherbrooke, a best-fit functional relationship for the secant shear modulus reduction data was proposed for granular materials. Table 4 compiles "sig 4" curve-fitting programmed in each model which matched the experimental reduction curves proposed for cohesionless soils and adjusted for effective confining pressures of 100 kPa and 300 kPa to cover the range confining pressure applicable to the dam conditions, that reach 400 kPa on the downstream area.

For placed clay fill (zone A), a degradation curve based on test results from the Université de Sherbrooke, was also retained (Table 5). Since the dynamic calculations are performed in effective stresses, these degradation curves were adjusted to fit particularly shear strain larger than 0.05 %.

Table 5. Curve-fitting matching Sherbrooke laboratory test on placed fill clay, rockfill and sand.

Shear modulus reduction curve - fitting	SIG 4 fitting parameters			
	a	b	x_0	y_0
Placed clay fill, zone A	1	-0.6	-0.75	0
0 – 100 kPa, Zones B and C	1	-0.65	-1.8	0
100 – 300 kPa, Zones B and C	1	-0.65	-1.8	0.01
> 300 kPa, Zones B and C	1	-0.65	-1.8	0.02
Sand filter, Zone E	1	-0.60	-2.6	0.02

Degradation curves obtained from Sherbrooke laboratory on equivalent soils

The strain-controlled energy-based approach is used in this study to evaluate the dynamic behaviour of the dam during seismic loadings (Horizontal and vertical components). Over the last decades, the energy-based approach has been used for different types of dynamic problems (e.g. Green et al. 2000, Kokusho and Mimory 2015, Karray et. 2015). The major factor to consider the energy-based approach is reliability of the laboratory-based models (Amirpour et al., 2020). In this study, the energy-based functions of the constituting materials of the simulated dam are defined from undrained simple shear tests conducted on similar soils.

The Fast Lagrangian Analysis of Continua in two and three-dimensions numerical platform (FLAC and FLAC3D) was employed to investigate the seismic response of a dam by considering the nonlinear "sig 4" models and the effect of generated pore pressure during earthquake excitation. Details of the sigmoid function ("sig 4" soil model) as well as energy-based pore water pressure models can be found in Karray et al. (2015).

The typical results of cyclic strain-controlled undrained simple shear tests were adapted to delineate a unique relation between pore pressure (Ru) and the normalized dissipated energy ($W0.5$/a) of the materials constituting the dam as follows:

Placed clay fill (zone A)
$Ru=-0.0114+0.824*(W^{0.5}/a)-0.368*(W^{0.5}/a)^2+0.08*(W^{0.5}/a)^3-0.00665*(W^{0.5}/a)^4$ With a=1.5

Rockfill (zone B) and Limestone (zone C)
$Ru=0.05+0.3754*(W^{0.5}/a)+1.0204*(W^{0.5}/a)^2-0.5091*(W/^{0.5})^3$ With a=2 for soil C and 2 for soil B

Filter (zone E)
$Ru=-0.005807+0.36091*(W^{0.5}/a)+1.12725*(W^{0.5}/a)^2-0.628024*(W^{0.5}/a)^3$ With a=2.5

The signals recorded from the station 4404 during the Elazing Sivrice earthquake on the 24th of January 2020, (17H 55 min) in Turkey were selected for the dynamic analysis. The input motions were adjusted based on the maximum acceleration from the signals, which occurs in the EW direction, and they were fitted proportionally to match a maximum accelerations of 0.3 g. Figure 8 shows the time histories of the adjusted input motion. The three signal components shown in this figure were applied at the base of the 2D and 3D models.
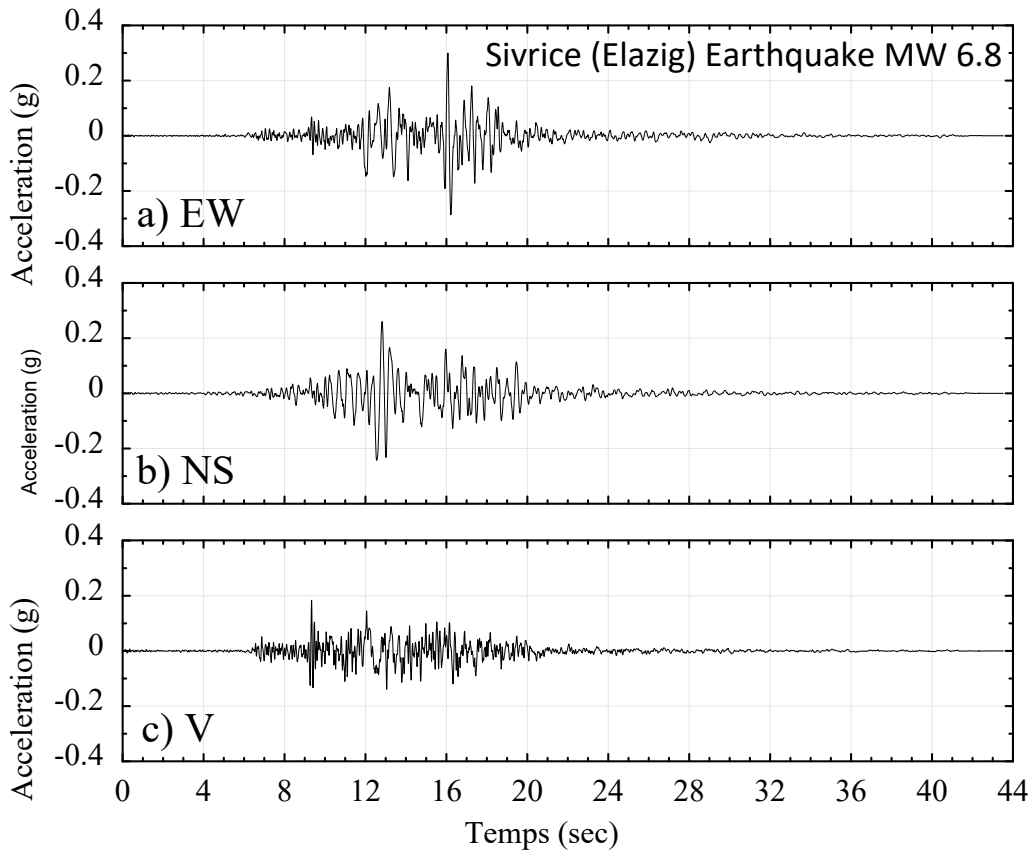

Figure 8. Time histories in the three directions adjusted proportionally to match a maximum acceleration of 0.3 g in the EW direction from recorded motion at the station 4404 during the Elazing Sivrice earthquake on 24 January 2020.

Figure 9 illustrates the maximums of the shear strain, the cyclic stress ratio and the excess pore water pressure ratio contours calculated by applying the Elazing Sivrice earthquake (EW and V components) at the base of the model. Overall, results show that the maximum shear strains are reasonable. Although they reach 5% in the upper portion of the upstream embankment (rockfill zone B), they are also evaluated at less than 0.5% for the rest of the entire dam. These deformations in the rockfill are associated with a more significant acceleration amplification on the upstream slope of the dam, reaching 1g near the surface. In addition to the dam geometrical effects, this amplification is influenced by the angle of friction and the stiffness of the clay fill material. This low level of deformations is mainly due to the high undrained shear strength, a strength which needs to be verified and documented. On the maximum shear strains figure, it is interesting to note that the potential failure surfaces are visible, especially the one passing through the upper filter in the downstream portion of the dam. As expected, the distribution of cyclic stress ratio (Figure 9b) exhibits an increase in values as we approach the surface. Obviously, in the rockfill and in the clay fill, there are low pore pressures (Ru) generated during the simulation, the Ru coefficient being less than 0.3. In the upper filter and the downstream slope, the Ru increases but does not exceed 0.6.
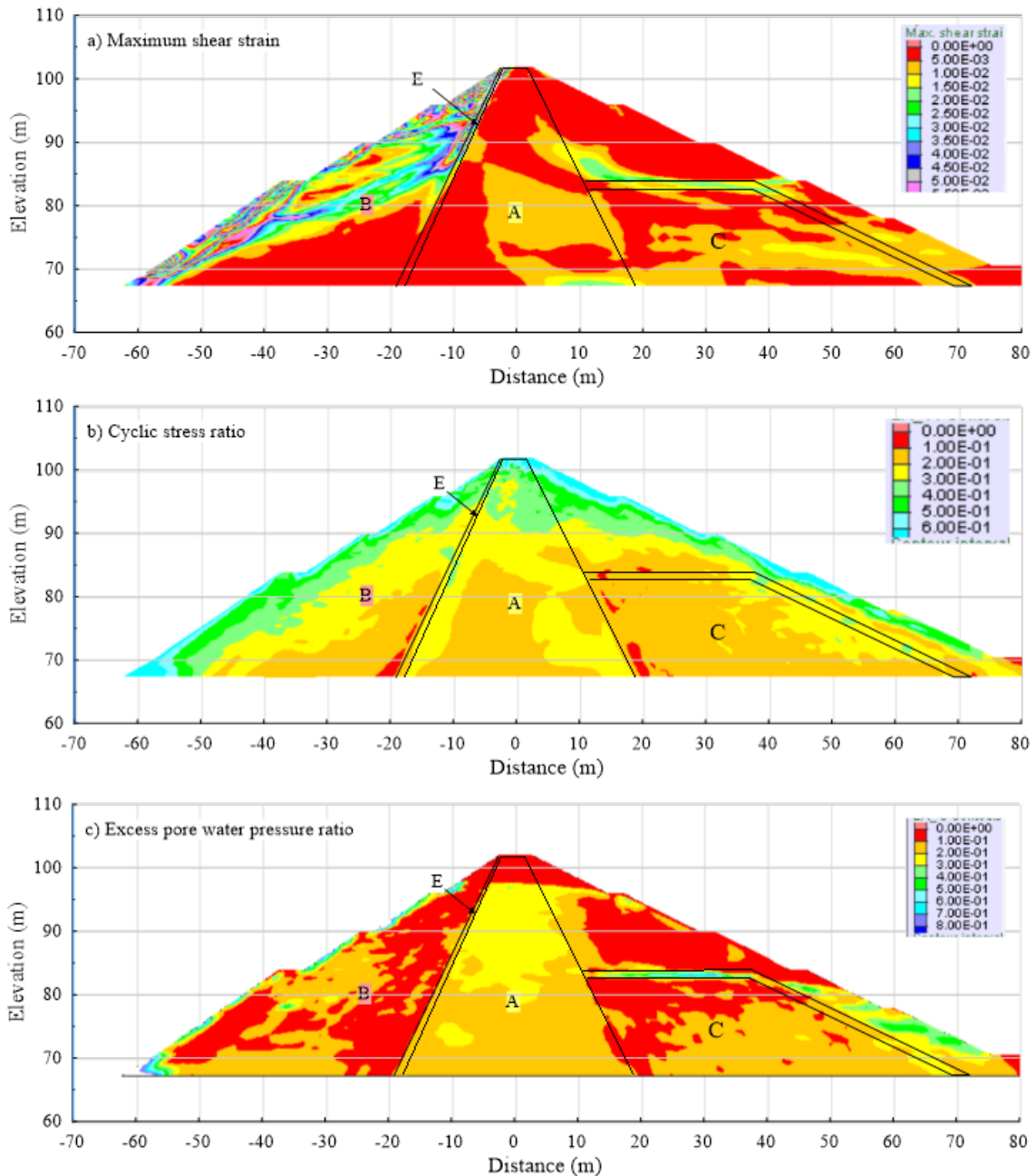
Figure 9. Dynamic analysis, a) Maximum shear strain b) Cyclic stress ratio and c) excess pore water pressure ratio contours.

Figure 10 compiles cumulative transverse displacements at the top of the dam berms during the simulation. In relation to shear deformations, the most important transverse displacements occur at the surface of the rockfill on the upstream face of the dam. These could reach 0.8 m at the base of the dam and near 0.5 m near the upper berm. For the downstream face of the dam, transverse displacements are estimated between 0.1 and 0.25 m.
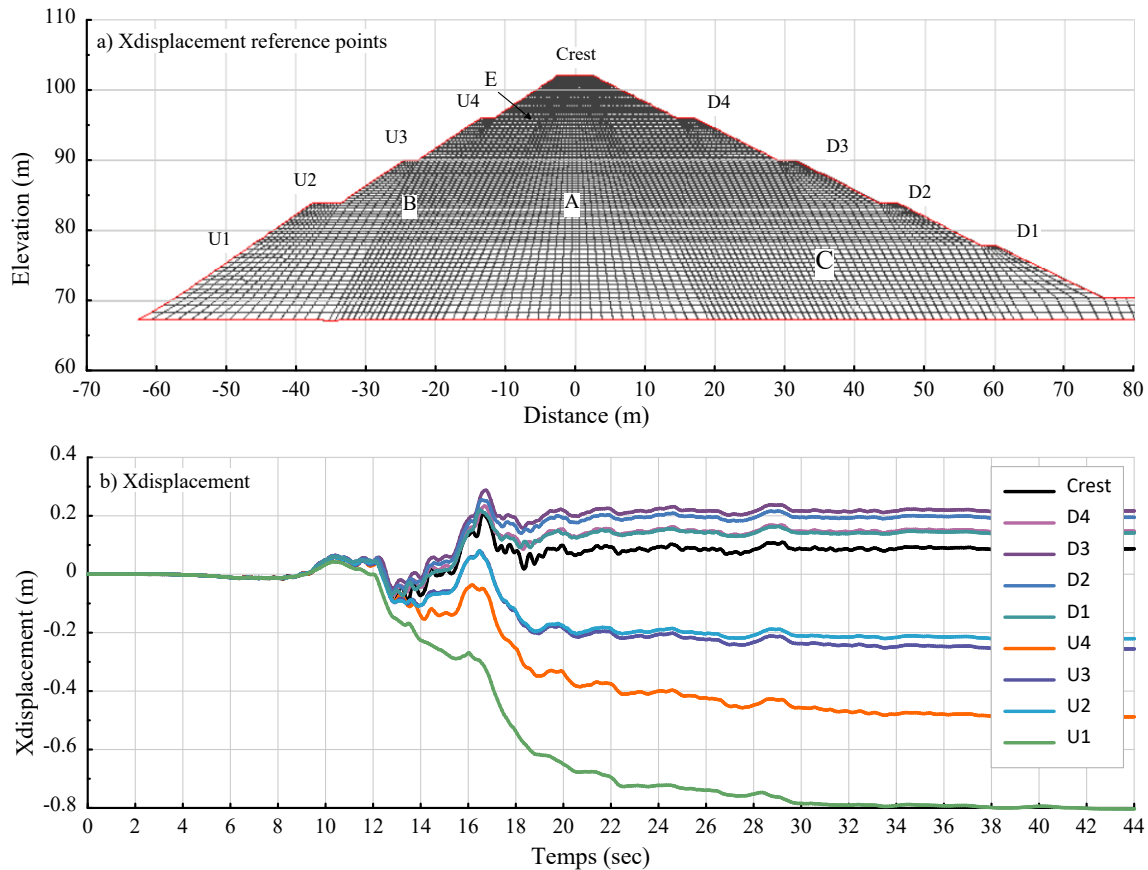
Figure 10. Dynamic analysis, X displacement at reference locations.

Overall, the dynamic analysis results show a good seismic behavior of the dam, based on this analysis, no uncontrolled release of the reservoir should be anticipated following an earthquake. However, it would be relevant to confirm the rockfill friction angle as well as the undrained strength of the clay fill.

7.4 *Creep*

The available data does not allow for a precise creep analysis. Instead of performing analyses with hypothetical parameters and speculating on the behavior of the structure, the authors recommend performing a few tests on placed clay to establish creep parameters that represents the actual structure conditions. Analysis to model the creep process is recommended once these parameters are available.

The authors are very interested to collaborate with the owner to perform accurate laboratory tests and to perform the appropriate analyses from a research perspective.

8 RECOMMENDATIONS

Based on the analyses performed, some recommendations are made to document or improve the robustness of this dam design:

8.1 *Upstream portion of the dam*

Perform the required verification in order to validate the rockfill friction angle (zone B). Based on the description of the materials a minimum angle of 45° is anticipated. This value would be consistent with the proposed density and would provide satisfactory static factor of safety for the upstream slope of 1.5H:1V. Otherwise, reinforcement work may be required.

8.2 *Core of the dam*

Conduct laboratory tests to characterize the clay fill of the core and to determine the appropriate parameters to allow an accurate creep analysis of this dam. It would also be relevant to validate the undrained shear strength of this clay. Based on available data on similar materials, an undrained shear strength of 75 kPa seems high. However, the undrained shear strength of this material does not appear to be an issue.

8.3 *Downstream portion of the dam*

After lowering the reservoir level, raising the downstream filter to the top of the core should be considered. Investigate the possibility of widening the future filter and thickening the existing upper filter on top of the draining fill (zone C) should be also considered. In general, the existing filters of this dam are very narrow. This design does not provide a large margin of safety in the event of local defects in this material. At first glance, concrete sand would be a good material for this filter. Downstream of this filter, an excellent transition must be provided in the areas with materials that meet the filter criteria. Although the use of draining material would be by far the best choice for this area of the dam, clay fill could be used downstream of the filter and transition zones.

It would also be preferable to remove the clay fill (zone A) in place on the downstream face, which cover the draining fill (zone C) and the filter (zone E) and place an inverted filter on the existing filter (zone E), the refill on the filter must meet the filter criteria and be a free-draining material.

8.4 *Pipes through the dam*

Where possible, all pipelines within the dam embankment should be decommissioned. The portion of each pipes between the upstream filters and the downstream filters should be injected with the most appropriate grout in order to ensure a permanent and sustainable sealing of the latter.

9 CONCLUSION

The embankment dam under study is an operating dam which has exhibited an atypical behavior after approximately 20 years of operation. The design of this structure, which incorporates pipes, suggested potential problems of internal erosion. The observations of erosion traces of the latter re-enforce this hypothesis. However, analysis of the downstream portion of the cross-section also shows a high potential of seepage on the downstream face of the dam, especially if the embankment has some anisotropic permeability. The delay before the appearance of these wet zones in the slope would also be consistent with the clayey nature of the backfill material (zone A) above the draining fill (zone C) and the filter (zone E).

A series of works are proposed in the downstream area of the dam to add lines of defense to the design. At a minimum, the downstream filter should be raised to the top of the core.

The dynamic analyses performed indicate that seismic stability would be ensured. Based on this analysis, no uncontrolled release of water from the reservoir should be anticipated following an earthquake. However, it would be relevant to verify if the signal adjustments is consistent with the seismic hazard applicable to this dam region. Moreover, these results should be confirmed with additional signals. Finally, it is recommended to validate the rockfill friction angle (zone B) and the clay fill (zone A) undrained shear strength.

After conducting laboratory tests to characterize the clay core fill and to determine the appropriate parameters to allow an accurate creep analysis of this dam, analysis to model the creep process is recommended. The authors are very interested to collaborate with the owner for this issue from a research perspective.

REFERENCES

Amirpour S., Ghlamallah N, Karray M. (2020). Seismic Assessment of Embankment Dams Using a Novel Energy-Based Approach, GeoVirtual 2020, Canada, September 14-16

Fell, R. & Foster, M. 1998, Embankment Dam incidents relating to piping associated with conduits.

FEMA, 2005, Technical Manual: Conduits through Embankment Dams, Best Practices for Design, Construction, Problem Identification and Evaluation, Inspection, Maintenance, Renovation, and Repair

Green, R.A., Mitchell,J.K. and Polito, C.P. 2000 « An Energy-Based Pore Pressure Generation Model for

Cohesionless Doils »in Proceedings of the John Booker Memorial Symposium–Developments in Theoretical Geomechanics, éd.Balkema, Rotterdam, Pays-Bas.

Itasca Consulting Group Inc. (2011). FLAC Software - Fast Lagrangian Analysis of Continua, Version 7. User's Manual. Itasca Consulting Group, Inc. Minneapolis, Minnesota, USA.

Itasca Consulting Group Inc. (2012) FLAC3D Software, Version 5. User's Manual. Itasca Consulting Group, Inc. Minneapolis, Minnesota, USA.

Karray, Mourad, Mahmoud N. Hussien, and Mohamed Chekired. 2015. —Evaluation of Compatibility between Existing Liquefaction Charts in Eastern Regions of North America.‖ Proc. 68e Conf. Can. de Géotech. et7e Conf. Can. Sur Le Pergélisol, 20 Au 23 Septembre2015, Québec, Québec. (Sept. 2015)

Kokusho, T., and Mimori, Y. 2015: Liquefaction potential evaluations by energy-based method and stress-based method for various ground motions. Soil Dynamics and Earthquake Engineering 75: 130–146.

Kuhlemeyer, R. L. and Lysmer, J. (1973) "Finite element method accuracy for wave propagation problems". Journal of the Soil Mechanics and Foundations Division, 99(5), pp. 421-427.

Lashin, Ibrahim & Karray, Mourad & Hussien, Mahmoud & Ghali, Michael & Chekired, Mohamed. (2021). Investigation of small-to large-strain moduli correlations of normally consolidated granular soils. Canadian Geotechnical Journal. 58. 1-22. 10.1139/cgj-2019-0741.

Wrachien, D. De. (2009). Dam-break Problems, Solutions and Case Studies, (September), 334. https://doi.org/10.2495/978-1-84564-142-9/04
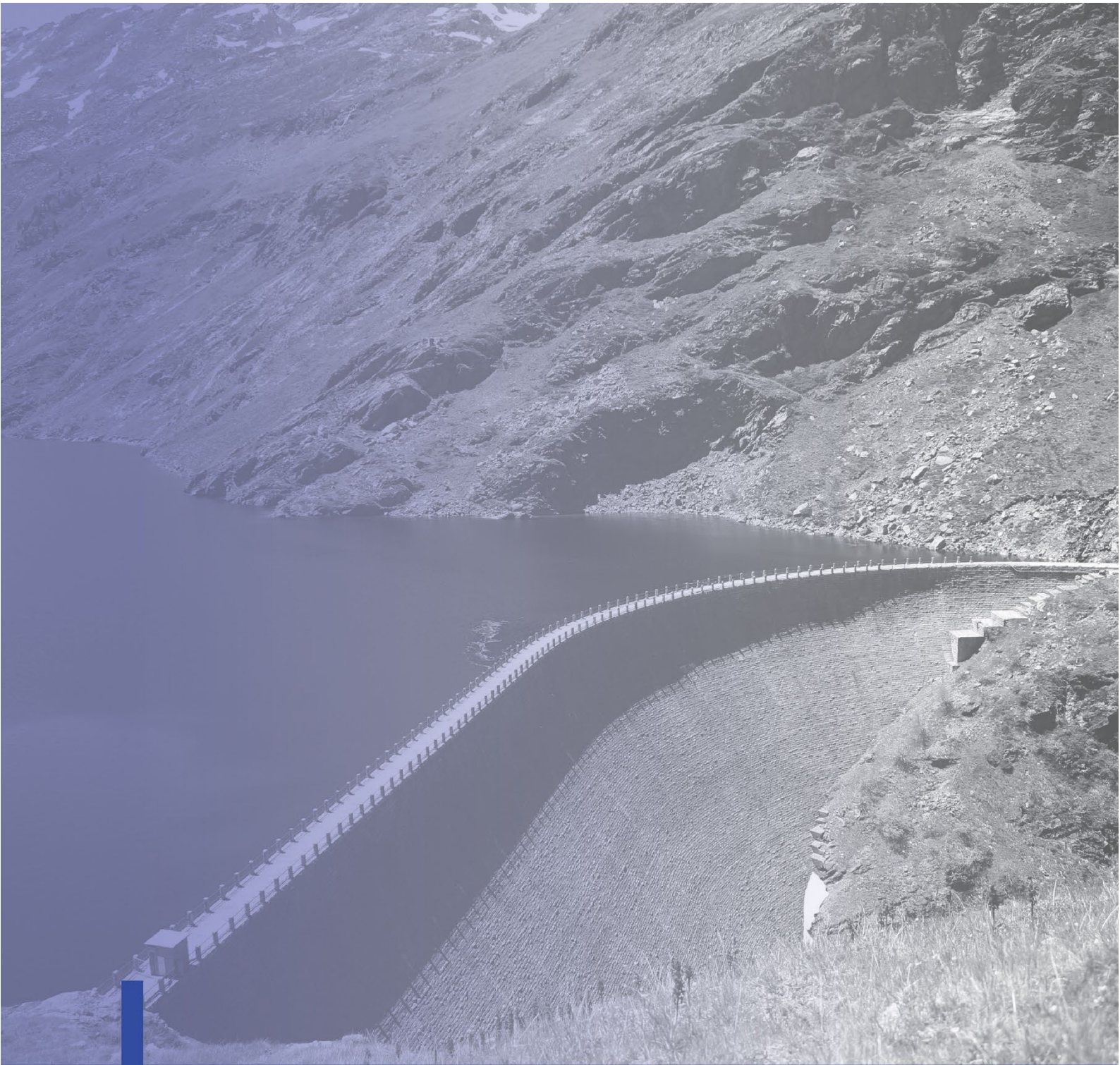
Choice of the contributor

Open theme

AMBIENT VIBRATION MEASUREMENTS: FEEDBACKS FROM MEASUREMENTS ON 20 CONCRETE DAMS AND COMPARISONS WITH FINITE-ELEMENT ANALYSES

Emmanuel Robbe

EDF Hydro Engineering Center, Le Bourget du Lac, France

Nicolas Humbert

EDF Hydro Engineering Center, Le Bourget du Lac, France

ABSTRACT: This paper presents the use of ambient vibration measurement to adjust finite-element analyses dedicated to seismic assessment of concrete dams. The paper describes not only the practical use of the recording devices and the processing of the signal but also some feedbacks from measurements on 20 concrete dams. In a second part, the calibration of finite-element model on measured frequencies on concrete dams (gravity and arch dams) is presented and discussed. Considering the relative simplicity of ambient vibration measurements, calibration of the numerical models with measured frequencies should be recommended when it is possible.

Robbe, Humbert

AMBIENT VIBRATION MEASUREMENTS: FEEDBACKS FROM MEASUREMENTS ON 20 CONCRETE DAMS
AND COMPARISONS WITH FINITE-ELEMENT ANALYSES

1 INTRODUCTION

EDF oversees the safety assessment of high number of concrete dams in France, including seismic safety assessment of dams located in certain areas. While engineers are used to calibrate numerical model with monitored displacements of the dam for static analyses, there was until recently no data to calibrate numerical model for dynamic analyses. That's why several years ago, the authors started using ambient vibration measurements to better understand the dynamic behavior of concrete dams and validate the numerical model of the structure analyzed.

The aim of this paper is to share with the dam engineers 'community our general feedback with ambient vibration measurements and the

2 AMBIANT VIBRATION MEASUREMENT

2.1 *Why?*

For the static assessment of existing concrete dam using finite-element analyses, physical properties of the numerical model are usually adjusted to reproduce the monitored behavior of the dam. This is generally done by adjusting the Young modulus of concrete and rock to reproduce the monitored displacement of the dam under hydrostatic load (usually obtained by a statistical analyses of the monitored displacements).

In the same spirit, for seismic assessment of concrete dams involving numerical analyses, dynamic properties of the materials should be calibrated to make sure the numerical model is reliable. Measurements and computations of the first frequencies of the structure provides an interesting way to perform such calibration.

As for static, comparison with measurements at the scale of the whole structure are more relevant compare to measurement of the dynamic properties of the concrete on core sample for example due to the size effects or the behavior of the vertical joints for instance.
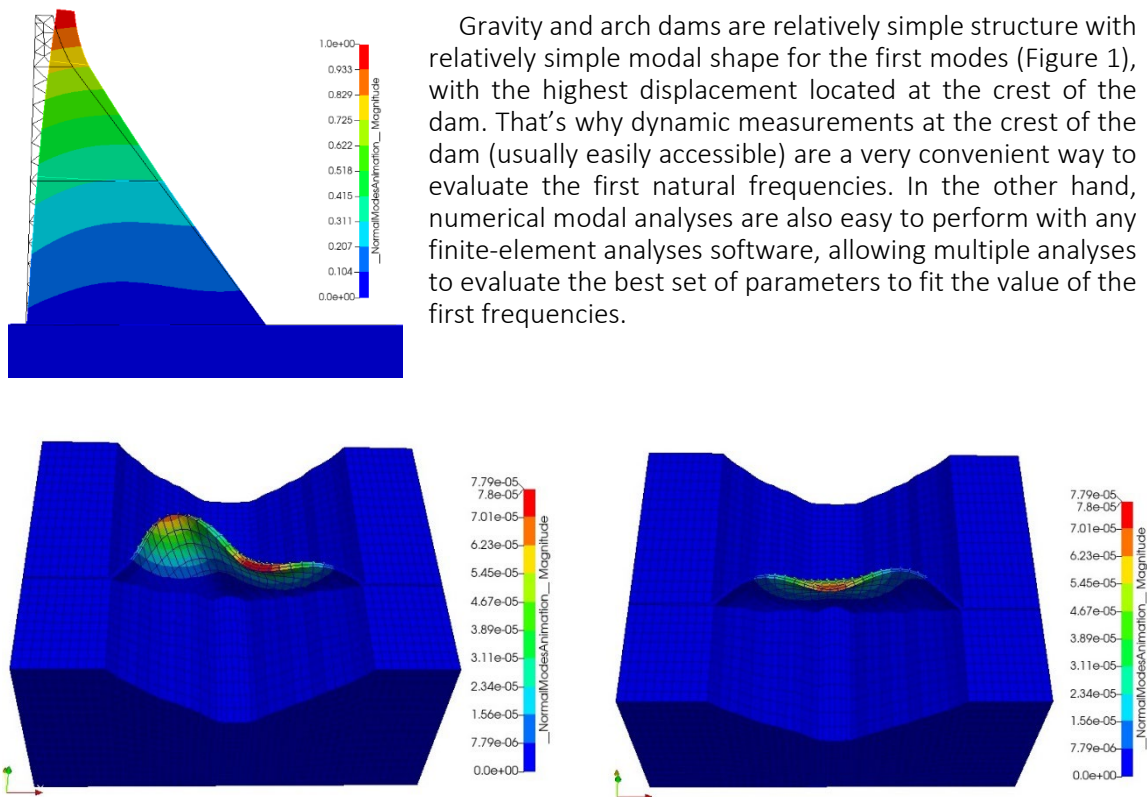

Gravity and arch dams are relatively simple structure with relatively simple modal shape for the first modes (Figure 1), with the highest displacement located at the crest of the dam. That's why dynamic measurements at the crest of the dam (usually easily accessible) are a very convenient way to evaluate the first natural frequencies. In the other hand, numerical modal analyses are also easy to perform with any finite-element analyses software, allowing multiple analyses to evaluate the best set of parameters to fit the value of the first frequencies.

Figure1. Modal shapes for gravity and arch dams

Robbe, Humbert

AMBIENT VIBRATION MEASUREMENTS: FEEDBACKS FROM MEASUREMENTS ON 20 CONCRETE DAMS
AND COMPARISONS WITH FINITE-ELEMENT ANALYSES

Finally, evaluation of the first frequency of a gravity dam in Japan by Kashima (2014) showed no clear difference between the first-order natural frequencies estimated based on seismic motion records and based on ambient vibration measurement records. Figure 2 shows that the first frequency evaluated from seismic event (recorded with permanent accelerometers) or ambient vibration measurements remain in the same rage. It should be reminded that the water level and the temperature conditions are responsible of variations of the value of the natural frequency (around 1 Hz). Such comparisons justify that natural frequency evaluated from ambient vibration measurements can be used for seismic assessment of concrete dams, at least if the dam remains under linear seismic behavior.
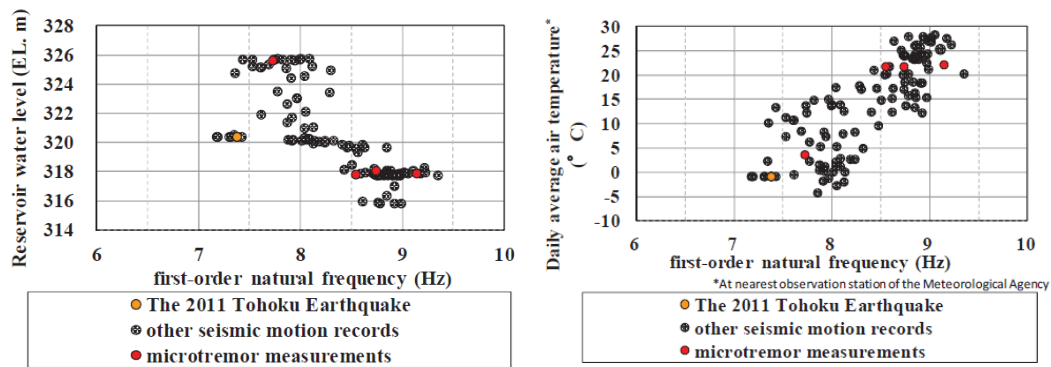
Figure 2. Comparison of the natural frequency estimated from seismic event or ambient vibration measurements (depending on the effect of the reservoir water level and the temperature). From Kashima (2014)

2.2 *Records*

Records on dams are achieved using Tromino © velocimeter devices, during approximatively 20 minutes. The device is positioned at the crest of the dam. The simplicity of the device allows for anybody to perform the measurement with a minimum knowledge of the device. Such measurements can be quickly done while visiting the dam for example.

Until recently, independent records were acquired, on several location of the dam, allowing to eventually identify different frequencies considering the modal shapes. Synchronized records (with 3 devices linked by a cable) are now used to be able to better distinguish modal shapes from the data's analyses (not described in this paper).

Miquel (2019) provides interesting advices to improve the quality of the records (for example, to cover the sensor with an isolated box to reduce spurious noise at low frequency).

Figure 3. Position of the recording device on the crest of dams

Robbe, Humbert

AMBIENT VIBRATION MEASUREMENTS: FEEDBACKS FROM MEASUREMENTS ON 20 CONCRETE DAMS
AND COMPARISONS WITH FINITE-ELEMENT ANALYSES

2.3 *Method for signal processing of the records*

First analyses of the records can be performed with the software Grilla provided with the Tromino© devices or with the open-source software Geopsy for more precise treatment. EDF Hydro choses to develop its own software called 'Modaloscope'.

The aim of the signal processing is to perform an averaging of frequency quantities on a high number of samples, coming from the input signal. This process is perfectly described in Dunand (2005) and rests on several steps described on the Figure 4 and summarized below:

- Filtering of the signal with a high pass filter (remove frequency content under 0.1 Hz),
- Cutting of the signal in 20 seconds length samples, with a 10s covering,
- Remove of the samples with standard deviation higher than the standard deviation of the whole signal (compare to a define criteria): this allows to remove part of the signal with high noise content because of a car passing nearby for example,
- Windowing of each sample with a Hanning window
- Computation of the power spectrum density (PSD) for each sample
- Averaging of all the PSD computed
- Modal identification using peak picking and evaluation of the frequency and modal damping.

The use of this method will be presented in the next chapter dedicated to the feedback from measurements on dams.
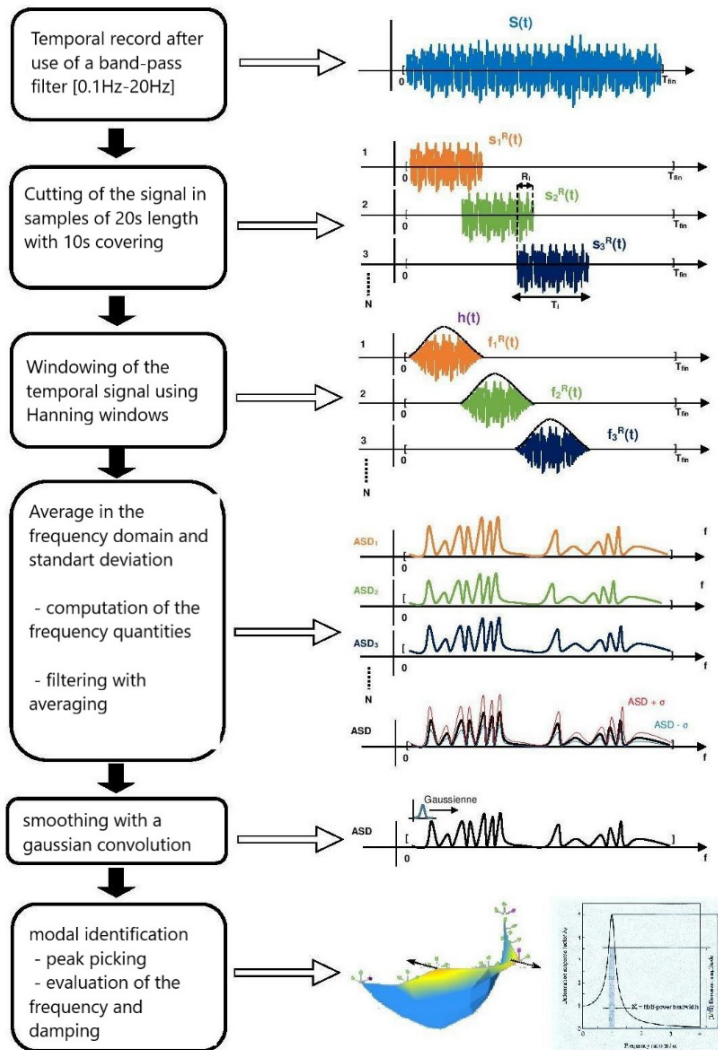
Figure 4. From records to modal identification

Robbe, Humbert

AMBIENT VIBRATION MEASUREMENTS: FEEDBACKS FROM MEASUREMENTS ON 20 CONCRETE DAMS
AND COMPARISONS WITH FINITE-ELEMENT ANALYSES

2.4 *Results from measurements on dams*

During the last 4 years, EDF engineers performed measurements on approximately 20 concrete dams: arch dams, gravity dams, multiple arch dams and gate-structure dams. The results of these measurements are summarized in Table 1, mainly for arch, gravity and multiple arch dams.

Velocity amplitudes range from 0.0001 mm/s for exceptionally low noise dam site to 0.03 mm/s for dam with loud noise, because of windy conditions, working powerhouse, or other reasons nearby. For such dam site, measurements do not allow to pick peaks corresponding to natural frequencies of the structure. Figure 5 shows the example of the frequency content at the crest of Sautet dam, with a working powerhouse nearby: sharp peaks with low damping (<1%) are characteristics of mechanical noise, covering the natural frequencies of the structure. Figure 6 shows the frequency content at Plan d'aval dam: a pipe of water near the crest of the dam also generated some noise at the frequency range of the structure.

Generally, velocities amplitudes lower than 0.005 mm/s provide clear results in the frequency domain, allowing to underline natural frequencies. Figure 7 shows the frequency content obtained for Gnioure 72m high gravity dam: first frequency at 5.4 Hz can clearly be seen. For arch dams, the first two frequencies are generally very close: symmetrical and anti-symmetrical modes are described in Figure 8 for Vouglans dam. Records at the center of the dam only shows the symmetrical 2nd mode at 2.8 Hz while records near the abutment only show the first anti-symmetrical mode at 2.7 Hz. In between, records show the two peaks simultaneously.

Table 1. Synthesis of the measurement and frequencies

Dam	Type of dam	Height (m)	average velocity amplitude (mm/s)	first mode frequency (Hz)	comments
Tech	Arch	33	0.025		lot of noise (wind)
Gage	Arch	41.75	0.002		measured at the abutment, first mode not clear
Plan d'aval	Arch	43.46	0.03		noise du to water pipe crossing the dam
Lanoux	Arch	45.2	0.001	4.5 & 4.78	small noise due to steps or wind - 2 first modes visible
Grangent	Arch	55.6	0.003	4.4	
Saint Guerin	Arch	70	0.002	3.76-3.93	
Couesque	Arch	70	0.001		measured at the abutment, first mode not clear
Chaudanne	Arch	73.9	0.025		powerhouse working
Sainte Croix	Arch	95	0.001	4.18	
Castillon	Arch	100			lot of noise (cars, pedestrian, wind)
Sautet	Arch	126	0.006		powerhouse working (maybe 11.6 Hz)
Vouglans	Arch	130	0.005	2.7 - 2.8	
Roselend	Arch - buttress	150	0.002	3.09 & 3.47	
Migoellou	Buttress	44	0.001	6.8	on buttress (+ low frequency content)
Girotte	Buttress	48.5	0.0003		several modes depending on the location
Pinet	Gravity	40	0.004		difficult to pick up the first modes
Plan d'amont	Gravity	50	0.0015	6.7	
Guerledan	Gravity	54.6	0.002	6.5	smothening might be useful
Eguzon	Gravity	61.1	0.007	6.8	
Gittaz	Gravity	66	0.0001	8.6	smothening might be useful
Gnioure	Gravity	72	0.002	5.4	
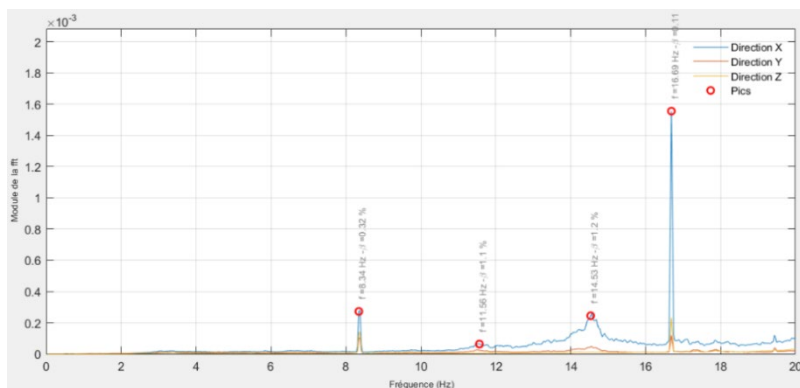
Figure 5. Frequency content at Sautet dam (effect of the working powerhouse)

Robbe, Humbert

AMBIENT VIBRATION MEASUREMENTS: FEEDBACKS FROM MEASUREMENTS ON 20 CONCRETE DAMS
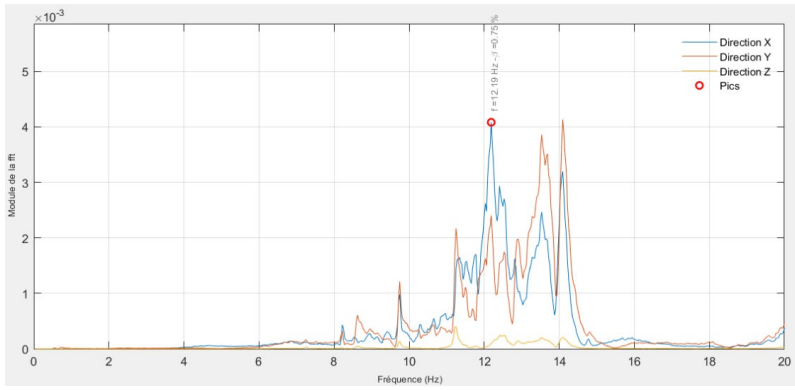AND COMPARISONS WITH FINITE-ELEMENT ANALYSES

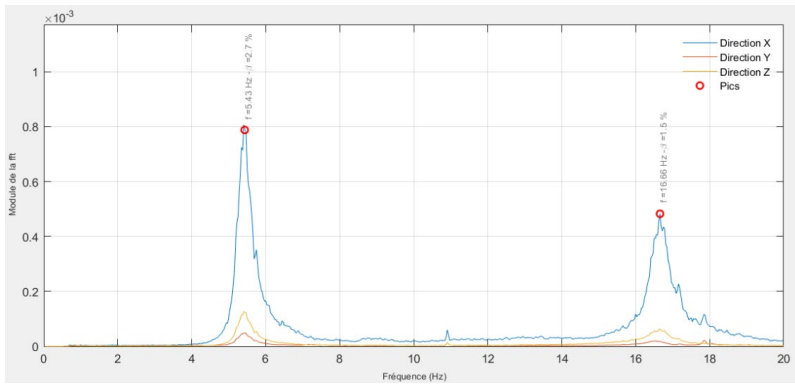Figure 6. Frequency content at Plan d'aval dam (effect of a water pipe nearby)

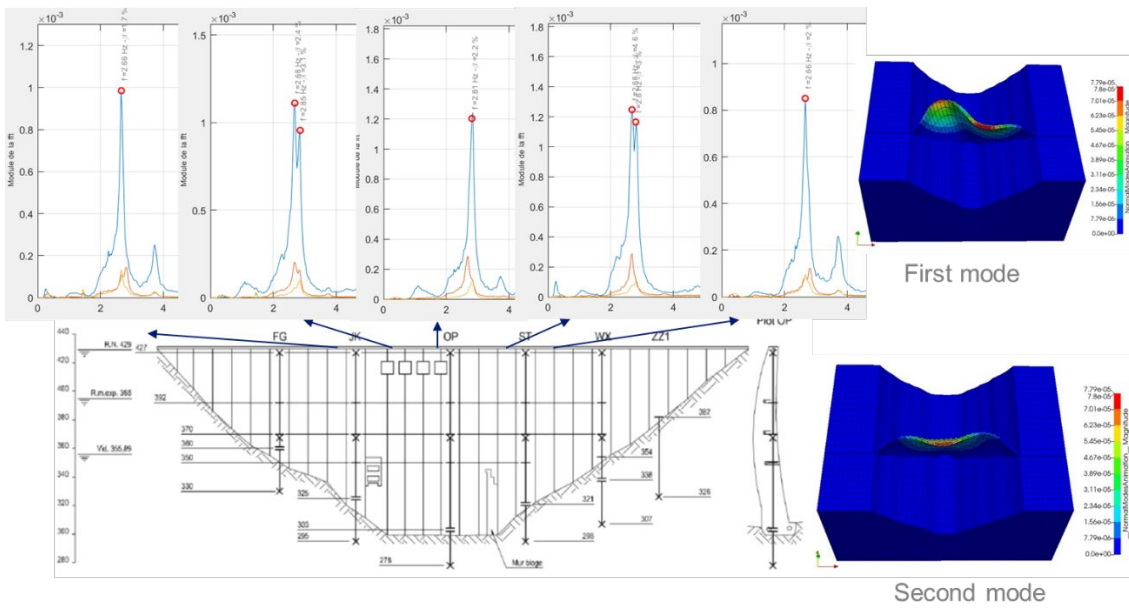Figure 7. Gnioure gravity dam frequency content

Figure 8. Vouglans frequency content: 2 first modes very close (2.7 & 2.8 Hz)

For the measured arch dams, first frequencies go from 2.7 to 4.5 Hz, depending on the height, the shape of the valley and how fin is the arch. Water level and thermal conditions are also responsible of variation of the frequencies.

Robbe, Humbert

AMBIENT VIBRATION MEASUREMENTS: FEEDBACKS FROM MEASUREMENTS ON 20 CONCRETE DAMS
AND COMPARISONS WITH FINITE-ELEMENT ANALYSES

For the fourth measured gravity dams (50 to 72m high) values go from 5.4 to 8.6 Hz. Table 2 presents some comparison between:

- Measured frequencies for each gravity dams (Guerledan, Eguzon, Gittaz and Gnioure)
- Computed frequency from Lokke & Chopra (2013) considering the dam-water-foundation interaction. For this method, the frequency relies on the moduli of elasticity of the concrete and the foundation. 3 sets of parameters will be used here: soft materials with Ec=20GPa, Ef=15 GPa, medium materials with Ec=30GPa, Ef=25 GPa, stiff materials with Ec=35GPa, Ef=35 GPa. For the water interaction, the reservoir is supposed full (almost the case during the measurements) and the wave reflection coefficient is set to 1.
- Computed frequency from Tardieu (1993) formula for the full reservoir: $N = 0.17 * \frac{S}{H}$ where S is velocity of the shear wave computed from the modulus of elasticity and the density of concrete, and H the height of the dam. 3 assumptions are considered with moduli of elasticity at 20, 30 and 40 GPa.

The comparison shows that frequency computed by Chopra are underestimated, even with the assumption of stiff materials. This is probably because the method was developed with the assumption of a 2D shape while some 3D effect tends to stiffen the structure. This is particularly the case for Gittaz, Eguzon and Gnioure dams that are curved. Tardieu formula, that doesn't consider the stiffness of the foundation, provide for that reason higher frequencies. In any case, with uncertainty of the stiffness of the materials, the gap between measured and computed frequency can be quite important, between 1 and 2 Hz, even higher for gravity dams in a narrow valley.

Table 2. Comparison between frequencies measured and computed from Chopra and Tardieu formulas with several assumptions (Ec=concrete modulus, Ef=foundation modulus)

Dam	Height(m)	Frequency measured (hz)	Density (kg/m3)	Frequency computed from Chopra (Hz)			Frequency computed from Tardieu (Hz)		
				Ec20/Ef15	Ec30/Ef25	Ec35/Ef35	Ec20	Ec30	Ec40
Guerledan	46.8	6.5	2200	4.9	5.8	6.1	7.1	8.7	10.0
Eguzon	62.1	6.8	2300	3.8	4.5	4.8	5.2	6.4	7.4
Gittaz	66	8.6	2400	3.6	4.2	4.5	4.8	5.9	6.8
Gnioure	72	5.4	2400	3.2	3.7	4.0	4.4	5.4	6.2

3 COMPARISON WITH FINITE-ELEMENT ANALYSES

Seismic assessment of concrete dams requires to deal with a lot of uncertainties: seismic hazard evaluation, accelerograms selection for time-history analyses, introduction of the seismic load in the numerical model, non-linear behavior of the structure, dam-water-foundation interaction model, selection of the damping value, dynamic properties of the materials (concrete and foundation). The knowledge of the measured first natural frequencies of the dam allows to reduce the uncertainty relative to this last assumption.

Without frequencies measurements on dams, dynamic moduli of elasticity are generally considered from sample core tests. Doing this, ratio between static and dynamic moduli of elasticity have been summarized in the ICOLD bulletin 2009, reminded in Table 3. In the engineer practice, the dynamic/static ratio of 1.25 is very often considered but it should be reminded that such value is valid for sample core tests only.

Robbe, Humbert

AMBIENT VIBRATION MEASUREMENTS: FEEDBACKS FROM MEASUREMENTS ON 20 CONCRETE DAMS
AND COMPARISONS WITH FINITE-ELEMENT ANALYSES

Table 3. Results from investigations for seismic moduli of elasticity (ICOLD Bulletin 2009)

Dynamic/static Ratio			Reference
max.	av./single value	min.	
	1.25		Bureau's of Reclamation test series
1.57	1.42	1.28	Big Tujunga dam, cores drilled from the dam. 2 concret
1,48	1.38	1,32	types: 25 MPa (1. row) and 36 MPa strength (2. row)
1.10	0.89	0.66	Bureau's of Reclamation test series
	1.18		Crystal Springs Dam
	1.15		Tests on Swiss dams
	1.04		extensive testing for Zervreila Dam (Switzerland)

For the static assessment of arch dams, the French guidelines (CFBR 2018) recommend calibrating the finite-element model with the monitored displacement of the dam. This is usually done with the following steps:

- Statistical analyses of the monitored displacements to evaluate the displacement due to the hydrostatic load only (using HST or HSTT analyses for example),
- Finite-element analyses of the dam with increasing hydrostatic load and computation of the displacements at the location of the displacement monitoring devices,
- Calibration of the static moduli of elasticity of concrete and foundation for the finite-element model to correctly reproduce the radial and tangential displacements of the arch for hydrostatic load only.

For the seismic assessment of concrete dams, the dynamic moduli of elasticity could also be adjusted compare to the measured natural frequencies of the dam, based on ambient vibration measurements, with the following steps:

- Calibration of the concrete and foundation moduli of elasticity as previously described
- Modal analyses of the dam considering fluid-structure and soil-structure interaction to evaluate the first frequencies (at least 1st frequency for a gravity dam, and 1st and 2nd frequency for arch dams)
- Evaluation of the ratio r_{sd} such $E_{dyn} = r_{sd}E_{stat}$ with E_{dyn} and E_{stat} the dynamic and static moduli of elasticity. This ratio is supposed identical for concrete and foundation.

In the engineering practice, this ratio rsd is considered at 1.25, misguided by the reference of the ratio proposed by ICOLD 2009 from core sample tests. The static moduli adjusted from the monitoring behavior are actually different from the static moduli from sample core tests: such moduli take into account the effect of the vertical contraction joint and some creep component coming from the time scale (weeks / month) of the hydrostatic loads change.

The following chapters describe the calibration process of finite-element model for the seismic assessment of gravity and arch dams.

3.1 *Gnioure gravity dam*

Gnioure dam is a 72m high gravity dam, with a curved part near the left abutment (Figure 9). A 2D finite-element model is developed (Figure 10). The static elastic moduli of the concrete and the foundation are calibrated to reproduce the monitored radial displacement of the crest and the toe of the dam as shown in Figure 11. The moduli of concrete and foundation are respectively 27.5 GPa and 50 GPa. The static modulus of foundation is particularly high, probably du the narrow shape of the valley at the bottom of the dam involving 3D effect.

Figure 12describes the several steps to adjust the finite-element model on the 5.4 Hz first frequency measured (Table 2) on the dam at almost full water level by gradually increasing the stiffness of the concrete and foundation by a constant ratio:

- With Westergaard added masses for the fluid-structure interaction, a dynamic/static ratio of 1.85 is required to reach the targeted frequency
- With acoustic fluid element for the fluid-structure interaction, the increase of the stiffness materials does not allow to reach the targeted frequency due to the 2D reservoir frequency at

$$f_r = {c}/{4H} = {1440}/{4 \times 72} = 5.1 \ Hz$$

Robbe, Humbert

AMBIENT VIBRATION MEASUREMENTS: FEEDBACKS FROM MEASUREMENTS ON 20 CONCRETE DAMS
AND COMPARISONS WITH FINITE-ELEMENT ANALYSES

- A 3D more realistic finite-element model of the reservoir shows that frequency of the reservoir is at 6.8 Hz
- The 2D finite-element model is artificially improved by considering a more realistic level of the foundation under the reservoir and slightly reducing the velocity of the wave in the fluid to get a more realistic reservoir frequency in 2D.
- Finally, a similar dynamic/static ratio of 1.85 is obtained for the finite-element model with fluid elements.

Despite the limitation of the representation of a 3D problem with a 2D finite-element model, the analysis shows that an important increase of the stiffness must be considered to adjust the dynamic elastic moduli from the static moduli. For gravity dams, this result need to be confirm with other examples.
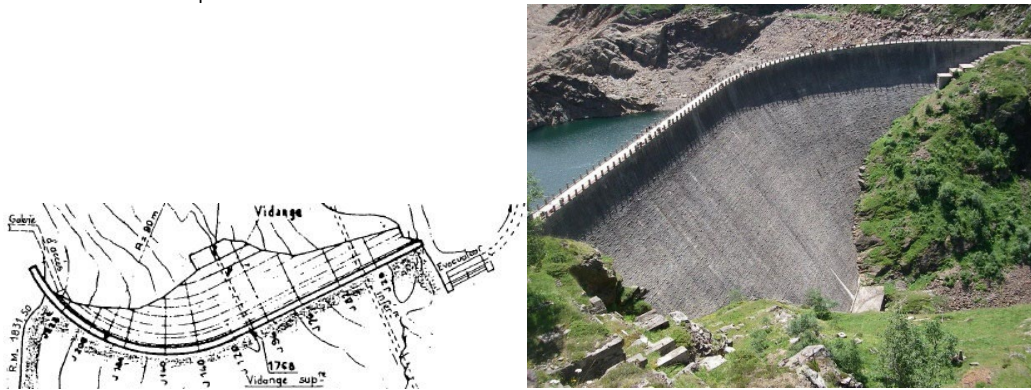
Figure 9. Gnioure gravity dam
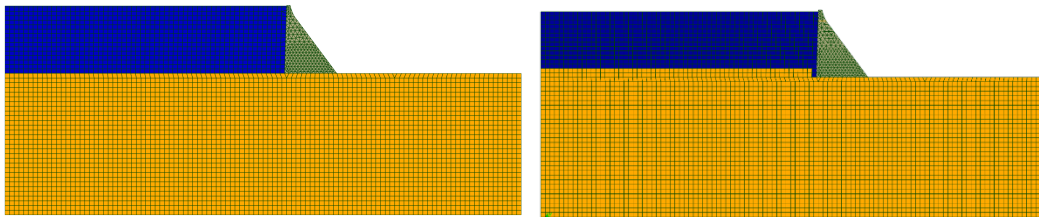
Figure 10. 2D finite-element model of Gnioure dam (initial and with raise foundation elevation in the reservoir
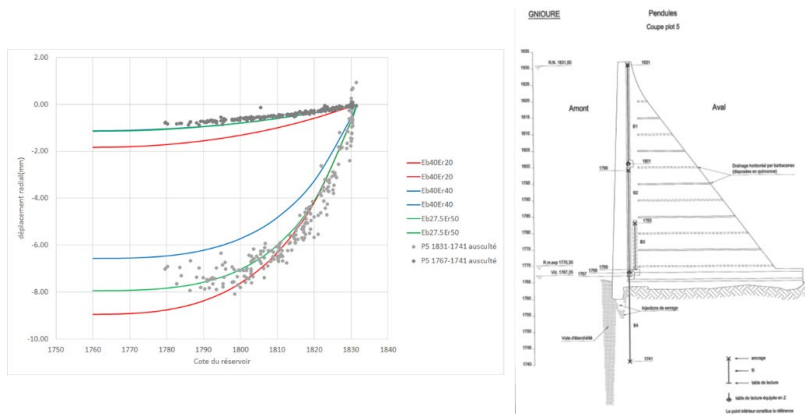
Figure 11. Calibration of the static moduli compared to monitored displacement at the crest and at the toe

Robbe, Humbert

AMBIENT VIBRATION MEASUREMENTS: FEEDBACKS FROM MEASUREMENTS ON 20 CONCRETE DAMS
AND COMPARISONS WITH FINITE-ELEMENT ANALYSES
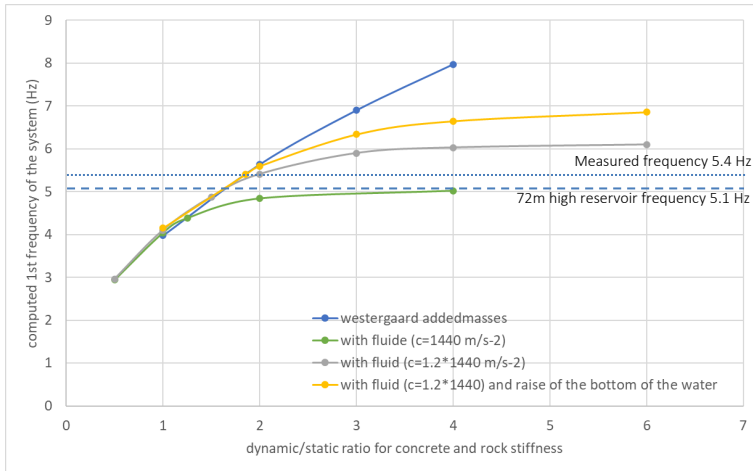
Figure 12. Evaluation of the dynamic / static ratio for Gnioure gravity dam

3.2 *Vouglans arch dam*

Vouglans dam is a 130m high arc dam with a normal reservoir level at 427m. Two sets of measurement were carried out, allowing to evaluate the first frequencies as previously presented:

- 9/03/2021, reservoir at 416.5, first frequencies are 2.7, 2.8, 3.7 Hz,
- 5/10/2021, reservoir at 420.2, first frequencies are 2.6, 2.75, 3.6 Hz.

A static finite-element analysis of the dam with an increasing hydrostatic load allows to calibrate the static moduli for concrete and foundation based on the monitored displacement of the arch.

Modal analyses with fluid element (mesh and modal shapes on Figure 13) are performed with an increasing dynamic/static ratio for elastic moduli assumptions. Figure 14 presents the evolution of the frequency computed and measured, function of the water level: when dynamic moduli are equal to static moduli, the frequencies are underestimated. A dynamic / static ratio of 1.5 allows to adjust measured and computed frequencies (the 2nd frequency become slightly overestimated).

With such assumptions for the dynamic moduli of elasticity, if the fluid elements are replaced by Westergaard added masses, these masses should be reduced by a factor 2 to keep similar frequencies under modal analyses.
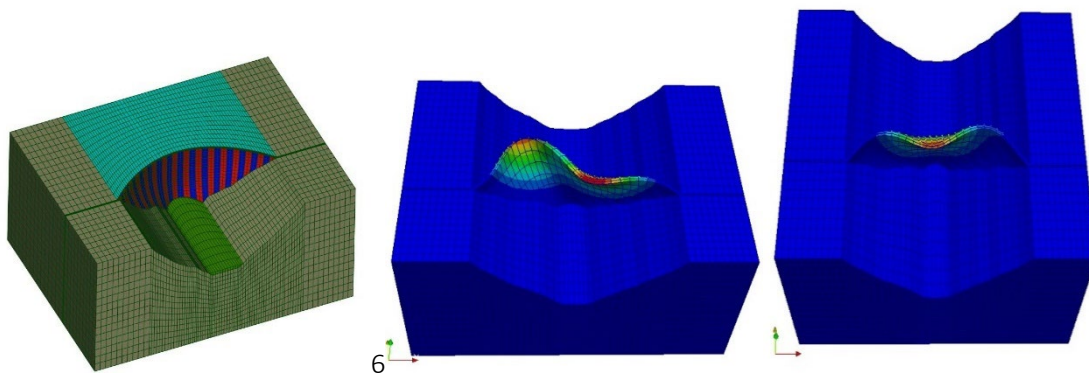
Figure 13. Mesh of Vouglans dam and shape of the first two modes

Robbe, Humbert

AMBIENT VIBRATION MEASUREMENTS: FEEDBACKS FROM MEASUREMENTS ON 20 CONCRETE DAMS
AND COMPARISONS WITH FINITE-ELEMENT ANALYSES
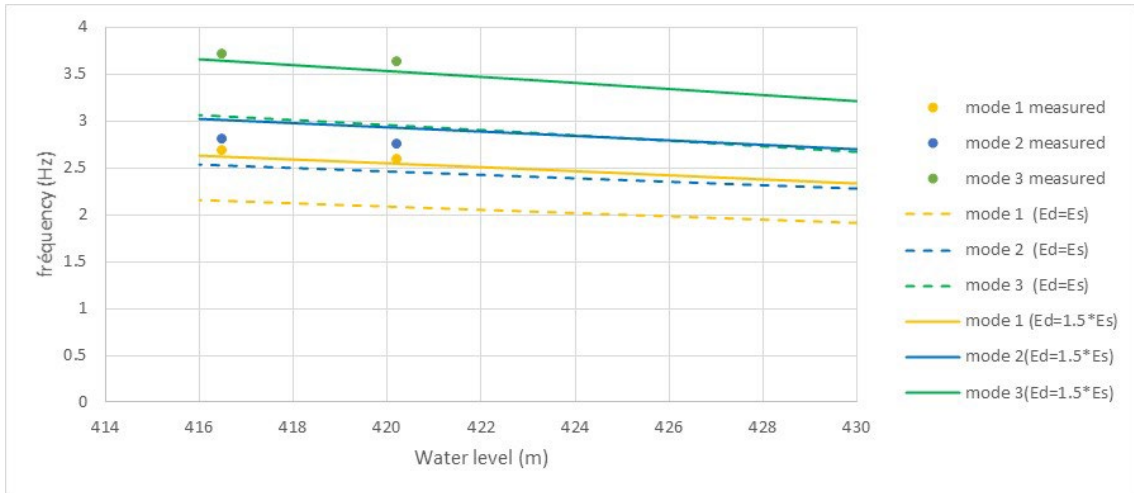
Figure 14. Evaluation of the dynamic / static ratio for Vouglans dam

3.3 *Other arch dams*

Similar analyses and comparison were performed on other arch dams. Table 4 describes the main results of the comparison based on the frequencies measurements. There are no constant rules that can be defined bases on the 4 dams studied nevertheless, on 3 cases, the dynamic/static ratio for elastic modulus is higher than 1.5. Such value would not have been considered without ambient vibration measurements.

Comparison between fluid-structure interaction based on Fluid elements or Westergaard added masses shows that an important reduction of the added masses is mandatory for arch dams to remain in a similar range of frequencies.

Table 4. Results from calibration on arch dams

Dam	first mode frequency (Hz)	modulus from static calibration(GPa)		Dynamic / static ratio from frequency calibration	reduction of Wstg added masses
		concrete	foundation		
Lanoux	4.5 & 4.8	20	(*)	1.75	0.6
Roselend	3.0 & 3.5	35	25, 12 & 8	1.8(**)	
Saint Guerin	3.8 & 3.9	32.5	15	1	0.5
Vouglans	2.7 & 2.8	38.5	32.5	1.5	0.5

(*) specific assumptions are considered due to the orthotropy of the foundation

(**) value with usual Westergaard added masses

4 CONCLUSION

This paper describes some practical advices for simple evaluation of the first natural frequencies of concrete dams using ambient vibration measurements. At the crest of the dams with one or few devices, performing a record is quite simple and can be done by non-specialist, during a routine visit of the dam. It's recommended to avoid all conditions that can generate disturbing noises: working powerhouse, wind conditions, pipe with running water nearby. Short duration noises such as cars or pedestrians crossing nearby can be removed from records and do not disturb the results. Processing the signal to extract the natural frequencies is a more complex task but fully documented and the authors chose to develop their own tools considering the number of dams managed by EDF. Results of measurements on 20 concrete dams are summarized.

Comparison between frequencies measured and computed (from simplified formula or FE analyses) shows significant gaps: comparison for gravity and arch dams shows that from a

Robbe, Humbert

AMBIENT VIBRATION MEASUREMENTS: FEEDBACKS FROM MEASUREMENTS ON 20 CONCRETE DAMS
AND COMPARISONS WITH FINITE-ELEMENT ANALYSES

dynamic point of view, dams are stiffer than expected at first. If the static elastic moduli for concrete and foundation were calibrated compare to monitored displacement under hydrostatic load, dynamic/static ratio reaches 1.8 for several dams. Considering the first frequencies of dams are generally lower than the peak of the design spectrum (for relatively high dams), underestimation of the dam frequency leads to an underestimation of the dam's response under earthquake. For arch dam, analyses also show that Westergaard added masses should be reduced to correctly fit the measured frequencies.

From the authors 'point of view, seismic assessment of dams is already full of uncertainty (seismic hazard definition, accelerograms selection, seismic loading on the numerical model, mechanical behavior of the structure (linear, non-linear, damping). Considering the relative simplicity of ambient vibration measurements, calibration of the numerical models with measured frequencies should be recommended when it is possible.

REFERENCES

Miquel B. The use of ambient vibration instrumentation for dams at Hydro-Québec, *12th Canadian conference on earthquake engineering*

Takeshi Kashima T. 2014. Effects of reservoir water level and temperature on vibration characteristics of concrete gravity dam, *ICOLD Symposium Bali*, 2014

Dunand F. 2005. Pertinence du bruit de fond sismique pour la caractérisation dynamique et l'aide au diagnostic sismique des structures de génie civil

Lokke A. & Chopra A. Response spectrum analysis of concrete gravity dams including Dam-Water-Foundation interaction, *Pacific earthquake engineering research center*, July 2013

Tardieu, Méthodes simplifiée de prédimensionnement des barrages-poids en zone sismique, 1993

ICOLD Bulletin. 2009. The physical properties of hardened conventional concrete in dams

CFBR 2018 Recommendations for the safety assessment of arch dams 'behavior

THE CONTRIBUTION OF NUMERICAL MODELLING TO ASSESS DAM SAFETY: THE CASE OF BUTTRESS, HOLLOW AND MULTIPLE ARCH/SLAB DAMS

Antonella Frigerio
Ricerca sul Sistema Energetico - S.p.A., Milan, Italy

Guido Mazzà
Chairman of ICOLD Tech. Committee "A" - Vice Chair of ITCOLD, Milan, Italy

ABSTRACT: Buttress (both solid or hollow) or multiple arch/slab dams are a type practically abandoned internationally, even if there are some relatively recent examples of the 70s-80s (e.g., Haen dams, 1963 and Storfoss, 1982, in Norway). In the Italian context there are numerous examples of this type of works built between the two World Wars and immediately after the II World War. A total of 37 dams are in operation (40% buttress, 30% hollow gravity, 30% multiple arch/slab). The problems of these structures are known: cracks (generally caused by phenomena of thermal origin, differences of the buttresses height, expansive chemical reactions, etc.), degradation associated with environmental conditions (e.g., due to corrosion of the reinforcement bars when present), phenomena of aging and degradation. To these problems some critical issues are added related to compliance with current legislation which requires the verification of more stringent conditions not foreseen in the design phase (e.g., higher seismic loads or more up-to-date criteria on the evaluation of uplift pressures). The verification of these structures has highlighted the need to systematize the knowledge of the phenomena that gave rise to the problems mentioned above, to deepen the evolutionary dynamics of decay and cracking states, to share the experiences on rehabilitation interventions. Numerical modelling has certainly contributed significantly to the understanding of the phenomena and to the evaluation of the structural behaviour depending on the applied actions. Some of the above-mentioned problems were topics of the Benchmarks proposed by the ICOLD Technical Committee "*Computational Aspects of Analysis and Design of Dams*". This article presents an overview of the problems concerning this type of dams and highlights the support that numerical models can offer for the evaluation of their safety and to identify the most effective interventions for long-term safety conditions.

1 INTRODUCTION

The construction of large dams is closely related to the development of the hydroelectric sector which was the backbone of the industrialization process in many European countries since the last part of the nineteenth century and the beginning of the twentieth.

The need to exploit the water resource for energy purposes leads to a great development of the dams; just think that Italy went from about a dozen dams at the end of the nineteenth century to almost 400 only in the first half of the twentieth century.

As in all industrial processes, the necessity to increase the hydroelectric production and development necessarily led to the need to maximize benefits above all by reducing the costs and construction times of dams. The goal was to achieve the maximum manufacturing economy while still ensuring an adequate degree of safety.

These are the principles, combined with the socio-economic context that characterized those years, which led to the evolution of the construction techniques of the dams.

At the base of this process there are then some fundamental elements such as:

- the evolution of material and labour costs;
- progress in geological and geotechnical investigations and in the treatment of foundation soils;
- advances in the static assessment of structures;
- the knowledge acquired on the basis of the monitoring of the although still few works in operation;
- advances in the material technology, in the construction machinery and equipment and in the entire production process.

Already at the beginning of the twentieth century there was a trend towards the optimization of the shape of dams marked by an economy of volume.

The first constructions based on this evolutionary trend, focused on a decisive saving of volume and therefore of materials, occurred in the first twenty-five years of the 1900s with concrete buttress dams connected by slabs or vaults. However, the collapse of the Gleno Dam, belonging to this type of construction, on 1st December 1923 effectively sanctioned the end of this type of dams [Barbisan, 2007]. Figure 1 shows two images of the Gleno Dam before and after the collapse.
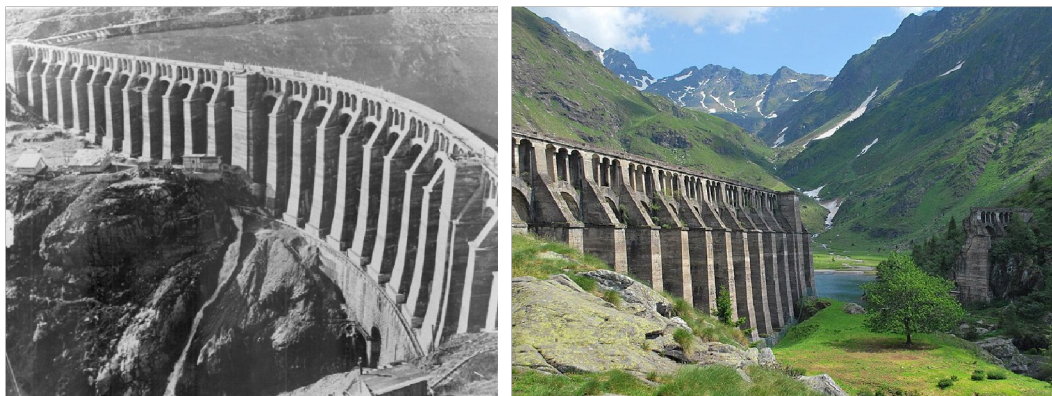
Figure 1. Gleno Dam before (left) and after (right) the collapse.

From the investigations conducted to identify the responsibilities, it appears that the cause of the collapse was attributable to the poor execution of the massive gravity foundation pad that blocked a gorge in the central part of the work.

This event generated a sense of mistrust towards "lightened" dams in general, which in the years immediately following led to the prevalence of more massive structures that found development in Italy until the early 1960s.

Subsequently, the increase in the cost of labour, having a much greater impact for these works than for gravity dams, no longer found compensation in the reduction of volumes. The evolution of construction machinery has also contributed to the abandonment of "lightened" gravity dams,

favouring the evolution of more massive gravity structures and, more recently, with a reduced cement content (this is the case of Rolled Compacted Concrete dams).

Figure 2, Figure 3 and Figure 4 show the three different types of dams that are the subject of this report: buttress, hollow gravity, multiple arch/slab dams, respectively.
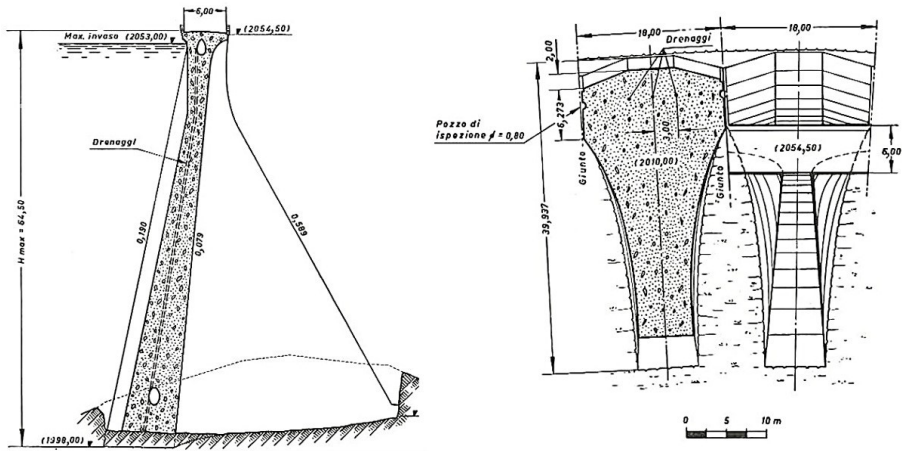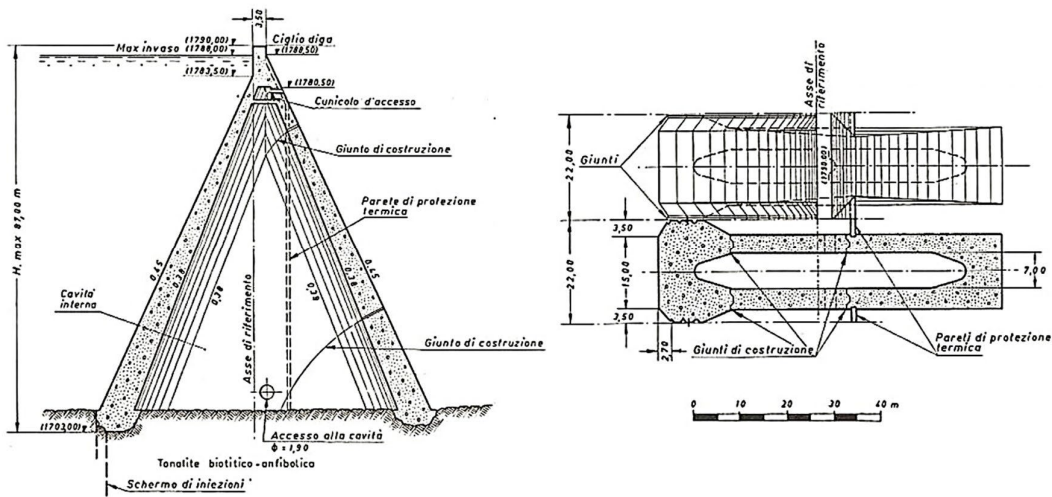
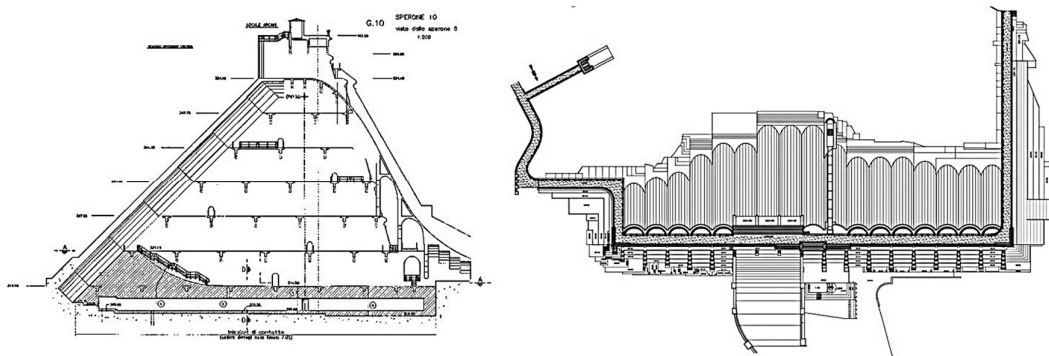

Figure 2. Buttress dam.

Figure 3. Hollow gravity dam.

Figure 4. Multiple arches dam.

2 MAIN PROBLEMS AND RESTORATION INTERVENTIONS

To systematize the knowledge relating to the behaviour of these structural types and the most appropriate criteria for assessing their safety, ITCOLD has set up the Working Group "*Behaviour, problems, rehabilitation of hollow gravity, buttress and multiple arch/slab dams*" and assigned the following Terms of Reference:
- Reconnaissance of the construction aspects.
- Reconnaissance on problems associated with this dam types.
- Reconnaissance of the remediation works.
- Methodologies of investigation.
- Monitoring methodologies.
- Criteria and methodologies for safety re-evaluation.

Figure 5 shows the trend of the construction of dams in Italy and the progression of rehabilitation interventions since the 1970s.
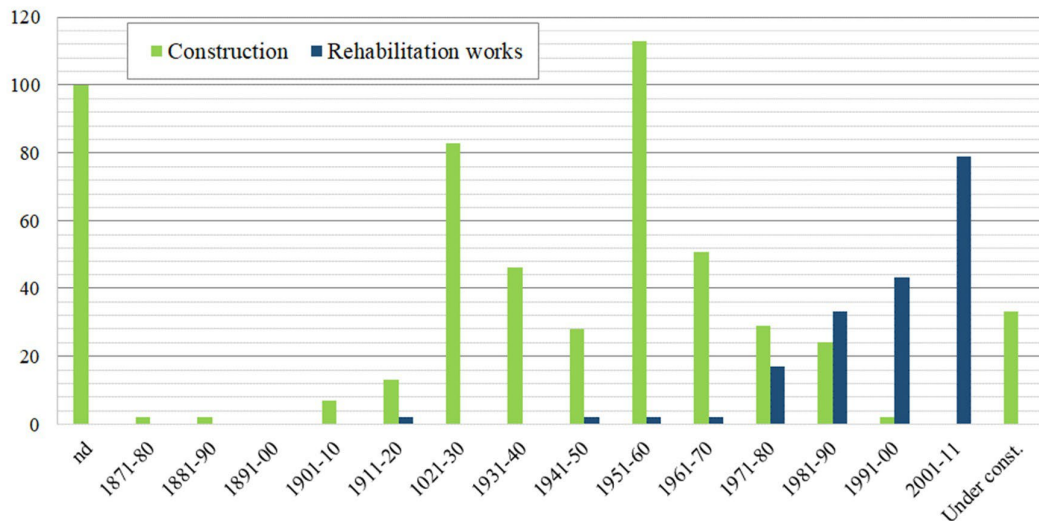
Figure 5. Progress of the construction of dams in Italy and the progression of rehabilitation interventions since the 1970s.

Before addressing the specific problems of this type of dams, it is appropriate to recall what is reported in the ITCOLD Bulletin [ITCOLD, 2018] regarding the various criticalities encountered in the dams of any type in operation and the related remediation interventions that mainly concerned structural deficiencies and inadequacy of the outlet works. Over 60% of the reports refer to:
- Structural problems.
- Insufficient impermeability of the dam body and of the grout cut off.
- Inadequate response to external or internal actions.

Over 30% of the reports belong to the category of inadequacy of the outlet works:
- Insufficient dimensioning of the outlet works.
- Inadequacy of the interception organs.
- Inadequate response to external actions (floating or sedimented material).

Table 1 shows the list of 37 Italian dams of this type indicating their main characteristics and whether rehabilitation works have been carried out.

Table 1. Italian multiple arch/slab, buttress and hollow gravity dams.

Dam name	Year of construction	Type	Hight (m)	Volume of reservoir (Mm³)	Rehabilitation works
Alto Temo	1984	Buttress	54.1	91.1	
Ancipa	1952	Hollow gravity	104.4	30.4	YES
Bau Muggeris	1949	Hollow gravity	58.7	61.4	YES
Bau Pressiu	1972	Buttress	52.9	8.5	
Brugneto	1964	Buttress	22.5	0.95	
Casoli	1958	Buttress	47.0	21.0	
Combamala	1916	Multiple slabs	35.0	0.4	Decommissioned
Corbara	1963	Buttress	52.0	192.0	YES
Fedaia	1954	Buttress	63.9	16.7	
Fontanaluccia	1928	Multiple arches	40.0	2.7	
Gioveretto	1956	Buttress	81.4	19.98	YES
Lago di Trona	1942	Hollow gravity	53.0	5.35	YES
Lago Eugio	1959	Buttress	48.5	4.95	YES
Lago Inferno	1944	Hollow gravity	37.0	4.17	YES
Lago Venina	1926	Multiple arches	44.5	11.19	YES
Liscia	1962	Hollow gravity	65.0	105.13	
Lomellina	1910	Buttress	19.9	0.25	YES
Malga Bissina	1957	Hollow gravity	81.0	61.0	
Malga Boazzo	1956	Hollow gravity	53.5	12.26	
Molato	1928	Multiple arches	52.6	8.24	YES
Montagna Spaccata2	1958	Buttress	14.4	9.05	
Ozola	1029	Multiple arches	27.5	0.09	
Pantano D'Avio	1952	Hollow gravity	59.0	12.67	YES
Pavana	1925	Multiple arches	52.0	0.9	
Pian Sapeio	1926	Multiple arches	17.5	0.22	YES
Poglia	1950	Hollow gravity	49.4	0.5	YES
Ponte Vittorio	1956	Hollow gravity	36.0	0.53	
Rio Lunato	1920	Multiple arches	24.0	0.11	YES
Sa Cantoniera	1996	Buttress	93.2	748.2	
Sabbione	1953	Hollow gravity	61.0	44.12	
San Domenico	1927	Multiple arches	28.9	1.16	
San Giacomo	1950	Hollow gravity	83.5	64.0	YES
Scais	1939	Hollow gravity	60.0	9.06	YES
Sos Canales	1959	Buttress	47.0	4.34	
Valgrosina	1959	Hollow gravity	51.5	1.34	YES
Veneracolo	1958	Hollow gravity	26.9	2.55	YES
Vinchiana	1952	Buttress	22.2	0.12	

3 THE CONTRIBUTION OF NUMERICAL MODELING TO THE ASSESSMENT OF STRUCTURAL SAFETY

The buttress, hollow gravity and multiple arch/slab dams were a clear example of an approach to structural optimization: the "lightened" shape was obtained, in fact, from a simple but somewhat articulated evaluation between the resistance of the material (concrete or reinforced concrete) and the real work rate of the same in operating conditions.

Also, for this typology of dams, the conceptual calculation model used in the past to carry out the regulatory assessment was traced back to a triangular static scheme that recalled the much better-known scheme adopted for massive gravity dams.

The possibilities offered by numerical modelling - and of the Finite Element Method (FEM) in particular - have allowed, since the early 1990s, to deal with the study of the behaviour of these structures in a particularly effective way, both in the design phase and in the verification of behaviour in different operating conditions or to analyse exceptional or extreme conditions such as seismic actions.

Already in the first Benchmark Workshops organized by the ICOLD Technical Committee "*Computational Aspects of Analysis and Design of Dams*" topics concerning this type of dams were proposed. The salient aspects of the three cases examined between 1994 and 2005 are summarized below.

3.1 *Benchmark Workshop # 3 - Theme A2: Evaluation of critical uniform temperature decrease for a cracked buttress dam (2D analysis) - Gennevilliers, France, 29th -30th September 1994.*

Theme A2 proposed in the BW3 [ICOLD TCA, 1994] concerned the numerical evaluation of a uniform temperature decrease capable to give rise to the propagation of a pre-existing cracks in an idealized 2D buttress dam.

With regard to numerical modelling of cracking phenomena, different methods can be adopted according to the kind of problem to be solved, namely: initiation, stability or growth of cracks. In Theme A2, a crack stability problem was proposed.

The participants were asked to evaluate the critical uniform temperature decrease which gives rise to a critical stress state at the tip of the crack that leads to the propagation of the crack itself. This temperature initial state has been conventionally assumed to correspond to a uniform temperature of 0º C. A uniform thermal distribution in the dam (both slab and webs) is to be considered. The foundation is assumed to remain at constant average temperature (0º C).

The temperature value capable to gives rise to a critical stress state at the tip of the crack was required to be defined for five different crack lengths: 0.5 m; 2.0 m; 10.0 m; 20.0 m; 40. m.

The analyses were executed for two different foundation scenarios: rigid and deformable foundation. For both cases, a plane (2D) analysis (plane stress for the buttress and plane strain for the foundation) was required.

The main geometrical data are reported in Figure 6.

The Finite Element (FE) meshes relevant to both rigid and deformable foundation were given by the formulators to the participants. However, considering that for this type of problems the adopted FE meshes are tightly connected with the algorithm adopted in the analyses, the proposed FE meshes were considered just as a suggestion.
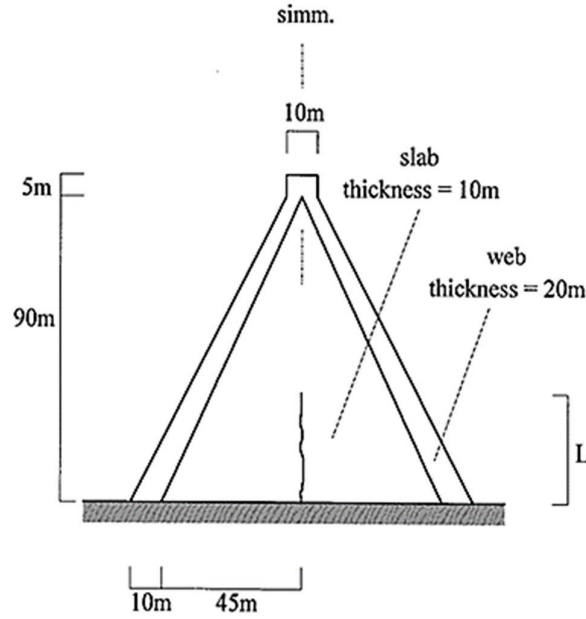
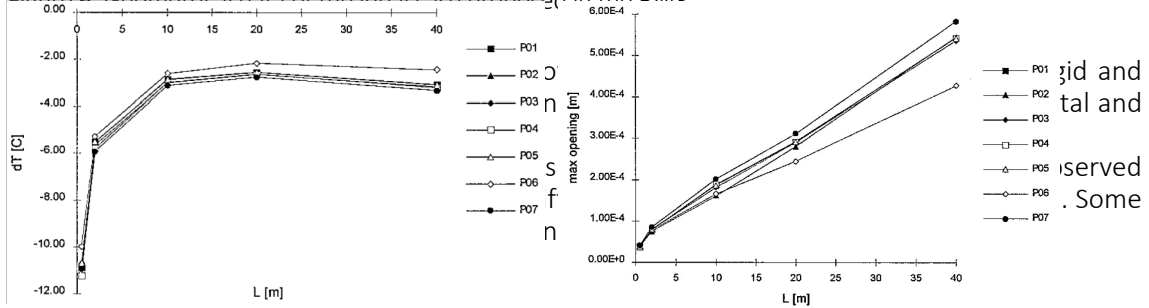Figure 6. Geometrical data of the ideal case proposed in the BW3

Figure 7. Rigid foundation. Relationship between crack length and the associated critical temperature (left). Maximum openings relative to different crack length (right).
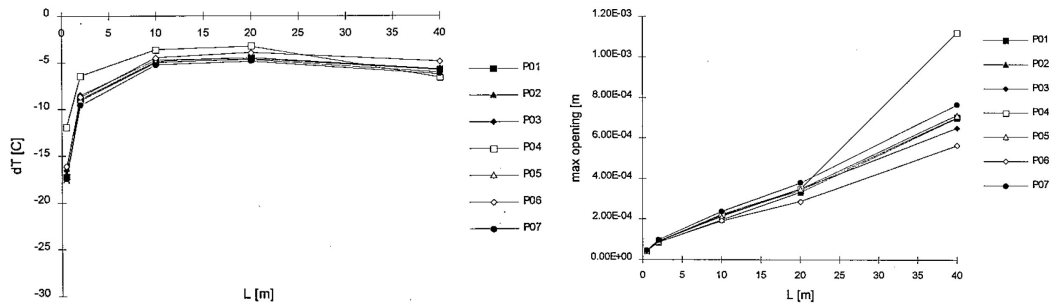

Figure 8. Flexible foundation. Relationship between crack length and the associated critical temperature (left). Maximum openings relative to different crack length (right).

3.2 *Benchmark Workshop # 4 - Theme A2: Evaluation of stress intensity factor KI along the tip of the crack in a buttress dam under thermal gradient effects (3D analysis). - Madrid, Spain, 25th -27th September 1996.*

The Theme proposed in the BW4 [ICOLD TCA, 1996] concerns the application of a thermal gradient across the thickness of a buttress dam, using a three-dimensional analysis. The geometrical data of the idealized dam are reported in Figure 9.
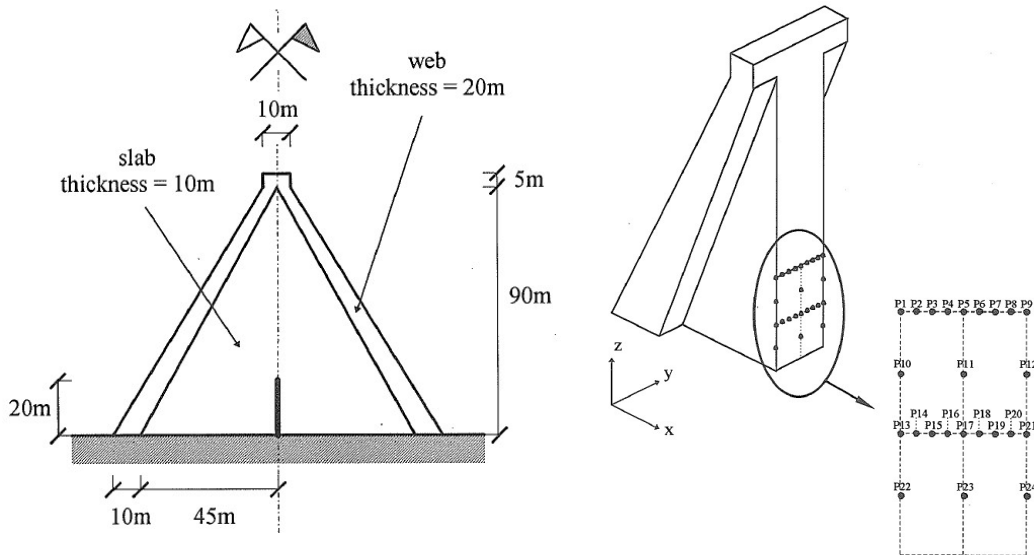
Figure 9. Buttress dam: a) cross section with vertical crack close to foundation; b) 3D illustration of computational references points along the crack surfaces and tip.

No FE mesh was provided since a suitable mesh for Stress Intensity Factor (SIF) evaluation is tightly connected with the algorithm adopted by each participant. Nevertheless, in order to allow the comparison of the results, SIF results were requested at nine points along the crack tip.

The crack tip develops into a line across the thickness of the buttress. For sake of simplicity, the crack tip follows a straight path across the thickness of the buttress, normal to the external surface.

The analysis followed two steps: a first step with time-constant temperature loading, varying per surface, for complete opening of the crack surfaces and a second step with a periodic time history for temperature, which generates opening-closing cycles of the crack surfaces. The main challenges were:

- the temperature field evaluation as a function of time for the assigned boundary conditions;
- the stress field evaluation (3D static non-linear structural analysis, with non-linearities arising from the unilateral behaviour of the crack surfaces interaction, i.e., joints);
- the Stress Intensity Factor KI evaluation across the thickness of the buttress as a function of the position along the crack tip for each time considered.

The contributors provided detailed results of temperature and SIF along the crack tip, as well as displacements at selected points, for both the time-constant scenarios and two temperature time histories (winter and summer conditions).

SIF distributions along the crack front for one of the exercises proposed (# A2.2) provided insight on the effect of contact modelling (Figure 10).

The results are considered satisfactory in terms of validation needs, taking into account that the solutions provided are characterized by the use of different codes, different methods of calculating the stress intensity factors, and use of different type of contact elements. Hence, it was concluded that different modelling approaches were able to provide a consistent and narrow band of solutions for the engineering problem.
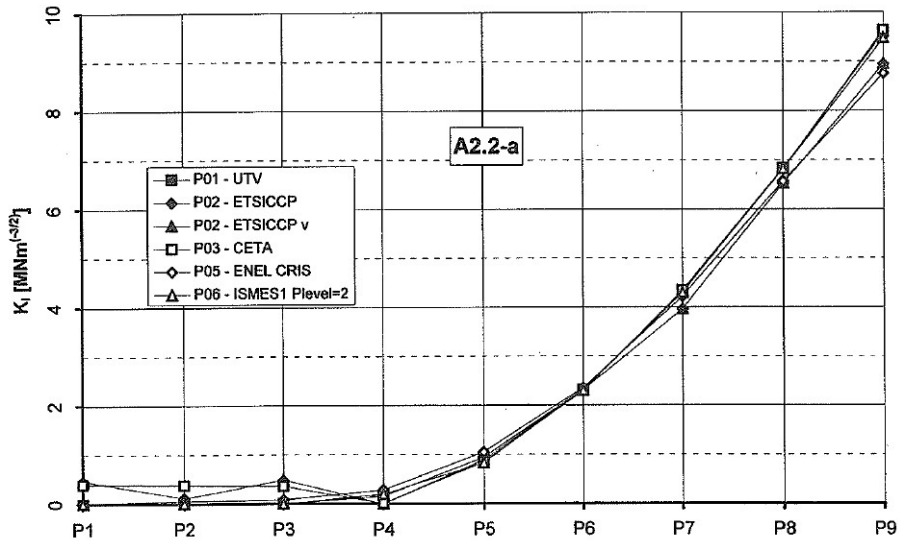
Figure 10. K_I variation along the crack tip.

3.3 *Benchmark Workshop # 8 - Theme A: Evaluation of alkali-aggregate reaction effects on the behaviour of an Italian hollow gravity dam. - Wuhan, China, 23rd -30th October 2005.*

The Poglia Dam is a large concrete hollow gravity structure, located in the northern part of Italy, for the purpose of hydroelectric power generation. The dam is 50 m high and the crest is 137 m long. The construction works took place in 1949-1950. The dam (Figure 11, left) consists of four
hollow diamond-head buttresses and two solid lateral gravity shoulders.

Since the seventies, hence roughly twenty years after its construction, the dam started to exhibit a drift in the displacements (detected by plumblines, collimation and levelling systems). In particular, in the main block the drift was estimated to be 1 mm per year in the vertical direction and 0.2 mm per year in the upstream-downstream direction. After a thorough investigation (i.e., laboratory tests and in situ investigations), the Alcali Aggregate Reaction (AAR) expansion phenomenon was recognized to be the cause of this drift.

Due to the non-straightness of the crown of the dam, the problem was particularly complex to establish BW parameters. Hence, for the sake of simplicity, in the benchmark the effects of AAR were only assessed for the main hollow gravity block for the evaluation of the stability against sliding. The provided geometry consisted of the block and a portion of the rock. The dam-foundation interface was included as well.

The aim of the proposed Theme [ICOLD TCA, 2005] was the evaluation of AAR effects on the operational and ultimate stability of the main block of the dam. Thus, the results of two loading paths had to be compared, with and without the AAR expansion:
- Dead weight + hydrostatic and uplift pressure.
- Dead weight + AAR expansion + hydrostatic and uplift pressure.

In both cases, two water levels were considered: the operational (630 m a.s.l.) and the ultimate reservoir elevation, which had to be found by participants (Figure 11, right). The presence of the drainage system was not considered.
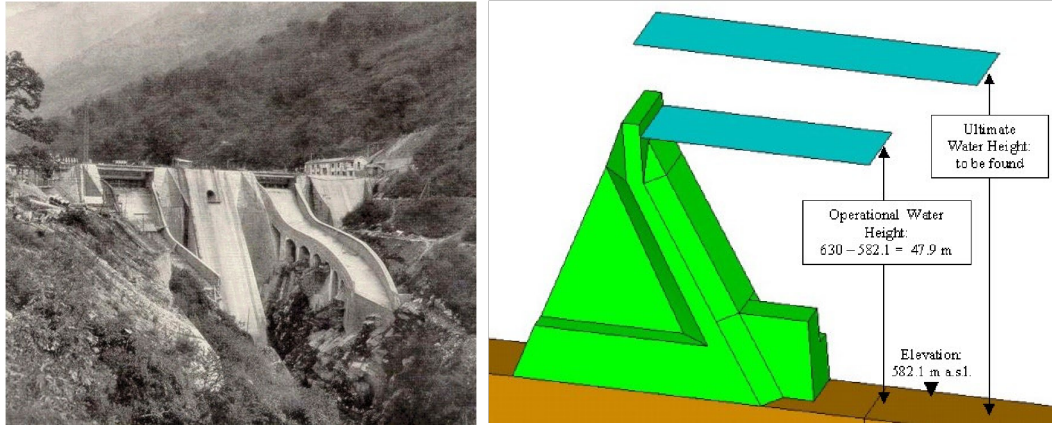
Figure 11. Downstream view of Poglia Dam (left) and geometry of the main block and water heights to be considered (right).

The total vertical drift displacement at the top of the main block was provided to allow the calibration of the AAR expansion phenomena.

In order to evaluate the AAR effects on the global behavior of the dam, the results related to the analyses with and without the AAR expansion had to be compared in terms of curves evaluated considering the water height vs the horizontal displacement at the top of the block.

The limited number of participants did not allow to carry out an extensive comparison of results obtained through different methodologies or models. Anyway, some interesting comparisons relative to the application of two computer codes (the general purpose ABAQUS and the in-house CANT-SD) have been possible. Figure 12 shows the comparison of results obtained with the two codes considering or neglecting the effects of AAR.

The different computed behavior is due to the different characteristics of the joint model adopted by CANT-SD and ABAQUS. In fact, the ABAQUS joint model did not consider cohesion, while CANT-SD did.

Some general considerations can be drawn:

- self-balanced actions such as AAR does not seem to influence sliding limit equilibrium condition provided that the stresses in the dam body do not give rise to the formation of (local or global) mechanisms caused by damages in the dam body;
- with reference to the statement described just above, different limit states relevant to the concrete strength capacity (tensile strength, in general) require the use of suitable models capable to keeping into account smeared or discrete crack formation and propagation or, at least, of damage models;
- the complexity level of the models used to carry out numerical analyses has to be adequate to the data completeness and quality. This last statement, in spite of its apparent obviousness, is sometime underestimated by numerical analysts.
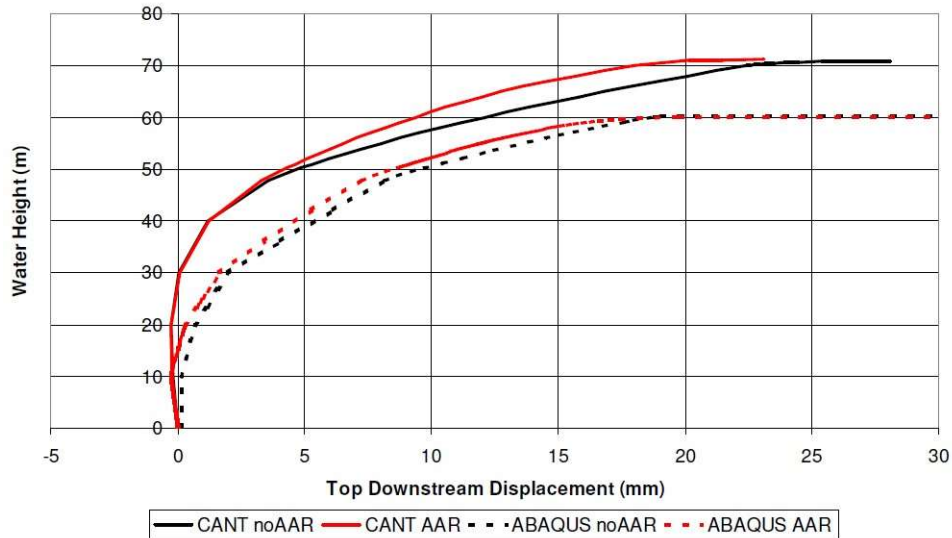
Figure 12. Comparison of displacements at the dam crest computed with CANT-SD and ABAQUS.

3.4 *Innovative methods to simulate crack propagation: the eXtended Finite Element Method*

The eXtended Finite Element Method (XFEM) is a numerical technique especially designed for modelling crack growth without remeshing [Moës et al., 1999]. A standard displacement-based approximation is enriched by local functions in conjunction with additional degrees of freedom to model cracks. This approach allows to simulate the crack propagations without modifying the mesh: a crack can develop inside a finite element (Figure 13, left).

To facilitate the evaluation of the enrichment functions and their derivatives, in most XFEM codes the Level Set Method (LSM) is employed. According to this method, surfaces are not represented explicitly but level set functions are used instead. In general, two levels set functions are considered, Φ and Ψ (Figure 13, right).

The nodal value of the function Φ represents the distance of the node from the crack face: the value is assumed positive on one side of the crack face and negative on the opposite face. The set of points for which the function Φ is zero describes the crack surface.

The nodal value of the function Ψ represents the distance of the node from an almost-orthogonal surface passing through the crack tip: the values of function are assumed negative on the side towards the crack. The intersection of the two levels sets gives the crack front.

Making reference to the example in Figure 13, the value of the function Φ in nodes 1 and 2 is respectively equal to 0.25 and -0.25; whereas the value of function Ψ in nodes 1 and 2 is respectively -1.5 and -1.0.

To model the crack propagation, different techniques can be used such as the cohesive segment approach or the Linear Elastic Fracture Mechanics (LEFM)-based approach.

The XFEM could be usefully applied to study the crack initiation and propagation in concrete dams. In Figure 14. a first XFEM application on a concrete buttress dam is provided [Frigerio, 2020]. Buttress dams exhibit a particular crack pattern generally due to the thermo-mechanical phenomena occurring during construction while further propagation of a crack is mainly related to the ambient temperature variation.
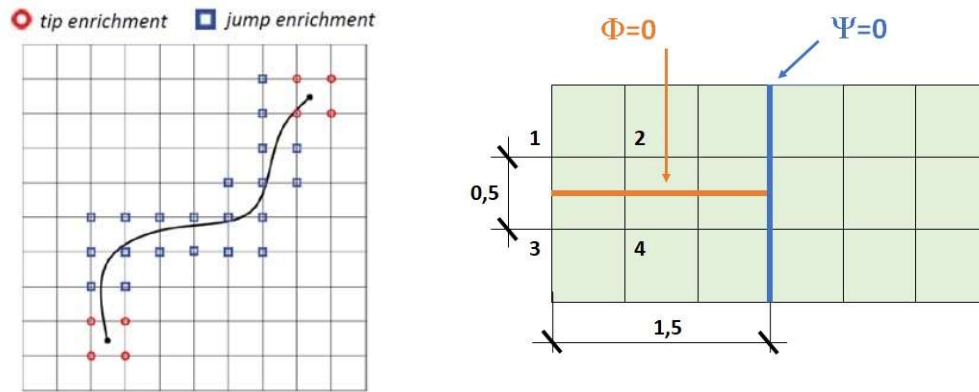
Figure 13. An arbitrary crack on a uniform mesh (left) and the two-levels set functions generally used in XFEM to describe a crack and tracking its motion (right).

The thermo-mechanical analysis has been carried out by means of ABAQUS which provides the XFEM, simulating a three-years period of seasonal temperature variation. In Figure 14. (left picture) the geometric model of the buttress is shown, whereas the contour (right picture) is related to the STATUSXFEM parameter which describes the status of an enriched element. This parameter is equal to 1.0 if the element is completely cracked and 0.0 if the element contains no crack. If the element is partially cracked, the value of STATUSXFEM lies between 1.0 and 0.0. A crack initiation surface was inserted a priori into the geometric model along the foundation interface (Figure 14., left), because this type of fractures takes place during construction but, in this test case, the thermal phenomena occurring during the casting sequence have not been modelled. The numerical results show how the crack propagates towards the upper part of the buttress due to temperature variation: the rate of propagation is greater in the first year and it slows down in the following ones.
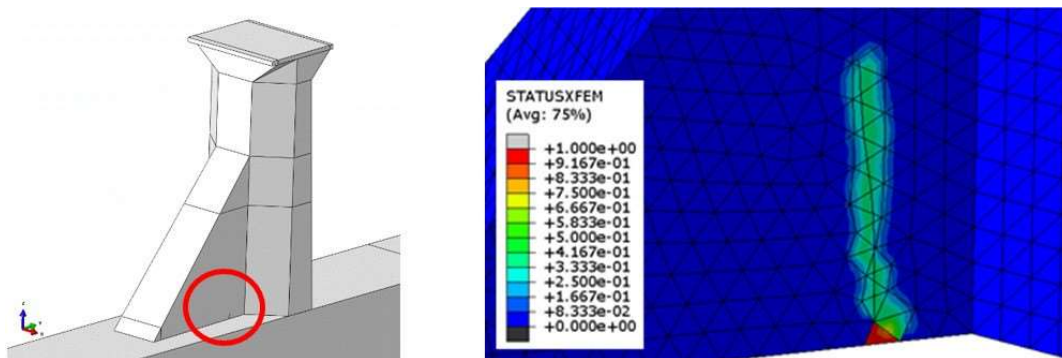
Figure 14. XFEM applied to model the crack propagation in a concrete buttress dam: geometric model with the crack initiation surface (left) and contour of the STATUSXFEM parameter (right).

3.5 *The seismic behaviour of buttress, hollow gravity, multiple arch/slab dams*

Strong earthquakes can cause major damage to all types of structures. Modern FEM numerical calculation methods allow today to face seismic analysis of dams with much greater reliability than in the past, even if further research and development activities are necessary due to the (fortunately!) limited number of dams that have suffered earthquakes of strong intensity.

The dams, in fact, have shown over time to be rather resilient structures with regard to seismic actions. On the other hand, to date, there is no information on dams that have suffered an earthquake of an intensity comparable to MCE (Maximum Credible Earthquake).

In 2011 an interesting article was published [Nuss et al., 2011] in which the performance of 19 concrete dams that have suffered earthquakes of medium-high seismicity with a PGA greater than 0.3g was reported. The survey included arch, gravity and buttress dams.

Of the 19 examined dams, only 5 had sustained significant damage. In 4 of these cases the damage was repaired, and the dam returned to normal service. The fifth case refers to the great river crossing of Shih Kang (Taiwan) built on a fault that suffered so severe damage that it was put out of service.

From the investigation conducted by Nuss et al., two buttress dams were damaged by earthquakes: the Hsinfengkiang Dam (China) and Sefid Rud Dam (Iran).

In both cases the cracks that formed in the structures were horizontal and were highlighted in the upper part of the dams where there is the variation of the profile of the downstream face, as can be clearly seen in Figure 15 and Figure 16, where there is a sudden change in stiffness in the geometry of the dams.
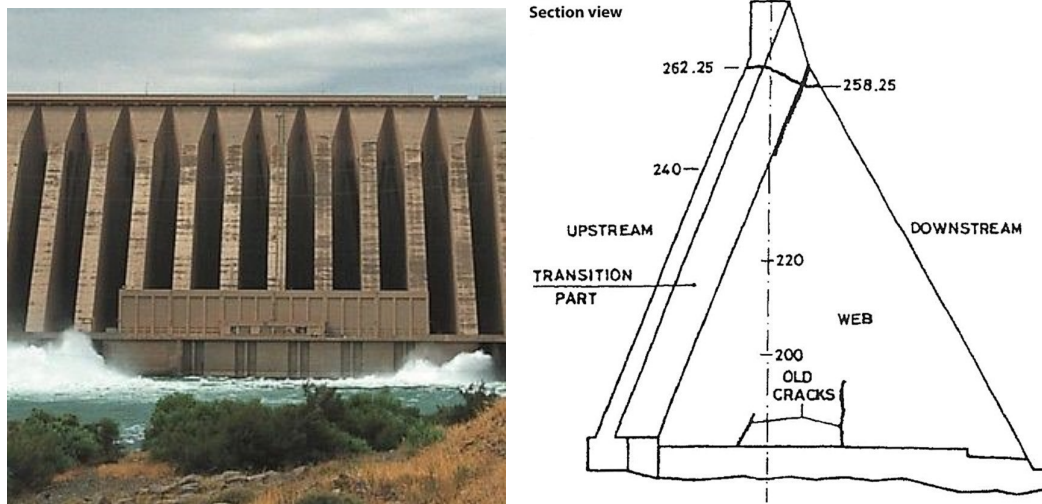
Figure 15. The downstream view of the Sefid Rud Dam (left) and cracks after the earthquake (right).
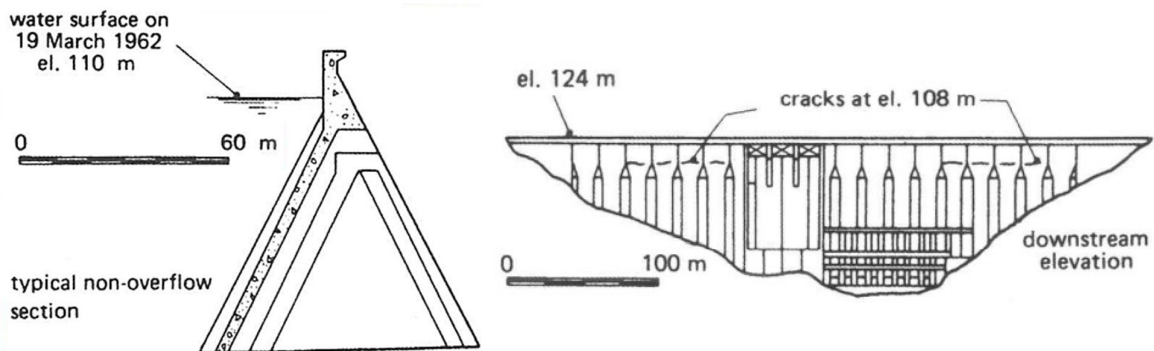
Figure 16. The Hsinfengkiang Dam after the earthquake.

In the case of the Sefid Rud Dam (and probably also in the case of the Chinese Hsinfengkiang Dam), the cracks in both faces created a substantial sub-horizontal rupture plane without associated significant sliding, probably due to the high value of the shear strength in concrete due to the roughness of the surface and the effect of the overlying weight.

A situation somewhat similar to the two described above is that relating to the well-known case of the Koyna Dam, in India (Figure 17).
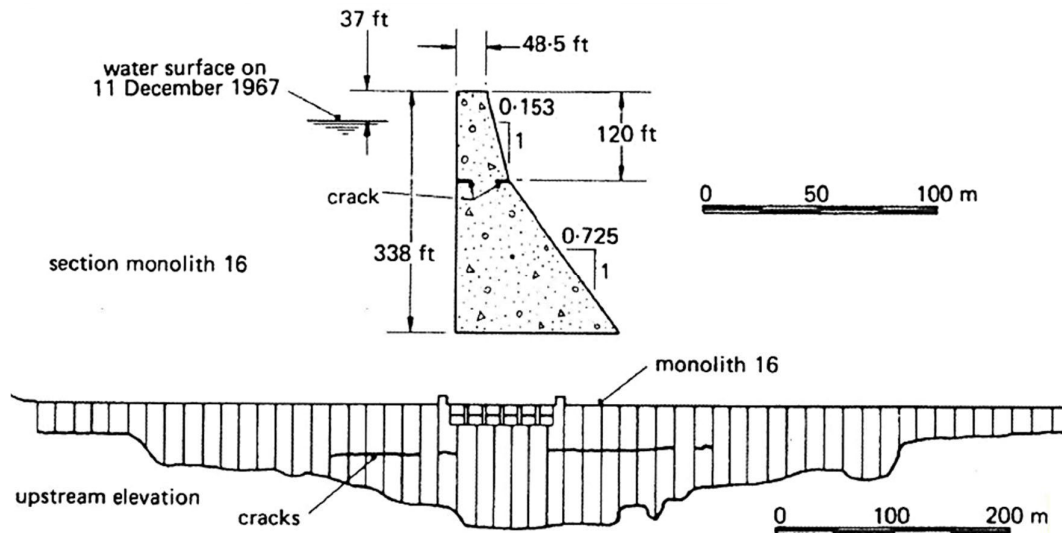
Figure 17. The Koyna dam after the earthquake.

In this case, the cracks that appeared on the two upstream and downstream sides in the upper part of the dam fortunately did not manage to create a rupture surface. In any case, the position of the cracks caused by the earthquake is substantially similar to what has been observed in the two cases of the aforementioned buttress dams.

The article by Nuss et al. cited above briefly describes some interesting cases of buttress dams that have been the subject of reinforcement interventions to cope with the expected stresses on the basis of the seismic re-evaluation of the sites where the works are located. Here below two cases are briefly described.

The Big Bear Dam (a multiple arches structure built in 1912, 28 m high, with a 110 m crest length) was rehabilitated in 1989 for a project earthquake with a PGA of 0.71 g. The adaptation project was necessary both for fear of seismic actions (the work is located just 16 km from the San Andreas fault in the S. Bernardino mountains, 80 km east of Los Angeles) and for the need to adaptation of outlets.

The structure was reinforced with the partial filling of the compartments by means of the massive concrete casting which substantially reduced the extension of the buttresses. The intervention involved the execution of completion castings to ensure the monolithic behaviour between the old and new structure (Figure 18). It is interesting to note that in 1992, at one day from each other, there were two events estimated with magnitudes equal to 7.3 and 6.6 located respectively at 28 and 9 miles from the dam site.

The estimated PGA at the dam site was 0.35 g. The inspection carried out immediately after the earthquakes did not show any damage to the structure.

The second case refers to the Littlerock Dam, California (a multiple arch structure built in 1924, 53 m high, with a crown of 219 m), rehabilitated in 1994 for a project earthquake with a PGA of 0.70 g. The dam is located just 1.5 miles from the San Andreas Fault.

The studies conducted for the evaluation of the safety conditions of the work had highlighted its potential vulnerability with regard to transversal actions. Therefore, it was decided to reinforce the structure with the partial filling of the compartments according to the scheme illustrated in Figure 19.
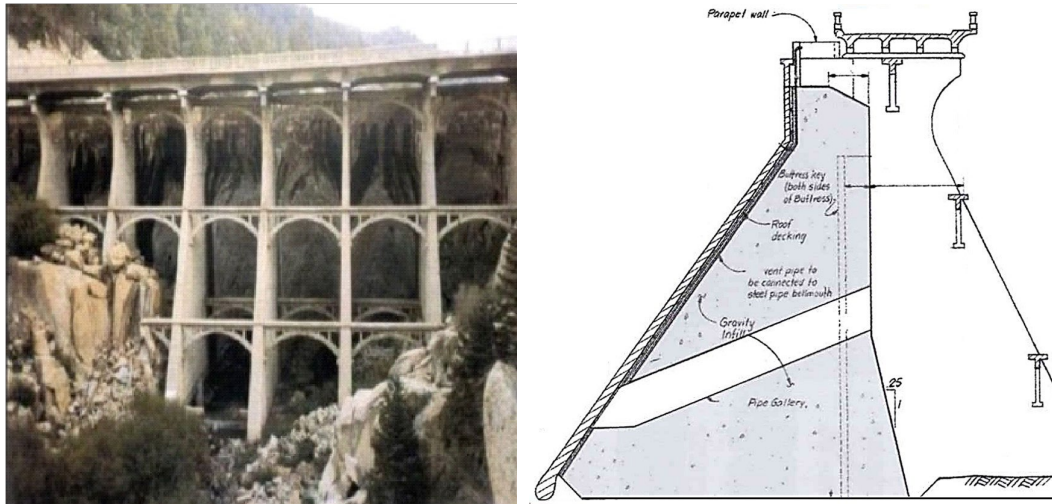
Figure 18. The Big Bear Dam: vertical section of the structure being filled with massive concrete.
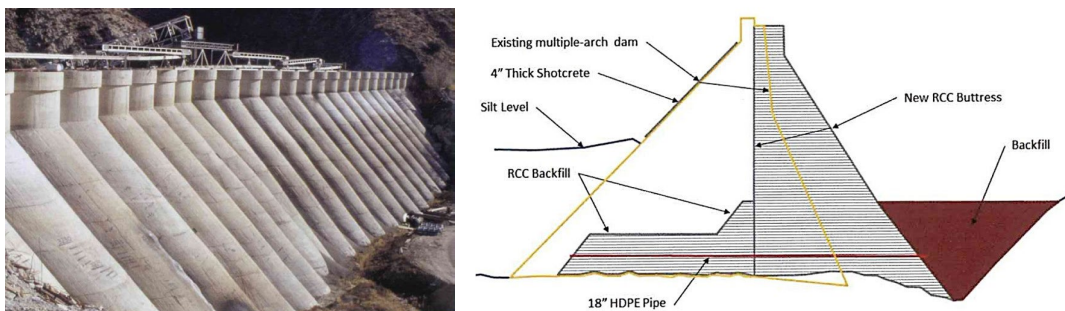

Figure 19. The Littlerock Dam: a) the structure seen from the mountain; b) vertical section of the intervention with partial filling of the rooms with concrete (RCC).

4 CONCLUSIONS

Water is an indispensable resource for human life and its use must primarily be aimed at satisfying human needs (water supply for drinking and irrigation purposes). A company must pay attention to the rational use of this strategic resource reconciling all these needs with the objectives of industrial development, energy production and environmental protection that each Country has to foster within the framework of a common European policy.

However, in Italy the construction of new dams is experiencing a very unfavourable phase both at the political level and in the public opinion due to numerous factors:

- Financial constraints (due to the persistent critical phase of public finance and the low propensity of the private one to long-term investments).
- Intense anthropization of the Italian territory.
- Reduction of favourable sites from a geo-morphological point of view.
- Administrative and legislative constraints (e.g., regional constraints on the Minimum Vital Outflow).
- Competition between the "multiple uses" of the water resource.
- Widespread hostility from pressure groups.

The managers of hydro and hydroelectric plants therefore have to face complex problems related to the safety of infrastructures that in some cases have also exceeded what is considered their design service life.

Dams are the product of the application of successive design and construction criteria. A further aspect to take into account when considering dam safety concerns the fact that the safety levels of the structures are inevitably not homogeneous due to the evolution of the construction

technologies, the investigation techniques, the calculation methods that took place over almost a century.

The dams covered by this article are fully part of this context and, taking into account their average life, in several cases close to a century, they require continuous surveillance and, in some cases, maintenance interventions (ordinary and, sometimes, extraordinary).

To this end, the modern calculation methods available today are able to offer operators responsible for dam management the necessary elements for a reliable assessment of structural safety.

5 ACKNOWLEDGEMENT

REFERENCES

Barbisan, U. 2007. Il crollo della diga di Pian del Gleno: errore tecnico? Tecnologos editor.

ITCOLD. 2018. Riabilitazione delle dighe. Osservatorio permanente. Bollettino.

ICOLD TCA. 1994. Theme A2. Evaluation of critical uniform temperature decrease for a cracked buttress dam. 3rd Benchmark Workshop on Numerical analysis of dams, Gennevilliers, France.

ICOLD TCA. 1996. Proceedings of the 4th Benchmark Workshop on Numerical analysis of dams, Madrid, Spain.ICOLD TCA. 2005. Proceedings of the 8th Benchmark Workshop on Numerical analysis of dams, Wuhan, P.R. China.

Moës N., Dolbow J., & Belytschko T. 1999. A finite element method for crack growth without remeshing. International Journal for Numerical Methods in Engineering.

Frigerio A. 2020. Attività scientifiche e di diffusione svolte nel 2020 a livello nazionale e internazionale per il settore idroelettrico. Ricerca di Sistema. RSE, n. 20010750. Milan, Italy.

Nuss L., Matsumoto N., Hansen K. 2011. Shaken, but not stirred – Earthquake performance of concrete dams. USSD Annual Conference, New Orleans, LA.

RE-ASSESSMENT OF HYDROLOGY AND HYDRAULICS RELATIVE TO THE OPERATION OF A LARGE DAM

dr. Primož Banovec
Assist. Prof. Faculty of civil and geodetic engineering, University of Ljubljana, Slovenia

Uroš Lesjak
Water Science Institute, Ljubljana, Slovenia

ABSTRACT: In the context of monitoring the operation of large dams, it is necessary to pay due attention to the various processes that affect the reliability of their operation. In addition to the monitoring the stability of high dams, it is also important to monitor the hydrological and hydraulic conditions that determine the filling and emptying of reservoirs during the performance of dam functions. This is particularly important due to recent changes in hydrologic conditions, which have been influenced primarily by climate change and changes in runoff. In addition to that hydraulic conditions may also be affected by a change in maintenance regime (vegetation) at various elements of the dam and reservoir system. Modelling results are also influenced by the use of advanced tools for modelling of both phenomena, as advanced modelling techniques and tools were not available at the time the dam and system were designed. The paper presents a re-modelling of the hydrological and hydraulic conditions for the operation of the large dam - the Drtijščica reservoir in the Lukovica municipality - and identifies the deviations from the design condition. The identified deviations lead to the need to study the modification of some elements and procedures that are crucial for the safe and reliable operation of the dam: Operating Rules, Contingency Plan in case of dam failure, Maintenance Program for the dam and its associated system, etc. We assume that the remodeling of the hydrological and hydraulic conditions that determine the operation of high dams would also be necessary for all other similar facilities, since the parameters and tools used at the time of their design may already differ significantly from the actual situation.

1 INTRODUCTION

In accordance with national (OG, 2008) and EU legislation - the Floods Directive (EU, 2007) - a comprehensive flood modelling of the main flood-prone areas in the Municipality of Lukovica (Lukovica) was carried out. The modelling requirements are based on the Slovenian regulation, which is in line with the EU requirements and prescribes the development of flood risk and flood management plans focused on prevention, protection and preparedness. As a result, a comprehensive flood hazard modelling with flood hazard maps, theoretical and actual flood waves with return periods of 10, 100 and 500 years, and proposals for the necessary mitigation measures for the planned urban development was carried out.

What makes the flood hazard mapping very specific for the addressed municipality is the existence of the Drtijščica dam/reservoir, which was built in 2002 as part of the mitigation measures for flood retention related to the construction of the Ljubljana - Maribor highway, which otherwise would have had serious negative impacts on the flood hazard in the addressed area.

The resulting hydrological and flood hydraulic modelling shows significant deviations from the design parameters of the dam/reservoir and the operation of the complex flood control system. The modelling and the resulting preparation of flood hazard maps were contracted by the Lukovica municipality and reviewed by the Slovenian Water Authority (DRSV). The results lead to quite restrictive conditions for the desired urban development in the studied area, but also to the need to review the operating parameters of the Drtijščica dam/reservoir.

2 BASIC DESCRIPTION

2.1 *Area description*

Lukovica is a medium-sized municipality in central Slovenia with 5,907 inhabitants, northeast of the capital Ljubljana. The entire area is hilly, with floodplains typically located in the valleys of the Radomlja and Drtijščica rivers, which are narrow and steep. In the 2000s, the construction of the Ljubljana - Celje highway significantly changed the hydraulic characteristics of the area, as well as the large-scale land reclamation works completed before the highway construction.

The Gradiško Lake behind the Drtijščica Reservoir attenuates the Drtijščica River near its confluence with the Radomlja River and was created as a compensatory measure to improve flood conditions. As part of the Drtijščica Reservoir, a 935 m long diversion tunnel from the Radomlja River was built to divert flood flows of up to 30 m3/s from the Radomlja River and allow them to flow directly into the Drtijščica Reservoir.
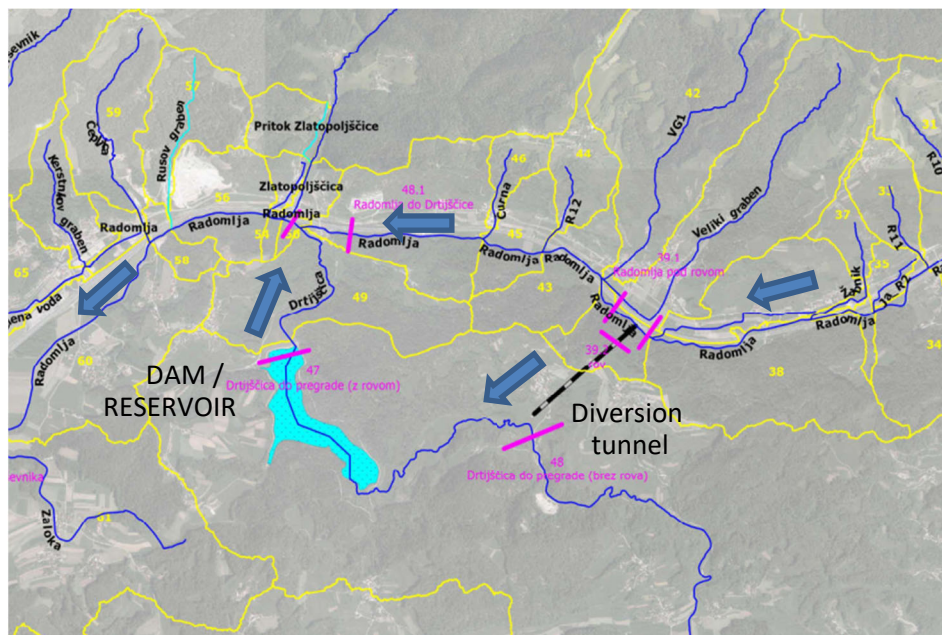

Figure 1. Addressed water retention system with diversion tunnel and Drtijščica reservoir.

2.2 *Drtijščica dam and reservoir*

The dam is located in the central part of Slovenia and is managed by the Slovenian Water Agency (DRSV). Basic data about the dam can be found in the following table. Its main function is to retain water and thus improve flood safety in the Radomlja river valley, which is achieved by reducing flood peaks. There are two main tributaries to the reservoir - the Drtijščica River (with 33.2 km^2 watershed) and the Radomlja River (which is partially diverted through gates through the tunnel to the reservoir). Several discharge measurements are carried out in the Drtijščica and Radomlja rivers to regulate the automatic inflow/outflow gates of the reservoir.

Table 1. Main characteristics of the Drtijščica dam

Dam height (m)	18.2
Dam length (m)	256
Permanent reservoir wetted area (ha)	29
Constant retention volume (mil m^3)	0.8
Max. retention volume (mil m^3)	6.7
Diversion tunnel length (m)	965
Max intake diversion tunnel (m^3/s)	30
Discharge return period safety (years)*	10000*
Critical volume Qn100 (mil m^3)*	3.13*

*estimated in original hydrology (VGI, 1996)

The diversion tunnel is operated according to operational rules (Table 2). The rules are based only on the measured discharges of the Radomlja River. The water levels and thus the free volume of the reservoir is not taken into account in the operating rules.

Table 20. Operational rules of the diversion tunnel based upon the 1996 baseline analysis

Rules (m^3/s)	Flow through the tunnel (m^3/s)	Flow in Radomlja river (m^3/s)
$Q_R <= 6$	0	Q_R
$6 < Q_R <= 36$	$6 < Q_T <= 30$	6
$Q_R > 36$	30	$Q_R - 30$

* Q_R is flow in Radomlja river

** Q_T is flow in the diversion tunnel

3 HYDROLOGY

3.1 *Baseline hydrology*

Design phase of the Drtijščica dam began in the 1990's and at that time the 0D hydrological model HEC-1 was a state-of-the-art approach to hydrologic modeling. Due to several numerical limitations of that model, designers had to perform extensive manual calculations as well.

To calculate rainfall losses, the SCS Curve method (SCS CN) was used, where the excess surface runoff is estimated as a function of runoff potential, antecedent soil moisture and land use. Flood wave propagation was calculated based on SCS unit hydrograph. Calculation assumed that precipitation with a given return period causes surface runoff with the same return period.

Precipitation values were defined based on a probabilistic analysis of daily measured precipitation at multiple ombrograph stations around the modeled area and increased by 15% as a precaution measure to measurements inaccuracies. The rainfall curves were further determined on the basis of the correlation of the rainfall curve (obtained by Gumbel probabilistic analysis and regression of the hourly rainfall) and the previously determined 24-hour rainfall.

Hydraulic calculations in terms of planning aid were performed only for the main hydraulic structures, flood propagation and inundation calculations of Radomlja and Drtijščica rivers were not carried out.

Elevation – volume chart (E-V) of the accumulation was calculated on the basis of topographical maps TTN5 of resolution 1:5000 which are to date still widely used in Slovenia.
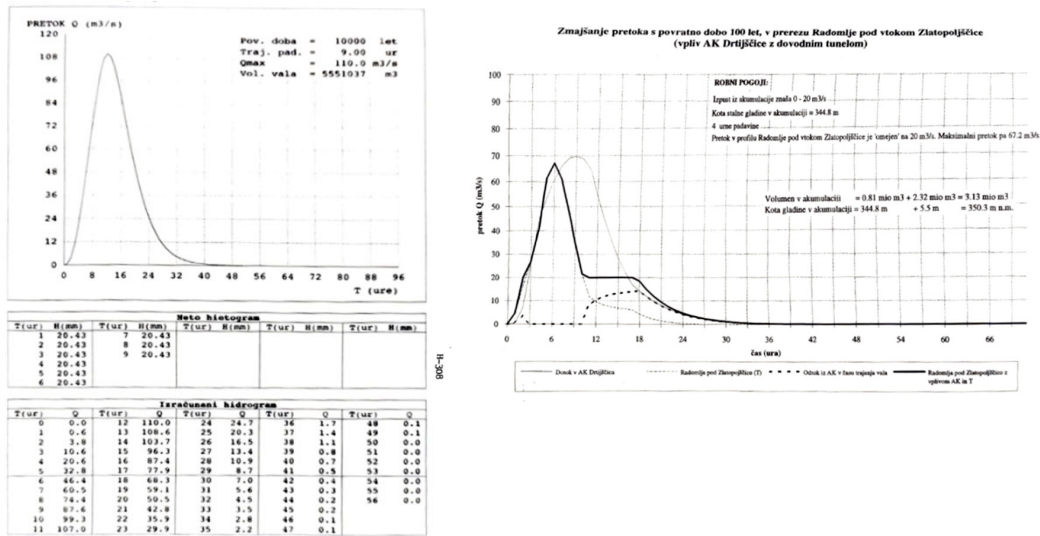
Figure 2. Results of hydrological modelling from baseline analysis (1996)

3.2 *Hydrology revised*

3.2.1 Radomlja watershed and methods used for the revised analysis

All hydrological calculations were performed from scratch. Modeling was done in HEC-HMS 4.7.1 which is a late successor of HEC-1 and offers combination of 0D, 1D and even 2D modeling. The same calculation method was used as in original hydrology, that is SCS CN method, as it is a method that is widely used in Slovenia and usually performs reasonably well for our climatologic and topographic conditions.

Precipitation data were used from calculated family of precipitation curves (Vertačnik et. al, 2019/2020) that was published by ARSO in 2020 and defines intensity-duration-frequency (IDF) curves for 22 duration intervals ranging from 5 minutes to 120 hours. Calculation was based on multi-parameter Generalized Theory of extreme values (GEV), which uses Fréchet's instead of Gumbel's distribution. The result is a spatial distribution of extreme rainfall events with spatial interpolation of the GEV distribution parameters. Analysis considered both, the geographical locations of the measurement sites as well as the lengths of the measurement arrays, where the input data were rainfall height measurements from the pluviographic stations measured at five-minute intervals.
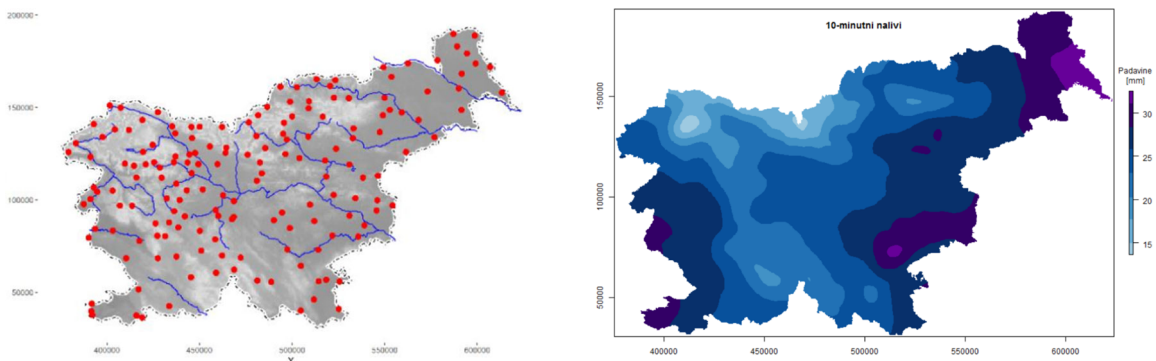
Figure 368. Pluviographic stations used for long rainfall intervals (left) and calculated 10-minute rainfall with 100 years return period (right), (Vertačnik et. al. 2019/2020)

Modeled part of Radomlja watershed covers approx. 160 km^2. Using modern GIS tools, all necessary hydrological parameters have been calculated, like average slopes, delineation areas, reach lengths, CN values etc, and the whole modeled area was subdivided into 83 smaller

watersheds in order to achieve the scope of the project. Wave transformation was calculated using Muskingum – Cunge method, which uses stream geometry defined by eight points and a uniform longitudinal slope within a reach.
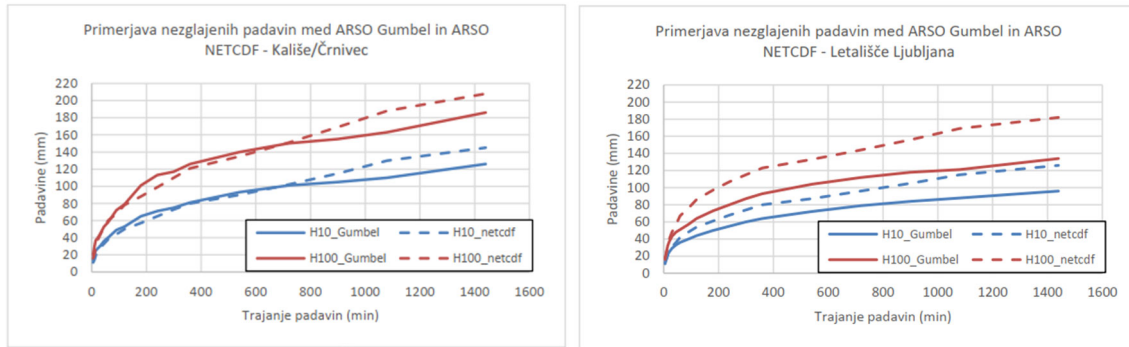
Figure 4. Comparison between original and new duration – precipitation curves for two measurement sites

Comparison of precipitation datasets between original and new hydrology reveals significant deviation as new datasets show increase from 27% to 44%. Cause of that increase can be different- weather in usage of more sophisticated methods where suspicious/erroneous precipitation datasets were omitted, as well as in climate changes. 30 years between the two studies is enough time to be able to statistically detect an increasing precipitation trend over the modeled area.
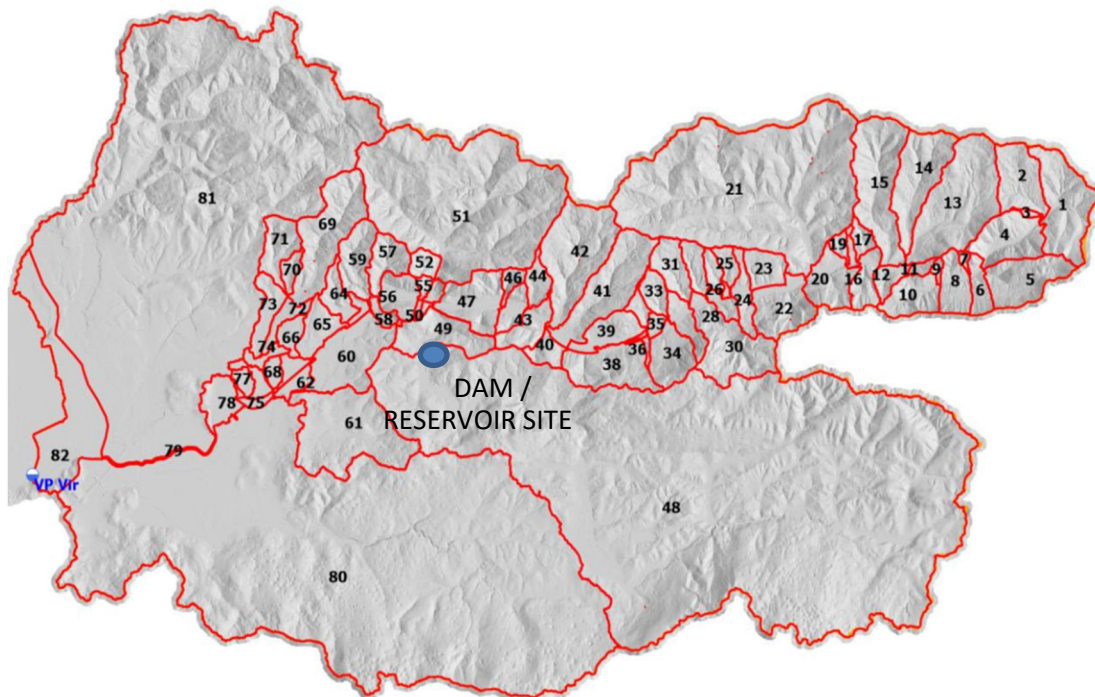
Figure 5. Radomlja watershed and location of the dam/reservoir

3.2.2 Hydrological model calibration

Hydrological model was calibrated to event that occurred in 2010, which clearly revealed unsatisfactory dam retention volume. Estimated return period of the event was 100 years, which means that accumulation should have accumulated all of the peak hydrograph without the need of activating emergency release. During the event water level in the dam reached critical value, so that emergency release had to be activated. That caused severe flooding downstream, and all

safety dam mechanism were put to a test including civil protection and firefighters being in full operative alert.

Model results for the 2010 event provide reasonably accurate predictions that follow actual course of events.
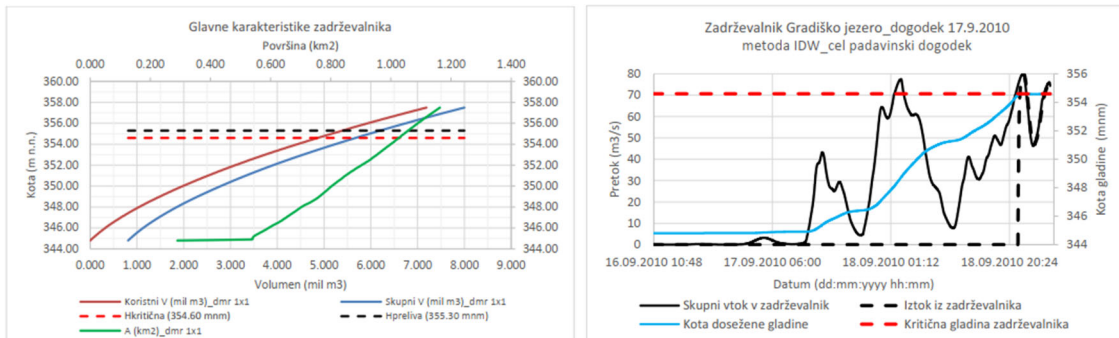
Figure 6. Elevation – volume table (left) and calculated inflow/water levels of the dam (right) for the 2010 event
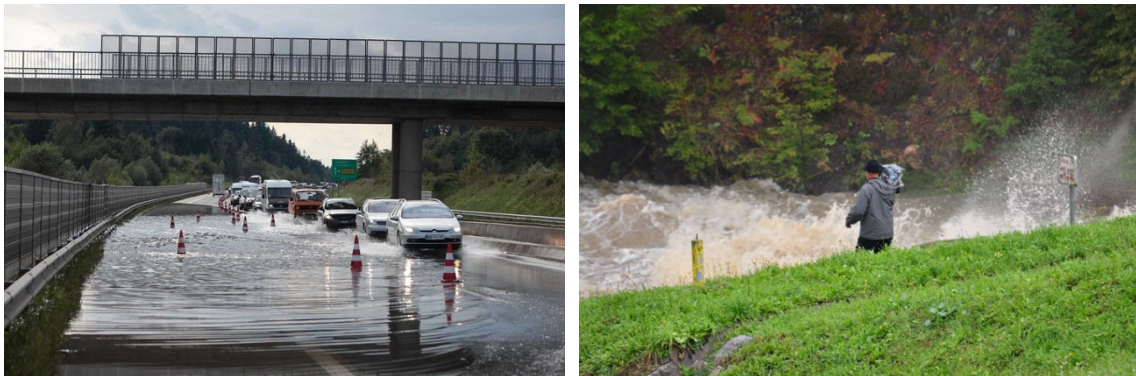
Figure 7. Flooded highway downstream of the dam (left) and ground discharge of the dam (right) for the 2010 event

4 HYDRAULICS

The whole area of interest has been model with full 2D hydraulic model HecRas 6.0. Calculation method is based on the finite volume method using depth-averaged shallow water equations (SWE). 2D geometry is defined by mesh elements (unstructured and structured) characterized by a detailed sub-grid bathymetry. Mesh density was modified according to the needs or spatial circumstances. Due to a very large modeled area, two independent hydraulic models were made, covering each other to the extent that possible boundary effects were diminished.

Sub-grid bathymetry in the flood plains was made from 1x1m DEM (ARSO, 2014), bathymetry inside streams was made from 0.1x0.1m DEM based on Lidar point cloud (ARSO, 2014) and updated with terrestrial land surveys.

Results show, that area is prone to a significantly greater flood risk than in calculated in in original studies in year 2000. The dam can not provide sufficient safety against flood risk during long-lasting events, (e.g., Q_{100}_24h precipitation and longer).

Figure 8. Hydraulic model mesh (left) and validation results (right)

5 CONCLUSIONS

Changes in hydrologic and hydraulic conditions require periodic reassessment of design parameters that include impact of changed IDF curves, land cover, land use, topography changes etc. All these changes induce changes in the runoff and consequently changes in flooding conditions at the area of interest.

LIDAR-based 2D hydraulic models provide a much better understanding of flood phenomena than 1D or 0D models made 30 years ago.

Hydraulics is also affected by the actual maintenance practices (in-stream vegetation), Therefore, operating rules, contingency plans, etc. need to be updated, based upon the results of the revised analysis of hydrological and hydraulic conditions. Re-assessment should become a regular practice for large, but also for small dams and other critical hydraulic structures.

Re-assessment is also one of the basic prerequisites of the climate proofing procedures for key infrastructure following the EC Technical guidance on the climate proofing of infrastructure in the period 2021-2027. A systematic implementation of these this guidance document on a national level should be obligatory in order to gradually adapt all key hydraulic structures of high importance to the target climate pathways, having in mind the defined long term time horizon.

REFERENCES

ARSO (2014) LIDAR DTM, downoadable: https://www.evode.gov.si/

Act on conditions and limitations for constructions and activities on flood risk areas (Official Gazette of RS [Uradni list], No 89/08)

European Environment Agency. (2007). Floods Directive. 2007/60/EC

Kozjek, K., Vertačnik, G. 2019/2020. Časovno in prostorsko glajeni povratni nivoji ekstremnih nalivov. Vetrnica 12/13: p.p. 77-85

European Commission. (2021). Technical guidance on the climate proofing of infrastructure in the period 2021-2027. (2021/C 373/01),
https://eur-lex.europa.eu/legal-content/EN/TXT/PDF/?uri=CELEX:52021XC0916(03)&from=EN

Vodnogospodarski inštitut RS (1996), Zadrževalnik Drtijščica, Hidrološki del, Projekt nizke gradnje, Ljubljana (Arhiv Republike Slovenije).

Dam behaviour prediction

Appendix: Theme A project presentation

Dam behaviour prediction

Suggested theme for the 16th ICOLD BW

Richard Malm, KTH Royal Institute of Technology, Sweden
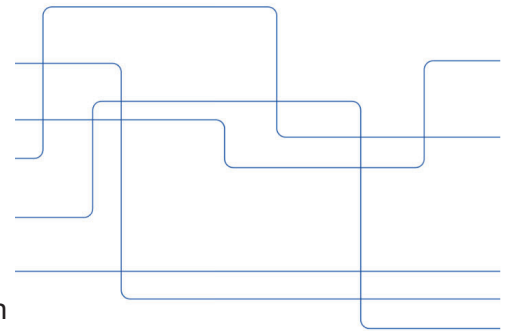
Mateja Klun, University of Ljubljana, Slovenia

Alexandre Simon, EDF Hydro, France

Fernando Salazar, CIMNE, Spain

Rikard Hellgren, KTH Royal Institute of Technology, Sweden

Background

- Monitoring is a vital tool to detect anomalies in the dam behaviour and thereby minimize the risk of catastrophic failures.

- To assess the measured behaviour and classify it as normal or unexpected, a prediction model is required. For this purpose, different types of models are available, based on finite element methods or data-based mathematical approaches.
    - Measurement prediction is becoming more and more common today and is something that all dam engineers are encountered with.

- Vast developments have occurred in the field of prediction models over the recent years, especially regarding machine learning and numerical modelling.
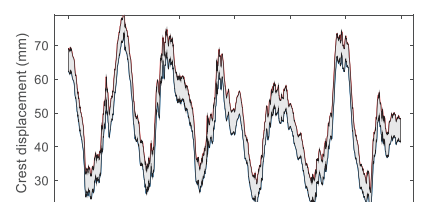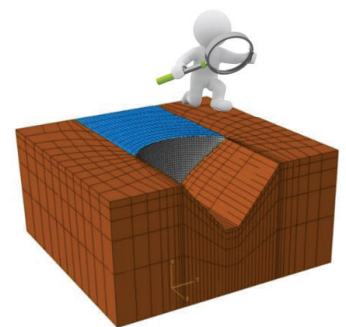
Background
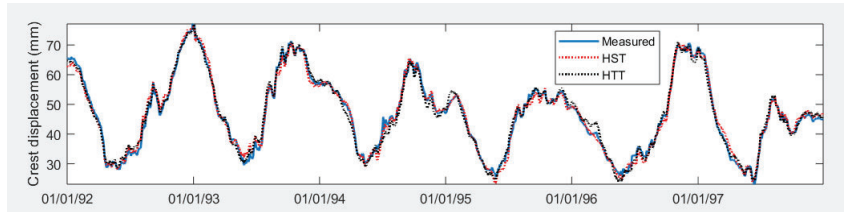
- 20 years ago, prediction of the measured behaviour of the Schlegeis dam was a theme in the 6th ICOLD BW.

- In the 14th ICOLD BW 2017, a theme was focused on predicting the dam behaviour, including cracking, caused by seasonal temperature variations.

- For the 2021 ICOLD Benchmark Workshop, we want to build from these experiences and see how modern tools can help in the prediction of dams
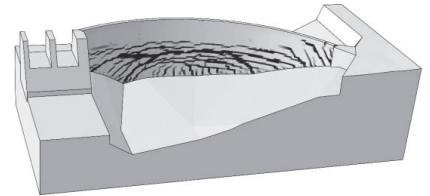
It is time to analyse the capabilities of the prediction models

Formulating team

- Collaboration between two ICOLD Committees
  - Com. A (COMPUTATIONAL ASPECTS OF ANALYSIS AND DESIGN OF DAMS)
  - Com. Q (DAM SURVEILLANCE)

- The formulating team has experience in working with prediction models from different roles in the dam engineering field (universities, research institutes, dam owners, consultants, etc.)

Theme; Concrete arch dam

- As the case study, a concrete arch dam has been selected which has been extensively monitored for more than 30 years.
  - 40 m high
  - 150 m crest length
- Monitoring
  - Displacements
    - > Along the crest
    - > Half dam height
    - > In the foundation
  - Uplift pressure
    - > Several points near the concrete rock interface
  - Leakage
  - Temperature
  - Water level
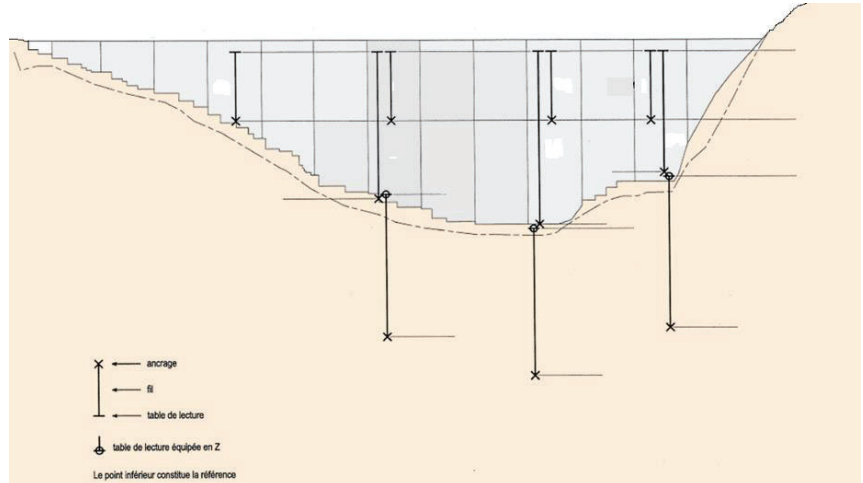
Theme formulation

- Contributors will be given
  - Measured data for 20 years (air temperature, water level, displacements, uplift pressure and leakage)
  - Measured input data for the prediction period (temperature, water level)
  - CAD geometry model and FE mesh
  - Material properties

- All types of models are welcome to use (statistical, hybrid, deterministic, machine learning, finite element modelling) from the simplest to the most complex ones.

- For all cases, the formulators will provide excel templates that the contributors should use for submittal of their results

Cases

- The theme consists of three subcases

- **Case A – Model calibration**
  - Develop a calibrated model that accurately can capture the provided measurement period (training period)

- **Case B – Short term prediction**
  - Short term predictions (3 months) to predict the dam behaviour without influence of time dependent effects

- **Case C – Long term prediction**
  - Long term predictions (5 years) to predict the dam behaviour including influence of time dependent effects

Tasks

- For each case, the contributors should perform
  - Predictions
  - Define warning levels
  - Interpret the influence of external parameters (water level, air temperature, time dependent effects)

- For the different output variables
  - Displacements
  - Uplift pressures
  - Leakage

- Six tasks are mandatory while the remaining are optional

Mandatory   *Optional*

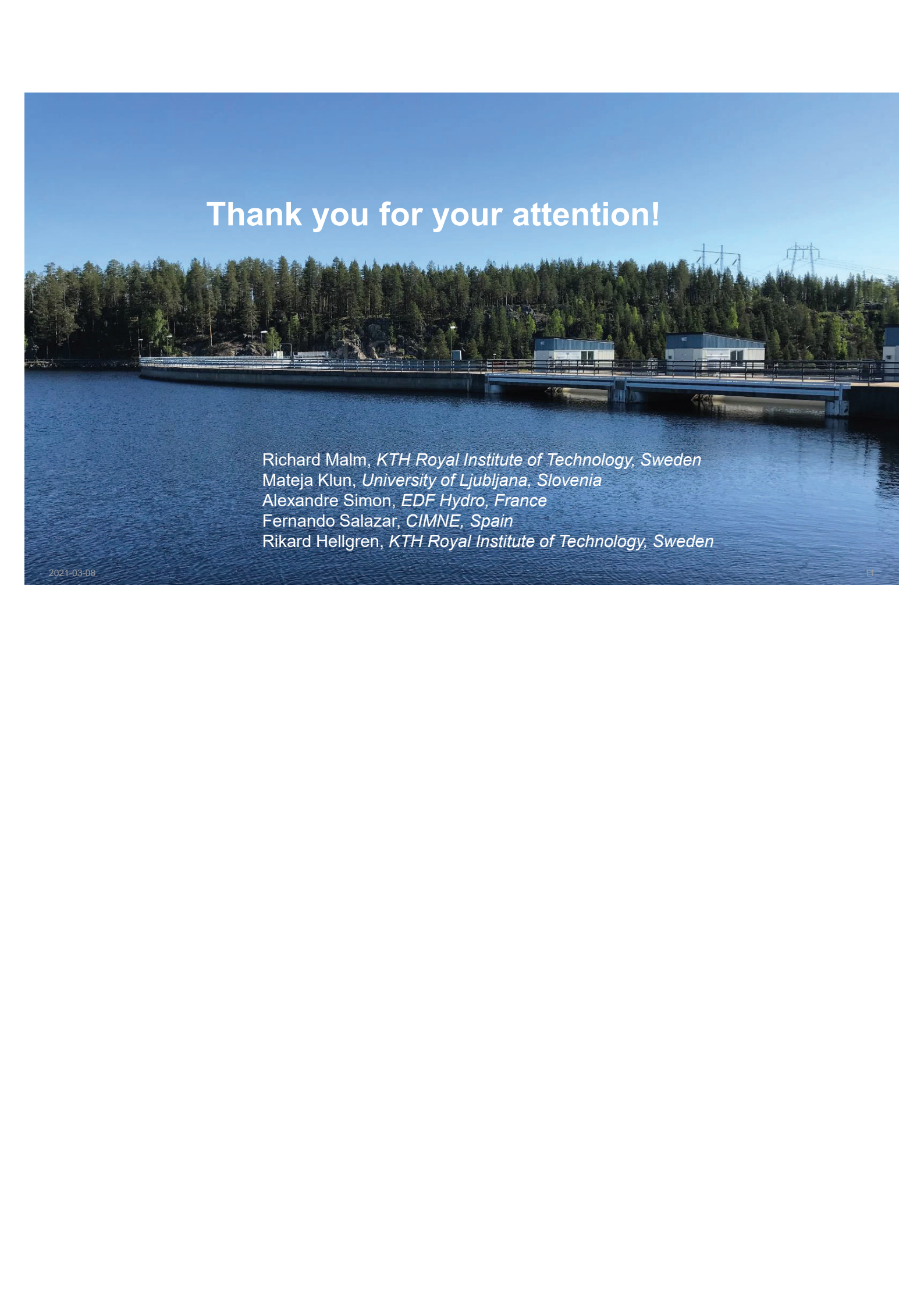|		Case A: Calibration	Case B: Short term	Case C: Long term
Predictions	Displacements	Mandatory	Mandatory	Mandatory
	Uplift pressure			
	Leakage			
Warning levels	Displacements		Mandatory	Mandatory
	Uplift pressure			
	Leakage			
Interpretation	Displacements	Mandatory		
	Pore pressure			
	Leakage			

Overall view of the theme

- The theme has been developed to be a realistic case study similar to what the analysts normally encounters when predicting the measured dam behaviour.
  - The results of the contributors will be assessed regarding the accuracy of their predictions.
  - The contributors defined of warning levels will be assessed in terms of classification accuracy (precision, recall)

- Several different type of models are expected to be used in this theme
  - The contributors can chose their level of engagement, depending on the number of tasks that they perform and also depending on which type of model/models they use.
  - The required effort will be quite low for those contributors using regression models and hence making the theme accessible for many contributors.

- This theme is expected to attract both data analysists (such as surveillance experts) and FE analysists (numerical experts) to participate

Expected outcomes

- Improve our understanding of dam behaviour and the applicability of theoretical methods and models compared to the real response of a dam.

- Highlight the development that has undergone within the industry especially in data-based models over the last 20 years (since Schlegeis, 2001)

- Evaluate the pros and cons of different type of models for dam behavioural analyses.

- Make the link between the FEA and data-based models. In dam prediction models both types of methods are vital for evaluation of dams.

- Discuss and evaluate methods to define warning thresholds from predictions.

Thank you for your attention!

Richard Malm, *KTH Royal Institute of Technology, Sweden*
Mateja Klun, *University of Ljubljana, Slovenia*
Alexandre Simon, *EDF Hydro, France*
Fernando Salazar, *CIMNE, Spain*
Rikard Hellgren, *KTH Royal Institute of Technology, Sweden*

AAR affected dams

Appendix: Theme B project presentation

Beauharnois dam

Proposition of a potential benchmark case for ICOLD BW 2021 (Slovenia): AAR affected dam

PRESENTED BY SIMON-NICOLAS ROTH

HYDRO-QUÉBEC PRODUCTION
DIRECTION DAMS AND INFRASTRUCTURES EXPERTISE

Past ICOLD AAR benchmarks workshops

- 2011 - Valencia, Spain

  - Case: Kariba dam (arch dam)
  - Exercise: Determining the adequate swelling law and parameters which allow the best identification with both horizontal and vertical movements of the dam vs time.
  - Number of participants: 9
  - Only one participant presented damage plots

- 2005 - Wuhan, China

  - Case: Poglia dam (hollow gravity dam)
  - Exercise: Structural behaviour of a large hollow gravity dam, with special reference to the ultimate strength against the hydrostatic load
  - Number of participants: 2

- 2001 - Salzburg, Austria

  - Case: Pian Telessio dam (arch dam)
  - Exercise: Forecast on stress-strain state generate by AAR
  - Number of participants:

- Presentation at the RILEM comitee revealed that a new benchmark case would be of interest;

- Evolution in the FE software industry (inclusion of damage and swelling laws) opens up perspectives to have a number of participants:

  - Merlin, Diana, Code_Aster, Atena, Grizzly, etc.

- The case should be formulated in a way that there is a number of steps to achieve with feedback and comparison with others before the workshop;

- Curve fitting of displacements is not enough for dam owners: damage plots, crack opening, seepage analysis, uplift pressure and potential failure modes should be given. Ideally safety factors would be nice to compute, but this is still a complex task with AAR affected dams;

- The benchmark will be used to discuss the type of physics required to correctly simulate AAR :

  - Creep, saturation, thermal effects, presence of reinforcements, uplift pressure evolution, two-way coupling, etc.
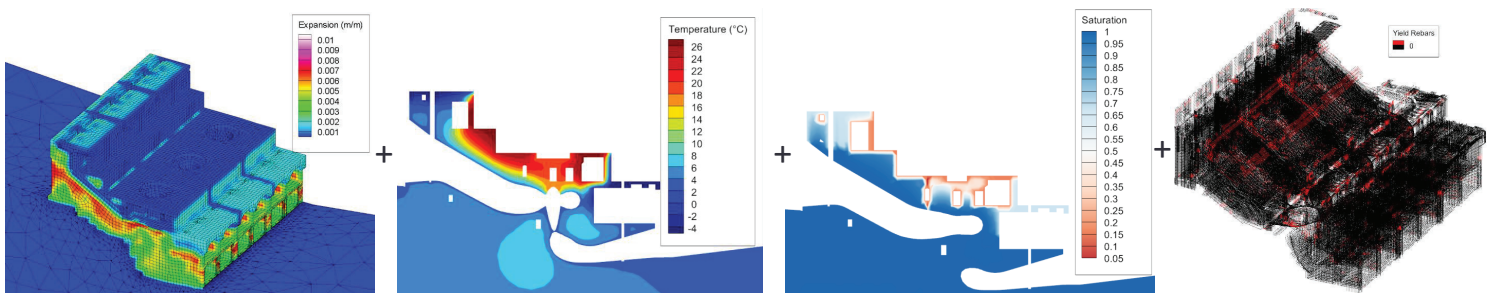
Chemical reaction   Temperature   Saturation   Reinforcement

Theme formulation

- Contributors will be given

  - Measured data for 85 years (air temperature, water level, displacements, hygral conditions)
  - CAD geometry model and FE mesh
  - Material properties
  - Reinforcements

- All types of models are welcome to use (thermal analogy, poroelasticity, multi-physic, chemo-mechanical model) from the simplest to the most complex ones.

- For all cases, the formulators will provide excel templates that the contributors should use for submittal of their results

Hydro-Québec -5

Theme formulation

To be realistic in the context of a benchmark, analysis of this section (3 groups with symetric boudary conditions)

Power house 1
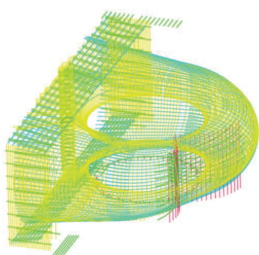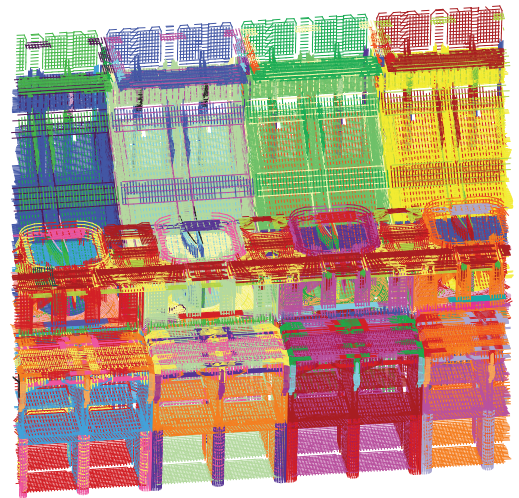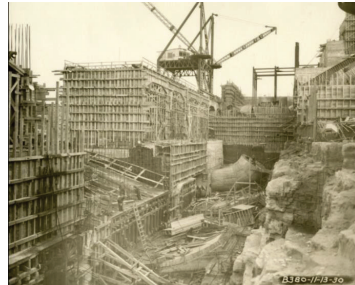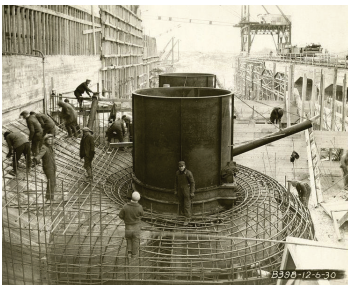
Power house 2

Power house 3
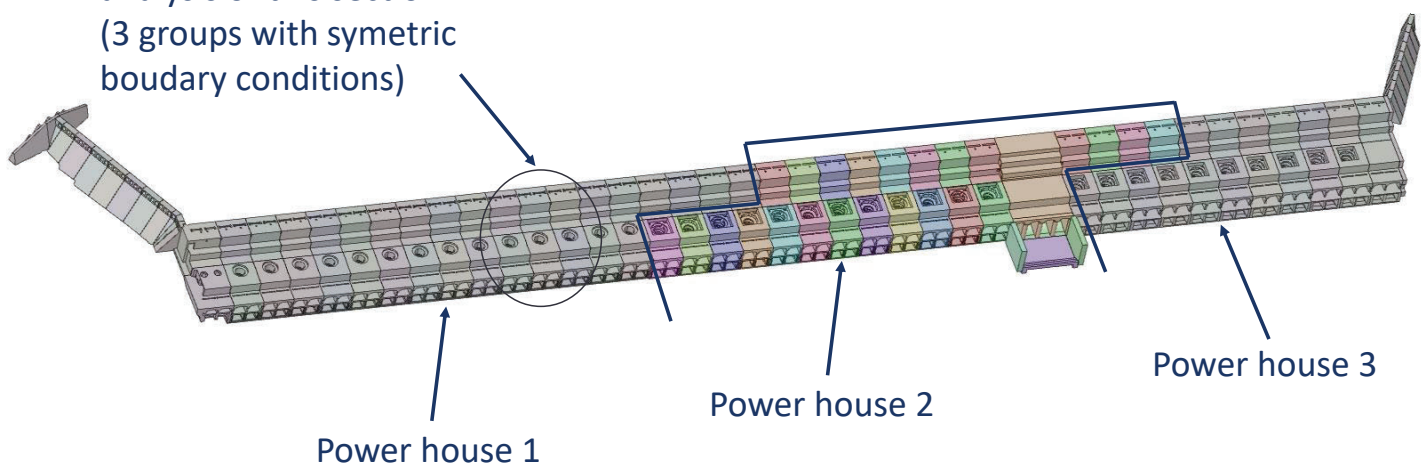
Hydro-Québec -6

Boundary conditions

The formulators will provide common set of basic boundary conditions
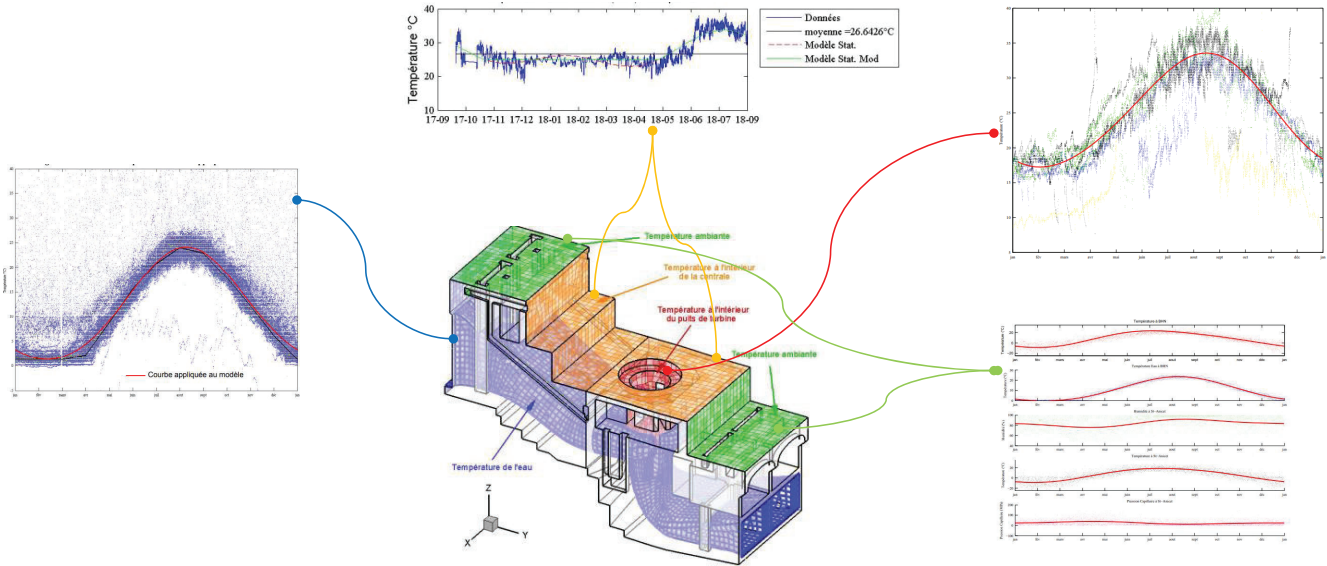
Consideration of reinforcement

The formulators will provide the reinforcement bars (discrete geometry, any modeling method is welcome)
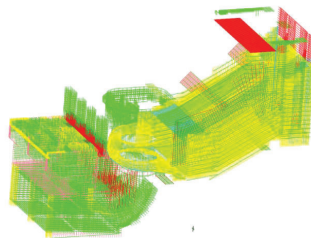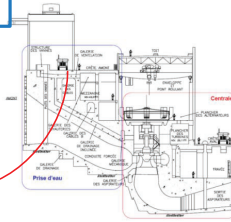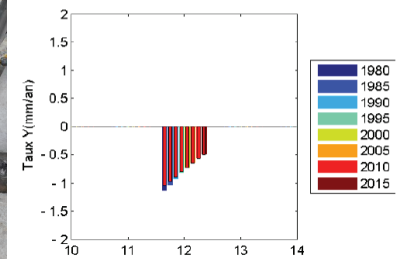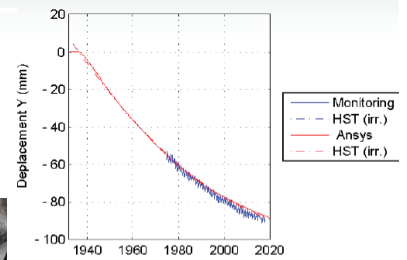
Model parameters and calibration

- Monitoring results will be available to calibrate the swelling kinetic (displacements and rates)
- Mechanical properties from:
  - Lab test (modulus, strength, …);
  - Ambient or vibration tests;
  - Slot testing.

Depending on data availability (postponed by COVID)
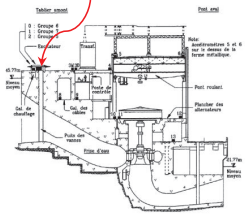
Cases

The theme consists of four subcases and include calibration (covered by the instrumentation records) + Prediction of damage for a period of 50 years

- **Case A – Chemical reaction only**

- **Case B – Chemical reaction + Temperature effects**

- **Case C – Chemical reaction + Temperature effects + Hygral effects**

- **Case D – Chemical reaction + Temperature effects + Hygral effects + Reinforcement**

Tasks

- For each case, the contributors should perform:
  - Displacement calibration/prediction (50 years period)
  - Define damage level (crack opening) at two time points
  - Interpret the effect of physic consideration
  - Loading (integration in different cross sections) and sliding safety analysis at end of prediction period
  - For two different water levels, provide the displacement differences at a specific location at the end of the 50 year period to compare the difference in stiffness with an intact structure

- Plot different output variables:
  - Hygral and thermal distribution at specific locations, rebar state (damage, plasticity)

Expected outcomes

- Give a complete benchmark case for improving the validation in the V&V process applied to complex multiphysic AAR model;

- Improve our understanding on the effect of physic integration to model AAR on full scale problems;

- Highlight the development that has undergone within industry, academic and commercial softwares to model AAR and damage;

- Compare simple and complex models on a full scale problem;

- Discuss and evaluate methods to asses the performance criteria of AAR affected structures (failure modes, safety factors).
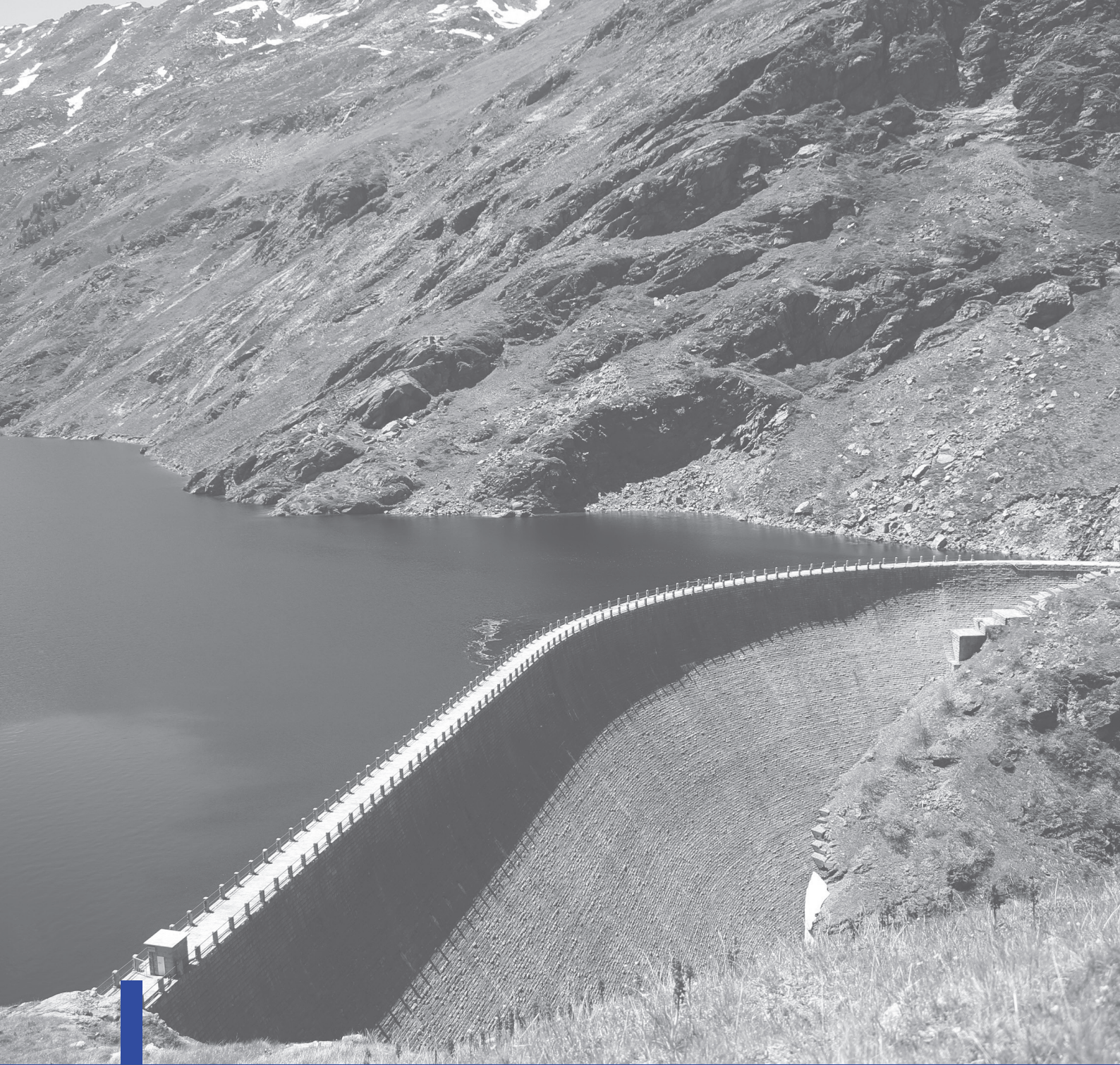
Behaviour of the embankment dam

Appendix: Theme C project presentation

Behaviour of the embankment dam

Suggested theme for the 16th ICOLD BW

Pavel Žvanut, Slovenian National Building and Civil Engineering Institute

Barbara Likar, Slovenian National Building and Civil Engineering Institute

Žiga Likar, Geoportal d.o.o.

Vanja Selan, Elea iC d.o.o.

Mateja Klun, University of Ljubljana, Faculty of Civil and Geodetic Engineering

Introduction

- Embankment dam is the most common dam type in the world, since they represent over 60% of all constructed dams worldwide.

- Seepage control plays an important role in embankment dam safety.

- The most common causes of embankment dam failures are associated with internal erosion.

Theme: The embankment dam

- The theme is devoted to the analysis of a zoned embankment dam in Slovenia.

- The dam is regularly monitored:
  - Geodetic measurements (vertical and horizontal displacements);
  - Vertical inclinations (4 inclinometers);
  - Water level, temperature and specific electrical conductivity (piezometers);
  - Drainage outflow, chemical analysis of water;
  - Water level in reservoir, ground accelerations, meteorological parameters;
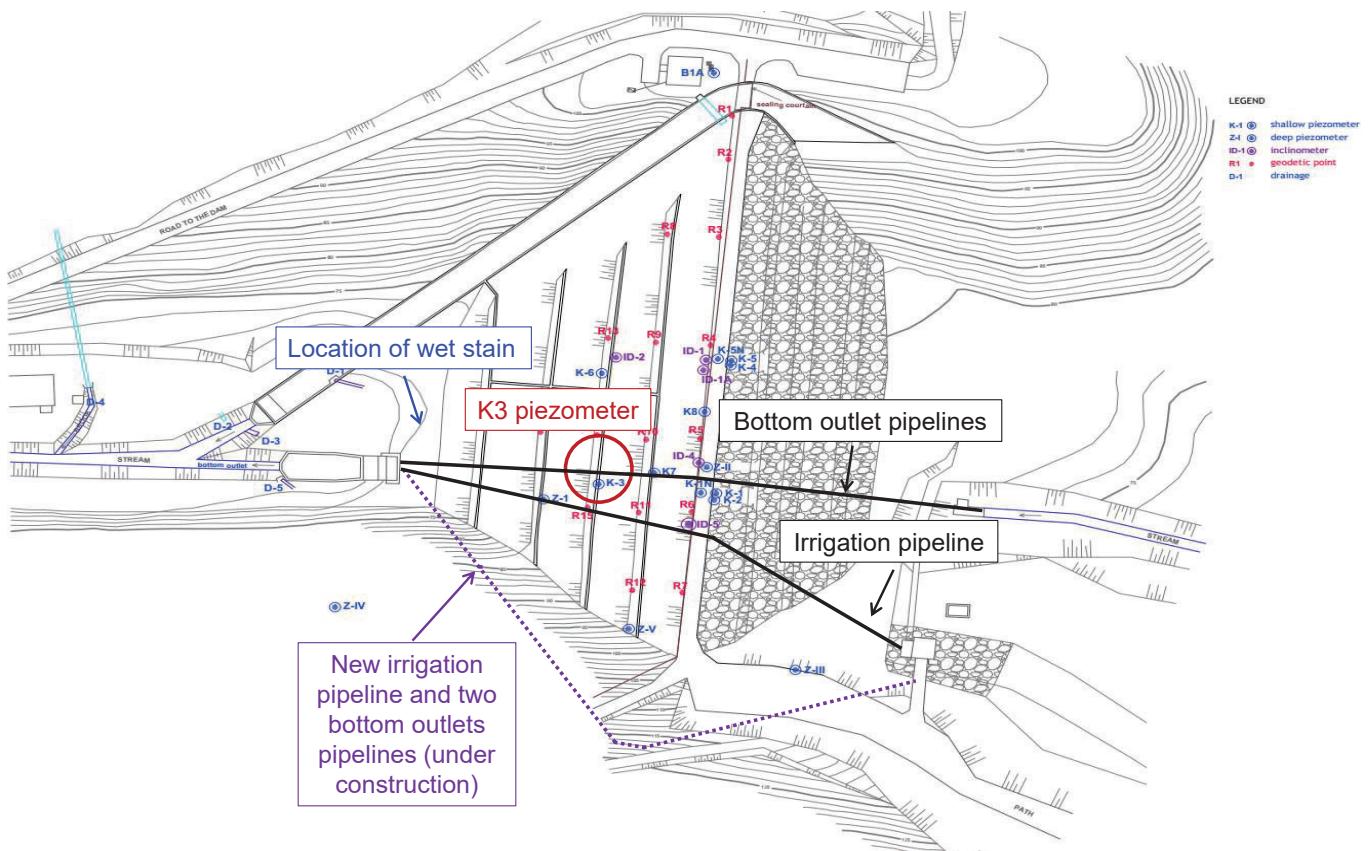 - Geological inspection.

Basic information on the dam

- Zoned embankment dam with a clay core.
- 35 m high, crest length 177 m.

The story of the dam

- The dam is over 30 years old.
- In 2007 during regular maintenance a wet stain was spotted. Moreover, one of the piezometer indicated rising levels of water in the dam body.
- The reservoir level was depleted from 98.8 m a.s.l. to 92 m a.s.l.
- There are three conduits passing through the body of the dam, irrigation pipeline and two bottom outlets. The origin of leakage was recognised to be the irrigation pipeline crossing the dam body. The irrigation pipeline was later filled with concrete.
- The reservoir has been drawdown for over 10 years, and after the remedial works, the owner expects to raise the reservoir level back to the nominal level.

Cross-section of the dam

LEGEND

(A) clayey silt material
(B) rockfill material
(C) tailing and clayey silt material
(D) clay material
(E) Impermeable rock base

(1) intake tower
(2) intake structure
(3) bottom outlets
(4) irrigation pipeline
(5) filter material
(6) maximal operating level
(7) minimal operating level
(8) access shaft for irrigation pipeline
(9) normal operating level
(10) depleted operating level

Theme formulation

- Contributors will receive:
  - CAD geometry model;
  - Measured monitoring data since construction;
  - Design material properties for the dam and foundation.

- Participants will be asked to:
  - Built a 2D and a simplified 3D models of the dam (full 3D optional);
  - Consider monitoring data;
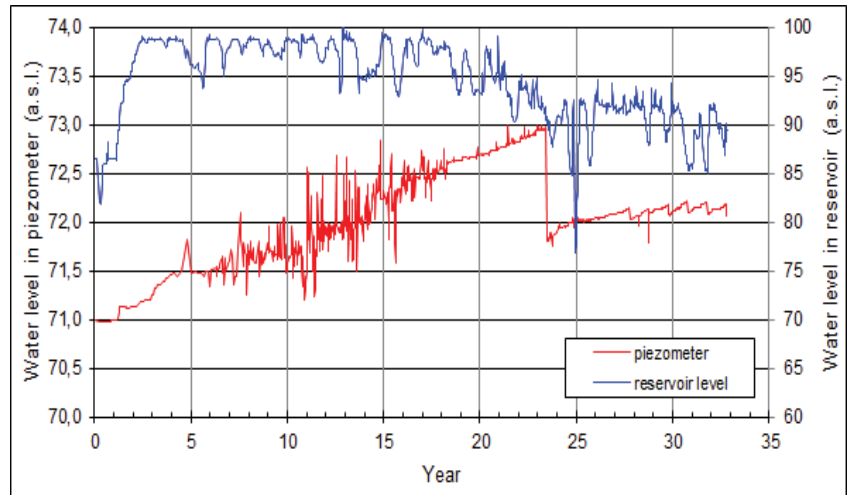 - Perform mandatory and optional tasks.

Monitoring data

Example of the piezometer measurements

- Rising water level in piezometer K3 was observed after 6 years of operation.

Tasks

Case	Tasks
Case 1 (Mandatory, Optional)	**Task 1:** Construction of a 2D model. Calibrate the model using dam surveillance. Estimate the as-built characteristics of the dam. **Task 2:** Evaluate the initial state after the reservoir is filled to the nominal level. Estimate the dam condition before the detection of leakage. **Task 3 (Optional):** Using calibrated data of 2D model, build a quasi 3D FE model (20 m wide section of the dam).
Case 2 (Mandatory, Optional)	**Task 1:** Consider the wet stain using 2D or quasi 3D model. **Task 2:** No action after the appearance of the wet stain.
Case 3 (Mandatory)	**Task 1:** Consider remedial works of the dam, consider long period of reservoir draw-down and its effect of the clay core. **Task 2:** Consider elevation of the reservoir back to nominal level according to the assumed filling times. Evaluate the safety of the dam under the final water level condition of the reservoir.
Case 4 (Optional)	**Task 1:** Seismic analysis.
Finalisation (Mandatory)	**Task 1:** Preparation of the technical paper. **Task 2:** Preparation of the presentation and presentation at the workshop.

* **as an optional case the participants can build a full 3D model and perform the required analysis.**

Outcomes and conclusions

- We expect that the results of this theme will improve our understanding of the dam behaviour, especially water seepage through the dam body and show the applicability of theoretical methods and models compared to the real response of a dam.
- The ageing dams will encounter various conditions in their life-time including longer periods of low-reservoir levels.
- Seepage is a complex phenomenon affected by various parameters; studies have shown that with careful evaluation of monitoring data, accidents and failures can be prevented.
- FEM provides a strong tool in hands of a qualified engineer, while such a complex phenomenon as seepage in an embankment dam can be studied using different modeling assumptions. BW provides a unique opportunity for dam experts to discuss various modelling approaches and assess their formulation on the final results.
- The formulators will provide templates for the participants to submit their results.
- The participants will be asked to describe their modelling approaches in detail. Based on comparison of various approaches, results and monitoring data, we will be able to improve our understanding of the seepage phenomena in embankment dams.

You are kindly invited to participate.

See you in Ljubljana in 2022.

Express your interest in the topic and get in touch with the formulating team.